S-2

II

SPACE SYSTEMS

Document No. 70SD4207
11 February 1970

EARTH RESOURCES TECHNOLOGY SATELLITE SPACECRAFT SYSTEM DESIGN STUDIES FINAL REPORT

VOLUME II

SUBSYSTEMS STUDIES

BOOK I OF 2

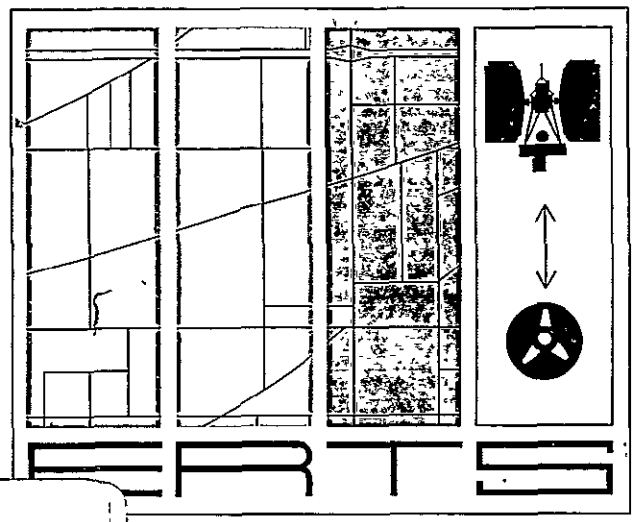

Prepared For
GODDARD SPACE FLIGHT CENTER
GREENBELT, MARYLAND 20771

GENERAL ELECTRIC

DOCUMENT NO. 70SD4207
11 FEBRUARY 1970

EARTH RESOURCES TECHNOLOGY SATELLITE SPACECRAFT SYSTEM DESIGN STUDIES FINAL REPORT

VOLUME II

SUBSYSTEMS STUDIES

BOOK I OF 2

PREPARED FOR:

GODDARD SPACE FLIGHT CENTER
GREENBELT, MARYLAND 20771

UNDER

CONTRACT NO. NAS 5–11529

GENERAL ELECTRIC

SPACE SYSTEMS ORGANIZATION
Valley Forge Space Center
P. O. Box 8555 • Philadelphia, Penna. 19101

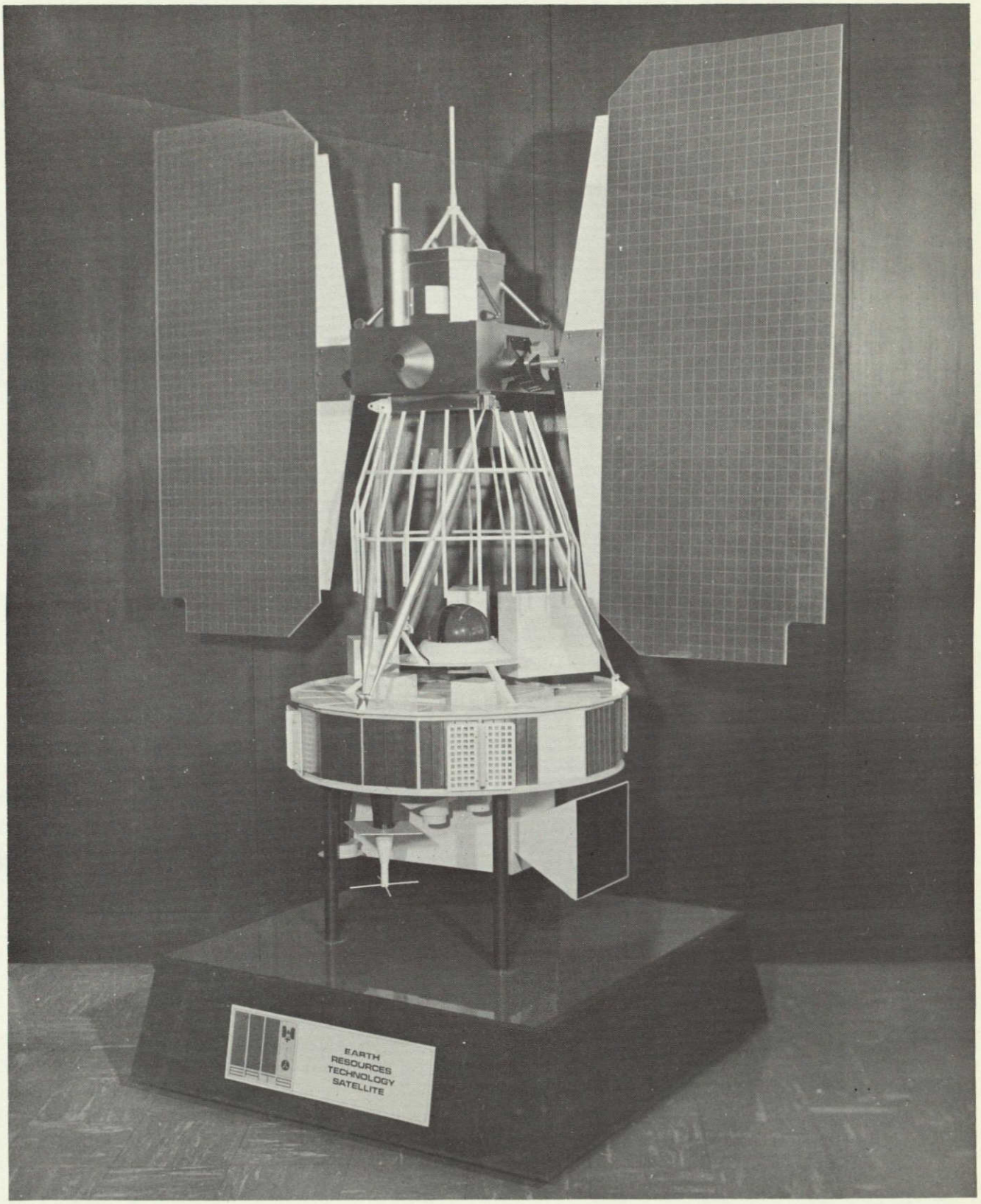
EARTH
RESOURCES
TECHNOLOGY
SATELLITE

TABLE OF CONTENTS

TABLE OF CONTENTS (Continued)

TABLE OF CONTENTS (Continued)

TABLE OF CONTENTS (Continued)

TABLE OF CONTENTS (Continued)

TABLE OF CONTENTS (Continued)

LIST OF ACRONYMS

NDPF	NASA Data Processing Facility
NTTF	NASA Tracking and Training Facility
WBVTR	Wide Band Video Tape Recorder
MSS	Multi-Spectral Scanner
RBV	Return Beam Vidicon
WB	Wide Band
RBVC	Return Beam Vidicon Camera
DCS	Data Collection System
OCC	Operations Control Center
TLM	Telemetry
NB	Narrow Band
MSFN	Manned Space Flight Network
nm	Nautical Mile
M	Meters
PCM	Pulse Code Modulated
I/O	Input/Output
STADAN	Satellite Tracking and Data Acquisition Network
AGE	Aerospace Ground Equipment (also equivalent to GSE or STE)
PMP	Premodulation Processor
CIU	Command Integration Unit
COMDEC	Command Decoder
PCM/FSK	Pulse Code Modulated/Frequency Shift Keyed
Nort.	Nortronics
FHC	Fairchild-Hiller Corp.
Cal Comp	California Computer Co.
PCM/PSK	Pulse Code Modulated/Phase Shift Keyed
IRLS	Interrogation, Recording and Location Subsystem
ITP	Integrated Test Plan
BIT	Bench Integrated Test
T/V	Thermal Vacuum
WTR	Western Test Range
GFE	Government Furnished Equipment
C&DH	Command and Data Handling Subsystem
VIP	Versatile Information Processor
SASS	Solar Array Sun Sensor
RWS	Reaction Wheel Scanner
SAD	Solar Array Drive
ADP	Automatic Data Processing
SWR	Standing Wave Ratio
RDT	Raw Data Tape
RMP	Rate Measuring Package
YIRU	Yaw Inertial Reference Unit
LN	Lead Network
RSAD	Right Solar Array Drive
HAC	Horizon Attitude Computer
ACS	Attitude Control Subsystem
PSA	Pneumatic Subassembly

SECTION 1

INTRODUCTION

1.1 STUDY OBJECTIVE

The primary objective of this study is to develop an observatory spacecraft capable of meeting the performance requirements of the ERTS mission. In attaining this objective, it was necessary to perform the analysis delineated in NASA Study Specification S-701-P-3, and other associated analysis and design tasks, to establish the overall Spacecraft Basline Design.

1.2 AREA OF STUDY

Heavy emphasis was placed on the Communications and Data Handling System, Image Location Requirements and Sensor, Electrical Integration, Thermal Control and Payload Integration. In addition, each of the other subsystems have been analyzed on the basis of mission requirements and constraints. With the completion of the analysis, a subsystem design, hence, a "black box" design was established.

1.2.1 COMMUNICATIONS AND DATA HANDLING SYSTEM

The Communications and Data Handling requirements were significantly changed after the General Electric submittal of June 1969' therefore, considerable effort was expended in this area. Complete analysis of the uplink capabilities and the downlink requirements was made to interface with both MSFN and STADAN equipment that is in place at Corpus Christi, Alaska and the NTTF facilities.

This analysis resulted in the establishment of the subsystem and "black box" requirements for the system. An industry and literature search of existing equipment was made to determine the availability of flight-proven components meeting the overall requirements. Subsystem and "block box" specifications were prepared, and RFP's sent to vendors of known capabilityin the specific technology areas. Evaluation of the proposals and existing hardware designs led to the baseline design in Section 1.4.

1.2.2 IMAGE LOCATION

Extensive analysis in this area has led to the design requirements for an Attitude Sensor enabling the location of a given point in a 100 by 100 nm scene to within 2 nm. The types of sensors available and in development have been reviewed. The specifications were prepared and sent out for quotes. The evaluation of the different types of sensors and the proposals has resulted in the selection of a flight-proven earth sensor that will meet the ERTS mission requirements.

1.2.3 ELECTRICAL INTEGRATION

The Electrical Integration Subsystem is critical in the overall spacecraft design. The grounding, shielding and power and signal distribution philosophy has been established to minimize the problems of electromagnetic interference. In addition, an Electromagnetic Control Plan has been prepared specifically for ERTS.

1.2.4 THERMAL CONTROL

Thermal Control on the spacecraft has been established by a complete analysis of the orbital and operational requirements placed on the system. The louvered control of the sensory ring bays temperatures is flight-proven on several spacecraft; the heat dissipation and rejection capability in each bay has been established. Analysis of the operational aspects of the center-section equipment has established the method of heat dissipation, and has sized the radiators and the insulation requirements.

1.2.5 PAYLOAD INTEGRATION

The integration of the various GFE items into the basic spacecraft structure and electrical system has been performed during this study. The data received from the GFE suppliers via NASA Goddard has been incorporated into the system design. Mechanical, Electrical and Thermal interfaces have been established for each item. The requirements for data transmission has been included in the design for the Return Beam Vidicon Cameras, Multispectral Scanner, Wideband Video Tape Recorder and the Data Collection System information flow.

1.3 DESIGN CONSTRAINTS

The following system level constraints were invoked on the spacecraft design:

1. Orbit - Sun-synchronous

Altitude	492.35 nm
Inclination	99.088°
Ascending Node Time	2130
Eccentricity	0

2. Thermal Environment

Temperature	$20^{\circ}C \pm 10^{\circ}C$

3. Attitude Control

Position Error (All Axes)	0.7°
Rate Error (Required)	$\leq 0.04^{\circ}$/sec
(Goal)	$\leq 0.015^{\circ}$/sec
Target Location	$\leq$ 2 nm in 100 x 100 nm Scene

4. Communications and Data Handling

   a. Command

Uplink Frequency	148-154 MHz	STADAN
	2106.4 MHz	MSFN

Real Time Digital Commands	≥ 256
Stored Digital Commands	≥ 30
Fail Safe Design	

b. Narrowband

Downlink Frequency	136-138 MHz 2287.5 MHz MSFN
Data Accuracy	8 bits
Real Time Data Rate	≤ 1kbs
Playback Data Rate	≥ 20 kbs

c. Wideband

Downlink Frequency	2265.5 MHz 2229.5 MHz
Bandwidth (RBV)	20 MHz
Power	20 watt Commandable
Operating Elevation	$\geq 5^{o}$
Receiving Antenna	30-ft or 85-ft dish
Bandwidth (MSS)	20 MHz

d. Tracking

USB Ranging (Prime)

Minitrack System (Back-up)

e. Storage

Wideband Video Tape Recorder	GFE-Supplied
Narrowband Tape Recorder	Contractor-Supplied

f. Timing

Common Spacecraft Clock

5. Power

Operate the payload at least 20 minutes per orbit

6. Lifetime

   One year in Orbit

7. Orbit Adjust

   Correct for Injection Error

   Provide for Drag Make-up

1.4 SPACECRAFT BASELINE DESIGN - SUMMARY

1.4.1 STRUCTURE

The basic structure is the same as the flight-proven Nimbus design.

1.4.1.1 SENSORY RING

The sensory ring is made up of 18 bays, each capable of supporting a 6 by 8 by 13-inch component, with indivudal bay thermal control. The different antenna systems are mounted below the ring and the three attachments for the Orbit Adjust System are on the top of the ring, as are the truss assembly attachments.

1.4.1.2 Cross Beam

The cross beam is mounted across the center of the sensory ring and is the support structure for the Return Beam Vidicon Cameras, the Multispectral Scanner, the Wideband Video Tape Recorders, the Narrowband digital tape recorders and the Power Switching Module.

1.4.1.3 Truss Assembly

The truss assembly is mounted to the top of the sensory ring and is the support structure for the Attitude Control Subsystem and the Solar Array Panels.

1.4.1.4 Adapter

The adapter is the interfacing structure between the spacecraft and the launch vehicle. It houses the RF reradiators and pick-ups for the Antenna Systems. In addition, stimulators for checkout of the sensors are mounted in the adapter.

1.4.2 ATTITUDE CONTROL SUBSYSTEM

The Attitude Control Subsystem (ACS) consists of 11 major component parts, plus a pneumatic subsystem. It is mounted to a structure composed of mounting surfaces on top of a honeycomb baseplate. Solar paddles are attached to two shafts, with individual drive motors to provide greater reliability in solar tracking.

The ACS is required to align the satellite with the local earth vertical and orbit velocity vectors to within 0.7 degree for all three axes. The instantaneous angular rates about the axes during normal operation are required to be less than 0.04 degree/second with a goal of 0.015 degree/second. To accomplish this, a 3-axis active ACS is provided, using horizon scanners for roll and pitch attitude error sensing and two gyros, one for sensing yaw rate and one to be used in a gyro compassing mode to sense yaw attitude. The torquing subsystem uses a combination of reaction jets to provide net momentum control and large control torques when required. Flywheels are utilized for fine control and residual momentum storage.

1.4.2.1 Roll Reaction Wheel Scanner
There are two roll reaction wheel scanners in the system. These reaction wheel scanners provide scanner pulses for pitch and roll attitude error computation and provide reaction torque for roll control.

1.4.2.2 Signal Processor
There are two signal processor units in the subsystem. These components process the signals from the scanners, reject sun and shape the signals for the control logic.

1.4.2.3 Control Logic
There is one control logic component in the subsystem. This unit calculates pitch and roll attitude errors, processes yaw signals, contains the wheel and pneumatic drivers, pulse modulators, command logic and compensation networks for all three axes.

1.4.2.4 Pitch Reaction Wheel
The pitch reaction wheel provides reaction torque for pitch control.

1.4.2.5 Yaw Reaction Wheel
The yaw reaction wheel provides reaction torque for yaw control.

1.4.2.6 Rate-Measuring Package
There are two rate-measuring packages in the subsystem, providing full redundancy of operation. The unit provides rate signals used to generate yaw axis rate and position signal.

1.4.2.7 Yaw Rate Gyro
This unit provides rate signals to reduce yaw rates during the acquisition mode.

1.4.2.8 Initiation Timer
The initiation timer enables the solar array drive and control logic at acquisition.

1.4.2.9 Solar Array Drive
There is a solar array drive for each panel, and their function is to orient the solar array toward the sun.

1.4.2.10 Magnetic Moment Assembly
The magnetic moment assembly provides compensation for the spacecraft magnetic moment.

1.4.2.11 Pneumatics
The pneumatics provide torque for acquisition, momentum wheel unloading, and momentum wheel back-up (coarse mode).

1.4.2.12 Attitude Sensor
The attitude sensor provides an independent attitude measurement to determine a given target location within 2 nm.

1.4.3 POWER SUBSYSTEM

The power subsystem is essentially the same as the one on Nimbus, the principal difference being the addition of another power regulator to the subsystem to increase the regulated bus capability for the payload units.

The subsystem has been designed to provide -24.5 vdc regulated to ± 0.5 volts to the experimental and service subsystems of the spacecraft. The basic functions performed to accomplish this may be summarized as follows:

1. Acquisition of incident solar radiation and photovoltaic conversion to electrical power.

2. Energy storage by electrochemical means.

3. Regulation of electrical power to provide voltage levels suitable for distribution to spacecraft loads.

1.4.3.1 Solar Array

There are two 4 by 8 foot solar panels capable of producing 14.26 amperes at -35 ± 0.2 volts. The purpose of this array is to provide power during operation of the spacecraft and to supply charging power for the batteries during non-operating periods.

1.4.3.2 Storage Modules

Each storage module contains a series string of 23 nickel-cadmium storage cells, each rated at 4.5 ampere-hour capabity. The charge current available during a satellite day is determined by the solar array output and the spacecraft subsystem load power requirements, and is regulated as a function of battery voltage and temperature with a closed-loop charge controller. The maximum charge current is also limited to a preset value. The charge current level is reduced when either the battery voltage or temperature reaches a predetermined limit. A ground commandable override circuit (in the power control module) opens the voltage-temperature control loop in the charge controller, permitting battery charge rates based on the battery voltage-solar array bus voltage relationship, and maximum limited to 1.1 amperes per battery. Battery voltages, current and temperature are telemetered. A shunt dissipator is provided in each module to control the dissipation of excess array power up to 50 watts. All shunt dissipators in the system are turned on at approximately the same time by a single feedback amplifier (shunt dissipator driver) in the power control module.

In the negative leg of each battery is a battery disconnect latching relay which can be actuated by ground command. This relay also disconnects the battery fuse blow tap line.

The storage module also contains a charge controller. The purpose of the charge controller is to protect the battery from overcurrent, overvoltage, and overtemperature conditions while it is being charged. The circuit performs this function by monitoring and operating upon the following parameters:

1. Battery charge current

2. Battery temperature

3. Battery terminal voltage

1.4.3.3 Power Control Module

The subsystem contains two identical power control modules. Each module has a completely redundant PWM regulator with an automatic switch over network. The regulated output is -24.5 ± 0.5 volts and is current-limited at 20 amperes.

1.4.3.4 Auxiliary Loads

There are two auxiliary load panels provided to minimize battery overchange. The loads can be individually commanded as required.

1.4.3.5 Auxiliary Load Controller

The auxiliary load controller provides the capability to operate the auxiliary loads individually.

1.4.4 ELECTRICAL INTEGRATION SUBSYSTEM

The Electrical Integration Subsystem is composed of all the harnesses, power and signal distribution components and the telemetry conversion modules. The design is based on previous experience with the Nimbus spacecraft.

1.4.4.1 Harnesses

The spacecraft harness is made up of many segments designed to distribute the signal and power, by classification, to minimize the electromagnetic interference effects.

1.4.4.2 Power Switching Module

The power switching module is a relay box logically designed to distribute the power and signals throughout the spacecraft system.

1.4.5 COMMUNICATIONS AND DATA HANDLING

The Communications and Data Handling Subsystem is composed of the wideband data link, the narrowband telemetry, tracking and command link and the transmission link for the Data Collection System.

1.4.5.1 Wideband Telemetry

The wideband telemetry equipment is designed to transmit the data from the multispectral scanner, return beam vidicon camera and the wideband video tape recorder to the ground network .

1.4.5.1.1 Wideband Antenna

The wideband antenna has been designed as a shaped-beam antenna operating at 2265.5 MHz and 2229.5 MHz. It has a nearly constant earth illumination for ± 60 degrees with a gain ≥ 4 dB at ± 60 degrees.

1.4.5.1.2 S-Band Power Amplifier
There are two S-Band power amplifiers in the system, each capable of operating at 2229.5 MHz or 2265.5 MHz, and each having a commandable 20-watt and 10-watt operating mode.

1.4.5.1.3 Wideband FM Modulator
The wideband FM modulator consists of two channels cross-strapped for redundancy. Each channel has the capability to modulate either a video input with a 3.5 MHz bandwidth or a PCM input with a transmission rate of 15 mbps. The outputs feed into the S-Band power amplifiers.

1.4.5.1.4 Signal Conditioner
The signal conditioner interfaces with the payload. It accepts stored and real-time information from the MSS, RBV, and two associated wideband video tape recorders. It commandably selects a pair of inputs, buffers and reconstitutes real-time or stored PCM (15 mbps) from the MSS, and buffers real-time or stored video (3.5 MHz BW) signals from the RBV. The MSS and RBV signals are routed to the FM modulators.

1.4.5.2 Narrowband Telemetry, Tracking and Command
The narrowband telemetry, tracking and command equipment provides the means for collecting and transmitting housekeeping data from the spacecraft to the ground net, providing a tracking beacon for the spacecraft, receiving commands from either the MSFN or STADAN net and implementing those commands aboard the spacecraft. In addition, it provides the link for transmitting data from the Data Collection System to the ground equipment.

1.4.5.2.1 PCM Telemetry Processor
The PCM telemetry processor samples the output of all the telemetry (housekeeping) sensors onboard the spacecraft, processes the data, and inserts it into an output bit stream to be stored on the narrowband digital tape recorder or transmitted real time. This unit is identical to the Nimbus D PCM telemetry processor.

1.4.5.2.2 VHF Transmitter
The VHF transmitter will operate as a minitrack beacon, and in a normal telemetry mode, receiving signals from the PCM telemetry processor at a 1 kbs rate, or in the playback mode at a 24 kbs rate. The unit is completely redundant, operates at a frequency of 137.86 MHz, and is a modification of a space-qualified transmitter.

1.4.5.2.3 Quadraloop Antenna
The quadraloop antenna is composed of four quadraloop elements spaced around the periphery of the spacecraft sensory ring. The antenna receives its input from the VHF transmitter

and operates at a frequency of 137.86 MHz. This antenna is identical to the Nimbus space-qualified antenna, except the feed point has been adjusted for an impedance match.

1.4.5.2.4 Command Antenna
The command antenna is a monopole-type antenna located on the top of the Attitude Control Subsystem package at the top of the vehicle. The antenna operates at a frequency of 154.2 MHz and is omnidirectional. This antenna is similar to the flight-proven unit on Nimbus, the only difference being in length for impedance matching. It receives commands from STADAN stations.

1.4.5.2.5 Command Receiver
The command receiver receives its input, at a frequency of 154.2 MHz, from the command antenna. The unit is composed of two redundant superhetrodyne receivers and two redundant PCM command demodulators. The function of the unit is to convert commands, received at 128 bps, from the STADAN ground station into intelligence suitable for storage and/or execution. One channel shall remain on continuously.

1.4.5.2.6 Unified S-Band Antenna
The unified S-Band equipment consists of a diplexer, hybrid, transponder and mixing amplifiers. Commands are received from the MSFN site through the unified S-Band antenna at a 1 kbs rate to the diplexer, hybrid, receiver portion of the transponder. The receiver output goes into a 70 khz discriminator packaged in the premodulation processor. Downlink information enters the equipment through a mixing amplifier, a S-Band transmitter, to a diplexer and out through the antenna. The power output of the transmitter is 2 watts. This equipment is similar to equipment flight-proven on Apollo.

1.4.5.2.8 Premodulation Processor
The premodulation processor forms a composite baseband for transmission of data via the unified S-Band equipment. In addition, it demodulates the 70 khz command subcarrier from the USB receiver for transfer of command data from MSFN site to the command integrator for further processing. This unit is similar in design to the Apollo premodulation processor.

1.4.5.2.9 Command Integrator Unit
The command integrator unit accepts signals from the VHF command link at 128 bps or the USB command link at 1 kbps, operates on the signals and provides an acceptable input for the command clock. Provision is made to inhibit commands that are being transmitted from one site while commands are going in via another site. The design is also such that commands from the same site for another spacecraft will not be accepted. The output of the command integrator is fed to the command clock, either at 128 bps rate (STADAN) or 200 bps rate (MSFN).

1.4.5.2.10 Command Clock
The command clock provides an accurate time base for spacecraft operations, generates time codes for transmission or storage, receives, processes and stores command information from the command integrator and executes these commands at predetermined times. The

capability for 30 stored commands and more than 256 real-time digital commands exist within the component. This component is identical to the Nimbus clock and is a space-qualified component.

1.4.5.2.11 Narrowband Digital Tape Recorder
The narrowband digital tape recorder accepts NRZ-L data from the PCM telemetry processor at a 1 kbx rate. The data is recorded directly in the tape and played back at a 32 kbs rate. The data can be played back either over the VHF transmitter link or through the USB equipment to the ground net. The unit is similar to those flown on other space programs.

1.4.6 Orbit Adjust Subsystem
The Orbit Adjust Subsystem will provide correction for initial vehicle-injection errors, and for orbit maintenance due to drag. It is composed of all space-qualified components, except for the tank which will be modified and requalifed for higher pressure levels. The total ΔV available is 45 ft/sec. This includes a margin of 30 percent. The subsystem is a hot gas system using monopropellant hydrazine (N_2H_4) for the propellant and nitrogen (GN_2) for the pressurant.

1.4.6.1 Tank
The tank is an 11-inch-diameter tank with an ethylene propylene rubber (EPR) diaphragm. There are two ports in the tank, one is the propellant inlet/outlet, and one is the GN_2 fill valve.

1.4.6.2 Thruster
The thrusters contains a combustion chamber, catalyst bed, expansion nozzle and an injector. It will produce a thrust of 1.0 to 0.7 pounds of force.

1.4.6.3 Propellant Valve
The propellant valve is a series redundant, normally closed, solenoid-actuated device and is directly attached to the thruster.

1.4.6.4 Normally-closed Explosive Valve
This unit is a squib-actuated parallel redundant valve which prevents premature engine firings. It is actuated through a fail-safe command.

1.4.6.5 Normally-Open Explosive Valve
This unit is a squib-actuated valve used for shutting off the gas supply in case of malfunction in the thruster. It is commanded by a fail-safe command.

1.4.6.6 Fill, Drain and System Test Valves
These manually operated valves are for preflight testing only.

1.4.6.7 Filter
The filter will prevent particulate contamination from entering the propellant valves.

1.4.6.8 Temperature Transducer

The Temperature Transducer is of the surface-temperature type. The gas temperature is monitored via the Narrowband Telemetry Subsystem.

1.4.6.9 Pressure Transducer

The pressure transducer utilizes semiconductor strain gauges bonded to a machined constant modulus steel diaphragm. The propellant pressure is monitored via the narrow-band telemetry link.

1.4.7 THERMAL SUBSYSTEM

The Thermal Subsystem provides control of the sensory ring heat absorption and rejection rates. Passive control, such as coatings and/or isulation, is used on the large areas of the top and bottom surfaces of the ring structure. Active control, in the form of thermal control shutters, is used on the peripheral areas of the sensory ring. Passive thermal control utilizes the absorptivity and emissivity of the external sensory ring structure surface to limit the operating temperature range. Insulation between the external surface and the inner volume of the sensory ring is in the form of a blanket consisting of 32 layers of 1/4-mil Mylar, aluminized on both sides. The insulation is described as multibarrier radiation insulation.

Active control is provided by sensing component temperatures and positioning movable insulation, in the form of shutters, to increase or decrease the heat rejection rate. Behind the shutters are surfaces which have high emissivities and low solar (and albedo) absorptivities. The coating, in conjunction with the shutter, maximizes the heat rejection at the full shutter open positions, but minimizes the heat absorption.

In flight, the spacecraft is permitted to seek its own thermal equilibrium level as a function of its orbital environment, internal heat dissipation, and inherent thermal design characteristics.

1.4.7.1 Passive Control

The top surface of the sensory ring will be insulated with super insulation blankets comprised of 32 layers of aluminized Mylar. One layer of AMFAB will be used to cover the exposed surface of the insulation.

With the exception of the selected cutouts, the lower surface of the sensory ring will be covered with 32 layers of aluminized Mylar. The fiberglass insulation support is coated, on the exposed surface, with D4D. Battery lower surfaces, exposed through the cutouts in the insulation, are coated with RV 100. A radiator of high emissivity and low absorbitivity will be provided in the center section for heat rejection in that area.

1.4.7.2 Active Control

The shutter array in each bay is controlled by a fluid bellows actuator. By opening the shutter array, the net heat exchange between the heat radiating surface(s) internal to the shutters and space is increased. This results from an increase in the effective emissivity of the heat radiating surface(s).

The shutter consists of a serpentine capillary tube connected to two bellows, which in turn are connected through a simple bar linkage to the individual shutters. The serpentine tube is fastened to the sensing plate, and the sensing plate is riveted to a bay separator. The capillary tube, referred to as the sensor tube, is filled with Freon-14.

In the event of a loss of the sensor fluid, the fail-safe bellows retract and bring the shutters to a midpoint position. The fail-safe positions can be mechanically adjusted through the use of a nylon screw on the fail-safe bellows. This setting will be predicated on the desired emissivity for each bay.

1.4.7.3 Thermal Strip Heaters (Compensation Loads)
Strip heaters will be used on ERTS for the purpose of maintaining a favorable thermal balance within the areas of the various subsystems as the operational modes, and thus, the thermal outputs of these subsystems are changed. These heaters are called the compensation loads and can be directly commanded on whenever the temperature of the surrounding subsystem areas becomes too low.

1.4.7.4 Thermistors
Thermistors identified by alphanumeric designators are used throughout the sensory ring to monitor temperatures and to evaluate the spacecraft heat balance. This is needed to perform operational thermal management. Thermistors (and shutter position indicators) are supplied with voltage derived from zener diode, resistor networks.

1.4.8 AGE
All Nimbus AGE has been reviewed to determine its application to the ERTS Program. All necessary AGE has been identified and designated as to whether it was identical or modified. The degree of modification has been defined in each case.

1.4.8.1 Mechanical AGE
The mechanical AGE consists of all that equipment necessary to handle the spacecraft and its subassemblies during the assembly, test, ship and prelaunch phase of the program.

1.4.8.2 Electrical AGE
The electrical AGE consists of all equipment necessary to perform electrical/electronic tests and integration and verification of performance during subsystem, system assembly and final systems test at Valley Forge Space Center and the Western Test Range prior to launch.

SECTION 2

STRUCTURE SUBSYSTEM

SECTION 2

STRUCTURE SUBSYSTEM

2.1 INTRODUCTION

The ERTS Spacecraft and Structure Subsystem meets the payload accommodation and requirements for the ERTS A and B missions. The ERTS spacecraft is shown in Figure 2.1-1. The spacecraft has four major configurational elements (Figure 2.1-2):

1. Attitude Control Subsystem (ACS)
2. Solar Array Paddles
3. Truss Structure
4. Sensory Ring

In the launch configuration, the solar arry is folded along its longitudinal axis to fit within the Sensory Ring envelope and is secured to the truss structure by a latch mechanism. The spacecraft is mounted on an adapter structure, which, in turn, is bolted to the launch vehicle adapter ring. Spacecraft/adapter separation occurs at the lower ring flange of the sensory ring.

The Structures Subsystem design is based on the existing design of Nimbus. The major elements have been developed and flight proven on the Nimbus program. Changes have been made only in the center section of the sensory ring assembly to accommodate ERTS payload and other new equipment. The spacecraft can accommodate up to 610 pounds of payload with a packaging volume of 48 cubic feet interfacing with the sensory ring structure. A total earth viewing area of 16.4 square feet is available to incorporate equipment such as payload sensors and antennas with an earth viewing requirement and without providing deployment functions. Additionally, the spacecraft and adapter is compatible with the Delta launch vehicle with an existing SACS ring and shroud.

The ERTS Structures Subsystem includes the Sensory Ring with cross beam, the truss structureture and the adapter. The ACS Package is part of the Attitude Control Subsystem, and the solar paddles are part of the Power Subsystem. The Structures Subsystem controls the interfaces between the ACS, the solar paddles, and the rest of the spacecraft, as well as allowing the solar paddle unfold system to deploy from the launch configuration.

2.2 SUBYSTEM REQUIREMENTS

The primary functional requirements of the Structural Subsystem are to provide volume, strength and stiffness to:

1. Support the payload and all other subsystems throughout all phases of the mission. As well as the basic housekeeping subystem accommodation, payload requirements are to accommodate 450 pounds and 12 cubic feet of payload equipment.

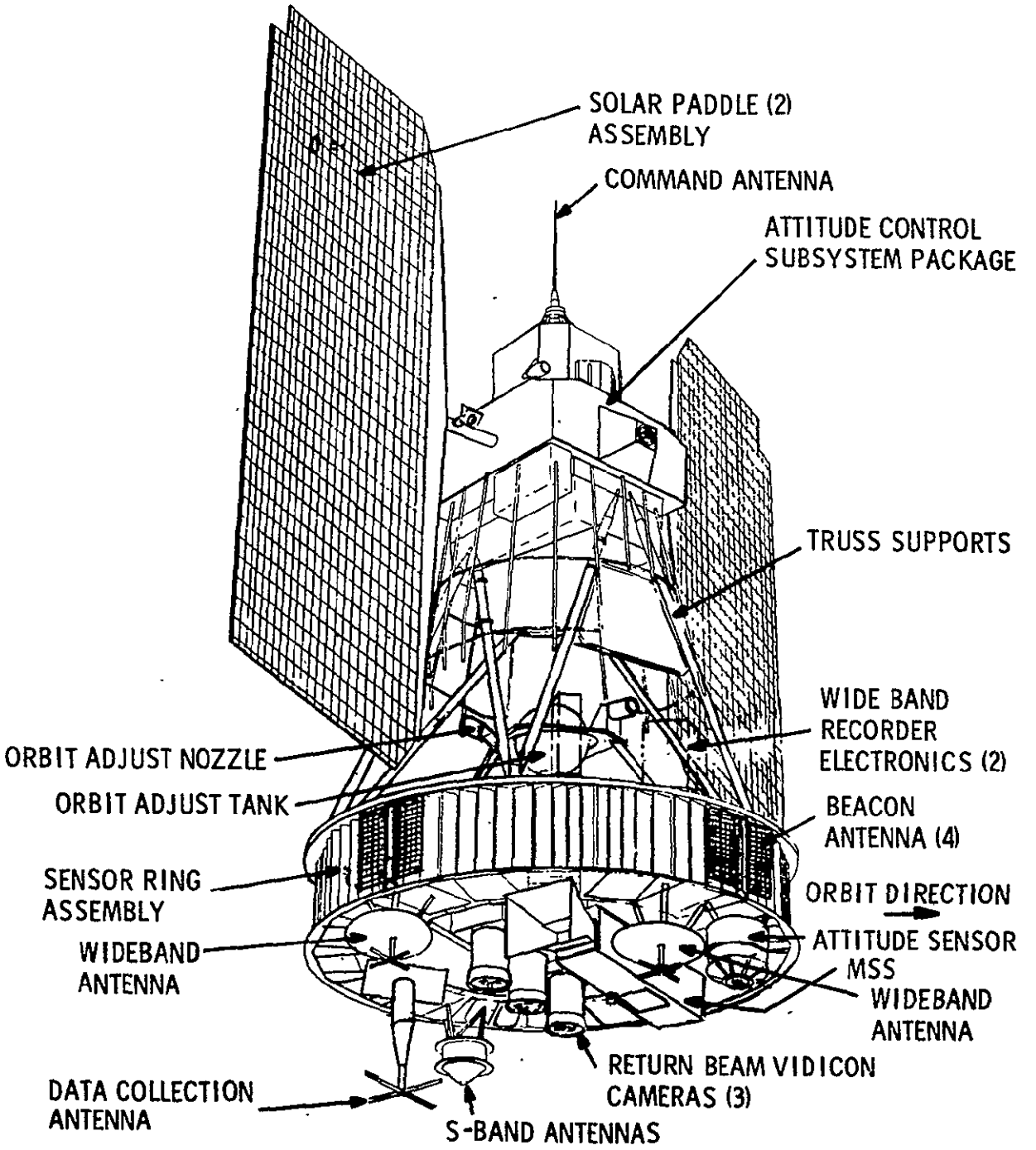

Figure 2.1-1. ERTS Spacecraft

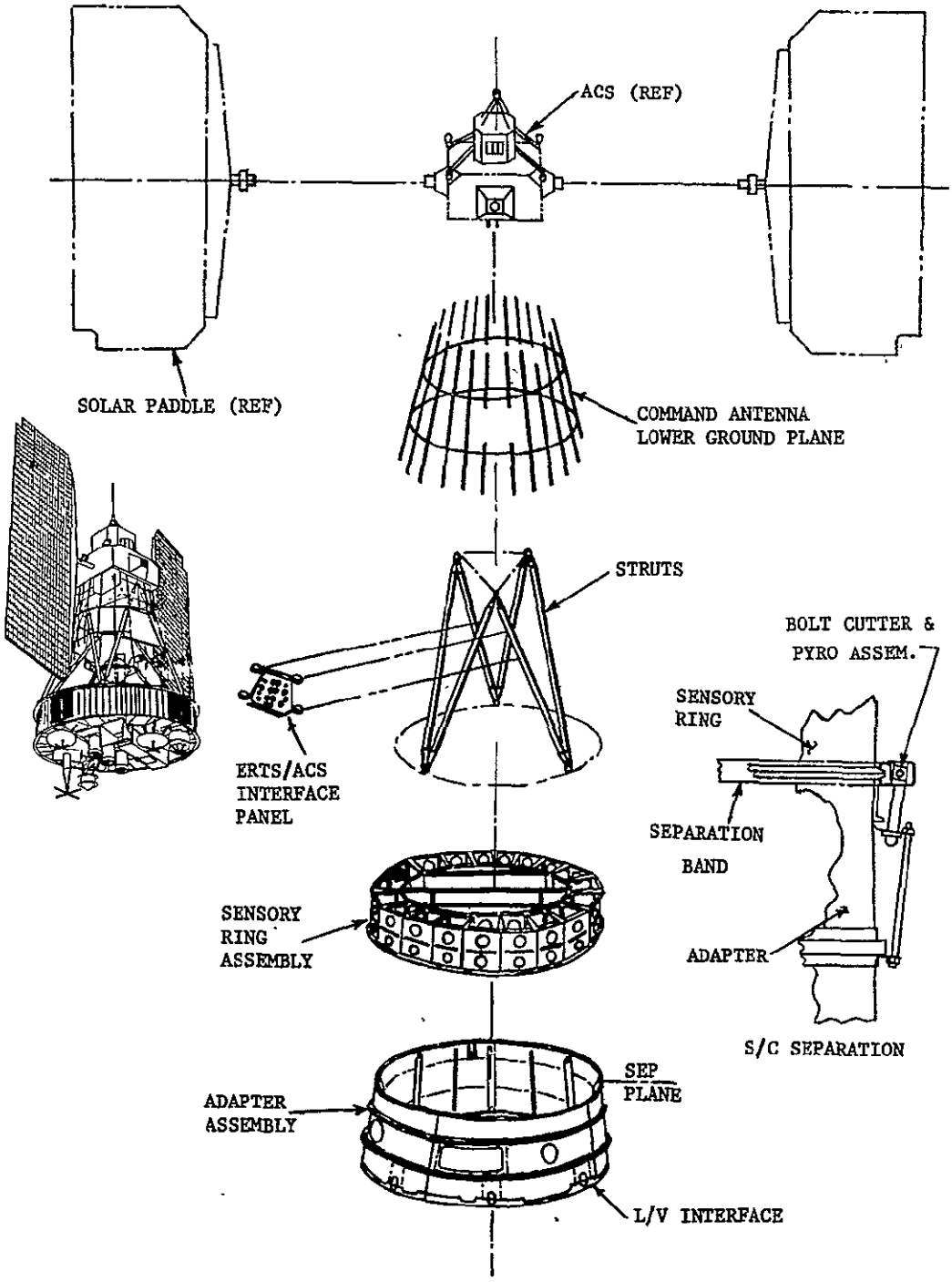

Figure 2.1.2. Configurational Elements of ERTS Spacecraft

2. Maintain the location and alignment of components within the specified tolerances. The payload sensors, attitude sensor, orbit adjust and Attitude Control Subsystem require 0.1 degree alignment of the components with respect to the vehicle axes.

3. Be compatible with the Delta launch vehicle and SACS shroud. Spacecraft space envelope, static and dynamics, must have clearance of 0.25 inch with surrounding shroud structure during ground handling and launch through shroud separation. The spacecraft adapter has a primary loads interface at a 58-inch diameter bolt circle consisting of eight bolts.

4. Withstand the environments through all mission phases. Principal requirements are to withstand launch environment of quasi-static and dynamic load requirements. All prelaunch phases will be attenuated with AGE as required.

The Structures Subsystem is further constrained to utilize existing spacecraft configurations to minimize development. For this purpose, General Electric has selected the Nimbus spacecraft configuration, which has a successful flight history and more than adequately meets the payload requirements for the ERTS system. Design studies have shown that the Structural Subsystem provides identical mechanical installation interfaces for the ERTS A and the ERTS B spacecraft.

2.2.1 SUBSYSTEM EQUIPMENT REQUIREMENTS

The ERTS Spacecraft Structure is required to accommodate components of the following subsystems:

1. Electrical Power Subsystem
2. Communication and Data Handling Subsystem
3. Thermal Subsystem
4. Attitude Control Subsystem
5. Orbit Adjust Subsystem
6. Payload Subsystem, including:
    a. Multispectral Scanner (MSS) and Electronics
    b. Return Beam Vidicon (RBV) and Electronics
    c. Wide Band Video Tape Recorder (WBVTR) and Electronics

The payload accommodation requirements are stated in the NASA-GSFC document, S-701-P-3, "Design Study Specifications for the Earth Resources Technology Satellite, ERTS-A and B, "dated October 1969. The spacecraft shall accommodate a payload weight of 450 pounds and a payload volume of 12 cubic feet. The spacecraft shall provide adequate earth looking area and space looking area to meet payload requirements. Additionally, the earth looking and space looking area requirements include a sensor field of view requirement for unobstructed view angles. These general payload requirements are more specifically defined in Section 2.3.4.

The equipment alignment and location with respect to the spacecraft structure are critical design requirements. In order to meet pointing accuracies, alignment must be held to within 0.1 degree (6 minutes) on the following equipment with respect to (WRT) the spacecraft axes:

1. Attitude Control S/S Package
2. Orbit Adjust
3. Multispectral Scanner
4. Return Beam Vidicon Assembly
5. Attitude Sensor
6. Magnetic Moment Assembly

Their location on the spacecraft is required to provide the following earth looking field of view (FOV) for the following equipment:

Item	FOV
Data Collection Antenna	120°
Unified S-Band Antenna	120°
Wide Band Antenna (2)	160°
Multispectral Scanner	30° crosstrack 20° in-track
Return Beam Vidicon	16.7°
Attitude Sensor	135°

2.2.2 STRUCTURAL DESIGN REQUIREMENTS

This section presents the basic requirements, environmental conditions, and structural design of the ERTS spacecraft. These requirements, when implemented, ensure the integrity and reliability of the structural design. The evaluation of system and mission requirements which lead to the major requirements are discussed in the following paragraphs. Figure 2.2.2-1 presents the sign conventions used for analyses of the ERTS spacecraft and Structural Subsystem.

2.2.2.1 Spacecraft Weight and Mass Properties

Weight and mass properties requirements which affect the design of the spacecraft structure and the spacecraft configuration have been identified and are discussed in the following paragraphs. In general, they consist of weight distributions, weight limits, center of mass restraints, and product of inertial restraints. In addition, co-contractor interface and reporting requirements as well as test requirements have been identified.

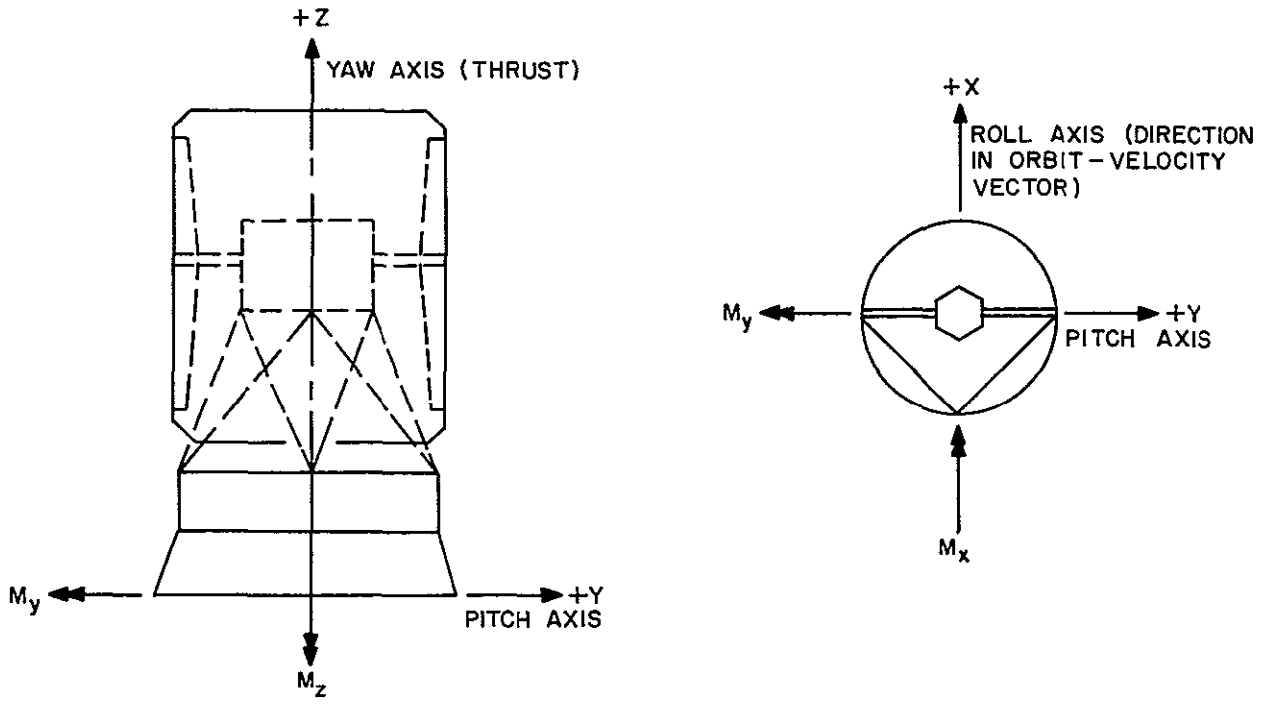

Figure 2.2.2-1. Sign Conventions

2.2.2.1.1 Spacecraft Weight Distribution

The presently estimated weights for the various spacecraft subsystems, and elements within the subsystems, are listed in Table 2.2.2-1. These values do not include an allowance for growth and represent only the baseline design status. A discussion of weight growth and estimated spacecraft flight weight is presented in Section 2.2.2.1.2. Table 2.2.2-2 presents the spacecraft system baseline design mass properties for various mission events: (1) with and without adapter; (2) with and without orbit adjust fuel; and (3) stowed and deployed solar arrays.

2.2.2.1.2 ERTS Weight Growth Predictions

An evaluation of expected weight growth of the current ERTS spacecraft baseline design was performed to arrive at a prediction of the flight spacecraft nominal weight. Current weight, nominal weight, and weight growth can be defined as follows:

- Current Weight - The present weight estimated based on the latest analytical and measured data including estimates for approved changes not yet incorporated into the design.
- Nominal Weight - The nominal weight is the weight which can be reasonably expected at flight. It is the current weight plus a weight growth allowance.

TABLE 2.2.2-1. SPACECRAFT WEIGHT DISTRIBUTION

	Weight - Pounds
Basic Spacecraft	1291.7
Structure	175.2
Sensory Ring	79.6
Crossbeam	45.2
Truss	13.4
Misc.	37.0
Thermal Controls and Insulation	80.8
Active	37.8
Passive Insulation	30.0
Thermal Radiator	10.0
TM Conversion Modules (3)	3.0
Independent Attitude Sensor	7.2
Attitude Control System	252.4
Magnetic Moments Module	10.0
Orbit Adjust	42.4
Mechanical System (Including Mount)	26.4
Fuel	11.0
Mounting Provisions	5.0
Electrical Harnesses and Installation	135.0
Electrical Power System	268.2
Solar Array	75.2
Storage Modules	122.5
Power Control	21.6
Power Switch Module (Including Pyro Mod)	15.2
Auxiliary Load Panels	12.4
Auxiliary Load Controller	6.0
Unfold Timer	3.3
Payload Regulator	12.0
Communications and Data Handling	320.5
VHF Transmitter	2.0
Quadraloop (Stadan)	5.7
Command Antenna (Including Ground Plane)	5.6
VHF CMD Receiver	5.5
VHF DCS Receiver	2.5
VHF/DCS Antenna (Including Mount)	4.2

TABLE 2.2.2-1. SPACECRAFT WEIGHT DISTRIBUTION (Continued)

		Weight - Pounds
USB Equipment		25.0
USB Pre-Mod Processor		4.0
USB Antenna (1) (Including Mount)		3.0
PCM Memory 1		5.7
PCM Memory 2		5.7
PCM Memory Sequencer		4.7
PCM Coder	43.0	9.7
PCM Reprogrammer		8.9
PCM Digital MUX		8.3
Command and Clock		27.0
CMD INT Unit		4.0
Narrowband Tape Recorders (2)		30.0
Wideband and Signal Cond		5.0
Wideband Power Amp (2)		19.0
Wideband Antenna (Including Mount)		3.0
Wideband Video Tape Recorders (2)		84.0
Wideband Recorder Electronics (2)		44.0
Wideband Diplexer		4.0
Payload Items		272.6
RBV System		143.8
Sensors (3)		91.8
Combiner		9.0
Controller		7.0
Electronics (3)		36.0
MSS System		128.8
Sensor		120.0
Multiplexer		8.8
Total Vehicle Less Adapter		1564.3
Adapter		122.7
Basic Structure		44.8
Separation Clamps, Fittings, etc.		12.2
Separation Spring Assemblies		9.7
Secondary Structure		28.2
Pre-Flight Disconnect & Instl.		4.0
Re-Radiator System		13.2
Harnesses		9.3
Separation Switches & Pushers		1.3
Total Vehicle With Adapter		1687.0

TABLE 2.2.2-2. SPACECRAFT MASS PROPERTIES SUMMARY

	With Adapter Full Fuel Array Closed	No Adapter Full Fuel Array Closed	No Adapter Full Fuel Array Open	No Adapter No OA Fuel Array Open	No Adapter No OA Fuel No ACS Fuel Array Open
Current Weight Pounds	1687.0	1564.3	1564.3	1553.3	1541.1
Nominal Weight (Including Growth (Pounds)	1782.5	1659.8	1659.8	1648.8	1636.6
Center of Gravity (Inches)					
X = Roll Axis (Measured from Pitch-Yaw Plane)	0.0	0.0	+ 0.6	+ 0.6	+ 0.6
Z = Yaw Axis (Stations) Separation Plane = 221.000	203.4	201.1	201.1	201.1	201.6
Y = Pitche Axis (Measured from	- 0.3	- 0.4	- 0.4	- 0.4	- 0.4
R = Radial CG Offset from Z Axis	0.3	0.4	0.7	0.7	0.7
Moment of Inertia About CG (Slug-Ft^2)					
I0X (Roll)	353	320	339	339	330
I0Z (Yaw)	130	114	131	131	131
I0Y (Pitch)	357	324	322	322	314
Products of Inertia About CG (Slug-Ft^2)					
POXZ (Roll-Yaw)	+ 9.44	+ 9.47	+ 1.13	+ 1.13	+ 1.04
POXY (Roll-Pitch	- 1.25	- 1.25	+ 5.53	+ 5.53	+ 5.53
POZY (Yaw-Pitch)	- 4.28	- 4.55	- 4.03	- 4.03	- 3.97
Angles Between Principal Axis and Corresponding Geometric Axis Through CG					
X (Roll)			17.2°	17.2°	17.2°
Z (Yaw)			1.2°	1.2°	1.3°
Y (Pitch)			17.2°	17.2°	17.2°

- Weight Growth - Weight growth is an allowance for the weight increases which are normally experienced during the various design phases. It does not provide for CCN type changes such as additions or deletions of systems or GFE equipment.

Although the ERTS spacecraft is a first generation vehicle, most of the structure, the Attitude Control System (ACS), and many electronic items are identical to the Nimbus D spacecraft. The weights of these identical items have been well established and no weight growth is anticipated in these areas. Therefore, an estimated weight growth factor of 10 percent was applied only to the items which are new to ERTS.

Nimbus Items	=	732.0 pounds
New Items	=	955.0 pounds
ERTS Current Weight	=	1687.0 pounds
Weight Growth (10% of 955)	=	95.5 pounds
ERTS Nominal Weight	=	1782.5 pounds

Table 2.2.2-3 lists items from the Nimbus spacecraft that are common to the ERTS spacecraft.

TABLE 2.2.2-3. NIMBUS ITEMS USED ON ERTS

	Weight - Pounds
Sensory Ring	79.6
Truss	13.4
Misc Structure	23.2
Active Thermal Controls	37.8
TM Conversion Modules (3)	3.0
ACS	252.4
Magnetic Moment Module	10.0
Command and Clock	27.0
Batteries (8)	122.5
Power Control Module	21.6
Auxiliary Load Panels	12.4
Auxiliary Load Controller	6.0
Unfold Timer	3.3
VIP System (PCM System)	43.0
VHF XMTR Antenna - Quadraloop	5.7
VHF Receive Antenna (Including Ground Plane)	5.6
VHF Antenna (WO/Mount)	2.2
USB Omni Antenna (WO/Mount)	1.0
Adapter Basic Structure	44.8
Separation Clamps, Fitting, Etc.	12.2
Preflight Disconnect and Instl.	4.0
Separation Switches and Pushers	1.3
Total	732.0

2.2.2.1.3 Weight Restraints

The presently projected weight capability of the various Delta N launch vehicles (GSFC SPEC S-701-P-3) is compared to the ERTS spacecraft nominal weight (including growth) in Table 2.2.2-4. Weight margins reflecting capability for additional payload is also shown. For the recommended Delta N-6 launch vehicle, a capability exists for 117 pounds of additional payload.

TABLE 2.2.2-4. WEIGHT MARGIN CAPABILITY

Launch Vehicle Configuration	Payload Weight Capability (pounds)	Nominal Weight Incl. Growth (pounds)	Weight Margin (pounds)
Delta N-3 (3 solid strapons)	1480	1783	Negative
Delta N-6 (6 solid strapons)	1900	1783	+ 117
Delta N-9 (9 solid strapons)	2120	1783	+ 337

2.2.2.1.4 Center of Mass Restraints

The center of mass of the spacecraft at separation is not on the vehicle centerline. In order to prevent the tumble rate at separation from exceeding acceptable limits, the separation spring constants and preloads are individually selected to compensate for the center-of-mass offset from the centerline. The separation system has been designed so that a radial center-of-mass offset from the yaw axis of 1.5 inches can be accommodated by the nonsymetrical choice of spring constants and preloads.

Radial Offset of Center of Mass
From Yaw Axis
In Launch Mode

Maximum Allowable	=	1.5 inches
Current	=	0.4 inches
Margin	=	1.1 inches

2.2.2.1.5 Products of Inertia Restraints

Due to the attitude control system capability, there is a restraint on the products of inertia of the spacecraft. Table 2.2.2-5 presents the allowable products of inertia, the current baseline design status, and the margin available.

TABLE 2.2.2-5. PRODUCT OF INERTIA*

		PZY	PXZ	PXY
Maximum Allowable	=	± 10	± 3	± 20
Current	=	- 4.03	+ 1.13	+ 5.53
Margin	=	5.97	1.87	+ 14.47

*Measurements in slug-ft^2 units.

2.2.2.1.6 Weight and Mass Property Measurement Requirements

During the ERTS phase B/C study, requirements for weight and mass property measurements were identified and are discussed in the following paragraphs.

2.2.2.1.6.1 Spacecraft Mass Property Measurements

The following mass property tests were identified as being required:

1. Measured weight of the complete spacecraft without adapter using a balance scale.
2. High speed Pelton test of the vehicle less adapter and solar array. This test provides the three centers of gravity and three products of inertia of the spacecraft.
3. Low speed Pelton test of the vehicle less adapter and with solar array folded. This test provides precise values of the center of gravity in the roll-pitch plane and is used to set the separation springs.

No moment of inertia tests are required. Over a period of five years, a total of 12 moment-of-inertia tests were performed on the Nimbus family of vehicles. The greatest difference between test results and analytical predictions was 4.5 percent, and the average difference was 1.9 percent. Since the testing accuracy is about 2 percent, no improvement in values results from testing.

2.2.2.1.6.2 Piece Part Measured Weights

During spacecraft fabrication, the individual piece parts will be weighted on a balance scale prior to installation on the spacecraft. This data will be used to verify and to update the mass properties computer weight tabulation as the fabrication cycle progresses.

2.2.2.1.7 Interface Requirements of Co-Contractors

Monthly weight status reports have been identified as being required from each of the Co-Contractors. These reports will contain the best assessment of the flight weight based on

the latest analytical and measured data. No other mass property parameters are required except for the following items which require individual considerations:

1. MSS Sensor - three-axis centers of gravity are required.
2. Wide Band Tape Recorders - center of gravity is required in pitch (Y) - yaw (Z) plane only.
3. RBV Sensors - center of gravity is required along optical axis only.
4. Orbit Adjust System with and without fuel - centers of gravity are required along the yaw (Z) axis only.
5. Solar Array - the centers of gravity must be reported separately for each of the transition sections and each of the paddles. For the paddle sections, the center of gravity is required in the solar cell plane only, whereas for the transition section, only the center-of-gravity location along the shaft centerline is required.

The accuracy required on the final figures submitted to General Electric on centers of gravity is ±0.2 inch. The data may be obtained by analytical means or by testing. A simple knife edge balance test generally can yield accuracies of better than ±0.1 inch for small items and is suggested as a low cost test procedure.

2.2.2.1.8 Spacecraft System Mass Property Reporting Requirements

The General Electric weight control and analysis organization will submit monthly mass property status reports to NASA. The reports will contain the following:

1. A functional current weight breakdown, and the percentage of the weights which are estimated, calculated, and actual will be indicated for each item.
2. A tabulation of the weight changes since the last report, together with an explanation of the changes.
3. Three-axis centers of gravity, moments of inertia, and products of inertia of the vehicle in each flight mode. This would include:
    a. Launch mode
    b. At separation from boost vehicle
    c. After array deployment
4. If applicable the following will also be included:
    a. Weight estimates of pending changes not yet approved.
    b. Realistic potential weight saving changes.
    c. Weight history curve together with weight growth curves for comparison.
    d. Discussion of unresolved problems.

2.2.2.2 Spacecraft Environment

This section discusses the types of loading environments that must be considered in the design of the ERTS spacecraft, and the general Delta Launch Vehicle environments. Sections 2.4.6 and 2.4.7 of this report provide the results of the specific analyses accomplished to determine the integrity of the ERTS Structures Subsystem.

The principle loads affecting the design of the ERTS structure result from the broad spectrum of static and dynamic environments occurring during launch. They are generally construed to include quasi-steady acceleration, shock, acoustic field, sinusoidal vibration, random vibration, and pyrotechnic shocks. These environments can be grouped into three basic categories with respect to the nature of the stimuli, frequency content, and effects on the spacecraft system and its components. These are:

1. Quasi-Steady Loadings - These environments provide the critical loading condition for the spacecraft primary structure and major mass items. The environments, experienced during lift-off and powered flight, are comprised of static (rigid body) accelerations onto which low-frequency, decaying sinusoidal vibrations are superimposed. These transients have frequency contents less than 100-150 Hz. Structural integrity under these environments is experimentally demonstrated through static loads and sinusoidal vibration tests.

2. Vibro-Acoustic Fields - These nondeterministic loadings, experienced during lift-off and powered flight, have frequency contents ranging from 10-10,000 Hz. Most of their potentially damaging energy content is concentrated approximately in the 1200 Hz bandwidth. These environments thus create the critical loading conditions for secondary (equipment support) structures and components. Structural integrity under these environments is experimentally demonstrated through random vibration and sinusoidal vibration tests.

3. Pyrotechnic Shocks - These deterministic environments, produced by the detonation of pyrotechnic devices during shroud and spacecraft separations, encompass shock pulses of durations far less than three milli-seconds (and induce decaying sinusoids of frequency content greater than 100-150 Hz). These phenomena do not cause significant participation of the spacecraft's principal structural resonances. Tests to these stimuli are best accomplished through detonation of pyrotechnic devices.

Two NASA GSFC documents specify the structural design requirements resulting from the aforementioned spacecraft environments. They are:

1. S-701-P-3, "Design Study Specifications for the Earth Resources Technology Satellite ERTS-A and -B", dated October 1969.

2. S-320-G-1, "General Environmental Test Specifications for Spacecraft and Components Using Launch Environment - Dictated by Delta, Centaur, Agena, and Scout Launch Vehicles."

Flight level limit load factors and flight level vibrations, acoustic, and shock environments specified in the above documents for design of the ERTS Spacecraft Structural Subsystem are presented in the following paragraphs.

2.2.2.2.1 Limit Load Factors

The following preliminary load factors are intended to generate static loads in the spacecraft structure which are equivalent to the worst case of combined effects due to rigid body and elastic accelerations (quasi-steady loading):

1. Longitudinal Aft: 9.2 g combined vectorially with 2.0 g in either direction along any lateral direction.
2. Longitudinal Forward: +3.0 g combined vectorially with 2.0 g in either direction along any lateral direction.

It is intended that loads generated by these load factors be verified by an overall launch vehicle spacecraft system dynamic analysis using measured spacecraft-vibration modal data. A preliminary analytical evaluation has been completed by GE during the ERTS phase B/C study and is discussed in Section 2.4.6.

2.2.2.2.2 Vibration

The following vibration levels represent maximum expected values due to combined effects at the interface between the forward section of the Delta N-6 and the spacecraft adapter. Levels given below will be limited so as not to exceed the design limit strength of the structure based on limit load factors. A preliminary vibration limiting evaluation has been completed by GE during the ERTS phase B/C study and is discussed in Section 2.4.6.

(a) Sinusoidal:

Delta Model	Axis	Frequency Range (Hz)	Level "G" (0-to-Peak)	Sweep Rate Octaves/Minute
N-6 (2 Stage)	Thrust (Z)	10-17	1.5	4.0
		17-23**	4.0	3.0
		23-200	1.5	4.0
	Lateral (X and Y)	5-14*	1.3	4.0
		14-200	1.0	4.0

*Because of shaker limitations, input levels may be limited to ±0.5 inch D.A. displacement.

**During the maximum POGO period, the steady-state acceleration is 6.0 g.

(b) Random:

Delta Model	Axis	Frequency Range (Hz)	PSD Level g^2/Hz	Duration	Acceleration (g's-rms)
N-6 (2 Stage)	Thrust (Z)	20-300 300-2000	+ 4 dB/OCT 0.04	2 Minutes	8.5
	Lateral (X and Y)	20-300 300-1000 1000-2000	+ 4 dB/OCT 0.06 - 6 dB/OCT	2 Minutes per axis	8.9

**The filter roll-off characteristics above 2000 Hz shall be at a rate of 40 dB/octave or greater.
Gaussian noise, peaks clipped to 3 times rms value, band-limited and shaped as above.

2.2.2.2.3 Acoustic Levels

The estimated acoustic spectra inside and outside the aerodynamic shroud during flight are given in Table 2.2.2-6.

TABLE 2.2.2-6. SPACECRAFT FLIGHT ACCEPTANCE DELTA ACOUSTIC NOISE

Octave Band Center Frequency (Hz)	Sound Pressure Level (db, ref. 0.0002)		Duration
	Exterior of Shroud	Interior of Shroud	
15.8	135	123	1 minute for complete exposure
31.5	136	123	
63	140	125	
125	142	130	
250	145	133	
500	145	134	
1000	143	134	
2000	140	131	
4000	136	127	
8000	131	121	
Overall	151	140	

2.2.2.2.4 Shock

Figure 2.2.2-2 envelopes the shock spectrum resulting from such events as engine ignition and burnout, stage separations, and shroud ejection. If shocks produced by firing of spacecraft separation ordnance are more severe, they will be used as the controlling design parameter where applicable.

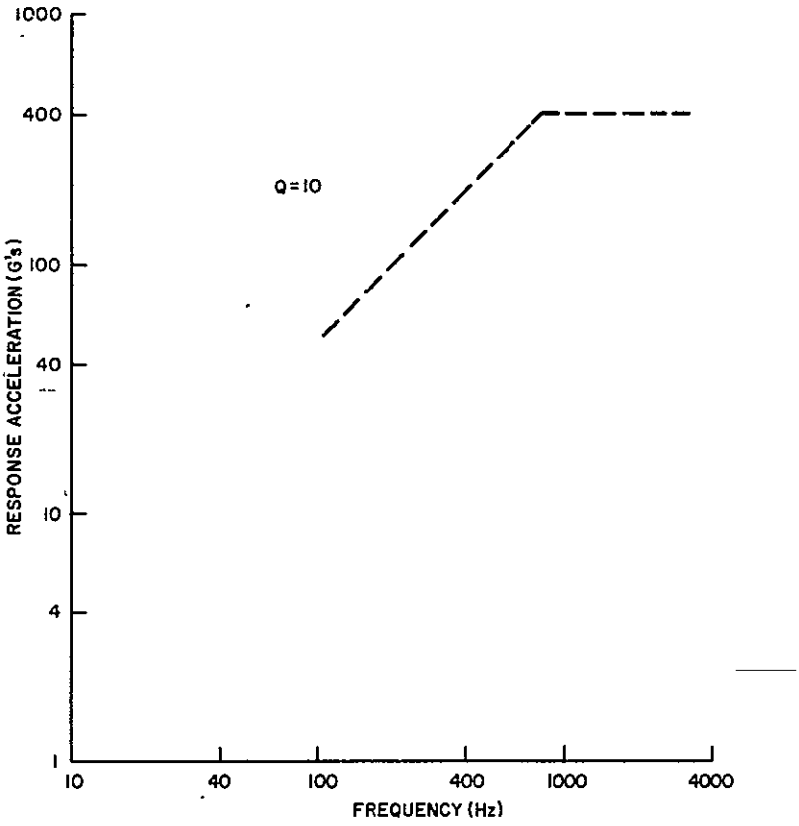

Figure 2.2.2-2. Delta Shock Spectra Input Spacecraft Flight Acceptance

2.3 SUBSYSTEMS DESCRIPTION

2.3.1 STRUCTURES SUBSYSTEM SUMMARY

2.3.1.1 Structure and Spacecraft Arrangement

The ERTS spacecraft and structures subsystem meets the payload accommodation and requirements for the ERTS A and B missions. The ERTS spacecraft is shown in Figure 2.3.1-1 and is similar to the Nimbus spacecraft. The spacecraft has five major configurational elements:

1. The Attitude Control Subsystem (ACS), a rectangular-shaped upper structure, that provides unobstructed, exposed mounting for the solar paddle sun sensors, horizon scanners, and gas nozzles. The necessary electronics, mechanical drives, pneumatics and the drive for the solar array paddles are assembled internally. The command antenna and the upper part of its ground plane are mounted on the top surface.
2. The solar array paddles, which attach to the shaft projecting from the ACS housing, are thermally isolated from the rest of the spacecraft.
3. A tripod truss structure provides a rigid connection between the ACS and sensory ring assemblies. Adjustment fittings at the tube ends allow the alignment of the ACS and the sensors. The truss also supports the command antenna lower ground plane and the auxiliary load panel.
4. The sensory ring is a torus structure composed of 18 rectangular module bays, 13 inches in depth. The bays house the electronic equipment and battery modules. The lower surface of the torus provides mounting space for payload and antennas. A crossbeam structure, mounted within the center of the torus, provides support for additional payload equipment and tape recorders.
5. The adapter (not shown) is the transition section between the spacecraft and the launch vehicle. The adapter is 24 inches high and interfaces with the spacecraft with a Marmon band separation device, and with the launch vehicle with eight one-half inch diameter bolts at a 58-inch diameter bolt circle. The adapter also provides a support beam to accommodate payload sensor stimulators and antennas pickups and reradiators.

2.3.1.2 Structure Assemblies

The arrangement and major features of the structural assemblies and their function are provided in Figure 2.3.1-2.

2.3.1.2.1 Solar Paddle Assemblies

The solar paddle assemblies are structurally supported during launch and orbit through a socket arrachment at the solar drive interface. This socket is built into the paddle transition section and secured by three tapered plugs. During launch, the solar paddles are folded toward each other and latched with additional support provided at the base of the latch line. The latch line consists of seven hinge line jaws spaced along the paddle (Figure 2.3.1-3). The jaws are

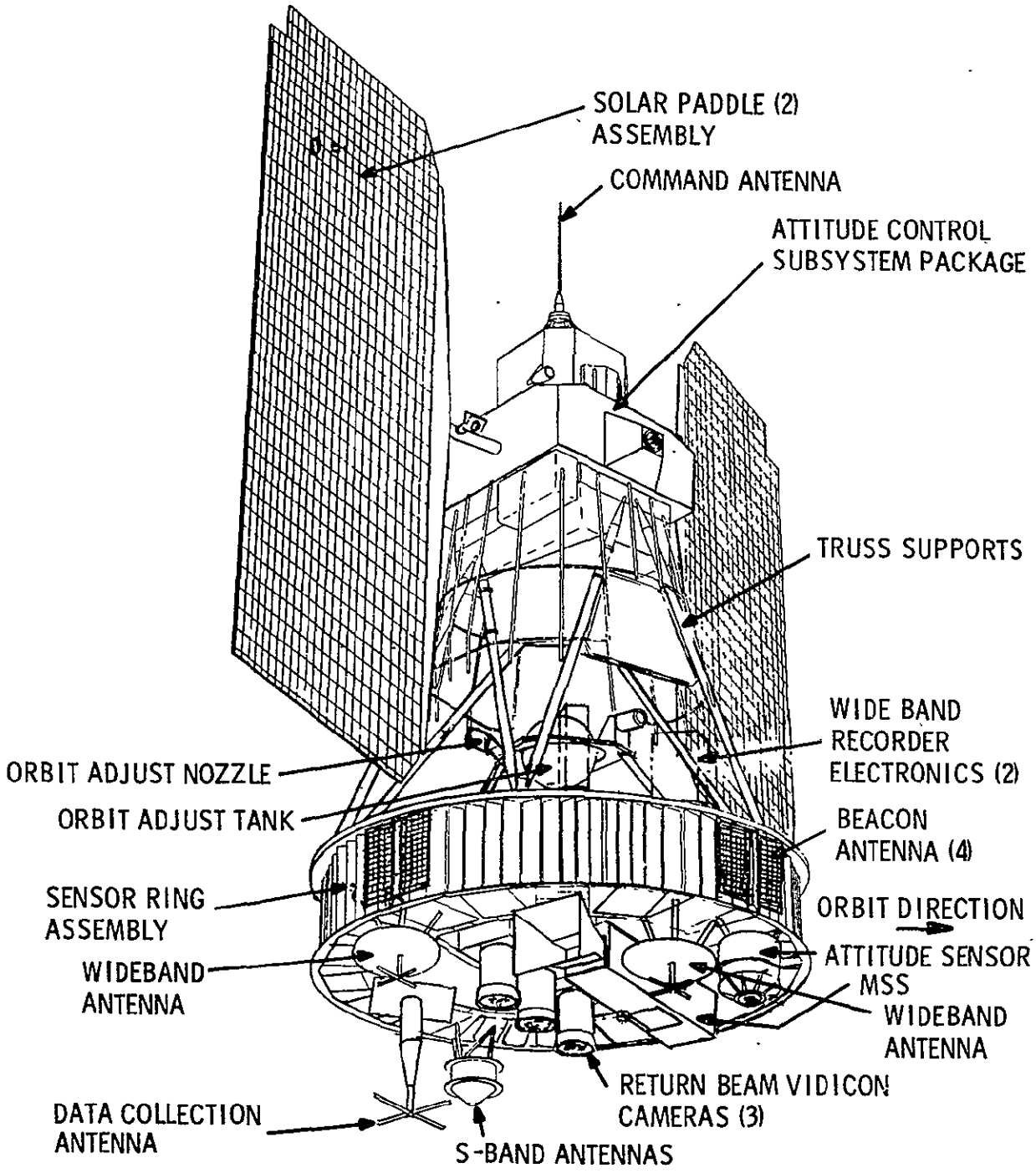

Figure 2.3.1-1. ERTS Spacecraft

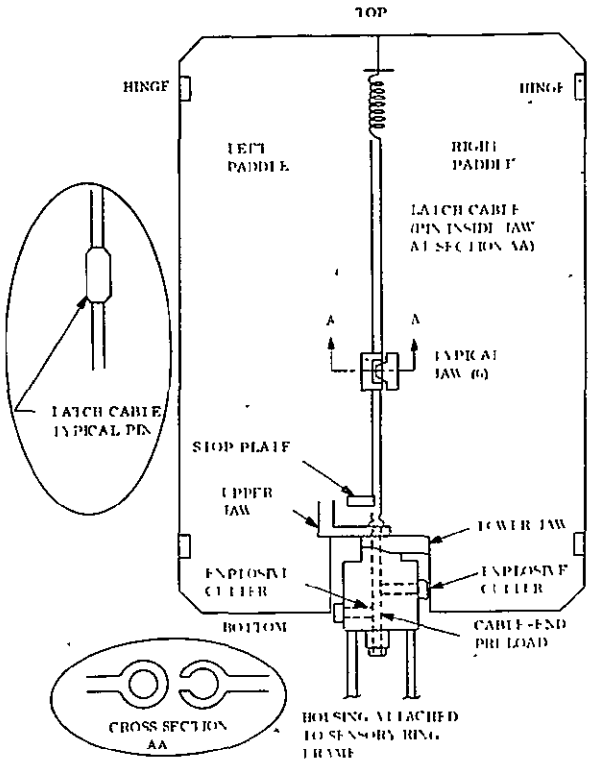

Figure 2.3.1-3. Unfold Subsystem Mechanical Arrangement

latched with pins that are connected by a cable. At the lower end, the cable has a rod anchored in the lower latch assembly and tensioned by a spring at the top. Unlatching occurs when a pyrotechnic cutter severs the anchor rod permitting the cable to be pulled upward by the upper tension spring. This motion withdraws the pins from the jaws and the unfold springs and paddle drive motor unfolds each array. The paddles are then latched in the full open position. Teflon-lined guides are strategically located to prevent hangup of the array during deployment.

2.3.1.2.2 Attitude Control Subsystem (ACS) Package

The structural subsystem interfaces with the ACS only as control of the interfaces of this package with the solar paddle assemblies, the truss tube support and special fittings on the ACS to serve as lift lugs for the entire spacecraft (Y-Y profile of Figure 2.3.1-2). The solar paddle/ACS package interface is defined on the Y-Y profile of Figure 2.3.1-2. The lift lug and truss tube interface is defined on Figure 2.3.1-4, which is a view of the ACS package at spacecraft station 162.140.

2.3.1.2.3 Strut Support

The strut support consists of six tubular assemblies forming a stable framework to support and connect the ACS package to the sensory ring assembly (Figure 2.3.1-2, X-X Profile and Y-Y Profile). The strut supports provide primary spacecraft structural continuity and provision to permit alignment adjustments of the ACS package to the vehicle axes. In the top

3. Solar Paddle Unfold Timer (1)
4. Power Switching Module (1)
5. TLM Conversion Module (1)

The upper plane of the sensory ring (view B-B of Figure 2.3.1-2) is utilized to support and accommodate the Orbit Adjust (O A) Subsystem, the Wide Band Video Tape Recorder Electronics (WBVTRE) and the Magnetic Moment Assembly. The O A interface is a simple three-point attachment of the mounting feet to pads on the upper plane of the sensory ring. The Structures Subsystem provides the support structure for the WBVTRE. Additionally, there is accommodation and interfaces for thermal insulation for the upper surface of the sensory ring, the O A subsystem and the WBVTRE, and a radiator panel for thermal control of the crossbeam equipment.

The lower plane of the Sensory Ring (view C-C of Figure 2.3.1-2) is utilized to support and accommodate the Multi-Spectral Scanner (MSS), Attitude Measurement Sensor (AMS), VHF-DCS Antenna, Wide Band Antennas, and the Unified S-Band Antenna. The Structures Subsystem provides the support structure for these components. The support structure has stand-off configurations to provide the proper fields of view for the components. In addition, there is accommodation and interfaces for the thermal insulation for the lower surface of the Sensory Ring, the MSS and the AMS.

2.3.1.2.5 Adapter

The adapter structure provides structural continuity between the spacecraft and the launch vehicle during the launch phase of this mission. It also provides a separation function to achieve an orbital spacecraft configuration. Additionally, the adapter supports and accommodates payload sensor stimulators (RBV and MSS), and antenna pickups and reradiators.

The adapter is a shell structure with longitudinal stiffeners, and upper and lower closure rings that are machined from forgings to mate with the spacecraft sensory ring and the launch vehicle ring respectively. Secondary structure is the adapter crossbeams necessary to support the payload sensor stimulators and antenna pickups.

The separation function is provided by the following hardware:

1. Two Marmon Band halves
2. Two pyrotechnic bolt cutters and bolts
3. Marmon Band retaining cables
4. Four separation spring assemblies with guides and brackets
5. Four separation switches and brackets

The spacecraft and adapter are clamped together with the Marmon Band, which is preloaded by a force computed to prevent gapping at the separation plane. Separation springs are provided to produce a nominal zero tumble rate and specified separation velocity. Separation

begins with the ignition of the pyrotechnic bolt cutters, which disconnects the Marmon Band halves. The bands displace from the separation rings, but are retained with the adapter by the retaining cables. Four separation springs provide velocity to separate the spacecraft and the adapter. Four switches monitor the event.

2.3.2 STRUCTURAL DESIGN CRITERIA

This section presents the criteria developed for design of the structural subsystem. Its purpose is to insure structural integrity, identify overall structural objectives, minimize structural weight, and provide uniformly acceptable and compatible structural components. The establishment of a comprehensive structural design criteria, along with the structural design requirements previously identified in Section 2.1.3, and the subsystem requirements discussed in Section 2.1.2, are of critical importance in order to insure that the structural design will have the capability of fulfilling all structural as well as functional requirements.

In general, the design criteria used for development of the ERTS spacecraft structure is based on the Nimbus D spacecraft criteria with modifications provided to account for differences in launch vehicle environments and payload requirements.

2.3.2.1 Definition of Terms

1. Limit Loads - Limit loads are defined as the maximum loads which the structure is expected to experience during launch or orbit. These loads are identified in GSFC specification S-701-P-3.
2. Qualification Loads - Qualification loads are equal to the limit loads multiplied by 1.5 or the maximum expected load or combination of loads the structure may be expected to experience during qualification testing. Qualification test levels are 1.5 times the flight acceptance levels.
3. Design Yield Loads - Design yield loads are the qualification loads multiplied by the design yield load factory of safety.
4. Design Ultimate Loads - Design ultimate loads are the qualification loads multiplied by the design ultimate load factor of safety.
5. Design Load Factor of Safety - Design load factor of safety is a factor used to account for uncertainties and variations from item to item in material properties, fabrication quality and detail, and internal and external load distributions.
6. Margin of Safety - Margin of safety is defined as the percentage by which the structural design capability exceeds the structural design requirement. Margins of safety are calculated comparing material yield strength with design yield loads and material ultimate strength with design ultimate loads.
7. Excessive Deflections - Deflections sufficient to jeopardize proper functioning shall be considered excessive if they result in:
   a. Detrimental contact between spacecraft components
   b. Spacecraft deflections which exceed the limitations of the allowable deflection envelope

c. Misalignment of structure and components which adversely affect performance or accuracy.

2.3.2.2 Factors of Safety

The following factors of safety shall be used to obtain structural design yield and design ultimate loads:

1. Yield Design Load = 1.2 x Qualification Loads
2. Ultimate Design Loads = 1.5 x Qualification Loads

2.3.2.3 Structural Design Margins of Safety

The structure shall be designed to the smallest practical margin of safety equal to or greater than zero. Minimum margins of safety shall be maintained on the following structural elements.

	Minimum Margin of Safety
Fasteners in Shear	+ 0.15
Bolts in Tension	+ 0.50
Fittings	+ 0.15
Lugs	+ 0.25
Welds - Electron Beam	+ 0.15
Welds - Other	+ 0.50
Bonded Joints	+ 0.50

2.3.2.4 Strength Criteria

The spacecraft structural subsystem shall be designed to survive the environmental loadings associated with launch and orbital flight.

The structure shall have sufficient strength to withstand simultaneously the design limit loads and other applicable environments associated with the limit design condition without experiencing significant permanent set or excessive deflections as defined in 2.3.2.1.

The structure shall have sufficient strength to withstand the design qualification loads and other applicable environments associated with the qualification design condition without experiencing structural failure.

2.3.2.5 Stiffness Criteria

Minimum resonant frequencies of the primary modes of the spacecraft, including launch vehicle adapter, cantilevered at the launch vehicle interface shall be:

1. Longitudinal > 22 Hz
2. Lateral > 10 Hz

For individual components or subsystems, when mounted to their secondary support, the following fundamental frequency requirements shall be satisfied:

1. Longitudinal > 100 Hz
2. Lateral > 100 Hz

For alignment of critical components, such as the RBV cameras, special stiffness requirements shall be established after more detailed studies have been completed.

2.3.3 LAUNCH VEHICLE INTERFACES

Establishment of the spacecraft launch-shroud interfaces is based on the use of a Standard Agena Clamshell Shroud (SACS), a SACS interface ring and a Delta-6 launch vehicle. A sketch of the spacecraft in the launch configuration mated to the launch vehicle is presented in Figure 2.3.3-1.

The following launch vehicle restraints are identified:

1. The spacecraft weight including the weight of the spacecraft adapter shall not exceed 1900 pounds.
2. The spacecraft adapter base shall be compatible for attachment to the SACS ring with eight bolts and one index hole. The bolt circle diameter will be 58.546 inches. The use of the standard Nimbus adapter will ensure this compatibility.
3. Based upon Nimbus experience, critical clearances between the spacecraft and the shroud are identified in Table 2.3.3-1. The relative spacecraft shroud dynamic deflections shall not exceed the minimum clearances listed in this table. Spacecraft-shroud relative deflections will be established by a coupled dynamic analysis for the spacecraft and launch vehicle.
4. Table 2.3.3-2 lists temperature critcal spacecraft components. The components shall not be subject to temperatures beyond the limits given in the table during the launch phase prior to orbit injection.
5. After mating the SACS ring to the Delta Launch Vehicle, the eight spacecraft mounting pads must be co-planer within .005 inches. In addition, the pad must be flat within 5 arc minutes in both the radial and tangential directions. This requirement is based on minimizing spacecraft and adapter distortion which contribute to tip-off rates at separation.

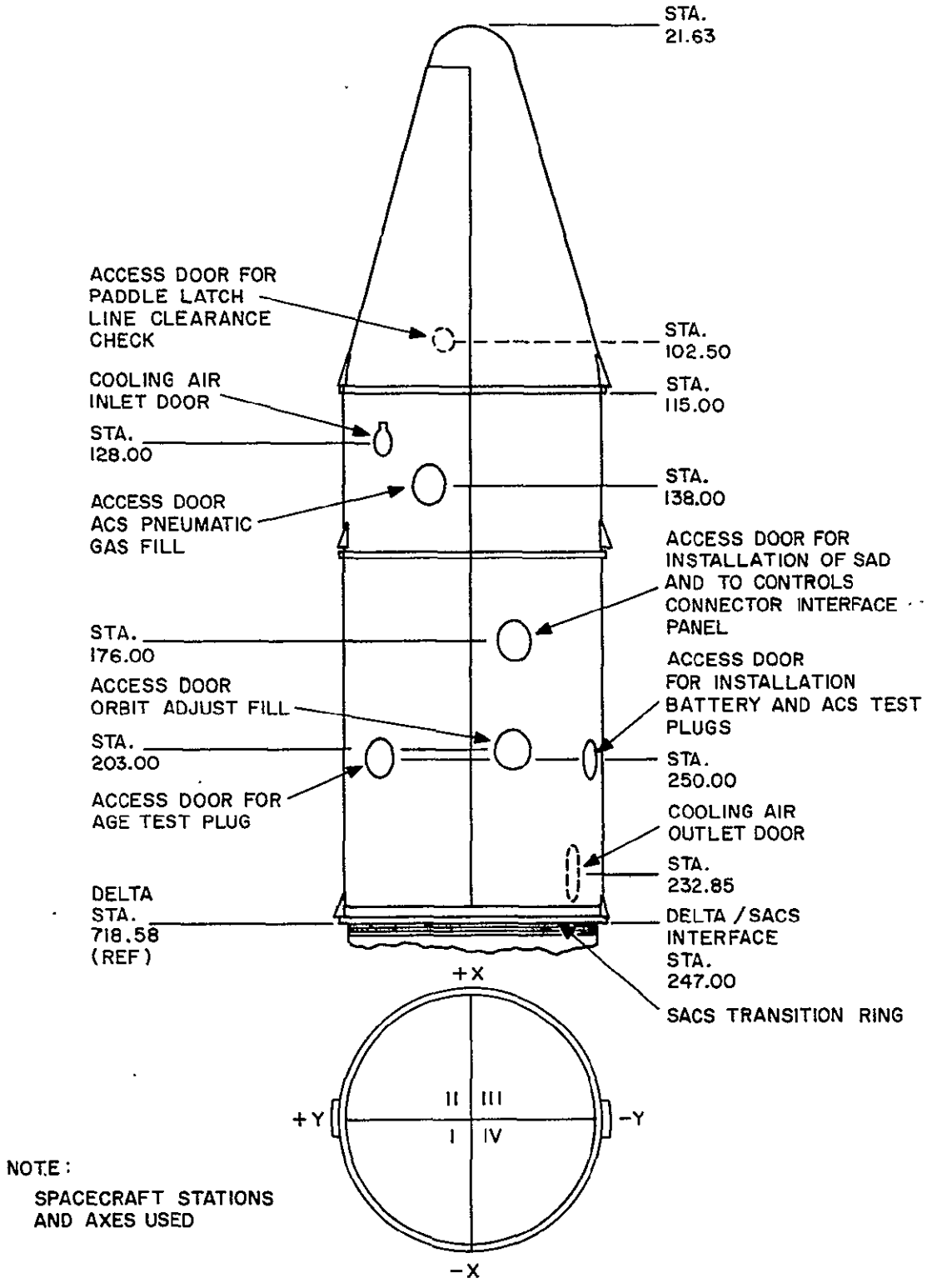

Figure 2.3.3-1. ERTS Shroud Access Doors

TABLE 2.3.3-1. SPACECRAFT SHROUD MINIMUM STATIC CLEARANCES

Components Spacecraft/Shroud	Nom Dim & Tolerance	Offset	Minimum Static Clearances
S/C Adapter Hat A/C Outlet Door	29.997 ± .093 30.280 ± .045	.024	.118
Bolt Cutters Shroud Frame	29.983 ± .153 30.523 ± .070	.058	.283
Quad Antenna Shroud Skin	30.903 ± .256 32.370 ± .020	.092	1.155
Bottom Paddle Jab Shear Strip Assembly	29.188 ± .000 30.400 ± .062	.132	1.102
Top Paddle Jan Shear Strip Assembly	28.074 ± .266 30.17 ± .062	.341	1.736

6. Access to the spacecraft after installation of the shroud is required for air conditioning test plugs and clearance checks. The ERTS spacecraft shroud access door requirements are indicated in Figure 2.3.3-1.

2.3.4 PAYLOAD

The nature of the payload to be carried on the spacecraft establishes varied requirements on the spacecraft design. Two payload items are proposed for the ERTS spacecraft; the Return Beam Vidicon Cameras (RBV) and the Multispectral Scanner (MSS). Both of these items look towards the earth and are used on ERTS A and B spacecrafts. The only difference being that the ERTS B has a mechanical radiative cooler attached to the MSS sensor to gain another spectral channel. In addition to accommodating the physical size and mass of the payload, the spacecraft must provide space for adequate view angles and close alignment to spacecraft reference axes to provide meaningful measurements. A summary of payload requirements and constraints is given in Table 2.3.4-1. The more significant requirements affecting the spacecraft are discussed in the following paragraphs.

2.3.4.1 Fields of View

The fields of view of the RBV and MSS require mounting in the center section and below the sensory ring which will permit unobstructed views of the earth. The three RBV's and the MSS are mounted such that their fields of view are cross track of the orbit direction. The arrangement of the experiments for this configuration was predicated on the basic size of the RBV and MSS. The spacecraft as shown in Figures 2.3.4-1 and 2.3.4-2, has several varied viewing requirements which dictate careful consideration in the location of the independent attitude sensor and the four telemetry antennas.

TABLE 2.3.3-2. ERTS TEMPERATURE CRITICAL COMPONENTS

Description	Max. Temp. (° F)	Min. Temp. (° F)
1. Horizon scanner case and window	131	23
2. Attitude control system insulation	300	Not critical
3. Thermal transfer plate (SAD)	131	23
4. Solar array drive sun sensors	131	23
5. Sensory subsystem insulation upper surface	300	Not critical
6. Separation devices (bolt cutters)	77*	5
7. Beacon/PCM antenna	160	-23
8. Solar platform aluminum channels	140	-112
9. Solar platform	140	-112
10. Solar platform transition section	140	-112
11. Solar platform motor drive assembly casing	140	23
12. Solar platform switch	140	23
13. Solar platform latch line	140	-112
14. Cable cutters	160	- 6

2.3.4.2 Physical Characteristics of the Experiments

Both the RBV and MSS have physical sizes and weights which are of major significance. The three RBV cameras are in line and mounted on a common baseplate. Their optical axes are parallel to each other and to the spacecraft yaw axis. Due to sensitive alignment restraints between each RBV during launch and orbit insertion, a three-point suspension system was incorporated. This suspension system minimizes any influence from structural/thermal distortions by isolating the RBV assembly from the spacecraft.

As shown in Figure 2.3.4-1, theRBV and the MSS sensors by their virtual size occupy the center section of the sensory ring. The MSS sensor with the cooler is 47-1/2 inches in length

TABLE 2.3.4-1. MOUNTING REQUIREMENTS

Description	Uncl. wt. (lb)	Unit Size (inches)	Alignment Field of View and Special Requirements	Location Pointing Requirements
Payload Subsystem				
RBV (3 Return Beam Vidicon Camera Dwg. No. RCA 2976696	30.6	22x5x6.25	Align: 0.008° between RBV's 0.1° wrt axes FOV: 16.7° clear FOV	All three sensors point earthward
MSS (Multi-spectral scanner) Dwg. No. Hughes Aircraft Co. 24469				
ERTS A	105	15x16x36	Align: 0.1° wrt axes FOV: SENSOR: ±15° from vert. of an enclosed 9" circular column in the cross track direction and ±10° from vert. of same column in the "along" track direction	Sensor to point earthward
			SUN CALIBRATE MIRROR: 55° x 40° clear FOV	Sun Calibrate Mirror is in the S/C pitch and roll plane and 10° off the orbit direction
ERTS B	120	15x16x36 SENSOR 13.85x18.25x16 COOLER	COOLER: (ERTS B ONLY) 90°x31°x28° clear FOV	Cooler is mounted below the S/C sensory ring, points away from the sun and cannot see either the earth or the S/C.

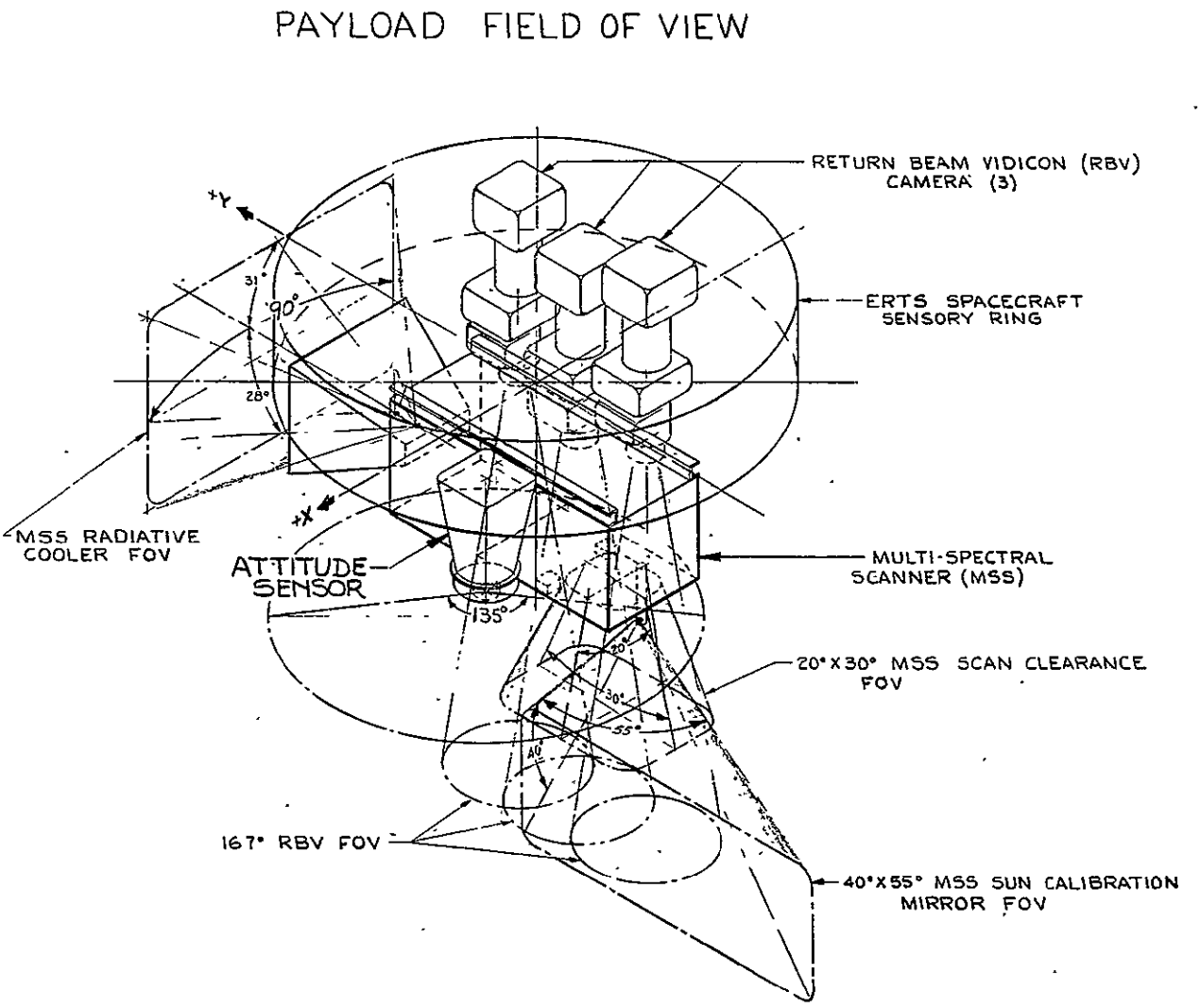

Figure 2.3.4-1. Payload Field of View

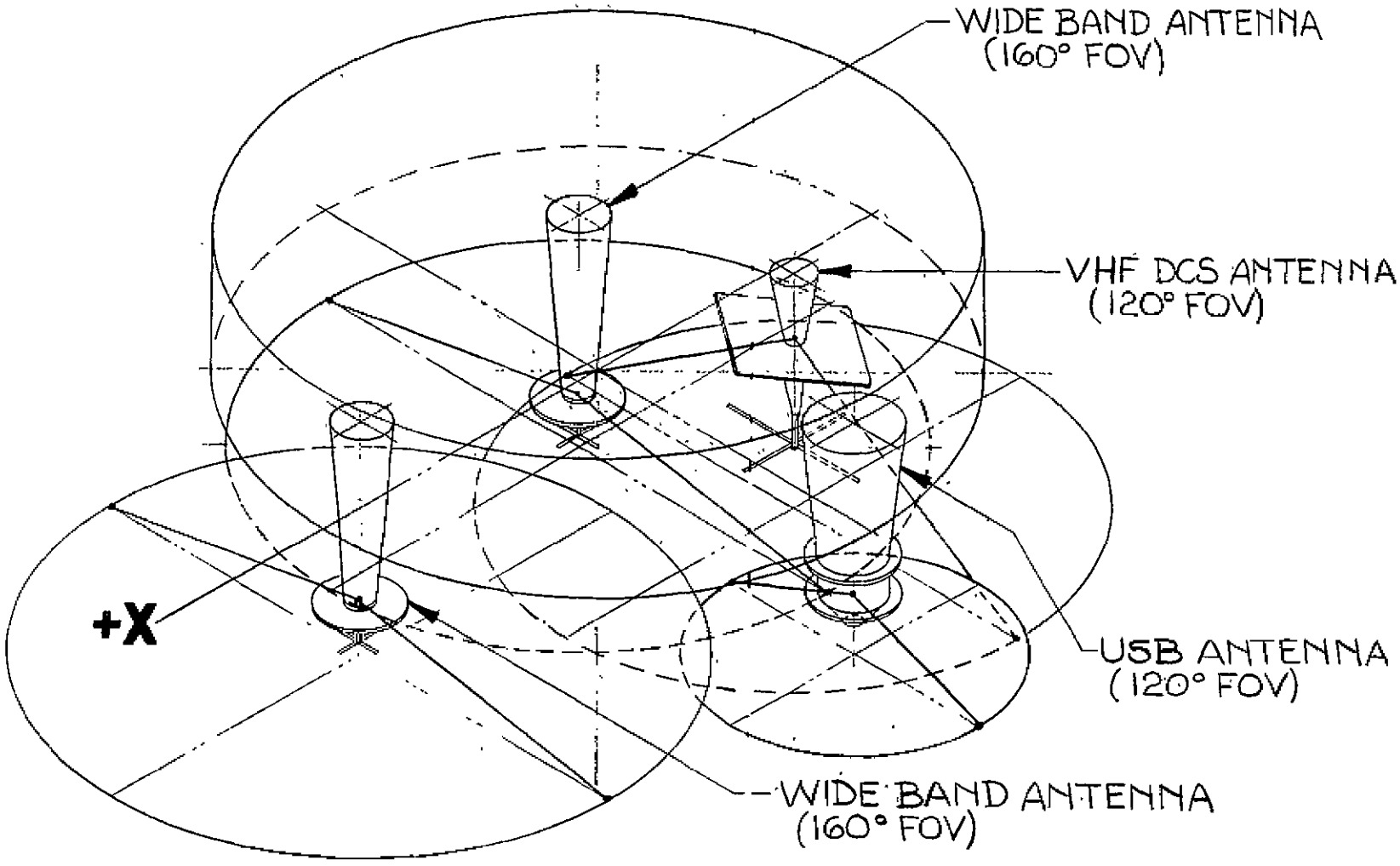

Figure 2.3.4-2. Field of View-Antennas

and must therfore be centered inside the 57-1/8 inch diameter sensory ring. The MSS weight, estimated at 120 pounds is mounted close to the primary torus and crossbeam structure to avoid vibration amplifications.

2.3.4.3 Alignment Requirements

The alignment requirements of the experiments have been evaluated for installation tolerances, structural hysteresis losses, thermal distortion, cross coupling, and internal alignment of the experiment. This evaluation shows that the requirements can be maintained with standard fabrication and assembly tooling by adjustment at installation.

2.3.4.4 Contamination

Two experiments (RBV & MSS) and the attitude sensor include optical equipment which must remain clean for proper operation. The only sources of spacecraft contamination are the attitude control and orbit adjust thrusters. In order to prevent thruster plume impingement of any of the optics, the thrusters are located such that their plumes are directed away from the spacecraft. An analysis which verifies that the MSS spectral surfaces will not be contaminated is presented in Section 7 Appendix of this volume.

2.3.5 MODULAR EQUIPMENT INTERFACES

The sensory ring structure provides 18 peripheral equipment bays. Each equipment bay accepts electronic packages up to 13 inches high x 8 inches deep x 6 inches wide. The packaging accommodation is modular and the preceding dimensions can be made up of modules 6.5 inches high x 2 inches deep x 6 inches wide in any combination up to the full bay dimensions. If a component fills one modular volume in the upper half of an equipment bay, its size is designated 1/0. If a component fills two modular volumes, side by side, on the lower half of an equipment bay, it is a 0/2 module. If a component is two modular volumes in line from top to bottom, the designation is 1/1. A bay completely filled is designated 4/4. The Module Mechanical Interface is defined in Figure 2.3.5-1.

The following are the specific modular equipment interface requirements:

1. Modules must conform to the dimensions and tolerances shown in the modular interface drawing (Figure 2.3.5-2).
2. Modules are preloaded radially with 144 pounds $\pm$72 pounds at four locations (2 locations for 1/2 depth modules) for good thermal contact. Each module must be capable of sustaining this preload (Figure 2.3.5-3).
3. Module mounting lugs must be attached to the module with at least two fasteners.
4. Integral mounting flanges should be avoided unless they are necessary for heat transfer requirements.
5. Full depth modules (i.e., 1/1, 2/2, 3/3 or 4/4) must have removable mounting lugs on the top or bottom.

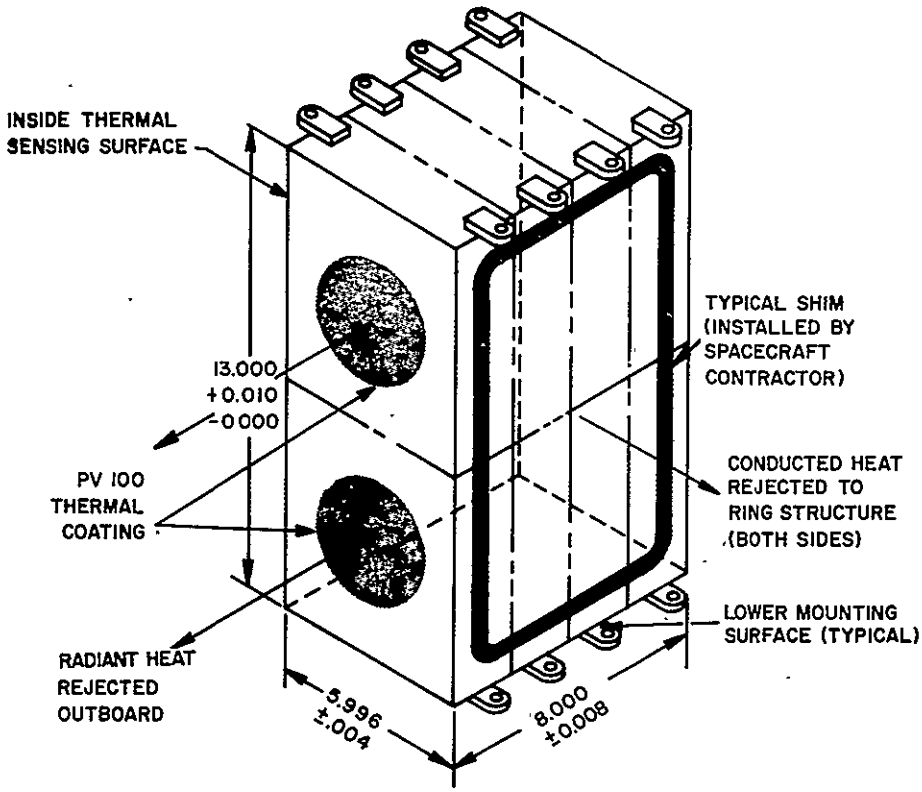

Figure 2.3.5-1. Mechanical Interface

6. High heat dissipation sources in modules should be located on the outboard face. The outboard facing surface should be indicated with a black dot as shown on the modules interface drawing.

7. All available mounting locations should be used on large modules to minimize load concentrations.

8. Inserts should be provided on all modules to facilitate removal from the bays.

9. Modules must be located within the bay in order of thermal dissipation with the highest dissipater in the most outboard location.

10. Equipment interfaces must have capability for static and dynamic load in all directions. Adequate load paths must be provided for shear and axial loads and bending moments.

11. Equipment mount must have a fundamental (first mode) frequency in excess of 100 cps in order to preclude interaction with the primary spacecraft vibration modes.

12. Equipment finishes must be compatible with the spacecraft structure at the mounting interface in order to inhibit electrolytic action.

FOLDOUT FRAME 1

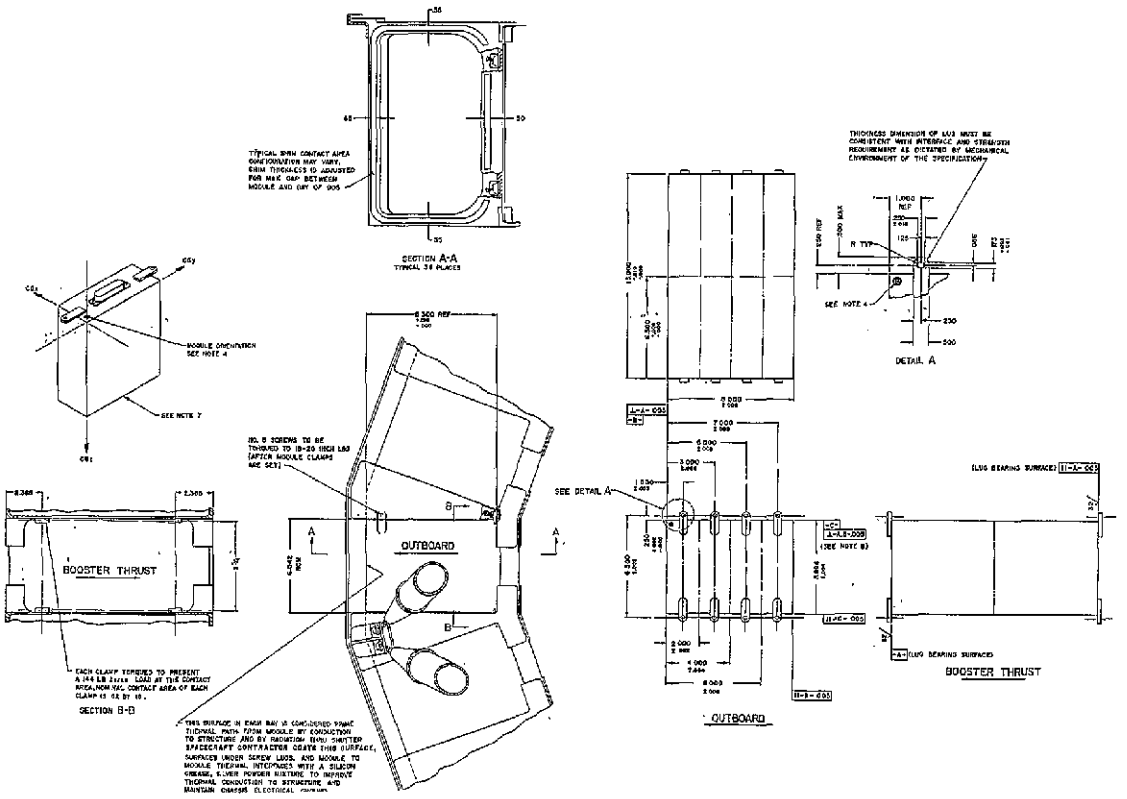

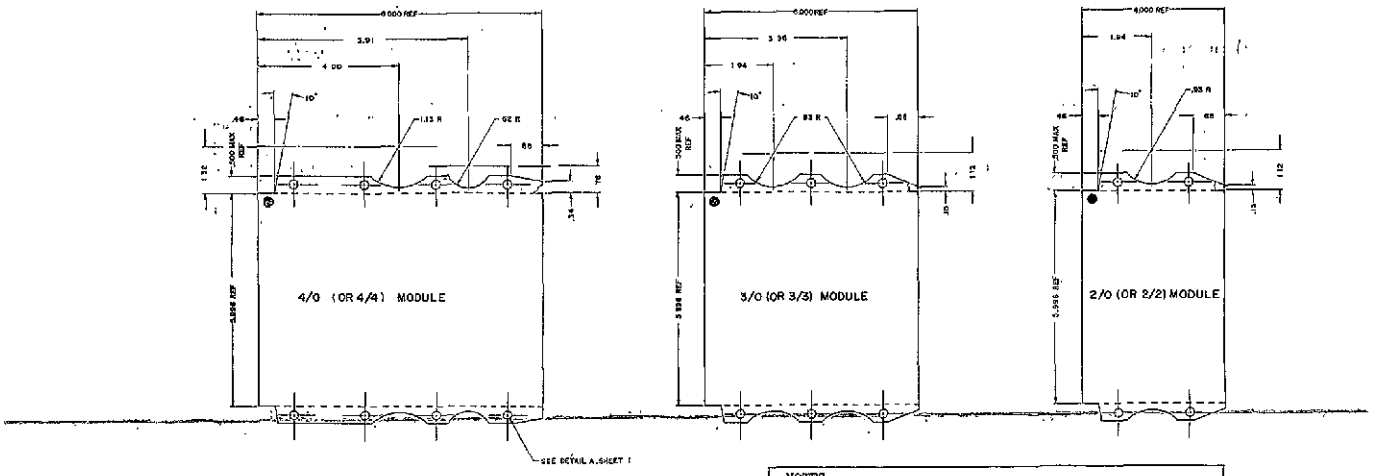

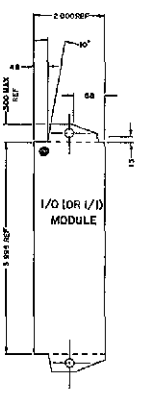

NOTES

1. All individual tabs must be attached to the module by at least two screws (No. 10-32) into tapped inserts. For continuous tabs (requiring approval of the spacecraft manager), at least four tapped holes utilizing inserts (No. 10-32) for each 1/0 module must be provided into the tabs (two for each tab). Screws and inserts must extend completely through the module face (or through the tab if a continuous tab).
2. Phantom lines indicate sizes of modules.
3. Where power dissipation requirement is critical, an integral tab or flange design (requiring approval of the spacecraft manager) may be used (as defined by sheets 3 and 4).
4. Each module shall have an orientation marking as shown to designate the outboard surface.
5. All connectors and identification labels shall be on the surfaces with the fastening lugs.
6. Parallelism and perpendicularity the same for all module configurations.
7. Center of gravity coordinate system.
8. Unless otherwise specified: Dimensions are in inches. Tolerances on decimals = ± 0.01, ± 0.005, Tolerances on fractions = ± 1/64, Tolerances on angles = ±0, 2°

Figure 2.3.5-2. Modular Interface Drawing

FOLDOUT FRAME 2

2-39/2-40

11 February 1970

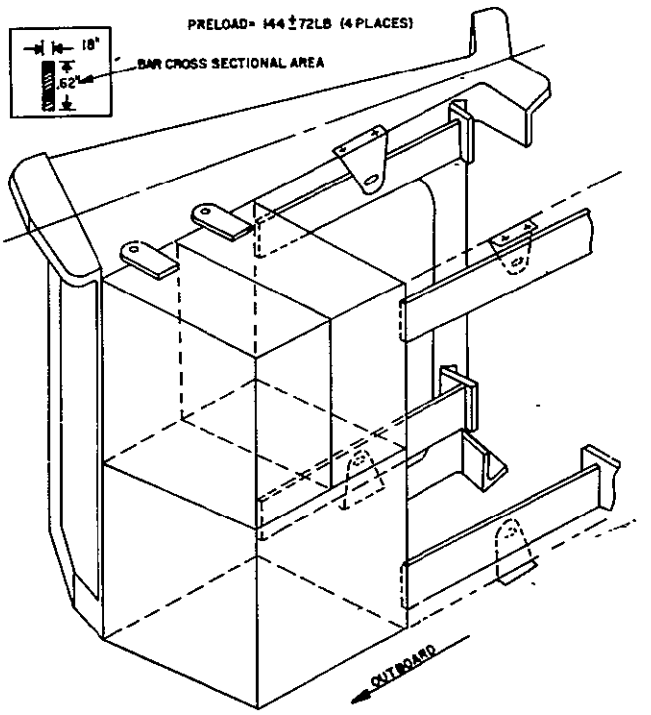

Figure 2. 3. 5-3. Module Preload Arrangement

13. The following finishes must be used:

a.	Magnesium	Dow 23
b.	Aluminum	Alodine 600
c.	Steel	Electroless Nickel

14. Equipment interfaces should have a $\surd$ 63 minimum surface finish for good thermal contact.

15. For equipment requiring alignment, reference alignment surfaces must be provided. For items requiring alignment to all three axes, two mutually perpendicular surfaces are required. For alignment with respect to two axes one surface will suffice.

The following geometric properties are required for alignment surfaces:

Alignment Limit	Surface Finish	Pad Flatness	Maximum Surface Slope	Pad Size (Minimum)
$\pm$0.5°	125 Min.	.001 in.	.005 in/ft	1.0 x 1.0 in.
$\pm$0.1°	32 Min.	.0005 in.	.0004 in/ft	1.0 x 1.0 in.

16. Where good heat transfer between the equipment and the spacecraft is required silver filled silicon grease must be used at the interface.

2.4 DESIGN STUDIES AND ANALYSES

2.4.1 SPACECRAFT STUDIES

2.4.1.1 Sensory Ring/Component Placement Study

Studies conducted on the placement of components in and on the sensory ring have demonstrated the capability of a basic Nimbus torus ring to accommodate the ERTS payload and subsystems, providing the internal or crossbeam structure is reconfigured. In addition, margin for subsystem growth is provided.

The rationale used in the placement of sensors and subsystems in the sensory ring is based on the following factors and considerations:

1. Sensor and antenna fields of view, size and thermal dissipation and control mounting requirements and weight.
2. Clearance with the spacecraft adapter during separation.
3. Subsystem and system interconnection, grouping, harness complexity, cable lengths and possible EMI problems.
4. Spacecraft center of gravity, moments and products of inertia, thermal control and balance, and crossbeam configuration.
5. Accessibility for interconnection, removal and installation,test and trouble shooting.

The order of placement is based on first - the field of view requirements and available space for experiments, sensors, antennas and large nonmodular components and then - tradeoffs between the above considerations to meet the mandatory and, if possible, desirable location restrictions.

The mounting arrangement for the ERTS Sensors is shown in Figure 2.4.1-1. The three Return Beam Vidicon (RBV) cameras are mounted on a common baseplate in the center area of the sensory ring. This baseplate will incorporate a three point universal mount which will preclude interaction with the spacecraft structure and guarantee maintenance of the close camera to camera alignment requirements.

The Multispectral Scanner (MSS) is mounted below the sensory ring forward [toward + X axis] of the YY axis. Mounting this unit with its center line directly below the YY axis would have provided a slightly larger available envelope, however, this arrangement would require descrete mounting of each RBV camera. This was considered undesirable because of alignment considerations.

The lower surface of the sensory ring also provides a mounting surface for the spacecraft antennas and the attitute sensor. As indicated in Figure 2.4.1-1 these units must be mounted on pedestals to provide clear fields of view over the MSS.

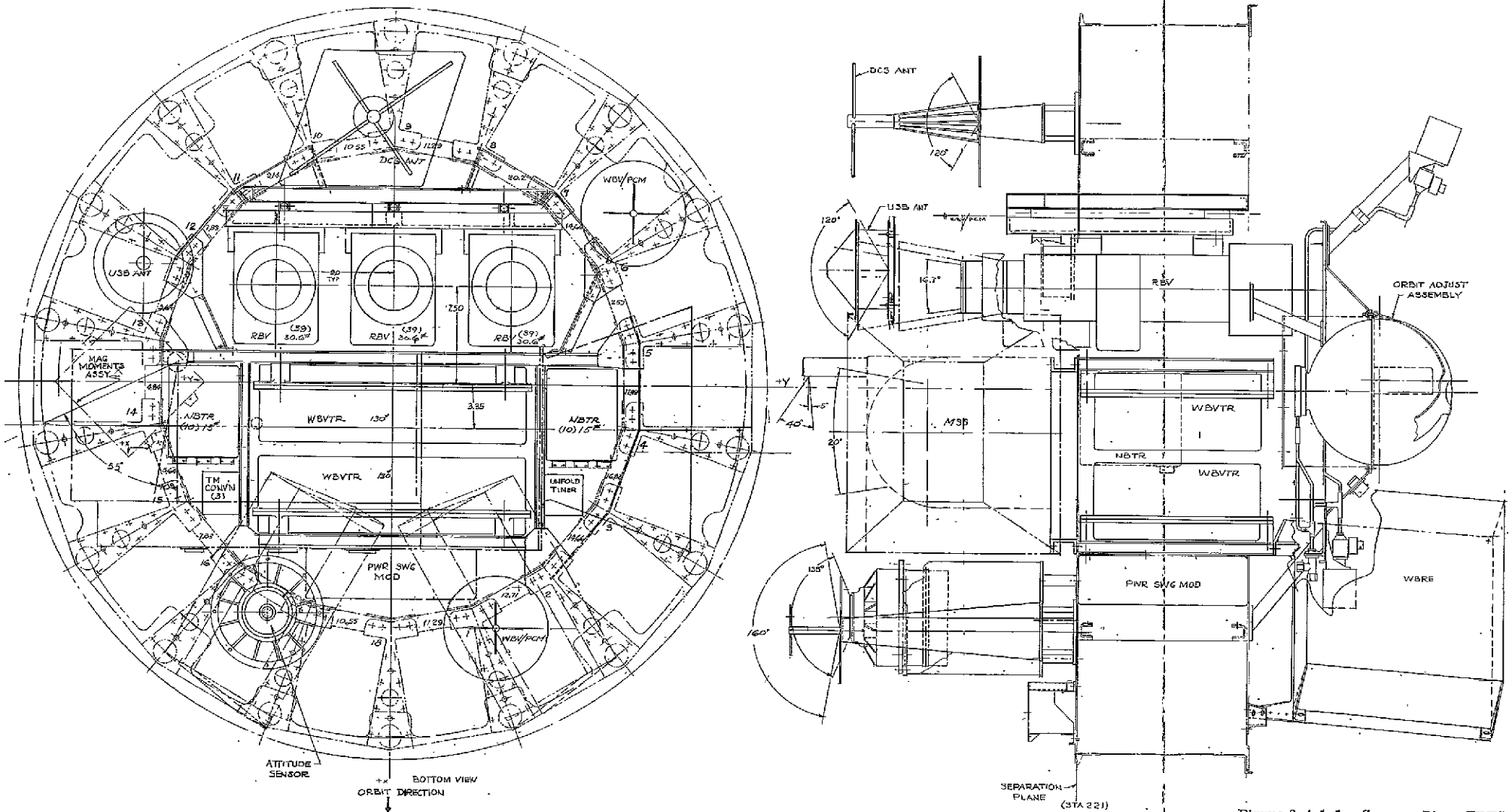

FOLDOUT FRAME 1

FOLDOUT FRAME 2

Figure 2.4.1-1. Sensory Ring, ERTS S/S Assembly

The upper surface of the sensory ring provides a mounting for the Orbit Adjust Subsystem, the two Wide Band Video Tape Recorder Electronic packages and the Magnetic Moment Package. These three packages are positioned such that clearance with the orbit adjust nozzles plumes is achieved.

The remaining nonmodular components are mounted in the center section along with the three RBV cameras. Adequate space is available to provide mounting structure for these components as described in section 2.4.5. Thermal dissipation from these components is accomplished via a radiator plate and opening in the lower insulation.

A placement study for the ERTS standard modules was completed. The modules are accommodated in the 18 bays of the sensory ring with 11 spaces unoccupied. The results of the study together with placement rationale are presented in Table 2.4.1-1. This table also presents the orbit average heat load per bay and the bay heat rejection capability. In addition the requirements for louvers and bay lower insulation are presented.

The highest thermal load occurs in bay 6 where the power control module is located. Bay 5 has a greater heat rejection capability, however bay 5 is blocked on the underside by the MSS and consequently Bay 6 with the lower insulation removed provides the optimum location for this module.

All other bays are loaded below their thermal dissipation capacity.

2.4.1.2 Structural Development Model (SDM)

During the Phase B & C study, the requirement to construct and test a structural dynamic model was identified. Although much structural testing has been conducted on Nimbus type spacecraft sturctures, the specific requirements for an ERTS structural model are based on the following:

1. The projected launch weight of the ERTS spacecraft including adapter is 1780 pounds. Previously the greatest weight tested was 1480 pounds (Nimbus B). The integrity of the basic Nimbus structure for this weight increase must be demonstrated.

2. The ERTS experiments have much tighter alignment tolerances than previous Nimbus experiments. The capability of the ERTS structural subsystem to maintain these tolerances through the launch vibration environment must be proven.

The following is a brief outline of the ERTS SDM test program. A more detailed description of the plan is contained in Volume IID of the proposal.

2.4.1.2.1 Test Objectives

The primary objectives of the SDM test program are:

1. To verify the structural integrity of the ERTS structural subsystem to withstand the launch environment imposed by the Delta N6 Launch Vehicle.

TABLE 2.4.1-1. ERTS MODULE LOCATIONS, LOUVER AND INSULATION REQUIREMENTS

Bay	Component	Module Size	Total Module Size	Component Heat Load (Avg.-Watts)	Total Bay Heat Load (Watts)	Bay Heat Rejection Capability (Watts)	Bay Louvers and Lower Insulation Requirements	Placement Rationale
1	Wide Band Power Amp.	2/2		7.2			Louvers -	Near antenna
	PCM Memory No. 1	2/0	4/4	.4	9.0	11.3	Btm Insulated	Near other PCM modules
	PCM Reprogrammer	0/2		1.4				Near other PCM modules
2	Wide Band Modulator	2/0	2/4	.6	6.6	12.7		Between Wide Band Power
	Battery	0/4		6.0			Btm Insulated	Amps
3	Wide Band Power Amp	2/2		7.2			Louvers -	Near antenna
	MSS Electronics	2/2	4/4	1.8	9.0	14.7	Btm Insulated	Near Sensor Connectors
4	Payload Regulator Mod.	4/4	4/4	2.0	2.0	16.8	Louvers- Btm Insulated	High heat rejection bay.
5	Auxiliary Load Controller	3/0		.7			Louvers-	
	Battery	0/4	3/4	6.0	6.7	17.5	Btm Insulated	
6	Power Control Mod.	4/4	4/4	33.0	33.0	25.7	No louvers- Btm Non-Insul.	Highest heat rejection bay without blockage on bottom [additional heat rejection relatively close to truss tube supporting I/F panel.
7	RBV Electronics	3/3		1.8			Louvers-	Near sensor
	Cmd. Int. Unit	1/1	4/4	3.0	4.8	14.7	Btm Insulated	Near clock
8	Command Clock	4/4	4/4	19.0		20.2	No louvers- Btm Non-Insulated	High heat rejection bay-no blockage on BTM
9	RBV Combiner	3/0		1.2			Louvers-	Central location
	Battery	0/4	3/4	6.0	7.2	11.3	Btm Insulated	between RBV Modules.
10	Battery USB, Pre-Mod	0/4	4/4	6.0	6.2	10.6	Louvers-	
	Proc.	4/0		0.2			Btm Insulated	
11	VHF Command Revr.	2/0		1.5			Louvers-	
	VHF DCS Revr.	1/0	3/4	1.5	9.0	9.1	Btm Insulated	Near Antenna - Antenna used
	Battery	0/4		6.0				as heat sink
12	VHF Transmitter	1/0		1.1			Louvers-	
			4/3	.3	3.2	7.8	Btm Insulated	Near USB Equip. &
	RBV Electronics	3/3		1.8				Antenna. Near sensor
								Low heat rejection bay
13	USB Equipment	4/4	4/4	3.1	3.1	5.6	Louvers- Btm Insulated	Near Antenna
14	RBV Electronics	3/3	3/3	1.8	1.8	4.8	Louvers- Btm Insulated	Near Sensor-Low heat rej. bay.
15	RBV Controller	3/3	3/3	1.2	1.2	5.6	Louvers- Btm Insulated	
16	PCM Coder	4/0		1.4			Louvers-	Near other PCM Mod.
	Battery	0/4	4/4	6.0	7.4	7.8	Btm Insulated	
17	PCM Dig. Mux.	3/0		2.6			Louvers-	Near other PCM Mod.
	Battery	0/4	3/4	6.0	8.6	9.1	Btm Insulated	
18	PCM Memory No. 2	2/0		.4			Louvers-	Near other PCM Mod.
	PCM Mem. Sequencer	2/0	4/4	1.0	7.4	10.6	Btm Insulated	Close to both PCM
	Battery	0/4		6.0				Memories.

2. To demonstrate the capability of the structural subsystem to maintain the payload alignment tolerances after exposure to the above vibration environment.

As a secondary objective, component environment levels will be verified for the subsystems and experiments.

2.4.1.2.2 Success Criteria

The tests conducted on the SDM will be considered successful providing:

1. The integrity of the structural subsystem is demonstrated, i.e., no failures cracks or permanent deformations.
2. Pre and post vibration alignment checks indicated that sensor alignment changes (if any) are within the tolerance requirements.
3. Meaningful component environment data is obtained.

2.4.1.2.3 Structural Development Model Description

The SDM will closely simulate the ERTS spacecraft configuration and will utilize as far as possible residual Nimbus hardware. New structural elements will be fabricated per engineering direction from design layouts. Mass simulations of the ERTS subsystems and experiments will be fabricated from engineering sketches. The following breakdown details the SDM structure:

1. Nimbus Residual Hardware

   Sensory Ring (Nimbus C Prototype Refurbished less X Beam)

   Dummy Modules - Mass simulated

   V-2 ACS Assembly

   Truss Tubes - Nimbus D Vibration Test

   A-4 Solar Paddles

   Adapter - Nimbus C Prototype

   Separation band assembly

   Paddle Latch Line

   Bolt and Cable Cutter Assemblies

   ACS Interface and Auxiliary Load Panels

   Ballast - As required to be added to the ACS, sensory ring and adapter.

2. New Structure

Sensory Ring Crossbeam

Secondary Structure - i.e., sensor, antenna and equipment mounts

Orbit Adjust Subsystem Structure

3. Mass Simulated Dummies

WB Video Tape Recorders (2)

WB Recorder Electronics (2)

Orbit Adjust Subsystem

NB Tape Recorders (2)

WB Antenna

Return Beam Vidicon Cameras (3)

Multi-Spectral Scanner

Magnetic Moment Assembly

2.4.1.2.4 Handling and Test Equipment

All the handling equipment and fixturing required exists in-house. There are no requirements for new equipment.

2.4.1.2.5 Instrumentation

Strain gages and accelerometers are required to monitor the spacecraft structure, control the test and notches, and to measure responses and component environment. Instrumentation will be minimized consistent with the test requirements. Based on past experience approximately 80 data channels will be required.

2.4.2 ERTS LAUNCH VEHICLE STUDIES

2.4.2.1 General

A study was performed under Program Directive Number 55 (Nimbus E&F) dated June 6, 1969 (NASA Contract No. 11570) to "Determine the impact on the Nimbus E&F spacecraft design using a Thorad/Delta launch vehicle for launching of the spacecraft with a payload as defined in GSFC Nimbus "E" configuration modified to include addition of the T&DR system and deletion of the SDR system." The study considered the mechanical and electrical interfaces, and the support equipment (AGE). In the course of the study various "Delta" problems arose for which "Nimbus" solutions were obvious. These problems were identified and proposed solutions were recommended.

This study was reviewed to determine the applicability of the results with respect to the ERTS spacecraft and its electrical and mechanical interface requirements.

2.4.2.1.1 Review Summary

The study was reviewed against the ERTS requirements. The conclusion reached was that while most of the potential mechanical and electrical problems identified for the Nimbus E/Delta L/V interface are extremely minor and readily solvable, there is one area which was not completely resolved. This area is the inadequate clearance between the upper paddle latch of the spacecraft and the Delta shroud.

This clearance problem is created by the method of shroud attachment to the launch vehicle. The Delta configuration has the shroud mounted directly to the forward end of the launch vehicle. The spacecraft adapter is mounted to a two inch adapter ring (or spacer) which in turn mounts to the forward end of the Delta. Because of this ring and the manner and position of mounting the shroud, the upper end of the paddle assembly protrudes into the conical portion of the shroud, thus creating an interference problem. Figure 2.4.2-1 illustrates this problem. Both Nimbus-B and Nimbus-D were mounted to two inch spacer rings which were mounted on top of the Agena, however, the shroud used was attached to the top of this spacer resulting in an adequate clearance for the upper paddle latch.

Several methods by which this problem can be resolved are:

1. Use a SACS type shroud with a SACS adapter ring (spacer) which raises the shroud two inches and attaches to the Delta booster, which requires modifying the front end of the Delta.
2. Use the present Delta shroud configuration except mounted to a new adapter ring.
3. Increase the length of the shroud by two inches.
4. Dimple the Delta shroud around the clearance problem area.
5. Design a new adapter to fit on top of the Delta booster, eliminating the need for an intermediate adapter ring (spacer).
6. Design a shorter adapter.

2.4.2.1.2 Baseline Configuration

Figure 2.4.2-2 shows the recommended approach which is to modify the upper end of the Delta to accept the SACS ring, thus permitting the use of the SACS shroud. This change has been requested by the NASA/GSFC Nimbus E&F Project Office.

2.4.2.2 Spacecraft Shroud Separation Study

One major difference between the SACS and Delta shroud is two pullaway connectors located in the spacecraft adapter which provide power to the ACS scanner stimulators and the shroud separation band bolt cutters. On the Nimbus B and D spacecrafts this function is provided within the launch vehicle adapter ring.

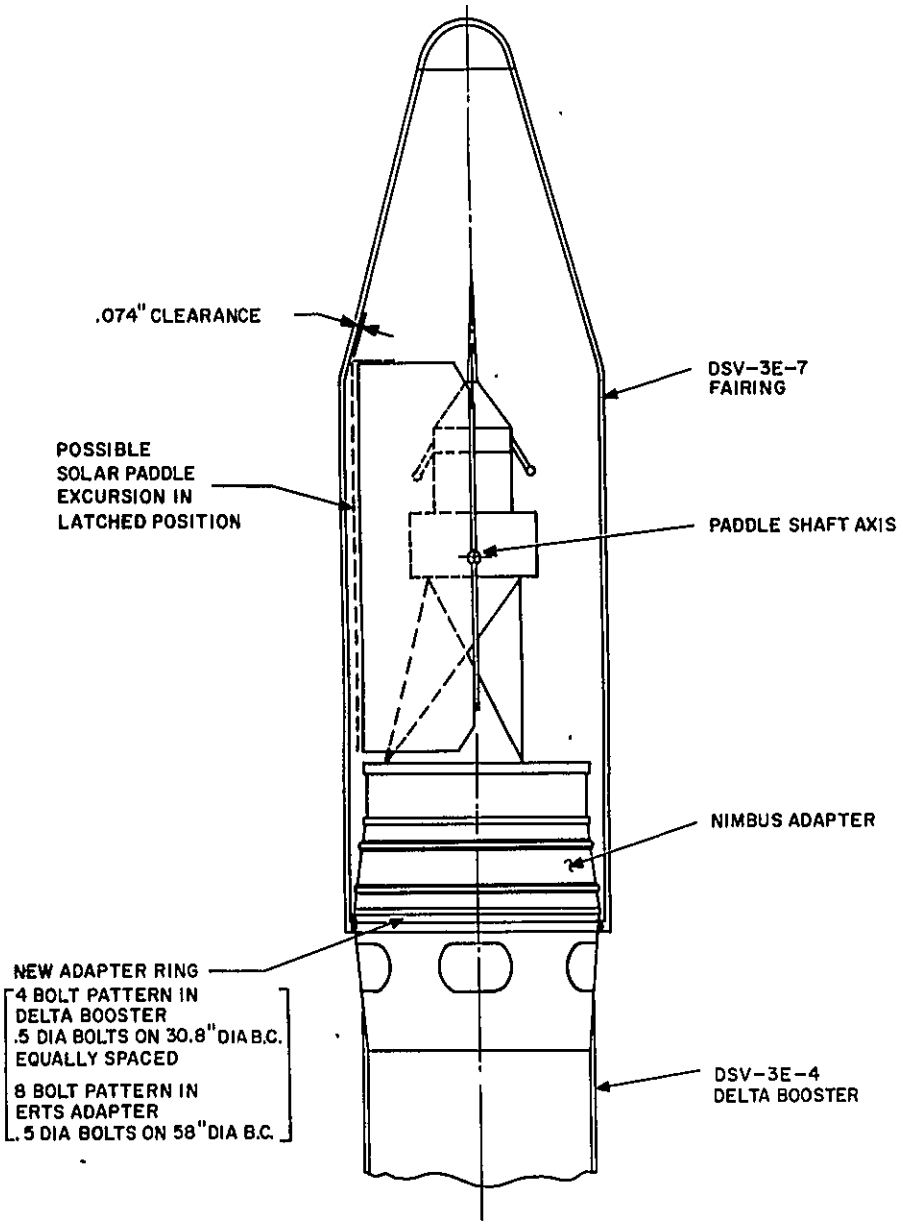

Figure 2.4.2-1. ERTS A&B Study with DSV-3E-4 Second Stage and DSV-3E-7 Fairing

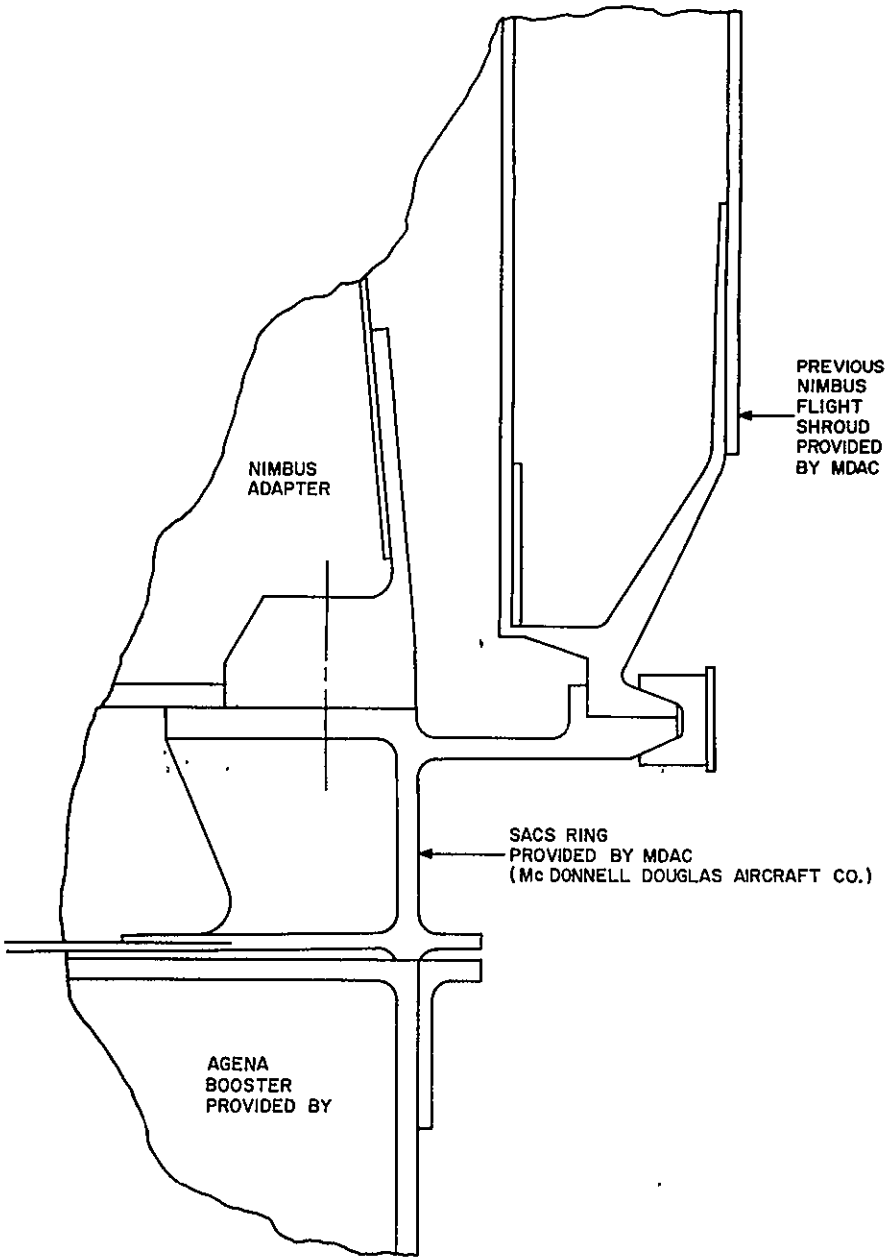

Figure 2.4.2-2. Modified Delta Booster

2.4.2.2.1 Interference

The location of the pullaway connectors have been scaled from a sketch in a Delta Report A2-260-ABA4-43, Page 3, Nimbus E&F on Delta Feasibility Study. There is an apparent interference between the pullaway connectors and the spacecraft cover lower support ring which bolts directly to the spacecraft adapter. A vertical repositioning of pullaway connectors of $\frac{1}{2}$ inch will provide ample clearance (see Figure 2.4.2-3).

2.4.2.2.2 Design

This figure also indicates the changes required in the spacecraft adapter. Since the pullaway connector location does not fall on a major structural member, only a doubler is required to stiffen the cut out in the skin. In addition, a new bracket must be designed to mount the pullaway connectors at the proper release angle. Although the ERTS adapters are the same as Nimbus, no problems are foreseen in modifying the adapter as indicated. The locations of the pullaway connector were also checked for compatibility with the ERTS A&B configurations. In particular, interference with possible targets, and antenna pickups and re-radiators was studied. No problems were discovered.

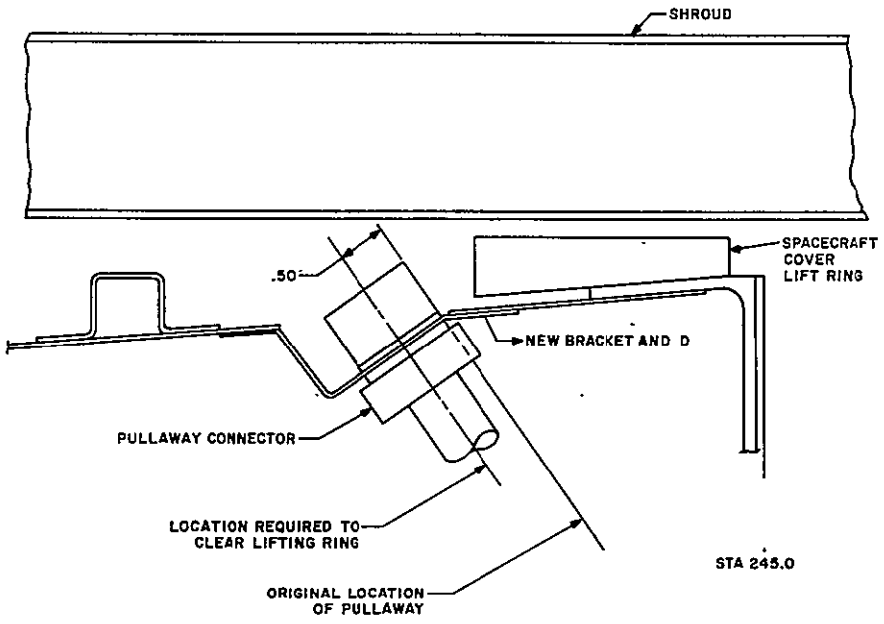

Figure 2.4.2-3. Repositioning of Pullaway Connector

2.4.2.2.3 Separation Analysis

Four areas of the spacecraft and shroud separation were analyzed:

1. Shroud/adapter physical impact during shroud ejection.
2. Adapter/launch vehicle transition ring shimming requirements to minimize launch vehicle/spacecraft separation tumble rates.
3. Delta Launch vehicle separation and retro-sequencing.
4. Separation Spring Analysis

2.4.2.2.4 Shroud/Adapter Physical Impact during Shroud Ejection

There was some question on the Nimbus A&C spacecrafts which used a similar shoud if the shroud actually hit the spacecraft adapter when ejected. These earlier spacecrafts had the shrouds directly mounted to the adapter and any slight inward "kick" would result in the lower shroud flange hitting the adapter sides. However, the new mounting arrangement (Delta forward section) prevents this problem from occurring since the shroud lower flange is three inches removed from the closest part of the adapter.

2.4.2.2.5 Adapter/Launch Vehicle Transition Ring Shimming Requirements to Minimize Launch Vehicle/Spacecraft Separation Tumble Rates

The interface between the spacecraft adapter and the launch vehicle transition ring is normally (Agena Launch Vehicle) shimmed to allow a maximum gap of 0.010 inches. This shimming is accomplished during a flight adapter and flight shroud matchmate at the launch vehicle facilities. If upon mating at the pad this maximum gap is exceeded, further shimming is performed. This process is relatively easy since it only involves measuring the gap and peeling a piece of laminated shim stock to the desired thickness. There has, however, been some question as to the real shimming requirements.

1. Analysis. The analysis performed was to assume a complete semicircular gap between the adapter and transition ring of 0.050 inch. It was then assumed that on torquing the bolts the gap would be closed. The analysis showed that a lower adapter ring deflection of 0.050 inches resulted in a deflection of only 0.010 inches at the spacecraft separation surface and represents a total stored energy of approximately 12 pounds. If a worst case tumble rate calculation were to be performed, all 12 pounds would be added to the force available at one of the four separation springs. This would result in an additional tumble rate of 0.2 degrees per second.

2. Conclusion. The present gap value of 0.010 inch instead of the 0.050 assumed would give a tumble rate of 0.04 degrees per second which is more in line. In addition, the analysis is conservative and values up to 0.02 degrees per second are more probable. Therefore, it is concluded that 0.010 max gap requirement between the spacecraft and launch vehicle remain unchanged.

2.4.3 ADAPTER SEPARATION STUDIES

2.4.3.1 Separation Spring Design for ERTS Spacecraft

An analysis of the Nimbus separation system was made to assess its applicability to the proposed ERTS spacecraft.

2.4.3.1.1 Conclusions

The existing Nimbus separation system design is directly applicable to the present ERTS spacecraft concept:

1. The existing spring design can be extended to cover the required spring rates. None of the presently available springs are adequate for the ERTS spacecraft weight as presently conceived - the spring rates are too low to achieve positive gaps between spacecraft and adapter for the required tumble rate calculations.

2. The analysis made used a spacecraft weight of 1529 pounds at separation and a Delta/spacecraft adapter total weight of 2102 pounds. A separate check of spring design for a possible spacecraft weight increase of 20 percent, to a total of 1830 pounds showed that only a change in spring wire diameter was required with higher spring rates.

3. The existing computer routines and analysis techniques can be used without change for the ERTS spacecraft.

4. Aside from the spring hardware details, no other spring actuator details will need redesign for either the present weight or the possible weight increase noted under (2) above.

5. No adapter structural details involved in the separation subsystem will need redesign for either the current weight or the possible weight increase noted under (2) above.

6. No spacecraft structural details will need redesign for separation loadings for either the current weight or the possible weight increase noted under (2) above.

2.4.3.2 ERTS Spacecraft Separation Clearance Study

An examination was made of the ERTS spacecraft to adapter separation in order to define clearance envelope criteria for the equipment mounted below the spacecraft sensory ring. Clearance between the bottom mounted sensory ring equipment and the adapter were assessed using the separation rates taken from Nimbus I, II and III flight data, shown in Table 2.4.3-1.

From the latest mass properties report for ERTS, the center of rotation is 19 inches above the separation plane, on the yaw axis, as shown in Figure 2.4.3-1.

The tip off rotation rates are approximately 10 times greater than the expected rates in flight (Table 2.4.3-1).

TABLE 2.4.3-1. ADAPTER CLEARANCES

	Separation Rates (ft/sec)	
	Nimbus I, II, III	Tolerance
Yaw Direction	4.5	± 0.5
Lateral Direction	Negligible	

	Tip Off Rates (deg/sec)			
	Flight Data for Nimbus			Worst Case Analysis
	I	II	III	
Roll/Pitch Rate	0.48	0.11	0.093	1.76
Yaw Rate	0.15	1.23	0.087	1.51

Suggested Separation Rates for ERTS	
Relative velocity, yaw direction	4 ft/sec (reduced due to heavier spacecraft)
Relative velocity, lateral direction	negligible
Roll pitch rotation rate	1.76 deg/sec
Yaw rotation rate	1.51 deg/sec

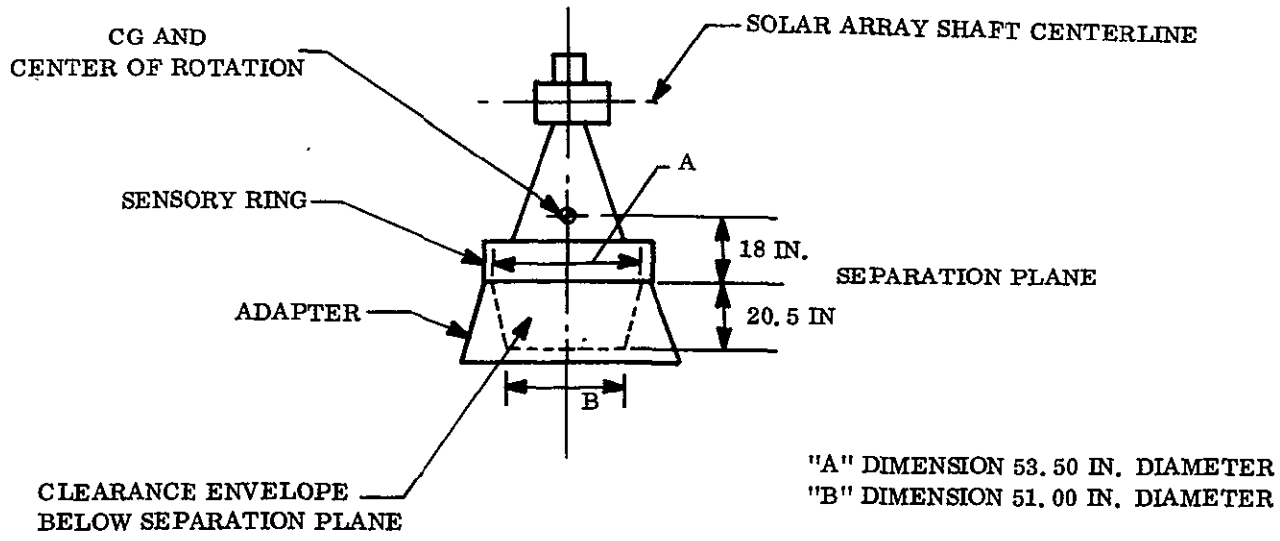

Figure 2.4.3-1. Clearance Envelope and Center of Rotation Diagram

Other ERTS components that must be cleared include four separation spring assemblies and six separation switch assemblies. The clearance envelope below the separation plane was determined from the suggested separation rates for ERTS plus allowance for thermal insulation. The multi-spectral scanner is the largest equipment mounted below the sensory ring.

2.4.4 SPACECRAFT SUBSYSTEM STUDIES

2.4.4.1 Solar Array Sun Sensor Shadowing Study

The Attitude Control Subsystem (ACS) contains two independent solar array drives. Sun sensors for these drives are currently mounted on the drive shaft extending from the ACS housing. For the proposed ERTS orbit shadowing of the +Y or right solar array sun sensor will occur. In order to remain outside any area shadowed by the ACS, the sun sensors on the +X or right side must be relocated.

2.4.4.1.1 Sun Sensor Configuration

The present sun sensor design is shown in Figure 2.4.4-1. There are two sets of sun sensors mounted on each side of the drive shaft. The albedo shield is located towards the earth-viewing side of the spacecraft and is attached to the ACS package. The purpose of this shield is to block out any reflected sun light off the surface of the earth.

The reason for having sun sensors on both sides of the array is in the event the sun does shine on the non-celled side of the paddle, it will rotate towards the sensitive side till it achieves sun acquisition.

2.4.4.1.2 Sun Sensor Shadowing

For this study, a worst case β angle of 40 degrees was used. Figure 2.4.4-1 shows the shadows cast by the ACS package and a plane taken through the solar array drive shaft for three spacecraft-to-sun positions. The figure also shows the composite shadow cast by the ACS package during any one orbit.

2.4.4.1.3 Sun Sensor Relocation

Several alternate methods for relocating the sun sensors were considered.

1. Place the sun sensors on the solar array transition section
2. Extend the sun sensors outward from their present location.
3. Place the sun sensors on the solar array.
4. Slave the right solar array by using the sun sensors on the left side.

These are discussed in the following paragraphs and summarized in Table 2.4.4-1.

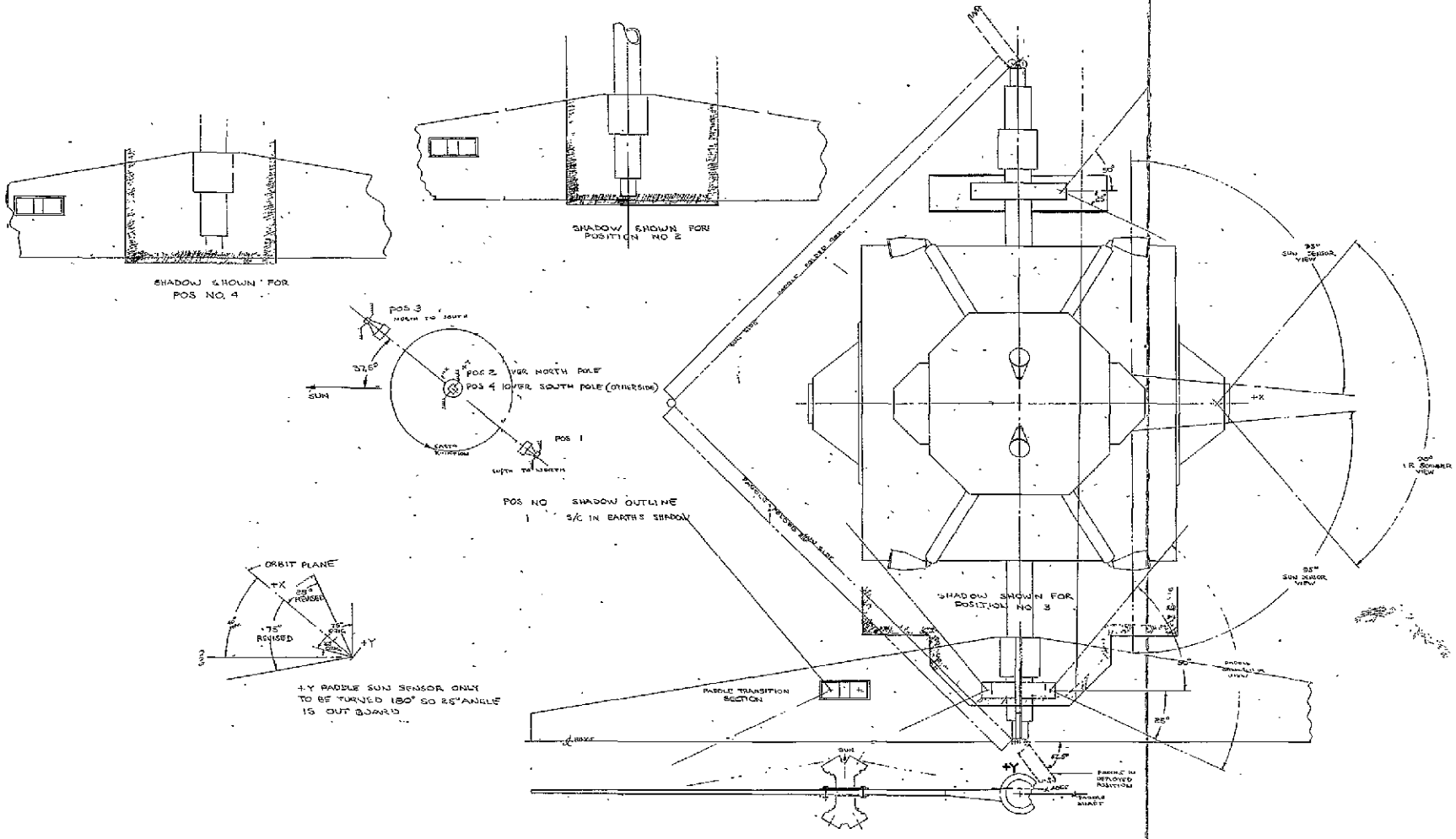

Figure 2.4.4-1. Paddle Sun Sensor Shadow Study

FOLDOUT FRAME 1

FOLDOUT FRAME 2

TABLE 2.4.4-1. SOLAR ARRAY SUN SENSOR RELOCATION STUDY

Sun Sensor Location	Advantages	Disadvantages
1 Sun Sensor on Solar Array Transition Section	No change required to present sun sensor design Clears shadow cast by ACS package Mounting onto transition honeycomb panel is feasible	Cannot accommodate a stationary albedo shield
2 Extended support Sun Sensor	The sun sensor can be supported from its present location An albedo shield can be incorpated	The -X sun sensor must be supported by a long stiff heavier boom The +X sun sensor must be made retractable to clear the stowed solar array
3 Sun Sensor on Solar Array	Clears all shadows cast by the ACS package	Placement of sun sensors on the array means loss of electrical power producing cells Cannot accommodate an albedo shield
4 Slave Solar Array from Left Side	Minimal hardware change	Loss of sun sensor redundancy Loss of solar array independence

1. Sun Sensors on Transition Section. The present configuration sun sensor (Figure 2.4.4-2 and 2.4.4-3) can be moved to the honeycomb transition section of the solar array. This can be done by placing standard threaded honeycomb inserts into the transition section. Thus, instead of clamping the sun sensors around a shaft, they are bolted to honeycomb inserts. The heat strap used to maintain thermal balance need only be lengthened a few inches. The disadvantage of this method, is that it cannot accommodate a simple stationary albedo shield.

2. Extended Support Sun Sensor. To keep the present Nimbus D drive shaft attachment configuration and still clear the shadow cast by the ACS package, the sun sensor support must be extended 15 inches beyond its present location (See Figure 2.4.4-4). The stowed or launch condition solar array interferes with the +X or sun acquisition and track sun sensor.

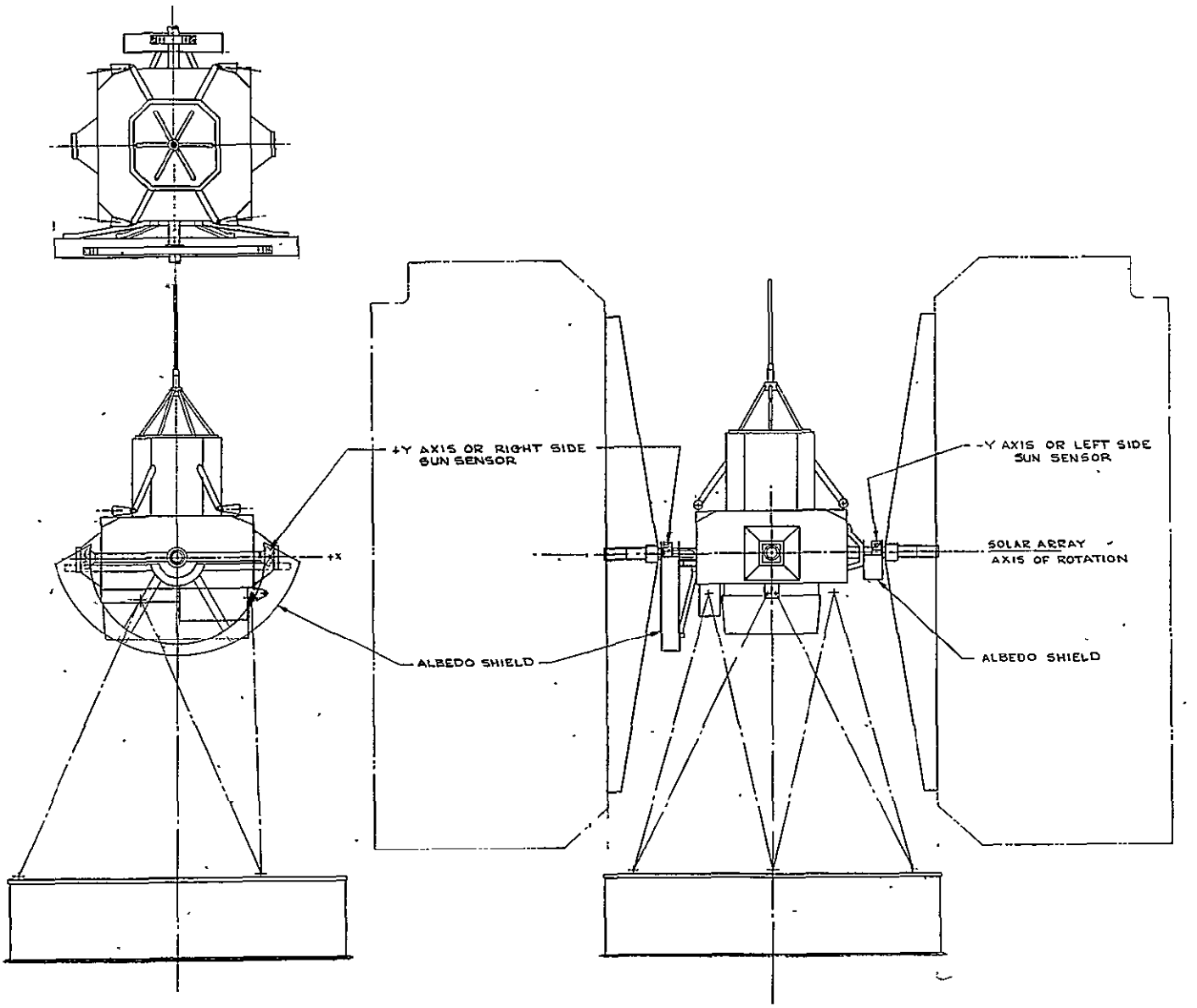

Figure 2.4.4-2. Sun Sensor Location on Nimbus

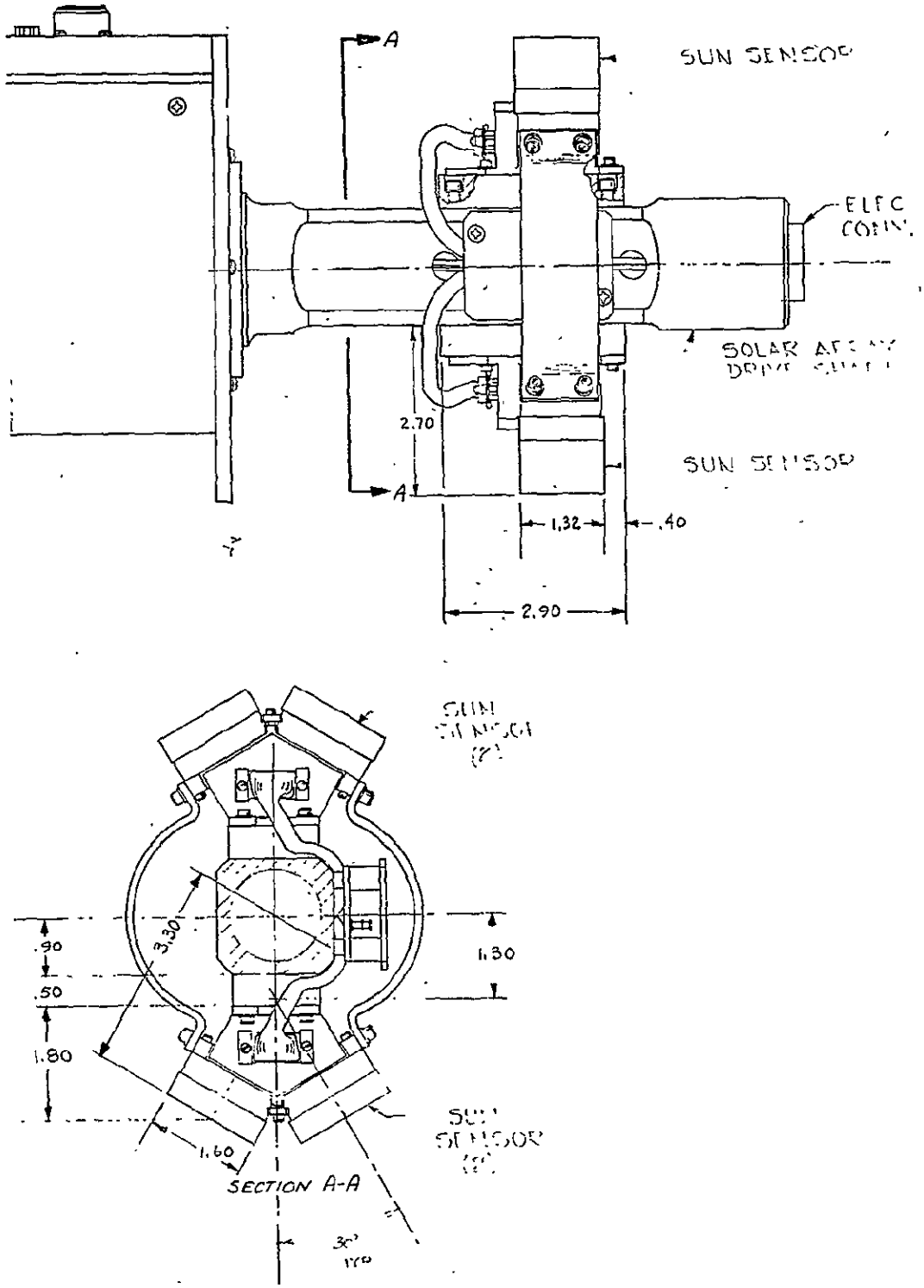

Figure 2.4.4-3. Solar Array Drive Sun Sensor

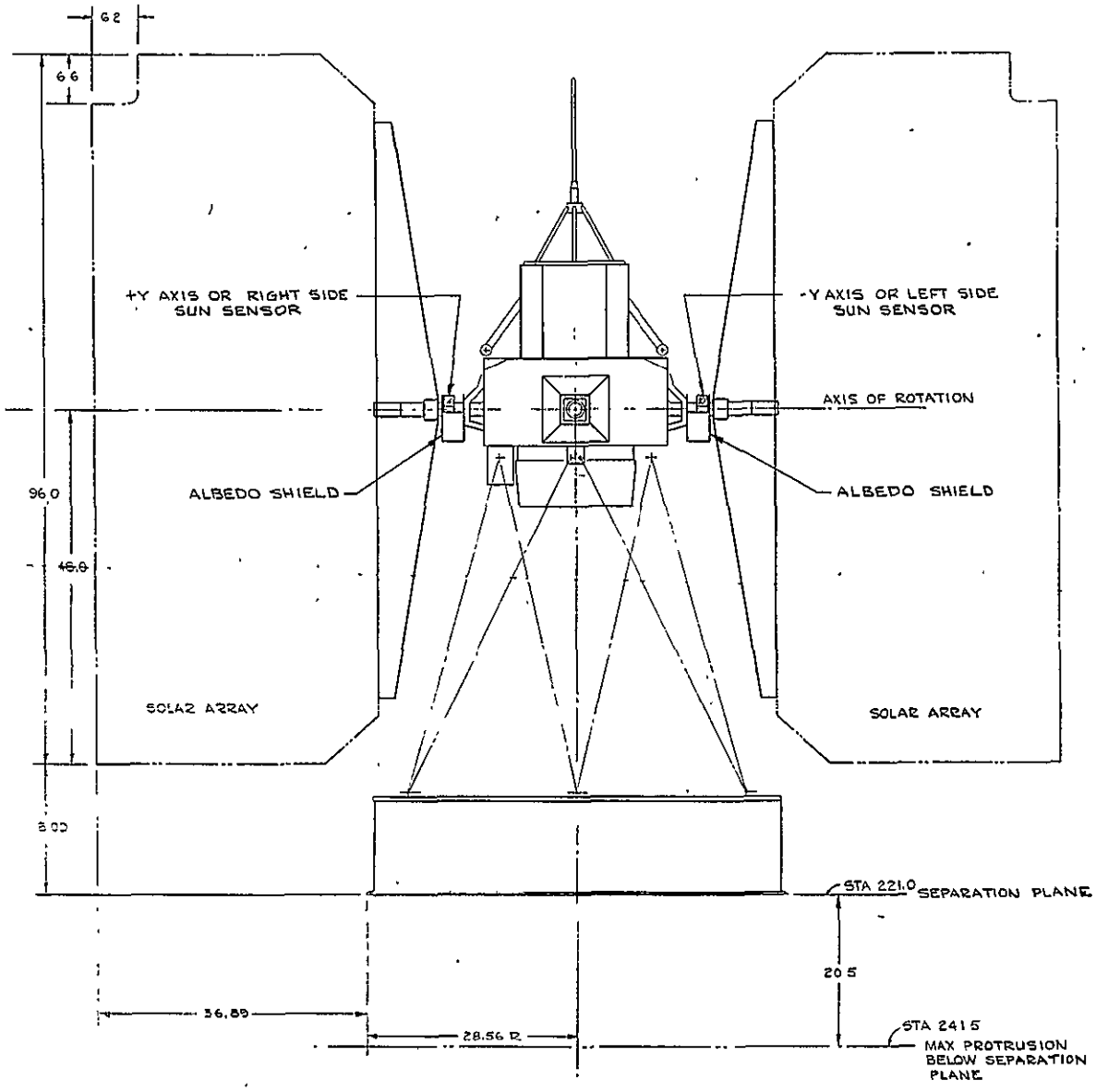

Figure 2.4.4-4. Extended Sun Sensor

The albedo shield will have the same earth blockage but enlarged to accommodate the extended sun sensors.

To maintain both sun sensors and a complementary albedo shield without interference, the +X sun sensor and a portion of the enlarged albedo shield must be made retractable and deployable.

This concept of retracting and deploying both the albedo shield and sun sensor poses a difficult design problem. It will require special retract and hold latching mechanism during launch when the solar arrays are stowed. After orbit insertion and during array deployment, the driven paddle can be used to activate a tripper mechanism which will in turn deploy the sun sensor and albedo shield to their respective positions.

The albedo shield will not only be larger but the support structure will also become larger and heavier.

The extended cantilevered sun sensor supporting arms will require "beefing up" to withstand launch loads.

3. Sun Sensor on Solar Array. The sun sensor can be feasibly moved to the center of the solar array, displacing 2.25 square inches of solar cells. Another 4 square inches of cells will be lost to shadowing effects from the newly located sun sensor. The total area of solar cells lost would be 6.25 square inches or 0.2 percent of the total solar cell area available. Approximately 2 to 3 square inches can be regained by simply canting the sensors towards the sun.

The present configuration sun sensors can be mounted with inserts located in the box tubing which runs through the center section of the solar array paddle. The electrical wires can also be routed into this box tubing through a grommet hole drilled on the shaded side of the sensor. In order to maintain thermal balance, a heat strap can be routed through this same hole to the cold side of the paddle. Both front and rear sun sensors can be accommodated.

The sensor wires inside the box tubing will be routed and snaked across the hinge line along with the solar cell power lines.

Aside from a 0.2 percent loss in electrical power, a few structural changes and no albedo shield requirement, this method offers one of the best solutions for clearing all shadows cast by the ACS package.

4. Slave Solar Array from the -Y or Left Sun Sensor. The +Y solar array can be driven using the sun sensors located on the left or -Y side.

Electrically slaving the right solar array from one side has several drawbacks:

1. Loss of sun sensor redundancy.
2. Loss of solar array independence, requiring electrical monitoring and coupling of both solar array positions.

3. No need for independent solar array drives.

4. Increased circuitry.

This method, however, offers several advantages:

1. Minimal hardware change.

2. Existence of an albedo shield.

2.4.4.1.4 Recommendation

For minimum modification to the sun sensor and circuitry, it is necessary that the sensors be mounted on the array. Further, they must be outside any area shadowed by the ACS. Suitable locations are on the array transition section and on the array itself (See Figure 2.4.4-5). Transition section mounting clears ACS shadows. Paddle mounting requires rearrangement of cells which is considered to be a major modification.

The recommendation is to mount the sun sensors on the transition section and inhibit the sensors from albedo effects.

2.4.4.2 Inclined ERTS Solar Paddle Study

In order that maximum power may be generated by the solar array during the ERTS orbit a study was conducted on the feasibility of reorienting the standard Nimbus paddles for direct sun viewing.

For maximum sun viewing, the right-hand paddle must open 167 degrees from the folded position and the left-hand paddle 103 degrees. Presently, the Nimbus paddles both open through a 135 degree angle.

In order to achieve the required inclination of the paddles changes must be made to the paddles transition section hinge line (Figure 2.4.4-6). The principal changes are in the area of the dog latch which locks the paddle in the open position however, the right-hand paddle edge members must be reconfigured from the present channel section to a zee section to provide clearance for the greater opening angle. In addition, the opening springs on the hinge line must be redesigned fro the greater travel.

Figure 2.4.4-6b, c, d, e shows the dog latch configuration for the inclined paddle and Figure 2.4.4-6 presents the present Nimbus arrangement as a reference. The dog latch is a simple, over center spring mechanism operating such that when the lug supporting the toggle spring on the paddle moves the toggle spring over the fulcrum of the toggle link, the moment on the link is reversed causing the dog latch toggle, which is guided in a slot, to snap to the latched position.

As shown in Figure 2.4.4-6c, d, and e, the elements of the latch are retained in the same relative orientation to each other, however, orientation with respect to the paddles and transition section is changed.

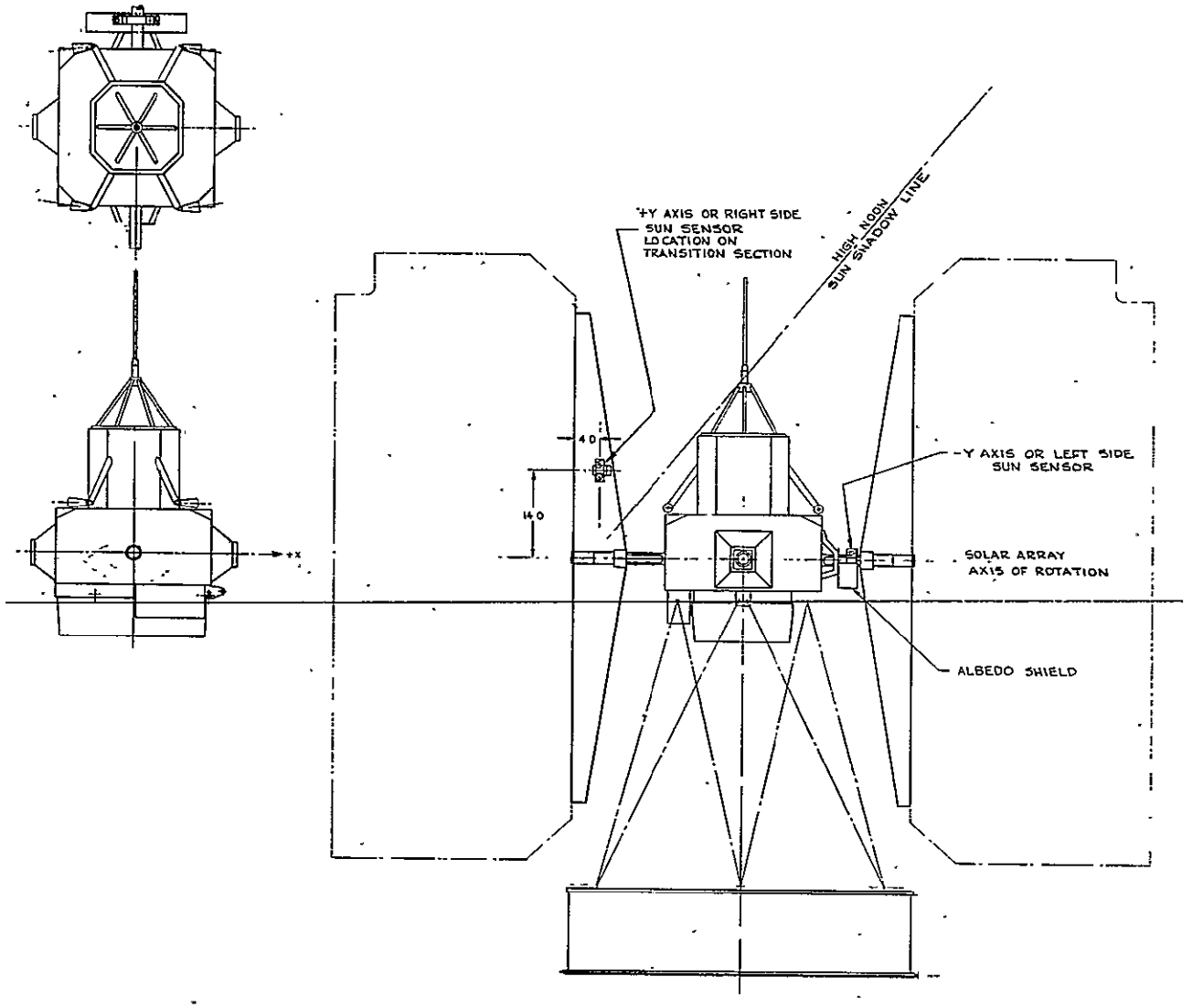

Figure 2.4.4-5. Sun Sensor on Transition Section

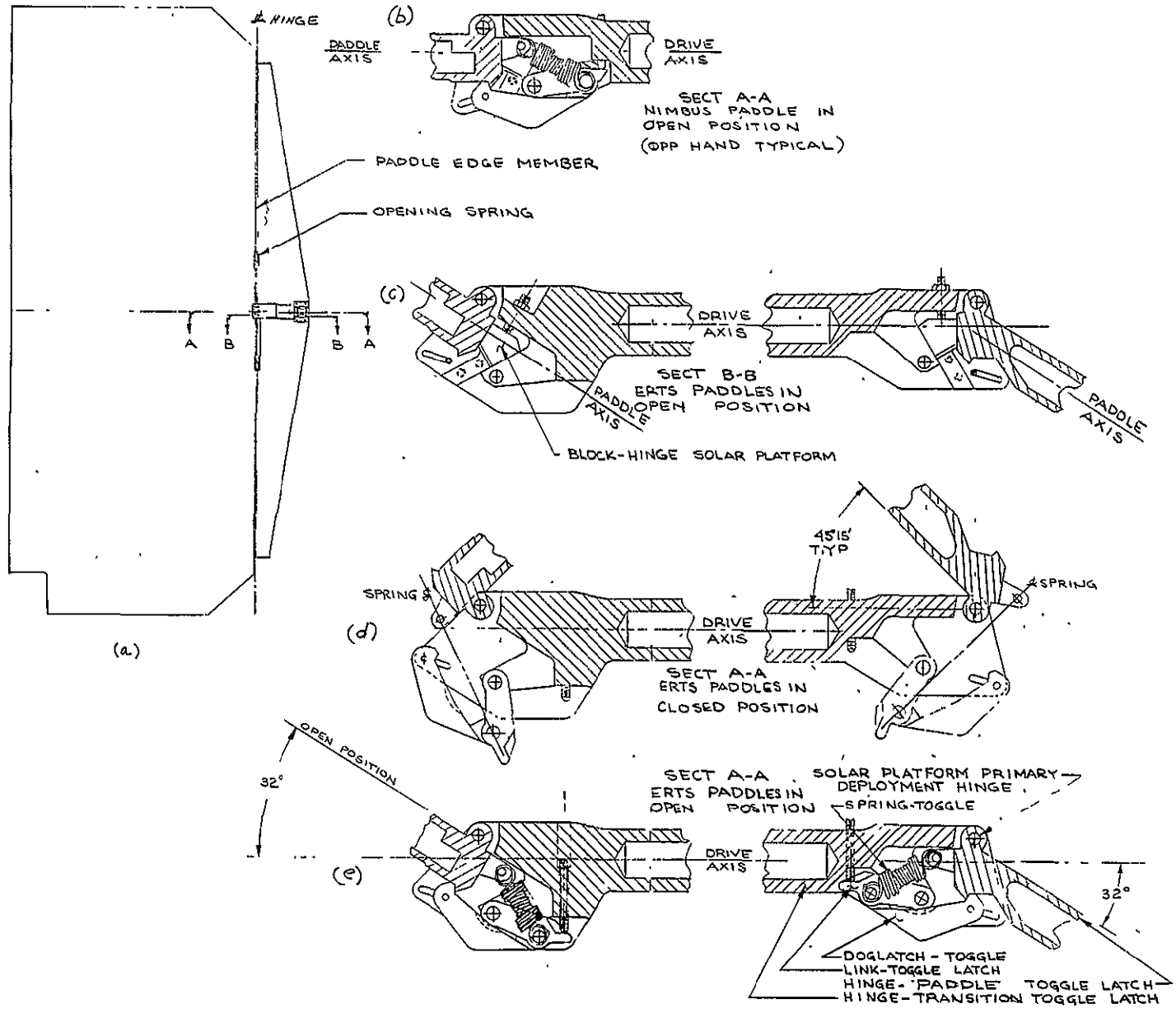

Figure 2.4.4-6. Inclined Paddle Study

2.4.4.3 Payload Sensor Sun Glint Study

There are three optical sensor systems on board the ERTS spacecraft that can be affected by sun glint. They are the MSS package, the independent attitude sensor and the three RBV's. This problem was studied by making a rough layout showing approximate positions of the ERTS spacecraft with its payload with respect to the earth and the sun. Figure 2.4.4-7 shows that as the spacecraft enters the sunlight from the dark side of the earth (see Position 1) the sun's rays directly enter the openings in the MSS package and the Attitude Sensor, till Position 2 is reached. The wide band antenna protrudes above the MSS and Attitude Sensor but is located away from the sun and sensor openings in such a manner that no detrimental reflections occur.

During this period, (Position 1 to 2) the RBV's are all in the shadow of the MSS package and will not receive any direct sunlight. However, they can receive reflections off the tops of the DCS and USB antennas.

From Position 2 to Position 3, the MSS and Attitude Sensor openings are in the shadows of the spacecraft sensory ring.

From Position 2 to Position 4, one or more of the RBV's can receive reflected sun light off the tops of the DCS and USB antennas. There is a definite increase in reflected sunlight into the RBV's, between Positions 3 and 4.

Positions 4 to 5 is the worst case condition in that the RBV's will not only receive direct sunlight of the wall of the MSS package but sunlight will directly enter all the sensor openings.

The recommendation is to use 9 and 1 inch long conical sun shades on the RBV and independent attitude sensors respectively. The MSS will not need a sun shade, if the sunlight entering the opening impinges upon a non-reflective surface. The field of view of the MSS sensor is comparatively small, so that it will never see the sun. If the sun's rays entering the opening is detrimental, then a truncated pyramid sun shade must be incorporated. This means relocating or extending the MSS sun calibration mirror.

2.4.5 PAYLOAD AND NEW EQUIPMENT ACCOMMODATION STUDY

All specified payload sensors and associated equipment are accommodated by the ERTS vehicle as shown in Figure 2.4.5-1.

Accommodation studies included are:

1. Payload and New Equipment Accommodation
2. RBV Common Plate Study
3. RBV and MSS Stimulator in Adapter Accommodation
4. Orbit Adjust Subsystem Accommodation

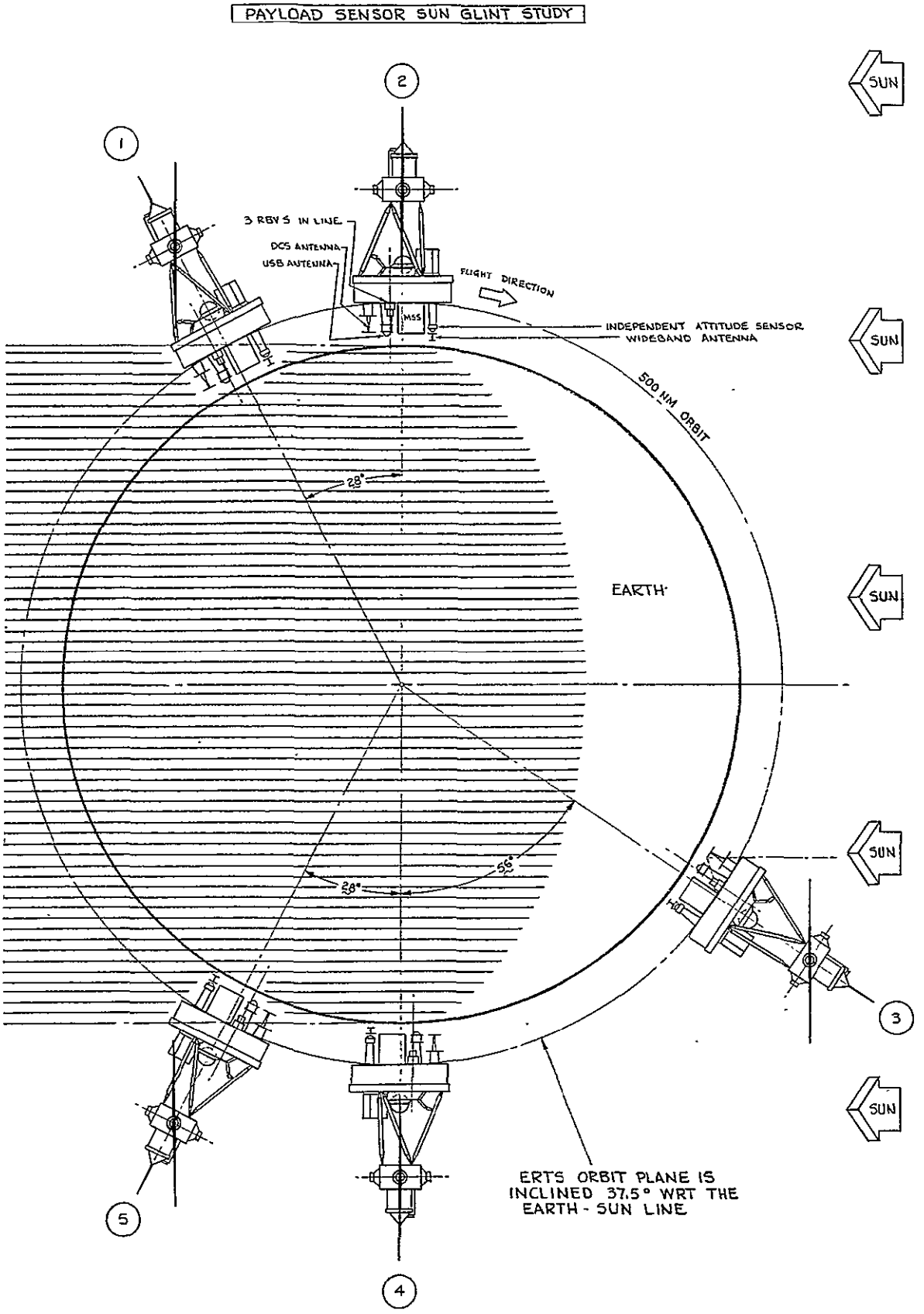

Figure 2.4.4-7. Payload Sensor Sun Glint Study

2.4.5.1 Payload and New Equipment Accommodation Study

Payload sensors and associated equipment accommodated are:

1. Return Beam Vidicon (RBV) camera system
2. Multispectral Scanner (MSS) system
3. Wideband Video Tape Recorders and Electronics
4. Data collection system for collecting data from sensors at known locations on the earth.

Approximately 48 cubic feet are made available by the ERTS structure for installation of sensors, components, and all associated equipment. This is considerably more than the specified mission required volume of 12 cubic feet (See Table 2.4.5-1).

The weight carrying capacity (as defined by S-701-P-3) of the Nimbus structure is approximately 610 pounds. This is based on a historical average of 38 percent for the capacity to-total-weight ratio of previous Nimbus spacecraft, and is applied to an approximate ERTS total weight of 1600 pounds. This definitely meets the specified required minimum weight capacity of 458.2 pounds.

Clear fields-of-view for all sensors are provided, as shown in Table 2.4.5-2. In addition, a 25 percent contingency increase in fields-of-view is easily accommodated with no change in sensor arrangement. The total earth looking surface available is approximately 2370 square inches or 16.4 square feet. The maximum earth viewing area required by the specified sensors including a 25 percent contingency and all antennas and attitude sensor is 10.4 square feet (See Table 2.4.5-2). Hence, an additional 6 square feet of viewing area is still available.

The preceeding discussion demonstrates that the basic Nimbus configuration possesses adequate capacity to accept the specified payload.

The ERTS configuration is well suited to accommodate additional equipment. Figure 2.4.5-2 shows that by placing the Wideband Video Tape Recorder equipment above the sensory ring, it leaves an additional 3 cubic feet of equipment that could be mounted inside the center section.

The placement of the Wide band Video Tape Recorder System above the sensory ring does three things:

1. Since the WBV Tape Recorders generate considerable heat, the placement above the sensory ring allows it to radiate its heat directly into space.
2. By surrounding the Orbit Adjust (OA) Subsystem, it can radiate heat inward and help control the O/A Subsystem temperature.
3. Allows room for additional equipment inside the center section.

TABLE 2.4.5-1. AVAILABLE VOLUME

Area	Volume (cubic inch)	Estimated Packaging Factor	Net Volume (cubic inch)
Bays	11,300	1.0	11,300
Center Section	14,000	0.8	11,200
Below Sensory Ring	47,500	0.8	38,000
Above Sensory Ring	34,800	0.6	20,900
On Periphery	1,200	1.0	1,200
Within Structure	3,500	0.6	2,100
			84,700 cu. in. or 48.7 cu. ft.

TABLE 2.4.5-2. EARTH VIEWING SURFACE AREA

Sensor	Area (square feet)		FOV Angle
3 RBV's		240	16.7 degree cone
MSS		750	12 degree x 9 inch pyramid
	25% Contingency	990	
	Subtotal	1239	
DCS Antenna		110	120 degree cone
WB Antenna		50	160 degree cone
USB Antenna		50	120 degree cone
Attitude Sensor		50	135 degree cone
	Total	1498 = 10.4 ft^2	

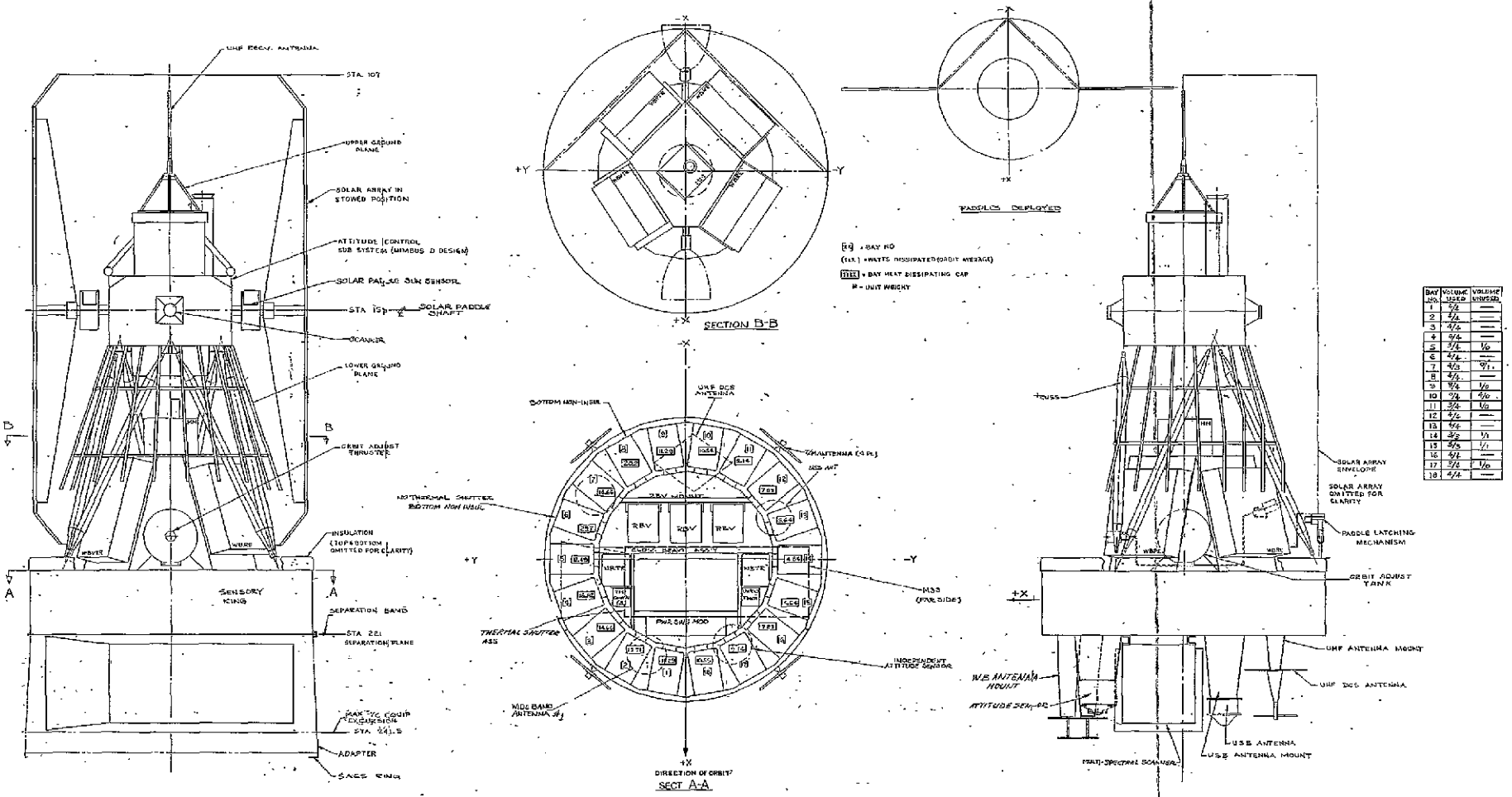

BAY NO.	VOLUME USED	VOLUME UNUSED
1	4/4	—
2	4/4	—
3	4/4	—
4	3/4	—
5	3/4	1/4
6	4/4	—
7	4/3	0/1
8	4/4	—
9	3/4	1/4
10	3/4	4/4
11	3/4	1/4
12	4/4	—
13	4/4	—
14	3/8	1/3
15	4/8	1/1
16	4/4	—
17	3/4	1/4
18	4/4	—

Figure 2.4.5-2. ERTS Configuration, Alternate

FOLDOUT FRAME 1

FOLDOUT FRAME 2

2.4.5.2 RBV Common Plate Study

2.4.5.2.1 General

Determination of the most appropriate method for mounting the RBV cameras to the ERTS spacecraft involved a tradeoff evaluation of how well the four major capabilities are carried out. These capabilities are:

1. Spacecraft interfacing
2. Structural isolation
3. Optical alignment
4. Thermal dissipation

The study was concentrated on two basic concepts: (1) individual RBV mounting configuration, and (2) common plate mounting of the RBV cameras (See Table 2.4.5-3)

2.4.5.2.2 Design Considerations

The RBV camera uses a foot mount configuration which provides a mounting plane parallel to the optical axis of the sensor. The mounting feet are separate from the camera housing, in that beveled brackets are used to mate with beveled machined surfaces on the camera housing as shown in Figure 2.4.5-3.

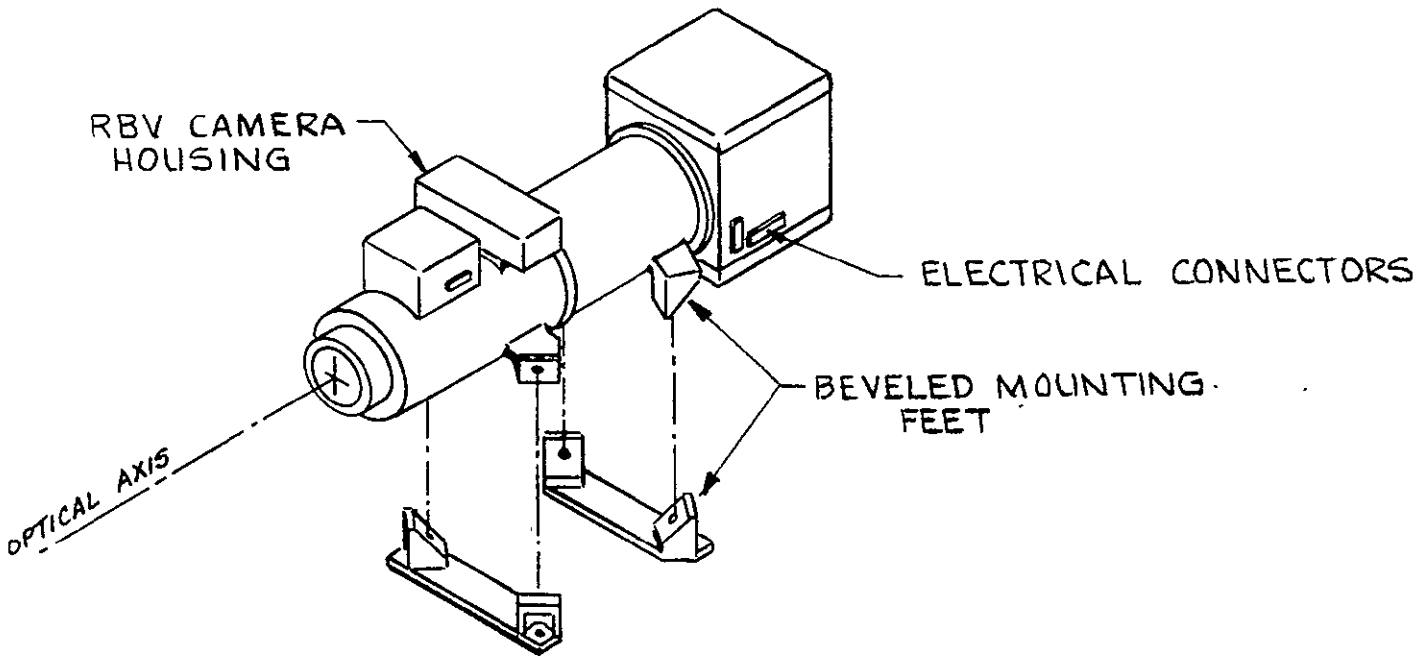

Figure 2.4.5-3. Return Beam Vidicon (RBV) Camera Mounting

TABLE 2.4.5-3. SUMMARY OF ADVANTAGES OF INDIVIDUAL VERSUS COMMON PLATE MOUNTING OF RBV's TO THE SPACECRAFT STRUCTURE

Design Considerations and Capabilities		Individual Mounting	Common Plate Mounting
1	Spacecraft Interfacing		
	a Ease of interfacing RBV's to spacecraft structure		X
	b Mounting flexibility	X	
	c. Least weight	X	
	d RBV orientation		X
	e Accessibility	X	X
2	Structural Isolation		
	a From vibration		X
	b From launch loads		X
	c From thermal distortions		X
3	Thermal Dissipation	X	X
4	Optical Alignment Capability		
	a Maintaining camera to camera alignment		X
	b Ease of camera adjustment		X
	c Replaceability of one camera		X

This allows the interface between the mounting feet and the camera housing to be in partial shear for any axis. It thus lends itself to dynafocal vibration isolation by simply placing damping pads between the feet and housing.

A moving slit focal plane shutter located in the RBV camera dictates it to be oriented in only one direction. Thus, in order to maintain one RBV configuration, all three cameras must be oriented the same way.

2.4.5.2.3 Common Plate RBV Mounting

The common mounting plate concept for supporting the three Return Beam Vidicon Cameras offers many design features. The RBV's can be assembled as a complete subassembly separate from the spacecraft (See Figures 2.4.5-4, 2.4.5-5 and 2.4.5-6). Bench alignments can be performed prior to spacecraft installation. Since alignment measurements between RBV's are quite critical, 30 arc seconds alignment checks can be easily performed in an environmentally controlled calibration laboratory prior to assembly into the spacecraft. The foot mounts provided on the RBV's are not easily accessible once they are mounted in the spacecraft. Thus, by mounting the cameras on a common plate, easily accessible attachment points can be provided.

This accessible attachment point can also be designed to provide alignment adjustment between the integrated RBV's and the spacecraft reference. The common platform will be a ribbed aluminum casting or machined plate. The ribs transmit loads from the RBV mounting points to the platform to sensory ring support points. The ribs also add to the overall stiffness of the common plate by unitizing the RBV cameras.

2.4.5.2.4 Individual RBV Mounting

Individual RBV mounting offers several distinct advantages:

1. Provides spacecraft arrangement flexibility
2. Efficient packaging
3. No intermediate interfacing plate, reducing weight
4. Spacing flexibility between RBV's
5. Leaves center section open for the MSS scanner.

Since each RBV is over 22 inches in length, weighs over 30 pounds and must look earthward, the logical location for it is in the central section of the sensory ring. With the MSS scanner occupying the center section, the staggered and closed-in-line arrangements for the RBV's are possible see Figures 2.4.5-7 and 2.4.5-8. The individual placement of RBV's inside the sensory ring, however, has a few drawbacks:

1. Difficult RBV insertion and withdrawal
2. Critical RBV alignment measurements required on the assembled spacecraft.
3. Mounting interface is open to thermal and structural distortions.
4. Due to RBV sensitivity, assembly and alignment must be performed late in the program.

2.4.5.2.5 Discussion and Recommendations

The type of alignment (5 to 30 arc seconds) measurements, necessitates controlled laboratory conditions. These alignment checks are necessary only between RBV's where the spacecraft

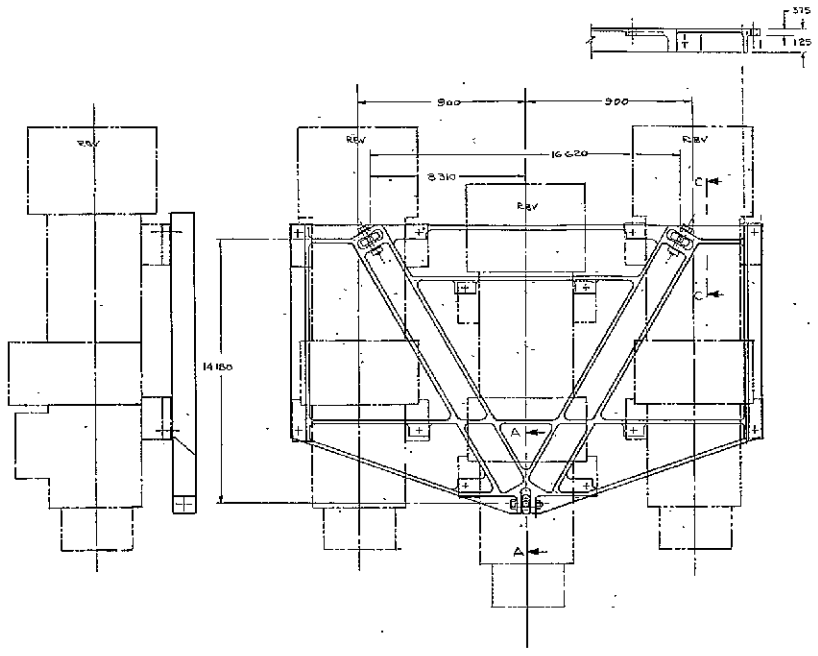

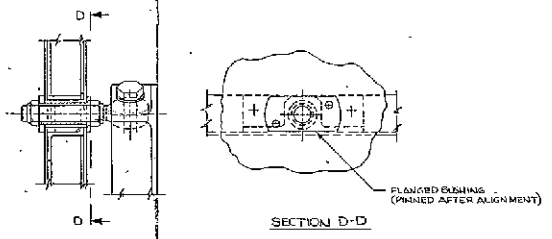

SECTION C-C
SCALE 1/1

SECTION D-D

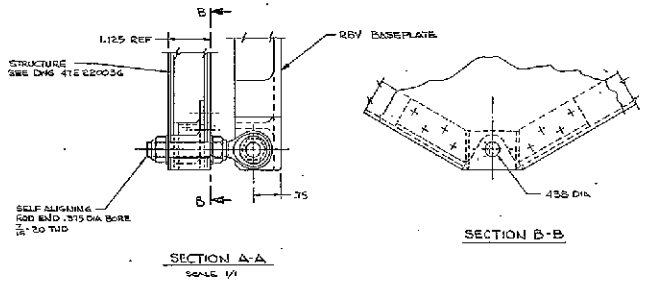

SECTION A-A
SCALE 1/1

SECTION B-B

Figure 2.4.5-4. Baseplate (Concept No. 1) RBV Cameras

FOLDOUT FRAME 1

FOLDOUT FRAME

FOLDOUT FRAME 2

2-81/2-82

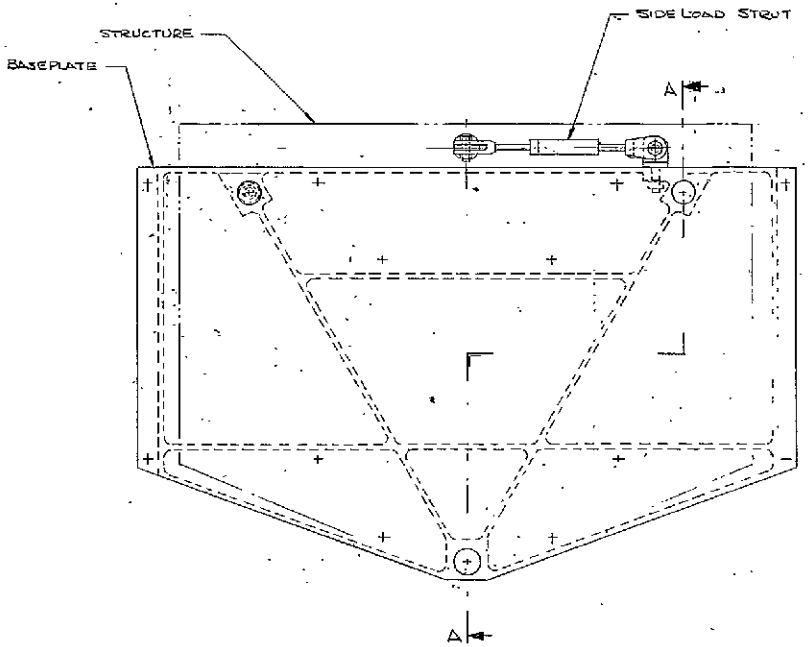

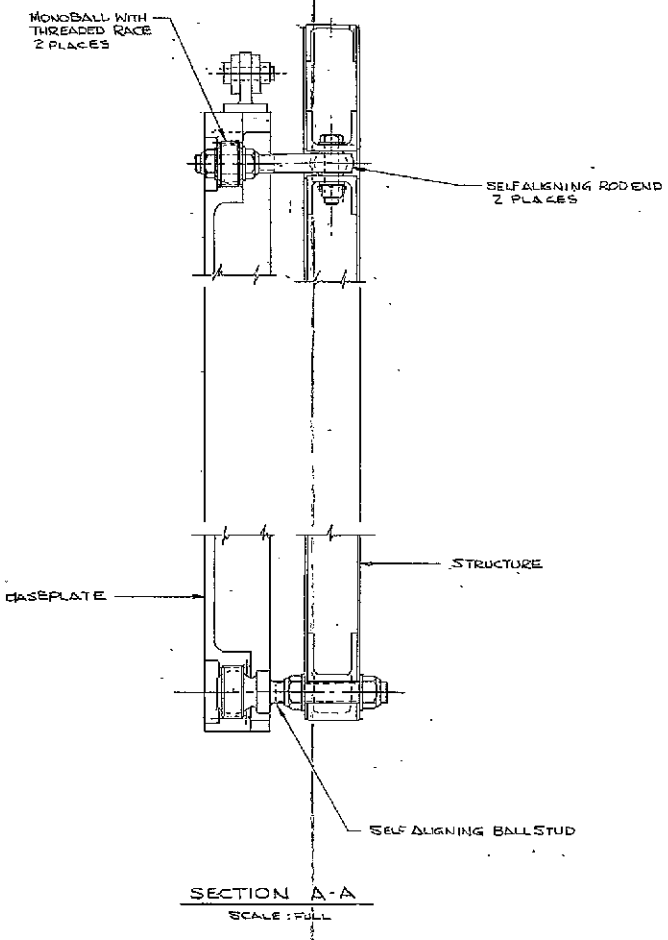

Figure 2.4.5-5. Baseplate (Concept No. 2) RBV Cameras

FOLDOUT FRAME 1

FOLDOUT FRAME 2

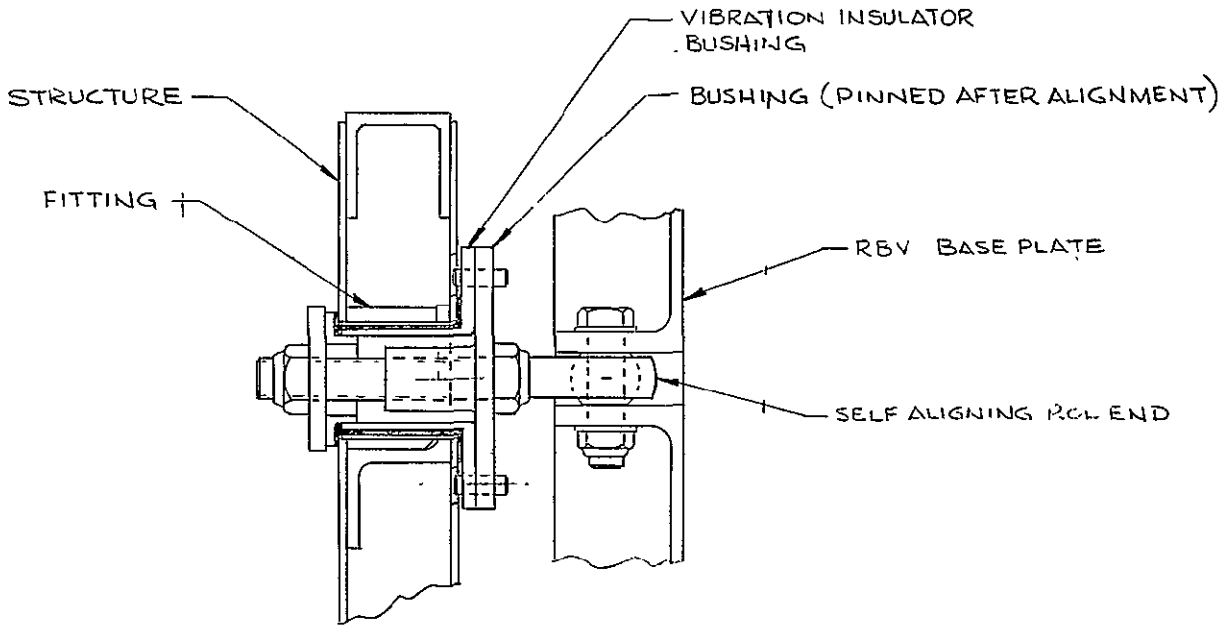

Figure 2.4.5-6. Method of Vibration Isolation of Baseplate from Spacecraft Structure

structure is not required. This lends itself to the common plate concept for mounting the RBV's. This method will also enhance early program subassembly alignment.

The common plate can be designed with the necessary stiffness to provide a stable non-influenced platform. This platform can be supported by three mono-balls with the base end attached to the common plate and the stud end to the box-beam/torus structure. Adjusting nuts on the stud on each side of the box beam can be used to raise and lower the platform to align the RBV system to the spacecraft reference.

The monoball support system is a proven concept used in all previous Nimbus flights to support the Attitude Control System (ACS). Table 2.4.5-4 shows a 3-axis post vibration (acceptance level) alignment shift on Nimbus "A" components. It shows that the 250 pound ACS package only shifted by 34 inch, 1 foot 44 inches and 49 inches (arc minutes and seconds) about the pitch, roll and yaw axes, respectively.

The AVCS system flown in the Nimbus A spacecraft was also a three TV camera mounted on a common plate system. Post three-axis vibration test has shown that the AVCS system shifted by 48 inch, 1 foot 59 inches and 55 inches (arc minutes and seconds) about the pitch, roll and yaw axes, respectively.

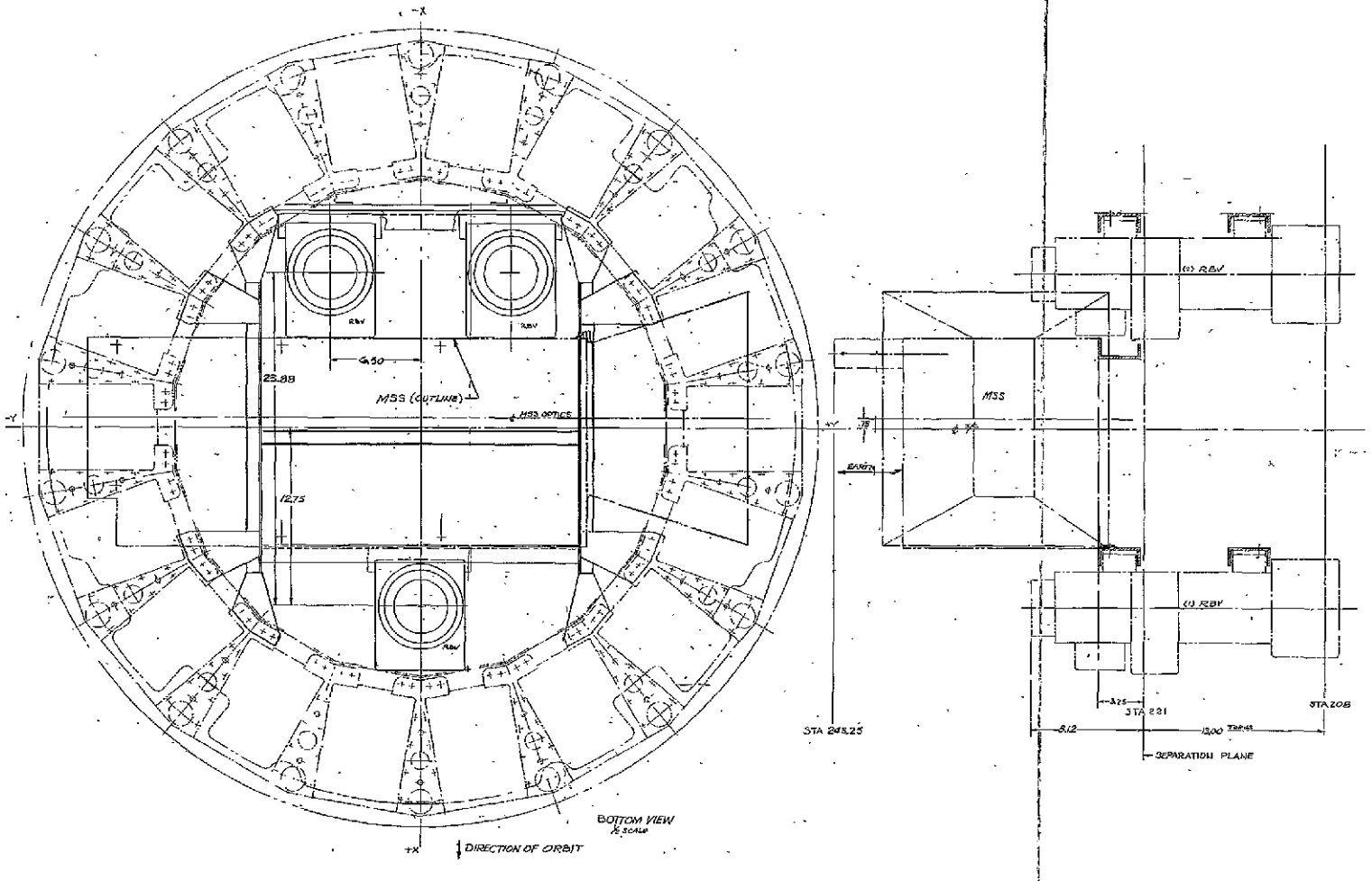

Figure 2.4.5-7. ERTS Sensory Ring, RBV Alternate Arrangement

FOLDOUT FRAME 1

FOLDOUT FRAME 2

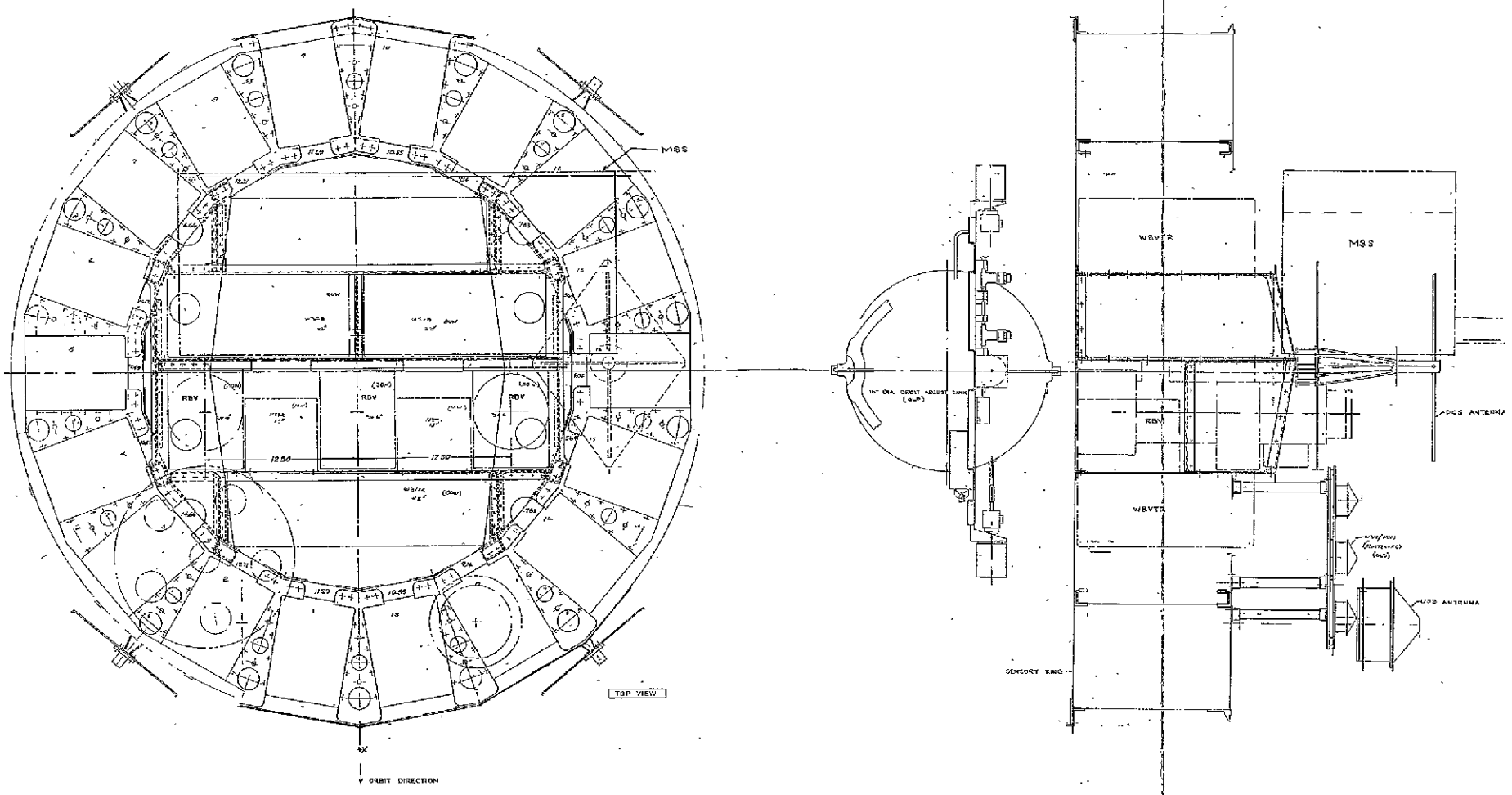

Figure 2.4.5-8. Individually Mounted In Line RBV's

FOLDOUT FRAME 1

FOLDOUT FRAME 2

TABLE 2.4.5-4. ALIGNMENT SHIFTS - NIMBUS COMPONENTS - AFTER 3-AXIS VIBRATION TESTS (ACCEPTANCE LEVELS)

Nimbus "A" Components	Alignment Change		
	Pitch Axis	Roll Axis	Yaw Axis
HRIR	-0' 18"	+0' 5"	-0' 40"
APTS	1' 25"	-1' 7"	0' 58"
AVCS	0 48'	-1' 59"	-0' 55"
ACS	0 34"	1' 34"	0' 49"

Data from GE Report 64SD4313, 1 August 1964, Changes were for before and after vibration tests during April 1964 and May 1964, respectively.

The above data and design features reveal that the common plate three monoball suspension system can satisfy the RBV mission requirements, and is therefore designed into the ERTS spacecraft.

2.4.5.3 RBV and MSS Stimulator Accommodation In Adapter

During pre launch checkout of the spacecraft, it is necessary to perform an end-to-end operational check of the MSS and RBV camera subsystem.

The verification can be satisfied by providing a signal stimulus into the sensors and producing a visible image on the hard copy from the sensor checkout console.

The only possible location for the checkout signal stimuli sources is in the flight adapter. In previous spacecraft such devices have been called the GO/NO-GO targets.

The problem in implementation of such test targets is the distance at which targets can be in a reasonable focus. The long focal lengths of optics, 126 mm for RBV Camera and 770 mm for the MSS scanner, will not keep these targets in focus, but will image them as a blur. If the target is sufficiently large in size, a recognizable image will be formed, although its definition is very poor. It is estimated that a square luminous panel subtending a cone of view of about 0.5 degree and having a radiant intensity of 4 $W\text{-}m^{-2} - \mu m^{-1}\text{-}sR^{-1}$ will be sufficient to be recognized adequately against the darkness of the flight adapter interior, provided the radiant intensity is sufficiently constant over the sensed band, from 0.5 to 1.1 μm.

The physical location of the targets as shown in Figure 2.4.5-9 will insure that they fall within the field of view of each of the sensors.

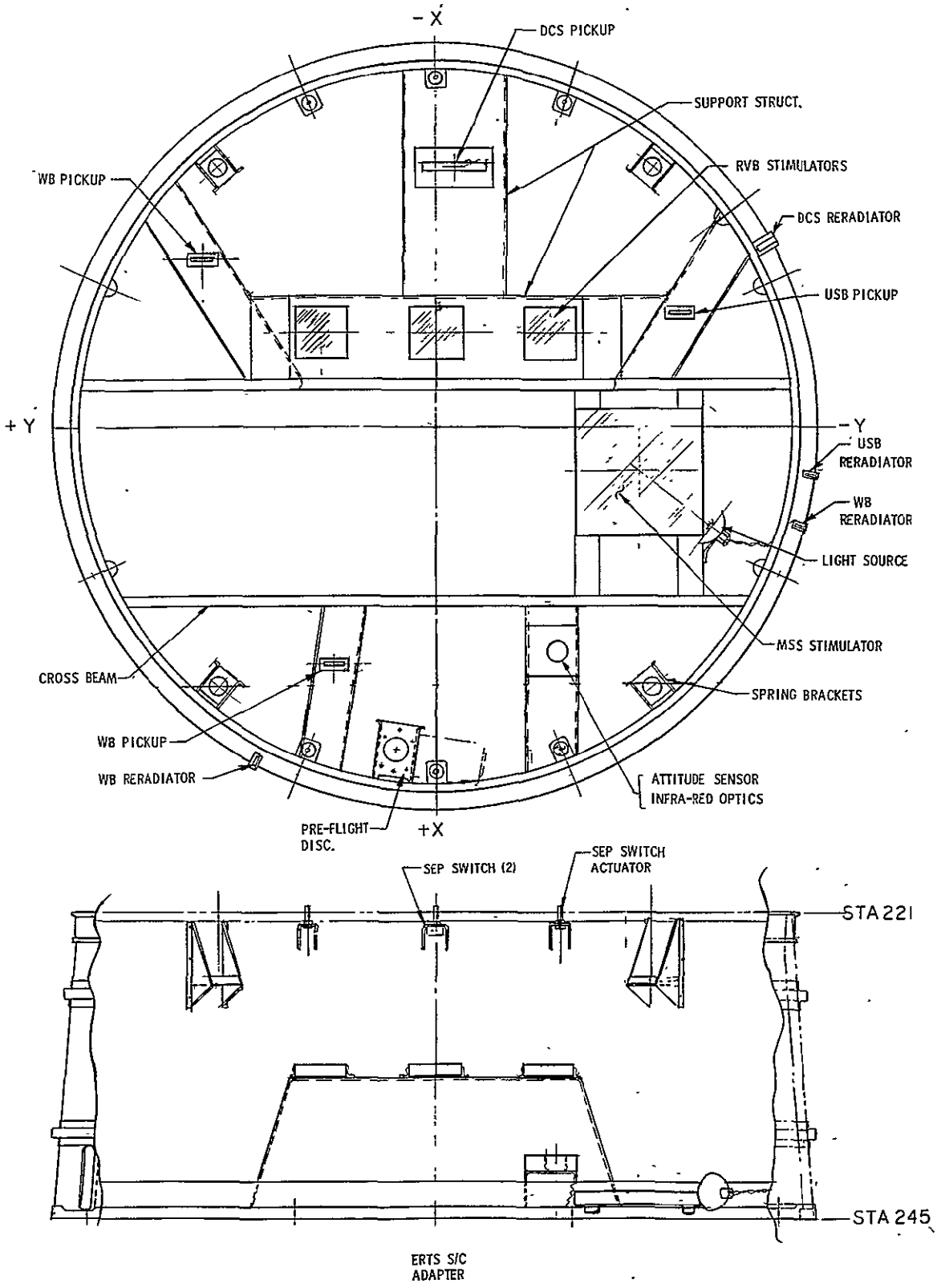

Figure 2.4.5-9. ERTS Adapter with Stimulators and Antenna Pickups

2.4.5.4 Orbit Adjust Subsystem Accommodation

2.4.5.4.1 General

The Orbit Adjust System is located above and centered over the sensory ring. It interfaces with the primary torus structure at three points. That is, the three orbit adjust support pads tie into the inner side of the torus castings on both sides of bays 6 and 13 and the casting between bays 1 and 18 (See Figure 2.4.5-10).

An estimate of the alignment requirements and methods of obtaining the alignment for the Orbit Adjust System was performed. Table 2.4.5-5 lists component misalignments possible. For a one pound thruster, the resulting disturbance torque of (1 lb. x 0.098 in. = .098 in.-lb) will cause gating of the ACS pneumatics. Approximately one pound of gas will be used. This appears to be acceptable per subsequent analysis.

2.4.5.4.2 Mounting Adjustment

For the previous Nimbus programs, the spacecraft center of gravity CG wandered as the design progressed. Past history has shown that X and Y center of gravity can be estimated to be within 0.5 inch of the geometric yaw axis and that the Z center of gravity will be within 1.0 inch of station 200.0 (separation plane is Station 221.0). Consequently, the orbit adjust system mounting plate should be capable of locating the system within a range of ±0.5 inch laterally and ±1.0 inch vertically. Furthermore, a fine adjustment capability of the thrusters, in .005 inch increments (the tolerance) over a range of .040 inch (approximately half of the total misalignment) would be desirable. In addition, the center of gravity of the full tank propellant should be 0.5 inch below the spacecraft center of gravity i.e., the spacecraft center of gravity should be 3.5 inches below the orbit adjust tank center.

Schematically shown in Figure 2.4.5-11 is the relative position of the Orbit Adjust system. Vertical adjust is achieved by shimming and lateral adjustment through the use of oversized mounting holes.

2.4.5.4.3 Thermal

The Orbit Adjust mounting pads are separated from the torus castings by the above alignment spacers. This imposes a heat resistance path between the isothermal torus ring and the Orbit Adjust thruster valves which must be maintained above 40°F. The tops of the castings and the surfaces of the spacers and orbit adjust mounting pads will be machined flat to provide good conductive contact. Silvered thermal grease will be used at each of the interfaces.

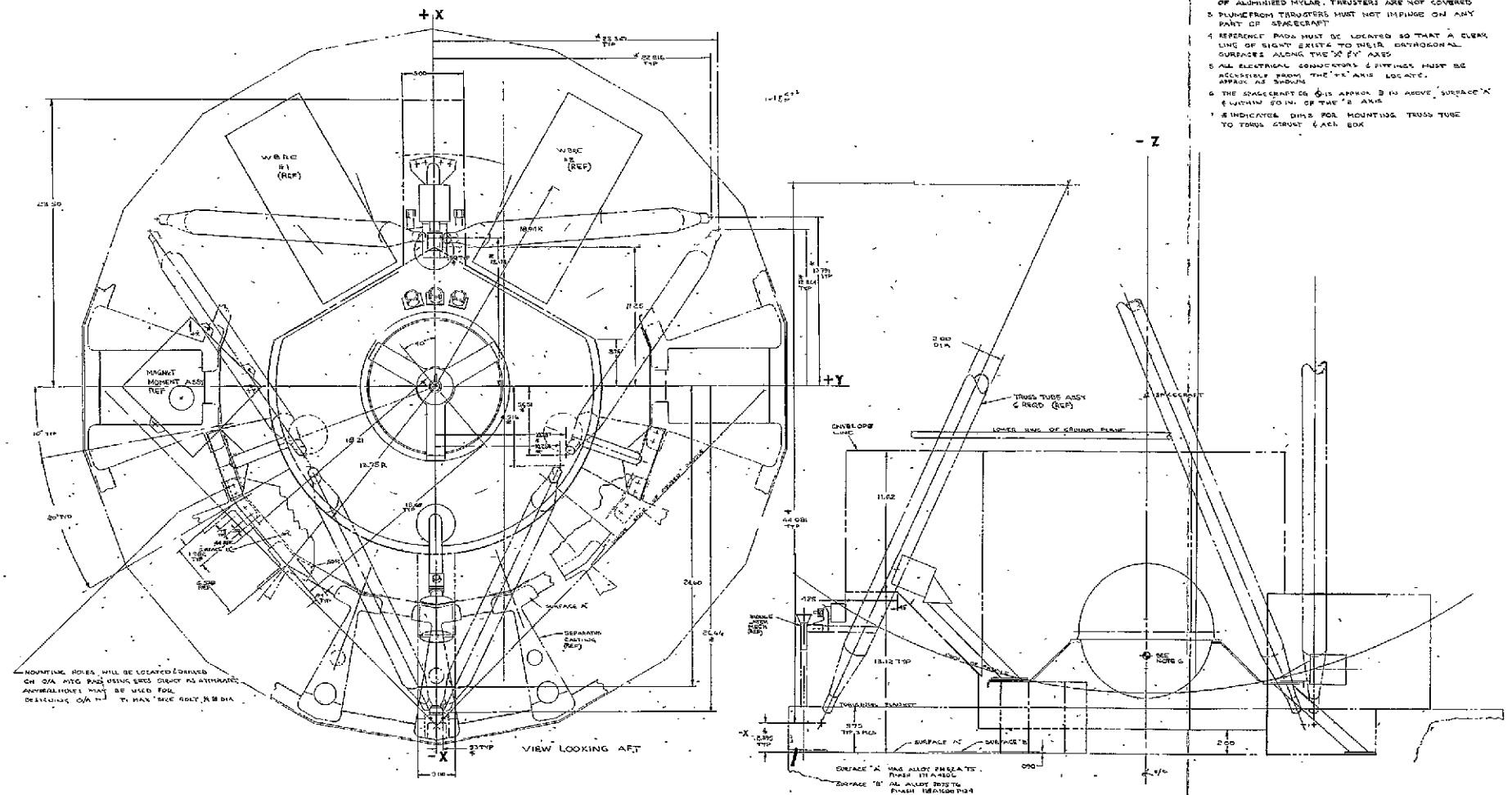

NOTES

1. ALL PHYSICAL COMPONENTS OF THE O/A INCLUDING INSULATION MUST FALL WITHIN DARK ENVELOPE LINES.
2. INSULATION WILL BE PROVIDED BY G.E. NOMINAL THICKNESS IS .150 IN. AND CONSISTS OF MULTI LAYERS OF ALUMIZED MYLAR. THRUSTERS ARE NOT COVERED
3. PLUME FROM THRUSTERS MUST NOT IMPINGE ON ANY PART OF SPACECRAFT
4. REFERENCE PADS MUST BE LOCATED SO THAT A CLEAR LINE OF SIGHT EXISTS TO NEAR ORTHOGONAL SURFACES ALONG THE "X" & "Y" AXES
5. ALL ELECTRICAL CONNECTORS & FITTINGS MUST BE ACCESSIBLE FROM THE "+X" AXIS LOCATE APPROX AS SHOWN
6. THE SPACECRAFT CG IS APPROX 3 IN ABOVE SURFACE "A" & WITHIN 50 IN. OF THE "Z" AXIS
7. ℄ INDICATES DIMS FOR MOUNTING TRUSS TUBE TO TORUS STRUT ℄ ASSY

Figure 2.4.5-10. Orbit Adjust Available Envelope

FOLDOUT FRAME 1

FOLDOUT FRAME 2

TABLE 2.4.5-5. COMPONENT MISALIGNMENTS POSSIBLE

1.	Thrust vector to nozzle centerline 1/4 degree at 10" (estimated by propulsion suppliers)	=	0.044"
2.	Accuracy of measuring center of gravity location (based on experience and analyses of equipment)	=	0.030"
3.	Accuracy of measuring nozzle location (based on experience)	=	0.004"
4.	Center of gravity motion due to propellant usage	=	0.010"
5.	Minimum practical nozzle alignment tolerance (based on experience)	=	0.005"
6.	Minimum practical tank center of gravity location tolerance (based on experience)	=	0.005"
	Total		0.098"

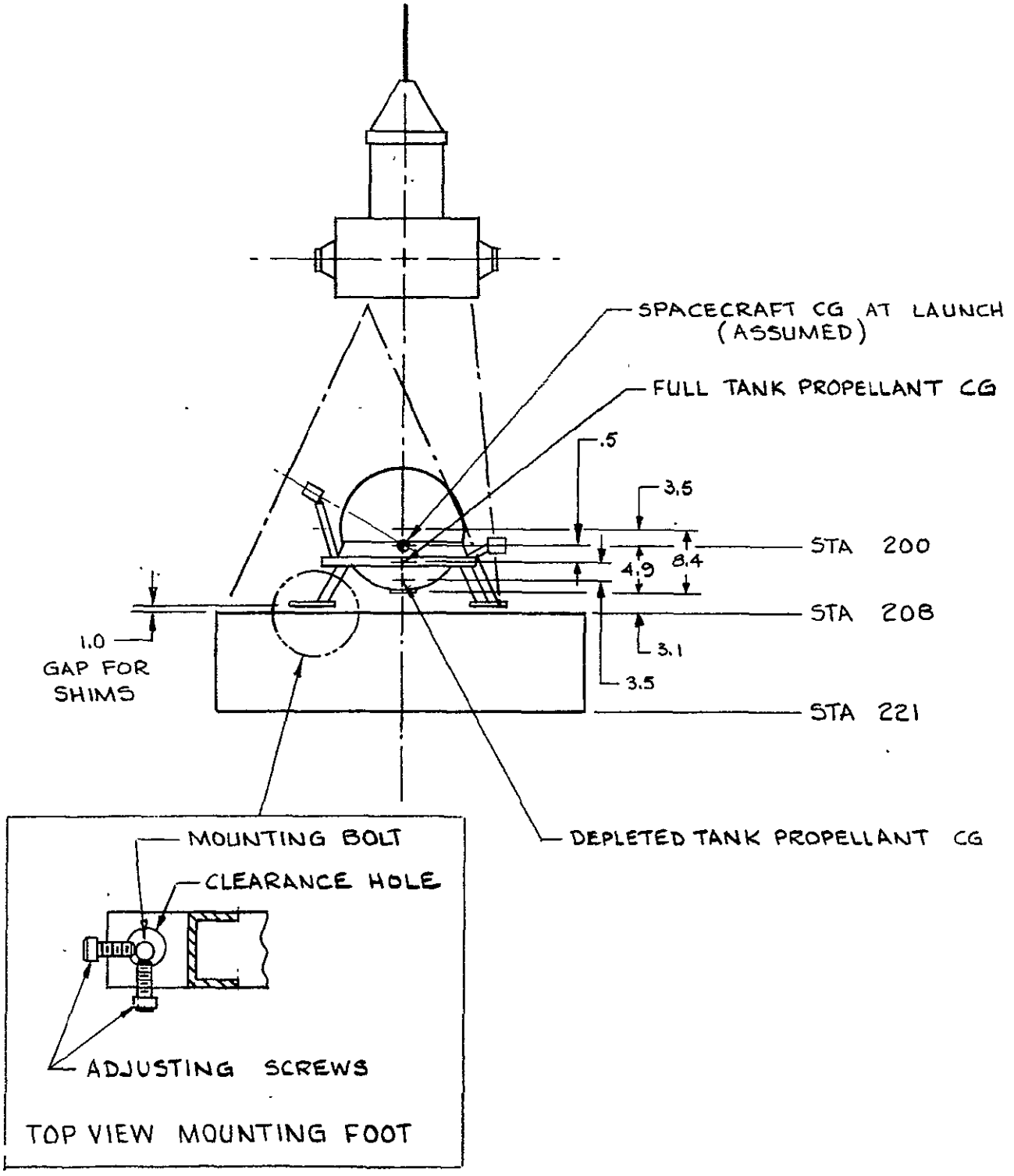

Figure 2.4.5-11. Relative Position of Orbit Adjust Subsystem

2.4.6 LOADS ANALYSES

2.4.6.1 Introduction and Summary

Loads analyses have been performed for ERTS spacecraft configurations having gross weights of 1621, 1675, 1800 and 1900 pounds. Coupled analyses were performed for the Delta/ERTS configuration for critical flight conditions. In addition, loads resulting from the spacecraft vibration test conditions have been determined. The ERTS spacecraft and launch vehicle configurations are very similar to those proposed for Nimbus E and, as a result, much of the recently conducted flight loads analysis activity is directly applicable. In this report, only launch and test structural loads are discussed because in-orbit loads are small due to the very low orbital force fields.

Detailed substantiation analyses are presented in appendices and the major study results and conclusions are presented herein. The three dynamic analysis appendices are:

2.A Launch Vehicle - Spacecraft Dynamic Analysis

2.B Dynamic Analysis - Vibration Test Loads

2.C Dynamic Analysis Model

The ERTS analyses utilized many parallel Nimbus studies to assess critical loading conditions and the adequacy of the structure for the ERTS mission. Of particular importance are the analyses of the Delta launch vehicle flight loads.

The following discussion shows that the primary structural design has been proof tested to structural load levels sufficiently great to assure successful mission performance. Furthermore, evincive data is presented which modifies preliminary design and vibratory test criteria so that the spacecraft structure can be designed for flight level load predictions.

2.4.6.2 Flight Loads

The flow plan for substantiation of the structural design is depicted in Figure 2.4.6-1. Attention must be focused on critical spacecraft interface loads in terms of forces and moments as shown in Table 2.4.6-1, which converts the quasi-steady load factors into interface loadings.

Flight load studies have been performed for the ERTS spacecraft configuration on the Delta launch vehicle, and these results have been included in Appendix 2.A. Table 2.4.6-2 presents a comparison of maximum interface loads resulting from the use of quasi-steady load factors and coupled L/V - S/C dynamic analysis. An 1800-pound spacecraft configuration is utilized in the comparison.

The quasi-steady factors and coupled L/V - S/C dynamic analysis interface loads agreed in the major mass sensory region and interface adapter. However, the forces and moments for the control system and paddle regions show significant discrepancies. The explanation is quite simple: the quasi-steady load factors are representative of single mass and spring gross

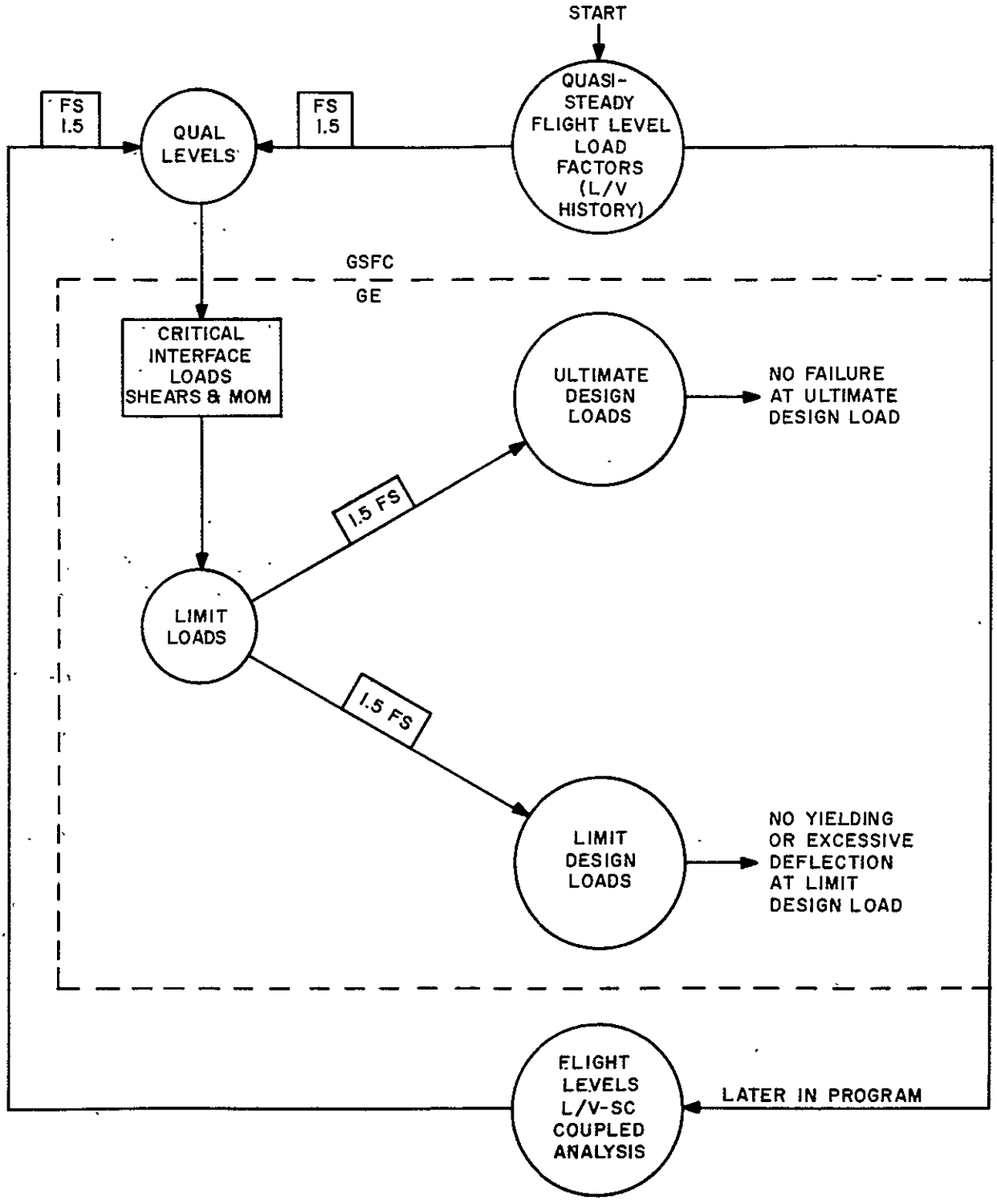

Figure 2.4.6-1. Structural Design Loads Philosophy

TABLE 2.4.6-1. INTERFACE LOADS FOR QUASI-STEADY LOAD FACTORS

Load Component		9.2 g Thrust	2 g Lat X	Combined 9.2 g Aft 2.0 g Lat X	3 g Thrust Forward	Combined 3.0 g Fwd 2.0 g Lat X
L/H Paddle	Fx	0	75	75	0	75
	Fy	0	35	35	0	35
Shaft	Fz	190	3	193	62	65
R/H Paddle	Fx	0	75	75	0	75
	Fy	0	35	35	0	35
Shaft	Fz	190	3	193	62	65
Paddle Tie Down	Fz	332	5	337	108	113
Control Box/ Truss Interface	Fx	0	629	629	0	629
	Fy	0	0	0	0	0
	Fz	2588	5	2593	844	849
	Mx	2342	0	2342	764	764
	My	2861	2582	5443	933	3515
	Mz	0	509	509	0	509
Truss/ Sensory System Interface	Fx	0	629	629	0	629
	Fy	0	0	0	0	0
	Fz	2920	0	2920	952	952
	Mx	2342	0	2342	764	764
	My	6602	32623	39225	2152	34775
	Mz	0	509	509	0	509
Sensory Ring/ Adapter Interface	Fx	0	3299	3299	0	3299
	Fy	0	0	0	0	0
	Fz	15207	0	15207	3995	3995
	Mx	1806	0	1806	474	474
	My	590	64303	64893	155	64458
	Mz	0	393	393	0	393
Adapter/ Delta Interface	Fx	0	3594	3594	0	3594
	Fy	0	0	0	0	0
	Fz	16560	0	16560	4351	4351
	Mx	5658	0	5658	1487	1487
	My	-1155	143483	144638	303	143786
	Mz	0	1228	1228	0	1228

Forces in pounds
Moments in inch pounds

TABLE 2.4.6-2. ERTS SPACECRAFT INTERFACE LOADS COMPARISON USING QUASI-STEADY LOAD FACTORS AND COUPLED LAUNCH VEHICLE/SPACECRAFT DYNAMICS

Load Component		Quasi-Steady Loads 9.2 g Long. (Fz) 2.0 g Lat (Fx)	Coupled L/V - S/C Loads
L/H Paddle	Fx	75	261
	Fy	35	168
Shaft	Fz	193	570
R/H Paddle	Fx	75	231
	Fy	35	92
Shaft	Fz	193	487
Paddle Tie Down	Fz	337	482
	Fx	629	1057
	Fy	0	201
Control Box/	Fz	2593	3432
Truss	Mx	2342	7297
Interface	My	5443	7213
	Mz	509	3389
	Fx	629	* 1057
Truss/	Fy	0	220
Sensory	Fz	2920	3462
System	Mx	2342	16715
Interface	My	64893	79051
	Mz	393	13928
	Fx	3299	* 3251
Sensory	Fy	0	455
Ring/	Fz	15207	13239
Adapter	Mx	1806	21560
Interface	My	64893	79051
	Mz	393	13928
	Fx	3594	* 3523
	Fy	0	442
Adapter/	Fz	16560	14384
Delta	Mx	5658	32478
Interface	My	144638	136993
	Mz	1228	13911

Notes:
1. Thrust Loads (Fz) are in a compressive sense.
2. *Asterisk denotes Max α Q condition generated load; all other loads generated by Meco-10 (POGO) condition.
3. All loads are flight levels.
4. Forces in pounds; Moments in inch-pounds.

simulations of spacecraft dynamics which is fine for preliminary design; the coupled L/V - S/C dynamic analysis is a much more detailed model and results in more realistic response predictions of spacecraft extremities. The higher response loads in the paddle and control regions not only occur in flight but also in test simulations. Care must be taken that these regions of the spacecraft are adequately exercised and yet not overtested because of shaker impedance mismatch and inability to simulate actual launch conditions. Section 2.4.8 presents a comparison of flight level load predictions and actual interface qualification test loads. As demonstrated by this table, it is virtually impossible to uniformly test the entire structure. However, the generally conservative vibration test loadings provide physical evidence of the structure's capability to withstand the predicted flight loads.

ERTS spacecraft vibratory environments are presented in Section 2.1.3. These data are extractions of several ERTS, Delta, and Nimbus documents and encompass structural design loads and flight-expected environmental estimates for vibro-acoustic field, pyrotechnic shock, and quasi-steady loads. Appendix 2.A compares quasi-steady and dynamic environments for the Agena and Delta launch vehicles.

The prime structure of the spacecraft is designed for analytically predicted flight loads. All environmental testing will be limited such that these loads are not exceeded. Unfortunately, test simulations of the flight environments with qualification level factors and inexact boundary conditions tend to result in over conservatism, even with input limiting and actually establish design loads in some areas of the structure. Analysis results are presented in the following section which predict the maximum test induced loads and environments for evaluation of the spacecraft structural adequacy.

2.4.6.3 Vibration Test Loads

Several payload configurations (1621, 1675, 1800 and 1900 pounds including adapter) have been investigated. Sections 2 and 3 of Appendix 2.B contain the complete modeling and response details for a 1621 pound configuration. Experience has shown that the major primary structural loads result from notched sinusoidal vibration testing, and these loadings determine the design of the structure.

Response loads analyses for the various payload configurations indicated a direct linear relationship with increasing weight and little change in response distributions for the major fundamental modes. In other words, changes in resonant frequencies and response mode shapes were within a few percent and the sensory ring interface load increases were directly proportional to the weight added in the sensory. Table 2.4.6-3 presents a summary of several key loadings which emphasize the trend. Section 2 of the Appendix 2.B contains a compilation of spacecraft interface loadings for the 19 fundamental resonances under roll-pitch-, and yaw-axis vibration testing for a 1621 pound spacecraft configuration.

A comparison of the unnotched loads in the appendix with the flight level load predictions of the previous section illustrates the unrealistically high loads resulting from an unnotched sinusoidal vibration test. Figures 2.4.6-2 and 2.4.6-3 present the results of notching the sinusoidal input to flight level load predictions.

TABLE 2.4.6-3. VIBRATION TEST INTERFACE LOADS COMPARISON

Loads	Input Axis	1621 pounds	1675 pounds	1800 pounds	1900 pounds
Paddle Tie Down					
F_z	X	1133	1173	1138	1139
Paddle Shaft Shear Force					
F_x	X	1984	2040	2113	2183
F_z	Z	1182	1172	1233	1260
Sensory Ring/ Adapter Interface Shear Force					
F_x	X	17931	19360	21797	24422
F_y	Y	10525	10965	11513	12034

The flight level loadings of the paddles and controls which dynamically are the most responsive usually control the basic notch levels. Of course, the basic objective of notching the vibration test inputs so that flight level load predictions are not exceeded, holds for the entire spacecraft. It is apparent from the discussion of quasi-steady load factors that the loadings on the spacecraft extremities will generally predominate.

The notches shown in the figures are for the Nimbus spacecraft and the referenced numbers and frequencies represent the key area dispositions at the major spacecraft resonances. The prefix F.L. denotes the input level for a response loading which equals the predicted flight level loading. As discussed earlier, the paddle shaft interface loadings are the limiting values for all notches.

The resulting ERTS flight level notch requirement predictions are very similar to those existing for Nimbus. This is an expected conclusion in view of the close similarities in launch vehicle performance and launch trajectory. Furthermore, sufficient confidence has been obtained with the prime spacecraft structure in test and through analysis to state its adequacy to withstand such a vibration test input spectrum. See Section 2.4.8.

2.4.6.4 Dynamic Analysis

The basic structural dynamic math model of the ERTS spacecraft consists of 19 resonant mode shapes and frequencies. A mass perturbation technique has been successfully used with this model for three spacecraft with significant weight and structural differences. The basic matrix equation for the math model can be stated as follows:

$$[K]\ \{X\} = [M]\ \{X\}\ \lambda$$

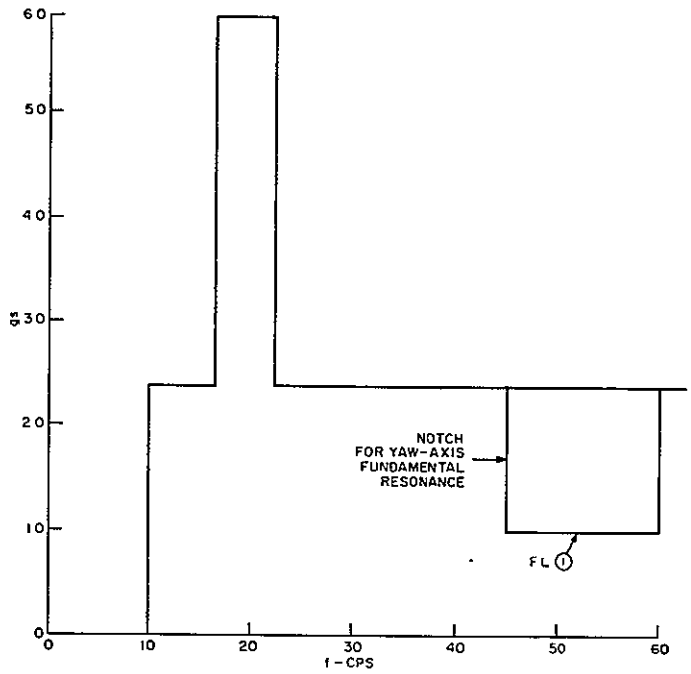

Figure 2.4.6-2. Yaw Axis Qualification Level Notching

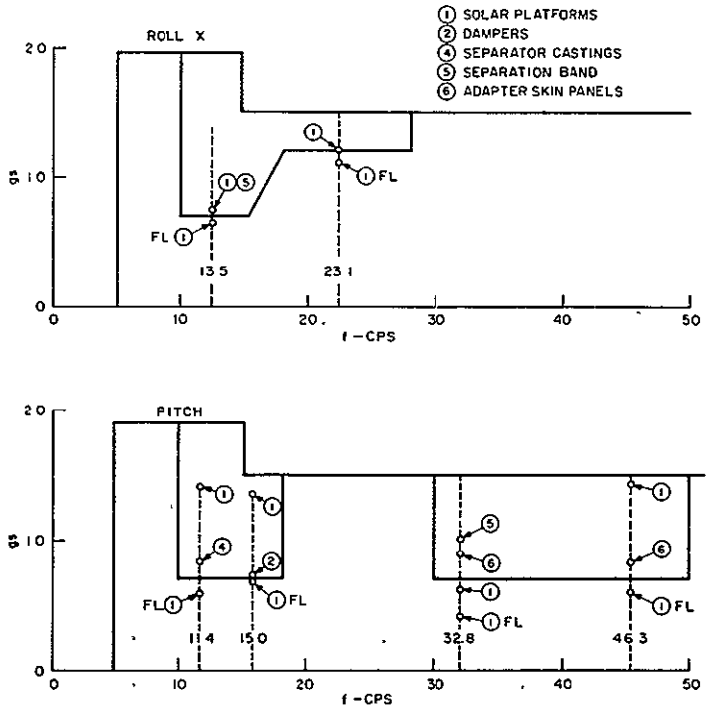

Figure 2.4.6-3. Lateral Axes Qualification Level Notching

Where

$[K]$ is a stiffness matrix

$\{X\}$ is a vector shape

$[M]$ is a mass matrix

λ is an eigenvalue (resonant frequency squared)

Sections 3 and 4 of the appendix present a detailed derivation and description of the modal math model which can be written in summary form as follows:

$$[K][\Phi] = [M][\Phi][\lambda]$$

where

$[\Phi]$ is a matrix of 19 mode shape vectors

$[\lambda]$ is a diagonal matrix of eigenvalues

The basic mode shapes consist of 51 three degree-of-freedom coordinates (X, Y, and Z) describing displacements through the spacecraft. By various manipulations and working in the generalized modal coordinate as discussed in the appendix, dynamic analyses extrapolations are readily obtainable. Figure 2.4.6-4 is a sample computer mode shape plot of the roll X axis fundamental mode.

An investigation was conducted for four payload weight configurations where the major changes consisted of sensory mass additions and redistributions. Table 2.4.6-4 presents the results of the computations for the spacecraft cantilevered vibration modes. Therein, only minor changes in dynamic characteristics of the ERTS spacecraft structure are indicated and a slight lowering of the spacecraft major resonant frequencies.

In conclusion, both the resonant frequencies and mode shapes evidenced insignificant changes on the order of 1 percent. It appears that additions to the sensory ring area have only a minor effect on the spacecraft dynamic characteristics.

Appendix 2.C contains the ERTS spacecraft math model used in these studies. This model can be utilized for further predictions of paddle-shroud clearances and spacecraft/launch vehicle coupled flight loads analyses similar to those presented in Appendix 2.A.

2.4.7 STRESS ANALYSIS

This section contains the significant results obtained from the structural analysis of the ERTS spacecraft during the study. In general, these consist of: 1. The development and assembly of a comprehensive structural computer model (SCM) 2. An analytical evaluation of the spacecraft primary structure to establish its integrity for ERTS structural load

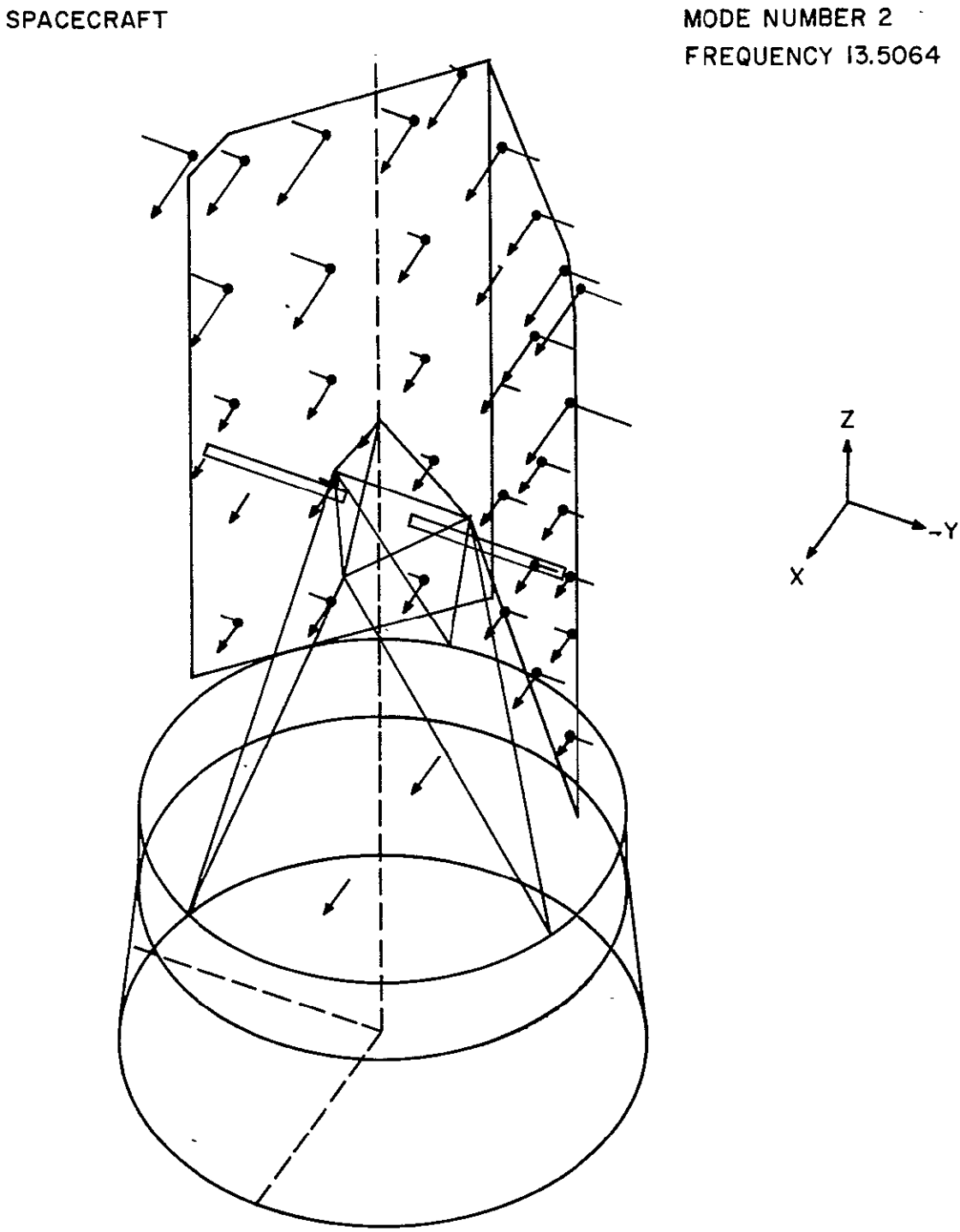

Figure 2.4.6-4. Plot of Roll X-Axis Fundamental Mode

TABLE 2.4.6-4. ERTS FREQUENCY COMPARISON TABLE

Mode Number	1621 pound S/C	1675 pound S/C	1800 pound S/C	1900 pound S/C
1	11.3	11.2	11.2	11.2
2	13.1	13.1	12.9	12.7
3	14.7	14.5	14.4	14.3
4	15.3	15.2	15.2	15.1
5	22.7	22.7	22.6	22.5
6	26.4	26.2	26.1	25.9
7	27.5	27.5	27.4	27.4
8	31.9	31.6	31.3	31.0
9	36.8	36.3	36.0	35.5
10	39.5	39.3	39.1	38.8
11	41.5	41.2	41.0	40.7
12	43.1	42.3	42.3	41.8
13	45.5	45.0	44.9	44.5
14	47.4	47.5	46.9	46.6
15	55.4	55.2	55.3	55.3
16	61.9	61.9	61.6	61.3
17	62.6	62.6	62.2	62.1
18	64.4	64.3	64.1	64.0
19	82.8	82.2	82.5	82.4

requirements 3. A structural analysis of the crossbeam design to determine its adequacy to meet loading and alignment requirements.

2.4.7.1 Structural Computer Model (SCM)

A comprehensive structural computer model (SCM) defining the primary structural elements of the ERTS spacecraft has been assembled during the Phase B/C study. The SCM is comprised of the following ERTS major substructures:

1. Attitude Control Subsystem (ACS)
2. Truss Assembly

3. Torus and Crossbeam Structures

4. Flight Adapter Structure

The component parts of these substructures are illustrated in Figures 2.4.7-1, 2.4.7-2, 2.4.7-3 and 2.4.7-4.

The SCM has been developed to simulate the structural complexities of the ERTS spacecraft in great detail and has been highly optimized to fully utilize the maximum capabilities of the GE 635 digital computer. The ERTS SCM has been developed from, and is equal in complexity to, the SCM utilized in the performance of the final structural analysis of the Nimbus D spacecraft and incorporates areas of structure unique to the ERTS spacecraft. The SCM, as presently configured, provides the capability for highly accurate determination of individual elemental internal loads, stresses, and deflections for the critical environmental design conditions of thermal, pressure, preload, or inertial loads, or any combination, thereof. In addition, the SCM provides the capability for generating detailed stiffness matrices for utilization in dynamic analyses to determine natural frequencies, mode shapes, and local amplifications of the ERTS spacecraft structure.

Briefly, the modeling of the individual substructures may be expressed in tabular form as follows:

Substructure	Number of Individual Elements		
	Joints	Beams	Plates
ACS	233	277	71
Truss	16	19	0
Torus/Crossbeam	185	248	58
Adapter	162	185	45
Total	596	729	174

The SCM described above provides the mathematical representation of the ERTS spacecraft structural elements for incorporation into the GE-developed structural analysis computer program "MASS" (Mechanical Analysis of Space Structures).

The MASS program is the most generally used computational tool at GE for analysis of stresses and deflections of complex structural systems. The program, because of its versatility, provides the capability of analyzing virtually any type of structural systems comprised of straight or curved beams, plates, and panels. This program has been used with success on a number of spacecraft programs (Nimbus, ATS F&G, MOL, GGTS, and various classified military programs) and has yielded good correlation with test data. ERTS structural analysis and results using the SDM is discussed in Section 2.4.7.4.

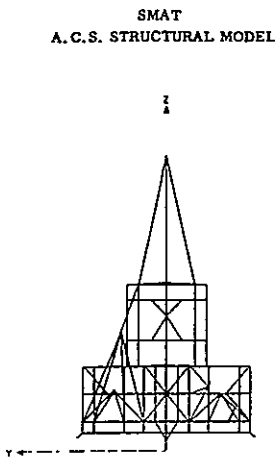

Figure 2.4.7-1(a). Substructural Model of ACS Subsystem

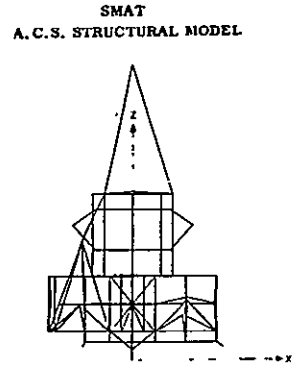

Figure 2.4.7-1(b). Substructural Model of ACS Subsystem

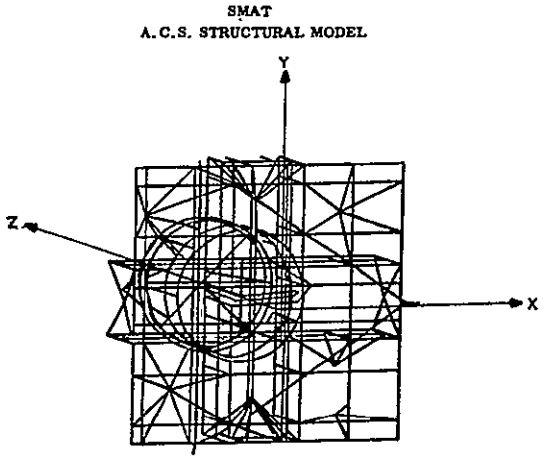

Figure 2.4.7-1(c). Substructural Model of ACS Subsystem

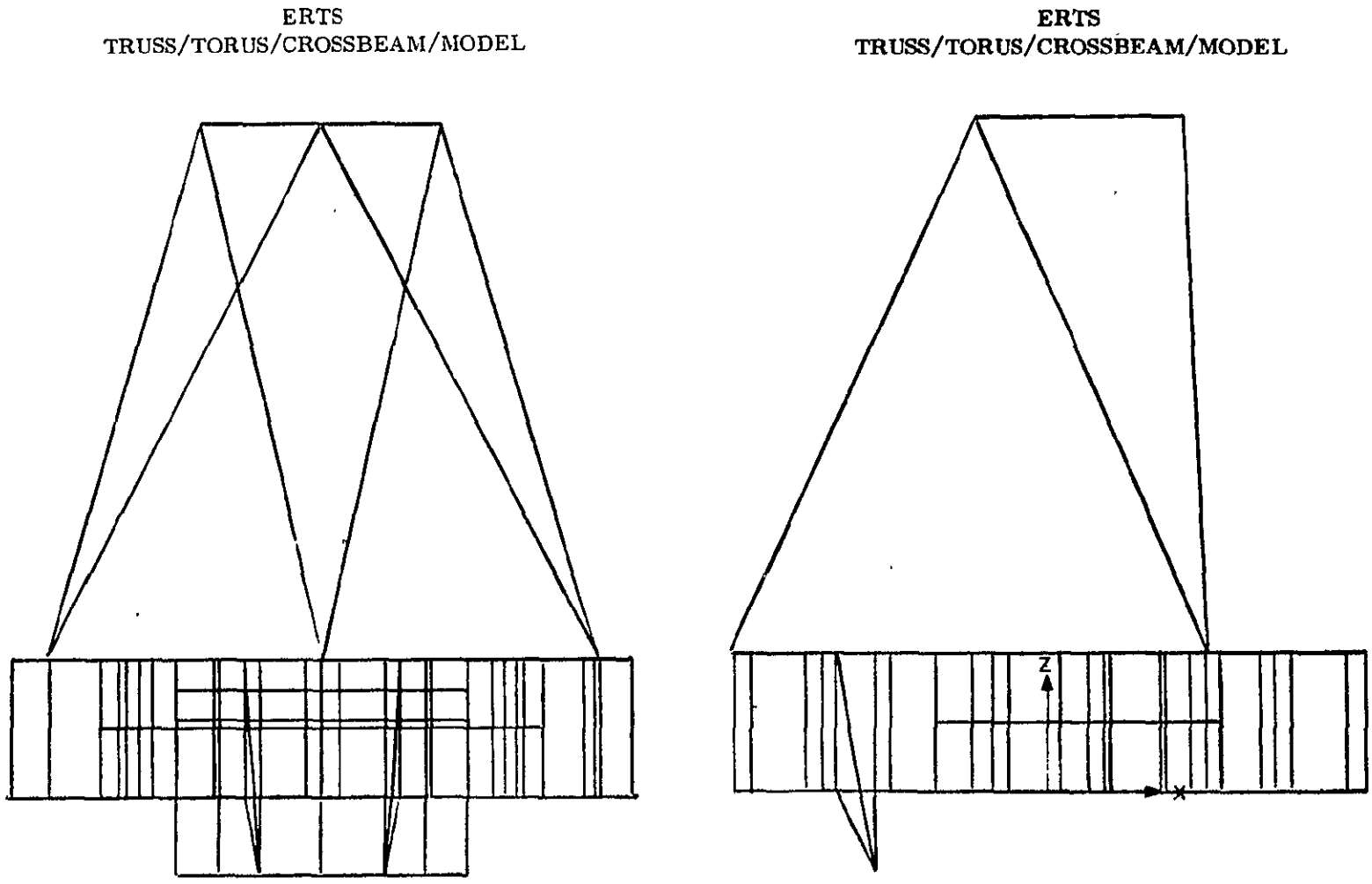

Figure 2.4.7-2. Model of Truss Assembly

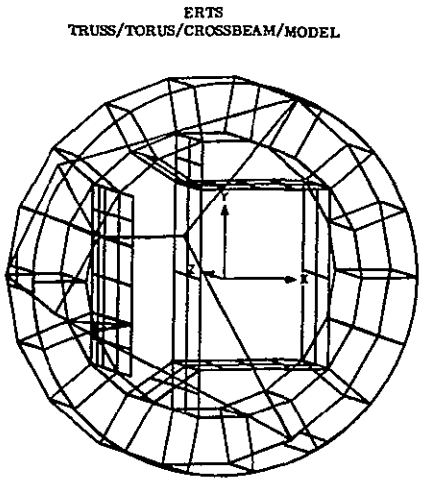

Figure 2.4.7-3. Model of Torus and Crossbeam Structure

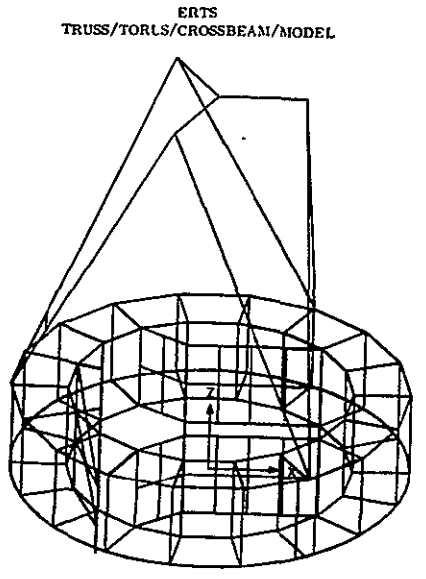

Figure 2.4.7-4. Model of Flight Adapter Structure

2.4.7.2 Evaluation of Primary Structure

Using the quasi-steady loads and the flight loads shown in table 2.4.7-1, the structural adequacy of the ERTS was determined. It was necessary that the structure withstand these loads and exhibit a positive margin of safety, based both on yield and ultimate stresses. Since much of the structure (paddle hinges, truss, ACS, torus ring, and adapter) remains essentially the same as the Nimbus structure, with only minor modifications, much of the Nimbus analytical data was applicable in evaluating the ERTS structure. Table 2.4.7-2 presents the design loads used to stress analyze the Nimbus D spacecraft structure, which is very similar to the ERTS structure. A comparison is made in Table 2.4.7-2 of ERTS flight loads and Nimbus vibration design loads at the critical strcutural interfaces. It can be seen, in this table, that the ERTS interface loads are lower than those used for Nimbus D thus ruling out any major structural modifications on the basis of strength limitations. The thrust load at the truss-to-sensory ring and sensory-ring-to-adapter interface for ERTS is higher than those evaluated for the Nimbus structure. However, it was found in previous structural analyses that the spacecraft structure is not critical for thrust loads since they do not induce significant stress levels. Critical loads are shear and bending.

Table 2.4.7-3 is a summary of minimum margins of safety of ERTS structural items which serves to substantiate the adequacy of the spacecraft structure. These margins were extrapolated from the Nimbus D structural analysis, using the loads in table 2.4.7-2 for ERTS and Nimbus. A further investigation of Table 2.4.7-1 shows the qualification vibration and acceleration test levels to which similar structures have been tested without failure. A comparison is made between the expected ERTS flight loads and the test loads in the table. This comparison is in the form of a ratio of the test load to the flight load. Since qualification loads are 1.5 times as high as flight loads, it is evident that in all cases where the ratio exceeds 1.5 (for that interface load) the ERTS structure exhibits the desired factor of safety. The ratio shows that in all cases (except thrust loading, which is not considered significant) the test loads are more than 1.5 times the design loads. Since the spacecraft is not critical for thrust loading and all test load conditions are higher than design, there is a high level of confidence in the ability of the spacecraft primary structure to survive the critical loading conditions.

2.4.7.3 Crossbeam Structural Analysis

Several crossbeam configurations were evaluated during the course of the study in an effort to find the structural arrangement which would provide the most optimum support for the RBV cameras. The resulting design is that which is presented in this report. Margins of safety in the crossbeam were computed and structural integrity verified for the critical loading conditions in Section 2.4.6. The minimum margin of safety was found to be +0.52 in the center beam flanges.

The vibration isolated RBV and mounting plate design concept was first analyzed and found to have a "rocking" mode frequency of approximately 28 cps. This mode occurs at a frequency near that of the primary longitudinal mode (17 to 23 cps) of the launch vehicle. The vibration isolators had been considered to limit the vibratory input to the mounting plate from the crossbeam structure in the sensory ring. The frequency of these isolators had been specified to

TABLE 2.4.7-1. COMPARISON OF CRITICAL STEADY STATE FLIGHT LOADS AND MAXIMUM QUALIFICATION VIBRATION AND ACCELERATION TEST LOADS

Spacecraft Structure Interface	Load Condition		Flight Loads	Quasi-Steady Loads	Qualification Vibration	Accelerating Tests	Max Test Load / Flight Load
L.H. Paddle at Hinge Line	Shear	Rx→ Rz	627	195	* 1520	346	2.42
	Axial	Ry	168	76	* 305	220	1.82
R.H. Paddle at Hinge Line	Shear	Rx→ Rz	539	182	* 1472	346	2.73
	Axial	Ry	92	74	* 403	220	4.38
Paddle Tie-Down	Axial	Rz	482	346	* 1823	390	3.78
ACS/Truss	Shear	Rx→ Ry	1076	618	* 2275	709	2.06
	Thrust	Rz	3432	3014	* 4418	2955	1.29
	Bending	Mx→ My	10224	7137	* 32900	5783	3.22
	Torsion	Mz	3389	-19	* 14058	2285	4.15
Truss/ Sensory Ring	Shear	Rx→ Ry	1080	716	* 2275	749	2.11
	Thrust	Rz	3462	3299	* 4418	3540	1.28
	Bending	Mx→ My	70771	52153	* 129500	50568	1.83
	Torsion	Mz	2818	174	* 14058	2285	4.99
Sensory Ring/ Adapter	Shear	Rx→ Ry	3283	3395	* 6520	3889	1.98
	Thrust	Rz	13239	15618	* 11307	* 19120	1.44
	Bending	Mx→ My	81938	84061	* 192500	86108	2.35
	Torsion	Mz	13928	2910	* 64105	2285	4.60
Adapter/ Delta	Shear	Rx→ Ry	3551	3600	* 6520	4129	1.84
	Thrust	Rz	14384	16560	* 11300	* 20342	1.41
	Bending	Mx→ My	140790	202503	* 315000	182388	2.24
	Torsion	Mz	13911	2910	* 2285	2285	4.60

*Maximum Test Value for Indicated Load

TABLE 2.4.7-2. INTERFACE DESIGN LOADS COMPARISON (ERTS - NIMBUS D)

Interface	ERTS Interface Load	Nimbus D Critical Cond. Interface Load			
		Cond 2X	Cond 4Z	Cond 8Y	Cond 14Z
Paddle Tie Down					
Fz	482	433	383	27	1936
Truss/Sensory Ring					
Fx + Fy	1076	2450	1690	2030	1100
Fz	3467	-216	448	-2	2429
Mx + My	70771	139000	75200	89350	59800
Mz	2818	899	-7367	-7077	985
Sensory Ring/ Adapter					
Fx + Fy	3883	5520	4190	4935	2380
Fz	13239	421	1236	331	10528
Mx + My	81938	207000	114200	146200	35100
Mz	13928	-21127	8433	-21145	23934

be in the 20-50 cps range. However, due to the overhang of the RBV from the centroid of the beam, a coupling will occur between the monting plate and the isolator thus, reducing the effectiveness of the isolation system. This coupling effect results in a frequency range between 12 and 15 cps, which is also near critical flight frequencies.

Subsequent analyses, for a design concept with the plate rigidly mounted to the crossbeam, resulted in a frequency of approximately 98 cps. The rigid mount concept for the RBV cameras is preferable and will result in acceptable RBV camera loading.

The most critical loading on the beams themselves is torsion. This occurs from excitation along the thrust axis and is due to the overhanging moment introduced by the positioning of the equipment on the structure. The most highly loaded beam is the one which supports the RBV cameras. Torsional stresses and distortions in this beam are minimized through the stiffness of the "box" type construction. The center beam, which must take some of the MSS weight, has a high bending load. This occurs about an axis normal to the beam about which the moment of inertia is the greatest, resulting in negligible stresses.

2.4.7.4 Thermal Distortion Analysis

A thermal distortion analysis of the ERTS structure has been completed, utilizing the MASS computer program, to determine the magnitude of any misalignments that might occur due

TABLE 2.4.7-3. SUMMARY OF MINIMUM MARGINS OF SAFETY.

Item	Drawing No.	Type of Stress	M.S.
Separator No. 10	242E501P4	Bending, Compression and Torsion	+ 0.01 (U)
Separator No. 4	242E501P4	Bending and Compression	+ 0.63 (Y)
Thermal Control Panel	47E213283G1	Shear	+ 3.48 (Y)
Side Plate (t = 0.040)	47C207625P1	Shear	+ 1.34 (Y)
Side Plate (t = 0.032)	108C7233P1	Shear	+ 1.77 (Y)
Ring-Top Outboard	242E502	Bending and Compression	+ 0.07 (U)
Ring-Top Inboard	237R450	Bending and Compression	+ 0.30 (U)
Ring-Lower Inboard	237R450	Bending and Compression	+ 0.02 (U)
Ring-Separation	242E507	Bending and Compression	+ 0.02 (U)
Web-Outboard	875D702G2	Shear	+ 0.66 (Y)
Web-Inboard	47E207680P5	Shear	+ 0.57 (X)
Fitting-Strut Support	884D315G2	Bending	+ 0.31 (Y)
Fitting-Support	875D708P1	Bending	+ 0.08 (Y)
Truss Tube Fitting	108C7201	Bending and Compression	+ 0.03 (Y)
Truss Tube Attachments	875D704	Bearing	+ 0.03 (U)
Truss Tube	875D704	Column Stability	+ 0.22 (U)
Tie-Down Strut	237R497	Column Stability	+ 1.41 (U)
Solar Platform Preload Adequacy	248E136	Preload Adequacy	+ 0.20 (Y)
Separation Band Preload Adequacy	1A01065	Preload Adequacy	+ 0.90 (Y)

Note: (U) Denotes M.S. based on ultimate design load criteria.
(Y) Denotes M.S. based on limit design load criteria (yield criteria).

to thermal distortion of the sensory/crossbeam structural subsystem. Primary area of interest was in the crossbeam supporting the RBV cameras. The thermal environment of concern was that of thermal gradients in the structure during orbit. Figure 2.4.7-5 shows the temperatures used in the structural computer model, described in Section 2.4.7.1, for the sensory ring. Figure 2.4.7-6 shows the temperatures on the crossbeam. It is noted that temperatures from the outside to inside of the sensory ring were assumed constant. In addition, the temperatures used were not necessarily absolute values but represented maximum ΔT thermal gradients expected in this area.

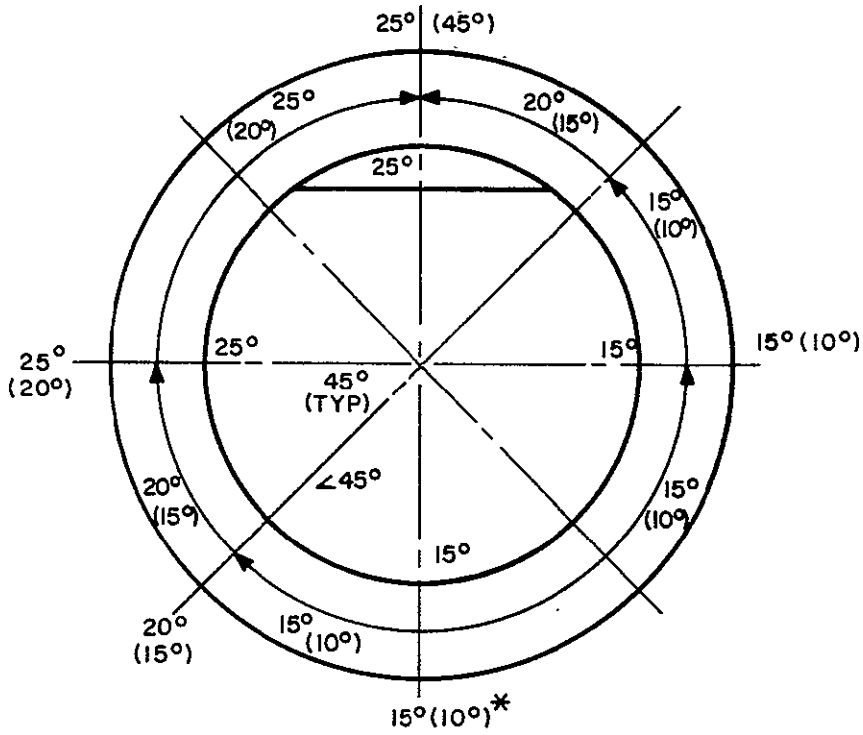

* TEMPERATURES IN PARENTHESES( ) OCCUR AT LOWER FACE OF SENSORY RING

Figure 2.4.7-5. Sensory Ring Temperature for SCM

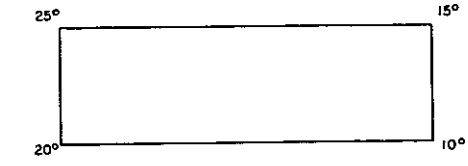

RBV MOUNTING BEAM

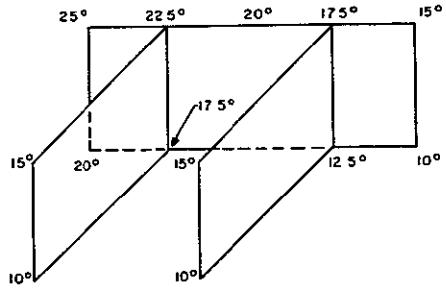

CENTER BEAM ASSY

Figure 2.4.7-6. Crossbeam Temperatures for SCM

Using the structural computer model developed during the study (described in Section 2.4.7.1, temperatures, and as shown in the aforementioned figures) were applied to the structure at the corresponding joints. The stresses and deflections at each joint were computed using the MASS structural computer program. Plate stress and deflections due to the temperatures were also calculated.

Of primary interest in the thermal distortion analysis were the deflections which occur on the crossbeam supporting the RBV cameras. These are reflected at joints 170 through 199 in Figure 2.4.7-7 with joints 184, 188 and 196 depicting the interfaces with the RBV mounting plate. The maximum deflection occurring at these three joints of 0.0243 inches (joint 184) and the maximum differential deflection between them is 0.010 inches.

Examination of the deflections for the other joints on this beam indicate that thermal distortion is negligible in the other directions of interest. Since this analysis represents a worst case thermal profile, it is not anticipated that thermal gradients will affect the alignment of the RBV cameras. Stresses incurred in these members are extremely low, with the maximum stress seen being 1610 psi at joint 182. Based on the allowables for this member, which is a 2024-T4 aluminum alloy extrusion, the margin of safety is greater than 10.

The remainder of the crossbeam, joints 200 through 260, indicate that deflections are much smaller than in the RBV support beam.

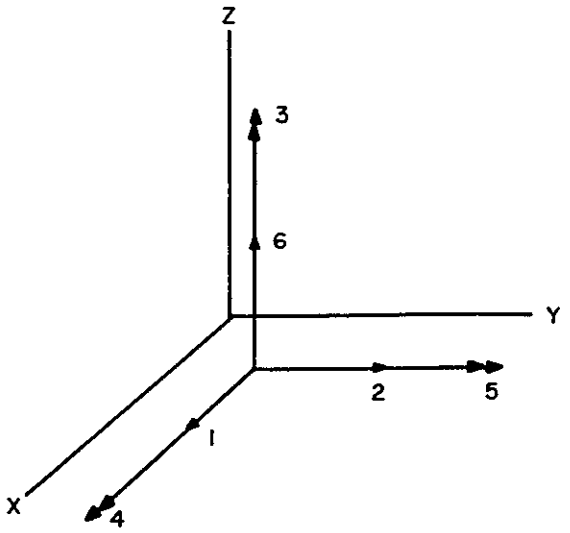

Figure 2.4.7-7. Deflection Direction, Coordinate Sign Convention

Table 2.4.7-4 presents the computer print-outs for the deflections at the joints of the sensory/crossbeam structure. Figure 2.4.7-7 presents the coordinate sign convention.

Alignment requirements for the RBV cameras specify that the cameras shall not be out of alignment with respect to each other by more than 30 arc-seconds. The mounting plate shall not be out of alignment with respect to the spacecraft coordinate axes by more than 6 minutes.

Evaluating the thermal distortion analysis results for the first requirement as stated above, it was determined that the maximum misalignment along the Y axis is 0.31 arc-seconds. Misalignment along the X axis is 0.21 arc-seconds. These are well within the 30 arc-second requirement and are based on the differential deflection between joints 174, 198, 172, 196, 170, and 194.

Evaluation of the thermal distortion analysis results for the second requirement shows a mounting plate misalignment with respect to the Y axis of 0.44 arc-seconds in the horizontal plane. A misalignment of 0.22 arc-seconds exists with respect to the Y axis in the vertical plane. These misalignments are well within the 6-minute requirement stated previously.

Based on these results, there are no appreciable effects on the alignment of the camera when exposed to the thermal environment anticipated during orbital operation.

TABLE 2.4.7-4. DEFLECTIONS OF CROSSBEAM STRUCTURE

* * DEFLECTIONS FOR SUBSTRUCTUR E 0 * *

JOINT	DIRECTION 1	DIRECTION 2	DIRECTION 3	DIRECTION 4	DIRECTION 5	DIRECTION 6
1	1.0111E-02	-4.3532E-03	-1.1134E-05	8.2709E-06	6.6225E-05	-6.7165E-05
2	9.0935E-03	-1.1730E-02	-1.2392E-05	4.6161E-05	6.0654E-05	1.5517E-04
3	5.6430E-03	-1.8347E-02	-2.7822E-06	8.4426E-05	1.1496E-04	-1.0228E-04
4	0.	-2.4244E-02	-7.5544E-06	1.8190E-04	6.7969E-06	0.
5	-7.9261E-03	-2.7609E-02	-1.2074E-05	2.0995E-04	-3.2714E-05	-8.5956E-04
6	-1.7099E-02	-2.8756E-02	-2.3371E-05	2.5005E-04	-9.5250E-05	-9.5634E-04
7	-2.6091E-02	-2.5015E-02	-5.9421E-05	1.9674E-04	-2.1856E-04	-1.6630E-03
8	-3.3099E-02	-1.8285E-02	-5.9265E-05	1.7002E-04	-3.1184E-04	-2.2034E-03
9	-3.7517E-02	-9.6796E-03	-7.4913E-05	2.8397E-04	-3.6442E-04	-2.3427E-03
10	-3.7905E-02	0.	-1.0943E-04	3.0477E-05	-2.2490E-04	0.
11	-3.4559E-02	8.6514E-03	-1.3530E-04	-3.2231E-04	-4.0745E-04	-2.5829E-03
12	-2.8655E-02	1.5054E-02	-1.4121E-04	-1.3203E-04	-2.4899E-04	-2.1524E-03
13	-2.1326E-02	1.8669E-02	-1.2720E-04	-1.8746E-04	-1.5192E-04	-2.2355E-03
14	-1.3938E-02	1.9981E-02	-1.0116E-04	-1.7993E-04	-1.4224E-04	-1.4560E-03
15	-6.5405E-03	1.8238E-02	-8.6895E-05	-1.8151E-04	-5.6302E-05	-6.5441E-04
16	0.	1.4581E-02	-5.4987E-05	-1.5394E-04	6.2328E-06	0.
17	5.4364E-03	9.5255E-03	-2.5659E-05	-1.1770E-04	8.6387E-05	3.6821E-04
18	8.9465E-03	2.9850E-03	-1.8029E-05	-1.3196E-05	9.1383E-05	3.7969E-04
19	9.8045E-04	-2.3371E-02	5.6293E-05	1.7707E-04	1.5163E-05	1.6028E-04
20	-3.7825E-02	-1.4823E-03	-1.3138E-04	7.3700E-05	-2.2434E-04	-1.9085E-05
21	8.6281E-03	-4.2212E-03	-2.9349E-05	1.5399E-05	5.6310E-05	-9.5106E-03
22	7.7302E-03	-1.0393E-02	-1.6090E-05	-1.5857E-06	6.9948E-05	-9.2894E-03
23	4.7494E-03	-1.5887E-02	5.0683E-06	1.5821E-04	6.7848E-06	-9.5433E-03
24	2.7676E-04	-2.1181E-02	8.7214E-06	1.4556E-04	-3.6260E-05	-1.0949E-02
25	-6.5300E-03	-2.4189E-02	6.9445E-06	1.8718E-04	-1.1162E-04	-1.1852E-02

TABLE 2.4.7-4. DEFLECTIONS OF CROSSBEAM STRUCTURE (Cont'd)

* * DEFLECTIONS FOR SUBSTRUCTUR E 0 * *

JOINT	DIRECTION 1	DIRECTION 2	DIRECTION 3	DIRECTION 4	DIRECTION 5	DIRECTION 6
26	-1.4545E-02	-2.5427E-02	-3.3404E-06	1.4870E-04	-1.7405E-04	-1.3505E-02
27	-2.2612E-02	-2.2443E-02	-2.7485E-05	1.5004E-04	-1.3664E-04	-1.4218E-02
28	-2.8432E-02	-1.5980E-02	-4.5178E-05	1.9189E-04	-3.5486E-04	-1.4708E-02
29	-3.2502E-02	-8.3542E-03	-6.5526E-05	2.8699E-04	-2.8786E-04	-1.4737E-02
30	-3.3779E-02	2.5568E-04	-9.7061E-05	5.2077E-05	-1.7328E-04	-1.2575E-02
31	-2.9941E-02	7.8404E-03	-1.2217E-04	-1.6021E-04	-2.1233E-04	-1.3438E-02
32	-2.4524E-02	1.3381E-02	-1.2658E-04	-1.7396E-04	-4.1233E-04	-1.3060E-02
33	-1.8135E-02	1.6486E-02	-1.3504E-04	-1.0555E-04	-2.0234E-04	-1.1669E-02
34	-1.1651E-02	1.7139E-02	-1.1804E-04	-1.6423E-04	-1.0795E-04	-1.0879E-02
35	-5.3667E-03	1.5279E-02	-1.0944E-04	-1.6222E-04	-5.9305E-05	-1.0070E-02
36	4.8000E-05	1.1869E-02	-9.1265E-05	-1.3701E-04	1.1826E-05	-9.4179E-03
37	4.3517E-03	7.3047E-03	-6.9167E-05	-9.6514E-05	7.3125E-05	-9.0565E-03
38	7.3957E-03	1.8823E-03	-4.7901E-05	1.8234E-06	8.6826E-05	-9.0766E-03
39	-1.2279E-03	-2.4708E-02	2.7974E-05	1.8540E-04	4.1989E-06	-8.3127E-05
40	-3.7457E-02	1.4152E-03	-1.5461E-04	-2.1168E-05	-2.2280E-04	6.5048E-05
41	3.1108E-03	-3.9823E-03	2.0147E-05	2.2660E-05	5.0981E-05	-9.2519E-03
42	2.5948E-03	-8.3874E-03	1.9301E-05	1.1276E-05	6.7693E-05	-8.8846E-03
43	5.5527E-04	-1.2300E-02	1.5832E-05	1.2087E-04	2.2913E-05	-8.7763E-03
44	-2.9543E-03	-1.5559E-02	3.7688E-05	1.8560E-04	-6.8629E-05	-1.0118E-02
45	-7.6283E-03	-1.7796E-02	4.2025E-05	1.7245E-04	-1.1458E-04	-1.0676E-02
46	-1.3157E-02	-1.8109E-02	2.0296E-05	2.5943E-04	-1.9246E-04	-1.1972E-02
47	-1.8712E-02	-1.6100E-02	-7.1307E-05	2.2478E-04	-1.8127E-04	-1.2551E-02
48	-2.2490E-02	-1.1455E-02	-9.2458E-05	1.9713E-04	-2.7287E-04	-1.1785E-02
49	-2.5357E-02	-6.2298E-03	2.2076E-06	1.2005E-04	-3.3998E-04	-1.1993E-02
50	-2.6389E-02	-4.1247E-04	-8.6675E-05	5.3236E-05	-2.1407E-04	-1.1217E-02

TABLE 2.4.7-4. DEFLECTIONS OF CROSSBEAM STRUCTURE (Cont'd)

* * DEFLECTIONS FOR SUBSTRUCTUR E 0 * *

JOINT	DIRECTION 1	DIRECTION 2	DIRECTION 3	DIRECTION 4	DIRECTION 5	DIRECTION 6
51	-2,4174E-02	4,8043E-03	-1,7644E-04	6,8377E-05	-4,7023E-04	-1,1010E-02
52	-2,0164E-02	8,5119E-03	-1,3646E-04	-1,0448E-04	-3,0556E-04	-9,9948E-03
53	-1,6228E-02	1,1253E-02	-1,1195E-04	-1,5119E-04	-1,6219E-04	-1,0175E-02
54	-1,1631E-02	1,1568E-02	-1,9491E-04	-1,6311E-04	-1,2585E-04	-9,5689E-03
55	-7,1790E-03	1,0003E-02	-1,7620E-04	-1,3875E-04	-5,8401E-05	-9,0657E-03
56	-3,3431E-03	7,4512E-03	-1,1142E-04	-1,2149E-04	-1,6508E-05	-8,6406E-03
57	-2,3724E-04	4,1754E-03	-3,7494E-05	-6,2866E-05	7,0764E-05	-8,2783E-03
58	2,0771E-03	3,5378E-04	9,4959E-06	2,0418E-05	7,0360E-05	-8,6063E-03
59	-7,7885E-04	-2,1579E-02	8,7214E-06	1,4556E-04	-3,6260E-05	-1,1072E-02
60	-3,3413E-02	1,5118E-03	-9,7061E-05	5,2077E-05	-1,7328E-04	-1,2455E-02
61	3,8972E-03	-4,2503E-03	2,5861E-05	2,0110E-05	5,1196E-05	2,0133E-04
62	3,3252E-03	-9,4512E-03	3,6234E-05	2,0537E-05	6,4029E-05	5,7681E-04
63	1,0545E-03	-1,4135E-02	-1,0772E-05	8,2501E-05	6,2455E-05	6,8660E-04
64	-3,4223E-03	-1,7598E-02	-1,3386E-05	1,0392E-04	9,2767E-06	8,9704E-04
65	-8,8803E-03	-2,0176E-02	4,2061E-05	1,6755E-04	-2,3196E-05	3,7863E-04
66	-1,5233E-02	-2,0534E-02	-2,9492E-05	1,2273E-04	-8,5990E-05	5,7588E-04
67	-2,1451E-02	-1,7919E-02	-6,9103E-05	1,3687E-04	-1,2277E-04	2,3634E-05
68	-2,6280E-02	-1,3174E-02	-5,3488E-05	1,1831E-04	-2,7290E-04	2,6745E-04
69	-2,9353E-02	-7,2824E-03	-7,8396E-05	1,6716E-04	-2,0158E-04	2,8036E-04
70	-2,9498E-02	-6,6079E-04	-1,0042E-04	-3,7715E-05	-2,0894E-04	1,5982E-03
71	-2,7786E-02	5,2656E-03	-1,4561E-04	-1,0901E-04	-4,1904E-05	-2,6966E-04
72	-2,3492E-02	9,4972E-03	-1,6880E-04	-9,6554E-05	-2,0708E-04	-9,6759E-05
73	-1,8766E-02	1,2623E-02	-9,4386E-05	-1,5007E-04	-1,2130E-04	-7,1189E-04
74	-1,3494E-02	1,3482E-02	-1,5742E-04	-1,4790E-04	-1,3423E-04	-1,1295E-04
75	-8,2220E-03	1,1928E-02	-1,6386E-04	-1,4021E-04	-5,8729E-05	4,0727E-04

TABLE 2.4.7-4. DEFLECTIONS OF CROSSBEAM STRUCTURE (Cont'd)

* * DEFLECTIONS FOR SUBSTRUCTUR E 0 * *

JOINT	DIRECTION 1	DIRECTION 2	DIRECTION 3	DIRECTION 4	DIRECTION 5	DIRECTION 6
76	-3,5814E-03	9.1291E-03	-7,5811E-05	-1,1828E-04	-1,1018E-05	8,2703E-04
77	3,3076E-04	5,4934E-03	-2,5686E-05	-6,9773E-05	4,7310E-05	1,1727E-03
78	2,8047E-03	8,7514E-04	-2,9952E-06	2,4324E-05	7,0305E-05	8,5586E-04
79	1,1329E-03	-2,0446E-02	8,7214E-06	1,4556E-04	-3,6260E-05	-1,0770E-02
80	-3,3694E-02	-1,0500E-03	-9,7061E-05	5,2077E-05	-1,7328E-04	-1,2606E-02
101	6,4958E-03	-4,2013E-03	-2,9349E-05	1,5399E-05	1,1482E-04	-4,8363E-03
102	5,9249E-03	-9,5003E-03	-1,6093E-05	2,2222E-05	1,3533E-04	-4,5380E-03
103	2,9359E-03	-1,5339E-02	5,0632E-06	2,0442E-04	6,1868E-05	-4,6100E-03
104	-1,3634E-03	-1,9703E-02	8,7183E-06	2,2654E-04	1,0493E-05	-5,2077E-03
105	-7,7399E-03	-2,2579E-02	6,9432E-06	2,7163E-04	-9,6730E-05	-5,9182E-03
106	-1,5079E-02	-2,3324E-02	-3,3405E-06	2,7175E-04	-1,9576E-04	-6,6459E-03
107	-2,1824E-02	-2,0758E-02	-2,7483E-05	2,5662E-04	-1,9819E-04	-7,2790E-03
108	-2,7632E-02	-1,4885E-02	-4,5160E-05	2,0253E-04	-3,6752E-04	-7,4016E-03
109	-3,0874E-02	-9,1674E-03	-6,5520E-05	3,0399E-04	-3,3454E-04	-7,4102E-03
110	-3,2032E-02	-4,4996E-04	-9,7061E-05	5,2077E-05	-3,2440E-04	-5,6700E-03
111	-2,8968E-02	7,4889E-03	-1,2218E-04	-1,9939E-04	-3,1994E-04	-7,0358E-03
112	-2,4428E-02	1,1582E-02	-1,2659E-04	-1,1795E-04	-3,4555E-04	-6,7598E-03
113	-1,8696E-02	1,4874E-02	-1,3505E-04	-1,7548E-04	-2,4272E-04	-6,3722E-03
114	-1,2365E-02	1,5731E-02	-1,1804E-04	-2,3265E-04	-1,2002E-04	-5,6775E-03
115	-6,5837E-03	1,3955E-02	-1,0944E-04	-2,2458E-04	-4,8306E-05	-5,0133E-03
116	-1,4333E-03	1,0746E-02	-9,1262E-05	-1,8742E-04	4,0931E-05	-4,4772E-03
117	2,7288E-03	6,5173E-03	-6,9161E-05	-1,3558E-04	1,1968E-04	-4,1235E-03
118	5,5578E-03	1,2063E-03	-4,7898E-05	-1,9474E-05	1,4531E-04	-4,2921E-03
121	8,6976E-03	-7,8044E-03	-1,6093E-05	5,4333E-05	6,0083E-05	-4,8598E-03
122	6,3965E-03	-1,4040E-02	5,0679E-06	1,2284E-04	2,7196E-05	-4,8755E-03

TABLE 2.4.7-4. DEFLECTIONS OF CROSSBEAM STRUCTURE (Cont'd)

* * DEFLECTIONS FOR SUBSTRUCTUR E 0 * *

JOINT	DIRECTION 1	DIRECTION 2	DIRECTION 3	DIRECTION 4	DIRECTION 5	DIRECTION 6
123	2,5973E-03	-1,9894E-02	8,7099E-06	1,5458E-04	-4,7053E-05	-5,5254E-03
124	-3,7942E-03	-2,4069E-02	6,9428E-06	1,8524E-04	-1,0631E-04	-6,1075E-03
125	-1,1534E-02	-2,6366E-02	-3,3407E-06	1,4870E-04	-1,7102E-04	-7,1821E-03
126	-2,0006E-02	-2,4772E-02	-2,7484E-05	1,2178E-04	-2,1421E-04	-7,7690E-03
127	-2,7464E-02	-2,0116E-02	-4,5168E-05	1,9937E-04	-3,4598E-04	-8,3672E-03
128	-3,2996E-02	-1,3004E-02	-6,5528E-05	1,2591E-04	-3,8087E-04	-8,6519E-03
129	-3,4604E-02	-4,1642E-03	-9,7053E-05	-2,2995E-04	-2,2303E-04	-7,5778E-03
130	-3,3655E-02	4,0586E-03	-9,7068E-05	2,5727E-04	-2,0948E-04	-7,5791E-03
131	-2,9309E-02	1,1043E-02	-1,2216E-04	-4,4258E-05	-2,7928E-04	-7,9778E-03
132	-2,3670E-02	1,6534E-02	-1,2659E-04	-2,1966E-04	-3,5789E-04	-7,6479E-03
133	-1,6230E-02	1,7604E-02	-1,3504E-04	-1,0864E-04	-1,9383E-04	-6,7443E-03
134	-9,5121E-03	1,7593E-02	-1,1804E-04	-1,6423E-04	-1,4563E-04	-5,9483E-03
135	-3,1886E-03	1,4801E-02	-1,0944E-04	-1,6845E-04	-7,6450E-05	-5,2169E-03
136	2,0285E-03	1,0549E-02	-9,1254E-05	-1,5066E-04	-4,4619E-06	-4,7064E-03
137	5,9441E-03	5,2693E-03	-6,9168E-05	-1,1275E-04	6,3756E-05	-4,5199E-03
138	8,1847E-03	-8,6696E-04	-4,7900E-05	-3,5493E-05	8,0244E-05	-4,7534E-03
141	3,2716E-03	-6,6247E-03	1,9301E-05	5,1906E-05	6,0520E-05	-4,5234E-03
148	-2,5989E-02	-9,5235E-03	2,2036E-06	1,2787E-04	-3,3546E-04	-6,0445E-03
149	-2,7522E-02	-3,5639E-03	-8,6683E-05	6,0769E-05	-2,1272E-04	-5,6498E-03
150	-2,6884E-02	2,2838E-03	-8,6658E-05	-2,1633E-05	-2,0084E-04	-5,7432E-03
151	-2,4655E-02	7,3971E-03	-1,7643E-04	-1,1439E-04	-3,6472E-04	-5,7350E-03
158	2,8816E-03	-1,6685E-03	9,4967E-06	-1,0975E-05	6,4818E-05	-4,3842E-03
170	-2,6115E-02	-9,5117E-03	-3,7162E-05	1,6929E-05	-1,8933E-04	3,6709E-04
171	-2,6009E-02	-5,9957E-03	-2,1637E-05	-4,7575E-06	-9,2927E-05	4,8682E-04
172	-2,5703E-02	-9,8934E-04	-8,9900E-05	-4,2835E-05	-9,6903E-05	2,6242E-04

TABLE 2.4.7-4. DEFLECTIONS OF CROSSBEAM STRUCTURE (Cont'd)

* * DEFLECTIONS FOR SUBSTRUCTUR E 0 * *

JOINT	DIRECTION 1	DIRECTION 2	DIRECTION 3	DIRECTION 4	DIRECTION 5	DIRECTION 6
173	-2,5055E-02	3,6166E-03	-1,4847E-04	-9,7230E-05	-3,7590E-05	-5,1753E-06
174	-2,4293E-02	6,5575E-03	-2,4322E-04	2,9316E-05	-1,3508E-04	-2,7670E-04
176	-2,5470E-02	-1,2831E-02	8,0435E-06	1,1885E-04	-3,0197E-04	-2,5981E-03
178	-2,5602E-02	-5,9548E-03	-3,6135E-06	4,1537E-05	-1,9256E-04	-2,1283E-03
180	-2,4735E-02	3,4140E-03	-1,8194E-04	-3,2906E-05	-1,8208E-04	-2,3024E-03
182	-2,2876E-02	9,0457E-03	-2,4049E-04	-1,3877E-04	-2,3256E-04	-2,5317E-03
183	-2,4593E-02	-1,2503E-02	6,4705E-05	1,2311E-04	-3,1998E-04	-5,3714E-03
184	-2,4815E-02	-9,1264E-03	5,3034E-05	1,0098E-04	-2,9114E-04	-4,9395E-03
185	-2,4948E-02	-5,7822E-03	1,5750E-05	6,6578E-05	-2,6933E-04	-4,6520E-03
186	-2,4802E-02	-1,0355E-03	-7,4986E-05	1,2526E-06	-2,5388E-04	-4,5203E-03
187	-2,4078E-02	3,3998E-03	-1,9885E-04	-2,6162E-06	-2,7676E-04	-4,5278E-03
188	-2,3214E-02	6,2307E-03	-2,6962E-04	-4,7121E-05	-2,6791E-04	-4,6398E-03
189	-2,2176E-02	8,8544E-03	-2,9251E-04	-3,4583E-05	-2,6735E-04	-4,8013E-03
190	-2,2685E-02	-5,1337E-03	5,5986E-06	1,0558E-04	-3,8043E-04	-1,0565E-02
192	-2,1698E-02	3,4806E-03	-1,9148E-04	2,0946E-05	-4,1212E-04	-9,7159E-03
193	-2,0671E-02	-1,0420E-02	-9,1536E-05	1,8028E-04	-2,6495E-04	-1,7794E-02
194	-2,0335E-02	-7,2578E-03	-9,4044E-05	2,5894E-04	-3,2820E-04	-1,6977E-02
195	-1,9981E-02	-4,2719E-03	-1,0185E-04	1,7740E-04	-4,0015E-04	-1,6106E-02
196	-1,9371E-02	-7,0838E-05	-1,2482E-04	1,6371E-04	-4,4957E-04	-1,5343E-02
197	-1,8623E-02	3,7506E-03	-1,5325E-04	7,3599E-05	-4,8144E-04	-1,4476E-02
198	-1,8165E-02	6,1678E-03	-1,0457E-04	-1,2076E-05	-4,2014E-04	-1,4412E-02
199	-1,7824E-02	8,5816E-03	-8,8355E-05	2,7800E-05	-3,6359E-04	-1,4411E-02
200	-1,8119E-02	-1,5978E-02	-6,7479E-05	5,8495E-05	-7,0967E-05	4,0992E-04
202	-1,5069E-02	-1,7242E-02	-5,7814E-05	1,9731E-05	-9,7658E-05	6,9979E-04
203	-1,4910E-02	-1,4020E-02	-2,6907E-05	6,7181E-05	-9,0655E-05	8,7796E-04

TABLE 2.4.7-4. DEFLECTIONS OF CROSSBEAM STRUCTURE (Cont'd)

* * DEFLECTIONS FOR SUBSTRUCTUR E 0 * *

JOINT	DIRECTION 1	DIRECTION 2	DIRECTION 3	DIRECTION 4	DIRECTION 5	DIRECTION 6
204	-1,4868E-02	-2,4492E-03	-1,6714E-06	6,8272E-07	-9,4475E-05	9,9016E-04
205	-1,4310E-02	8,1948E-03	-1,0839E-04	-1,0945E-04	-1,2493E-04	7,1099E-04
206	-1,3943E-02	1,0880E-02	-1,1505E-04	-1,1898E-04	-1,3101E-04	3,0140E-04
208	-1,6580E-02	1,0454E-02	-1,6856E-04	-1,2091E-04	-1,4318E-04	1,3076E-06
210	-1,0830E-02	-1,4096E-02	-9,4579E-06	1,1895E-04	-3,5012E-05	1,1821E-03
211	-6,9178E-03	-1,4115E-02	-3,9809E-07	1,4844E-04	2,9834E-05	1,1699E-03
212	-2,7365E-03	-1,4112E-02	-2,6594E-07	1,4209E-04	5,0916E-05	9,4724E-04
214	6,4517E-04	-4,3177E-03	5,1952E-05	2,5594E-05	5,3284E-05	7,8333E-04
216	-3,3668E-03	5,9243E-03	-1,3932E-04	-9,4674E-05	-3,9984E-06	1,2094E-03
217	-7,2313E-03	6,7513E-03	-1,8727E-04	-1,0956E-04	-3,8589E-06	1,2175E-03
218	-1,0741E-02	7,5591E-03	-1,7429E-04	-1,2507E-04	-5,4917E-05	1,1510E-03
220	-2,0178E-02	-1,7148E-02	-6,5933E-05	1,2925E-04	-2,5478E-04	-6,4741E-03
224	-1,4366E-02	-1,9487E-02	-1,1147E-05	1,9725E-04	-1,8112E-04	-5,9026E-03
226	-1,4175E-02	-1,3356E-02	-6,2845E-06	1,5575E-04	-1,2976E-04	-4,7961E-03
228	-1,3628E-02	7,4779E-03	-1,5871E-04	-1,1522E-04	-1,1630E-04	-4,2213E-03
230	-1,2562E-02	1,2461E-02	-1,7298E-04	-1,5341E-04	-1,6001E-04	-5,0451E-03
232	-1,7535E-02	1,1931E-02	-1,1777E-04	-9,0254E-05	-2,3566E-04	-5,6535E-03
234	-6,7485E-03	-1,3191E-02	9,2774E-06	1,4929E-04	-4,6507E-05	-4,1473E-03
236	7,4921E-04	-1,3180E-02	4,4436E-06	1,7073E-04	3,8952E-05	-4,2283E-03
238	7,8951E-05	4,7831E-03	-3,8219E-05	-1,2601E-04	3,9086E-05	-3,7374E-03
240	-7,0417E-03	6,0725E-03	-1,7120E-04	-1,0886E-04	-3,8686E-05	-3,6138E-03
242	-1,5960E-02	-1,4295E-02	2,4919E-05	2,3557E-04	-2,8191E-04	-1,0971E-02
244	-1,3243E-02	-1,5189E-02	3,0590E-05	3,3144E-04	-1,6707E-04	-1,0708E-02
245	-1,3360E-02	-1,2334E-02	3,8207E-05	1,2380E-04	-1,3947E-04	-1,0052E-02
246	-1,3763E-02	-2,1722E-03	2,7560E-06	4,2712E-05	-9,0994E-05	-9,2747E-03

TABLE 2.4.7-4. DEFLECTIONS OF CROSSBEAM STRUCTURE (Cont'd)

* * DEFLECTIONS FOR SUBSTRUCTUR E 0 * *

JOINT	DIRECTION 1	DIRECTION 2	DIRECTION 3	DIRECTION 4	DIRECTION 5	DIRECTION 6
247	-1,2854E-02	7,0389E-03	-1,6900E-04	1,2357E-05	-1,1363E-04	-8,7552E-03
248	-1,2264E-02	9,3479E-03	-1,8120E-04	-1,4334E-04	-1,2405E-04	-8,8754E-03
250	-1,4579E-02	9,2394E-03	-2,3250E-04	-8,8808E-05	-1,7775E-04	-9,1691E-03
252	-9,8409E-03	-1,2245E-02	5,5305E-06	1,6465E-04	-1,1234E-04	-9,4310E-03
253	-6,4151E-03	-1,2261E-02	-9,9238E-06	1,4998E-04	-8,6671E-05	-9,0697E-03
254	-2,7788E-03	-1,2312E-02	-7,4379E-06	1,3593E-04	-2,8955E-05	-8,5952E-03
256	-9,8908E-06	-4,0719E-03	5,2326E-05	1,4986E-05	5,2261E-05	-8,0151E-03
258	-3,4713E-03	4,6082E-03	-1,3209E-04	-1,0670E-04	2,9509E-05	-7,8425E-03
259	-6,7962E-03	5,3998E-03	-1,8385E-04	-1,0799E-04	-5,1599E-05	-8,0543E-03
260	-9,8248E-03	6,2356E-03	-1,9362E-04	-7,2453E-05	-7,9235E-05	-8,2709E-03

2.5 DESIGN DESCRIPTION

2.5.1 OVERALL VEHICLE

The ERTS vehicle is shown in Figure 2.5.1-1 in the orbit configuration.

Basically, the ERTS spacecraft is a two-body vehicle. The lower body is the sensory ring which houses the experiments and subsystems, and the upper body is the attitude control system (ACS) assembly that houses the components which provide for orientation of the spacecraft and drive the solar arrays.

The sensory ring and the ACS are connected by a six-member truss with each member of the truss of identical design. A secondary function of the truss is to support the auxiliary load panels which reject excess power from the spacecraft and the ACS/Sensory Ring connector interface panel. In addition, the truss tubes support the command antenna lower ground plane which is the birdcage-like structure shown in Figure 2.5.1-1 and the solar array paddle dampers which limit dynamic deflections of the paddles.

In addition to housing the solar array drives and the ACS components, the ACS assembly provides support for the comand antenna upper ground plane and the command antenna stub.

In the launch configuration, the paddles are rotated about the hinge axis and latched together and tied down to the sensory ring at the -X axis intersection with the sensory ring.

The launch configuration and spacecraft adapter are illustrated in Figure 2.5.1-2. The adapter is connected to the spacecraft with a segmented marmon clamp and separation band. Separation is achieved by pyrotechnically severing two bolts in the separation band, one located at the +Y axis and one located at the -Y axis.

The primary function of the adapter is to provide conformance with the launch vehicle and to support the spacecraft during the launch vibration environment. The adapter also houses the four separation springs which supply the velocity increased to separate the spacecraft from the launch vehicle. In addition, the adapter provides accomodation for sensor "go no-go" targets for stimulation on the launch pad and the antenna pick ups and re-radiators.

2.5.2 ATTITUDE CONTROL SYSTEM PACKAGE SUPPORT AND INTERFACES

The ERTS Attitude Control System (ACS) is based on the ACS assembly designed by NASA for the Nimbus D and subsequent Nimbus spacecraft. The ERTS ACS is identical with the Nimbus D design, subject to the following exceptions:

1. The yaw sun sensors are eliminated.
2. The right-hand solar array drive sun sensor must be relocated on the solar paddle transition section to provide a clear field of view.
3. The gravity gradient experiment is replaced by a back up Rate Measuring Processor.

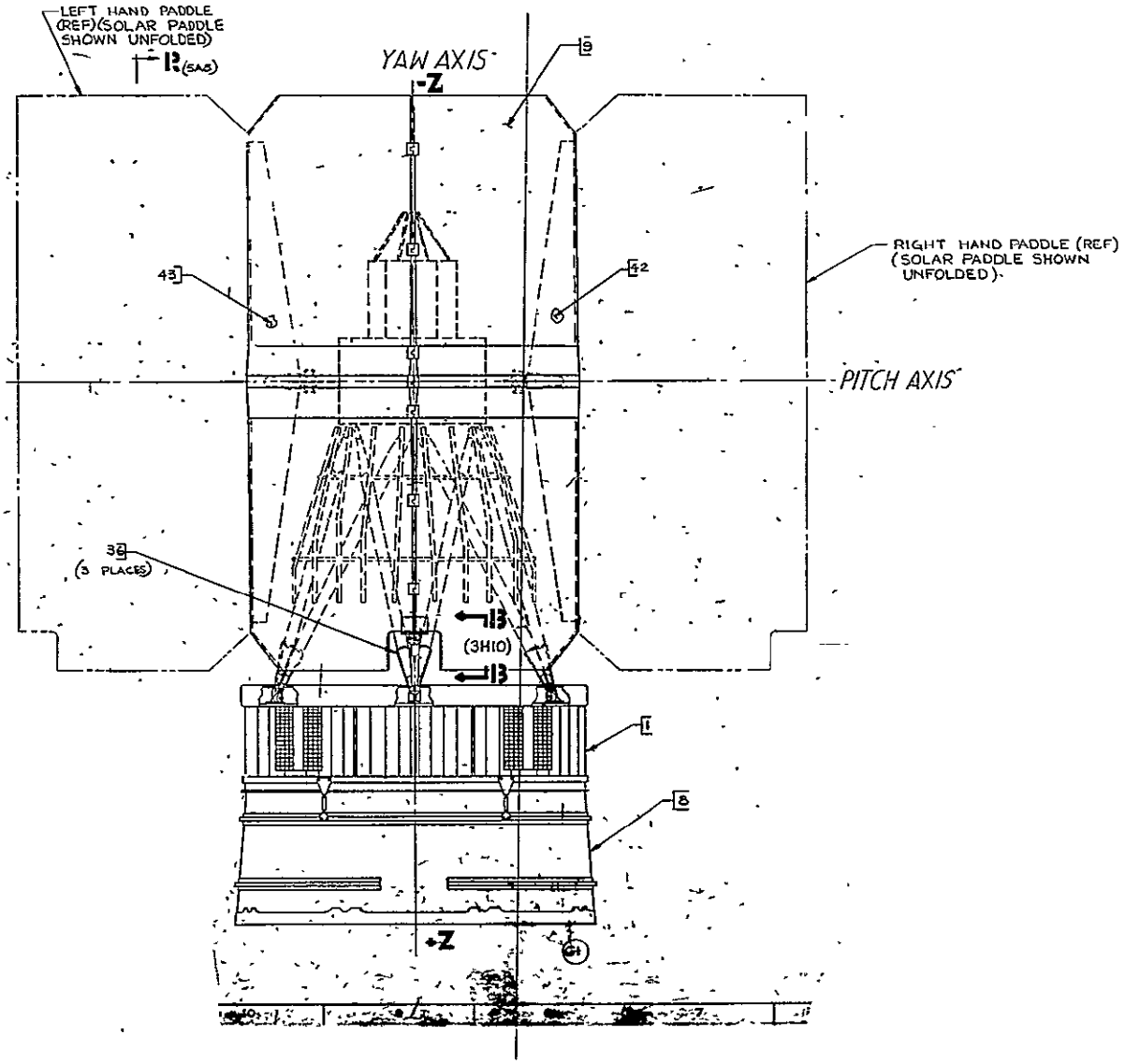

Figure 2.5.1-2. Spacecraft Launch Configuration

The ACS assembly is shown in Figure 2.5.2-1. A triangular arrangement of aluminum alloy I-beams form the foundation of the ACS structure. This triangular frame is oriented parallel to the spacecraft roll pitch plane.

The I-beams are interconnected at each corner by a machined fitting. Each of the three fittings are identical with its counter-parts and incorporates a clevis for attachment of the spacecraft truss tubes (two per fitting) and a hoisting lug. The hoisting lug provides structural integrity for lifting the entire spacecraft, but is normally used for ACS handling only.

A square aluminum sandwich plate mounts over the I-beam structure and a network of sheet metal beam provides eight compartments in an "egg box" arrangement. These compartments provide accommodation for some of the ACS components, i.e., pitch Reaction Wheel, Control Logic Box, Rate Measuring Processor (two for ERTS), Horizon Scanners (2), the Solar Array Drives (2), and the Yaw RateGyro. The yaw reaction wheel is located below the sandwich plate within the confines of the I-beams.

A cylinder of sandwich construction is mounted over the assembly previously described. The function of this cylinder is to support the pneumatics assembly. This assembly consists of the pneumatic tank and regulator and six nozzles integrated on a baseplate which attaches to the upper end of the cylinder. The tank mounts to the underside of the baseplate and consequently is located inside the sandwich cylinder upon assembly. The pitch-yaw nozzles are mounted on a long stand offs to provide plume clearance.

Thermal control for the ACS is provided by a shutter assembly actuated by bi-metal spring and mounted below the baseplate. Excess heat is radiated through the shutters to a thermal cover which surrounds the shutter assembly. With the exception of thethermal cover, the ACS is completely covered with insulation.

2.5.2.1 Solar Paddle Support and Interfaces

The solar paddle interfaces with the spacecraft are shown in Figure 2.5.2-2 (4 Sheets), the Solar Power Subsystem.

View JJ and Section NN of Figure 2.5.2-2 (Sheet 4) show the solar paddle equal to the solar array drive interface. A socket built in to the paddle transition section engages over the SAD shaft and three tapered plugs provide a structural connection. Two clamps, one on each side of the transition section, surround this point for additional rigidity.

In the launch configuration, the paddles are folded back and connected together by seven latches and two yaw fittings. The latch pins are mounted on a cable which runs the entire length of the paddles. This cable is tensioned by a spring at the upper latch fitting.

The main structural tie for the paddles is comprised of the two jaw fittings at the lower end of the latch line. The two jaws are connected by a preload pin and attached to spacecraft with a 2000-pound preload. The preload pin connects to the lower end of the latch cable; however, a shoulder on the pin sustains the 2000-pound preload such that the only cable load is that induced by this spring at the upper end.

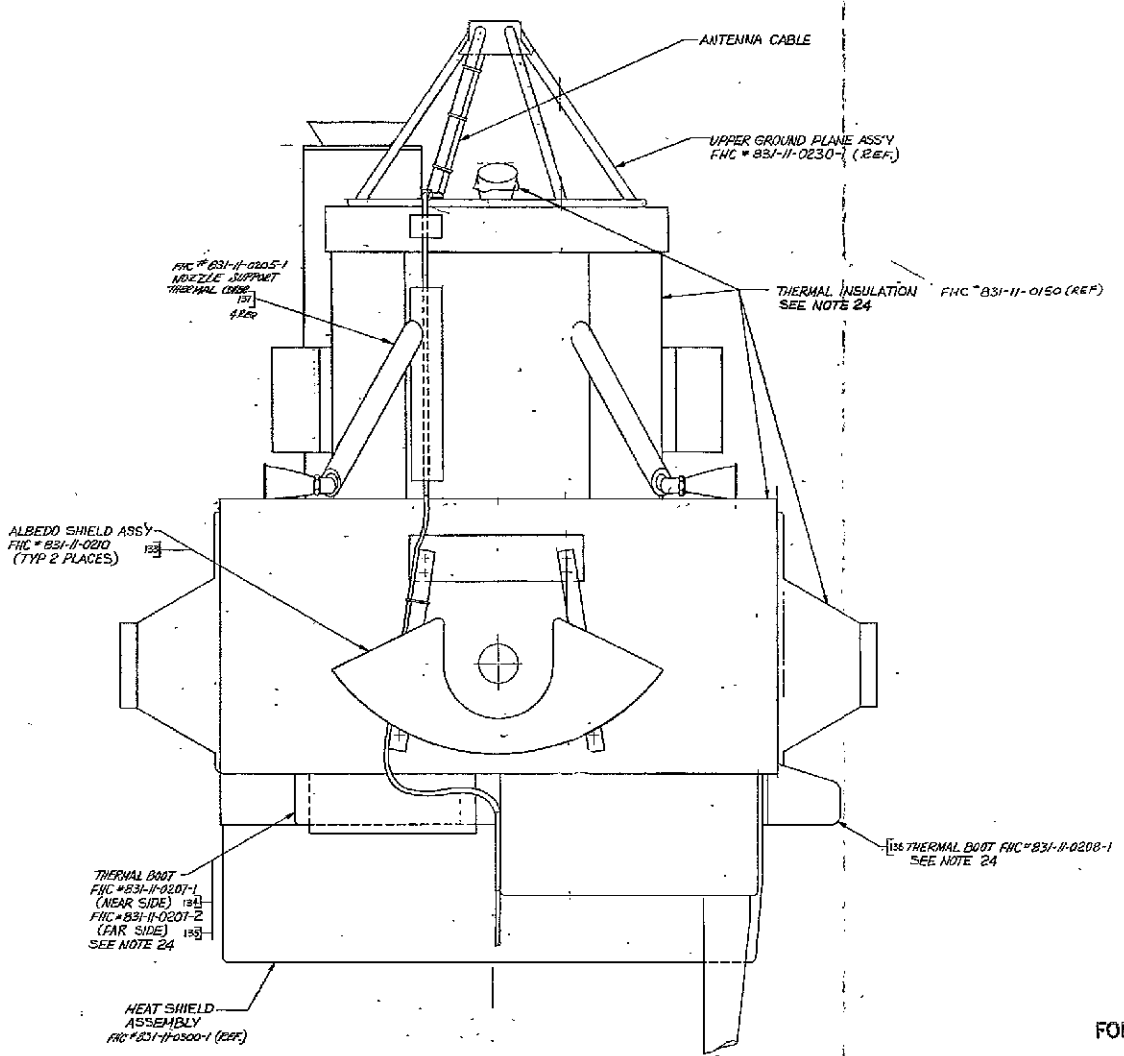

FOLDOUT FRAME 2

FOLDOUT FRAME 1

Figure 2.5.2-1. ACS Assembly
(Sheet 3 of 3)

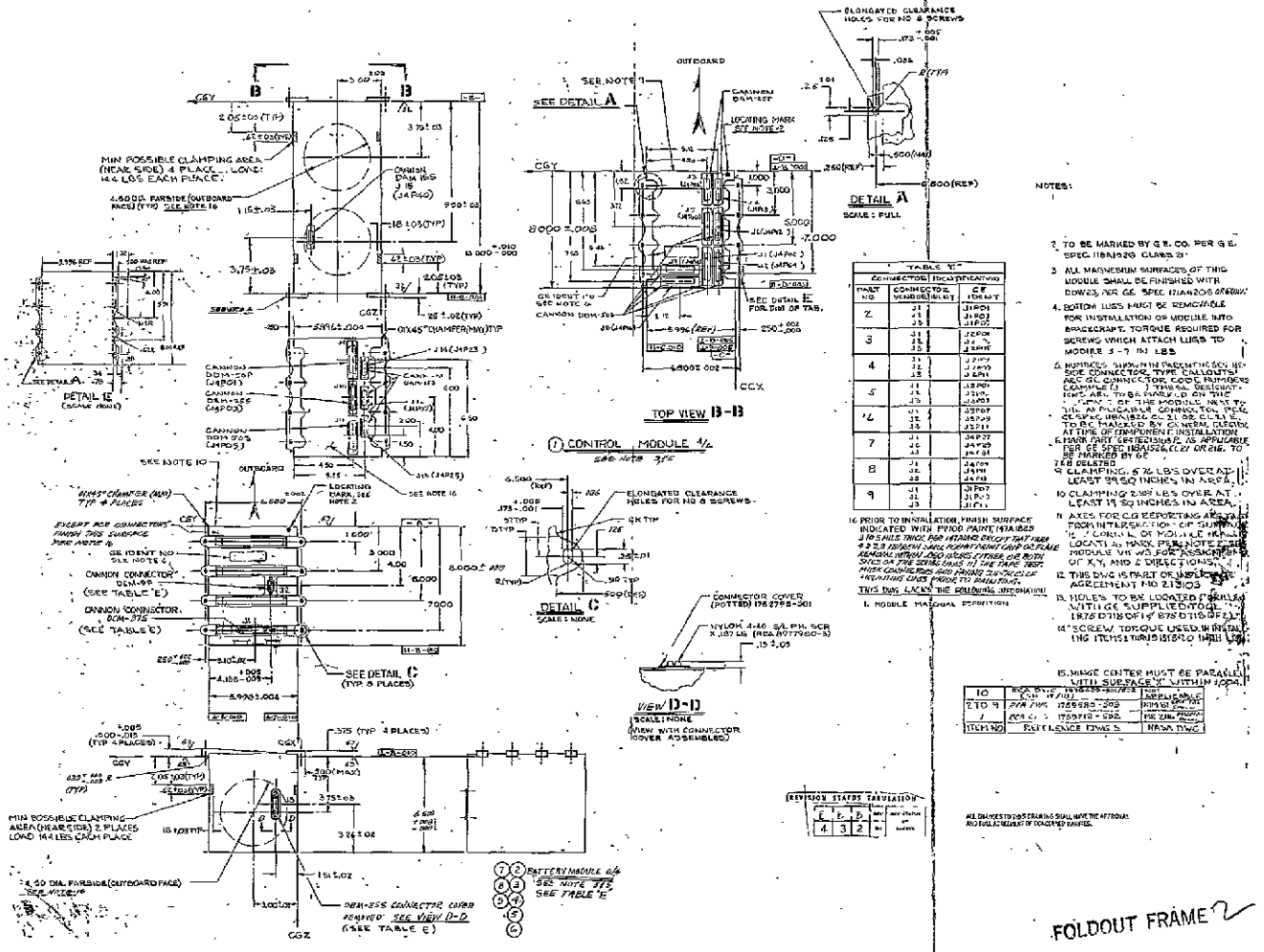

TABLE "E"		
CONNECTOR LOCATION/IDENTIFICATION		
PART NO	CONNECTOR VENDOR/SERIES	CP IDENT
2	J1 J2 J5	J1P01 J2P01 J5P02
3	J1 J2 J5	J2P01 J2P02 J5P01
4	J1 J2 J5	J1P01 J2P01 J5P01
5	J1 J2 J5	J1P01 J2P01 J5P03
6	J1 J2 J5	J1P07 J2P09 J5P11
7	J1 J2 J3	J1P07 J2P09 J3P01
8	J1 J2 J3	J1P07 J2P11 J3P01
9	J1 J2 J3	J1P07 J2P03 J3P01

16 PRIOR TO INSTALLATION, FINISH SURFACE INDICATED WITH PAINT, (MIL-P-23377) TO 5 MILS THICK PER MIL-C-27427 EXCEPT THAT OVER ± 2.5 S (SILICON) RAD. RADIATING SURFACE PLANE REMOVAL WITH ZERO LOSSES EITHER OR BOTH SIDES OF THE SETBACK LINES IS THE TAPE TEST. MASK CONNECTORS AND GROUND SURFACES OF MOUNTING LUGS PRIOR TO PAINTING.

THIS DWG LACKS THE FOLLOWING INFORMATION:

1. MODULE MATERIAL PERMITTION

NOTES:

2. TO BE MARKED BY G.E. CO. PER G.E. SPEC. MBM1320 CLASS 2.
3. ALL MAGNESIUM SURFACES OF THIS MODULE SHALL BE FINISHED WITH DOW 17, PER G.E. SPEC. (MIL-M-3171) GRADE
4. BOTTOM LUGS MUST BE REMOVABLE FOR INSTALLATION OF MODULE INTO SPACECRAFT. TORQUE REQUIRED FOR SCREWS WHICH ATTACH LUGS TO MODULE 5 - 7 IN LBS
5. NUMBERS SHOWN IN PARENTHESIS ADJ. TO SIDE CONNECTORS, TYPE CALLOUTS, ARE GE CONNECTOR CODE NUMBERS EXAMPLE (1) THESE DESIGNATIONS ARE TO BE PANEL ID ON THE "OUT" SIDE OF THE MODULE NEXT TO ITS APPLICABLE CONNECTOR. PER GE SPEC MBM1322 CL 21 OR CL 23 TO BE MARKED BY CAMERA OR OTHER METHOD AT TIME OF COMPONENT INSTALLATION
6. ERROR (PART OF SPECIFICATION, AS APPLICABLE PER GE SPEC MBM1526, CLEI OR 216. TO BE MARKED BY GE
7 & 8 DELETED
9. CLAMPING: 6.76 LBS OVER AT LEAST 19.50 INCHES IN AREA.
10. CLAMPING: 2.98 LBS OVER AT LEAST 19.50 INCHES IN AREA.
11. AXES FOR C.G REPORTING ARE TAKEN FROM INTERSECTION OF SURFACES
12. THIS DWG IS PART OF UNIT DWG AGREEMENT NO 213103
13. HOLES TO BE LOCATED FROM LUG WITH GE SUPPLIED TOOL
14. SCREW TORQUE USED IN INSTALLING ITEMS
15. IMAGE CENTER MUST BE PARALLEL WITH SURFACE "E" WITHIN

ITEM NO	ELECT. SPACE DWG S	NASA DWG
1		
ZTO 9		
10		

FOLDOUT FRAME 1

FOLDOUT FRAME 2

Figure 2.5.2-2. Solar Power Subsystem Mechanical Interface (Sheet 1 of 4)

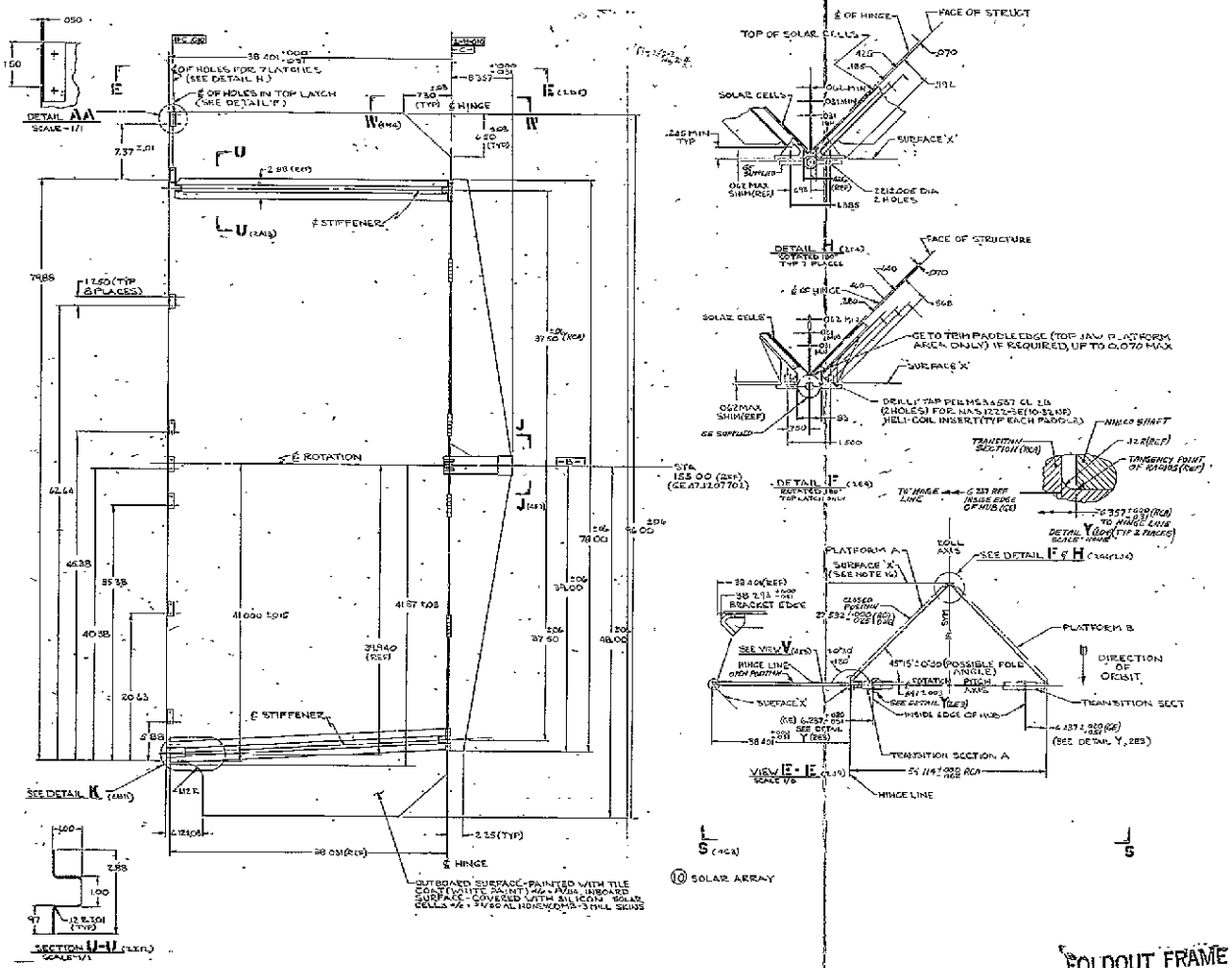

FOLDOUT FRAME 1

FOLDOUT FRAME 2

Figure 2.5.2-2. Solar Power Subsystem Mechanical Interface (Sheet 2 of 4)

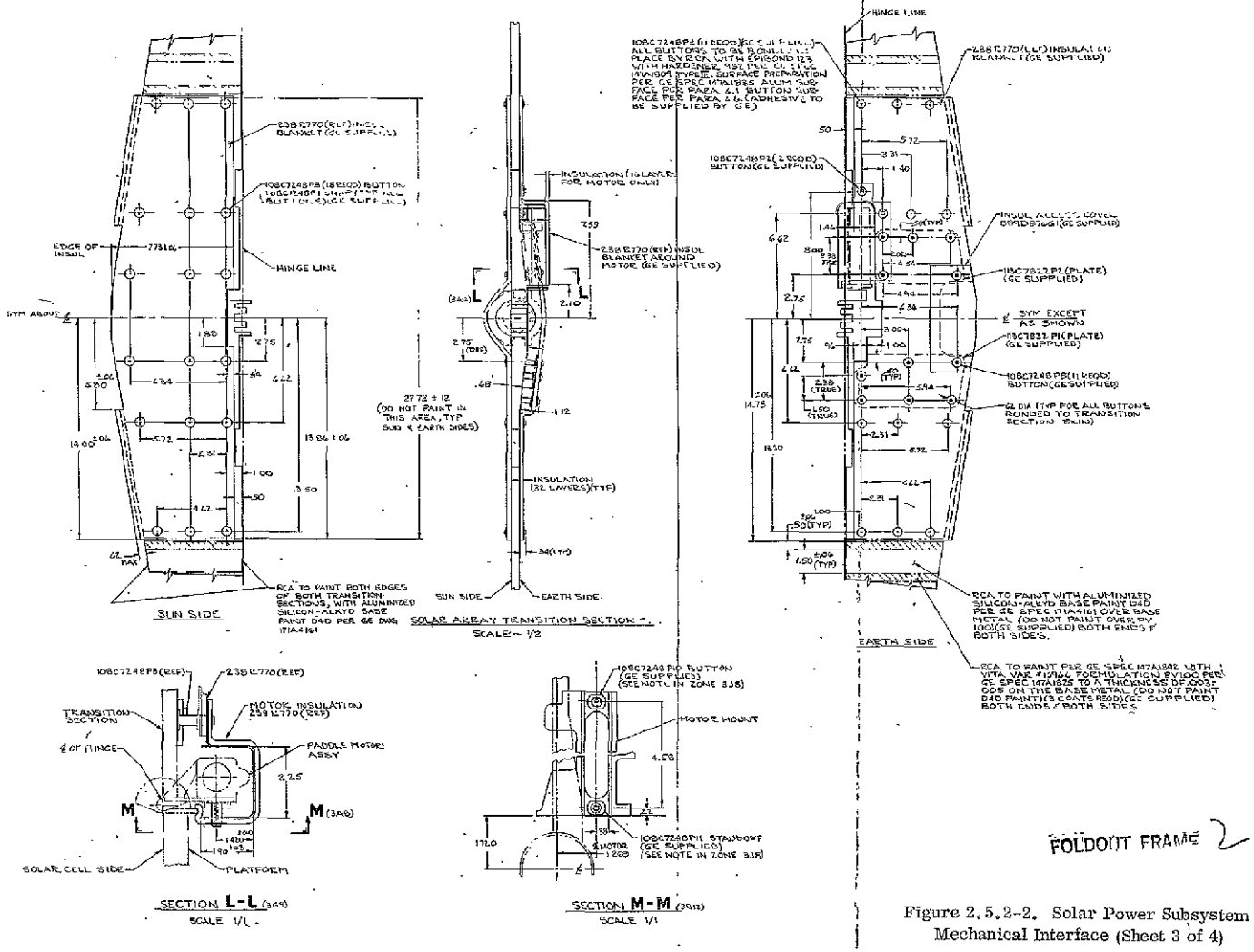

FOLDOUT FRAME 1

FOLDOUT FRAME 2

Figure 2.5.2-2. Solar Power Subsystem Mechanical Interface (Sheet 3 of 4)

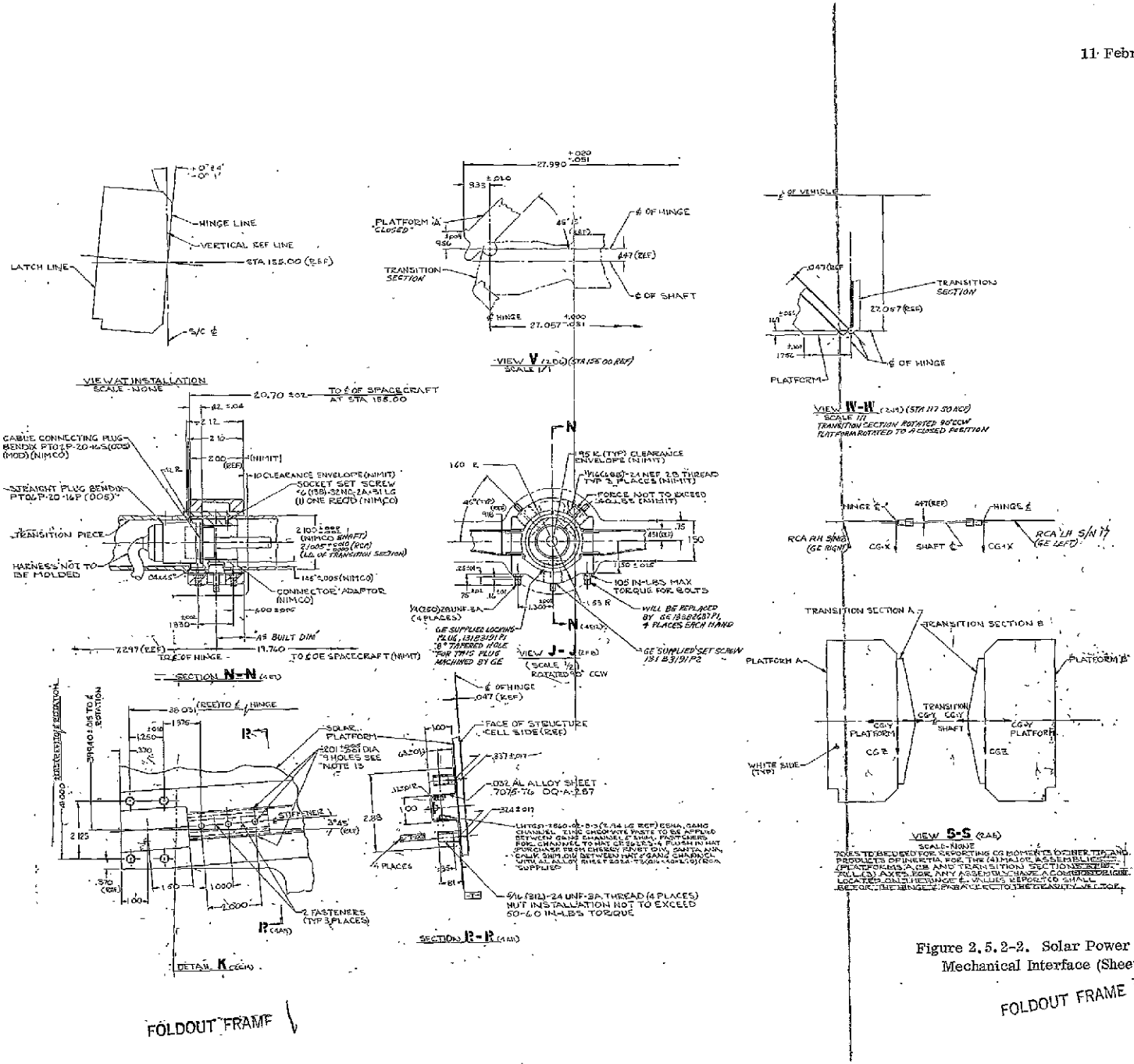

Figure 2.5.2-2. Solar Power Subsystem Mechanical Interface (Sheet 4 of 4)

When the preload pin is severed by a pyrotechnically initiated bolt cutter, the upper spring withdraws each latch pin and the preload pin. The latches and jaw on the left-hand paddle are split to allow the cable to pass through and connect the paddles.

The paddles are opened by spring located at the paddle hinge and the opening rate is controlled by a motor located on the transition section.

2.5.3 SENSORY RING ASSEMBLY AND INTERFACES

The sensory ring structural assembly is comprised of 18 magnesium alloy separator castings connected by the upper and lower outer ring. These outer rings are machined from 7075-T6 forgings and the lower ring incorporates the marmon clamp flange which is the interface with the spacecraft adapter.

Each separator casting has a "fish tail" shaped lug at the top and bottom on the inboard side. A series of channels connect these lugs together to provide structural continuity.

Shear webs are provided about the outer periphery of the ring and are riveted to the upper and lower rings and the separator castings. Shear webs are also positioned in the radial direction on each casting. One web per casting is the sensing plate of the temperature controlled assembly.

Three machined lugs equally spaced on the upper surface of the ring provide the interface. In addition, the lug positioned on the -X axis also supports the solar paddle tie down links.

The Nimbus D sensory ring is shown in Figure 2.5.3-1 during assembly. The ERTS cross beam, although of different configuration, would feature the same gusseting techniques as illustrated in this photograph.

2.5.4 PAYLOAD AND NEW EQUIPMENT

The ERTS spacecraft relies on previously proven components. Modular-sized components are mounted within the 18 sensory ring compartments in a manner identical to Nimbus D. Good thermal contact is made between the outboard component and the outboard face, and between all components and the temperature sensor. Furthermore, components are rigidly mounted with the resonant mount frequency above 100 Hz. This precludes destructive coupling with spacecraft major modes, all of which fall below 100 Hz.

Nonmodular components, such as antennas, cameras, and the Orbit Adjust Subsystem, are mounted on the top and bottom sensory ring surface and in the crossbeam area. For some of these components, additional mounting bases were designed to locate components as dictated by field of view, and structural and dynamic requirements. Construction is of sheet stock and extruded shapes. A harness deck will be used for optimum harness routing and to provide convenient interface connector locations.

Six truss tubes and associated fittings are used to mount the packaged attitude control system, which contains the pneumatics, gyros, scanners, solar array drive, and shafts, etc.

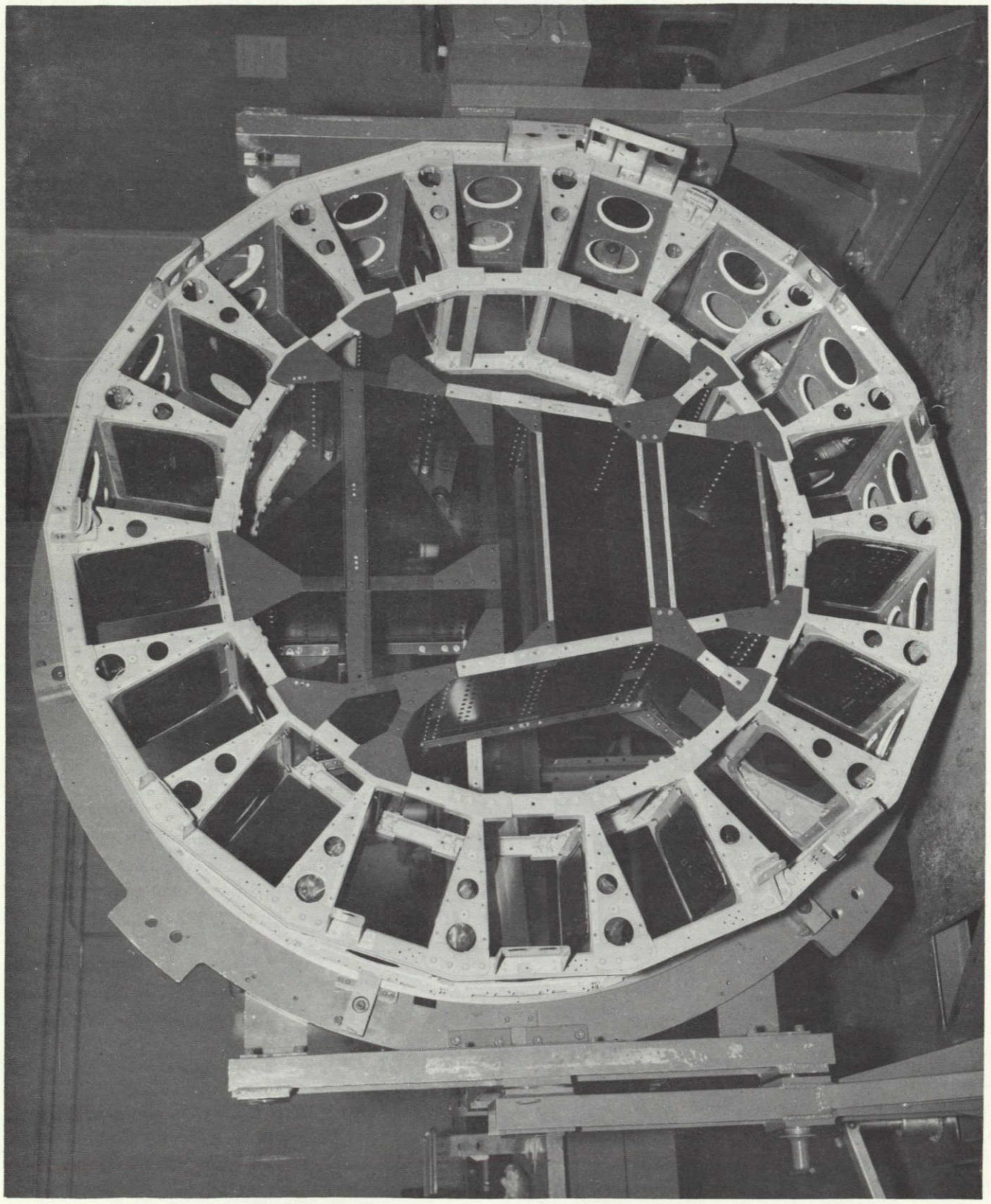

Figure 2.5.3-1. Nimbus D Sensory Ring

2.5.4.1 Center Section Equipment Support

2.5.4.1.1 RBV Support

The RBV cross beam support structure (Figure 2.5.4-1) consists primarily of riveted extruded channels and sheet metal panels. The channel structure is riveted together with clips and this subassembly is sandwiched between the sheet metal panels forming a rigid reinforced box beam. This beam assembly is located symmetrically about the X-axis of the spacecraft. The ends of the box beam are connected to the inboard post of separator castings numbers 8 and 12. The center section is supported by two intercostals attached to castings numbers 9 and 11. Gusset plates are used to tie the box beam to the upper and lower caps of the torus structure. This construction with the torus structure forms an extremely rigid torque box which is essential to the support of the RBV cameras. The structure provides a rigid base with sufficient mounting area to support the three point RBV common plate suspension system.

All extruded channels and sheet metal panels are fabricated from 7075-T6 and 2024-T3 aluminum alloy, respectively. The material selected was the best choice considering the factor of stiffness, cost, ease of fabrication, and availability.

2.5.4.1.2 Center Section Cross Beam

The center section cross beam supports the following equipment:

1. Wide-band Video Tape Recorder Transport (2)
2. Narrow-band Tape Recorder (2)
3. Telemetry Conversion Modules (3)
4. Power Switching Module (1)
5. MSS Scanner (1)
6. Unfold Timer (1)

The cross beam structure (Figure 2.5.4-2) is "Π" shaped and consists primarily of riveted extruded channel/angle caps with sheet metal webs. These primary members are jointed to each other by side beams and to the torus structure by intercostals. The ends of the "Π shaped cross beam are connected to the inboard post of separator castings numbers 3, 6, 7, 13, 14 and 17. Gusset plates are used to join and reinforce the ends of the "Π" shaped cross beam to the upper and lower caps of the torus structure.

The WBVTR's are inserted into the center section of the cross beam from the top side of the sensory ring and bolted to the upper and lower caps of the horizontal beam. One-inch square aluminum pads are fastened to the upper and lower caps where the WBVTR's mount to the crossbeam. To provide adequate interface, the mounting pads are machined flat within ±0.005 inch, after the center crossbeam section has been rivited together as a subassembly. Upon installing the center section crossbeam subassembly into the spacecraft torus structure, jig plates are fastened across the WBVTR mounting points to maintain flatness between pads. The electrical connectors in the WBVTR's point upward and are readily accessible

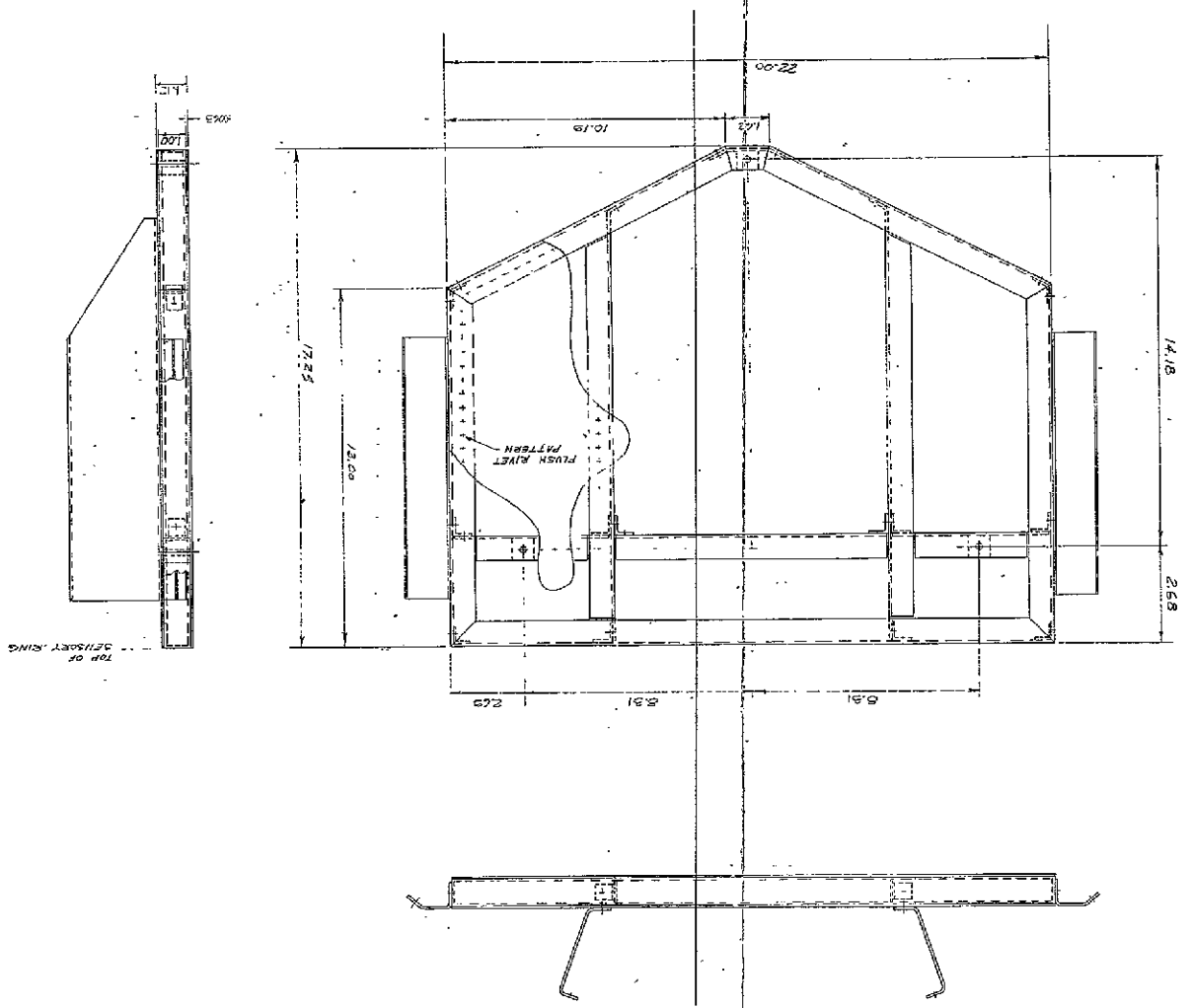

FOLDOUT FRAME 2

Figure 2.5.4-1. Mounting Structure, RBV Baseplate

FOLDOUT FRAME 1

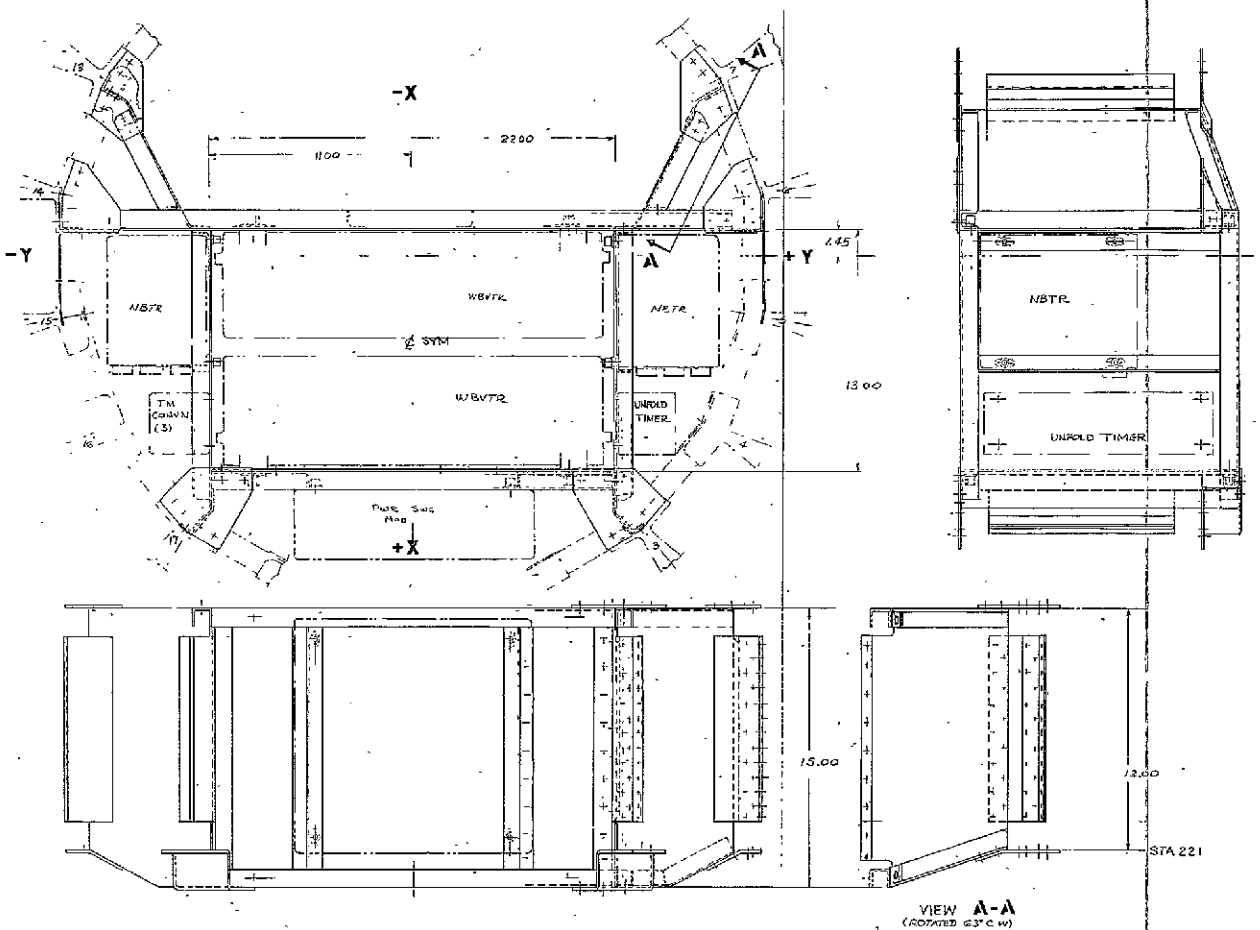

1. RIVETED CONSTRUCTION.
2. AL ALY 2024 SHEET METAL & SHAPES
3. AIR-FRAME NUT PLATE FASTENERS

FOLDOUT FRAME 1

FOLDOUT FRAME 2

Figure 2.5.4-2. Cross Beam, Center Section

from above the sensory ring. The two NBTR's, the three Telemetry Conversion Modules, and the Unfold Timer are mounted on either side of the vertical cross beams.

The Power Switching Module, which is connector laden, is located along the horizontal beam opposite one of the Wide-band Video Tape Recorders. The electrical connectors are readily accessible from both top and bottom.

The MSS scanner support is also a "Π" shaped structure which overlaps the center section cross beam and consists of extruded channels and riveted gusset plates. This frame is bolted into inserts located in the caps on the bottom side of the torus structure and cross beam. The MSS channel structure can be maintained quite shallow so as to keep the MSS scanner (weight of 120 pounds) close to the primary torus and cross beam structure and thus avoid vibration amplifications.

The overlapping "Π" sections for the crossbeam and MSS support structure provides several unique features:

1. The load path from the MSS Scanner can be dumped directly from its mounting feet into the crossbeam and torus structure with almost no bridging.
2. The MSS can be mounted close to the primary structure minimizing vibration amplification.
3. MSS channel structure provides:
    a. Simple construction
    b. Change in height flexibility
    c. Lateral freedom, i.e., the ERTS A and B MSS's can be centered about the spacecraft Z axis with only minor mounting hole modifications.

2.5.4.2 Above Sensory Ring Equipment Support

Nonmodular equipment is mounted in the Sensory Ring Assembly in an area above the sensory ring and attached to the Sensory Ring structure. The following nonmodular components are mounted to the top of the Torus ring and center crossbeam in this area of packaging:

1. Orbit Adjust Subsystem
2. Wideband Vidio Tape Recorder Electronics
3. Magnetic Moments Assembly

Super insulation is used to cover all three components with opening only for the O/A thrusters. (See Figure 2.5.4-3.)

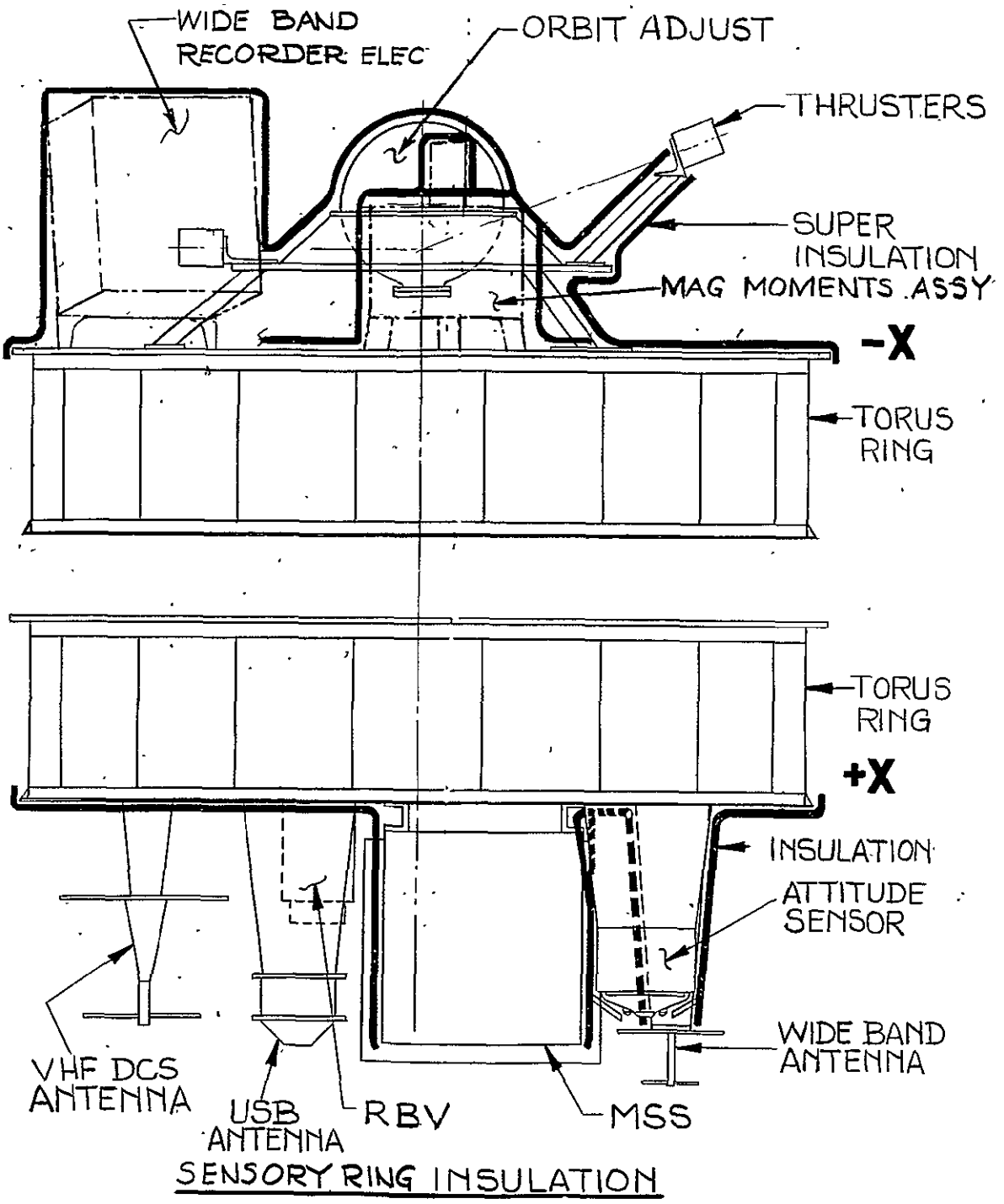

Figure 2.5.4-3. Sensory Ring Insulation

The subsystem will be mounted on the spacecraft and positioned to the nominal calculated center-of-mass location (±0.5 inch center-of-mess accuracy at this point). Thrusters will then be aligned optically to the measured nominal center-of-mass location using existing data from the Nimbus Program and a thrust axis tool. No vertical or lateral positioning is required after initial mounting on the spacecraft.

The misalignment of the Orbit Adjust Subsystem thrusters with respect to the center of mass of the spacecraft results in disturbance torques. Furthermore, the center-of-mass moves somewhat during the mission due to consumption of ACS fuel. This motion is vertical only and does not contribute additional yaw torques. The O/A Subsystem thrusters are aligned to within 0.1 inch (approximately) of the spacecraft center-of-mass to minimize disturbance torques in pitch and to average out orbital effects of pitch axis attitude control.

Adequate clearance for installation, maintenance, accessibility, and thruster firing exists for this subsystem installation. One thruster (-X axis) has been offset to eliminate interference with the existing strut assembly and solar paddle tie down. However, the angle of thrust vector on the -X axis is established to pass through the spacecraft center of gravity. By this means, enough clearance has been provided for the -X and +X thrusters to fire between the support struts (-X) and the Wideband Recorder Electronics (+X) respectively.

The O/A Subsystem assembly is a completely self supporting structural assembly to facilitate a simple installation on the spacecraft. The O/A interfaces with the ERTS spacecraft by means of three mounting pads on the spacecraft, picking up the O/A tripod support legs. The electrical interface is by means of three connectors. The trhee support legs are bolted to the inner side of the torus separator castings on both sides of bays 6 and 13 and the casting between bays 1 and 18. Spacers are used between the O/A and torus ring interface. This is to position the O/A center of gravity with respect to the spacecraft center of gravity. In order to maintain a good thermal interface, all mating surfaces are machined to a flatness of 0.001 inch. Silvered thermal grease will also be applied at each mating surface.

The support brackets or legs are designed with a natural frequency above 100 Hz to preclude dynamic coupling with the spacecraft major resonances. As a result, load inputs to the tank can be maintained below 15g.

2.5.4.2.2 Wideband Video Tape Recorder Electronic Mounting

Two Wideband Video Tape Recorder Electronic (WBVTRE) packages are mounted over the sensory ring generally in the +X area of the sensory ring. The WBVTRE's are mounted to an "A" frame located over bays 1, 2, 17 and 18. (See Figure 2.5.4-4.) Construction of the frame consists of riveted aluminum 2024-T3 sheet metal shear panels and extruded aluminum 707S-T6 angle stiffeners. The structure is designed to bridge over all harnessing of the above listed bays. A four-point base of the "A" frame is riveted to machined brackets which are fastened to the torus separator castings and center section crossbeam. The design incorporates mechanical fasteners for manual disassembly and assembly to ease the Orbit Adjust Subssystem equipment insertion and removal. All mating surfaces between "A" frame and torus/crossbeam structure are machined to provide a godd thermal interface.

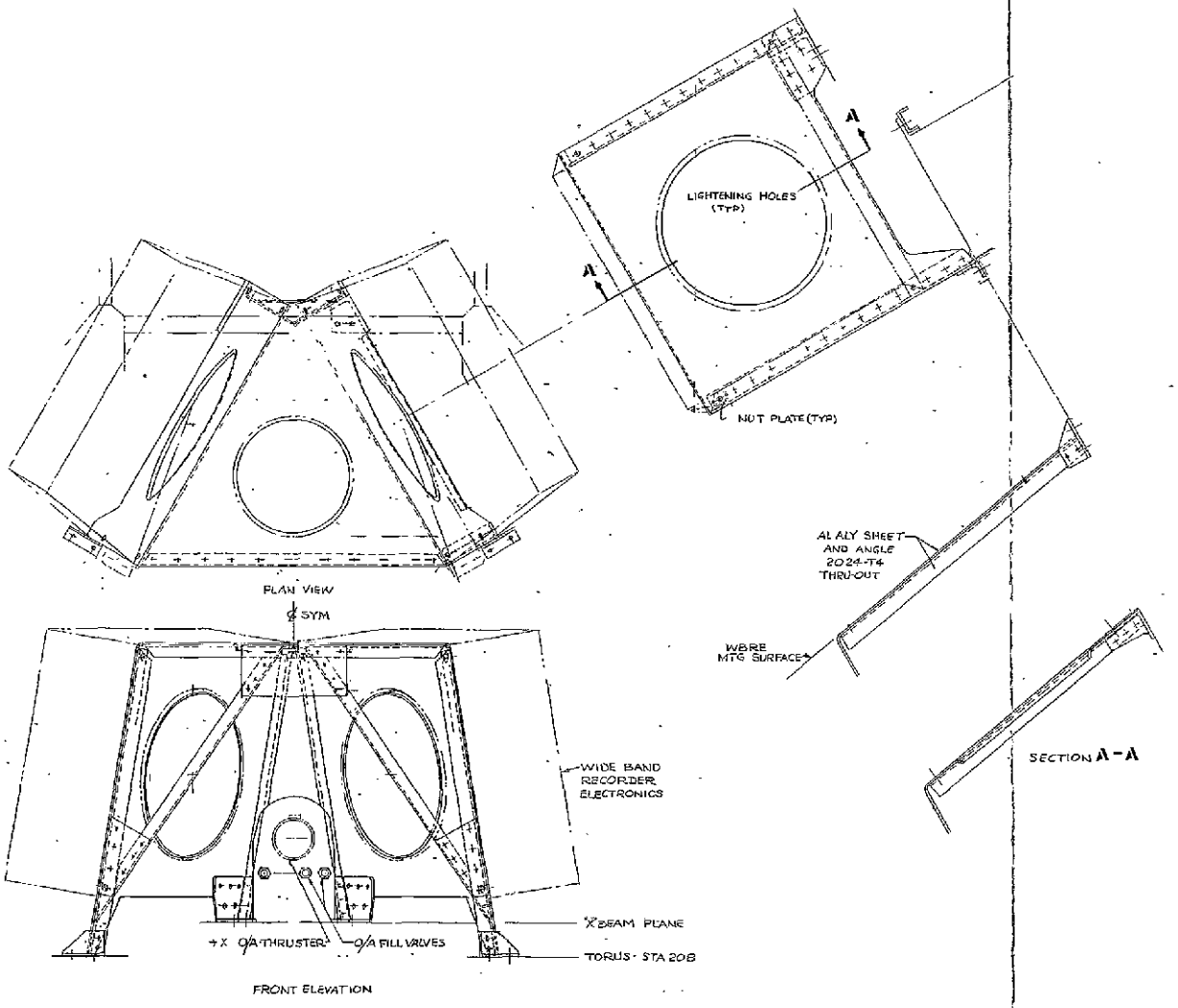

FOLDOUT FRAME

Figure 2.5.4-4. Wide-Band Video Tape Recorder Electronic Components

FOLDOUT FRAME 2

The WBVTRE Tape Recorder packages were positioned on the "A" frame to provide easy access to connectors and to harness tie points. The "A" frame also bridges the Orbit Adjust +X thruster, but leaves ample room for access to its thruster and fill valves.

2.5.4.2.3 Magnetic Moments Assembly (MMA) Mounting

The Magnetic Moments Assembly is used on the Nimbus D Program. The MMA is similarly mounted on the ERTS spacecraft above the sensory ring (see Figure 2.4.5-5). It is mechanically fastened to a machined standoff bracket. This bracket has four support flanges that are installed over the sensory ring into separator castings 14 and 15. The package is oriented such that its mounting surface lies in the pitch and roll plane of the spacecraft. The package is then rotated about its yaw axis until the X and Y axes are parallel to the spacecraft reference axes. The assembly is mounted within ±0.5° tolerance about all three axes. Figure 2.5.1-1 shows the location of the Magnetic Moments Package on the ERTS spacecraft.

2.5.4.3 Equipment Below Sensory Ring

The following nonmodular components are mounted below the sensory ring separation planes and center crossbeam:

1. Multispectral Scanner (MSS)
2. Attitude Sensor
3. Antennas
   a. Unified S-Band
   b. Wideband No. 1
   c. Wideband No. 2
4. Preflight Disconnect Connector

2.5.4.3.1 MSS Installation

The MSS consists of two basic assemblies, the multispectral scanner housing, and associated electronics. The electronics is located just above the scanner in bay 3. The housing contains the scan mirror, optics, and spectral photo-sensors. These are all mated into a single package (rigid) and mounted as a single entity on the earth side of the sensory ring adjacent to the center crossbeam section and bays 3, 4, 5, 15 and 16.

The MSS structure is a "II" shaped structure consisting primarily of extruded channels and gusset plates riveted together. (See Figure 2.5.4-6). Machined standoffs are provided below separator castings 14 and 16 to support the cantilevered ends of the structure.

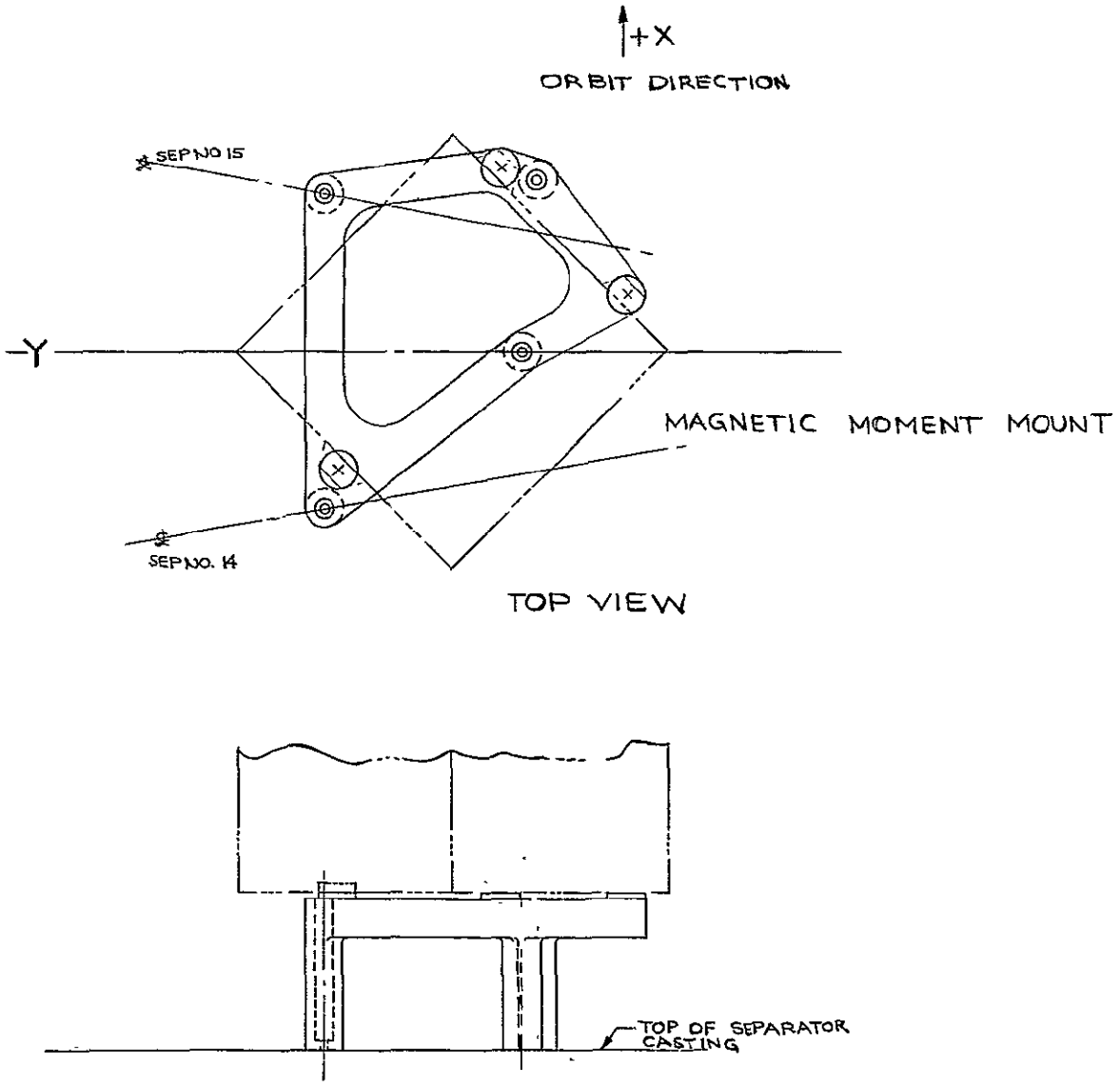

Figure 2.5.4-5. Magnetic Moments Assembly

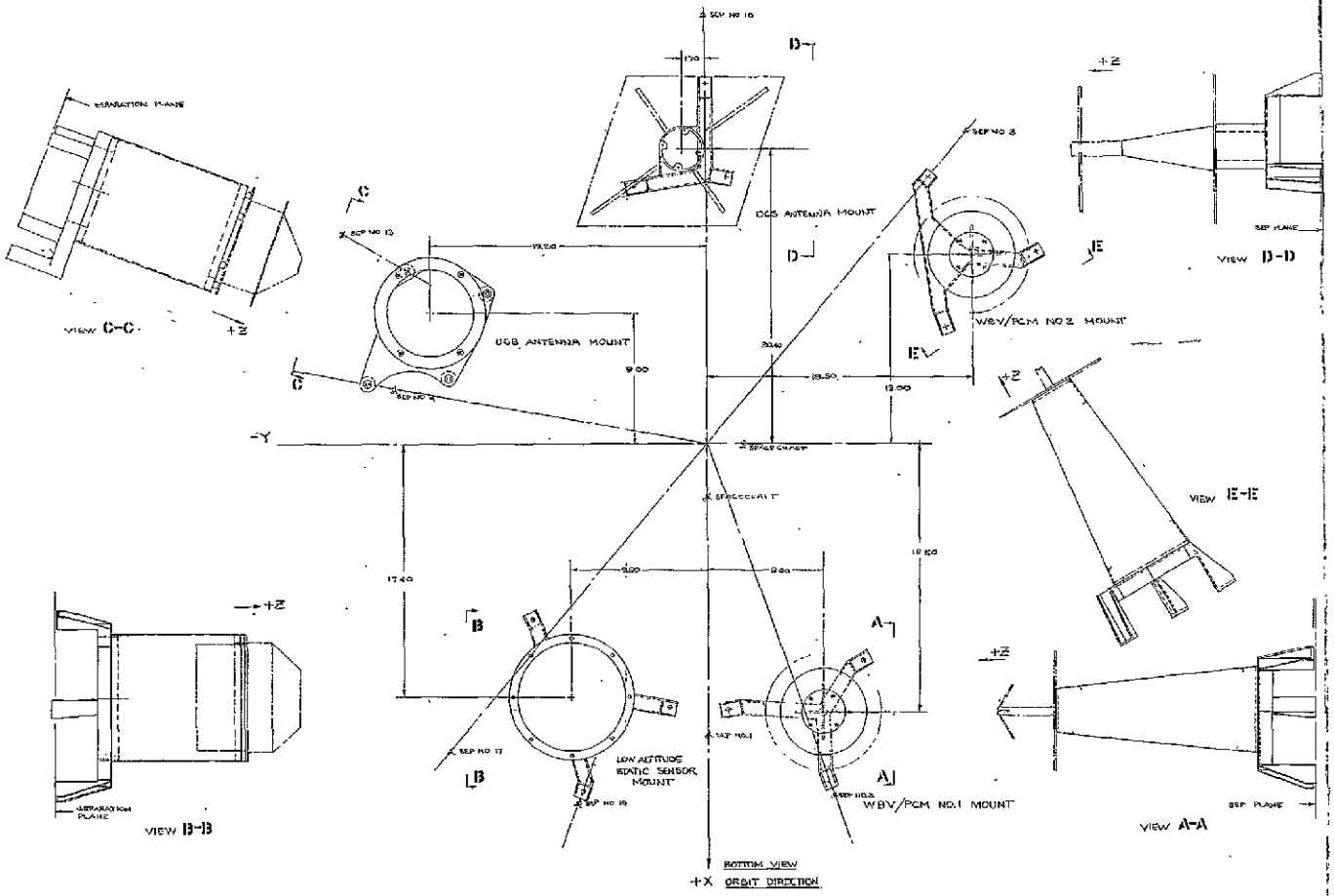

NOTES

1. INTERPRETATION OF DRAWING TERMS & TOL PER MIL-STD-100
2. ALL DIM SHOWN ARE APPROX & FOR REFERANCE ONLY
3. MATL:
   MAG MOMENT & DCS ANTENNA MOUNTS ARE MACHINED PART MADE OF 6061-T6 ALUM ALY
   ALL OTHER MOUNTS HAVE MACHINED SUB MOUNTS OF 6061-T6 ALUM ALY
   TOP PLATES OF 6061-T6 ALUM ALY & FORMED SHEET METAL OR TUBING SPACERS OF 6061-T6 ALUM ALY

FOLDOUT FRAME 1

FOLDOUT FRAME 2

Figure 2.5.4-7. Mounting Structure for DCS/MAG Moment, WBV, USB and Attitude Sensor

This structure is bolted over flat machined pads placed on the crossbeam and separator castings to allow accessibility to bays 14 and 16 and to the center area. The structure in turn provides machined pads, flat and coplanar to within 0.001 inch and 0.005 inch, respectively, as mounting interface for the MSS housing.

The MSS unit will be positioned such that the telescope axis is parallel to the pitch axis of the spacecraft. Additionally, the MSS is positioned such that sunlight enters the sun calibration opening when the spacecraft approaches the North Pole on each orbit. The field of view of the scan mirror will not be obstructed in the pitch yaw plane for an angle of ± 15° from NADIR and in the roll yaw plane of ±10° from NADIR. The field of view of the sun calibration mirror will not be obstructed in the roll pitch plane for an angle of ±25° offset from the + roll axis toward the pitch axis by 35°. Shims will be used to align the MSS package with respect to the spacecraft reference axes to within 0.1°. The two orthogonal reference alignment mirrors provided on the sides of the MSS housing will be used for this purpose.

The MSS scanner will be fully insulated except for the following areas: scan mirror opening, sun calibration opening, mounting surfaces, radiation cooler opening, and the flat radiative surface facing the earth. A thin film of thermally conductive grease will be applied at all mating joints.

2.5.4.3.2 Attitude Sensor Installation

The Attitude Sensor is an independent infrared earch attitude sensor for low altitude, stabilized space vehicles. It is a completely static two-axis sensor intended primarily for vehicles in a near circular orbit. The total weight, including all electronics is approximately 7 pounds. The Attitude Sensor unit will be positioned such that its optical axis is parallel to the spacecraft yaw axis or NADIR. The field of view is a 160 degree cone about its optical axis.

The Attitude Sensor support consists of a thin wall aluminum tubing which is riveted to a flange at one end and a closely machined three-legged standoff bracket at the other.

The sensor is bolted to the flange end of the support standoff bridge connectors and harnessing and is bolted to torus separator castings number 17 and 18. The three-point interfacing allows shimming and sensor alignment to within 0.1 degree with respect to the spacecraft reference axes. An alignment mirror is provided on the face of the sensor for this purpose; locating dowel pins is used to provide easy sensor insertion and withdrawal. Thermal grease will be used on all mating surfaces to provide a good thermal-electrical interface.

The sensor will be fully insulated with 1/2 inch thick aluminized mylar except for the optical openings and it's mounting surface.

2.5.4.3.3 Preflight Disconnect Connector Installation

The Preflight Disconnect Connector has been used on all Nimbus spacecraft to provide electrical power to the spacecraft during the time prior to launch. It consists of a plug, receptacles (spacecraft and auxiliary), and a remote disconnect motor to drive the plug and auxiliary receptacle. The receptacle is soft mounted to the ERTS spacecraft. The plug and drive motor assembly is installed in the spacecraft adapter. The support bracket is similar in design to that used on Nimbus "D". It is designed to bridge bay No. 1 in the sensory ring.

2.5.4.3.4 Antenna Installation

Antenna subsystem provides the necessary transducer (radiator and/or pick-up) to transmit processed spacecraft data and other signals to ground stations or to receive signals from ground stations.

The following antenna installation restraints are presented:

1. Component placement restraints
   a. Antennas mounted on the bottom of the spacecraft sensory ring shall be mounted as far below the spacecraft separation plane as is feasible to minimize interference effects. Once a location has been selected, it shall not be changed without conducting radiation tests to verify acceptability of antenna patterns.
   b. Insulation and/or cover position, shape, and composition shall not be changed on the bottom of the spacecraft sensory ring without conducting similar radiation tests.
   c. All portions of all antennas and all structural parts of the spacecraft shall have low resistance (20 milli-ohm max) paths or be properly bonded together.
   d. Adjacent equipment, flight hardware, insulation, etc., should permit antenna field-of-view area to be free from obstruction.
2. Thermal Surfaces - All antenna ground planes shall be finished with D4D paint to enhance their thermal properties.
3. Alignment - Alignment of antennas on the spacecraft is not critical.
4. Flatness of mating surfaces is not critical.

The antennas (DCS, USB, and WB) are mounted below the sensory ring to permit earth view.

They are supported by monocoque aluminum sheet metal structure, of conical, cylindrical or rectangular box sections, riveted to 3 inch high machined standoff brackets. (See Figure 2.5.4-7). These antennas are attached to the spacecraft structure at three or four tie down points mainly in the torus separator casting area. The mounting feet are designed

so that they can be used for alignment of each unit and also provide limited thermal dissipation surface. The standoffs consist of an antenna matching plate so that the electrical characteristics and attachment to the sensory ring structure are maintained. They are also designed to minimize installation interference with the sensory ring structure.

1. USB Antenna - The Unified S-Band (USB) antenna is a conical spiral antenna which is installed on mounts that position the antenna 14 inches below the spacecraft sensory ring - adapter separation plane over bay 13.
2. DCS Antenna - The Data Collection System (DCS) is a turnstile (crossed dipole) antenna mounted to the bottom of the sensory ring, 7 $\frac{1}{2}$ inches below the spacecraft sensory ring - adapter separation plane over bays 9 and 10.
3. WB Antenna - Two Wideband Antennas are used on the ERTS spacecraft. They are similarly mounted to the bottom of the sensory ring over bays 2 and 7, respectively.

2.5.4.3.5 Insulation Installation

The insulation configuration and location on the bottom of the spacecraft sensory ring/and the environment surrounding the antenna (MSS, attitude sensor and RBV's) will be developed by use of the antenna model.

Fiberglass shells are used to support the lower insulation which is comprised of 32 layers of aluminized mylar. In addition, the shells prevent the insulation from encroaching in the field of view of the antennas and sensors.

2.5.5 ADAPTER ASSEMBLY

The adapter structure provides structural continuity between the spacecraft and the launch vehicle. In addition, it houses the spacecraft adapter separation springs, the stimulators for the payload (RBV and MSS) antenna pickups and reradiators, and mounts sensing devices for spacecraft separation. The adapter assembly consists of the following components:

1. Adapter structure
2. Separation springs and supports
3. Separation switches and supports
4. Bolt cutters
5. Separation band
6. Internal mounting for harness, targets and preflight connector
7. Mounting for antenna pickups and reradiators for data transmission on the pad.

The ERTS adapter will be similar to the Nimbus adapter. The current ERTS baseline adapter interfaces with an eight bolt pickup on the SACS ring, the same interface as on Nimbus. At the adapter to spacecraft interface, the Marmon band separation on ERTS will be identical to Nimbus.

While on the launch pad, the stimulator housed within the adapter is used to check continuity within the RBV and MSS subsystems. The antenna pickups and reradiators mounted in and on the adapter are used to verify the data transmission function during on-pad checkout. Power for these is supplied through the umbilical, which is the only interface between the spacecraft and the adapter, and is broken immediately prior to launch.

After the launch phase, upon reaching the correct altitude and orbit, and upon initiation of the launch vehicle firing circuit, the spacecraft is separated from the adapter. This action is accomplished by firing a set of pyro operated bolt cutters, which releases the separation band assembly that had been the structural connection between the spacecraft and adapter. Separation is accomplished by a set of four springs mounted in the adapter, exerting a force against the spacecraft; the springs provide the required separation velocity and acceptable tumbles rates. It also should be noted that the separation band is restrained from becoming free by means of four restraining spring clips that capture the separation band and hold it with the separated adapter.

Guillotine type, explosively powered, bolt cutters are used to release the separation band clamp and permit spacecraft/booster separation. The bolt cutters are designed to cut 0.156 inch diameter bolts located 180 degrees apart on the band perifery which are used to tension the band and provide required clamping force. The booster vehicle provides the signal and electrical power for simultaneous initiation of the bolt cutters. Cutting of eigher bolt will release the separation band and permit separation to occur. Upon release, the band clamp halves, and the expended bolt cutters and bolts are tethered to or are captured by the adapter so that no space debris is generated.

Figure 2.5.5-1 illustrates the structural configuration of the adapter. The adapter structure is a hollow truncated core, 60 inches outside diameter on the bottom flange, 57.12 inches outside diameter on the upper flange, and 24 inches high. The shell is magnesium sheet with upper and lower channel shaped stiffening rings, vertical hot section stiffeners, and circumferential intermediate rings. The adapter is riveted construction. The upper ring provide a flange for mounting to the spacecraft through the use of the separation band. The lower ring secures the adapter to the SACS ring by means of eight interface bolts with one index hole. Internal secondary structure shown in the figure is the separation spring bracket and the separation switch bracket, with a separation switch installed. The secondary structure will require modification to add a revised stimulator and antenna pickup crossbeam in the adapter to incorporate these at the proper locations.

The existing Nimbus separation spring design, directly applicable to the ERTS spacecraft, can be extended to cover the required spring rates required by the heavier spacecraft. For the ERTS spacecraft weight, only an increase in spring wire diameter is required; an increase in spring diameter is not required. Therefore all brackets and interfaces will remain the same.

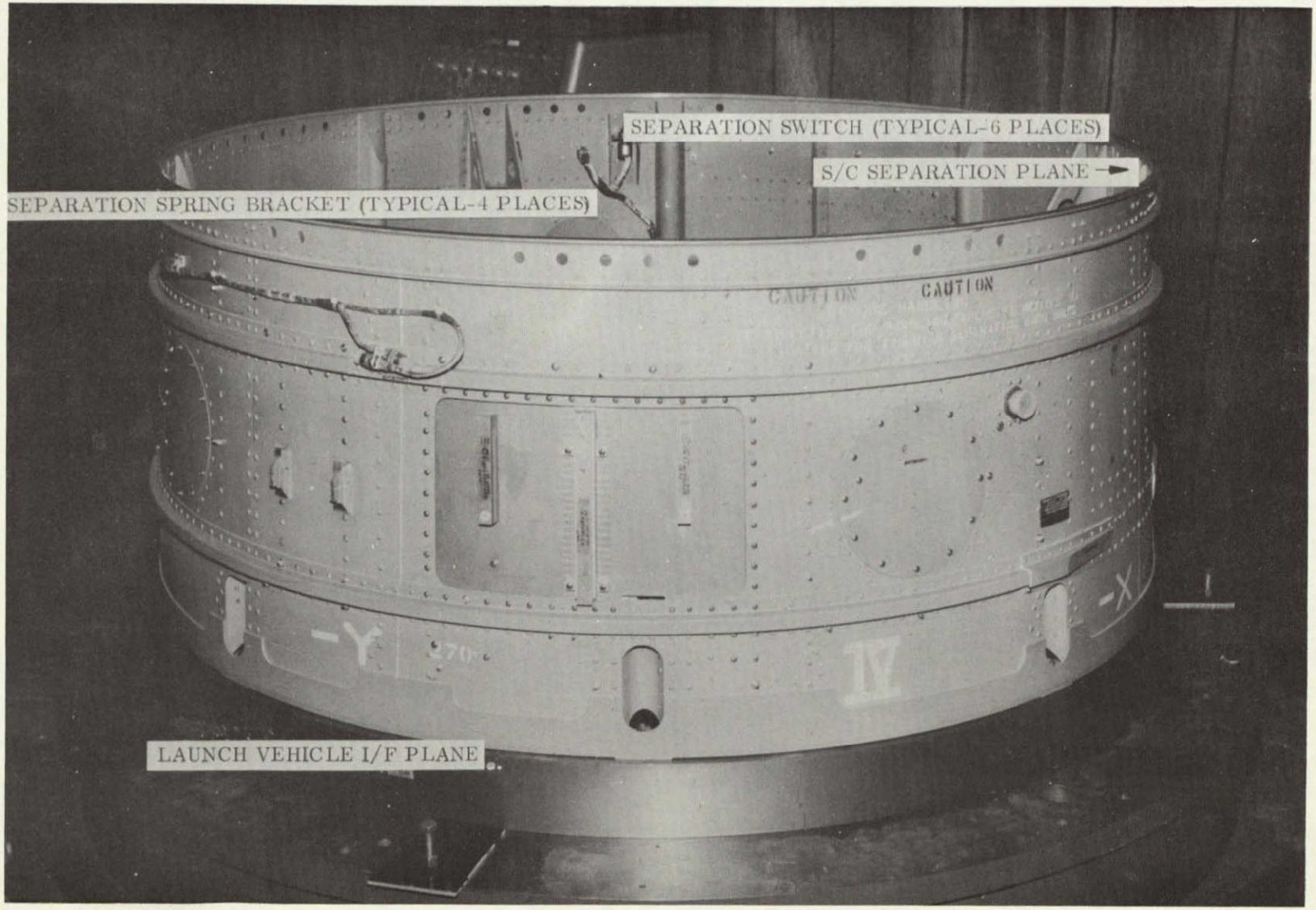

Figure 2. 5. 5-1. Structural Configuration of the Adapter

APPENDIX 2.A

LAUNCH VEHICLE - SPACECRAFT DYNAMIC ANALYSIS

2.A.1 ABSTRACT

This appendix presents results of launch vehicle dynamic analysis. In particular, Thorad Delta and Thorad Agena launch vehicles are compared in the areas of spacecraft structural environments and shroud deflections. Additionally, expected spacecraft flight loads at four trajectory points (Liftoff, maximum α Q, Meco-10, Seco II) are presented as is a comparison of flight loads with test loads.

2.A.2 LAUNCH VEHICLE ENVIRONMENT COMPARISON

2.A.2.1 COMPARISON OF NOMINAL AEROELASTIC FORCING DATA

The Thorad Agena, TAT Agena, and Thorad Delta all utilize the basic Thor vehicle with thrust augmentation. As indicated by Table 2.A.2-1, the thrust at liftoff for the Thorad Agena is the least severe, of the three. This reduced liftoff acceleration is perhaps the most significan difference in the launch vehicles in terms of transient loads imparted to the spacecraft.

TABLE 2.A.2-1. BASIC COMPARISON OF NOMINAL AEROELASTIC FORCING DATA

1. Thrust (lb)	Nimbus B/D Thorad/Agena	Nimbus C TAT-Agena	Thorad-Delta
a. Liftoff	243,300	336,450	322,659
b. Maximum airload bending	187,800	190,400	371,683
c. Maximum long oscillation (POGO)	184,900 (90%)	185,700	182,410
d. MECO	176,800	177,300	174,007
e. SECO	15,955		6,631
2. Maximum dynamic pressure(psf)	840	1400	977.89
3. MECO (g)			
a. Longitudinal load factor	6.7	7.4	7.33
4. POGO oscillation condition	(MECO-10)	(MECO-8)	(MECO-?)
a. Longitudinal load factor	5.5 ± 4.1 @ 245	6.05 ± 2.35 @ 409	5.9 ± 3.5 @ 725.8*
b. Lateral load factor	0.047 ± 0.3 @ 245	0.056 ± 0.3 @ 245	0 ± .5 @ 725.8*
5. Spacecraft Weight (lb)	1475	900	680 (Tiros M)
6. Launch vehicle weight at lift-off (lb)	201,997		226,394

*Launch vehicle station 725.8 is equivalent to spacecraft Station 245

The data presented is for a 3 solid thrust engine augmented configuration with the exception that the Thorad Delta includes a second set of three solid thrust engines which are ignited after the first set burnout. This second burn results in a higher thrust and vibration environment during maximum α Q. The final notable difference occurs in the thrust of the second stage vehicles where the Agena 15,000-pound level is over twice the Delta value.

The effects of these vehicle variations on the launch vehicle and spacecraft structural environments are discussed further in following sections of the report.

2.A.2.2 COMPARISON OF ANALYTICAL AND TEST OBSERVED VIBRATION SPECTRA

The Thorad Agena and Thorad Delta have many similarities in their vibratory spectra. Table 2.A.2-2 presents comparative analytical vibration modal frequencies for the Thorad Delta/OSO and the Thorad Agena/Nimbus B vehicles. The first two modes show close agreement for the main booster phase of flight. Modes 3 and 4 show the effects of spacecraft responses. The major vibratory loadings tend to occur at these fundamental vehicle resonances. This is substantiated by the actual flight observed data of Table 2.A.2-3.

TABLE 2.A.2-2. COMPARISON ANALYTICAL AGENA AND DELTA FREQUENCIES

		Liftoff		MAX α Q *		MECO-10	
		Agena	Delta	Agena	Delta	Agena	Delta
Axis	Mode No.	Frequency (cps)	Frequency (cps)	Frequency (cps)	Frequency (cps)	Frequency (cps)	Frequency (cps)
X-X	1	2.238	2.52	2.627	2.89	4.862	
	2	5.460	5.19	6.777	5.20	10.07	
	3	9.639	5.66	9.964	6.76	14.41	
	4	12.81	8.24	14.41	8.47	16.97	
Y-Y	1	2.239	2.50	2.629	2.89	4.877	
	2	5.469	5.62	6.795	6.72	10.06	
	3	9.673	8.07	9.969	8.36	12.07	
	4	11.78	11.23	12.10	13.39	15.26	
Longit.	1	9.567	11.77	10.70		15.59	20.35
	2	15.35	21.38	15.55		18.91	50.07
	3	15.83		16.51		26.69	
	4	22.20					

Notes: *Delta maximum α q frequency for transonic condition
**Delta lateral frequency for OSO-G delta
***Agena frequencies for Nimbus D/Agena

TABLE 2.A.2-3. LAUNCH VEHICLE MEASURED FLIGHT VIBRATION ACCELERATIONS

Flight Configuration	THORAD AGENDA						THORAD DELTA					
	X Axis (longitude)		Y Axis (lateral)		Z Axis (lateral)		Z Axis (longitude)		X Axis (pitch)		Y Axis (yaw)	
	Hz	g's	Hz	g's	Hz	g's	Hz	g's	Hz	g's	Hz	g's
Liftoff	14.3	±0.26	5.3 11.0 24.0 42.0	±0.5 ±0.12 ±0.15 ±0.28	5.3 11.0 24.0 42.0 90.0	±0.5 ±0.08 ±0.08 ±0.08 ±0.25	12-13 12-13 28	±1.0 ±1.0 ±0.5	13 13 12	±0.22 ±0.22 ±0.13		Bios 43 Bios 51
POGO	17.6	±2.49	17.6 49.0	±0.10 ±0.16	17.6 49.0	±0.07 ±0.08	19.7 49.7	±3.5	~	±0.3		±0.3 DSV-BL 2000#P1
MECO	21.2	±0.17	5.5 42.0 52.0	±0.04 ±0.12 ±0.13	5.5 26.4	±0.04 ±0.04						
SECO II	50	±0.65	19.3 52.0	±0.17 ±1.01	19.3 52.0 70.0	±0.08 ±0.15 ±0.60	50 55	±0.5 ±0.4	27 50 48	±0.1 ±0.175 ±0.095	22 48	±0.1) TOS E ±0.04) TOS F

The flight data ensemble presented herein represents OSO and Bios-Delta launch data and Nimbus B-Agena launch vehicle data. The Thorad mainstage was common to all spacecraft except Nimbus A and C. TheThorad Agena is also scheduled for Nimbus D launch.

2.A.2.3 QUASI STEADY LOAD CRITERIA COMPARISON

Table 2.A.2-4 presents a comparison of the sustained and fundamental vibratory loading criteria for the two launch vehicles. This compliation reflects a judicious envelope of flight and analytically anticipated environment for use in primary structural sizing. The most obvious difference shown here is in the increased lift-off loading environment on the Delta.

The high dynamic loads of ± 2 G's longitudinally and ± 1 G laterally result primarily from the greater thrust and flexibility of the third stage spin-up table. Since ERTS will not use a third stage, ±0.5 G's was felt to be a more realistic value for lateral vibratory loadings at liftoff.

Maximum α Q on the Delta is more severe in terms of spacecraft dynamic loads because of the additional solid booster thrust loads at this time. MECO-10 on the Delta is anticipated to follow the same trends as the Agena with regard to magnitude and frequency. At present, the Thorad Delta "POGO" occurs about 19 Hertz and 3.5 g's O-peak maximum and the Thorad Agena evidences 17 Hertz and 4.1 g's maximum O-peak.

Thrust transient events during second stage flight of the Delta appear to cause vibratory loadings of equivalent severity even though the engine thrust is half as great. This may be due to close tuning of the longitudinal vibration modes of the spacecraft and launch vehicle second stage.

2.A.2.4. SUMMARY OF DELTA/AGENA LOAD RATIOS

In view of the recent coupled launch vehicle and Nimbus D spacecraft analysis activity, it was possible to extrapolate the results in a preliminary fashion on the basis of flight and analytically anticipated behavior of an ERTS/Delta launch (Table 2.A.2-5). The vibratory and sustained components were individually considered.

The most drastic changes in transient loading occur at liftoff and maximum α Q along the thrust axis. Fortunately, the spacecraft is fairly rigid along the longitudinal axis at those flight times and no serious structural problems result. However, the addition of sustained accelerative loadings at maximum α Q does complicate matters and the total summation of flight loadings make it the most severe condition for the spacecraft on the Delta launch vehicle. The tabulations of flight loads at several interfaces on the ERTS are computed in the next section using these factors and provide numerical comparitive data.

TABLE 2.A.2-4. SPACECRAFT INTERFACE QUASI-STEADY LOAD FACTORS

Flight Condition Limit Level	Nimbus E Delta Acceleration (g's)	Nimbus B Agena Thorad Acceleration (g's)
1. Liftoff		
a. Steady state, longitude	1.25	1.28
b. Oscillating, longitude	±2.0	-0.0005
c. Oscillating, latitude	±0.5	±0.19
2. Transonic - near maximum α Q		
a. Steady state, longitude	2.4	1.22
b. Steady state, latitude	0.3	0.22
c. Oscillating, longitude	±1.5	±0.3
d. Oscillating, latitude	±1.0	±1.0
3. POGO		
a. Steady state, longitude	5.9	5.33
b. Steady state, latitude	0	0.047
c. Oscillating, longitude	±3.5	±4.0
d. Oscillating, latitude	±0.5	±0.30
4. MECO		
a. Steady state, longitude	7.7	6.4
b. Steady state, latitude	0.5	
5. Agena 1st ignition		
a. Steady state, longitude		1.91
b. Steady state, latitude		0.075
c. Oscillating, longitude		-0.46
d. Oscillating, latitude		+0.017 to -0.074
6. Agena 2nd ignition		
a. Steady state, longitude		6.1
b. Steady state, latitude		0.34
c. Oscillating, longitude		-0.11
d. Oscillating, latitude		+0.252 to -0.077
7. Agena 2nd cutoff		
a. Steady state, longitude	2.5	5.42
b. Steady state, latitude		0
c. Oscillating, longitude		-2.03
d. Oscillating, latitude		+0.072 to -0.006

TABLE 2.A.2-5. SUMMARY OF DELTA/AGENA LOAD RATIOS

	Transient			Sustained		
	X	Y	Z	X	Y	Z
Liftoff	$\frac{0.5}{0.19}$	$\frac{0.5}{0.19}$	$\frac{2.0}{0.1}$	same	same	same
Maximum α Q	same	same	$\frac{1.5}{2.0} \times \frac{2.0}{0.1}$	$\frac{0.3}{0.22}$	$\frac{0.3}{0.22}$	$\frac{2.4}{1.22}$
MECO-10	$\frac{0.5}{0.3}$ same	$\frac{0.5}{0.3}$ same	$\frac{3.5}{4.1}$ ~same	same	same	$\left(\frac{5.9}{5.33}\right)$ ~same
SECO	same	same	same	same	same	$\frac{2.5}{5.42}$

2.A.3 FLIGHT LOADS ANALYSIS

Interface loads within the spacecraft structure were determined at the following locations and are shown in Figure 2.A.3-1:

1. Right-hand paddle shaft (+Y Axis)
2. Left-hand paddle shaft
3. Paddle tie-down
4. Control box/truss
5. Truss/sensory system
6. Sensory system/adapter
7. Adapter/booster

Four flight conditions were selected as shown by the load summary table:

1. Liftoff
2. Maximum αQ
3. Meco-10
4. SECO II

These flight conditions are the most critical in terms of structural loads for both launch vehicles. Furthermore, in view of the close similarity in their dynamic envrionment, extrapolations of the recently completed Nimbus D/Agena flight loads results, provide a good estimate of ERTS load levels until more definitive analyses are completed. Tables 2.A.3-1 through 2.A.3-4 present the detailed tabulations for a 1450-pound spacecraft.

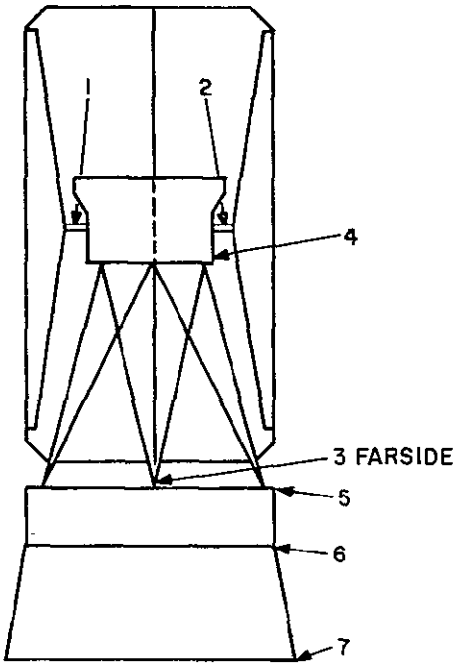

INTERFACE	LOCATION
1	RIGHT-HAND PADDLE SHAFT
2	LEFT-HAND PADDLE SHAFT
3	PADDLE TIE-DOWN
4	CONTROL BOX / TRUSS
5	TRUSS / SENSORY SYSTEM
6	SENSORY SYSTEM / ADAPTER
7	ADAPTER / BOOSTER

Figure 2.A.3-1. ERTS Spacecraft Structure Interfaces

2.A.4 SHROUD DEFLECTIONS

The equations utilized in the clearance deflections extrapolations are summarized below:

$$\delta_{\substack{\text{ERTS}\\\text{Delta}}} = \delta_{\substack{\text{Nimbus B}\\\text{Agena}}} \times \begin{matrix}\text{Flight Load}\\\text{Factor Ratio}\end{matrix} \times \begin{matrix}\text{Stiffness}\\\text{Factor Ratio}\end{matrix}$$

$$\delta_{\substack{\text{Delta Minimum}\\\text{Clearance}}} = \delta_{\substack{\text{Minimum Net}\\\text{Clearance}}} - \sum \left(\delta_{\substack{\text{Static}\\\text{Shroud}}} + \delta_{\substack{\text{Spacecraft}\\\text{Static}}} + \delta_{\substack{\text{Relative}\\\text{Dynamic}\\\text{S/C-Shrous}}} \right)$$

Where δ = deflection dimension in inches

Table 2.A.4-1, 2.1.4-2 and 2.A.4-3 are tabulations of the data used in calculation of the shroud spacecraft clearances. All of the data was computed for the Maximum δ q flight condition. Since the highese combination of flight and aerodynamically induced deflection occurs at this time. Figure 2.A.4-1 is a comparison of shroud deflections.

TABLE 2.A.3-1. LIFTOFF LOADS

Load Component		Transient Response X	Transient Response Y	Transient Response Z	Sustained Load X	Sustained Load Y	Sustained Load Z	Total Loading (X+Z)	Total Loading (Y+Z)
L/H(Left-hand) paddle shaft	Fx	42	37	0	7	3	0	49	40
	Fy	18.5	66	0	3	7	0	21.5	73
	Fz	8	47.5	20	0	0	27	55	94.5
R/H(Right-hand) paddle shaft	Fx	39.5	34	0	7	3	0	46.5	37
	Fy	21	66	0	3	7	0	24	73
	Fz	5.2	45	1	0	0	26	32.2	72
Paddle tie-down	Fz	16	5.2	40	1	0	46	103	91.2
Control box/ Truss Interface	Fx	287	18.5	20	60	0	0	367	38.5
	Fy	5.2	490	20	0	60	0	25.2	570
	Fz	18.5	5.2	140	1	60	360	519.5	505.2
	Mx	190	4650	2600	0	259	326	3116	7835
	My	1350	216	180	25	0	398	1953	794
	Mz	310	1418	100	48	122	0	532	1640
Truss/sensory System Interface	Fx	284	18.5	20	0	0	0	364	38.5
	Fy	5.2	490	20	0	60	0	25.2	570
	Fz	21	5.2	20	0	0	406	447	431.2
	Mx	140	27750	760	3099	3099	326	1226	31935
	My	15300	1230	500	0	0	918	19817	2648
	Mz	310	1415	100	48	122	0	458	1637
Sensory ring/ Adapter Interface	Fx	950	116	20	252	0	0	1222	136
	Fy	21	1470	20	0	252	0	41	1742
	Fz	31.5	13	680	0	0	1704	2415.5	2397
	Mx	198	41550	700	0	492	202	1100	42944
	My	24400	1325	300	4921	0	66	29687	1691
	Mz	926	4900	560	30	24	0	1516	5484
Adapter/delta Interface	Fx	1010	116	20	275	0	0	1305	136
	Fy	21	1520	20	0	275	0	41	1815
	Fz	31.5	13	740	0	0	1865	2636.5	2618
	Mx	547	76600	740	0	10980	633	1920	88961
	My	47500	2330	320	10980	0	129	58929	2779
	Mz	1100	4900	540	94	34	0	1734	5474

TABLE 2.A.3-2. MAXIMUM ALPHA-Q LOADS

Load Component		Transient Response			Sustained Load		Total Loading	
		X	Y	X	Y	Z	(X+Z)	(Y+Z)
Left-hand paddle shaft	Fx	22	10	63	2.7	0	85	12.7
	Fy	11	20	30	63	0	41	83
	Fz	6	12	2.7	2.7	61	69.7	75.7
Right-hand paddle shaft	Fx	20	9	63	30	0	83	39
	Fy	9	19	30	63	0	39	82
	Fz	4	11	2.7	2.7	61	67.7	74.7
Paddle tie-down	Fz	8	1	4.1	0	108	120.1	109
Control box/ Truss Interface	Fx	155	3	525	0	0	680	3
	Fy	4	160	0	53	0	4	213
	Fz	12	2	4.1	0	841	857.1	843
	Mx	113	1361	0	2281	761	874	4403
	My	270	42	2160	0	930	3360	972
	Mz	160	332	426	1069	0	1555	1401
Truss/Sensory System Interface	Fx	155	3	525	0	0	680	3
	Fy	4	160	0	525	0	4	685
	Fz	16	4	0	0	949	965	953
	Mx	91	8811	0	27200	761	852	36772
	My	8176	198	27200	0	2140	37516	2338
	Mz	160	332	426	1069	0	586	1401
Sensory ring/ Adapter Interface	Fx	498	24	2218	0	0	2716	24
	Fy	13	444	0	2218	0	13	2662
	Fz	23	7	0	0	3990	4013	3997
	Mx	107	13224	1.4	43200	472	580.4	56896
	My	13036	222	43200	1.4	153	56839	376.4
	Mz	584	886	264	212	0	948	1098
Adapter/Delta Interface	Fx	526	24	2414	0	0	2940	24
	Fy	13	470	0	2414	0	13	2884
	Fz	24	7	0	0	4350	4374	4357
	Mx	355	23978	0	96500	1480	1835	120487
	My	25074	648	96500	0	303	121877	951
	Mz	628	893	823	294	0	1451	1187

TABLE 2.A.3-3. MECO-10 LOADS

Load Component		Transient Response			Sustained Load			Total Loading
		X	Y	Z	X	Y	Z	(X+Y+Z)
Left-hand paddle shaft	Fx	234	9	15	2	1	0	261
	Fy	95	6	64	1	2	0	168
	Fz	80	37	310	0	0	115	542
Right-hand paddle shaft	Fx	195	6	27	2	1	0	231
	Fy	56	1	32	1	2	0	92
	Fz	24	38	283	0	0	114	459
Paddle tie-down		6	9	219	0	0	200	434
Control box/ Truss Interface	Fx	931	1	100	20	0	0	1052
	Fy	38	13	125	0	20	0	196
	Fz	182	22	1296	0	0	1556	3056
	Mx	1495	1395	2532	0	102	1408	6932
	My	4092	202	795	9	0	1702	6800
	Mz	1722	635	961	16	41	0	3375
Truss/Sensory System Interface	Fx	931	1	100	20	0	0	1052
	Fy	38	132	125	0	20	0	215
	Fz	176	30	1077	0	0	1755	3038
	Mx	294	4904	8468	0	1048	1408	16122
	My	48500	45	2288	10481	0	3967	65281
	Mz	1722	64	961	16	41	0	2804
Sensory ring/ Adapter Interface	Fx	2075	138	221	73	0	0	2507
	Fy	120	166	78	0	73	0	437
	Fz	250	60	3789	0	0	7363	11462
	Mx	27	10449	7915	5	1674	874	20944
	My	73774	1055	1776	1680	5	285	78575
	Mz	4748	3687	5480	10	1	0	13926
Adapter/Delta Interface	Fx	2086	138	226	79	0	0	2529
	Fy	120	145	79	0	79	0	423
	Fz	250	63	4115	0	0	8020	12448
	Mx	2800	15040	6970	0	3441	2736	30987
	My	124158	4466	3407	3443	3	559	136026
	Mz	4719	3695	5463	26	2	0	13905

TABLE 2.A.3-4. SECO II LOADS

Load Component		Transient Response		Sustained Load			Total Loading	
		X	YZ	X	Y	Z	(XZ+XZ)	(YZ+XZ)
Left-hand paddle shaft	Fx	29	22	3	1	0	32	23
	Fy	92	90	1	3	0	93	93
	Fz	407	408	0	0	51.5	458.5	459.5
Right-hand paddle shaft	Fx	43	35	3	1	0	46	36
	Fy	107	102	1	3	0	108	105
	Fz	310	310	0	0	51.5	361.5	361.5
Paddle tie-down		557	555.5	0	0	90	647	645.5
Control box/ Truss Interface	Fx	311	247	23	0	0	334	247
	Fy	90	88	0	23	0	90	111
	Fz	1222	1222	0	0	704	1926	1926
	Mx	4927	4925	0	98	636	5563	5659
	My	1263	953	93	0	776	2132	1729
	Mz	1507	1530	18	46	0	1525	1576
Truss/Sensory System Interface	Fx	311	247	23	0	0	311	247
	Fy	90	88	0	23	0	90	111
	Fz	1386	1385	0	0	794	2180	2179
	Mx	9176	9088	0	1174	636	9812	10898
	My	16453	13031	1174	0	1790	19417	14821
	Mz	1507	1530	18	46	0	1525	1576
Sensory ring/ Adapter Interface	Fx	892	655	96	0	0	988	655
	Fy	363	382	0	96	0	363	478
	Fz	1774	1777	0	0	3330	5104	5107
	Mx	13859	14185	0	1865	396	14255	16446
	My	19221	13442	1865	0	129	21215	13571
	Mz	6596	6422	11	9	0	6607	6431
Adapter/Delta Interface	Fx	916	671	104	0	0	1010	671
	Fy	362	433	0	104	0	362	507
	Fz	1686	1697	0	0	3625	5305	5322
	Mx	22315	35104	0	4161	1281	23596	40546
	My	35885	24284	4161	0	252	40298	24536
	Mz	6688	6431	36	13	0	6724	6444

TABLE 2.A.4-1. CLEARANCE TABLE TABULATION

Static Shroud Deflections

Station	Nimbus B Shroud	Load Factor	Deflection Factor	Delta Shroud	Deflection Factor	Delta Shroud
107	0.222	1.36	2.0	0.604	2.76	0.833
196.6	0.078	1.36	2.0	0.212	2.76	0.293
209	0.058	1.36	2.0	0.158	2.76	0.218
223	0.034	1.36	2.0	0.092	2.76	0.128
237	0.012	1.36	2.0	0.033	2.76	0.045

TABLE 2.A.4-2. RELATIVE DYNAMIC DELFECTIONS OF SPACECRAFT SHROUD

Station	Nimbus B RDS	Deflection Factor	ERTS RDS	Deflection Factor	ERTS RDS
107	0.160	2.0	0.230	2.76	0.441
196.6	0.125	2.0	0.250	2.76	0.345
209	0.139	2.0	0.278	2.76	0.384
223		2.0		2.76	
237	0.0273	2.0	0.0546	2.76	0.076

TABLE 2.A.4-3. STATIC SPACECRAFT DEFLECTIONS

Station	Nimbus G Spacecraft	Load Factor	Deflection Factor	ERTS Spacecraft 1 x 2 x 3	Total Static Deflection Shroud Spacecraft	Total Deflection (Deflection Factor = 2.0)
107	0.018	1.36	0.775	0.019	0.623	0.858
196.6	0.008	1.36	0.775	0.0085	0.2205	0.304
209					0.158	0.218
223					0.092	0.128
237					0.033	0.045

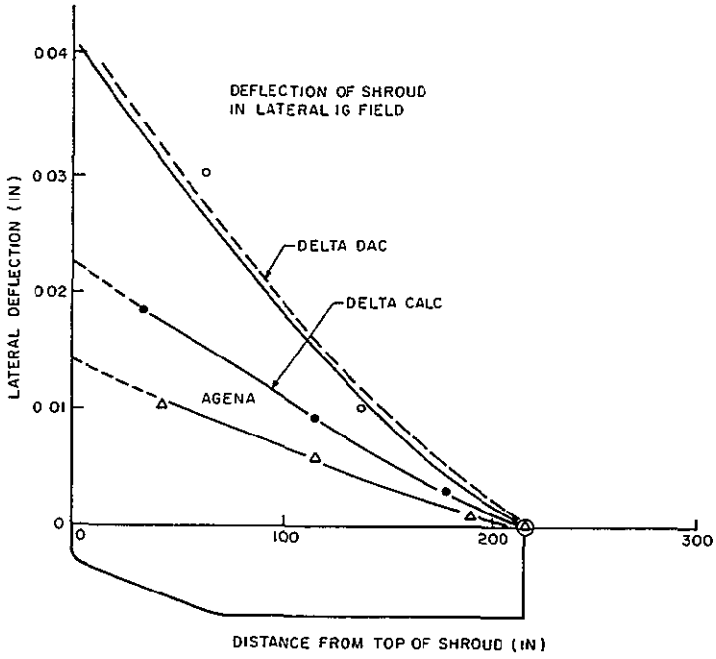

Figure 2.A.4-1. Comparison of Shroud Deflection

2.A.5 REFERENCES FOR APPENDIX 2.A

2.A.1. McDonnell Douglas Report DAC 61864, "Detailed Test Objectives for Long Tank Delta (Six Solids-Retrofit) Launch Vehicle, Spacecraft: Tiros M," May 1969.

2.A.2. McDonnell Douglas Report DAC 61731, "Mode Shapes and Dynamic Response Functions for the OSO-G Spacecraft Model DSV-3L," October 17, 1968.

2.A.3. LMSC Report A879342, "Nimbus B Vehicle Structural Dynamic Analysis" June 5, 1967.

2.A.4. LMSC Report A730557, "Nimbus A Agena 6201 Environmental Data Analysis Report," 25 January 1965.

2.A.5. LMSC Report A824514, "Nimbus C NASA Agena Vehicle 6202 Flight Evaluation and Performance Analysis Report," 24 June 1966.

2.A.6. LMSC Report D051821, "Report No. 67-5 for the Nimbus B-2 Mission Tag Design Trajectory (U)," dated 7 February 1969.

2.A.7. GE Document 68SD4221, "Nimbus B Spacecraft Structural Loads Analysis for Launch Environment," February 1968.

APPENDIX 2.B

DYNAMIC ANALYSIS VIBRATION TESTS LOADS

2.B.1 ABSTRACT

This appendix presents the results of the basic vibratory loads analysis for a projected 1621-pound spacecraft. These loads represent the dynamic response of the primary structure undergoing unnotched sinusoidal qualification test level vibration environment on a dynamic exciter. Delta vehicle vibration specification input level without notching was applied to the base of the adapter.

2.B.2 SUMMARY

This report presents prototype loads for the initial sizing of the ERTS strcuture. The loads given here are considered preliminary because they utilize a weight distribution effective at the time the analysis was performed but no longer current. The primary structural loads predictions contained herein are representative and will not be significantly altered by subsequent changes in the vehicle. As such, they are considered adequate for sizing of the structure and notching studies. However, an updated analysis will be released with the final notching study.

The information contained herein are basic vibratory load magnitudes which are imparted to the primary structure undergoing an unnotched sinusoidal qualification test level vibration environment on a dynamic exciter.. They are considered the maximum structural loading that is imparted to the spacecraft and provide the basis upon which investigations are made on the spacecraft structural integrity.

This analysis forms the first part of a structural evaluation underway, utilizing the existing Nimbus structural design with some minor changes, weighted to the ERTS configuration. The objective of these studies is to determine:

1. The capability of the existing structure to survive a qualification level vibration test.
2. The amount of test level vibration input limiting (notching) necessary to assure that flight level loads are not exceeded

Vehicle modal frequencies, responses, and major interface loads were extrapolated from modal test data of a Nimbus spacecraft using a matrix analysis technique for the extrapolation. Results of this study, when compared with a similar study for the Nimbus "D" 1500-pound spacecraft, indicate slightly lower resonant frequencies for the ERTS. Dynamic loads for ERTS have increased due to increased input levels and increased weight. Evaluation of stresses due to these increased loads is currently underway.

2.B.3 INTRODUCTION

An interface dynamic loads analysis was performed using the projected weight for the ERTS spacecraft given in Reference 1.

This differs from the Nimbus "D" 1500-pound spacecraft mainly in the weight of the sensory ring--1191 pounds for ERTS vs. 1046 pounds for Nimbus "D" and adapter. The modal extrapolation technique and matrix methods are similar to the analysis of Reference 2, and a brief description of the analytical approach is given under Section 2.B.4.

The Delta vehicle vibration specification input level without limiting (notches) was applied to the base of the adapter (spacecraft/booster interface). The mathematical model weight breakdown derived from Reference 1 is given in Table 2.B-1 Input levels and modal damping values are given in Table 2. B-3. The lateral input level for the first four modes has increased by 30 percent over those for Nimbus "D".

2.B.4 LOAD ANALYSIS METHOD

2.B.4.1 EXTRAPOLATION OF NATURAL FREQUENCIES AND MODE SHAPES

The extrapolation of the Nimbus modal test data to the ERTS included the effects of increased weight eccentrically located in the sensory ring and a stiffened crossbeam. Simple vibration analysis of the weighted crossbeam indicated its fundamental resonance to be above 100 cps which is beyond the significant fundamental spacecraft resonance range and justified the use of a rigid beam. This results in an equation of the form:

$$[K + \Delta K]\{X\} = [M + \Delta M]\{X\}\lambda \qquad (2.B.4\text{-}1)$$

which can be written is partitioned form as:

$$\left[\begin{bmatrix} K_{11} & K_{12} \\ K_{21} & K_{22} \end{bmatrix} + \begin{bmatrix} 0 & 0 \\ 0 & \Delta K_{22} \end{bmatrix}\right]\begin{Bmatrix} X_1 \\ X_2 \end{Bmatrix} = \left[\begin{bmatrix} M_1 & 0 \\ 0 & M_2 \end{bmatrix} = \begin{bmatrix} \Delta M_1 & 0 \\ 0 & \Delta M_2 \end{bmatrix}\right]\begin{Bmatrix} X_1 \\ X_2 \end{Bmatrix}\lambda \qquad (2.B.4\text{-}2)$$

where K is a matrix of stiffness coefficients

M is a matrix of mass items

X is a vector of displacement

λ is a scalar resonant frequency

subscript $_1$ coordinates associated with original Nimbus

$_2$ coordinates associated with modified structure

The vector X can be represented by a new vector Y as:

$$\begin{Bmatrix} X_1 \\ X_2 \end{Bmatrix} = \begin{bmatrix} \phi_1 \\ \hline \phi_2 \end{bmatrix}\{\gamma\} \qquad (2.B.4\text{-}4)$$

where

$\begin{bmatrix} \phi_1 \\ \phi_2 \end{bmatrix}$ are the partitioned mode shapes of the original Nimbus vehicle (19 flexible modes, 154 coordinates per mode)

Substituting for X in equation 2. B. 4-2 and multiplying both sides of equation 2. B. 4-2 by

$$\begin{bmatrix} \phi_1^T & \phi_2^T \end{bmatrix}$$

yields

$$\left[[\lambda 1] + [\phi_2^T \Delta K_{22} \phi 2]\right] \{Y\} = \left[[I] + [\Delta M^*]\right] \{Y\} \quad \lambda \qquad (2.B.4\text{-}4)$$

Since

$$\lambda_1 = \begin{bmatrix} \phi_1^T & \phi_2^T \end{bmatrix} \begin{bmatrix} K_{11} & K_{12} \\ K_{21} & K_{22} \end{bmatrix} \begin{bmatrix} \phi_1 \\ \phi_2 \end{bmatrix}$$ = generalized stiffness of original spacecraft structure

$$I = \begin{bmatrix} \phi_1^T & \phi_2^T \end{bmatrix} \begin{bmatrix} M_1 & 0 \\ 0 & M_2 \end{bmatrix} \begin{bmatrix} \phi_1 \\ \phi_2 \end{bmatrix}$$ = generalized mass of original spacecraft

$$\Delta M^* = \begin{bmatrix} \phi_1^T & \phi_2^T \end{bmatrix} \begin{bmatrix} \Delta M_1 & 0 \\ 0 & \Delta M_2 \end{bmatrix} \begin{bmatrix} \phi_1 \\ \phi_2 \end{bmatrix}$$ = change in generalized mass

If the matrix

$$\Delta\lambda = \begin{bmatrix} \phi_2^T \Delta K_{22} \phi 2 \end{bmatrix}$$

is known, equation (2.B.4-4) is the familiar eigenvalue problem for which a computer program exists.

Solution of equation (2.B.4-4) yields a new set of mode shapes and resonant frequencies of the ERTS configuration where:

$$\begin{bmatrix} \phi^T \text{NEW} \end{bmatrix} \begin{bmatrix} I + \Delta M^* \end{bmatrix} \begin{bmatrix} \phi \text{NEW} \end{bmatrix} = \begin{bmatrix} I \end{bmatrix}$$ the identity matrix

Returing to equation (2.B.4-4) and considering the equality of both sides, it is possible to alter the stiffness of a particular portion of the structure (i.e., ΔK_{22}) by redistributing the mass into adjacent coordinates.

Since ERTS crossbeam mass and structure are being designed to a fundamental resonance above 100 cps, it appears rigid to the lower vehicle resonances and can be treated as an

integral part of the sensory ring. This effect was accomplished by the redistribution of the crossbeam masses into the surrounding sensory ring coordinates.

2.B.4.2 LOADS ANALYSIS

The fixed-free natural frequencies and associated normal mode shapes of the ERTS were determined by the methods described herein and in Reference 2. These mode shapes together with their frequencies and generalized masses were used to obtain loads in the ERTS structure at six interfaces:

1. ends of the paddle shaft
2. paddle tie-down
3. base of the control box
4. base of the truss
5. base of the sensory subsystem
6. base of the adapter

Loads are calculated by summing the inertia forces which must be carried across the interfaces. That is:

$$F = T\ W\ Y$$ (See Table 2B-6)

where

F is a column of force components at the interfaces

T is a matrix which sums the inertia forces

W is a diagonal matrix of weights

Y is a column of accelerations in gravitational units

At resonance the acceleration response vector Y is:

$$Y = \phi^{(r)}\ \xi_q^{(r)}$$

where

$\phi^{(r)}$ is the mode shape associated with the resonant frequency

$\xi_q^{(r)}$ is the quadrature modal acceleration of the resonant mode shape in gravitational units

and

$$\ddot{\xi}_q^{(r)} = \frac{1}{g}\ \phi^{(r)T}\ W\ \phi_{RB}\ X_B \qquad \text{Where } \phi^{(r)T}\ W\ \phi^{(r)} = 1$$

where

ϕ_{RB} is the rigid body mode shape

g is the structural damping

$\phi^{(r)T}$ is the transposal of $\phi^{(r)}$

X_B is the base acceleration in gravitational units.

2.B.5 CONVENTIONS

2.B.5.1 Axes

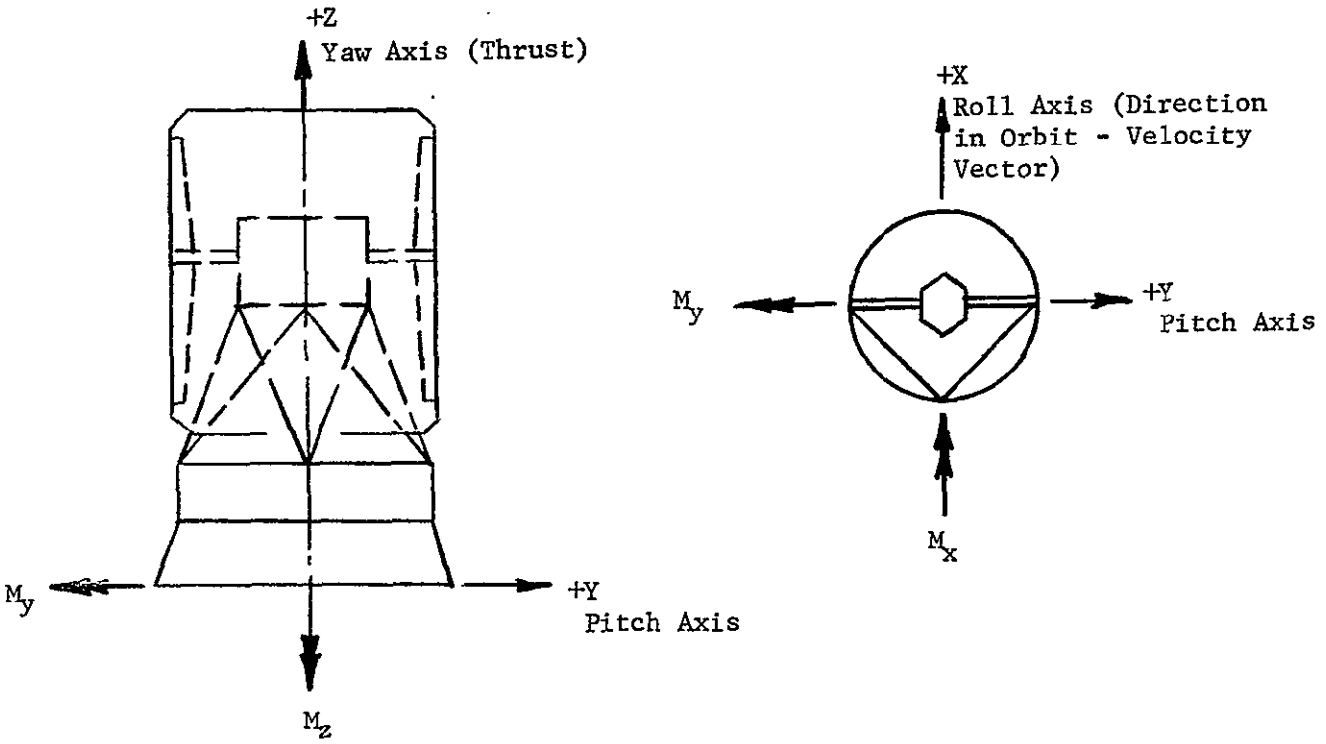

2.B.5.1.1 Roll Axis

The roll (X) axis is tangential to the orbit, and angular motions about this axis are described as roll motions. Components of linear displacement or acceleration along this axis are described as "Roll Components," although no angular motion is implied, and the "Roll Axis" defines direction only.

2.B.5.1.2 Yaw Axis

The yaw (Z) axis of the spacecraft is maintained along the zenith by the control system when the spacecraft is in orbit. During power flight, the rocket thrust acts along this axis. It should be noted that the spacecraft rotates 90 degrees about the pitch axis upon separation from the adapter.

2.B.5.1.3 Pitch Axis

The pitch (Y) axis is mutally perpendicular to the yaw and roll axes.

2.B.5.1.4 Origin

The origin may be considered at the geometric center of a plane at the bottom of the Nimbus adapter. Dimensions to points on the spacecraft are measured from this origin.

2.B.5.1.5 Axis Symbols

Yaw Axis	Z
Roll Axis	X
Pitch Axis	Y

Subscripts x, y, z will be used to denote acceleration, displacement, or force components.

2.B.6 SIGN CONVENTIONS

2.B.6.1 DISTANCES

Positive directions of axes are as shown in the Figure under Section 2.B.4.1.

2.B.6.2 FORCES

Forces are positive when acting along the positive axis shown in the Figure under Section 2.B.5.1.

2.B.6.3 MOMENTS

Moments are positive as indicated by double arrows in the Figure under Section 2.B.5.1. Moments are positive in the sense of the motion of a right hand screw.

2.B.7 RESULTS

The loads at six major interfaces (see Table 2B-6) are presented in tabular computer output form. Resonant frequencies for ERTS are shown in Table 2B-4 which also contains Nimbus "D" frequencies for comparison.

The increased weight lowers the ERTS frequencies to values, at most, two percent below Nimbus "D". A comparison of loads at three of the interfaces is shown in Table 2B-5. As expected, increased weight in the sensory ring combined with higher input levels has caused loads to be higher for the ERTS spacecraft. In particular, paddle tie down axial force has increased by 31 percent input level coincidentally increased 30 percent. Shear force in the paddle shaft area has increased 42 percent, while sensory ring base shear force has increased 63 percent.

The stresses due to the increased loads are currently being evaluated and critical members will be identified. Based on this, appropriate modifications to the structure will be recommended.

2.B.8 REFERENCES

1. ERTS November Weight Status Report, 114E-ERTS-047, 12/10/69.
2. Nimbus B Loads Analysis, PIR 4145d-912-083, 3/25/65.

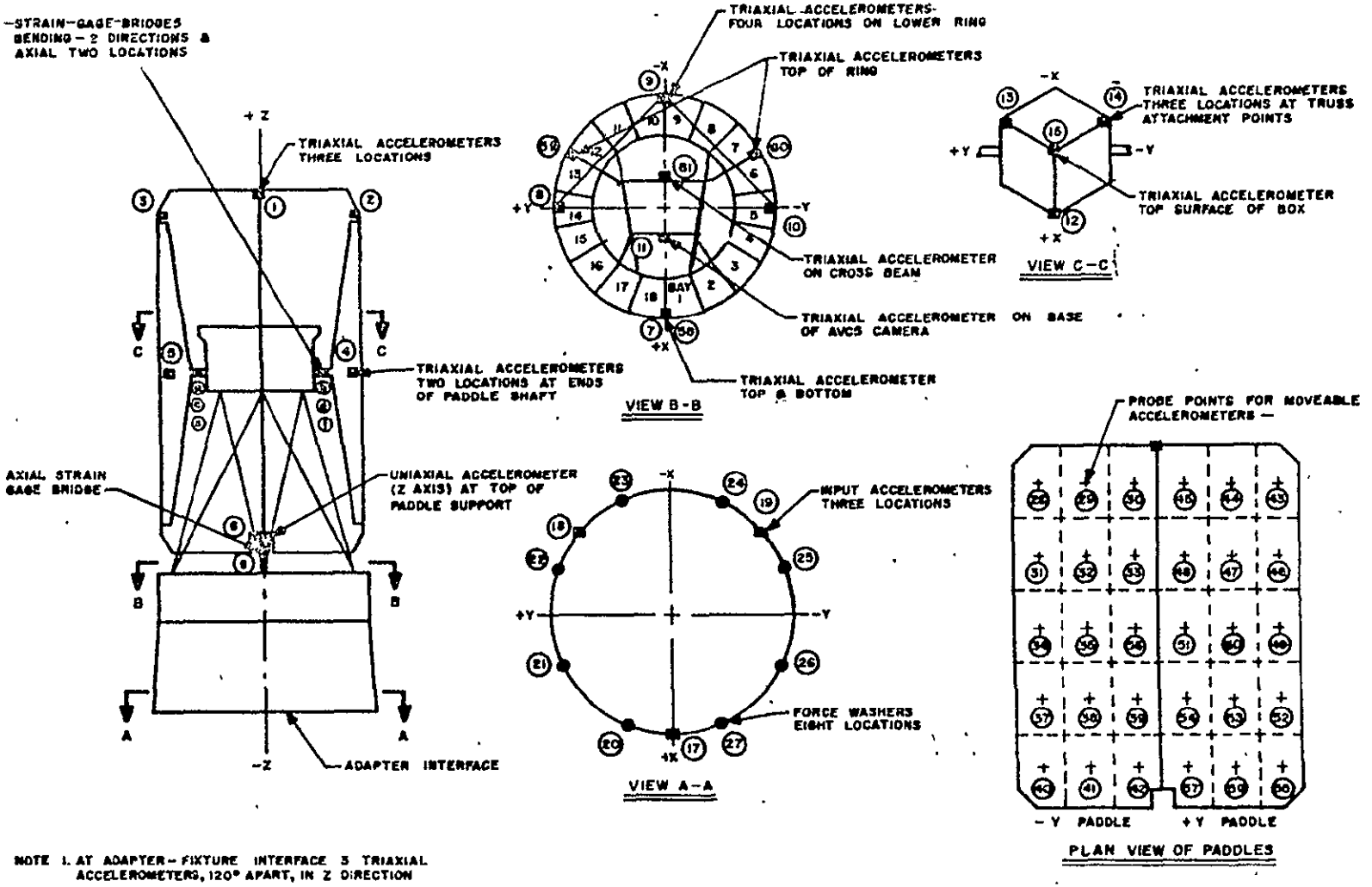

NOTE 1. AT ADAPTER – FIXTURE INTERFACE 3 TRIAXIAL ACCELEROMETERS, 120° APART, IN Z DIRECTION

2. (X) DESIGNATES INSTRUMENTATION IDENTIFICATION – REFER TO SECTION 10.7 IN G.E. DOCUMENT 64 SD 4254 FOR DESCRIPTION. (Reference 2)

Figure 2. B-1. Transducer Locations

TABLE 2.B.1. ERTS WEIGHT, GEOMETRY (REF. FIGURE 1)

Accel. No.	Wt. Lbs.	X ins.	Y ins.	Z ins.	Accel. No.	Wt. Lbs.	X ins.	Y ins.	Z ins.
1	1.65	-25.73	1.414	135.59	32	1.61	-13.69	-13.36	109.59
2	.80	-2.12	-25.03	132.59	33	1.90	-22.17	-4.88	109.59
3	.79	-2.12	25.03	132.59	34	4.39	-6.61	-20.44	90.09
4	2.2	-1.0	-23.55	85.59	35	3.22	-12.65	-14.4	90.09
5	2.2	-1.0	-23.55	85.59	36	3.52	-22.17	-4.88	90.09
6	2.71	-28.50	0	47.47	37	2.78	-4.47	-22.58	72.59
7	173.59	28.45	-1.5	24.09	38	1.61	-14.05	-13.0	71.09
8	169.19	5.0	28.0	24.09	39	1.90	-22.53	-4.52	71.09
9	232.40	-28.45	1.5	24.09	40	1.79	-6.97	-20.80	52.59
10	144.76	-5.0	-28.0	24.09	41	1.79	-13.69	-13.36	53.59
11	1.0	9.62	2.4	28.59	42	2.08	-22.17	-4.88	52.59
12	87.53	10.4	0	84.84	43	0.98	-6.97	20.8	129.59
13	42.73	-5.05	9.0	84.84	44	1.79	-13.69	13.36	131.09
14	72.6	-5.05	-9.0	84.84	45	1.27	-21.	5.85	129.59
15	49.13	0	0	101.84	46	2.76	-4.95	22.1	109.59
16					47	1.60	-14.05	13.0	108.59
17	33.	28.0	-8.6	-1.0	48	1.88	-22.10	4.95	109.59
18	33.	-13.5	28.0	-1.0	49	4.37	-5.66	21.39	90.09
19	33.	-13.25	-28.0	-1.0	50	3.19	-14.05	13.0	90.09
20		27.6	10.77	0	51	3.48	-22.17	4.88	90.09
21		11.57	26.7	0	52	2.76	-5.66	21.39	72.84
22		-11.57	26.7	0	53	1.60	-13.69	-13.36	72.84
23		-27.6	10.77	0	54	1.88	-22.53	4.52	72.84
24		-27.6	-10.77	0	55	1.79	-5.66	21.39	54.09
25		-11.7	-26.7	0	56	1.79	-13.69	13.36	53.59
26		11.7	26.7	0	57	2.07	-21.81	5.24	53.59
27		27.6	-10.77	0	58	155.15	28.0	0	37.09
28	0.99	-6.61	-20.44	129.59	59	164.26	-14.23	24.6	37.09
29	1.79	-13.69	-13.36	129.59	60	151.26	-14.23	-24.6	37.09
30	1.69	-21.81	-5.24	129.59	61	1.0	-8.87	0	34.09
31	2.78	-5.2	-21.85	109.59					

TABLE 2.B.2. IDENTIFICATION OF ROWS OF IBM PRINTOUT

Row No.	Accel.	Description	Row No.	Accel.	Description	Row No.	Accel.	Description
1	1X	Paddle	53	61X	Cross Beam	104	44X	Right
2	1Y	Perimeter	54	61Y	Cross Beam	105	44Y	Paddle
3	1Z	↓	55	61Z	Cross Beam	106	44Z	↓
4	2X		56	28X	Left	107	45X	
5	2Y		57	28Y	Paddle	108	45Y	
6	2Z		58	28Z	↓	109	45Z	
7	3X		59	29X		110	46X	
8	3Y		60	29Y		111	46Y	
9	3Z		61	29Z		112	46Z	
10	4X		62	30X		113	47X	
11	4Y		63	30Y		114	47Y	
12	4Z		64	30Z		115	47Z	
13	5X		65	31X		116	48X	
14	5Y		66	31Y		117	48Y	
15	5Z		67	31Z		118	48Z	
16	6Z	↓	68	32X		119	49X	
17	12X	Control	69	32Y		120	49Y	
18	12Y	Box	70	32Z		121	49Z	
19	12Z	↓	71	33X		122	50X	
20	13X		72	33Y		123	50Y	
21	13Y		73	33Z		124	50Z	
22	13Z		74	34X		125	51X	
23	14X		75	34Y		126	51Y	
24	14Y		76	34Z		127	51Z	
25	14Z		77	35X		128	52X	
26	15X		78	35Y		129	52Y	
27	15Y		79	35Z		130	52Z	
28	15Z	↓	80	36X		131	53X	
29	7X	Sensory	81	36Y		132	53Y	
30	7Y	System	82	36Z		133	53Z	
31	7Z	↓	83	37X		134	54X	
32	8X		84	37Y		135	54Y	
33	8Y		85	37Z		136	54Z	
34	8Z		86	38X		137	55X	
35	9X		87	38Y		138	55Y	
36	9Y		88	38Z		139	55Z	
37	9Z		89	39X		140	56X	
38	10X		90	39Y		141	56Y	
39	10Y		91	39Z		142	56Z	
40	10Z		92	40X		143	57X	
41	58X		93	40Y		144	57Y	
42	58Y		94	40Z		145	57Z	↓
43	58Z		95	41X		146	17X	Input
44	59X		96	41Y		147	17Y	↓
45	59Y		97	41Z		148	17Z	
46	59Z		98	42X		149	18X	
47	60X		99	42Y		150	18Y	
48	60Y		100	42Z	↓	151	18Z	
49	60Z	↓	101	43X	Right	152	19X	
50	11X	Cross Beam	102	43Y	Paddle	153	19Y	
51	11Y	Cross Beam	103	43Z	Right Paddle	154	19Z	↓
52	11Z	Cross Beam						

TABLE 2.B.3. NIMBUS D VIBRATION DATA SINUSOIDAL VIBRATION LEVEL INPUTS TO SPACECRAFT ADAPTER BASE AND AXIS MODAL DAMPING

Listing Column No.	Resonant Frequency Hertz	Input Accelerations g's 0 to peak			Modal Damping			Major Response Region	
		X-Axis	Y-Axis	Z-Axis	X-Axis	Y-Axis	Z-Axis		
1	11.3	1.95	1.95	2.3	.06	.06	.06	Upper Paddles	Y-Axis
2	13.1	1.95	1.95	2.3	.07	↑	↑	Upper Paddles	X-Axis
3	14.7	1.95	1.95	4.6	.06	↕	↕	Lower Paddles	Y-Axis
4	15.3	1.95	1.95	4.6	↕	↕	↓	Lower Paddles	X-Axis
5	22.7	1.5	1.5	2.3	↕	↕	.06	ACS	X-Axis
6	26.4	↕	↕	↕	↓	↓	.06	ACS	Y-Axis
7	27.5	↕	↕	↕	.06	.06	.12	Paddle Shaft	Z-Axis
8	31.9	↕	↕	↕	.12	.09	.06	Paddle Twist	Y-Axis
9	36.8	↕	↕	↕	.12	.12	↑	Paddle Twist	X-Axis
10	39.5	↕	↕	↕	.06	.06	↕	Paddle Rock	X-Axis
11	41.5	↕	↕	↕	↕	↕	↕	Sensory	X-Axis
12	43.1	↕	↕	↕	↕	↕	↕	Sensory	Y-Axis
13	45.5	↕	↕	↕	↕	↕	↕	Paddles/ACS	Z,Y-Axis
14	47.4	↕	↕	↕	↕	↕	↕	ACS	Z-Axis
15	55.4	↕	↕	↕	↕	↕	↕	Paddles	Z,X-Axis
16	61.9	↕	↕	↕	↕	↕	↕	Paddles	Y,X-Axis
17	62.6	↕	↕	↕	↕	↕	↕	Paddle Tie Down	Z,X-Axis
18	64.4	↕	↕	↕	↕	↕	↕	Upper Paddles	Z,X-Axis
19	82.8	1.5	1.5	2.3	.06	.06	.06	ACS / Sensory	Z-Axis

* Loads in 4th Mode Should Be Multiplied By $\frac{6.0}{4.6}$ To Produce Z Axis 6.0 g Pogo Input Qualification Levels

TABLE 2.B.4. FREQUENCY COMPARISON

Listing Column Number	Frequency (Hz)	
	ERTS - 1621 lb S/C	NIMBUS D - 1500 lb S/C
1	11.3	11.3
2	13.1	13.4
3	14.7	14.8
4	15.3	15.4
5	22.7	22.8
6	26.4	26.6
7	27.5	27.6
8	31.9	32.4
9	36.8	37.4
10	39.5	39.9
11	41.5	42.2
12	43.1	43.5
13	45.5	45.9
14	47.4	48.0
15	55.4	55.4
16	61.9	62.0
17	62.6	63.5
18	64.4	64.7
19	82.8	82.6

TABLE 2.B.5. LOADS COMPARISON

Loads	Input Axis	Mode	ERTS 1621-lb S/C	Nimbus D 1500-lb S/C
Paddle Tie Down				
F_z	X	2	1133.	865.
Paddle Shaft Shear Force				
F_x	X	2	1984.	1395.
F_z	Z	8	1182.	
F_z	Z	7		1118.
Sensory Ring/ Adapter Interface Shear Force				
F_x	X	2	17931.	10963.
F_y	Y	8	10525.	9497.

SPFX = Solar Platform Forces Due to X Axis Excitation

	SPFX	11.3	1	13.1	2	14.7	3	15.3	4	22.7	5	26.4	6	
F_{x_4}	1	-1.3343145 /	2	1.9246348 /	3	-7.3468595 /	1	1.1491054 /	1	-8.5552609 /	2	-1.9963343 /	1	-Y Axis Paddle Shaft
F_{y_4}	2	1.9612742 /	2	-4.8443945 /	2	1.0882491 /	2	-1.5012332 /	2	4.5967163 /	2	3.8353919 /	1	End
F_{z_4}	3	2.2113189 /	2	-6.0671304 /	2	2.1957773 /	2	-1.3264418 /	2	1.9928798 /	2	-9.5934514 /	1	
F_{x_5}	4	6.8063450 /	1	1.9836976 /	3	8.6770532 /	1	-3.0007846 /	2	-7.1472772 /	2	2.4863560 /	1	
F_{y_5}	5	1.4535543 /	2	5.6261107 /	2	1.0014447 /	2	-2.2481778 /	2	-3.9435995 /	2	5.0969574 /	1	+Y Axis Paddle Shaft
F_{z_5}	6	-2.0094732 /	2	-5.6072525 /	2	-2.2775935 /	2	4.1910290 /	2	2.2372830 /	2	8.6293203 /	1	End
F	7	4.2620247 /	1	4.7800291 /	2	6.2251023 /	1	-4.8953050 /	2	1.7745536 /	2	2.2519857 /	1	Tie Down
F_{z_6}	8	-6.8882021 /	1	6.5482109 /	2	-1.0442940 /	2	-3.1030261 /	2	1.0773674 /	2	-2.0422522 /	1	
	9	-2.6261774 /	1	1.1328240 /	3	-4.2178383 /	1	-7.9963612 /	2	2.8519211 /	2	2.0973349 /	0	Total Tie Down Force

SPFX	27.5	7	31.9	8	36.8	9	39.5	10	41.5	11	43.1	12
1	1.2074228 /	0	5.8991594 /	1	5.8341679 /	1	-8.2925289 /	1	-2.1649932 /	2	7.3461996 /	1
2	7.2646791 /	0	-1.3690863 /	2	-3.4881315 /	2	3.2236999 /	2	2.2847574 /	2	-1.9492722 /	1
3	7.9329886 /	1	1.4624591 /	2	1.1435283 /	2	1.4363775 /	2	-7.0843816 /	1	-1.6278577 /	2
4	5.8173519 /	0	-8.3213995 /	1	9.6840484 /	1	1.2539331 /	2	-2.2066072 /	2	-7.2410782 /	1
5	9.2965857 /	-1	-1.8643815 /	2	3.3613295 /	2	3.0322294 /	2	-2.0285169 /	2	-4.7701333 /	1
6	8.2964050 /	1	-1.4514687 /	2	1.1456178 /	2	-1.3437808 /	2	-4.1058770 /	1	2.0705038 /	2
7	-3.5045374 /	1	-6.5618533 /	1	-1.0351552 /	2	-1.1921137 /	2	-5.6356840 /	1	-2.1373354 /	2
8	-3.6494878 /	1	2.4115091 /	1	-2.3640102 /	1	8.8055150 /	1	-6.1774084 /	1	1.8068199 /	2
9	-7.1940252 /	1	-4.1503441 /	1	-1.2715562 /	2	-3.2958629 /	1	-1.1813092 /	2	-3.3051540 /	1

SPFX	45.5	13	47.4	14	55.4	15	61.9	16	62.6	17	64.4	18
1	2.2466342 /	1	-7.9970982 /	0	-1.0317838 /	1	5.3563057 /	0	-6.5240311 /	0	-2.4738049 /	1
2	-1.8444114 /	2	2.4592295 /	1	5.2425896 /	1	1.9127417 /	1	-7.2220685 /	-2	3.3301352 /	1
3	3.3797254 /	1	1.7972359 /	2	1.3657129 /	1	-1.5595365 /	1	-3.3265180 /	-1	-1.5898009 /	1
4	-5.2985810 /	1	1.7768370 /	1	3.9602828 /	-1	2.3306115 /	1	-1.1147520 /	1	2.3698575 /	1
5	-1.7193741 /	2	-1.3415793 /	1	4.9691161 /	1	-1.4742692 /	1	4.7834046 /	-1	2.4874240 /	1
6	-1.0539905 /	2	1.7350720 /	2	-2.7304897 /	1	-1.8500079 /	1	5.1447109 /	-1	5.8475197 /	-1
7	2.9871141 /	1	-1.9012573 /	2	-2.2612762 /	0	1.2051219 /	1	4.7624180 /	0	-9.4069711 /	1
8	-4.8619698 /	1	-1.7629549 /	2	1.2745982 /	0	4.8955734 /	1	4.5163534 /	0	3.2273980 /	1
9	-1.8748556 /	1	-3.6642122 /	2	-1.0066779 /	0	6.1006953 /	1	9.2787714 /	0	-6.1795730 /	1

SPFX	82.8	19
1	5.4302835 /	1
2	-1.1732429 /	-1
3	1.1204062 /	1
4	2.8356133 /	1
5	-3.0784655 /	1
6	-2.5864675 /	1
7	7.7385638 /	1
8	4.3769791 /	1
9	1.2115542 /	2

CBFX = Control Box Base Forces for X-Axis Excitation

CBFX	11.3	1	13.1	2	14.7	3	15.3	4	22.7	5	26.4	6
F_x 1	-7.2198534 /	1	7.2901717 /	3	1.2463693 /	2	2.6144670 /	3	1.2129779 /	3	-4.2032346 /	1
F_y 2	1.6015368 /	3	3.0111293 /	2	-3.0454873 /	2	2.0826849 /	2	-1.7970439 /	1	-1.3766012 /	1
F_z 3	9.8839687 /	0	-7.4629466 /	2	-8.1944180 /	1	-7.6786746 /	2	5.3013383 /	2	-1.2490873 /	2
M_x 4	1.9514557 /	4	1.4751596 /	3	1.0410762 /	4	-1.6426267 /	4	-2.8349356 /	2	-5.7979588 /	3
M_y 5	-1.0094364 /	3	6.1340248 /	4	-7.6629954 /	2	-1.3877386 /	4	5.8145320 /	3	-1.7130554 /	1
M_z 6	-2.1618857 /	3	2.5845671 /	3	-6.4428963 /	3	1.3947711 /	4	3.7283483 /	2	-1.8127655 /	3

CBFX	27.5	/	31.9	8	36.8	9	39.5	10	41.5	11	43.1	12
1	2.6460352 /	1	-1.3600798 /	2	-5.8575514 /	2	-1.7087449 /	0	-1.5262672 /	3	-4.5091101 /	1
2	5.0588748 /	0	-9.4194622 /	2	-4.4388705 /	1	9.3651990 /	2	9.7403677 /	1	7.7823682 /	0
3	3.5191317 /	2	5.1419916 /	0	3.5828786 /	2	-1.3271450 /	2	-2.5181676 /	1	3.2483326 /	1
4	2.6239575 /	2	5.1269393 /	3	2.9048113 /	2	1.4068396 /	4	-2.0857046 /	2	-8.4468602 /	3
5	-1.4513976 /	2	-9.8496684 /	2	-2.9468974 /	3	3.8568405 /	2	-4.2582744 /	3	-5.3942573 /	2
6	-8.1271771 /	1	3.0304172 /	3	-1.2314335 /	3	-7.0017208 /	3	-1.9073115 /	3	4.2445675 /	3

CBFX	45.5	13	47.4	14	55.4	15	61.9	16	62.6	17	64.4	18
1	-1.6844579 /	2	1.1547214 /	2	-1.6745951 /	1	4.9136892 /	1	-1.3637054 /	0	-3.5094732 /	2
2	2.6444048 /	1	-1.7166700 /	1	-3.0634239 /	2	-8.6512640 /	0	-1.8563700 /	0	-1.6485986 /	1
3	-4.1708823 /	2	-2.3942139 /	2	-9.9946877 /	1	5.7547367 /	1	3.7726011 /	1	-4.5353630 /	2
4	4.0393863 /	3	-7.9018533 /	2	-7.0153441 /	1	-7.4227899 /	1	1.8372500 /	1	-1.5712079 /	3
5	-7.0301836 /	2	6.5258619 /	2	6.3058809 /	1	4.8622631 /	1	-1.4502608 /	2	-2.7005690 /	3
6	1.0688758 /	3	-1.2991071 /	2	1.0514372 /	3	-2.2058034 /	2	1.9317917 /	2	-3.7592453 /	3

CBFX	82.8	19
1	-1.6586526 /	2
2	1.6407089 /	1
3	-2.5013854 /	2
4	4.6576832 /	2
5	-5.4391944 /	3
6	-3.0859059 /	1

TRUSFX = Truss Base Forces for X-Axis Excitation

TRUSFX		11.3	1	13.1	2	14.7	3	15.3	4	22.7	5	26.4	6
F_x	1	-7.2198534 /	1	7.2901717 /	3	1.2463693 /	2	2.6144670 /	3	1.2129779 /	3	-4.2032346 /	1
F_y	2	1.6015368 /	3	3.0111293 /	2	-3.0454873 /	2	2.8826849 /	2	-1.7970439 /	1	-1.3766012 /	1
F_z	3	9.8839687 /	0	-7.4629466 /	2	-8.1944180 /	1	-7.6746746 /	2	5.3013383 /	2	-1.2490873 /	2
M_x	4	9.5907862 /	4	1.5838246 /	4	-4.1162116 /	3	-6.4918603 /	3	-1.1406835 /	3	-6.4545976 /	3
M_y	5	-4.4533065 /	3	4.0908143 /	5	5.1788822 /	3	1.1083268 /	5	6.3673577 /	4	-2.0220734 /	3
M_z	6	-2.1618857 /	3	2.5845671 /	3	-6.4428963 /	3	1.3947711 /	4	3.7283483 /	2	-1.8127655 /	3

TRUSFX	27.5	7	31.9	8	36.8	9	39.5	10	41.5	11	43.1	12
1	2.6460352 /	1	-1.3600796 /	2	-5.8575514 /	2	-1.7087349 /	0	-1.5262672 /	3	-4.5091101 /	1
2	5.0588748 /	0	-9.4194622 /	2	-4.4388705 /	1	9.3051090 /	2	9.7403677 /	1	7.7823682 /	0
3	3.5191317 /	2	5.1419916 /	0	3.5828786 /	2	-1.3271450 /	2	-2.5181676 /	1	3.2483326 /	1
4	5.0370408 /	2	-3.9803894 /	4	-1.8268600 /	3	5.8739965 /	4	4.4375847 /	3	-8.0756412 /	3
5	1.1170190 /	3	-7.4725477 /	3	-3.0887417 /	4	3.0217439 /	2	-7.7061220 /	4	-2.6902711 /	3
6	-8.1271771 /	1	3.0304172 /	3	-1.2314335 /	3	-7.0017208 /	3	-1.9073115 /	3	4.2445675 /	3

TRUSFX	45.5	13	47.4	14	55.4	15	61.9	16	62.6	17	64.7	18
1	-1.6844579 /	2	1.1547214 /	2	-1.6745951 /	1	4.9136892 /	1	-1.3637054 /	0	-3.5094732 /	2
2	2.6444048 /	1	-1.7166700 /	1	-3.0634239 /	2	-8.6312640 /	0	-1.8563700 /	0	-1.6485986 /	1
3	-4.1708823 /	2	-2.3942139 /	2	-9.9946877 /	1	5.7547367 /	1	3.7726011 /	1	-4.5353630 /	2
4	5.3007674 /	3	-1.6090369 /	3	-1.4682685 /	4	-4.8593918 /	2	-7.0176348 /	1	-2.3575895 /	3
5	-8.7378827 /	3	6.1606072 /	3	-7.3572306 /	2	2.3924523 /	3	-2.1007483 /	2	-1.9440756 /	4
6	1.0688758 /	3	-1.2991071 /	2	1.0514322 /	3	-2.2058034 /	2	1.9317917 /	2	-3.7592453 /	3

TRUSFX	82.8	19
1	-1.6586526 /	2
2	1.6407089 /	1
3	-2.5013854 /	2
4	1.2483864 /	3
5	-1.3350967 /	4
6	-3.0859059 /	1

SCBFX = Sensory Cross Base Forces for X-Axis Excitation

SCBFX	11.3	1	13.1	2	14.7	3	15.3	4	22.7	5	26.4	6
F_x 1	1.2910203	-1	3.2274077	1	4.8044710	-1	-4.4028507	0	6.9896172	0	-5.1265120	-1
F_y 2	-3.1826872	-1	-1.3318628	0	2.3529529	0	-2.5971529	0	9.3804453	-2	-7.1743777	-1
F_z 3	-3.2998675	-1	-3.7413714	0	7.1430159	-1	7.6020754	0	-2.2956894	0	-5.0265779	-1
M_x 4	-3.0711284	-2	9.5388043	0	-1.2620794	1	2.0581322	1	3.2997603	0	3.3745884	0
M_y 5	-1.1775098	0	-1.9061048	2	2.9582356	0	1.1347612	2	-4.2730293	1	-1.1066068	0
M_z 6	7.0798501	0	-3.3080682	1	-3.0944024	0	-6.4159857	0	-1.3454285	1	3.0680582	0

SCBFX	27.5	7	31.9	8	36.8	9	39.5	10	41.5	11	43.1	12
1	2.5288273	-2	1.4534904	0	9.3129432	0	1.8752097	0	7.4342818	0	2.4937679	0
2	3.3203137	-2	-1.5605272	0	-4.3875959	-1	-1.4635023	0	2.1665273	-1	3.2272330	0
3	2.4900660	-1	-1.0610850	0	-4.2220568	0	-1.3988252	0	-5.6395092	0	-5.3905602	-1
4	-1.8895072	-1	7.6241160	0	3.3360497	0	9.3712150	0	6.8295933	-1	-1.8271742	1
5	2.4433709	0	-1.7979749	1	-7.4925663	1	-2.1092968	1	-8.3444859	1	-1.8434689	1
6	1.4034309	-1	2.1724367	0	-7.0045987	0	-5.6100314	0	-1.1229754	1	-2.5382216	0

SCBFX	45.5	13	47.4	14	55.4	15	61.9	16	62.6	17	64.4	18
1	1.1276938	0	-9.1190086	-3	2.0417028	-1	-1.3908610	-1	1.1923322	-2	1.8655631	0
2	4.4160970	-1	-3.1061754	-1	5.8051634	-3	8.5213273	-2	8.8867599	-2	-4.3119824	-1
3	-2.4528447	0	-1.2198500	0	-6.2092676	-1	6.1226156	-1	7.0465525	-1	-8.3906616	-1
4	-1.5537098	0	1.8142541	0	1.5358286	0	-4.6400998	-1	-3.2425202	-1	1.4077808	0
5	-2.3737027	1	-1.0508599	1	-2.9577351	0	6.0387343	0	5.7772805	0	-3.6941938	1
6	-2.5454227	0	-7.6916597	-2	-3.8925658	0	2.4410661	-2	-7.8818120	-1	-6.9667906	0

SCBFX	82.8	19
1	-1,7585655 /	0
2	-6,5386160 /	-2
3	1,4436071 /	0
4	3,7878667 /	-1
5	2.1104849 /	1
6	1,2802565 /	0

SSFX = Sensory Ring Base Forces for X-Axis Excitation

SSFX	11.3	1	13.1	2	14.7	3	15.3	4	22.7	5	26.4	6
F_X 1	6,2440600 /	2	1.7931757 /	4	2.8762951 /	2	7,3251598 /	3	4,0978987 /	3	7,3756200 /	1
F_Y 2	1,4014180 /	3	3,1329755 /	3	1.2909722 /	3	-1,3212661 /	2	-6,0235090 /	1	-3,0950041 /	2
F_Z 3	-3,6775001 /	1	1,0624723 /	3	-1.9540670 /	2	-2,3241969 /	3	1,3978176 /	3	-2,8926318 /	2
M_X 4	1,1612535 /	5	2.2627501 /	4	6.6531181 /	3	-1,4639884 /	4	2,9044897 /	3	-9,0799019 /	3
M_Y 5	-5,1518838 /	2	6,2169973 /	5	1.1596527 /	4	1,7173198 /	5	1,1836506 /	5	1,0234956 /	3
M_Z 6	2,6636600 /	4	-9,6861173 /	4	-1.4443320 /	3	-2,0882611 /	4	-5,4644846 /	3	4,7825311 /	3

SSFX	27.5	7	31.9	8	36.8	9	39.5	10	41.5	11	43.1	12
1	2,4782221 /	1	7.4314611 /	2	3.3965800 /	3	6,8021662 /	2	7,3897240 /	2	5,7009087 /	2
2	1.3956790 /	1	-2.4219897 /	3	-2.9058240 /	2	-1,8360216 /	2	3,8600794 /	2	1,9754273 /	3
3	4.1499625 /	2	-1.4961892 /	2	-2.5405309 /	1	-4,1396367 /	2	-1,5837382 /	2	-1,1964725 /	2
4	6.7648607 /	2	-6.8027842 /	4	-6.2586266 /	3	6,0948152 /	4	9,6480435 /	3	1,4537499 /	4
5	7.3586138 /	2	-6.4016977 /	3	-1.1723446 /	4	5,6994779 /	3	-9,0712469 /	4	5,9744220 /	3
6	-2.5599732 /	2	1.1130103 /	4	2.1466713 /	4	-3,1999664 /	4	-1,9024367 /	4	1,4915217 /	4

SSFX	45.5	13	47.4	14	55.4	15	61.9	16	62.6	17	64.4	18
1	3,5010763 /	2	1.9968837 /	2	1.3109086 /	2	5.8526550 /	1	1.7866096 /	1	6.7761650 /	2
2	6,8837947 /	2	-1.9193338 /	2	-1.6544611 /	2	3.0436790 /	1	1.2239645 /	1	3.6891139 /	1
3	-1,0947781 /	3	-1.4443330 /	3	-1.9212069 /	2	3.5211970 /	2	2.7291750 /	2	-8.7679247 /	2
4	1,5076971 /	4	-3.2656411 /	3	-1.8240011 /	4	-1.2865433 /	3	-3,2604458 /	2	-1.0960945 /	3
5	5,9502720 /	3	-8.6758473 /	3	2.6982842 /	3	6.2642152 /	3	1.9207187 /	3	-1.1190620 /	4
6	-5,1272266 /	3	-2.6506202 /	3	5.6003240 /	1	-8.7713306 /	2	-2.9929794 /	2	-6.8555935 /	3

SSFX	82.8	19
1	1,8000959 /	2
2	8,6385033 /	1
3	-3,0434116 /	2
4	2,1281302 /	3
5	-6,6357875 /	3
6	2,5935303 /	3

BASEFX = Adapter Base Forces for X-Axis Excitation

BASEFX		11.3	1	13.1	2	14.7	3	15.3	4	22.7	5	26.4	6
F_x	1	6,2437375 /	2	1.7931136 /	4	2.8760651 /	2	7.3258908 /	3	4,0977495 /	3	7,3826087 /	1
F_y	2	1,4014201 /	3	3.1330138 /	3	1.2909735 /	3	-1.3217146 /	2	-6.0226197 /	1	-3.0950362 /	2
F_z	3	-3,6770242 /	1	1.0625582 /	3	-1.9540377 /	2	-2,3242922 /	3	1,3978293 /	3	-2,8925983 /	2
M_x	4	1,4989967 /	5	9.8134743 /	4	3.7765634 /	4	-1.7820965 /	4	1,4532090 /	3	-1,6538810 /	4
M_y	5	1,4533056 /	4	1.0538562 /	6	1.8528439 /	4	3.4826703 /	5	2,1712466 /	5	2.8009432 /	3
M_z	6	2,6636716 /	4	-9.6859129 /	4	-1.4442725 /	3	-2.0864715 /	4	-5,4644517 /	3	4,7830130 /	3

BASEFX	27.5	7	31.9	8	36.8	9	39.5	10	41.5	11	43.1	12
1	2.2314871 /	1	7.4313060 /	2	3.3965843 /	3	6.8014471 /	2	7.3920503 /	2	5.7024024 /	2
2	1.4049062 /	1	-2.4219874 /	3	-2.9058288 /	2	-1.8359966 /	2	3.8598698 /	2	1.9754137 /	3
3	4.1468023 /	2	-1.4960672 /	2	-2.5407806 /	1	-4.1595853 /	2	-1.5840464 /	2	-1.1966344 /	2
4	1.0059287 /	3	-1.2639746 /	5	-1.3261728 /	4	5.6523724 /	4	1.8949882 /	4	6.2144786 /	4
5	1.3350706 /	3	1.1508189 /	4	7.0134117 /	4	2.2237437 /	1	-7.2903639 /	4	1.9713368 /	4
6	-2.8388087 /	2	1.1130727 /	4	2.1466595 /	4	-3.1999213 /	4	-1.9025315 /	4	1.4914804 /	4

BASEFX	45.5	13	47.4	14	55.4	15	61.9	16	62.6	17	64.4	18
1	3.4986676 /	2	2.1901070 /	2	1.3107650 /	2	5.7448521 /	1	1.5813415 /	1	6.7736746 /	2
2	6.8840216 /	2	-1.9384476 /	2	-1.6544186 /	2	3.0318731 /	1	1.2208049 /	1	3.6894767 /	1
3	-1.0947704 /	3	-1.4435146 /	3	-1.9216094 /	2	3.4809328 /	2	2.7275786 /	2	-8.7666325 /	2
4	3.1667308 /	4	-7.8867840 /	3	-2.2226223 /	4	-6.0612935 /	2	-1.3809573 /	1	-2.0289677 /	2
5	1.4388183 /	4	-3.8827730 /	3	5.8574219 /	3	7.6589964 /	3	2.3530482 /	3	5.1407771 /	3
6	-5.1274243 /	3	-2.5642036 /	3	5.6076845 /	1	-9.7901469 /	2	-2.7159692 /	2	-6.8485044 /	3

BASEFX	82.8	19
1	1.8002518 /	2
2	8.6384239 /	1
3	-3.0434782 /	2
4	4.2098258 /	3
5	-2.2976031 /	3
6	2.5932362 /	3

SPFY = Solar Platform Forces Due to Y-Axis Excitation

	SPFY	11.3	1	13.1	2	14.7	3	15.3	4	22.7	5	26.4	6	
F_{x_4}	1	-2,9948973 /	2	3.9232826 /	2	-3.2977699 /	2	-2.4187808 /	-1	1.2573995 /	1	8.3693006 /	1	-Y Axis Paddle Shaft
F_{y_4}	2	4.4021217 /	2	-9.8750837 /	1	4.8848019 /	2	3.1598920 /	0	-6.7559704 /	0	-1.6079244 /	2	End
F_{z_4}	3	4.9633522 /	2	-1.2367576 /	2	9.8561413 /	2	2.7919798 /	0	-2.9290120 /	0	3.9380486 /	2	
F_{x_5}	4	1.5276985 /	2	4.0435982 /	2	3.8948513 /	2	6.4425358 /	0	1.0504627 /	1	-1.0423635 /	2	
F_{y_5}	5	3.2625337 /	2	1.1466577 /	2	4.7644855 /	2	4.7321089 /	0	5.7960595 /	0	-2.1368148 /	2	+Y Axis Paddle Shaft
F_{z_5}	6	-4.5103054 /	2	-1.1430136 /	2	-1.0223388 /	3	-8.8215467 /	0	-3.2882207 /	0	-3.6176993 /	2	End
F	7	9.5662051 /	1	9.7438777 /	1	2.7942491 /	2	1.9303951 /	1	-2.6081296 /	0	-9.4410766 /	1	Tie Down
F	8	-1.5460716 /	2	1.3348238 /	2	-4.6875017 /	2	6.5315116 /	0	-1.5834483 /	0	8.5618038 /	1	
F_{z_6}	9	-5.8945111 /	1	2.3092115 /	2	-1.8932526 /	2	1.6835463 /	1	-4.1915779 /	0	-8.7927289 /	0	Total Tie Down Force

SPFY	27.5	7	31.9	8	36.8	9	39.5	10	41.5	11	43.1	12
1	7.6017283 /	-1	-2.5635135 /	2	-4.9912181 /	0	2.8188772 /	1	-1.1304836 /	2	2.5448542 /	2
2	4.5737181 /	0	5.9494429 /	2	2.9841487 /	1	-8.6258381 /	1	1.1930203 /	2	-6.7526258 /	1
3	4.9944743 /	1	-6.3552000 /	2	-9.7830567 /	0	-3.8433974 /	1	-3.6992159 /	1	-5.6391887 /	2
4	3.6625056 /	0	3.6161117 /	2	-8.2848486 /	0	-3.3552206 /	1	-1.1522130 /	2	-2.5084383 /	2
5	5.8529718 /	-1	8.1017768 /	2	-2.8756675 /	1	-8.8135096 /	1	-1.0592205 /	2	-1.6524590 /	2
6	5.2232751 /	1	6.3074407 /	2	-9.8009320 /	0	3.5954439 /	1	-2.1439452 /	1	7.1725936 /	2
7	-2.2063970 /	1	2.8514909 /	2	-8.8559082 /	0	3.8828409 /	1	-2.9427568 /	1	-7.4041101 /	2
8	-2.2976553 /	1	-1.0479351 /	2	2.0224461 /	0	-2.2116510 /	1	-3.2256263 /	1	6.2591459 /	2
9	-4.5040523 /	1	1.8035558 /	2	1.0878354 /	1	8.7118984 /	0	-6.1683832 /	1	-1.1449641 /	2

SPFY	45.5	13	47.4	14	55.4	15	61.9	16	62.6	17	64.4	18
1	4.4205053 /	1	7.0781726 /	0	1.3022947 /	1	2.8268159 /	0	-5.0365903 /	0	-1.3474290 /	0
2	-3.6290867 /	2	-2.1589441 /	1	-6.6170803 /	1	1.0094366 /	1	-5.5754793 /	-2	1.8138539 /	0
3	6.6499895 /	1	-1.5907202 /	2	-1.7237726 /	1	-8.2385269 /	0	-2.5680914 /	-1	-8.6593084 /	-1
4	-1.0425553 /	2	-1.5726653 /	1	-4.9985812 /	-1	1.2299914 /	1	-8.6059514 /	0	1.2908111 /	0
5	-3.3830618 /	2	1.1874220 /	1	-6.2719082 /	1	-7.7805268 /	0	3.6928164 /	-1	1.3548470 /	0
6	-2.0738447 /	2	-1.5356995 /	2	3.4463636 /	1	-9.7035955 /	0	3.9717471 /	-1	3.1850198 /	-2
7	5.8774826 /	1	1.6827888 /	2	2.8793762 /	0	6.3000885 /	0	3.6766147 /	0	-5.1237774 /	0
8	-9.5664719 /	1	1.5603783 /	2	-1.6087696 /	0	2.5836424 /	1	3.4866513 /	0	1.7578952 /	0
9	-3.6889892 /	1	3.2431672 /	2	1.2706065 /	0	3.2196711 /	1	7.1632680 /	0	-3.3658822 /	0

SPFY	82.8	19
1	2,6056960 /	1
2	-5,6297511 /	-2
3	5,3762167 /	0
4	1,3606557 /	1
5	-1,4771872 /	1
6	-1,2411042 /	1
7	3,7133134 /	1
8	2,1002728 /	1
9	5,8135862 /	1

CBFY = Control Box Base Forces for Y-Axis Excitation

CBFY		11.3	1	13.1	2	14.7	3	15.3	4	22.7	5	26.4	6
F_x	1	-1,6205114 /	2	1,4860692 /	3	5,5945530 /	2	-5,5030977 /	1	-1,7827601 /	1	1,7621363 /	2
F_y	2	3,5946834 /	3	6,1380540 /	1	-1,3670217 /	3	-4,3837687 /	0	2,6411844 /	-1	5,7711722 /	1
F_z	3	2,2184777 /	1	-1,5212886 /	2	-3,6782118 /	2	1,6154347 /	1	-7,7915805 /	0	5,2365914 /	2
M_x	4	4,3800838 /	4	3,0070475 /	2	4,6750580 /	4	3,4575060 /	2	4,1666136 /	0	2,4306980 /	4
M_y	5	-2,2657015 /	3	1,2503938 /	4	-3,4396733 /	3	2,9210014 /	2	-8,5458409 /	1	7,1817007 /	1
M_z	6	-4,8523985 /	3	5,2685256 /	2	-2,8920098 /	4	-2,9358030 /	2	-5,4796967 /	0	7,5997186 /	3

CBFY		27.5	7	31.9	8	36.8	9	39.5	10	41.5	11	43.1	12
	1	1,6658986 /	1	5,9103050 /	2	5,0112230 /	1	4,5721598 /	-1	-7,9696330 /	2	-1,5620360 /	2
	2	3,1849813 /	0	4,0932812 /	3	3,7975202 /	0	-2,5058757 /	2	5,0860789 /	1	2,6959508 /	1
	3	2,2155853 /	2	-2,2344819 /	1	-3,0652064 /	1	3,5911478 /	1	-1,3148989 /	1	1,1252802 /	2
	4	1,6519989 /	2	-2,2279408 /	4	-2,4851096 /	1	-3,7643611 /	3	-1,0890819 /	2	-2,9261427 /	4
	5	-9,1377524 /	1	4,2802297 /	3	2,5211149 /	2	-1,0266373 /	2	-2,2235218 /	3	-1,8686667 /	3
	6	-5,1167321 /	1	-1,3168851 /	4	1,0535098 /	2	1,8734904 /	3	-9,9593133 /	2	1,4703937 /	4

CBFY	45.5	13	47.4	14	55.4	15	61.9	16	62.6	17	64.4	18
1	-3.3143603 /	2	-1.0220354 /	2	2.1136368 /	1	2.5932229 /	1	-1.0527886 /	0	-1.9115355 /	1
2	5.2031637 /	1	1.5194119 /	1	3.8665858 /	2	-4.5551904 /	0	-1.4331285 /	0	-8.9795669 /	-1
3	-8.2066797 /	2	2.1191011 /	2	1.2615073 /	2	3.0370898 /	1	2.9124701 /	1	-2.4703159 /	1
4	7.9479464 /	3	6.9938721 /	2	8.8546118 /	1	-3.9174328 /	1	1.4183677 /	1	-8.5580364 /	1
5	-1.3632676 /	3	-5.7759923 /	2	-7.9591431 /	1	2.5060826 /	1	-1.1196099 /	2	-1.4709426 /	2
6	2.1031333 /	3	1.1498302 /	2	-1.3270944 /	3	-1.1641236 /	2	1.4913545 /	2	-2.0475811 /	2

CBFY	82.8	19
1	-7.9589667 /	1
2	7.8728646 /	0
3	-1.2002780 /	2
4	2.2349674 /	2
5	-2.6099718 /	3
6	-1.4807574 /	1

TRUSFY = Truss Base Forces for Y-Axis Excitation

TRUSFY		1	2	3	4	5	6
F_x	1	-1.6205114 / 2	1.4860692 / 3	5.5945530 / 2	-5.5030977 / 1	-1.7827601 / 1	1.7621363 / 2
F	2	3.5946834 / 3	6.1380540 / 1	-1.3670217 / 3	-4.3837687 / 0	2.6411844 / -1	5.7711722 / 1
	3	2.2184777 / 1	-1.5212886 / 2	-3.6782118 / 2	1.6154147 / 1	-7.7915805 / 0	5.2365914 / 2
	4	2.1526723 / 5	3.2285564 / 3	-1.8476355 / 4	1.3664483 / 2	1.6765063 / 1	2.7059829 / 4
	5	-9.9955410 / 3	8.3389438 / 4	2.3246344 / 4	-2.3328774 / 3	-9.3583501 / 2	8.4772073 / 3
	6	-4.8523985 / 3	5.2685256 / 2	-2.8920098 / 4	-2.9358036 / 2	-5.4796967 / 0	7.5997186 / 3

TRUSFY	27.5	7	31.9	8	36.8	9	39.5	10	41.5	11	43.1	12
1	1,6658986 /	1	5.9103050 /	2	5.0112230 /	1	4.5721598 /	-1	-7,9696330 /	2	-1.5620360 /	2
2	3,1849813 /	0	4.0932812 /	3	3.7975202 /	0	-2.5058757 /	2	5,0860789 /	1	2.6959508 /	1
3	2,2155853 /	2	-2.2344819 /	1	-3.0652064 /	1	3.5511173 /	1	-1.3148989 /	1	1.1252802 /	2
4	3,1712349 /	2	1.7297010 /	5	1.5629061 /	2	-1.5717388 /	4	2.3171514 /	3	-2.7975458 /	4
5	7,0325612 /	2	3.2472384 /	4	2.6424648 /	3	-8.0854526 /	1	-4,0238670 /	4	-9.3195782 /	3
6	-5,1167321 /	1	-1.3168851 /	4	1.0535098 /	2	1.8734904 /	3	-9,9593133 /	2	1.4703937 /	4

TRUSFY	45.5	13	47.4	14	55.4	15	61.9	16	62.6	17	64.4	18
1	-3,3143603 /	2	-1.0220354 /	2	2.1136368 /	1	2.5932229 /	1	-1.0527886 /	0	-1.9115355 /	1
2	5,2031637 /	1	1.5194119 /	1	3.8665658 /	2	-4.5551906 /	0	-1,4331285 /	0	-8.9795669 /	-1
3	-8,2066797 /	2	2.1191011 /	2	1.2615073 /	2	3.0370898 /	1	2,9124701 /	1	-2.4703159 /	1
4	1,0429855 /	4	1,4241467 /	3	1.8532160 /	4	-2.5645672 /	2	-5,4176552 /	1	-1.2841289 /	2
5	-1,7192766 /	4	-5,4527080 /	3	9,2861335 /	2	1,2626281 /	3	-1,6217900 /	2	-1.0588967 /	3
6	2,1031333 /	3	1.1498302 /	2	-1.3270944 /	3	-1,1041234 /	2	1,4913545 /	2	-2.0475811 /	2

TRUSFY	82.8	19
1	-7,9589667 /	1
2	7,8728646 /	0
3	-1,2002780 /	2
4	5,9903237 /	2
5	-6,4063989 /	3
6	-1,4807574 /	1

SCBFY = Sensory Cross Base Forces for Y-Axis Excitation

	SCBFY	11.3	1	13.1	2	14.7	3	15.3	4	22.7	5	26.4	6
F_x	1	2,8977226	-1	6,5789278	0	2,1565732	0	9,3936945	-2	-1,0272908	-1	2,1492050	0
F_y	2	-7,1436091	-1	-2,7149433	-1	1,0561652	1	5,4066541	-2	-1,3786800	-3	3,0077388	0
F_z	3	-7,4066228	-1	-7,6266200	-1	3,2062710	0	-1,6422508	-1	3,3740628	-2	2,1073094	0
M_x	4	-6,8932130	-2	1,9444430	0	-5,6650707	1	-4,3320677	-1	-4,8497843	-2	-1,4147402	1
M_y	5	-2,6429459	0	-3,8855102	1	1,3276572	1	-2,3885181	0	6,2802353	-1	4,6392654	0
M_z	6	1,5890874	1	-6,7433506	0	-1,3889782	1	1,3504778	-1	1,9774280	-1	-1,2862324	1

SCBFY	27.5	7	31.9	8	36.8	9	39.5	10	41.5	11	43.1	12
1	1,5921065	-2	-6.3162259	0	-7.9673625	-1	-5,0176058	-1	3,8819217	0	8.6388559	0
2	2.0904128	-2	6.7813607	0	3.7536540	-2	3,8357041	-1	1,1312847	-1	1.1179709	1
3	1,5677031	-1	4,6110058	0	3,6120329	-1	3,7429167	-1	-2,9447542	0	-1,8673860	0
4	-1,1896015	-1	-3,3131032	1	-2,8540405	-1	-2,5075095	0	3,5661744	-1	-6,3296567	1
5	1,5383046	0	7,8132032	1	6,4100028	0	5,6437251	0	-4,3571983	1	-6,3861044	1
6	8,8357617	-2	-9,4404484	0	5,9925391	-1	1,5011881	0	-5,8637844	0	-8,7928516	0

SCBFY	45.5	13	47.4	14	55.4	15	61.9	16	62.6	17	64.4	18
1	2,2188644	0	8.0711673	-3	-2,5769920	-1	-7,3403388	-2	9,2048752	-3	1,0161326	-1
2	8,6891672	-1	2,7492529	-1	-7,3271485	-3	4,4971712	-2	6,8606309	-2	-2,3486453	-2
3	-4,8262477	0	1,0796802	0	7,6371999	-1	3,8512397	-1	5,4399799	-1	-4,5702152	-2
4	-3,0570986	0	-1,6057829	0	-1,9384888	0	-2,4488348	-1	-2,5032447	-1	7,6678835	-2
5	-4,6705268	1	9,3010841	0	3,7331877	0	3,1869709	0	4,4600945	0	-2,0121489	0
6	-5,0084052	0	6,8078313	-2	4,9131102	0	1,2882843	-2	-6,0848052	-1	-3,7946630	-1

SCBFY	82.8	19
1	-8.4383941 /	-1
2	-3.1375241 /	-2
3	6.9270809 /	-1
4	1.8175900 /	-1
5	1.0127062 /	1
6	6.1432507 /	-1

SSFY = Sensory Ring Base Forces Y-Axis Excitation

	SSFY	11.3	1	13.1	2	14.7	3	15.3	4	22.7	5	26.4	6
F_x	1	1.4014925 /	3	3.6553092 /	3	1.2910767 /	3	-1.5418466 /	2	-6.0228389 /	1	-3.0921063 /	2
F_y	2	3.1455126 /	3	6.3864319 /	2	5.7947609 /	3	2.7810856 /	0	8.8529825 /	-1	1.2975291 /	3
F_z	3	-8.2542272 /	1	2.1658028 /	2	-8.7711811 /	2	4.8921188 /	1	-2.0544261 /	1	1.2126879 /	3
M_x	4	2.6064583 /	5	4.6125160 /	3	2.9863717 /	4	3.0814967 /	2	-4.2688400 /	1	3.8065982 /	4
M_y	5	-1.1563512 /	3	1.2673073 /	5	5.2053096 /	4	-3.6147248 /	3	-1.7396568 /	3	-4.2908358 /	3
M_z	6	5.9786416 /	4	-1.9744721 /	4	-6.4851443 /	3	4.3955059 /	2	8.0313629 /	1	-2.0049968 /	4

SSFY	27.5	7	31.9	8	36.8	9	39.5	10	41.5	11	43.1	12
1	1.5602464 /	1	-3.2293839 /	3	-2.9058251 /	2	-1.8381490 /	2	3.8586551 /	2	1.9748962 /	3
2	8.7869573 /	0	1.0524695 /	4	2.4859760 /	1	4.9127480 /	1	2.0155983 /	2	6.8432320 /	3
3	2.6127456 /	2	6.5017758 /	2	2.1734622 /	0	1.1076662 /	2	-8.2697264 /	1	-4.1447939 /	2
4	4.2590409 /	2	2.9561888 /	5	5.3543489 /	2	-1.6306245 /	4	5.0378705 /	3	5.0360486 /	4
5	4.6328578 /	2	2.7818944 /	4	1.0029584 /	3	-1.5250416 /	3	-4.7366875 /	4	2.0696461 /	4
6	-1.6117155 /	2	-4.8366504 /	4	-1.8365095 /	3	8.5623384 /	3	-9.9338587 /	3	5.1668966 /	4

SSFY	45.5	13	47.4	14	55.4	15	61.9	16	62.6	17	64.4	18
1	6.8887611 /	2	-1.7674270 /	2	-1.6545998 /	2	3.0687659 /	1	1.3792731 /	1	3.6908332 /	1
2	1.3544639 /	3	1.6987882 /	2	2.0882241 /	2	1.6063161 /	1	9.4490784 /	0	2.0093820 /	0
3	-2.1540991 /	3	1.2783685 /	3	2.4249048 /	2	1.8583285 /	2	2.1069391 /	2	-4.7757024 /	1
4	2.9665634 /	4	2.8903949 /	3	2.3022137 /	4	-6.7897934 /	2	-2.5170833 /	2	-5.9701943 /	1
5	1.1707828 /	4	7.6789285 /	3	-3.4057145 /	3	3.3059695 /	3	1.4828061 /	3	-6.0952932 /	2
6	-1.0088394 /	4	2.3460444 /	3	-7.3210404 /	1	-4.6291416 /	2	-2.3105977 /	2	-3.7340962 /	2

SSFY	82.8	19
1	8.6376759 /	1
2	4.1451452 /	1
3	-1.4603667 /	2
4	1.0211733 /	3
5	-3.1841514 /	3
6	1.2444933 /	3

BASEFY = Adapter Base Forces for Y-Axis Excitation

BASEFY	11.3	1	13.1	2	14.7	3	15.3	4	22.7	5	26.4	6
F_x 1	1.4014201 /	3	3.6551827 /	3	1.2909735 /	3	-1.5420004 /	2	-6.0226197 /	1	-3.0950362 /	2
F_y 2	3.1455173 /	3	6.3865099 /	2	5.7947670 /	3	2.7020298 /	0	8.8516753 /	-1	1.2975425 /	3
F_z 3	-8.2531590 /	1	2.1659780 /	2	-8.7710497 /	2	4.8923892 /	1	-2.0544434 /	1	1.2126738 /	3
M_x 4	3.3645300 /	5	2.0004332 /	4	1.6951764 /	5	3.7523339 /	2	-2.1358370 /	1	6.9336218 /	4
M_y 5	3.2619753 /	4	2.1482392 /	5	8.3166232 /	4	-7.3305478 /	3	-3.1911644 /	3	-1.1742489 /	4
M_z 6	5.9786675 /	4	-1.9744304 /	4	-6.4828772 /	3	4.3959486 /	2	8.0313145 /	1	-2.0051988 /	4

BASEFY	27.5	7	31.9	8	36.8	9	39.5	10	41.5	11	43.1	12
1	1,4049062 /	1	-3.2293165 /	3	-2.9058288 /	2	-1.8359960 /	2	3,8598698 /	2	1.9754137 /	3
2	8,8450502 /	0	1.0524885 /	4	2.4859801 /	1	4.9125740 /	1	2,0154888 /	2	6.8431846 /	3
3	2.6107559 /	2	6.5012461 /	2	2.1736759 /	0	1.1076311 /	2	-8.2713361 /	1	-4.1453546 /	2
4	6.3331556 /	2	5.4926743 /	5	1.1345607 /	3	-1.5124375 /	4	9.8949651 /	3	2.1528059 /	5
5	8.4053770 /	2	-5.0009494 /	4	-6.0000787 /	3	-5.9501981 /	3	-3.8067728 /	4	6.8290617 /	4
6	-1.7872655 /	2	-4.8369213 /	4	-1.8364994 /	3	8.5622122 /	3	-9.9343535 /	3	5.1667536 /	4

BASEFY	45.5	13	47.4	14	55.4	15	61.9	16	62.6	17	64.4	18
1	6,8840216 /	2	-1.9384476 /	2	-1,6544186 /	2	3,8318731 /	1	1,2208049 /	1	3.6894768 /	1
2	1,3545086 /	3	1.7157057 /	2	2,0881704 /	2	1,6000855 /	1	9,4246857 /	0	2,0095797 /	0
3	-2,1540838 /	3	1,2776442 /	3	2,4254128 /	2	1,8370789 /	2	2,1057067 /	2	-4,7749986 /	1
4	6,2308987 /	4	6.9805344 /	3	2,8055970 /	4	-3,1988766 /	2	-1,0661071 /	1	-1.1051356 /	1
5	2,8310366 /	4	3.4366137 /	3	-7,3931081 /	3	4,0420719 /	3	1,8165671 /	3	2.8000721 /	2
6	-1,0088783 /	4	2.2695577 /	3	-7,0778951 /	1	-5,1687968 /	2	-2,0967442 /	2	-3.7302349 /	2

BASEFY	82.8	19
1	8,6384239 /	1
2	4,1451071 /	1
3	-1,4603987 /	2
4	2,0200651 /	3
5	-1,1024940 /	3
6	1,2443522 /	3

SPFZ - Solar Platform Forces Due to Z-Axis Excitation

	SPFZ	11.3	1	13.1	2	14.7	3	15.3	4	22.7	5	26.4	6	
F_{x_4}	1	9.26836B7 /	0	1.5693987 /	2	1.1774952 /	2	-6.0202071 /	0	-4.4748508 /	2	1.1993560 /	2	-Y Axis Paddle Shaft
F_{y_4}	2	-1.3623333 /	1	-3.9502488 /	1	-1.7441577 /	2	7.8650180 /	1	2.4043241 /	2	-2.3042235 /	2	End
F_{z_4}	3	-1.5360185 /	1	-4.9473004 /	1	-3.5192144 /	2	6.9492790 /	1	1.0423809 /	2	5.6433897 /	2	
F	4	-4.7277993 /	0	1.6175274 /	2	-1.3906879 /	2	1.6035366 /	2	-3.7384014 /	2	-1.4937508 /	2	
F_{x_5}	5	-1.0096628 /	1	4.5876612 /	1	-1.7011978 /	2	1.1778269 /	2	-2.0627097 /	2	-3.0621457 /	2	+Y Axis Paddle Shaft
F_{y_5}	6	1.3958132 /	1	-4.5723037 /	1	3.6503428 /	2	-2.1956960 /	2	1.1702165 /	2	-5.1843156 /	2	End
F_{z_5}	7	-2.9604725 /	0	3.8977636 /	1	-9.9770908 /	1	2.5046886 /	2	9.2818479 /	1	-1.3529461 /	2	Tie Down
F	8	4.7846587 /	0	5.3395863 /	1	1.6757101 /	2	1.6257028 /	2	5.6351979 /	1	1.2269426 /	2	
F_{z_6}	9	1.8241861 /	0	9.2373499 /	1	6.7600104 /	1	4.1903717 /	2	1.4917045 /	2	-1.2600351 /	1	Total Tie Down Force

	SPFZ	27.5	7	31.9	8	36.8	9	39.5	10	41.5	11	43.1	12
	1	1.7202235 /	1	-3.6420230 /	1	-1.3383517 /	0	7.6710692 /	1	7.1137096 /	1	-2.3637575 /	1
	2	1.0350038 /	2	8.4524649 /	1	8.0017355 /	0	-2.9821418 /	2	-7.5072294 /	1	6.2720957 /	0
	3	1.1302163 /	3	-9.0289302 /	1	-2.6232416 /	0	-1.3287336 /	2	2.3277778 /	1	5.2378931 /	1
	4	8.2880212 /	1	5.1374655 /	1	-2.2215101 /	0	-1.1599618 /	2	7.2504443 /	1	2.3299330 /	1
	5	1.3244909 /	1	1.1510318 /	2	-7.7108527 /	0	-2.8049904 /	2	6.6652775 /	1	1.5348668 /	1
	6	1.1819945 /	3	8.9610779 /	1	-2.6280347 /	0	1.2430815 /	2	1.3491042 /	1	-6.6621779 /	1
	7	-4.9929385 /	2	4.0511569 /	1	2.3746348 /	0	1.0657951 /	2	1.8517664 /	1	6.8772192 /	1
	8	-5.1994503 /	2	-1.4888174 /	1	5.4230135 /	-1	-7.6460871 /	1	2.0297656 /	1	-5.8137329 /	1
	9	-1.0192388 /	3	2.5623394 /	1	2.9169361 /	0	3.8118645 /	1	3.8815321 /	1	1.0634863 /	1

	SPFZ	45.5	13	47.4	14	55.4	15	61.9	16	62.6	17	64.4	18
	1	-1.0779269 /	2	8.0821120 /	1	2.3193463 /	1	4.9764493 /	1	-1.7254572 /	2	4.9091973 /	1
	2	8.8494188 /	2	-2.4651600 /	2	-1.1784813 /	2	1.7770911 /	2	-1.9100722 /	0	-6.6085611 /	1
	3	-1.6215799 /	2	-1.8163416 /	3	-3.0699852 /	1	-1.4489350 /	2	-8.7978809 /	0	3.1549159 /	1
	4	2.5422398 /	2	-1.7957258 /	2	-8.9023170 /	-1	2.1693258 /	2	-2.9482646 /	2	-4.7029167 /	1
	5	8.2494943 /	2	1.3558411 /	2	-1.1170072 /	2	-1.3697149 /	2	1.2651012 /	1	-4.9362241 /	1
	6	5.0570080 /	2	-1.7535169 /	3	6.1378660 /	1	-1.7188863 /	2	1.3606585 /	1	-1.1604240 /	0
	7	-1.4332064 /	2	1.9214688 /	3	5.1280791 /	0	1.1196953 /	2	1.2595508 /	2	1.8667873 /	2
	8	2.3327553 /	2	1.7816961 /	3	-2.8651686 /	0	4.5483820 /	2	1.1944723 /	2	-6.4046820 /	1
	9	8.9954892 /	1	3.7031649 /	3	2.2629105 /	0	5.6080373 /	2	2.4540231 /	2	1.2263191 /	2

SPFZ	82.8	19
1	-1.4076543 /	2
2	3.0413155 /	-1
3	-2.9043506 /	1
4	-7.3505618 /	1
5	7.9800907 /	1
6	6.7047184 /	1
7	-2.0060136 /	2
8	-1.1346136 /	2
9	-3.1406273 /	2

CBFZ = Control Box Base Forces for Z-Axis Excitation

CBFZ	11.3	1	13.1	2	14.7	3	15.3	4	22.7	5	26.4	6
1	5.0150291 /	0	5.9446009 /	2	-1.9975800 /	2	-1.3697291 /	3	6.3445116 /	2	2.5252157 /	2
2	-1.1124538 /	2	2.4553554 /	1	4.8810610 /	2	-1.8911265 /	2	-9.3994839 /	0	8.2703352 /	1
3	-6.8655675 /	-1	-6.0854862 /	1	1.3133350 /	2	4.0207911 /	2	2.7728784 /	2	7.5042564 /	2
4	-1.3555132 /	3	1.2028846 /	2	-1.6685528 /	4	8.6057835 /	3	-1.4828202 /	2	3.4832928 /	4
5	7.0117117 /	1	5.0018479 /	3	1.2281629 /	3	7.2704855 /	3	3.0413057 /	3	1.0291680 /	2
6	1.5016814 /	2	2.1075252 /	2	1.0326153 /	4	-7.3072985 /	3	1.9501220 /	2	1.0890717 /	4

CBFZ	27.5	7	31.9	8	36.8	9	39.5	10	41.5	11	43.1	12
1	3.7698245 /	2	8.3968610 /	1	1.3437159 /	1	1.5806802 /	0	5.0149911 /	2	1.4508784 /	1
2	7.2074136 /	1	5.8153873 /	2	1.0182720 /	0	-8.6632762 /	2	-3.2004786 /	1	-2.5041017 /	0
3	5.0137311 /	3	-3.1745627 /	0	-8.2190846 /	0	1.2276871 /	2	8.2741660 /	0	-1.0452031 /	1
4	3.7383703 /	3	-3.1652697 /	3	-6.6636053 /	0	-1.3014093 /	4	6.8531841 /	1	2.7179126 /	3
5	-2.0676162 /	3	6.0809881 /	2	6.7601505 /	1	-3.5492751 /	2	1.3991788 /	3	1.7356887 /	2
6	-1.1578845 /	3	-1.8709189 /	3	2.8248951 /	1	6.4770033 /	3	6.2670221 /	2	-1.3657576 /	3

CBFZ	45.5	13	47.4	14	55.4	15	61.9	16	62.6	17	64.4	18
1	8.0819679 /	2	-1.1669967 /	3	3.7643212 /	1	4.9652130 /	2	-3.6066894 /	1	6.9644525 /	2
2	-1.2687758 /	2	1.7349192 /	2	6.8862686 /	2	-8.0191392 /	1	-4.9096748 /	1	3.2715983 /	1
3	2.0011741 /	3	2.4196658 /	3	2.2467051 /	2	5.3466139 /	2	9.9776684 /	2	9.0003023 /	2
4	-1.9380828 /	4	7.9858547 /	3	1.5769787 /	2	-6.8963695 /	2	4.8591067 /	2	3.1180187 /	3
5	3.3730564 /	3	-6.5952357 /	3	-1.4174985 /	2	4.5174340 /	2	-3.8356088 /	3	5.3592045 /	3
6	-5.1284273 /	3	1.3129174 /	3	-2.3635137 /	3	-2.0493690 /	3	5.1091481 /	3	7.4601182 /	3

CBFZ	82.8	19
1	4.2996090 /	2
2	-4.2530948 /	1
3	6.4841664 /	2
4	-1.2073786 /	3
5	1.4099642 /	4
6	7.9993778 /	1

TRUSFZ = Truss Base Forces for Z-Axis Excitation

TRUSFZ	11.3	1	13.1	2	14.7	3	15.3	4	22.7	5	26.4	6
1	5.0150291 /	0	5.9446009 /	2	-1.9975800 /	2	-1.3697291 /	3	6.3445116 /	2	2.5252157 /	2
2	-1.1124538 /	2	2.4553554 /	1	4.8810610 /	2	-1.0911265 /	2	-9.3994839 /	0	8.2703332 /	1
3	-6.8655675 /	-1	-6.0854862 /	1	1.3133350 /	2	4.0207911 /	2	2.7728784 /	2	7.5042564 /	2
4	-6.6619181 /	3	1.2914930 /	3	6.5971312 /	3	3.4011101 /	3	-5.9663739 /	2	3.8777876 /	4
5	3.0933400 /	2	3.3357594 /	4	-8.3002938 /	3	-5.8065664 /	4	3.3304625 /	4	1.2148195 /	4
6	1.5016814 /	2	2.1075252 /	2	1.0326153 /	4	-7.3072585 /	3	1.9501220 /	2	1.0890717 /	4

TRUSFZ	27.5	7	31.9	8	36.8	9	39.5	10	41.5	11	43.1	12
1	3.7698245 /	2	8.3968610 /	1	1.3437159 /	1	1.5806802 /	0	5.0149911 /	2	1.4508784 /	1
2	7.2074136 /	1	5.8153873 /	2	1.0182720 /	0	-8.6632762 /	2	-3.2004786 /	1	-2.5041017 /	0
3	5.0137311 /	3	-3.1745627 /	0	-8.2190846 /	0	1.2276871 /	2	8.2741660 /	0	-1.0452031 /	1
4	7.1763065 /	3	2.4574127 /	4	4.1907970 /	1	-5.4337920 /	4	-1.4580964 /	3	2.5984669 /	3
5	1.5914246 /	4	4.6134014 /	3	7.0855398 /	2	-2.7952906 /	2	2.5320686 /	4	8.6563789 /	2
6	-1.1578845 /	3	-1.8709189 /	3	2.8248951 /	1	6.4770033 /	3	6.2670221 /	2	-1.3657576 /	3

TRUSFZ	45.5	13	47.4	14	55.4	15	61.9	16	62.6	17	64.4	18
1	8.0819679 /	2	-1.1669967 /	3	3.7643212 /	1	4.5052130 /	2	-3.6066894 /	1	6.9644525 /	2
2	-1.2687758 /	2	1.7349192 /	2	6.8662686 /	2	-8.0191592 /	1	-4.9096748 /	1	3.2715983 /	1
3	2.0011741 /	3	2.4196658 /	3	2.2467051 /	2	5.3466139 /	2	9.9776684 /	2	9.0003023 /	2
4	-2.5432888 /	4	1.6261419 /	4	3.3005198 /	4	-4.5147662 /	3	-1.8560041 /	3	4.6785711 /	3
5	4.1924042 /	4	-6.2260981 /	4	1.6538313 /	3	2.2227809 /	4	-5.5559996 /	3	3.8579642 /	4
6	-5.1284273 /	3	1.3129174 /	3	-2.3635137 /	3	-2.0493690 /	3	5.1091481 /	3	7.4601182 /	3

TRUSFZ	82.8	19
1	4.2996090 /	2
2	-4.2530948 /	1
3	6.4841664 /	2
4	-3.2361047 /	3
5	3.4608777 /	4
6	7.9993778 /	1

SCBFZ = Sensory Cross Base Forces for Z-Axis Excitation

SCBFZ	11.3	1	13.1	2	14.7	3	15.3	4	22.7	5	26.4	6
F_x 1	-8.9676401	-3	2.6317146	0	-7.7002179	-1	2.3381044	0	3.6559370	0	3.0799014	0
F_y 2	2.2107469	-2	-1.0860365	-1	-3.7711227	0	1.3606582	0	4.9064657	-2	4.3102165	0
F_z 3	2.2921423	-2	-3.0508143	-1	-1.1448248	0	-4.0875368	0	-1.2007661	0	3.0198632	0
M_x 4	2.1332563	-3	7.7781963	-1	2.0227589	1	-1.0782580	1	1.7259479	0	-2.0273823	1
M_y 5	8.1791776	-2	-1.5542886	1	-4.7412210	0	-5.9450569	1	-2.2350188	1	6.6482630	0
M_z 6	-4.9177805	-1	-2.6974673	0	4.9594561	0	3.3013592	0	-7.0372982	0	-1.8432254	1

SCBFZ	27.5	7	31.9	8	36.8	9	39.5	10	41.5	11	43.1	12
1	3.6028377	-1	-8.9735591	-1	-2.1363790	-1	-1.7346792	0	-2.4427476	0	-8.0240981	-1
2	4.7304737	-1	9.6343832	-1	1.0065097	-2	1.3260739	0	-7.1187501	-2	-1.0384139	0
3	3.5476141	0	6.5509267	-1	9.6853522	-2	1.2939955	0	1.8530233	0	1.7344991	-1
4	-2.6919939	0	-4.7069766	0	-7.6528617	-2	-8.6689246	0	-2.2440596	-1	5.8792260	0
5	3.4810873	1	1.1100337	1	1.7187865	0	1.9511402	1	2.7418214	1	5.9316566	0
6	1.9994776	0	-1.3412189	0	1.6068472	-1	5.1896087	0	3.6898595	0	8.1671352	-1

SCBFZ	45.5	13	47.4	14	55.4	15	61.9	16	62.6	17	64.4	18
1	-5.4106340	0	9.2159491	-2	-4.5895422	-1	-1.2922224	0	3.1534466	-1	-3.7021584	0
2	-2.1188272	0	3.1391958	0	-1.3049422	-2	7.9169993	-1	2.3503450	0	8.5570097	-1
3	1.1768659	1	1.2328177	1	1.3957808	0	5.6884029	0	1.8636522	1	1.6651035	0
4	7.4546431	0	-1.8335406	1	-3.4523880	0	-4.3110263	0	-8.5757258	0	-2.7937021	0
5	1.1388939	2	1.0620312	2	6.6486907	0	5.6104705	1	1.5279587	2	7.3310253	1
6	1.2212845	1	7.7734265	-1	8.7500960	0	2.2679470	-1	-2.0845593	1	1.3825403	1

SCBFZ	82.8	19
1	4.5586062 /	0
2	1.6949596 /	-1
3	-3.7421615 /	0
4	-9.8190217 /	-1
5	-5.4708621 /	1
6	-3.3187192 /	0

SSFZ = Sensory Ring Base Forces for Z-Axis Excitation

	SSFZ	11.3	1	13.1	2	14.7	3	15.3	4	22.7	5	26.4	6
F_x	1	-4.3372270 /	1	1.4622034 /	3	-4.6096933 /	2	-3.8376789 /	3	2.1434162 /	3	-4.4311167 /	2
F_y	2	-9.7344809 /	1	2.5547120 /	2	-2.0690658 /	3	6.9221633 /	1	-3.1506117 /	1	1.8594139 /	3
F_z	3	2.5544521 /	0	8.6636637 /	1	3.1316206 /	2	1.2176555 /	3	7.3113204 /	2	1.7378329 /	3
M_x	4	-8.0662585 /	3	1.8451070 /	3	-1.0663079 /	4	7.6698907 /	3	1.5192007 /	3	5.4550157 /	4
M_y	5	3.5785833 /	1	5.0695059 /	4	-1.8585976 /	4	-8.9971035 /	4	6.1911147 /	4	-6.1489486 /	3
M_z	6	-1.8502221 /	3	-7.8983192 /	3	2.3146587 /	3	1.0940478 /	4	-2.8582125 /	3	-2.8732450 /	4

SSFZ	27.5	7	31.9	8	36.8	9	39.5	10	41.5	11	43.1	12
1	3.5307400 /	2	-4.5880353 /	2	-7.7917175 /	1	-6.3479070 /	2	-2.4281069 /	2	-1.8343587 /	2
2	1.9884335 /	2	1.4952879 /	3	6.6659286 /	0	1.6984279 /	2	-1.2683404 /	2	-6.3562543 /	2
3	5.9124800 /	3	9.2371728 /	1	5.8279501 /	-1	3.8294972 /	2	5.2038285 /	1	3.8498423 /	1
4	9.6379434 /	3	4.1999028 /	4	1.4357221 /	2	-5.6380623 /	4	-3.1701426 /	3	-4.6776736 /	3
5	1.0483867 /	4	3.9522800 /	3	2.6893458 /	2	-5.2723521 /	3	2.9806197 /	4	-1.9223660 /	3
6	-3.6472114 /	3	-6.8715034 /	3	-4.9244406 /	2	2.9601588 /	4	6.2510045 /	3	-4.7992102 /	3

SSFZ	45.5	13	47.4	14	55.4	15	61.9	16	62.6	17	64.4	18
1	-1,6798036 /	3	-2.0181117 /	3	-2,9467907 /	2	5,4375864 /	2	4,7251746 /	2	-1.3447111 /	3
2	-3,3028195 /	3	1,9397375 /	3	3,7190620 /	2	2,8276229 /	2	3,2371068 /	2	-7.3209444 /	1
3	5,2527057 /	3	1,4596871 /	4	4,3166798 /	2	3,2714756 /	3	7,2160448 /	3	1,7399703 /	3
4	-7,2338758 /	4	3,3003568 /	4	4,1001708 /	4	-1,1953823 /	4	-8,6231347 /	3	2,1751692 /	3
5	-2,8549187 /	4	8,7680766 /	4	-6,0654712 /	3	5,8199605 /	4	5,0798625 /	4	2,2207475 /	4
6	2,4600246 /	4	2,6767978 /	4	-1,3038544 /	2	-8,1492725 /	3	-7,9157472 /	3	1,3604735 /	4

SSFZ	82.8	19
1	-4,6662627 /	2
2	-2,2392987 /	2
3	7,8892227 /	2
4	-5,5166030 /	3
5	1,7201487 /	4
6	-6,7230269 /	3

BASEFZ = Adapter Base Forces for Z-Axis Excitation

BASEFZ	11.3	1	13.1	2	14.7	3	15.3	4	22.7	5	26.4	6
F_x 1	-4,3370029 /	1	1,4621526 /	3	-4,6095248 /	2	-3,6380619 /	3	2,1433382 /	3	-4,4353174 /	2
F_y 2	-9,7344951 /	1	2,5547432 /	2	-2,0690631 /	3	6,9245133 /	1	-3,1501464 /	1	1,8594332 /	3
F_z 3	2,5541216 /	0	8,6643644 /	1	3,1317737 /	2	1,2177054 /	3	7,3113816 /	2	1,7378128 /	3
M_x 4	-1,0412278 /	4	8,0021694 /	3	-6,0527707 /	4	9,3396146 /	3	7,6010466 /	2	9,9361724 /	4
M_y 5	-1,0094900 /	3	8,5934255 /	4	-2,9695885 /	4	-1,8245841 /	5	1,1356760 /	5	-1,6827483 /	4
M_z 6	-1,8502301 /	3	-7,8981525 /	3	2,3147633 /	3	1,0941581 /	4	-2,8581953 /	3	-2,8735345 /	4

BASEFZ	27.5	7	31.9	8	36.8	9	39.5	10	41.5	11	43.1	12
1	3,1792150 /	2	-4,5879396 /	2	-7,7917273 /	1	-6,3472418 /	2	-2,4288712 /	2	-1,8348394 /	2
2	2,0015795 /	2	1,4952865 /	3	6,6659396 /	0	1,6983677 /	2	-1,2682715 /	2	-6,3562102 /	2
3	5,9079776 /	3	9,2364200 /	1	5,8285231 /	-1	3,8292859 /	2	5,2048415 /	1	3,8503631 /	1
4	1,4331536 /	4	7,8035267 /	4	3,0422259 /	2	-5,2287766 /	4	-6,2265303 /	3	-1,9996081 /	4
5	1,9020842 /	4	-7,1049256 /	3	-1,6088689 /	3	-2,0570936 /	4	2,3954592 /	4	-6,3430923 /	3
6	-4,0444702 /	3	-6,8718683 /	3	-4,9244136 /	2	2,9001152 /	4	6,2513158 /	3	-4,7990773 /	3

BASEFZ	45.5	13	47.4	14	55.4	15	61.9	16	62.6	17	64.4	18
1	-1,6786479 /	3	-2,2133691 /	3	-2,9464678 /	2	5,3374302 /	2	4,1822872 /	2	-1,3442169 /	3
2	-3,3029264 /	3	1,9590544 /	3	3,7189664 /	2	2,8168543 /	2	3,2287502 /	2	-7,3216644 /	1
3	5,2526684 /	3	1,4588600 /	4	4,3195845 /	2	3,8340669 /	3	7,2138226 /	3	1,7397139 /	3
4	-1,5193858 /	5	7,9706252 /	4	4,9966808 /	4	-5,6314298 /	3	-3,6523168 /	2	4,0264302 /	2
5	-6,9033976 /	4	3,9240491 /	4	-1,3166894 /	4	7,1158244 /	4	6,2232753 /	4	-1,0201729 /	4
6	2,4601194 /	4	2,5914626 /	4	-1,2605510 /	2	-9,0958349 /	3	-7,1831185 /	3	1,3590667 /	4

BASEFZ	82.8	19
1	-4,6666667 /	2
2	-2,2392781 /	2
3	7,8893957 /	2
4	-1,0912836 /	4
5	5,9559156 /	3
6	-6,7222647 /	3

APPENDIX 2. C

DYNAMIC ANALYSIS MODEL

2. C. 1 ABSTRACT

A dynamic analysis model of a 1621-pound spacecraft is presented. The spacecraft (with adapter) includes a sensory ring with an ERTS peculiar weight distribution. Analytic results include mode shapes and resonant frequencies normalized to a generalized mass of one. Also included herein is a description of the launch vehicle coupling technique.

2. C. 2 SUMMARY

Experimentally determined frequencies and mode shapes are extrapolated to the ERTS 1621-pound spacecraft configuration. The revised frequencies, mode shapes, and masses are presented.

2. C. 3 DISCUSSION

This report presents the ERTS 1621-pound spacecraft frequencies and mode shapes normalized to a generalized weight of one and follows the same general format as used for the Nimbus "B" presentation of frequencies and mode shapes in Reference 1 and in Appendix 2. B.

The ERTS weights and geometry are presented in Table 2. C-1 and Figure 2. C-1.

Frequencies, computer listing format identification, and mode shape listings are given in Tables 2. C-2 through 2. C-5.

Coupling between rigid body and ERTS flexible mode shapes are presented in Table 2. C-6, while Table 2. C-7 contains the rigid body inertia matrix.

2. C. 4 CONVENTIONS

2. C. 4. 1 AXES

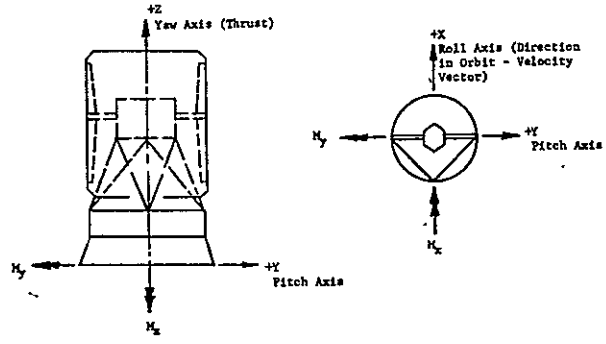

[1] Nimbus "B" Modes, Frequencies, and Generalized Mass--GE Document No. 65SD5261, 11 May 1965

TABLE 2. C-1. ERTS WEIGHT, GEOMETRY (REF. FIGURE 1)

Total Wt. (Including Adapter) = 1621 lbs. Nominal

Accel. No.	Wt. Lbs.	X ins.	Y ins.	Z ins.	Accel. No.	Wt. Lbs.	X ins.	Y ins.	Z ins.
1	1.65	-25.73	1.414	135.59	32	1.61	-13.69	-13.36	109.59
2	.80	-2.12	-25.03	132.59	33	1.90	-22.17	-4.88	109.59
3	.79	-2.12	25.03	132.59	34	4.39	-6.61	-20.44	90.09
4	2.2	-1.0	-23.55	85.59	35	3.22	-12.65	-14.4	90.09
5	2.2	-1.0	-23.55	85.59	36	3.52	-22.17	-4.88	90.09
6	2.71	-28.50	0	47.47	37	2.78	-4.47	-22.58	72.59
7	173.59	28.45	-1.5	24.09	38	1.61	-14.05	-13.0	71.09
8	169.19	5.0	28.0	24.09	39	1.90	-22.53	-4.52	71.09
9	232.40	-28.45	1.5	24.09	40	1.79	-6.97	-20.80	52.59
10	144.76	-5.0	-28.0	24.09	41	1.79	-13.69	-13.36	53.59
11	1.0	9.62	2.4	28.59	42	2.08	-22.17	-4.88	52.59
12	87.53	10.4	0	84.84	43	0.98	-6.97	20.8	129.59
13	42.73	-5.05	9.0	84.84	44	1.79	-13.69	13.36	131.09
14	72.6	-5.05	-9.0	84.84	45	1.27	-21.	5.85	129.59
15	49.13	0	0	101.84	46	2.76	-4.95	22.1	109.59
16					47	1.60	-14.05	13.0	108.59
17	33.	28.0	-8.6	-1.0	48	1.88	-22.10	4.95	109.59
18	33.	-13.5	28.0	-1.0	49	4.37	-5.66	21.39	90.09
19	33.	-13.25	-28.0	-1.0	50	3.19	-14.05	13.0	90.09
20		27.6	10.77	0	51	3.48	-22.17	4.88	90.09
21		11.57	26.7	0	52	2.76	-5.66	21.39	72.84
22		-11.57	26.7	0	53	1.60	-13.69	-13.36	72.84
23		-27.6	10.77	0	54	1.88	-22.53	4.52	72.84
24		-27.6	-10.77	0	55	1.79	-5.66	21.39	54.09
25		-11.7	-26.7	0	56	1.79	-13.69	13.36	53.59
26		11.7	26.7	0	57	2.07	-21.81	5.24	53.59
27		27.6	-10.77	0	58	155.15	28.0	0	37.09
28	0.99	-6.61	-20.44	129.59	59	164.26	-14.23	24.6	37.09
29	1.79	-13.69	-13.36	129.59	60	151.26	-14.23	-24.6	37.09
30	1.69	-21.81	-5.24	129.59	61	1.0	-8.87	0	34.09
31	2.78	-5.2	-21.85	109.59					

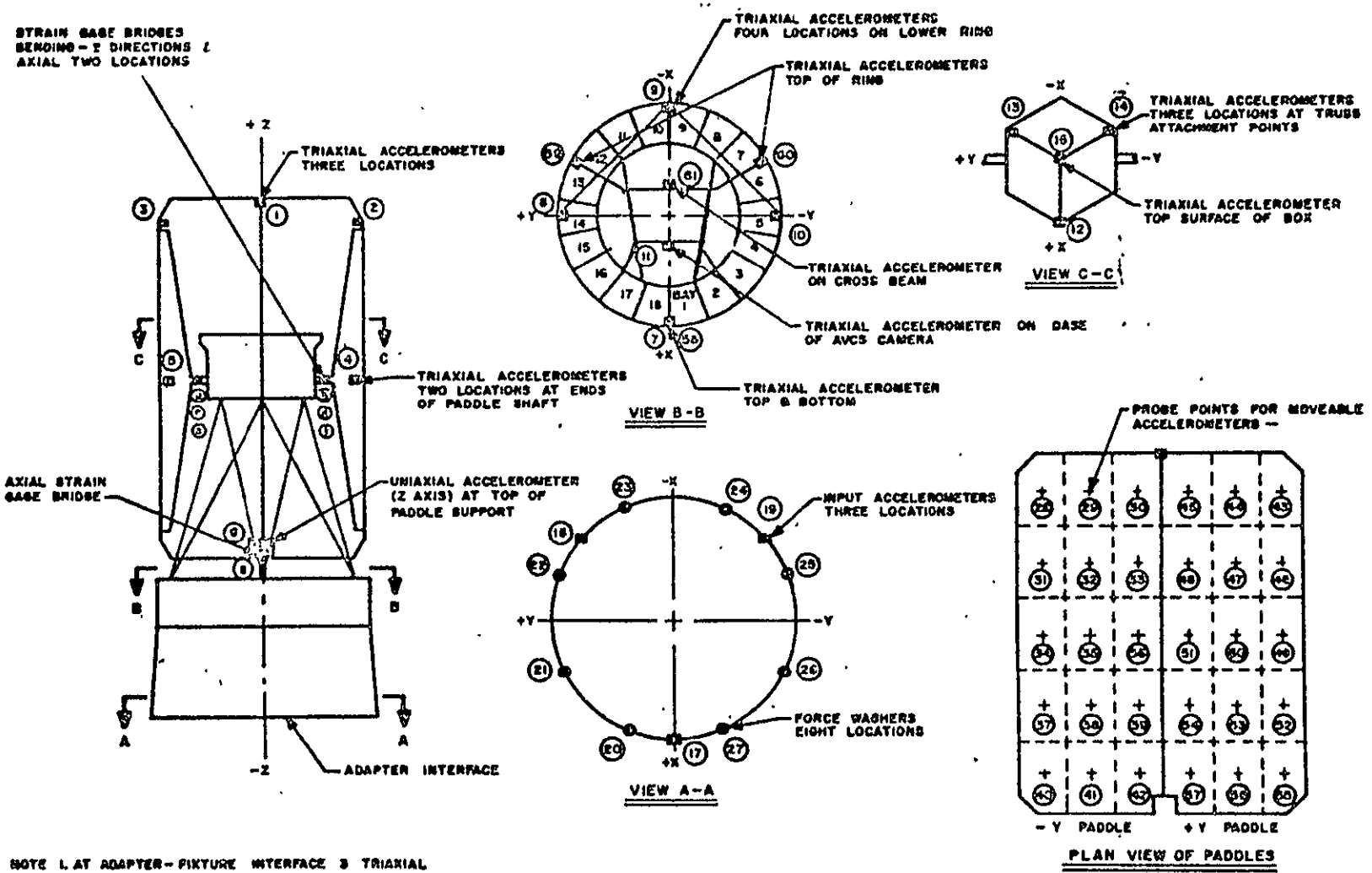

NOTE 1. AT ADAPTER - FIXTURE INTERFACE 3 TRIAXIAL ACCELEROMETERS, 120° APART, IN Z DIRECTION

2. (K) DESIGNATES INSTRUMENTATION IDENTIFICATION - REFER TO SECTION 10.7 IN G.E. DOCUMENT 64 SD 4254 FOR DESCRIPTION. (Reference 2)

Figure 2. C-1. Transducer Locations

TABLE 2.C-2. IDENTIFICATION OF ROWS OF IBM PRINTOUT

Row No.	Accel.	Description	Row No.	Accel.	Description	Row No.	Accel.	Description
1	1X	Paddle Perimeter	53	61X	Cross Beam	104	44X	Right Paddle
2	1Y		54	61Y	Cross Beam	105	44Y	
3	1Z		55	61Z	Cross Beam	106	44Z	
4	2X		56	28X	Left Paddle	107	45X	
5	2Y		57	28Y		108	45Y	
6	2Z		58	28Z		109	45Z	
7	3X		59	29X		110	46X	
8	3Y		60	29Y		111	46Y	
9	3Z		61	29Z		112	46Z	
10	4X		62	30X		113	47X	
11	4Y		63	30Y		114	47Y	
12	4Z		64	30Z		115	47Z	
13	5X		65	31X		116	48X	
14	5Y		66	31Y		117	48Y	
15	5Z		67	31Z		118	48Z	
16	6Z		68	32X		119	49X	
17	12X	Control Box	69	32Y		120	49Y	
18	12Y		70	32Z		121	49Z	
19	12Z		71	33X		122	50X	
20	13X		72	33Y		123	50Y	
21	13Y		73	33Z		124	50Z	
22	13Z		74	34X		125	51X	
23	14X		75	34Y		126	51Y	
24	14Y		76	34Z		127	51Z	
25	14Z		77	35X		128	52X	
26	15X		78	35Y		129	52Y	
27	15Y		79	35Z		130	52Z	
28	15Z		80	36X		131	53X	
29	7X	Sensory System	81	36Y		132	53Y	
30	7Y		82	36Z		133	53Z	
31	7Z		83	37X		134	54X	
32	8X		84	37Y		135	54Y	
33	8Y		85	37Z		136	54Z	
34	8Z		86	38X		137	55X	
35	9X		87	38Y		138	55Y	
36	9Y		88	38Z		139	55Z	
37	9Z		89	39X		140	56X	
38	10X		90	39Y		141	56Y	
39	10Y		91	39Z		142	56Z	
40	10Z		92	40X		143	57X	
41	58X		93	40Y		144	57Y	
42	58Y		94	40Z		145	57Z	
43	58Z		95	41X		146	17X	Input
44	59X		96	41Y		147	17Y	
45	59Y		97	41Z		148	17Z	
46	59Z		98	42X		149	18X	
47	60X		99	42Y		150	18Y	
48	60Y		100	42Z		151	18Z	
49	60Z		101	43X	Right Paddle	152	19X	
50	11X	Cross Beam	102	43Y		153	19Y	
51	11Y	Cross Beam	103	43Z	Right Paddle	154	19Z	
52	11Z	Cross Beam						

TABLE 2. C-3. ERTS FREQUENCIES

Listing Column No.	Frequency CPS	Principal Response Axis
1	11.3	Y
2	13.1	X
3	14.7	Y
4	15.3	X,Z
5	22.7	X
6	26.4	Y,Z
7	27.5	Z
8	31.9	Y
9	36.8	X
10	39.5	X,Z
11	41.5	X,Y
12	43.1	Y
13	45.5	Z,Y
14	47.4	Z
15	55.4	Z,Y
16	61.9	Z
17	62.6	Z
18	64.4	Z,X
19	82.8	Z,X

NOTE: Where two axes are given, the first is the major response axis.

2. C. 4. 1. 1 Roll Axis

The roll (X) axis is tangential to the orbit, and angular motions about this axis are described as roll motions. Components of linear displacement or acceleration along this axis are described as "Roll Components," although no angular motion is implied, and the "Roll Axis" defines direction only.

2. C. 4. 1. 2 Yaw Axis

The yaw (Z) axis of the spacecraft is maintained along the zenith by the control system when the spacecraft is in orbit. During power flight, the rocket thrust acts along this axis. It should be noted that the spacecraft rotates 90 degrees about the pitch axis upon separation from the adapter.

2. C. 4. 1. 3 Pitch Axis

The pitch (Y) axis is mutually perpendicular to the yaw and roll axes.

TABLE 2. C-4. RIGID BODY MODE SHAPES

ROW	RBM	X	1	Y	2	Z	3	M_X	4	M_Y	5	M_Z	6 ← MODE
1		1.0000000 /	0		0		0		0	1.3558999 / 2		-1.4139999 /	0
2			0	1.0000000 /	0		0	1.3558999 /	2		0	-2.5729999 /	1
3			0		0	1.0000000 /	0	-1.4139999 /	0	2.5729999 / 1			0
4		1.0000000 /	0		0		0		0	1.3258999 / 2		2.5029999 /	1
5			0	1.0000000 /	0		0	1.3258999 /	2		0	-2.1199999 /	0
6			0		0	1.0000000 /	0	2.5029999 /	1	2.1199999 / 0			0
7		1.0000000 /	0		0		0		0	1.3258999 / 2		-2.5029999 /	1
8			0	1.0000000 /	0		0	1.3258999 /	2		0	-2.1199999 /	0
9			0		0	1.0000000 /	0	-2.5029999 /	1	2.1199999 / 0			0
10		1.0000000 /	0		0		0		0	8.5589999 / 1		2.3549999 /	1
11			0	1.0000000 /	0		0	8.5589999 /	1		0	-1.0000000 /	0
12			0		0	1.0000000 /	0	2.3549999 /	1	1.0000000 / 0			0
13		1.0000000 /	0		0		0		0	8.5589999 / 1		-2.3549999 /	1
14			0	1.0000000 /	0		0	8.5589999 /	1		0	-1.0000000 /	0
15			0		0	1.0000000 /	0	-2.3549999 /	1	1.0000000 / 0			0
16			0		0	1.0000000 /	0		0	2.8499999 / 1			0
17		1.0000000 /	0		0		0		0	8.4839999 / 1			0
18			0	1.0000000 /	0		0	8.4839999 /	1		0	1.0399999 /	1
19			0		0	1.0000000 /	0		0	-1.0399999 / 1			0
20		1.0000000 /	0		0		0		0	8.4839999 / 1		-9.0000000 /	0
21			0	1.0000000 /	0		0	8.4839999 /	1		0	-5.0499999 /	0
22			0		0	1.0000000 /	0	-9.0000000 /	0	5.0499999 / 0			0
23		1.0000000 /	0		0		0		0	8.4839999 / 1		9.0000000 /	0
24			0	1.0000000 /	0		0	8.4839999 /	1		0	-5.0499999 /	0
25			0		0	1.0000000 /	0	9.0000000 /	0	5.0499999 / 0			0
26		1.0000000 /	0		0		0		0	1.0183999 / 2			0
27			0	1.0000000 /	0		0	1.0183999 /	2		0		0
28			0		0	1.0000000 /	0		0		0		0
29		1.0000000 /	0		0		0		0	2.4089999 / 1		1.4999999 /	0
30			0	1.0000000 /	0		0	2.4089999 /	1		0	2.8449999 /	1
31			0		0	1.0000000 /	0	1.4999999 /	0	-2.8449999 / 1			0
32		1.0000000 /	0		0		0		0	2.4089999 / 1		-2.7999999 /	1
33			0	1.0000000 /	0		0	2.4089999 /	1		0	5.0000000 /	0
34			0		0	1.0000000 /	0	-2.7999999 /	1	-5.0000000 / 0			0
35		1.0000000 /	0		0		0		0	2.4089999 / 1		-1.4999999 /	0
36			0	1.0000000 /	0		0	2.4089999 /	1		0	-2.8449999 /	1
37			0		0	1.0000000 /	0	-1.4999999 /	0	2.8449999 / 1			0
38		1.0000000 /	0		0		0		0	2.4089999 / 1		2.7999999 /	1
39			0	1.0000000 /	0		0	2.4089999 /	1		0	-5.0000000 /	0
40			0		0	1.0000000 /	0	2.7999999 /	1	5.0000000 / 0			0
41		1.0000000 /	0		0		0		0	3.7089999 / 1			0
42			0	1.0000000 /	0		0	3.7089999 /	1		0	2.7999999 /	1
43			0		0	1.0000000 /	0		0	-2.7999999 / 1			0
44		1.0000000 /	0		0		0		0	3.7089999 / 1		-2.4599999 /	1
45			0	1.0000000 /	0		0	3.7089999 /	1		0	-1.4224999 /	1
46			0		0	1.0000000 /	0	-2.4599999 /	1	1.4224999 / 1			0
47		1.0000000 /	0		0		0		0	3.7089999 / 1		2.4599999 /	1
48			0	1.0000000 /	0		0	3.7089999 /	1		0	-1.4224999 /	1
49			0		0	1.0000000 /	0	2.4599999 /	1	1.4224999 / 1			0
50		1.0000000 /	0		0		0		0	2.8589999 / 1		-2.3999999 /	0
51			0	1.0000000 /	0		0	2.8589999 /	1		0	9.6199998 /	0
52			0		0	1.0000000 /	0	-2.3999999 /	0	-9.6199998 / 0			0
53		1.0000000 /	0		0		0		0	3.4089999 / 1			0
54			0	1.0000000 /	0		0	3.4089999 /	1		0	-8.8699999 /	0

TABLE 2. C-4. RIGID BODY MODE SHAPES (Continued)

RBM	1	2	3	4	5	6
55	0	0	1.0000000 / 0	0	8.8699999 / 0	0
56	1.0000000 / 0	0	0	0	1.2958999 / 2	2.0439999 / 1
57	0	1.0000000 / 0	0	1.2958999 / 2	0	-6.6099999 / 0
58	0	0	1.0000000 / 0	2.0439999 / 1	6.6099999 / 0	0
59	1.0000000 / 0	0	0	0	1.2958999 / 2	1.3359999 / 1
60	0	1.0000000 / 0	0	1.2958999 / 2	0	-1.3689999 / 1
61	0	0	1.0000000 / 0	1.3359999 / 1	1.3689999 / 1	0
62	1.0000000 / 0	0	0	0	1.2958999 / 2	5.2399999 / 0
63	0	1.0000000 / 0	0	1.2958999 / 2	0	-2.1809999 / 1
64	0	0	1.0000000 / 0	5.2399999 / 0	-2.1809999 / 1	0
65	1.0000000 / 0	0	0	0	1.0958999 / 2	2.1849999 / 1
66	0	1.0000000 / 0	0	1.0958999 / 2	0	-5.1999999 / 0
67	0	0	1.0000000 / 0	2.1849999 / 1	5.1999999 / 0	0
68	1.0000000 / 0	0	0	0	1.0958999 / 2	-1.3359999 / 1
69	0	1.0000000 / 0	0	1.0958999 / 2	0	-1.3689999 / 1
70	0	0	1.0000000 / 0	1.3359999 / 1	1.3689999 / 1	0
71	1.0000000 / 0	0	0	0	1.0958999 / 2	4.8800000 / 0
72	0	1.0000000 / 0	0	1.0958999 / 2	0	-2.2169999 / 1
73	0	0	1.0000000 / 0	4.8800000 / 0	2.2169999 / 1	0
74	1.0000000 / 0	0	0	0	9.0089999 / 1	2.0439999 / 1
75	0	1.0000000 / 0	0	9.0089999 / 1	0	-6.6099999 / 0
76	0	0	1.0000000 / 0	2.0439999 / 1	6.6099999 / 0	0
77	1.0000000 / 0	0	0	0	9.0089999 / 1	1.4400000 / 1
78	0	1.0000000 / 0	0	9.0089999 / 1	0	-1.2649999 / 1
79	0	0	1.0000000 / 0	1.4400000 / 1	1.2649999 / 1	0
80	1.0000000 / 0	0	0	0	9.0089999 / 1	4.8800000 / 0
81	0	1.0000000 / 0	0	9.0089999 / 1	0	-2.2169999 / 1
82	0	0	1.0000000 / 0	4.8800000 / 0	2.2169999 / 1	0
83	1.0000000 / 0	0	0	0	7.2589999 / 1	2.2579999 / 1
84	0	1.0000000 / 0	0	7.2589999 / 1	0	-4.4699999 / 0
85	0	0	1.0000000 / 0	2.2579999 / 1	4.4699999 / 0	0
86	1.0000000 / 0	0	0	0	7.1089999 / 1	1.2999999 / 1
87	0	1.0000000 / 0	0	7.1089999 / 1	0	-1.4049999 / 1
88	0	0	1.0000000 / 0	1.2999999 / 1	1.4049999 / 1	0
89	1.0000000 / 0	0	0	0	7.1089999 / 1	4.5199999 / 0
90	0	1.0000000 / 0	0	7.1089999 / 1	0	-2.2530000 / 1
91	0	0	1.0000000 / 0	4.5199999 / 0	2.2530000 / 1	0
92	1.0000000 / 0	0	0	0	5.2589999 / 1	-2.0799999 / 1
93	0	1.0000000 / 0	0	5.2589999 / 1	0	-6.9700000 / 0
94	0	0	1.0000000 / 0	2.0799999 / 1	6.9700000 / 0	0
95	1.0000000 / 0	0	0	0	5.3589999 / 1	1.3359999 / 1
96	0	1.0000000 / 0	0	5.3589999 / 1	0	-1.3689999 / 1
97	0	0	1.0000000 / 0	1.3359999 / 1	1.3689999 / 1	0
98	1.0000000 / 0	0	0	0	5.2589999 / 1	4.8800000 / 0
99	0	1.0000000 / 0	0	5.2589999 / 1	0	-2.2169999 / 1
100	0	0	1.0000000 / 0	4.8800000 / 0	2.2169999 / 1	0
101	1.0000000 / 0	0	0	0	1.2958999 / 2	-2.0799999 / 1
102	0	1.0000000 / 0	0	1.2958999 / 2	0	-6.9700000 / 0
103	0	0	1.0000000 / 0	-2.0799999 / 1	6.9700000 / 0	0
104	1.0000000 / 0	0	0	0	1.3108999 / 2	-1.3359999 / 1
105	0	1.0000000 / 0	0	1.3108999 / 2	0	-1.3689999 / 1
106	0	0	1.0000000 / 0	-1.3359999 / 1	1.3689999 / 1	0
107	1.0000000 / 0	0	0	0	1.2958999 / 2	-5.8499999 / 0
108	0	1.0000000 / 0	0	1.2958999 / 2	0	-2.1199999 / 1

TABLE 2. C-4. RIGID BODY MODE SHAPES (Continued)

RBM	1	2	3	4	5	6
109	0	0 1.0000000 / 0	-5.8499999 / 0	2.1199999 / 1		0
110	1.0000000 / 0	0	0	1.0958999 / 2	-2.2100000 / 1	
111	0	1.0000000 / 0	0	1.0958999 / 2	-4.9499999 / 0	
112	0	0 1.0000000 / 0	-2.2100000 / 1	4.9499999 / 0		0
113	1.0000000 / 0	0	0	1.0858999 / 2	-1.2999999 / 1	
114	0	1.0000000 / 0	0	1.0858999 / 2	-1.4049999 / 1	
115	0	0 1.0000000 / 0	-1.2999999 / 1	1.4049999 / 1		0
116	1.0000000 / 0	0	0	1.0958999 / 2	-4.9499999 / 0	
117	0	1.0000000 / 0	0	1.0958999 / 2	-2.2100000 / 1	
118	0	0 1.0000000 / 0	-4.9499999 / 0	2.2100000 / 1		0
119	1.0000000 / 0	0	0	9.0089999 / 1	-2.1389999 / 1	
120	0	1.0000000 / 0	0	9.0089999 / 1	-5.6599999 / 0	
121	0	0 1.0000000 / 0	-2.1389999 / 1	5.6599999 / 0		0
122	1.0000000 / 0	0	0	9.0089999 / 1	-1.2999999 / 1	
123	0	1.0000000 / 0	0	9.0089999 / 1	-1.4049999 / 1	
124	0	0 1.0000000 / 0	-1.2999999 / 1	1.4049999 / 1		0
125	1.0000000 / 0	0	0	9.0089999 / 1	-4.8800000 / 0	
126	0	1.0000000 / 0	0	9.0089999 / 1	-2.2169999 / 1	
127	0	0 1.0000000 / 0	-4.8800000 / 0	2.2169999 / 1		0
128	1.0000000 / 0	0	0	7.2839999 / 1	-2.1389999 / 1	
129	0	1.0000000 / 0	0	7.2839999 / 1	-5.6599999 / 0	
130	0	0 1.0000000 / 0	-2.1389999 / 1	5.6599999 / 0		0
131	1.0000000 / 0	0	0	7.2839999 / 1	-1.3359999 / 1	
132	0	1.0000000 / 0	0	7.2839999 / 1	-1.3689999 / 1	
133	0	0 1.0000000 / 0	-1.3359999 / 1	1.3689999 / 1		0
134	1.0000000 / 0	0	0	7.2839999 / 1	-4.5199999 / 0	
135	0	1.0000000 / 0	0	7.2839999 / 1	-2.2530000 / 1	
136	0	0 1.0000000 / 0	-4.5199999 / 0	2.2530000 / 1		0
137	1.0000000 / 0	0	0	5.4089999 / 1	-2.1389999 / 1	
138	0	1.0000000 / 0	0	5.4089999 / 1	-5.6599999 / 0	
139	0	0 1.0000000 / 0	-2.1389999 / 1	5.6599999 / 0		0
140	1.0000000 / 0	0	0	5.3589999 / 1	-1.3359999 / 1	
141	0	1.0000000 / 0	0	5.3589999 / 1	-1.3689999 / 1	
142	0	0 1.0000000 / 0	-1.3359999 / 1	1.3689999 / 1		0
143	1.0000000 / 0	0	0	5.3589999 / 1	-5.2399999 / 0	
144	0	1.0000000 / 0	0	5.3589999 / 1	-2.1809999 / 1	
145	0	0 1.0000000 / 0	-5.2399999 / 0	2.1809999 / 1		0
146	1.0000000 / 0	0	0	-1.0000000 / 0	8.4299999 / 0	
147	0	1.0000000 / 0	0	-1.0000000 / 0	2.7999999 / 1	
148	0	0 1.0000000 / 0	8.4999999 / 0	-2.7999999 / 1		0
149	1.0000000 / 0	0	0	-1.0000000 / 0	-2.7999999 / 1	
150	0	1.0000000 / 0	0	-1.0000000 / 0	-1.3500000 / 1	
151	0	0 1.0000000 / 0	-2.7999999 / 1	1.3500000 / 1		0
152	1.0000000 / 0	0	0	-1.0000000 / 0	2.7999999 / 1	
153	0	1.0000000 / 0	0	-1.0000000 / 0	-1.3249999 / 1	
154	0	0 1.0000000 / 0	2.7999999 / 1	1.3249999 / 1		0

TABLE 2. C-5. ERTS FIXED-FREE FLEXIBLE MODE SHAPES

	11.3	1	13.1	2	14.7	3	15.3	4	22.7	5	26.4	6
1	-1.1982304 / -2		1.1284138 / -1		-4.7271832 / -3		1.8823452 / -2		-6.9892016 / -2		3.1680934 / -3	
2	-4.9742477 / -2		-2.0530536 / -2		-1.2049269 / -1		1.3490362 / -2		-3.3014077 / -3		-1.7927578 / -2	
3	1.6521119 / -3		4.4321878 / -3		-6.6318553 / -3		1.4998259 / -2		1.0589549 / -2		-8.2059783 / -2	
4	1.5131883 / -1		1.2329035 / -1		-3.5193620 / -2		1.2795032 / -1		-4.1657980 / -3		-2.1753694 / -2	
5	3.9130004 / -2		5.5307244 / -2		-1.2957168 / -1		1.9985736 / -1		1.3944571 / -1		5.1659403 / -2	
6	1.1691829 / -2		-5.2111062 / -3		-6.6167404 / -3		2.5439924 / -2		4.0400719 / -2		7.9317199 / -2	
7	-1.1556903 / -1		1.1483135 / -1		7.7629961 / -2		1.2893330 / -1		2.1365071 / -2		-1.0235646 / -2	
8	5.7351281 / -2		-6.3994027 / -2		-1.8953519 / -1		-1.1290058 / -1		-1.4138049 / -1		1.1945340 / -1	
9	-1.4196228 / -2		9.4431165 / -6		2.9372979 / -2		2.3481479 / -2		4.1546612 / -2		-6.3900997 / -2	
10	-7.4057787 / -3		3.8742801 / -2		3.2535445 / -2		-2.2202852 / -2		-7.0835495 / -2		2.9206441 / -2	
11	-7.8131680 / -2		1.6648446 / -2		3.3771173 / -2		1.1272982 / -2		1.7068482 / -3		2.9397648 / -2	
12	-2.4690569 / -2		-5.8762717 / -3		-1.3886179 / -2		2.3925423 / -2		2.9899551 / -2		7.8487840 / -2	
13	2.0541638 / -2		3.2085766 / -2		-4.4889510 / -2		-1.0547803 / -2		-6.5203705 / -2		-3.5614233 / -2	
14	-7.1919348 / -2		-8.2966028 / -3		4.0229155 / -2		-3.1976333 / -2		-7.1896402 / -3		1.7976506 / -2	
15	2.7100452 / -2		6.0635292 / -3		4.2005807 / -2		1.4926459 / -2		3.0657319 / -2		-5.9024625 / -2	
16	-1.1341272 / -3		1.1112009 / -2		-2.1537653 / -3		9.1984937 / -4		7.1843341 / -3		5.5415198 / -4	
17	1.4720204 / -3		1.3088475 / -2		-7.8823745 / -3		-3.1949551 / -2		3.7160598 / -2		3.7775870 / -3	
18	-3.3788584 / -2		3.4033404 / -3		2.7566726 / -2		-5.3006247 / -3		3.0147862 / -3		1.0222435 / -2	
19	-9.2403962 / -4		-1.4151444 / -2		-4.0099193 / -3		-1.1750595 / -2		-6.9355331 / -3		7.9326767 / -3	
20	9.2775555 / -3		1.3002023 / -2		-1.2890107 / -2		-3.2406986 / -2		2.9778502 / -2		2.0444978 / -3	
21	-3.5159068 / -2		-3.1415739 / -5		1.3304474 / -2		-3.0087455 / -3		-5.2594234 / -3		1.8120961 / -3	
22	5.0336048 / -3		1.3384682 / -2		1.2866127 / -3		2.9023065 / -2		5.0366600 / -3		7.5285237 / -3	
23	-9.4712152 / -3		1.2193001 / -2		1.0584795 / -3		-3.4104960 / -2		3.0426504 / -2		8.9601700 / -3	
24	-2.7214439 / -2		4.4646965 / -4		1.6176482 / -2		-5.6479644 / -3		-1.9473595 / -3		-2.3944743 / -4	
25	-2.1474102 / -3		1.3208710 / -2		1.2519013 / -2		2.1324980 / -2		7.2609014 / -3		1.6730335 / -2	
26	4.2601650 / -3		4.4751090 / -2		2.5088473 / -4		4.4330764 / -3		3.9928263 / -2		4.8689220 / -4	
27	-4.9052030 / -2		-2.7527419 / -4		2.4779215 / -2		-5.8707349 / -3		-3.2153842 / -3		2.9407511 / -2	
28	1.9134382 / -3		6.1810507 / -3		3.0947291 / -3		1.4023342 / -2		4.0582154 / -3		1.0156321 / -2	
29	-3.7825146 / -3		1.0852740 / -2		-2.7695402 / -3		-7.2894019 / -3		6.4614496 / -3		1.8939513 / -4	
30	-9.7367457 / -3		4.8873353 / -3		-8.5802197 / -3		-3.3897628 / -3		2.5528741 / -3		-1.4771039 / -2	
31	4.4052367 / -6		3.1658454 / -4		2.6836163 / -3		-3.2239870 / -3		1.7311233 / -3		5.0918877 / -3	
32	1.7303486 / -3		1.3841180 / -2		7.8329197 / -4		-7.9481468 / -3		8.2647919 / -3		-5.3172804 / -3	
33	-6.4719475 / -4		-3.2887724 / -3		-3.6105593 / -3		-8.9064141 / -5		-6.2049690 / -4		5.2782654 / -3	
34	1.6010694 / -3		7.1449642 / -5		2.0013723 / -3		4.2281684 / -3		4.1994569 / -5		3.2105115 / -3	
35	-3.0412937 / -3		1.1129042 / -2		-1.6752581 / -4		-6.9126450 / -3		5.7990641 / -3		-7.1942636 / -5	
36	2.8823104 / -3		1.4986551 / -2		-1.0492637 / -2		-5.8186411 / -3		-4.8293735 / -3		7.5767165 / -3	
37	1.0531914 / -4		2.5935745 / -3		-2.0477905 / -3		-2.0076857 / -4		3.7867126 / -3		2.3954180 / -3	
38	-1.2573015 / -2		9.2294985 / -3		-5.2912561 / -3		-5.1364887 / -3		4.8640728 / -3		-5.4614623 / -3	
39	3.1386414 / -3		2.8929745 / -4		-1.9711832 / -2		4.1004370 / -3		1.1307906 / -3		1.1285903 / -2	
40	-1.3010411 / -3		2.5116993 / -4		-2.7760068 / -4		2.8100364 / -3		9.0438107 / -4		1.0481206 / -3	
41	-4.2682550 / -3		1.4038995 / -2		-3.3738166 / -3		-1.0803720 / -2		9.3934852 / -3		5.3046479 / -5	
42	1.9623375 / -3		-1.7431131 / -3		-1.9262523 / -2		8.0480247 / -3		-2.2222954 / -3		8.2477595 / -3	
43	1.8931023 / -3		-1.8815079 / -3		4.7689258 / -3		1.0465364 / -2		-1.9701445 / -3		1.2397258 / -2	
44	2.9066529 / -3		1.6655167 / -2		8.3003945 / -3		-1.3856465 / -2		1.1458568 / -2		-1.8467143 / -3	
45	6.1427381 / -3		1.8888654 / -3		-1.9559255 / -2		2.5534119 / -3		3.4116332 / -3		1.1516737 / -2	
46	4.3250995 / -4		1.4480428 / -3		2.0654596 / -3		-2.0979336 / -3		1.9371841 / -3		-6.0668540 / -4	
47	-1.1990988 / -2		1.2885692 / -2		-9.0423885 / -3		-1.0082594 / -2		7.8871083 / -3		-4.9786557 / -3	
48	5.0549093 / -3		1.0059937 / -3		-1.9127019 / -2		2.9419496 / -3		1.8017580 / -3		1.3038472 / -2	
49	-2.1927446 / -3		2.0468054 / -3		-4.4143106 / -3		-6.6943124 / -4		3.2881783 / -3		-1.4151351 / -3	
50	7.8407469 / -5		2.0743842 / -2		-3.8080160 / -3		8.7346815 / -4		1.0774150 / -2		6.9722779 / -3	
51	-1.6058777 / -3		-7.4288993 / -4		-1.0438327 / -2		3.6394391 / -3		-7.3434929 / -4		5.0538210 / -3	
52	7.8842457 / -4		-1.5676641 / -3		5.2259947 / -5		3.4321950 / -3		-2.9803285 / -3		2.0323201 / -4	
53	-9.8470145 / -4		2.4920967 / -2		-1.1613906 / -3		9.8055587 / -3		1.1063740 / -2		4.9606507 / -3	
54	3.8402165 / -3		-1.1415717 / -3		-1.3896961 / -2		2.1096459 / -3		1.0274256 / -3		1.1645903 / -2	

TABLE 2. C-5. ERTS FIXED-FREE FLEXIBLE MODE SHAPES (Continued)

	11.3	1	13.1	2	14.7	3	15.3	4	22.7	5	26.4	6
55	1.5280765	/ -3	-3.7360274	-3	-7.4404926	/ -3	-2.0702920	/ -2	-4.1921692	/ -3	1.1497081	/ -2
56	1.2359926	/ -1	1.0674656	/ -1	-3.4667713	/ -2	6.8446641	/ -2	-4.0903305	/ -2	-4.3586743	/ -2
57	5.5463540	/ -3	3.5053210	/ -2	-1.1926036	/ -1	1.1740173	/ -1	8.2980675	/ -2	5.8429015	/ -2
58	8.7039395	/ -5	-1.2815692	/ -2	-1.4370815	/ -2	3.5059490	/ -3	1.9630862	/ -2	6.7348667	/ -2
59	7.4585197	/ -2	6.3825422	/ -2	-3.9751060	/ -2	1.6015162	/ -2	-6.9804401	/ -2	-8.1673312	/ -2
60	-3.0464042	/ -2	5.3143810	/ -2	-8.8163932	/ -2	1.0303836	/ -1	6.2792756	/ -2	3.0331305	/ -2
61	-1.1555820	/ -2	1.8074528	/ -3	-7.7736997	/ -3	1.7937432	/ -2	2.5959708	/ -2	5.8604912	/ -2
62	5.8339662	/ -2	1.0672873	/ -1	-1.4539322	/ -2	2.9322345	/ -2	-9.9158665	/ -2	-4.4079812	/ -2
63	-3.1675861	/ -2	4.0227614	/ -2	-6.7312625	/ -2	6.9932354	/ -2	3.1972254	/ -2	8.3024546	/ -2
64	-3.2757145	/ -3	5.2670246	/ -3	7.5160979	/ -4	1.3514907	/ -2	1.2817738	/ -2	2.6388233	/ -2
65	-3.9876338	/ -2	1.2978124	/ -1	-1.1758613	/ -2	1.2720951	/ -1	-3.9875678	/ -2	-7.7810946	/ -2
66	-9.6631467	/ -2	7.9633234	/ -2	-3.5904110	/ -2	1.6260774	/ -1	5.8329225	/ -2	1.5869526	/ -2
67	-3.2167534	/ -2	-1.0002459	/ -2	-2.6396582	/ -2	2.9439788	/ -2	3.7614680	/ -2	5.5838402	/ -2
68	-6.4651317	/ -2	1.1094211	/ -1	-7.1494434	/ -2	6.3572469	/ -2	-6.1167942	/ -2	-1.8720377	/ -1
69	-1.4080604	/ -1	5.3598346	/ -2	-1.0904287	/ -1	9.8242990	/ -2	3.2424442	/ -2	-1.3173204	/ -1
70	-1.7306767	/ -2	7.2107096	/ -3	-1.2044594	/ -2	2.5988314	/ -2	2.9050073	/ -2	7.6420920	/ -3
71	-4.1086233	/ -2	7.5630716	/ -2	-3.3365975	/ -2	-1.3094360	/ -3	-9.1661[illegible]	/ -2	-1.0326317	/ -1
72	-1.2759627	/ -1	-2.2483216	/ -3	-1.1465125	/ -1	-2.0320653	/ -3	1.0061159	/ -2	-8.1102097	/ -2
73	-7.4893263	/ -3	2.4983461	/ -4	-5.4495472	/ -3	-1.3710859	/ -3	1.2737203	/ -2	1.7372414	/ -2
74	-6.7519700	/ -3	5.7397607	/ -2	2.0666853	/ -2	-6.5532936	/ -3	-6.9827840	/ -2	3.0184451	/ -2
75	-6.2649804	/ -2	2.6257644	/ -2	-8.1527120	/ -5	-2.7707522	/ -3	1.1295483	/ -2	1.5330205	/ -2
76	-2.4359467	/ -2	-8.5130800	/ -3	-1.6594691	/ -2	3.7771852	/ -2	4.9532947	/ -2	5.5575525	/ -2
77	-6.9226495	/ -3	7.0490915	/ -2	-2.0722252	/ -2	-1.7720443	/ -2	-7.1810875	/ -2	-6.0252702	/ -3
78	-5.4296703	/ -2	5.9170201	/ -2	-3.4571976	/ -2	2.8810874	/ -3	1.8634880	/ -2	-6.6954043	/ -3
79	-1.1024113	/ -2	1.3630119	/ -2	-3.1[illegible]1670	/ -3	2.6799153	/ -2	3.4511763	/ -2	2.1567157	/ -2
80	4.4061428	/ -3	9.4240291	/ -2	-2.2866353	/ -2	1.6837859	/ -3	-7.4563804	/ -2	-1.5222979	/ -2
81	4.6211716	/ -2	2.1569325	/ -2	-4.0551992	/ -2	6.9839499	/ -3	1.3464212	/ -2	-2.3026603	/ -2
82	-9.2853381	/ -3	4.5949292	/ -3	-4.8924041	/ -3	9.7310120	/ -3	2.1895778	/ -2	1.2585114	/ -2
83	2.4572257	/ -2	2.1559476	/ -2	3.7243774	/ -2	-1.1473975	/ -1	-1.0965364	/ -1	5.9150074	/ -2
84	-2.7556342	/ -2	-9.3267044	/ -3	2.7659107	/ -2	-1.5726137	/ -1	-6.2130728	/ -2	-1.2104630	/ -3
85	-3.3646779	/ -2	-7.6852603	/ -3	-2.4262358	/ -2	3.1034964	/ -2	4.9040094	/ -2	7.9136115	/ -2
86	7.1038253	/ -2	8.4145468	/ -2	-2.5176672	/ -2	-3.3994829	/ -2	-8.1618463	/ -2	4.4526516	/ -2
87	2.6253965	/ -2	2.5201583	/ -2	-2.8875133	/ -2	-5.7532347	/ -2	-3.4364440	/ -2	-2.1625422	/ -2
88	-9.5319270	/ -3	4.1676498	/ -3	-8.3519658	/ -3	1.2763834	/ -2	2.6691572	/ -2	2.5408570	/ -2
89	7.0685860	/ -2	5.8287307	/ -2	-2.7010296	/ -2	2.8423273	/ -2	-6.3116386	/ -2	1.6847282	/ -2
90	5.5476437	/ -2	2.3563185	/ -2	-3.3464585	/ -2	1.1523878	/ -2	-6.7965770	/ -3	-5.7941900	/ -2
91	-1.6006039	/ -2	2.4444686	/ -3	-4.4683172	/ -3	9.3266793	/ -4	1.8962697	/ -2	2.1623596	/ -2
92	3.2952426	/ -2	5.5239682	/ -2	3.9842899	/ -2	-8.3074853	/ -2	-1.1262332	/ -1	4.9519601	/ -4
93	3.2427235	/ -2	3.7580200	/ -2	5.5961299	/ -2	-1.0782069	/ -1	-6.1820291	/ -2	-1.2314043	/ -1
94	-1.8392677	/ -2	-4.6349661	/ -3	-4.7067976	/ -3	1.1046314	/ -2	2.1830274	/ -2	4.0917874	/ -2
95	8.4124722	/ -2	8.9983287	/ -2	2.4921986	/ -3	1.3493363	/ -2	-5.9986944	/ -2	-2.1317517	/ -2
96	5.5572399	/ -2	5.5302809	/ -2	5.4295220	/ -3	-5.9084257	/ -2	-5.8693590	/ -2	-1.1732424	/ -1
97	-1.1045312	/ -2	-2.3562283	/ -3	-1.0719231	/ -2	6.0164179	/ -3	2.2547648	/ -2	4.3668656	/ -2
98	4.3807089	/ -2	4.9943386	/ -2	1.5377939	/ -2	6.3019957	/ -2	-3.5692870	/ -2	-1.9660971	/ -2
99	4.3022400	/ -2	3.2421909	/ -2	1.4021230	/ -2	1.6704867	/ -2	-6.1066136	/ -3	-1.1552341	/ -1
100	2.7065852	/ -3	5.4305270	/ -3	-1.5175400	/ -3	7.0417126	/ -3	1.2474512	/ -2	1.1165196	/ -3
101	-1.1498866	/ -1	1.0926446	/ -1	5.9837294	/ -2	4.8637464	/ -2	-4.1566568	/ -2	3.2567566	/ -2
102	2.1501561	/ -2	-2.0603223	/ -2	-1.6334501	/ -1	-6.5001962	/ -2	-7.5760823	/ -2	6.8129696	/ -2
103	-4.9591629	/ -3	-5.0695175	/ -3	2.4736146	/ -2	1.3020383	/ -2	2.2546419	/ -2	-5.1222100	/ -2
104	-4.5881456	/ -2	1.3973816	/ -1	6.3472416	/ -2	5.3987161	/ -2	-5.1799232	/ -2	9.5900226	/ -2
105	-2.5241583	/ -2	-4.8635064	/ -2	-1.3373859	/ -1	-3.5084963	/ -2	-6.5510469	/ -2	8.4085788	/ -3
106	1.3997372	/ -4	4.5414484	/ -3	7.2053590	/ -3	2.4086901	/ -2	2.4871465	/ -2	-2.4423710	/ -2
107	-3.9289966	/ -2	1.0739856	/ -1	2.0799199	/ -2	1.5316136	/ -2	-1.2024745	/ -1	6.9890858	/ -2
108	-3.5911219	/ -2	-4.9142575	/ -2	-1.0745547	/ -1	-2.6473064	/ -2	-2.1192009	/ -2	2.8286823	/ -2

TABLE 2.C-5. ERTS FIXED-FREE FLEXIBLE MODE SHAPES (Continued)

	11.3 1	13.1 2	14.7 3	15.3 4	22.7 5	26.4 6
109	-1.2957335 / -3	6.8.02309 / -3	4.9157178 / -3	1.0305802 / -2	9.8509727 / -3	3.2876163 / -3
110	6.05-3626 / -2	1.0587453 / -1	3.6206555 / -2	7.7066929 / -2	-2.2431997 / -2	5.5163499 / -2
111	-1.2390801 / -1	-5.5427577 / -2	-1.0148905 / -1	-7.4006433 / -2	-6.1149126 / -2	-2.1640560 / -2
112	2.9291864 / -2	-1.2539631 / -2	4.5177067 / -2	5.6355916 / -3	4.1596792 / -2	-5.2790966 / -2
113	1.0369275 / -1	1.1863129 / -1	6.8857774 / -2	3.1217091 / -2	-5.2194365 / -2	1.4793225 / -1
114	-1.4270954 / -1	-5.9566009 / -2	-1.3786825 / -1	-9.0232865 / -3	-3.0386296 / -2	-1.3172360 / -1
115	2.4734554 / -3	-4.7126591 / -3	8.9461624 / -3	6.9223028 / -3	2.4257607 / -2	-1.8549858 / -2
116	5.3642226 / -2	8.4663805 / -2	4.3561524 / -2	-2.8382795 / -2	-8.9309741 / -2	1.3459284 / -1
117	-1.2105734 / -1	-2.3714869 / -2	-1.1159946 / -1	4.1763052 / -2	7.6714969 / -4	-8.2058002 / -2
118	9.6860568 / -3	4.3554424 / -3	1.6965413 / -2	-1.7965359 / -3	1.4561653 / -2	-4.6597747 / -3
119	2.1529517 / -2	5.7169659 / -2	-3.0183013 / -2	1.5867839 / -5	-4.9598991 / -2	-2.0456771 / -2
120	-5.5752041 / -2	-2.0965908 / -2	2.3329742 / -3	1.1689122 / -2	-1.5812326 / -2	2.8400993 / -3
121	3.4570852 / -2	-1.0984781 / -2	4.4446009 / -2	1.5980498 / -2	4.9335033 / -2	-5.8250160 / -2
122	1.4261674 / -2	8.0464459 / -2	8.5444037 / -3	-1.1766575 / -2	-4.7291435 / -2	-8.5565755 / -4
123	-4.6522877 / -2	-3.0296256 / -2	-3.7406253 / -2	2.5983427 / -2	-9.8044134 / -3	-1.8072655 / -2
124	1.0564997 / -2	3.4282529 / -3	1.9069429 / -2	2.0276802 / -2	2.8751640 / -2	-1.9371916 / -2
125	9.6403448 / -3	6.9613969 / -2	1.4187740 / -2	-8.0669774 / -3	-5.8664757 / -2	-2.0732259 / -3
126	-4.2081312 / -2	-1.7882726 / -2	-4.1312316 / -2	2.6719168 / -2	3.4709853 / -3	-2.4798978 / -2
127	1.6158112 / -2	4.9849197 / -3	1.7204092 / -2	6.0132601 / -3	1.9755479 / -2	-1.1027725 / -2
128	-1.1366069 / -2	3.7882156 / -2	-8.8733569 / -2	-3.6405928 / -2	-9.1321819 / -2	-3.7256172 / -2
129	2.3462602 / -3	2.0546029 / -4	1.0397455 / -1	7.2761919 / -2	6.1030075 / -2	-1.2989206 / -2
130	3.4024035 / -2	-1.2235062 / -2	4.3196849 / -2	1.4792421 / -2	4.5048507 / -2	-6.2676984 / -2
131	-1.0240133 / -1	7.0293771 / -2	-1.2898442 / -2	-2.3231277 / -2	-7.0739560 / -2	-6.1485998 / -2
132	8.0210781 / -2	-2.9423524 / -2	2.2671351 / -2	4.3931191 / -2	3.0355410 / -2	-2.3015354 / -2
133	1.9305964 / -2	9.1585465 / -4	1.9631320 / -2	1.5218263 / -2	2.9267337 / -2	-2.2402063 / -2
134	-6.7312045 / -2	5.7713112 / -2	2.6165221 / -2	9.4276897 / -3	-6.0619273 / -2	-3.9346896 / -2
135	6.4839803 / -2	-1.1427439 / -2	-1.7665406 / -2	2.6435609 / -2	2.5316281 / -2	-4.0032854 / -2
136	9.1766224 / -3	4.9287299 / -3	1.0889581 / -2	2.6793650 / -3	1.6670171 / -2	-1.1024911 / -2
137	-4.4837335 / -2	6.8366015 / -2	-7.0194375 / -2	-2.4123360 / -2	-9.8665011 / -2	6.5899311 / -3
138	4.1545295 / -2	-2.8843568 / -2	1.0394558 / -1	6.6395863 / -2	8.6917376 / -2	-1.2284245 / -1
139	1.8153092 / -2	-5.9262369 / -3	2.6193463 / -2	8.3956996 / -3	3.7325191 / -2	-6.1884384 / -2
140	-5.6436822 / -2	6.5264139 / -2	-2.6054231 / -3	1.7127720 / -2	-6.5102481 / -2	3.0989610 / -2
141	5.0956765 / -2	-3.8097362 / -2	4.2041391 / -2	4.0465030 / -2	5.5979697 / -2	-1.4937664 / -1
142	7.6451245 / -3	-1.4915731 / -4	1.9273399 / -2	8.3484725 / -3	2.6006019 / -2	-2.8943910 / -2
143	-3.5236822 / -2	5.9011785 / -2	7.7161345 / -2	5.5320441 / -2	-3.4565532 / -2	8.6525518 / -3
144	3.1780042 / -2	-2.1456309 / -2	1.6745511 / -2	1.1186952 / -3	2.6257167 / -2	-1.4097842 / -1
145	4.0437703 / -3	4.3338685 / -3	1.2406865 / -2	2.9631406 / -3	1.5550669 / -2	-1.0908643 / -3
146	1.4651963 / -6	-5.5738020 / -6	1.4141996 / -6	-1.0056733 / -5	-2.4741269 / -6	-3.0733310 / -6
147	-4.2633380 / -7	1.5650435 / -6	-3.8302009 / -7	2.7421210 / -6	4.8652694 / -7	-1.1484585 / -6
148	-1.6287869 / -7	6.5500315 / -7	-1.5861722 / -7	1.1159164 / -6	1.5693596 / -7	-8.7920926 / -7
149	3.1417470 / -6	-1.2142212 / -5	3.2567852 / -6	-2.2193821 / -5	-6.0822548 / -6	-1.8824130 / -5
150	1.5732615 / -6	-6.1936105 / -6	1.7296601 / -6	-1.1425750 / -5	-3.3607121 / -6	-1.4327230 / -5
151	8.2135794 / -8	-3.5085638 / -7	8.7243990 / -8	-6.3907982 / -7	-1.6660722 / -7	-2.6322750 / -7
152	2.2544857 / -6	-8.9033946 / -6	2.5369859 / -6	-1.6786169 / -5	-5.5678014 / -6	-2.7398035 / -5
153	-1.5782141 / -6	6.2667178 / -6	-1.7776977 / -6	1.1142799 / -5	3.7162629 / -6	1.7737280 / -5
154	-9.1155986 / -7	3.3817716 / -6	-8.4612205 / -7	5.9081764 / -6	1.1169718 / -6	-1.2198349 / -6

TABLE 2. C-5. ERTS FIXED-FREE FLEXIBLE MODE SHAPES (Continued)

	27.5	7	31.9	8	36.8	9	39.5	10	41.5	11	43.1	12
1	1,2290521	-1	1.3919563	-2	-1.6429426	-2	-1.9760915	-2	4.0130259	-2	7.6980916	-3
2	-1,6034651	-2	-1.3592628	-2	-1.0592367	-3	9.4365693	-2	-2.8277510	-3	-7.7668265	-2
3	-1,6510777	-2	-8.0871309	-3	-3.2648991	-3	-6.3317665	-2	1.2277737	-2	7.7278713	-3
4	1.2174254	-1	-1.1394618	-1	2.4917943	-2	3.6197963	-2	7.1516869	-2	-1.4771467	-1
5	-1,4709062	-2	-7.4203815	-2	8.0586530	-2	1.0810725	-1	7.3180879	-3	-1.7081729	-1
6	-6,6862833	-2	3.6800066	-2	-7.3557690	-3	4.5653456	-2	5.0197001	-2	1.6457948	-2
7	9.2403384	-2	1.2917445	-1	-1.9243860	-2	1.6781736	-2	1.0272318	-1	1.6017152	-1
8	-7,8086857	-3	-8.7833886	-2	-3.5187853	-2	6.8972069	-2	-4.5638835	-2	-2.3132293	-1
9	-7,1869487	-2	-5.3337739	-2	-6.0045961	-3	-3.6442535	-2	4.7421000	-2	-1.0057084	-2
10	1.6639499	-2	-1.5974499	-2	-5.6511942	-2	-1.0165475	-2	8.2628846	-2	1.4783933	-3
11	5,5305645	-3	-7.2699168	-2	6.4809326	-5	2.0423844	-2	1.2847431	-2	-4.8142855	-2
12	-8,1643035	-2	4.3996137	-2	-2.1825788	-2	4.8066695	-2	3.2873726	-2	2.1457255	-2
13	1,3609104	-2	1.0656380	-2	-5.2581502	-2	6.3741065	-3	8.4999179	-2	-1.9774380	-2
14	-4.1002946	-3	-8.4250383	-2	-1.0229890	-3	1.0710196	-2	-9.3284906	-3	-3.5107380	-2
15	-7,8948466	-2	-3.5336239	-2	-4.4924653	-3	-4.2933178	-2	1.9812836	-2	-8.2229348	-3
16	-2.1002435	-3	1.0439383	-2	4.6971346	-4	1.6052475	-3	1.6157206	-2	9.9557949	-4
17	-3,4616428	-3	-3.7456664	-3	1.5252564	-2	-7.1585900	-4	3.3714123	-2	-1.2830191	-3
18	3.9710071	-4	-2.5585223	-2	6.6458463	-4	1.7745808	-3	3.3048005	-3	3.4869113	-3
19	-3,2329820	-2	2.7984530	-3	-2.4063752	-3	-4.5673160	-3	3.8239744	-3	1.0163714	-3
20	-3.2489030	-3	-4.4294336	-3	1.3146661	-2	5.3001220	-3	3.2631523	-2	1.7137758	-3
21	1,0857597	-2	-2.8503012	-2	-8.4888077	-4	1.3803218	-2	-8.8206386	-3	-5.1179038	-3
22	-2,9999565	-2	-9.9699727	-3	-2.0581644	-3	-1.5520409	-2	-9.3079510	-3	-7.5248664	-3
23	-3,9332792	-3	-4.1817854	-3	9.4476204	-3	-6.2922527	-3	3.2748459	-2	-2.1448898	-3
24	-3,8642741	-3	-2.6842589	-2	2.7212931	-3	8.4203971	-3	-3.1963713	-3	-1.0932961	-3
25	-3.6031405	-2	4.2503594	-3	-2.2941864	-3	3.2319507	-3	-5.2160923	-3	3.3656246	-3
26	-2.0913669	-3	-6.9024406	-3	2.0553964	-2	-9.6077115	-4	2.6056456	-2	-3.9011846	-3
27	-1,7383697	-3	-2.0601430	-2	-1.3344332	-3	2.0670735	-2	-4.2402765	-3	1.2635925	-2
28	-2.6471694	-2	-1.7414521	-3	-3.4453202	-3	-5.3793474	-3	-3.9939547	-3	-2.2479495	-3
29	-2,6962004	-4	6.5499456	-3	-1.5988795	-2	3.0373431	-3	-1.4274868	-2	5.1401629	-3
30	1.2899868	-4	-1.0582429	-2	-3.6556964	-3	-1.4444960	-2	-3.1128814	-3	7.4644667	-3
31	-5,4005477	-3	-4.6080306	-4	1.9213065	-3	-2.1318877	-3	-1.5884165	-3	-4.6442455	-3
32	1,6048897	-3	2.6396651	-3	-1.2054382	-2	7.4524066	-3	-1.8873679	-2	-1.3237387	-3
33	-1.4360356	-3	-8.2063219	-3	3.5698841	-4	-3.9090333	-3	3.4236794	-3	6.3569845	-3
34	-9,5015815	-4	2.4265357	-3	-8.7423740	-4	-1.0663807	-3	-8.8564745	-4	-5.6136351	-3
35	8,1044533	-4	8.1099996	-3	-1.3136324	-2	6.1250277	-3	-1.2132825	-2	4.7039002	-3
36	-1,9404182	-4	-1.2044538	-2	5.5377605	-3	-3.9394854	-3	-2.3513009	-4	7.6253798	-3
37	-9,7963977	-3	-1.1061503	-3	8.6924863	-4	-6.0298269	-4	2.3798742	-3	1.9407572	-3
38	2,7365287	-4	9.4972665	-3	-1.7425944	-2	-5.7847598	-3	-7.3729652	-3	9.0492940	-3
39	-7,4510564	-4	-1.1601815	-2	-3.6096592	-5	-7.6978334	-3	-3.7503621	-3	2.1241223	-2
40	-2,3323436	-3	-6.2892519	-3	1.5853465	-3	-3.7674769	-3	-6.2429492	-4	2.7133042	-3
41	-1,1908319	-3	6.9231861	-3	-2.1370652	-2	3.9461244	-3	-1.7782769	-2	6.5148373	-3
42	3,6407829	-4	-1.1652751	-2	-3.3874128	-3	-5.7079831	-3	2.1245753	-3	2.3210679	-2
43	-2,3172360	-3	-5.0869401	-4	3.6516794	-3	-2.4146342	-3	4.6554572	-4	-2.6238285	-3
44	-1,2363811	-3	9.9509341	-3	-1.5284118	-2	1.8090473	-2	-1.7746834	-2	-2.9427075	-3
45	-1,6481283	-3	-1.7794551	-2	4.1020566	-3	-6.5211035	-3	-4.4607528	-3	1.8329994	-2
46	-4,7296673	-3	2.7139154	-3	-1.0647949	-3	1.9055624	-3	1.0060260	-3	-3.0599507	-3
47	7,4217673	-4	1.0278692	-2	-2.0254546	-2	-5.6272994	-3	-9.0992754	-3	1.0132012	-2
48	1,4045043	-3	-1.9206675	-2	2.2495449	-3	-9.0333767	-3	-7.6666201	-3	1.7336245	-2
49	-5,5547210	-3	-4.8119939	-3	-8.6625401	-4	-3.9038657	-3	-1.3573060	-3	5.4810296	-3
50	2,2632598	-3	9.6179152	-3	-2.2353377	-2	8.9914095	-3	-2.8622883	-2	1.1663667	-2
51	-7,0195610	-4	-5.2998499	-3	-4.1051918	-5	-6.4000926	-3	-1.2116068	-5	1.3330579	-2
52	3,8442559	-5	-5.0808865	-4	4.1694771	-3	-1.4191906	-3	4.1198536	-3	-6.8507024	-4
53	-3,3339208	-3	5.4628925	-3	-2.2846741	-2	5.3262486	-3	-2.6064427	-2	9.2224206	-3
54	-7,0380627	-4	-1.0891527	-2	2.1704184	-3	-4.5450275	-3	1.5816027	-3	1.3698508	-2

TABLE 2. C-5. ERTS FIXED-FREE FLEXIBLE MODE SHAPES (Continued)

	27.5	7	31.9	8	36.8	9	39.5	10	41.5	11	45.1	12
55	-1,0580944	/ -2	-1.0501285	/ -2	1.6320801	/ -2	-9.2011622	/ -3	3,7364932	/ -2	-3.8296928	/ -3
56	1,1736332	/ -1	-1.1424054	/ -1	2.5725832	/ -2	1.1156945	/ -2	5.3252989	/ -2	-1.3910882	/ -1
57	-1,3689872	/ -2	-5.21[illegible]871	/ -2	8.1398885	/ -2	1.3008499	/ -1	-1.3029556	/ -2	-1.3930850	/ -1
58	-7,4925943	/ -2	4.5340739	/ -2	-6.0653374	/ -3	3,1102451	/ -2	3.3515872	/ -2	1.7308715	/ -2
59	5,7224620	/ -2	-8.5145374	/ -2	7.5681971	/ -2	4.1080281	/ -2	6.0404385	/ -2	-9.4209699	/ -2
60	-5,0810323	/ -2	-5.4241448	-2	1.2756240	/ -1	1.6552160	/ -1	-3.2193103	/ -2	-1.1013369	/ -1
61	-5,6112181	/ -2	1.7833681	/ -2	-7.2984673	/ -3	3.5226090	/ -2	2.4389311	/ -2	-4.8088455	/ -3
62	7.5195178	/ -2	-5.5981765	/ -2	-1.3917701	/ -2	3.9753017	/ -2	4.5019378	/ -2	-6.2039964	/ -2
63	-2,6923813	/ -2	-1.9970844	/ -2	4.7146093	/ -2	1.3794735	/ -1	-1.5813256	/ -2	-8.3440257	/ -2
64	-2,5420876	/ -2	2.8667141	/ -3	-3.0074267	/ -3	9.6254130	/ -3	1.4909730	/ -2	-7.8235308	/ -4
65	6.1269422	/ -2	9.7856268	/ -3	-1.6609875	/ -2	-3.1560820	/ -2	5.5272738	/ -3	9.6618339	/ -3
66	-3,5603032	/ -3	3.5449073	/ -2	4.0425542	/ -2	1.0000999	/ -1	-6.7538742	/ -2	4.9666661	/ -4
67	-8,7222486	/ -2	3,5405204	/ -2	-2.6186464	/ -2	3.9165296	/ -2	3.8528593	/ -2	7.4859013	/ -3
68	2,4666131	/ -2	4,7531540	/ -2	5.6289188	/ -2	-2.1416767	/ -2	1.0208320	/ -2	3.7645774	/ -2
69	-3,7226843	/ -2	4.1556543	/ -2	1.0784530	/ -1	4.1467694	/ -2	-5.9040231	/ -2	2.2411721	/ -2
70	-6,0670912	/ -2	1.3973373	/ -2	-7.8711463	/ -4	1.3004033	/ -2	1.9860125	/ -2	2.3156111	/ -3
71	2,3406449	/ -2	2.6339106	/ -2	1.4671274	/ -3	-3.7125891	/ -2	5.3016226	/ -2	2.7076025	/ -2
72	-1,0672325	/ -2	1.9552764	/ -2	6.7085430	/ -2	5.7126827	/ -2	1.0718187	/ -2	-6.2355906	/ -5
73	-2,4591337	/ -2	4.8294056	/ -3	-2.4564167	/ -3	5.1501189	/ -3	2.4328149	/ -2	5.4480190	/ -4
74	6.3339427	/ -3	2.1492724	/ -3	-2.5022456	/ -2	-9.3100941	/ -3	4.9042817	/ -2	2.0284584	/ -2
75	5,1534602	/ -3	-3.9361417	/ -2	6.5992140	/ -2	1.5360574	/ -2	-4.2814604	/ -2	-1.0962765	/ -3
76	-7,7960175	/ -2	3.7177304	/ -2	-2.2813388	/ -2	3.6445960	/ -2	3.0069319	/ -2	1.5237524	/ -2
77	3,0356575	/ -2	2.8446764	/ -2	3.6761084	/ -2	3.5529528	/ -4	1.0006229	/ -2	3.8464261	/ -2
78	1,4483791	/ -2	-1.4662799	/ -2	1.1484316	/ -1	2.4782665	/ -2	-7.1650217	/ -2	1.7114695	/ -2
79	-5,4126877	/ -2	1.2220417	/ -2	-2.2633028	/ -3	7.7706016	/ -3	1.5624909	/ -2	4.9312690	/ -3
80	1,2556374	/ -2	1.7574279	/ -2	-2.4861640	/ -2	-9.6663945	/ -3	5.7605773	/ -2	2.3690292	/ -2
81	3,4951184	/ -3	-2.4567316	/ -2	5.7672911	/ -2	2.6214947	/ -4	-3.4555795	/ -2	-2.1641512	/ -4
82	-2,1268246	-2	3.4429486	/ -3	-3.1873501	/ -4	-4.4821490	/ -4	1.5038150	/ -2	-7.4800172	/ -4
83	-5,2556674	/ -2	1.6603466	/ -2	-5.3414521	/ -3	6.7192335	/ -2	6.6224006	/ -2	7.7841473	/ -2
84	-1,6494297	/ -2	-7.7943363	/ -2	9.1121852	/ -2	5.7356859	/ -2	-3.2475203	/ -2	3.4462415	/ -2
85	-7,2420036	/ -2	3.8066881	/ -2	-1.8418949	/ -2	2.6077249	/ -2	3.4510859	/ -2	-3.0152015	/ -3
86	-4,2509842	/ -2	7.7464490	/ -2	4.6444929	/ -2	1.3604501	/ -1	5.6260141	/ -3	1.2718567	/ -1
87	-3,4701537	/ -3	-1.0037547	/ -2	1.3043679	/ -1	1.2461657	/ -1	-8.3253245	/ -2	8.2724522	/ -2
88	-4, 2[illegible]715	/ -2	9.7875578	/ -3	3.1643134	/ -3	1.2982595	/ -2	1.7873642	/ -2	3.4648040	/ -3
89	-3,2159941	/ -2	6.1696781	/ -2	-3.5401598	/ -2	9.0062965	/ -2	4.6814154	/ -2	7.9611525	/ -2
90	-7,1453347	/ -4	-6.4947126	/ -2	5.9809704	/ -2	8.0094676	/ -2	-5.7973854	/ -2	6.8918056	/ -3
91	-2,4522856	/ -2	2.4146353	/ -3	3.0231763	/ -3	-1.4449592	/ -3	1.5670456	/ -2	-4.5760247	/ -3
92	-1,8544839	/ -1	1.7085944	/ -2	3.7311187	/ -3	1.3191210	/ -1	1.4533588	/ -2	1.5160563	/ -1
93	-6,1872684	/ -2	-1.3157942	/ -1	1.1202656	/ -1	8.4014406	/ -2	-8.7428753	/ -2	7.7048344	/ -2
94	-6,8251402	/ -2	2.3514545	/ -2	2.4184123	/ -4	2.9239980	/ -2	1.2117466	/ -2	1.2112179	/ -2
95	-1,8558829	/ -1	2.8331665	/ -2	-1.9701140	/ -2	1.3586092	/ -1	1.9552555	/ -2	1.1384286	/ -1
96	-9,8944585	/ -2	-5.8261881	/ -2	1.0053725	/ -1	1.0985166	/ -1	-1.2207905	/ -1	8.3159414	/ -2
97	-4,8639595	/ -2	1.2744582	/ -2	-2.4493525	/ -3	2.8053982	/ -2	1.9069496	/ -2	-2.3507874	/ -3
98	-1,2729052	/ -1	2.8150118	/ -2	-9.0969110	/ -2	8.1813776	/ -2	5.9519993	/ -2	6.5481126	/ -2
99	-3,1356527	/ -2	-9.1670619	/ -2	4.1805208	/ -2	4.7396484	/ -2	-6.9070458	/ -2	1.9358048	/ -2
100	-1,2143899	/ -2	-5.0917094	/ -4	6.1834667	/ -4	9.1544076	/ -3	9.9135655	/ -3	1.4539112	/ -3
101	8,8356552	/ -2	1.1270240	/ -1	-1.2056272	/ -2	8.4033017	/ -3	8.5950827	/ -2	1.5201436	/ -1
102	1,5082457	/ -3	-9.0737435	/ -2	-3.1601561	/ -2	1.1127855	/ -1	-1.3988613	/ -2	-1.7912886	/ -1
103	-6,8039045	/ -2	-4.5947577	/ -2	-6.3052534	/ -3	-3.3636140	/ -2	2.8378149	/ -2	-7.3723526	/ -3
104	5,8699611	/ -2	3.6505732	/ -2	1.0791251	/ -2	-4.1971441	/ -2	3.5148736	/ -2	7.4443755	/ -2
105	4,8726957	/ -2	-9.5075126	/ -3	-8.6074096	/ -2	1.5420835	/ -1	2.0190999	/ -2	-9.9304650	/ -2
106	-3,7465645	/ -2	-1.0248979	/ -2	-7.9285393	/ -3	-1.0422023	/ -2	2.0813376	/ -2	2.2544835	/ -4
107	8,0987938	/ -2	4.0765028	/ -2	-2.9682910	/ -2	-5.0720876	/ -2	6.2948077	/ -2	4.6589502	/ -2
108	3,2751236	/ -2	-1.4156395	/ -2	-5.4129220	/ -2	1.4752057	/ -1	2.1978043	/ -2	-7.0539241	/ -2

TABLE 2. C-5. ERTS FIXED-FREE FLEXIBLE MODE SHAPES (Continued)

	27.5	7	31.9	8	36.8	9	39.5	10	41.5	11	43.1	12
109	-2,3071790	-2	-8.7648281	-3	-6.3644462	-3	-9.3822267	-3	1.2827205	-2	-5.6105513	-5
110	4,7369964	-2	-3.5762183	-2	-2.3104205	-2	5,2946764	-2	2.2266566	-2	-1.0875031	-2
111	6,8032108	-3	1.1218317	-2	-6.0149345	-2	2.0176251	-2	5.6647683	-2	-2.8395999	-2
112	-7,7436262	-2	-5.5349287	-2	-2.9204871	-3	-4.1962780	-2	2.8948613	-2	-1.7052226	-3
113	2.4143261	-2	-7.0572686	-2	3.3843089	-2	4.5003443	-2	-4.6671423	-3	-4.6411450	-2
114	2,3105527	-2	5.1920385	-2	-1.1124581	-1	4.3938147	-2	-,3615305	-2	9.9790184	-3
115	-4,5691724	-2	-1.7505703	-2	-1.2960073	-2	-1.3717606	-2	2.9517758	-2	-7.8874728	-4
116	3,6354613	-2	-5.1253535	-2	-1.2665556	-2	2.2157940	-2	5.4091522	-2	-4.2430803	-2
117	9,4351101	-3	2.7581961	-2	-7.6360653	-2	6.7412754	-2	2.5380432	-2	-1.5322938	-3
118	-2,5608883	-2	-2.1574379	-2	-2.3705239	-3	-1.4807410	-2	2.0848245	-2	-5.3527571	-3
119	8,1378197	-3	-1.5585991	-2	-1.9704965	-2	1.8023866	-2	5.0755069	-2	3.0734253	-2
120	-7,3459751	-3	-6.0046866	-2	-7.8833421	-2	2.0953432	-2	1.7634233	-2	-1.2037736	-2
121	-7,5062852	-2	-5.6981275	-2	-7.1387345	-3	-3.9065123	-2	1.9346008	-2	-2.2634531	-3
122	2,6644215	-2	-1.9750405	-2	3.5049107	-2	-2.6536472	-4	8.6980516	-3	-3.8222851	-2
123	-9,0144375	-3	-4.0517001	-2	-1.1271011	-1	4.1954816	-2	4.9846226	-2	-6.1993536	-4
124	-4,5391177	-2	-2.1516953	-2	-1.1824740	-2	-6.7946782	-3	2.1509891	-2	-3.9134512	-3
125	1,4659623	-2	-2.7434266	-2	-1.5205854	-2	4.0712435	-3	4.8256438	-2	-3.1230142	-2
126	-1,9960734	-3	-4.6991419	-2	-7.1125440	-2	3.9453815	-2	4.6122365	-2	-1.1768423	-2
127	-2,3059279	-2	-2.0716938	-2	-4.6210528	-4	-8.0963545	-3	1.5303527	-2	-1.8881838	-3
128	-5,9867166	-4	2.7796625	-3	-2.5473697	-2	-3.4080606	-2	6.6987668	-2	-6.4771741	-4
129	1,6411753	-2	-1.3036604	-1	-7.2068838	-2	4.1760319	-2	2.3602420	-2	9.6808700	-3
130	-7,1091194	-4	-6.2789150	-2	-9.4536100	-3	-3.9321078	-2	2.4430773	-2	-6.5437762	-3
131	-3,0819824	-2	-3.4168826	-2	4.6021463	-2	-1.2374955	-1	9.6287002	-3	-8.6761671	-2
132	-9,1704385	-3	-4.6310317	-2	-1.2046462	-1	1.1434652	-2	7.3900114	-2	2.8016175	-4
133	-4,2024925	-2	-2.2763158	-2	-1.1459411	-2	-3.3635757	-3	2.5465218	-4	-2.9674939	-3
134	-1,9515134	-4	-4.0539149	-2	-4.5574561	-2	-5.4294424	-2	4.4542922	-4	-4.5329685	-4
135	-7,2127399	-3	-8.1556996	-2	-5.0719588	-2	6.7136056	-2	1.2621279	-2	-,0464797	-3
136	-2,6946755	-4	-1.6661416	-2	-1.4551950	-4	-9.9627926	-3	1.6643416	-2	-3.1399320	-3
137	-1,4657202	-1	-7.6156635	-4	-4.2603464	-3	-1.0934696	-1	2.2194929	-2	-1.1565484	-1
138	3,0164810	-4	-1.1961995	-1	-1.1691625	-1	8.5598178	-2	5.7741059	-2	9.7908346	-4
139	-6,9995862	-2	-3.3801837	-2	8.3370984	-3	-4.3299679	-2	1.3614653	-2	9.5153110	-3
140	-1,4454762	-1	-5.3892379	-2	-1.5581023	-2	-1.3991891	-1	2.2870025	-2	-1.2230581	-1
141	1,9316654	-4	-6.5235729	-2	-1.0654939	-1	1.1711209	-1	9.7951499	-2	1.0828297	-1
142	-3,1640761	-2	-2.6763110	-2	-3.7705353	-3	-3.4066456	-2	2.0045711	-2	-2.8188943	-3
143	-1,2360898	-1	-5.2293867	-2	-7.8452855	-2	-7.8039494	-2	7.4060974	-2	-6.9312207	-2
144	6,2504370	-3	-8.8221910	-2	-4.0640875	-2	5.1490340	-2	4.5749711	-2	3.1075370	-2
145	-1,7104246	-2	-1.0215419	-2	1.2652295	-3	-8.1980968	-3	1.2981747	-2	-1.0333957	-3
146	-1,9123963	-5	-4.0811117	-6	-3.7152645	-7	-5.5013448	-6	-1.5949672	-5	1.1330087	-5
147	1,8793494	-4	1.7668208	-6	1,6315355	-7	1.5214764	-6	3.7375147	-6	-2.3854468	-6
148	1,1442679	-4	8.4691106	-7	7,9741233	-8	5.9697796	-7	1.2837861	-6	-7.3636326	-7
149	1,1125052	-3	-3.3865248	-6	-3.8622546	-7	-7,5776532	-6	-2.2473159	-5	1.5930311	-5
150	1,0202509	-3	4.7275913	-7	-2.5944237	-8	-1.9637497	-6	6.0426818	-6	4.1624175	-6
151	6,5517143	-6	-2.3004086	-7	-1.7587651	-8	-,9811325	-7	-8.8503757	-7	5.9192250	-7
152	2,0721722	-3	2.5919375	-6	1,3494546	-7	-3,9991725	-6	-1.3438459	-5	1.0649683	-5
153	-1,3265687	-3	-1.5230218	-6	-6,6811358	-8	1.9443252	-6	6.9785642	-6	-5.2583053	-6
154	2,8448069	-4	3.2161506	-6	3.0552498	-7	2,.955454	-6	8.4733809	-6	-3.9633981	-6

TABLE 2. C-5. ERTS FIXED-FREE FLEXIBLE MODE SHAPES (Continued)

	45.5	13	47.4	14	55.4	15	61.9	16	62.6	17	64.4	18
1	2.7104323	-4	-1.3246804	-1	1.5265351	-2	-1.7297437	-1	-4.5312151	-2	-3.6494022	-2
2	3.2550539	-3	3.7529290	-2	-9.1117603	-3	-1.2032016	-1	6.1378015	-2	3.3946984	-2
3	-1.3661170	-2	-3.6434631	-2	8.4381808	-2	4.4004423	-4	4.3750141	-2	3.2517155	-2
4	-1.5199429	-2	-7.1[illegible]3204	-2	1.2770031	-1	-1.5040774	-1	1.2483502	-1	-2.3525820	-1
5	-5.3839945	-2	7.0963588	-2	6.3431860	-2	-8.4308575	-2	-1.1157420	-2	-2.5873401	-1
6	-2.4661715	-2	4.1001864	-2	-1.2252295	-2	-2.0096032	-2	2.5826561	-3	1.8224420	-2
7	1.3500624	-1	1.0730599	-2	-1.1264857	-1	-2.8014921	-1	9.8699545	-2	1.8931093	-1
8	-1.0319906	-1	-4.0713726	-2	5.0451975	-2	1.0381652	-1	1.8517769	-2	-1.9592183	-1
9	-4.9907562	-3	4.7039396	-2	5.0795182	-3	-4.6379451	-2	-2.4042183	-2	6.2281127	-2
10	-1.1010225	-2	3.4711150	-2	-5.0358229	-2	-3.2736942	-2	-2.6215366	-2	3.0840141	-2
11	-3.0341565	-2	9.1053946	-3	-8.2742377	-2	-1.5190188	-2	-2.0838061	-2	-4.8037928	-3
12	-9.2329632	-3	2.4515019	-2	-8.4040737	-3	-8.4715880	-3	-2.4583666	-2	5.7619204	-4
13	3.0412590	-2	1.0498019	-2	6.0814445	-2	-3.8306826	-2	-4.0227039	-2	-1.7702572	-2
14	-4.2540164	-2	-1.1024362	-2	-1.0214224	-1	2.4433217	-2	2.8450539	-2	-1.9539699	-2
15	-2.2272145	-2	2.4553513	-2	1.4088283	-2	-1.1437478	-2	-3.0702439	-2	5.5081336	-3
16	6.7883364	-3	-3.4664360	-2	-7.2157498	-4	4.0763344	-3	5.1684294	-2	-5.1536511	-3
17	-7.6645485	-3	6.9303251	-3	1.76[illegible]726	-3	-1.1790588	-3	3.3704806	-3	7.0459437	-3
18	9.5198677	-3	3.4495562	-3	1.2866210	-2	-3.7561860	-3	1.5141286	-3	6.2070850	-3
19	-6.3326407	-3	-2.7849828	-2	4.9326504	-3	-1.0799215	-2	7.6355843	-3	5.0069552	-3
20	3.1750154	-3	6.2333140	-3	1.6639081	-2	-2.3651490	-3	4.1688613	-3	-7.8146344	-4
21	1.7428911	-2	7.1[illegible]34229	-4	3.6618238	-2	-1.0598235	-2	-9.4079889	-3	-3.5060589	-4
22	-2.4966851	-2	-3.1267417	-2	8.3877110	-3	-1.4249311	-2	4.3345973	-3	1.8363248	-2
23	-1.2640485	-2	4.209798	-3	-9.0106392	-3	-5.0708650	-3	3.9365594	-3	1.7669106	-2
24	1.5660825	-2	-7.7753965	-3	3.8835310	-2	9.3014524	-3	2.5349021	-3	-3.5176835	-3
25	-1.5777569	-2	-3.[illegible]447487	-2	6.0340871	-3	-1.3050285	-2	6.3050212	-3	1.0758227	-2
26	-4.4507452	-4	6.4299565	-3	-1.8414622	-3	6.5436871	-4	1.2465066	-3	1.6759972	-2
27	2.4044911	-2	-3.7[illegible]0272	-3	3.4466186	-2	9.1253457	-3	-5.7708390	-4	6.1225098	-3
28	-1.8876962	-2	-3.8845522	-2	5.6969356	-3	1.6079382	-3	1.1743278	-2	1.4455037	-2
29	1.7552251	-3	2.4356333	-4	-1.9229525	-3	-5.5865536	-5	1.5916841	-4	-5.3093273	-3
30	1.5076935	-2	-2.7583623	-3	-3.1493231	-3	-5.1163400	-4	-1.0119817	-3	-2.8334668	-3
31	-1.2117091	-2	7.[illegible]289741	-3	2.9899324	-3	-4.1332223	-3	4.8623177	-3	6.2841561	-3
32	8.3641874	-3	4.[illegible]381279	-3	-7.1452625	-4	3.1263419	-4	1.0783809	-3	-5.4724971	-3
33	2.9563441	-3	-5.[illegible]097050	-4	-2.6976476	-4	1.1626040	-3	-1.3759270	-3	4.0009428	-4
34	-1.0986569	-2	-3.[illegible]581570	-3	4.6211161	-4	-5.0466013	-3	1.0498908	-2	2.6769691	-3
35	5.4796761	-3	1.1265840	-3	-1.9789177	-3	1.7708900	-4	-6.4890473	-4	-6.7598736	-3
36	2.5315317	-4	-6.9755[illegible]81	-4	-4.1117950	-3	-8.0088042	-4	1.2570706	-3	2.8608354	-4
37	-1.0874429	-3	-1.7451684	-2	-4.9768438	-4	-8.9816743	-3	1.1459805	-2	1.7850007	-3
38	-2.4117160	-3	-3.8148746	-4	-2.7425183	-3	-1.4283823	-4	-1.9515031	-4	-3.9620803	-3
39	6.5506305	-3	-2.8697442	-3	-6.8802495	-4	-2.8990583	-3	6.9700566	-3	4.6938996	-4
40	-1.7842946	-3	-4.1661956	-3	2.4[illegible]955	-3	-1.3531940	-3	4.8102333	-3	1.3108224	-3
41	3.8445859	-3	-1.7121835	-3	-2.0[illegible]371	-3	-8.7460330	-4	5.0394378	-3	-7.1521615	-3
42	3.2438184	-3	-2.4786767	-3	3.0417732	-3	-1.9746150	-4	-1.6067139	-3	-4.6560906	-4
43	-1.8982699	-2	-4.[illegible]123177	-3	6.3752917	-3	-5.6485897	-3	6.1218422	-3	7.6031628	-3
44	1.5047350	-2	2.6371482	-3	-6.0011746	-4	-1.4970736	-3	-1.2182698	-3	-1.2208100	-2
45	1.0364774	-2	-4.1766207	-3	-3.7915927	-3	-2.1634419	-3	4.2814507	-3	-4.1279261	-3
46	-1.3272803	-3	-8.9550824	-3	-5.5469209	-5	-5.1598204	-3	1.1379679	-2	-1.2724113	-3
47	-1.1885563	-3	2.5541141	-4	-5.6441174	-3	3.9280735	-4	2.3386307	-3	-5.1742656	-3
48	4.9100662	-3	-1.4047087	-3	-4.4796266	-3	-9.4762767	-4	-4.1536170	-4	-2.9576589	-4
49	4.0752526	-3	-1.1652689	-2	-1.5594849	-3	-4.3736421	-3	1.6710712	-2	-2.2992671	-3
50	6.8198849	-3	-6.7009146	-4	-1.0449686	-3	1.9723411	-3	4.8229402	-3	-9.6664353	-3
51	1.6784276	-3	-2.1569671	-3	3.4933328	-3	-8.5748661	-4	6.2621946	-4	3.2303086	-3
52	-2.8463615	-3	-8.2695094	-6	3.3005316	-3	-3.1650348	-4	-2.4561898	-4	-7.0509858	-3
53	5.2379651	-3	5.4685340	-4	-2.5216780	-3	1.6977502	-3	-4.2232672	-3	-4.6695580	-3
54	3.0434775	-3	-2.0408479	-3	-3.5947431	-3	-1.3710386	-3	3.8432977	-3	6.3251138	-5

TABLE 2. C-5. ERTS FIXED-FREE FLEXIBLE MODE SHAPES (Continued)

	13	47.4	14	55.4	15	61.9	16	62.6	17	64.4	18
55	-2.3380644 / -2	-1.6477294 / -2		7.5464261 / -3		-1.5839265 / -2		3.5685631 / -2		1.5498822 / -2	
56	4.9054695 / -2	-0.0186687 / -2		4.4296172 / -2		-1.4419750 / -1		4.4037523 / -2		-6.8268972 / -2	
57	1.3028206 / -2	6.3137207 / -2		6.2860788 / -3		-8.0035455 / -2		-1.1274866 / -2		-1.0264182 / -1	
58	-2.0260801 / -2	3.1908066 / -2		-3.2394257 / -3		-8.4062365 / -3		-1.0673421 / -2		-1.3668340 / -2	
59	6.7326845 / -2	-1.9028326 / -1		-2.8081712 / -2		1.3562529 / -1		-7.7610932 / -2		1.4942075 / -1	
60	4.5332874 / -2	-7.6782823 / -2		-9.4774655 / -2		1.5007641 / -1		-1.5263633 / -1		1.5508290 / -1	
61	-7.5298677 / -3	6.4191568 / -3		-1.1747197 / -2		-9.2188781 / -3		-6.1439392 / -3		1.2672320 / -2	
62	6.6735268 / -2	-2.0596522 / -1		-5.3374919 / -2		2.1334259 / -1		-2.1533701 / -2		1.2732541 / -1	
63	4.3325024 / -2	-9.7252697 / -2		-1.3682879 / -1		2.4296798 / -1		-9.4443183 / -2		1.2919957 / -1	
64	-8.2610613 / -3	-3.6795389 / -2		-6.7340196 / -3		-6.5014061 / -3		1.3468132 / -2		2.5408823 / -2	
65	-3.4327875 / -2	-1.4886971 / -2		1.1198257 / -2		-9.5203850 / -2		5.2956859 / -2		1.9630873 / -2	
66	-5.6661105 / -2	3.7774045 / -2		-3.9377812 / -2		-5.4101323 / -2		2.8261168 / -2		-5.9770179 / -2	
67	-5.5381997 / -3	2.5115293 / -2		1.0565823 / -3		-6.5995268 / -3		-3.6681175 / -3		4.2569943 / -3	
68	-1.6550276 / -2	-9.5660829 / -2		5.5466141 / -2		-4.0552343 / -2		-9.2719458 / -2		5.1229114 / -2	
69	-5.6527918 / -2	-3.4982679 / -2		4.8714510 / -3		-1.3007329 / -2		-1.1950611 / -1		1.0088662 / -2	
70	-4.1775740 / -3	-1.0516555 / -2		5.1912787 / -3		2.9905125 / -3		2.7019638 / -2		1.7231025 / -2	
71	2.0379879 / -2	-9.4366551 / -2		3.1039740 / -2		-1.5980067 / -2		-1.1349107 / -1		1.9164906 / -2	
72	-3.7189253 / -2	-1.3751476 / -2		-2.3583292 / -2		7.1596824 / -3		-4.9648037 / -2		-2.2588356 / -2	
73	-1.1978345 / -3	-3.9237085 / -2		2.8163927 / -4		-5.9034305 / -3		3.8394503 / -2		1.6604811 / -2	
74	-5.3005442 / -2	1.7046690 / -2		-6.5301549 / -3		-3.4033977 / -2		-3.6517535 / -2		3.5241952 / -2	
75	-1.1316928 / -1	1.1274449 / -2		-4.5771728 / -2		-2.1613789 / -2		-2.7221388 / -2		8.6907919 / -3	
76	-1.1751490 / -2	3.0083804 / -2		-3.3626082 / -3		-1.5724471 / -2		-2.9218140 / -2		1.9891634 / -3	
77	-1.0151578 / -1	2.2563459 / -2		8.0626258 / -2		1.6928803 / -2		6.5955174 / -2		5.7516935 / -2	
78	-1.5217283 / -1	4.0822196 / -2		1.2594570 / -2		-7.3406336 / -3		-1.7391529 / -2		8.1182464 / -3	
79	-1.1337509 / -2	3.3668583 / -4		-3.5793621 / -3		-7.4671553 / -3		4.[illegible]3817 / -3		6.8288472 / -3	
80	-6.6580575 / -2	2.6910481 / -2		5.6023169 / -2		-1.6833661 / -2		-3.2477551 / -2		2.2298353 / -2	
81	-1.1080052 / -1	1.1216569 / -2		1.5183301 / -2		-6.3573052 / -4		-7.4134047 / -3		-2.8756324 / -2	
82	-7.8988399 / -3	-2.9482920 / -2		-3.7356043 / -3		-1.3632785 / -2		2.8703074 / -2		1.6818022 / -2	
83	-4.2955479 / -3	2.3027541 / -2		-6.5086610 / -2		-3.0387601 / -2		-5.2352560 / -2		1.1078744 / -2	
84	-6.5911432 / -2	-1.7860111 / -2		-1.3202820 / -1		-2.6458207 / -2		5.5324483 / -3		1.4064230 / -2	
85	-3.6042400 / -2	2.5729664 / -2		8.1521780 / -3		-2.2367890 / -3		-4.2932334 / -3		1.7381854 / -2	
86	-2.2897412 / -2	7.1377273 / -2		1.0821521 / -1		1.1011791 / -1		1.8503519 / -1		4.4906713 / -2	
87	-7.3368642 / -2	2.3904813 / -2		6.7976519 / -2		1.0914645 / -1		1.2392766 / -1		1.6921520 / -2	
88	-1.3807352 / -2	2.6295485 / -3		1.0888168 / -3		-1.9396066 / -3		1.2860073 / -2		3.4515959 / -3	
89	-4.6590288 / -4	7.4292572 / -2		1.4542310 / -1		1.0067165 / -1		.2347559 / -1		-4.4130172 / -2	
90	-3.2973567 / -2	1.7764241 / -2		1.2486694 / -1		4.0563457 / -2		5.8602436 / -2		-6.3861751 / -2	
91	-1.3420972 / -2	-2.1329157 / -2		-7.3540838 / -3		-5.7217206 / -3		3.8507943 / -2		1.2688943 / -2	
92	-6.9320950 / -3	5.5048778 / -2		-1.0013059 / -1		-5.8865961 / -2		-1.3365194 / -1		-1.5415998 / -1	
93	-3.7231561 / -2	-2.6422967 / -2		-1.1223772 / -1		-9.9697992 / -2		-4.3644735 / -2		-1.7598228 / -1	
94	-2.6603463 / -3	7.4091353 / -3		-2.2046550 / -2		-9.2077711 / -3		-2.6460119 / -2		3.3434639 / -2	
95	-3.5286430 / -2	1.0955920 / -1		1.5469478 / -2		4.1947449 / -2		-2.1015819 / -2		4.9835938 / -2	
96	-6.8097422 / -2	3.6852436 / -2		-2.3656610 / -3		-6.6591653 / -3		2.5778222 / -2		8.4232696 / -2	
97	1.2602621 / -3	-2.0174109 / -2		-8.3776328 / -4		6.1076903 / -4		2.5555249 / -2		-1.7201090 / -3	
98	5.9657199 / -3	9.6059465 / -2		3.5982901 / -2		9.2535916 / -2		9.8201962 / -3		8.6850568 / -2	
99	-4.3903994 / -2	3.0005219 / -2		1.5019209 / -2		3.7745944 / -2		4.0952403 / -2		7.1912968 / -2	
100	-1.1311635 / -3	-3.4664407 / -2		1.2123979 / -2		-1.6410677 / -2		3.5564901 / -2		-1.0054837 / -2	
101	-3.3248134 / -2	-3.4619683 / -2		-6.5462780 / -2		-1.2039154 / -1		6.0281034 / -2		2.2486113 / -2	
102	1.8879172 / -2	-3.8953404 / -2		3.7066121 / -3		7.6355978 / -2		1.2970167 / -2		-9.2012105 / -2	
103	-6.5328611 / -3	2.3168392 / -2		3.9046950 / -3		-2.6606321 / -2		-2.1526570 / -2		3.4887433 / -2	
104	-1.0520733 / -1	-1.2487387 / -1		-4.1707583 / -3		1.5930052 / -3		-1.1652066 / -1		-1.6211656 / -1	
105	9.0431021 / -2	4.4391273 / -2		-4.2606028 / -2		-1.0983 45 / -1		1.0542395 / -1		6.2133537 / -2	
106	-8.4371575 / -3	-1.3952188 / -2		7.2637818 / -3		-1.5018860 / -2		-1.7369504 / -2		1.3626246 / -2	
107	-1.0376163 / -1	-1.9107453 / -1		3.5268510 / -2		1.5243660 / -1		1.4063911 / -2		-1.6751148 / -1	
108	8.5591462 / -2	9.6714824 / -2		-9.4537706 / -2		-2.4524[illegible] / -1		7.2771759 / -2		1.1270653 / -1	

TABLE 2.C-5. ERTS FIXED-FREE FLEXIBLE MODE SHAPES (Continued)

	45.5	13	47.4	14	55.4	15	61.9	16	62.6	17	64.4	18
109	-2,7406617	-2	-3.8102882	-2	6.7065825	-3	-4.2510035	-4	2.7151532	-2	5.0287989	-3
110	3.8843551	-2	-5.3963811	-3	8.6794487	-3	-7.5078442	-2	2.6621072	-2	-4.9795820	-2
111	-5.6143234	-2	-3.0476971	-2	-3.8192168	-2	1.4306810	-2	-2.3349274	-2	2.0030450	-2
112	-2,4364603	-2	1.9709265	-2	7.3522933	-3	-8.1001335	-4	7.3368797	-4	6.2735450	-3
113	-3,3385840	-2	-5.3777661	-2	-5.3282883	-2	-5.3300737	-2	-9.6836489	-2	-2.4715482	-2
114	2,9653342	-3	2.9463439	-2	-2.4100439	-3	2.7021155	-3	1.2530558	-1	-3.1536731	-3
115	-1.7364536	-2	-1.1294553	-2	1.8283430	-3	-4.7845457	-3	2.5099376	-2	-9.0211624	-3
116	-3,0270497	-2	-8.1983260	-2	-3.2674126	-2	-2.7232628	-2	-1.0174140	-1	1.8927225	-3
117	9,4696162	-3	2.1046062	-2	-1.7794267	-2	-1.5019866	-2	4.4514728	-2	-4.6346035	-2
118	-2.0798968	-2	-2.7796806	-2	-8.1627592	-4	-7.8857599	-3	4.5736396	-2	-1.7863704	-3
119	4,2667060	-2	1.9921738	-2	1.5845494	-2	-4.4564596	-2	-3.0721700	-2	-1.6598687	-2
120	-7.9521900	-2	-8.7140988	-3	-5.4532736	-2	1.6023471	-2	1.6644867	-2	-1.5924402	-2
121	-1,5109716	-2	2.6719494	-2	8.4564150	-3	-2.9495216	-3	-1.4269849	-2	5.5927265	-3
122	7,6590506	-2	1.9656699	-2	-4.1584177	-2	-2.0988202	-2	4.3757758	-2	-2.8822934	-3
123	-9,3250104	-2	-2.3392145	-2	1.0722038	-2	2.8170244	-2	3.3194059	-2	-2.9995914	-2
124	-9,6530969	-3	-1.9438259	-3	5.4059922	-3	-1.3924151	-2	7.6410968	-4	-5.1253339	-3
125	5.1764234	-2	2.4365135	-2	-4.1783922	-2	-4.5694175	-2	-3.8593211	-2	2.2172496	-2
126	-7.4526921	-2	-4.1709634	-3	1.2095612	-2	1.7023719	-3	6.1860697	-3	-6.7193808	-2
127	-7,2112844	-3	-2.8068563	-2	3.9763779	-3	-1.9301335	-2	1.5206850	-2	-2.8146918	-4
128	1,4798891	-3	3.6363810	-2	7.9058233	-2	-3.7651631	-2	-4.8674885	-2	9.2357259	-3
129	-4,4644169	-2	1.1749576	-2	-1.4580377	-1	2.2964974	-2	1.4528445	-3	-8.3818176	-4
130	-1.1169770	-2	2.5869457	-2	5.3146162	-3	-7.2610002	-3	-1.6389565	-2	5.2388771	-3
131	2,5376253	-2	7.7686525	-2	-1.2755456	-1	7.1920265	-2	1.7276875	-1	-7.2404537	-2
132	-6.2137162	-2	-2.1449165	-2	9.2175658	-2	-8.5365124	-2	-2.1777314	-1	3.5721094	-2
133	-8.0887560	-3	-2.9485009	-4	1.8011093	-2	-9.0146964	-3	9.9173044	-3	1.8305441	-2
134	2,7923144	-2	7.4998533	-2	-1.5021209	-1	7.3779765	-2	1.1459282	-1	3.0858049	-2
135	-6.1443197	-2	-7.4170928	-3	1.4302679	-1	-3.3758656	-2	-6.3389910	-2	-5.5706711	-2
136	-8,1427346	-3	-1.9090092	-2	2.5924707	-3	-1.8690047	-2	2.2756913	-2	1.1035271	-2
137	-1,6359361	-2	8.9.44229	-2	8.3417691	-2	-1.2096207	-1	1.7518296	-1	6.7406087	-2
138	-6,3978599	-2	-1.8543204	-2	-1.0946742	-1	8.0343497	-2	3.2185488	-2	-1.0508336	-1
139	-4.0698815	-2	-4.4207971	-3	1.6396190	-2	-5.8719678	-3	-1.9706636	-2	-2.1591811	-2
140	-3.5593553	-2	9.9030501	-2	3.2982435	-3	5.7304721	-2	-2.5330162	-2	-8.3811079	-2
141	-3.4552101	-2	-1.4735233	-2	-2.7167023	-3	-2.1080869	-2	-3.6064854	-2	7.9966049	-2
142	-2,9623604	-2	-2.1073654	-2	4.1466234	-3	-5.9355964	-3	1.3591816	-2	3.3899240	-3
143	-7,2362275	-3	8.9179100	-2	-3.4686304	-2	1.1080854	-1	-3.8637803	-2	-1.0104212	-1
144	-4,6473364	-2	-7.9903239	-3	3.2805351	-2	-3.2024127	-2	-2.5165468	-2	9.7973810	-2
145	-1,4980288	-2	-3.2215333	-2	-9.5367726	-3	-2.9068042	-2	2.2958551	-2	2.1732607	-2
146	-2,1484473	-3	2.8225996	-3	-2.2042779	-6	1.3513840	-4	-1.1930639	-3	2.3041174	-5
147	2,7525749	-6	-6.6868125	-5	7.2277222	-6	9.3979281	-4	1.1711567	-4	-1.2490166	-5
148	2.0466505	-7	1.0924937	-4	4.7041573	-6	7.2240836	-4	-1.0642045	-5	-6.3018975	-6
149	-3.0077444	-5	2.7535727	-3	-7.7547756	-6	-4.6008246	-4	-1.8021704	-3	4.1352308	-5
150	-7.4975139	-6	5.8977183	-4	-6.4486319	-6	-2.1545720	-5	-1.0983190	-3	2.1915365	-5
151	-1,2084686	-6	1.1095375	-4	-2.2604130	-8	6.0164360	-4	-5.6592207	-4	4.2994917	-6
152	-2,6485022	-5	3.1368612	-3	1.7062848	-5	1.1289335	-3	-1.3918350	-4	-6.4033513	-6
153	1,2096749	-5	-1.3056636	-3	-3.0320053	-6	-8.2384937	-4	9.3814827	-4	-1.0270071	-5
154	3.5274279	-6	1.1494484	-4	1.6625179	-5	1.9059074	-3	3.9325542	-4	-2.8092576	-5

TABLE 2. C-5. ERTS FIXED-FREE FLEXIBLE MODE SHAPES (Continued)

	82.8 19
1	-2.3967681 / -2
2	-1.9883145 / -3
3	-1.0667456 / -3
4	1.5992044 / -1
5	2.2330234 / -1
6	7.4861075 / -2
7	1.5527512 / -1
8	-1.8227539 / -1
9	6.9532552 / -2
10	2.1371559 / -2
11	1.0459615 / -2
12	2.3446617 / -2
13	1.7609261 / -2
14	-2.0680351 / -3
15	2.6725673 / -2
16	1.5362731 / -4
17	-8.0432404 / -3
18	-5.1692630 / -3
19	1.8344192 / -2
20	1.5372724 / -3
21	1.0495403 / -2
22	-3.4124052 / -2
23	-2.1745775 / -3
24	5.1869236 / -3
25	-3.7260111 / -2
26	-5.9196213 / -2
27	6.7672256 / -3
28	-1.9356065 / -2
29	5.1061516 / -3
30	4.4252354 / -3
31	1.1536163 / -3
32	2.2271869 / -3
33	1.9005971 / -3
34	-5.0054701 / -3
35	2.4568437 / -3
36	-1.6427626 / -3
37	3.0942712 / -3
38	4.1700854 / -3
39	1.1069683 / -3
40	-3.4079027 / -3
41	7.2179371 / -3
42	-1.0202110 / -3
43	-1.0718364 / -2
44	3.9796231 / -3
45	7.3058577 / -4
46	7.9458161 / -4
47	6.4535085 / -3
48	1.4157460 / -3
49	1.9103396 / -4
50	-6.0822925 / -3
51	-2.2493538 / -4
52	-6.1474114 / -4
53	-2.0131021 / -2
54	-7.4971577 / -4

TABLE 2. C-5. ERTS FIXED-FREE FLEXIBLE MODE SHAPES (Continued)

82.8 19

55	2.2133260 / -2
56	8.6421404 / -2
57	1.5428219 / -1
58	5.2874052 / -2
59	1.7660708 / -1
60	1.7669586 / -1
61	2.0973155 / -2
62	-4.4743801 / -3
63	5.4478018 / -2
64	-1.4256679 / -3
65	-4.2632502 / -2
66	-2.0397540 / -2
67	3.0977369 / -2
68	4.5778152 / -2
69	6.7897455 / -2
70	3.0554638 / -2
71	3.3223079 / -2
72	1.1327369 / -1
73	1.3854119 / -2
74	9.6191426 / -3
75	9.9568901 / -3
76	2.7594491 / -2
77	8.8448066 / -3
78	1.9489432 / -2
79	2.2617353 / -2
80	1.4371462 / -2
81	7.2344159 / -3
82	2.2123949 / -3
83	4.7038158 / -2
84	1.8974064 / -2
85	3.9317729 / -2
86	1.8063520 / -2
87	-5.5743566 / -3
88	2.5530270 / -2
89	7.1714137 / -3
90	-3.0980975 / -2
91	6.2734137 / -3
92	-3.7366448 / -2
93	-6.8006933 / -2
94	2.7720897 / -2
95	-3.6383795 / -2
96	-1.3116901 / -1
97	2.9915043 / -2
98	-3.0816200 / -2
99	-7.8457962 / -2
100	5.8870936 / -3
101	7.1949319 / -2
102	-1.3362410 / -1
103	3.6641780 / -2
104	5.3652461 / -2
105	-1.4524576 / -1
106	2.1434111 / -2
107	1.7115078 / -2
108	-5.8708207 / -2

TABLE 2.C-5. ERTS FIXED-FREE FLEXIBLE MODE SHAPES (Continued)

	828	19
109	-8.6714815	/ -4
110	-2.1555183	/ -2
111	-2.1706447	/ -2
112	4.2072872	/ -2
113	3.2526191	/ -2
114	-7.4893589	/ -2
115	1.6482146	/ -2
116	3.7704507	/ -2
117	-9.0467302	/ -2
118	6.7961547	/ -3
119	4.7353119	/ -3
120	-3.1977836	/ -2
121	3.5213068	/ -2
122	2.0351284	/ -2
123	-3.5808100	/ -2
124	1.3696174	/ -2
125	1.7514411	/ -2
126	-2.0996905	/ -2
127	2.3264002	/ -3
128	1.3477573	/ -2
129	-9.4337793	/ -3
130	2.6025494	/ -2
131	2.2683940	/ -2
132	-1.6617600	/ -2
133	2.1366872	/ -2
134	1.3098230	/ -2
135	-5.8261705	/ -3
136	4.0596332	/ -3
137	-2.3755710	/ -2
138	5.5801653	/ -2
139	3.2260952	/ -2
140	-2.5396322	/ -2
141	6.1737573	/ -2
142	1.3632155	/ -2
143	7.5188386	/ -3
144	2.8536484	/ -2
145	6.6055540	/ -4
146	2.3841842	/ -6
147	-1.2099954	/ -6
148	-6.2564224	/ -7
149	4.2477593	/ -6
150	1.9434153	/ -6
151	2.0116333	/ -7
152	4.1016755	/ -7
153	-1.0924050	/ -8
154	-2.5875228	/ -8

TABLE 2. C-6. COUPLING BETWEEN RIGID BODY AND NIMBUS "D" FIXED-FREE FLEXIBLE MODE SHAPES (GENERALIZED WEIGHT)

	X	1	Y	2	Z	3	M_X	4	M_Y	5	M_Z	6
1	-4.3830925 /	0	-9.8379444 /	0	2.5812644 /	-1	-1.0522930 /	3	-1.0202179 /	2	-1.8698927 /	2
2	2.5370885 /	1	4.4329223 /	0	1.5034208 /	0	1.3885850 /	2	1.4911082 /	3	-1.3704663 /	2
3	-2.9747993 /	0	-1.3352922 /	1	2.0211190 /	0	-3.9062814 /	2	-1.9164513 /	2	1.4938539 /	1
4	-1.6216679 /	1	2.9257635 /	-1	5.1450810 /	0	3.9461984 /	1	-7.7092808 /	2	4.6230657 /	1
5	1.2802733 /	1	-1.8816668 /	-1	4.3672840 /	0	4.5403087 /	0	6.7836971 /	2	-1.7072766 /	1
6	-1.7184421 /	0	7.2042837 /	0	6.7330712 /	0	3.8497217 /	2	-6.5197265 /	1	-1.1133369 /	2
7	-9.4477240 /	-1	-5.9481258 /	-1	-1.7556831 /	1	-4.2589253 /	1	-5.6524540 /	1	1.2019018 /	1
8	7.7104117 /	0	-2.5129526 /	1	-1.5522567 /	0	-1.3114471 /	3	1.1940414 /	2	1.1548776 /	2
9	-1.6484136 /	1	1.4102425 /	0	1.2330792 /	-1	6.4361867 /	1	-3.4037145 /	2	-1.0418062 /	2
10	5.2388728 /	0	-1.4017951 /	0	-3.1606078 /	0	4.3157465 /	2	1.6978795 /	2	-2.4432136 /	2
11	-5.4376650 /	0	-2.8393583 /	0	1.1652402 /	0	-1.3939720 /	2	5.3628636 /	2	1.3995209 /	2
12	4.7759408 /	0	1.6544708 /	1	-1.0022188 /	0	5.2048205 /	2	1.6510563 /	2	1.2491615 /	2
13	3.7409451 /	0	7.3607299 /	0	-1.1705816 /	1	3.3860224 /	2	1.5384543 /	2	-5.4824908 /	1
14	2.9598020 /	0	-2.6196989 /	0	-1.9508260 /	1	-1.0038529 /	2	-5.2473414 /	1	-3.4653718 /	1
15	-2.2897729 /	0	2.8901006 /	0	3.3568559 /	0	3.8830441 /	2	-1.0232319 /	2	-9.7960535 /	-1
16	-1.5158960 /	0	-8.0002140 /	-1	-9.1851491 /	0	1.5993955 /	1	-2.0209819 /	2	2.5833293 /	1
17	7.9532171 /	-1	6.1399302 /	-1	1.3718115 /	1	-6.9454025 /	-1	1.1834447 /	2	-1.3659726 /	1
18	-5.2052568 /	0	-2.8351929 /	-1	6.7367531 /	0	1.5591682 /	0	-3.9504503 /	1	5.2627600 /	1
19	2.6834692 /	0	1.2876501 /	0	-4.5366323 /	0	6.2751989 /	1	-3.4248250 /	1	3.8654980 /	1

TABLE 2. C-7. INERTIA

	1	2	3	4	5	6
1	1.6182899 / 3	0	0	0	6.3772692 / 4	-5.4252908 / 2
2	0	1.6182899 / 3	0	6.3772692 / 4	0	-2.2729826 / 3
3	0	0	1.6209999 / 3	-5.4252908 / 2	2.3502176 / 3	0
4	0	6.3772692 / 4	-5.4252909 / 2	4.2195866 / 6	1.5411239 / 4	-1.0160932 / 5
5	6.3772692 / 4	0	2.3502176 / 3	1.5411240 / 4	4.2896040 / 6	-7.9528204 / 3
6	-5.4252909 / 2	-2.2729826 / 3	0	-1.0160932 / 5	-7.9528204 / 3	1.1091311 / 6

2. C. 4. 1. 4 Origin

The origin may be considered at the geometric center of a plane at the bottom of the Nimbus adapter. Dimensions to points on the spacecraft are measured from this origin.

2. C. 4. 1. 5 Axis Symbols

Yaw Axis: Z

Roll Axis: X

Pitch Axis: Y

Subscripts x, y, z will be used to denote acceleration, displacement, or force components.

2. C. 5 SIGN CONVENTIONS

2. C. 5. 1 DISTANCES

Positive directions of axes are as shown in the Figure under paragraph 2. C. 4. 1.

2. C. 5. 2 FORCES

Forces are positive when acting along the positive axis shown in the Figure under paragraph 2. C. 4. 1.

2. C. 5. 3 MOMENTS

Moments are positive as indicated by double arrows in the Figure under paragraph 2. C. 4. 1. Moments are positive in the sense of the motion of a right-hand screw.

SECTION 3

PAYLOAD

SECTION 3

PAYLOAD

3.1 INTRODUCTION

The payload for ERTS A and B is described in "Design Study Specification for the Earth Resources Technology Satellite, ERTS-A and -B," dated April 1969, revised October 1969 (S-701-P-3), issued by NASA/GSFC. This document specifies the basic payload requirements and characteristics which have been used in the performance of the Phase B/C Spacecraft System Design Study.

To supplement the information contained in S-701-P-3, the government has provided many documents, reports, and memos as advisory information and has held a series of interface meetings with the payload contractors in order to assist the overall Phase B/C study effort. This section of the SSD final report documents the major payload characteristics and interfaces as used by the General Electric Company in the conduct of this study. In some instances, estimates were made where specific information was not available. These are noted accordingly. The RBV camera subsystem, the MSS, the WBVTR and the DCS are discussed in Sections 3.3 through 3.6, respectively.

Many of the study tasks performed relate directly to one or more of the payload items. In an effort to summarize those studies related to a particular payload item, a table listing the type of study task and its location within the total SSD final report has been compiled (i.e., RBV camera alignment... see Volume II, Section 2.4.5). This table is contained in Section 3.7.

A summary of recommended changes to the payload equipment is contained in Section 3.8. These recommendations have been made where the results of the studies performed indicated that modification to the payload other than the spacecraft equipment is preferred.

3.2 PAYLOAD CHARACTERISTICS SUMMARY

The ERTS payload consists of the following:

1. Return Beam Vidicon Subsystem (RBVC)
2. Multispectral Scanner Subsystem (MSS)
3. Two Wideband Video Tape Recorder Subsystem (WBVTR)
4. Data Collection Subsystem (DCS)

The overall block diagram is shown in Figure 3.2-1. All items that are shown, except for the DCS and switching module, are Government Furnished Equipment (GFE). The payload/spacecraft interface is at the input to the switching and signal conditioning module and, for the DCS, at the output of the limiter.

Both RBVC and MSS outputs can be either transmitted directly (real time) or can be recorded for delayed playback. This is accomplished by using two identical and switchable WBVTR's. There is no on-board recording capability of the DCS data.

As a result of this interconnection scheme for the imaging sensors (RBVC and MSS) the Wideband Communication Subsystem input is supplied with six outputs, namely:

1. RBVC Video - Real-Time Signal
2. RBVC Video - WBVTR No. 1, Playback Signal
3. RBVC Video - WBVTR No. 2, Playback Signal
4. MSS Signal - Real Time Signal
5. MSS Signal - WBVTR No. 1, Playback Signal
6. MSS Signal - WBVTR No. 2, Playback Signal

Switching of these six outputs is provided by the Wideband Telemetry Subsystem so that any combination of two of these signals may be transmitted simultaneously to the ground.

The following four sections document the individual characteristics and interfaces for each payload subsystem that were used as a basis for the SSD study.

3.3 RETURN BEAM VIDICON (RBV) CAMERA SUBSYSTEM

3.3.1 SUBSYSTEM DESCRIPTION

The RBV Multispectral Camera System (Figure 3.3-1) consists of:

1. Three sensor housings, each containing a 2-inch Return Beam Vidicon, lens, mechanical shutter, focusing and deflection coils, and associated circuitry
2. Three camera electronics packages containing most of the required circuitry
3. One camera controller which provides all the required synchronizing signals to the cameras
4. One video combiner which combines the video output signals to provide one single video output.

The three sensor housings are boresighted in the spacecraft to view a common 100 x 100 nautical mile scene on the ground in three different spectral regions. Each lens has a diagonal field-of-view of 16.25 degrees. Each sensor housing has four mounting feet for attaching to the spacecraft. The three camera electronic packages, camera controller, and video combiner are configured to the sizes given in paragraph 3.3.2.

Power is applied to all three cameras by means of a main switch located in the spacecraft and actuated by a command. Upon application of power to the RBV Subsystem, a self-generated power reset pulse (0.5-second nominal duration) causes the logic to enter the warmup mode, which has a duration of 50 seconds. During this time the shutter is inhibited. During the warmup, the 1-Hz clock line is examined for the presence of a clock signal. If a signal is present, the camera will use it to synchronize the internal counter so that the exact time of the shutter exposure pulse may be related to the phase of the 1-Hz reference clock. This rephasing will occur only at the beginning of the first picture cycle when operating in the continuous mode, and at the beginning of each picture when operating in the single-cycle mode. Should the 1-Hz signal fail to be present during the warmup period, the programmer will inhibit this rephasing function and develop the shutter phasing internally. It is intended that shutter actuation time be known to within 10 milliseconds.

Two modes of operation are possible after the warmup period are selected by ground command:

1. NORMAL - the cameras continues taking picture every 25 seconds until commanded "off" by either stored or direct command.

2. SINGLE-PICTURE - the cameras will take one picture and then revert back to the "warm-up" mode until another single-picture command is received. This mode allows single pictures to be taken of selected areas.

Each camera has an "on-off" switch in series with the main switch (located on the S/C but not part of RBVC) and is also actuated by command.

The three sensors are exposed simultaneously every 25 seconds and are read out sequentially in 3.5 seconds per camera. The three video outputs are then summed in the video combiner to provide a single output to the video tape recorder.

The video signal characteristics are shown in Figure 3.3-2. The combined video signal begins at To + 13.5 seconds with horizontal sync pulses phased with an on-board,rotating head, wideband video tape recorder. These phased pulses are present until To + 25 seconds. Between To + 13.5 to To + 14.5 seconds, a 1.6 MHz test signal is added during the active portion of each horizontal line, (see Figure 3.3-3). At To + 14.5 seconds, the first vertical sync signal is generated indicating the start of readout for camera No. 1. The vertical sync signal consists of a 50 kHz tone added during the active portion of each horizontal line and it lasts for 0.2 second (see Figure 3.3-4). The composite video signal is then transmitted.

The three RBV cameras will be photometrically calibrated prior to launch, but there will be provisions for a commandable in-flight calibration. This calibration sequence will provide three calibration points on the video output waveform, i.e.:

1. Black level

2. Midbrightness

3. Peak brightness and for each spectral band camera.

The signals for the midbrightness and peak calibration points will be provided by the erase lamps, utilized for this purpose, modulated in a pulse-width mode and operated with the shutter closed. The signal for the black level calibration point is obtained with lamps extinguished, but read cycle energized.

3.3.2 GENERAL SPECIFICATIONS AND REQUIREMENTS

3.3.2.1 RBV Camera Performance Specifications

See Table 3.3-1.

Table 3.3-1. RBV Camera Performance Specifications

Item	Camera No. 1	Camera No. 2	Camera No. 3.
Spectral Bandwidth (nanometers)	475-575	580-680	690-830
Resolution (at maximum scene highlight contrast)	4500 TVL*	4500 TVL*	3400 TVL*
Edge Resolution (percentage of center)	80	80	80
Signal-to-Noise Ratio (at 10 RVL)	33 dB	33 dB	25 dB
Dynamic Range	50:1	50:1	30:1
Gray Scale ($\sqrt{2}$ transmission steps)	10	10	8
Horizontal Scan Rate (lines/sec)	1250	1250	1250
Number of Scan Lines	4200	4200	4200
Readout Time (seconds)	3.5	3.5	3.5
Video Bandwidth (MHz)	3.5***	3.5***	3.5***
Time Between Picture Sets (seconds)	25	25	25
Exposure Time, Nominal (milliseconds)	12 ± 5%	12 ± 5%	12 ± 5%
Exposures, Optional, Commandable (milliseconds)	8 ± 5% 16 ± 8%	8 ± 5% 16 ± 8%	8 ± 5% 16 ± 8%
Picture Smear	12 TVL	12 TVL	1 TVL
Image Distortion (maximum)	1%**	1%**	1%**
Deflection Skew (maximum) (degree arc)	+0.5%	+0.5%	+0.5%
Size and Centering Shift (maximum)	± 2%	± 2%	± 2%
Residual Image Retention (maximum)	3%	3%	3%
Shading (maximum vertical and horizontal)	15%	15%	15%

* TVL - Television Lines

** The 1 percent distortion includes: 1. Optics distortion, 2. deflection nonlinearities, and 3. electron optics distortion. The test method to measure the geometric distortion in each camera will utilize a reseau pattern, consisting of 81 (9 x 9 array) points.

*** Video signal characteristics are shown in Figure 3.3-2.

3.3.2.2 Optics

Focal Length: 126 MM

Field of View: 16.25 degrees (diagonal); 11.5 degrees (on side)

T/No: 3.2

Shutter: Double blade, focal plane; running time 20 milliseconds
Direction of motion: from mounting feet upwards

Shutter Momentum Compensation: 0.025 ft-lb-sec

Exposure: Simultaneous, actuated on the positive going transition of 1 Hz S/C clock pulse.

Readout: Sequential; refer to Figures 3.3-3 and 3.3-4.

3.3.2.3 Clock Requirements

Clock Inputs: 1 Hz, 50 kHz, and 1.6 MHz

Clock Stability: 1 part in 10^6 (Short and long term)

3.3.2.4 Physical
See Table 3.3-2.

Table 3.3-2. RBV Camera Subsystem Clock Requirements

Item	Unit Size	Unit Weight (lbs)	Unit Dissipation (watts)
Camera Head (3 required)	22L x 8.75H x 7.75W	31.2 (See note)	30 (estimated)
Camera Electronics (3 required)	6" x 6" x 13" (3/3)	12.0	15 (estimated)
Camera Controller (1 required)	6" x 6" x 6.5" (3/0)	7.0	10 (estimated)
Video Combiner (1 required)	6" x 6" x 6.5" (3/0)	9.0	10 (estimated)

NOTE: Weights exclude harnesses and baseplate

3.3.3 POWER

Power Supplies Required:	-24.5 volts +2 percent
Peak System Power:	193 watts
25 Sec. Average System Power:	185 watts (Also refer to Figure 3.3-5)
Warm-up Power (50 Seconds):	75 watts
Telemetry, Continuous Power:	2 watts (estimate)
Peak Transient Power (Exposure Transient): (Shutter Operation)	30 amperes (may be supplied by a -26 volts unregulated source). This transient occurs during exposure and it lasts approximately 100 milliseconds.
(Turn-on Transient): (RBVC S/S ON)	12 amperes on the regulated bus during initial turn-on. This transient has a rise of 90 ma/microseconds.

The regulated and unregulated power interface is described in Figure 3.3-6.

3.3.4 THERMAL

Thermal Constraints: Sensor baseplate temperature must be maintained between 10°C and 30°C, preferably at 20°C. Each sensor housing dissipates approximately 30 watts during operation.

3.3.5 TELEMETRY

A total of 17 digital and 17 analog telemetry points (Table 3.3-3) are required per camera head and electronics.

3.3.6 COMMANDS

A total of thirty-four commands are required (Table 3.3-4).

All command pulse inputs will conform to Nimbus D handbook specifications.

3.3.7 WIDEBAND VIDEO TAPE RECORDER INTERFACE

1. Wideband Video Tape Recorder - will provide the 312.5 kHz phasing pulses to the RBV camera to phase-in the horizontal scan frequency in the three cameras.

Table 3.3-3. RBV Camera Subsystem Telemetry Points

Item No.	Function	Type
	Telemetry Points	
1	Vidicon Filament Current	Digital
2	G1 Voltage	Analog
3	Target Voltage	Analog
4	Anode Voltage	Digital
5	G2 Voltage	Digital
6	Vidicon Cathode Current	Analog
7	Video Output	Analog
8	Focus Current	Analog
9	Alignment Currents	Analog
10	Horizontal Deflection Output	Analog
11	Vertical Deflection Output	Analog
12	Deflection Power Supply	Analog
13	Low Voltage Power Supply	Analog
14	-24.5 Volt Input Voltage	Digital
15	-28 Volt (Shutter) Current	Analog
16	Temperature - Faceplate	Analog
17	Temperature - Yoke/Focus Coil	Analog
18	Temperature - Electronics	Analog
19	Temperature - L.V. Power Supply	Analog
20	Anode/Target Mode (Command Verification)	Digital
21	Power ON/OFF (Command Verification)	Digital
22	One cycle per second rephasing	Digital
23	Thermoelectric cooler current	Analog
	Controller Telemetry	
24	Clock Input (50 kHz)	Digital
25	Horizontal Sync	Digital
26	Vertical Sync	Digital
27	Clock A/B (Command Verification)	Digital
28	Cycle continuous/Single (Command Verification)	Digital
29	P3-Auto/P2-P1 (Command Verification)	Digital
30	P2-Auto/P3-P1 (Command Verification)	Digital
31	Mode Record/Direct-Record (Command Verification)	Digital
32	Mode Direct/Direct-Record (Command Verification)	Digital
33	Dynamic Beam Regulator - In-Out (Command Verification)	Digital
34	Temperature - Camera Controller	Analog
	Video Combiner Telemetry	
	Later	

Table 3.3-4. RBV Camera Subsystem Commands

Item No.	Function	Item No.	Function
1	S/S Power ON (Not part of RBVC S/S. Located on spacecraft power system)	18	Single Cycle
2	S/S Power OFF	19	Continuous (Normal) Cycle
		20	Record Mode
3	Start Prepare	21	Direct Mode
4	Camera 1, ON	22	Direct/Record Mode
5	Camera 2, ON	23	Clock A (Spacecraft)*
6	Camera 3, ON	24	Clock B (Spare)*
7	Camera 1, OFF	25	Calibrate 1 (tentative)
8	Camera 2, OFF	26	Calibrate 2 (tentative)
9	Camera 3, OFF	27	Calibrate 3 (tentative)
10	Anode Mode	28	Peaking IN
11	Target Mode	29	Normal
12	Beam IN	30	Undetermined commands*
13	Beam OUT	31	Undetermined commands*
14	Expose Auto	32	Undetermined commands*
15	Preset 8 msec	33	Undetermined commands*
16	Preset 12 msec	34	Undetermined commands*
17	Preset 16 msec		

*The exact function of these commands is uncertain at this time.

2. RBV Camera - will provide a "Tape Run" signal to the WBVTR at To +11.5 seconds. Refer to Figure 3.3-4.

3. The Video Input Line - is routed from the RBVC video combiner and will carry the time multiplexed video as shown in the subsystem block diagram.

Other pertinent details are described in the wideband video tape recorder discussion of Section 3.5.

3.3.8 MECHANICAL

The outline of the RBV camera head is shown in Figure 3.3-7. Other modules, camera electronics, camera controller and video combiner are standard Nimbus modules and their sizes are as indicated in Paragraph 3.3.2.

3.3.8.1 Mass Properties

The maximum weights and centers of gravity for each individual RBVC component module will be shown on their respective interface control drawings:

1. RBV Camera Head - Drawing No. (later)
2. Camera Electronics - Drawing No. (later)
3. Camera Controller - Drawing No. (later)
4. Camera Video Combiner - Drawing No. (later)

Momentum levels will be below 0.025 ft-lbs-sec.

3.3.8.2 Location-Mounting

The camera heads shall be located on the spacecraft so that their optical axes are parallel to the "Z" axis of the spacecraft and the scan raster at 90 degrees to the x - x axis.

The field of view for each camera shall be unobstructed within a 17-degree cone and shall be mounted down toward the earth, assuming an orbiting spacecraft.

Thermal considerations shall assume a 30-watt dissipation in each camera head and requirement to maintain the mounting feet at +20 $\pm$10°C.

The distances between each module within the return beam vidicon camera and wideband video tape recorder shall be kept small to reduce signal line lengths and corresponding signal level attenuation.

3.3.8.3 Alignment (Tentative) (In Degrees)

		Initial		Recheck	
		Alignment (±)	Accuracy (±)	Alignment (±)	Accuracy (±)
RBV					
	Roll	0.0055	0.0016	0.011	0.0016
	Pitch	0.0055	0.0016	0.011	0.0016
	Yaw	0.008	0.0016	0.011	0.0016
RBV to Spacecraft Axes					
	Roll	0.05	0.008	0.10	0.01
	Pitch	0.05	0.008	0.10	0.01
	Yaw	0.05	0.008	0.10	0.01

3.3.8.4 Environment Levels

The environmental levels conform to Nimbus D requirements.

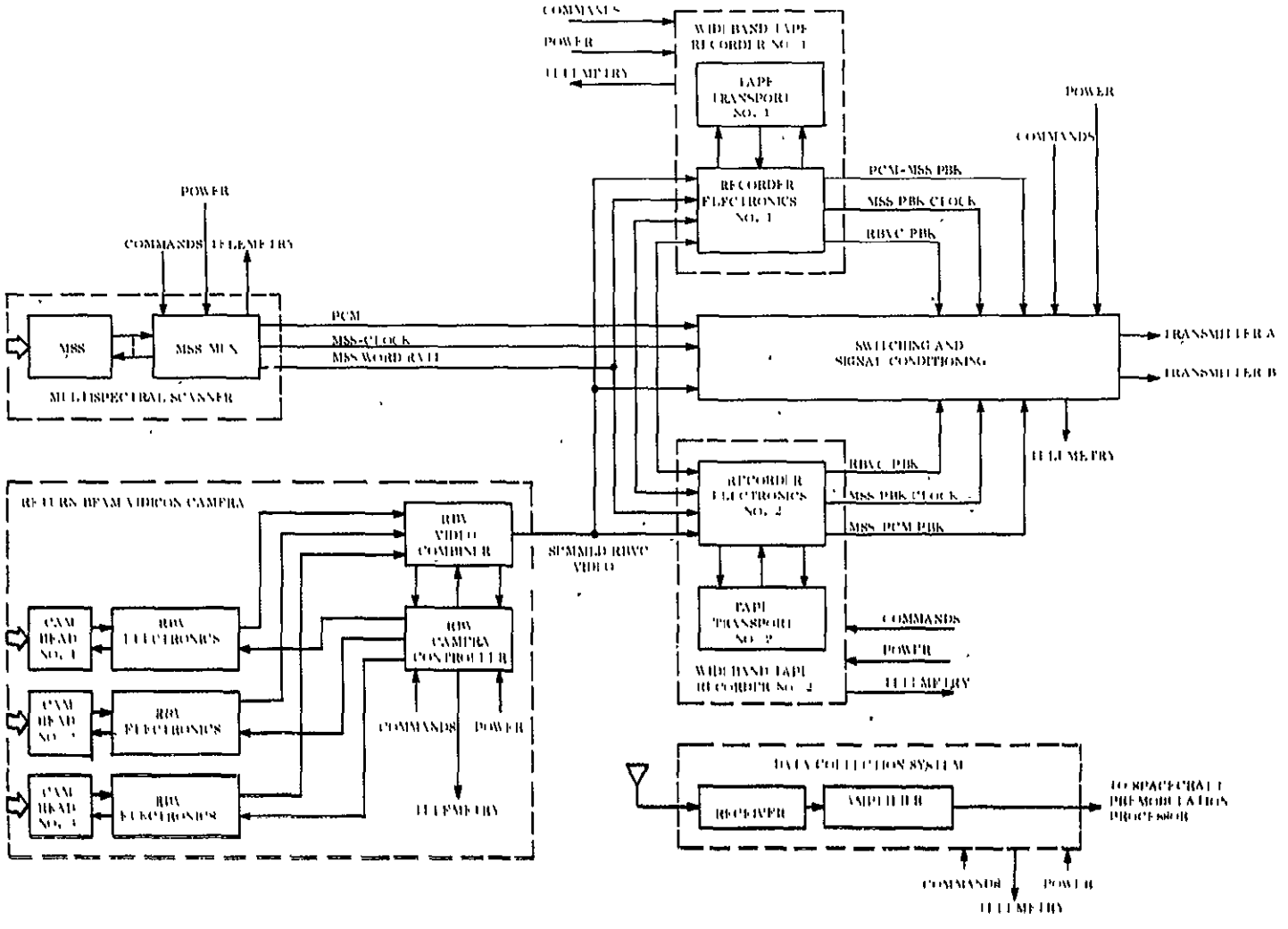

Figure 3.2-1. ERTS Payload Subsystems

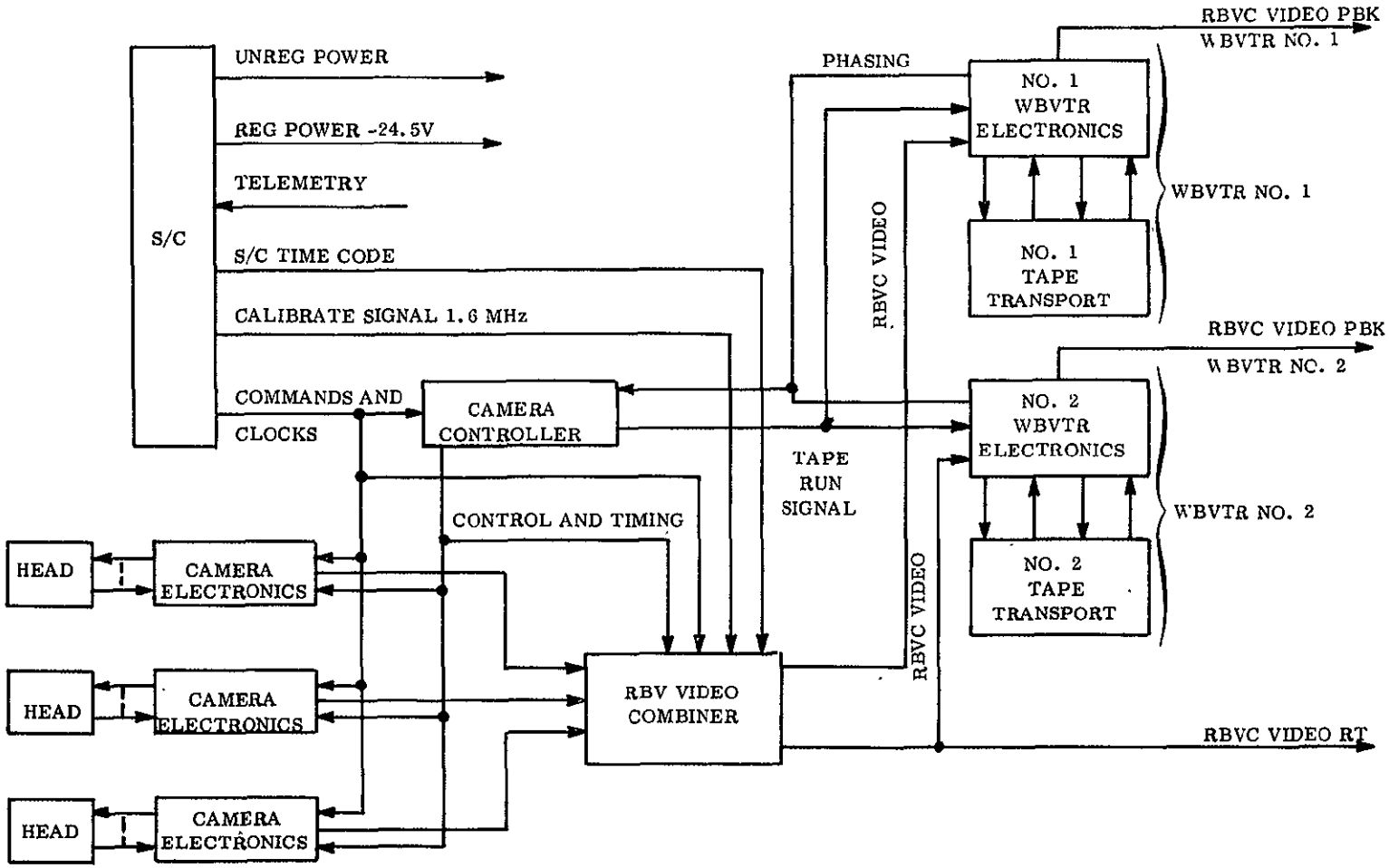

Figure 3.3-1. Return Beam Vidicon Camera Block Diagram

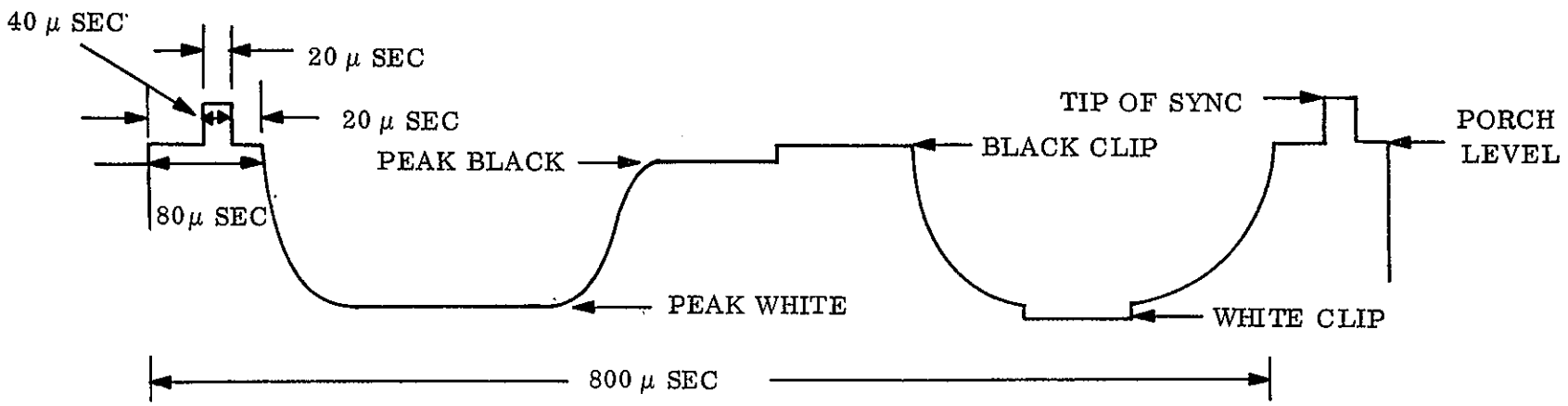

TIP OF SYNC	0 ± 0.05 VOLTS
PORCHES	- 0.3 ± 0.05 VOLTS
BLACK CLIP	-0.3 ± 0.05 VOLTS
PEAK BLACK	-0.35 ± 0.05 VOLTS
PEAK WHITE	-11.5 ± 0.1 VOLTS
WHITE CLIP	-1.65 ± 0.1 VOLTS

Figure 3.3-2. Video Signal Characteristics (One Line of Video Shown)
RBV Camera

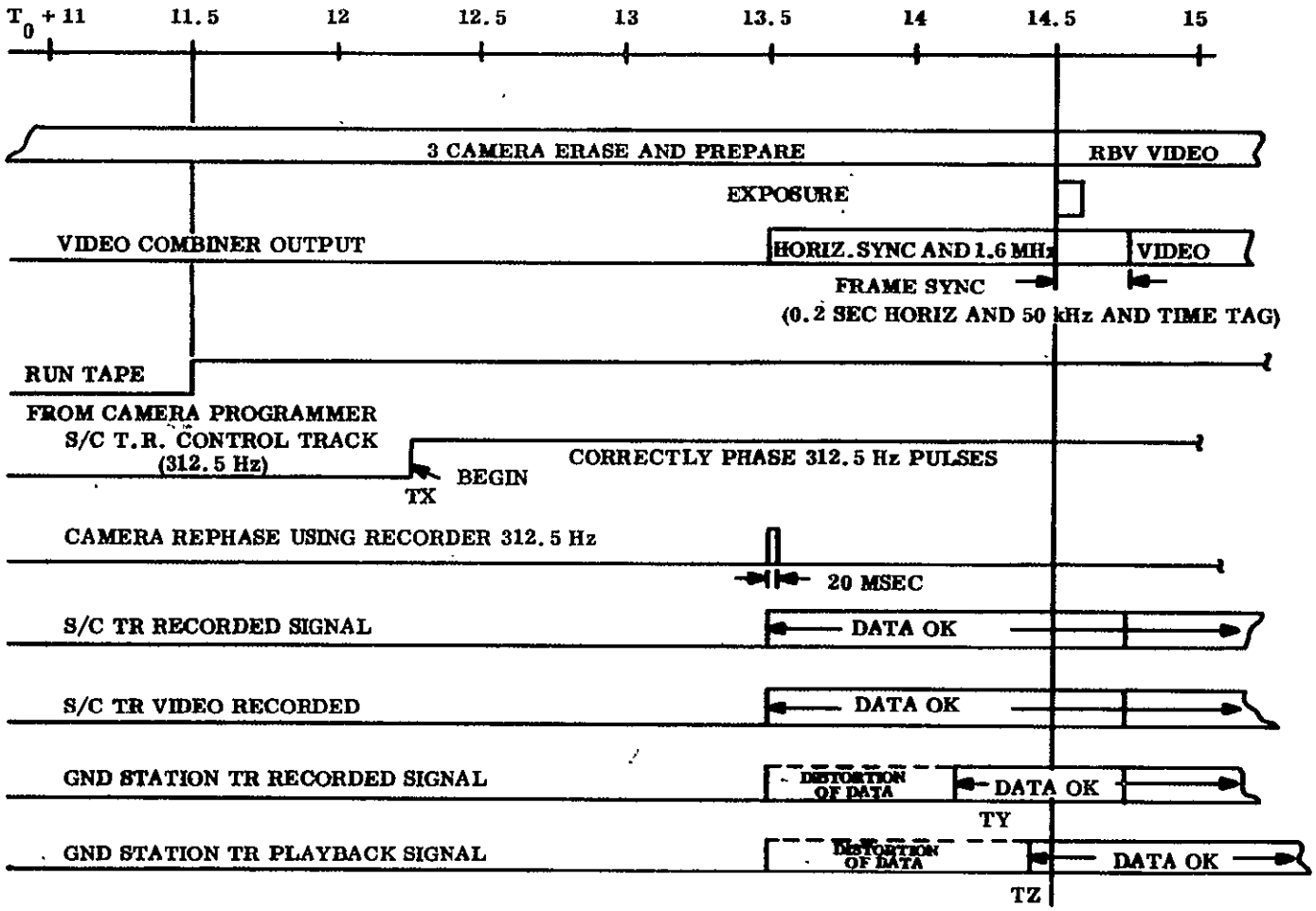

NOTES:

1. TIMES TX, TY, TZ ARE UNDEFINED
2. NEED ASSURANCE THAT TZ ≤ 14.5 SECONDS WHEN FRAME SYNC STARTS
3. "DATA OK" MEANS THE SIGNAL HAS CORRECT TIME BASE AND AMPLITUDE
4. "DISTORTION OF DATA" MEANS THE SIGNAL DOES NOT HAVE THE CORRECT TIME BASE AND AMPLITUDE.

Figure 3.3-3. Composite Video Format (Spacecraft Storage - Ground Station Storage Mode)

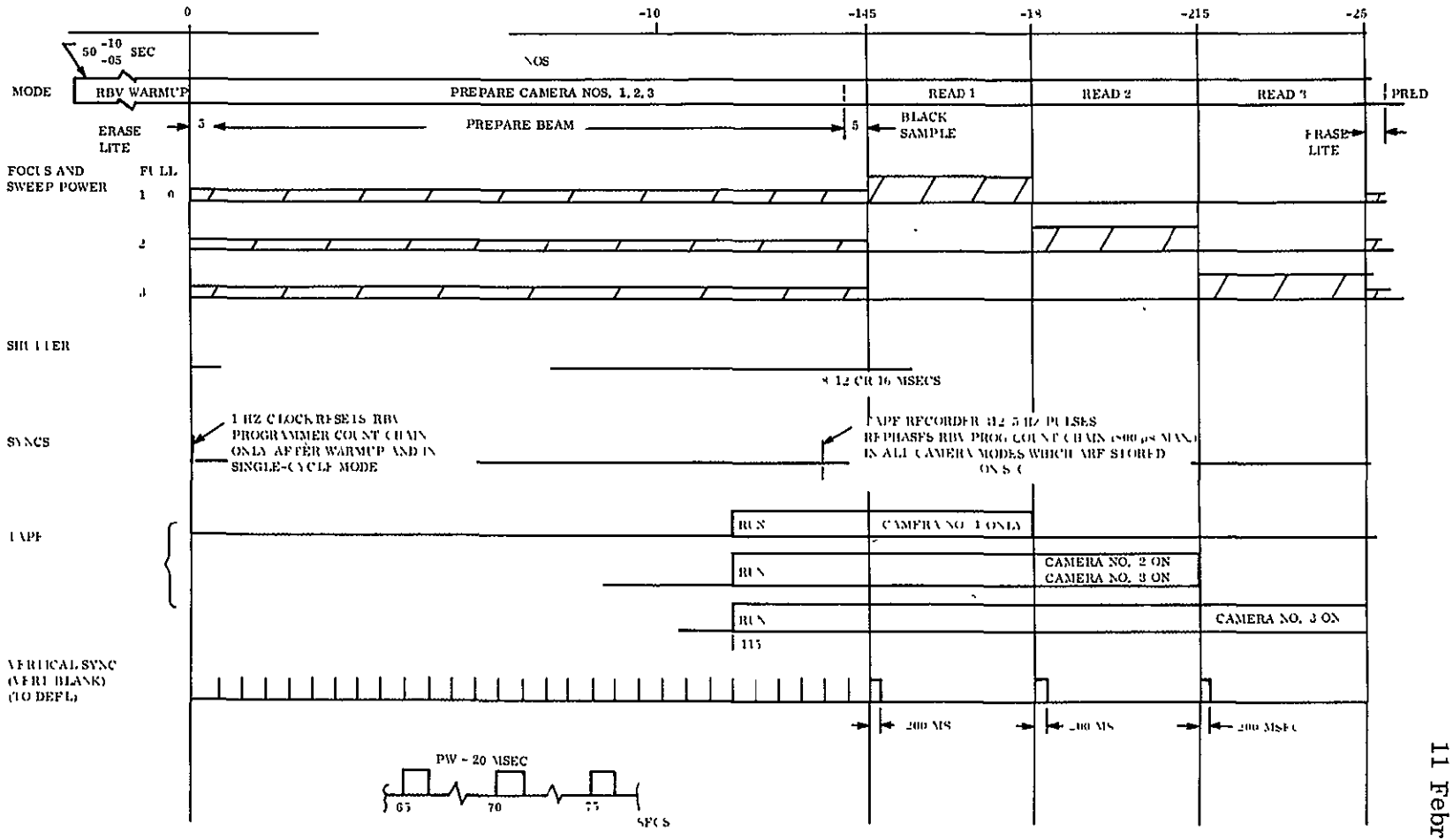

Figure 3.3-4. Single Picture Timing Cycle

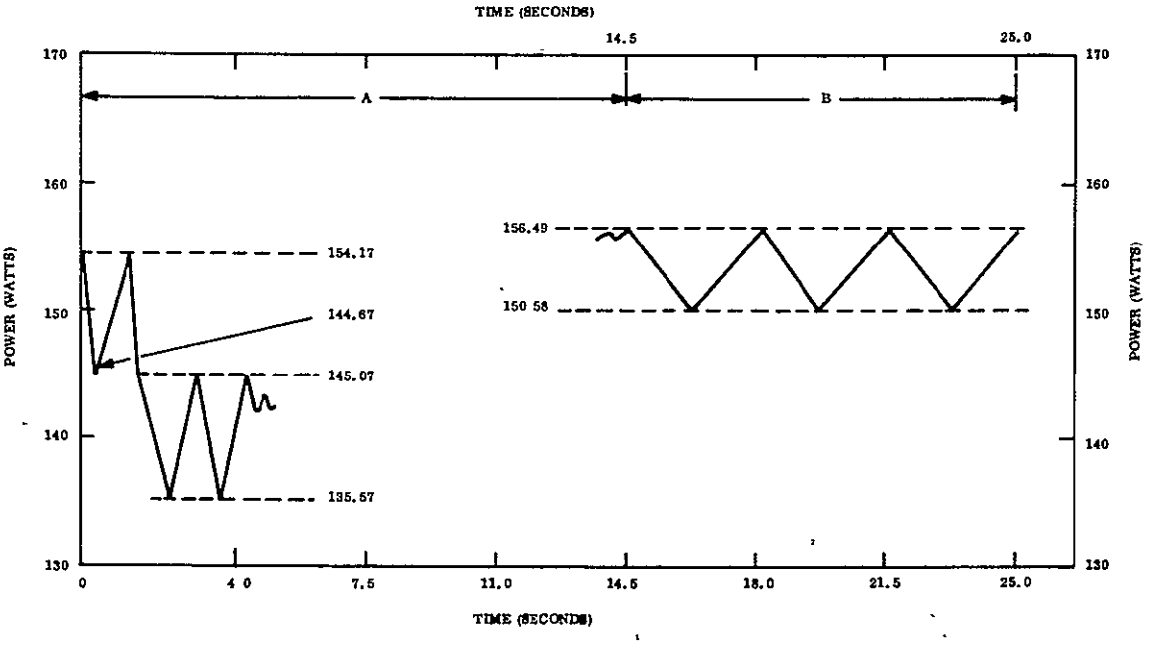

Figure 3.3-5. Two-Inch Return - Beam Camera System - Power Profile

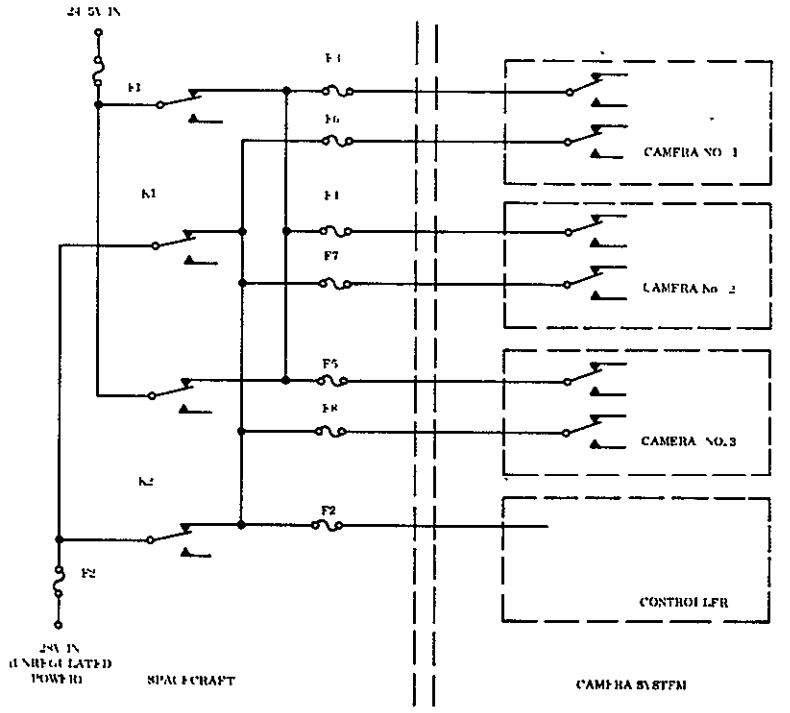

Figure 3.3-6. Camera Power Wiring Configuration

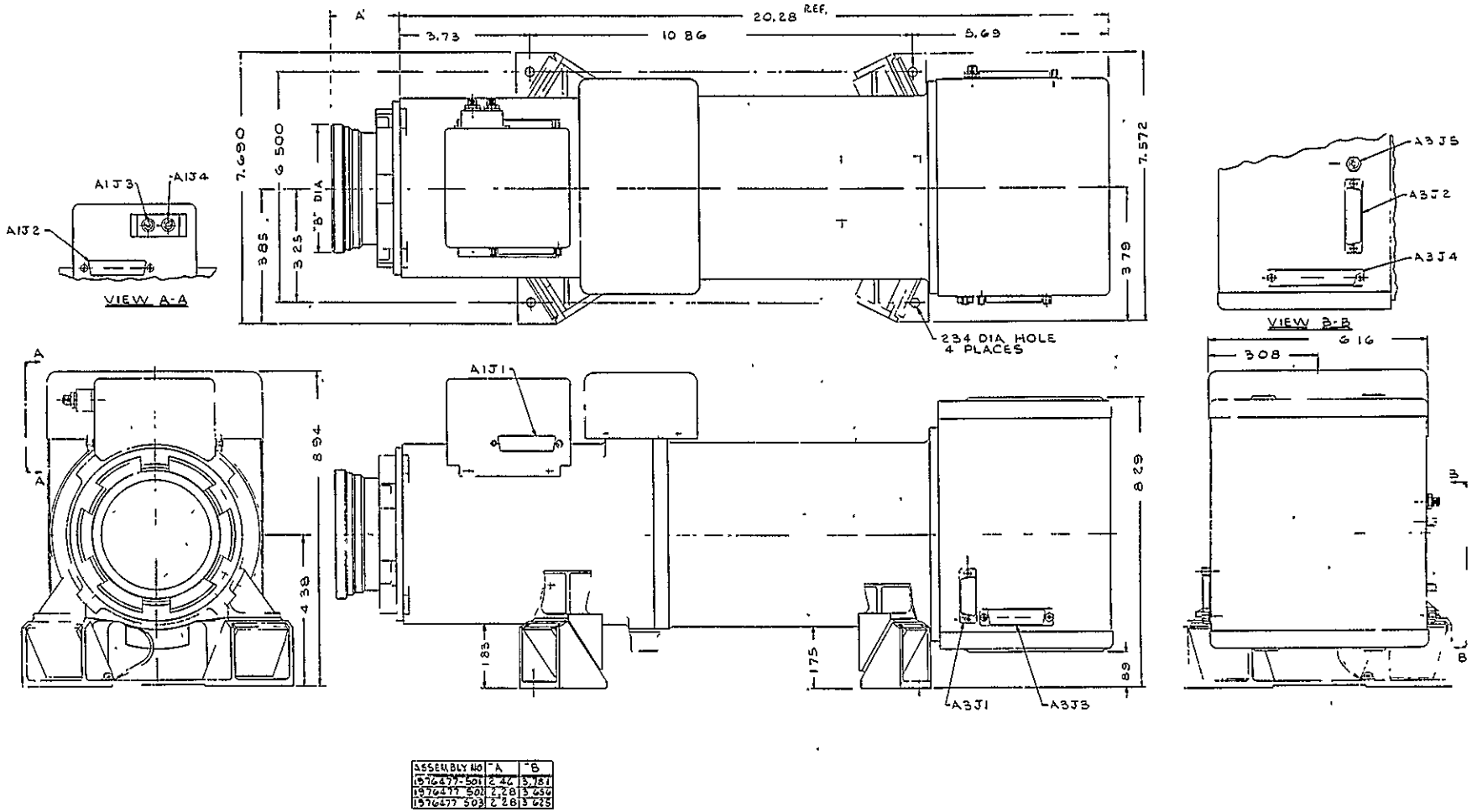

ASSEMBLY NO	"A"	"B"
1976477-501	2.42	3.781
1976477-502	2.28	3.636
1976477-503	2.28	3.625

Figure 3.3-7. RBV Camera Head Outline

3.4 MULTISPECTRAL SCANNER (MSS) SUBSYSTEM

3.4.1 SUBSYSTEM DESCRIPTION

The Multispectral Scanner Subsystem uses an object plane scanner. A flat scan mirror oscillating at 15.2 Hz provides the cross track scan. The optics are all reflecting to accommodate the very wide spectral range of sensing. A simplified scanner cross section is shown in Figure 3.4-1 and the overall system block diagram is shown in Figure 3.4-2.

The spectral bands used for sensing are:

1. Band 1 (0.5 - 0.6 micrometers)
2. Band 2 (0.6 - 0.7 micrometers)
3. Band 3 (0.7 - 0.8 micrometers)
4. Band 4 (0.8 - 1.1 micrometers)
5. Band 5 (10.4 - 12.6 micrometers) (ERTS-B only)

The cross track scanning is provided by a high duty cycle (65 pecent) scan mechanism. The scan timing is shown in Figure 3.4-3. The scan width is $\pm$50 nautical miles ($\pm$5.8 degrees) from an orbital altitude of 492 nautical miles. The instantaneous field of view is 0.077 milliradian (MR).

Each spectral band has six detectors, except for Band 5 where only two are used but with an increased field of view of 0.24 MR.

The image is focussed on a bundle of fiber optics, layed out as shown in Figure 3.4-4. Each fiber corresponds to a remotely located detector. The energy for Band 5 however is split off by reflective means onto two proportionately larger detectors which also form the instantaneous field-of-view field stops.

The instantaneous field of view for Band 5 is larger by a factor of three in order to achieve the temperature differential of 1 degree and also be compatible with diffraction spreading.

The detectors for Bands 1 through 3 are photomultiplier tubes. The Band 4 detector is a silicon photodiode and in Band 5 a passively cooled HgCdTe detector is used.

The passive radiation cooler, for HgCdTe detectors, is a three-stage design and develops temperature of about 80° Kelvin.

The primary calibration is provided by a small mirror designed to reflect the sun into the telescope when the spacecraft is in view of Alaska.

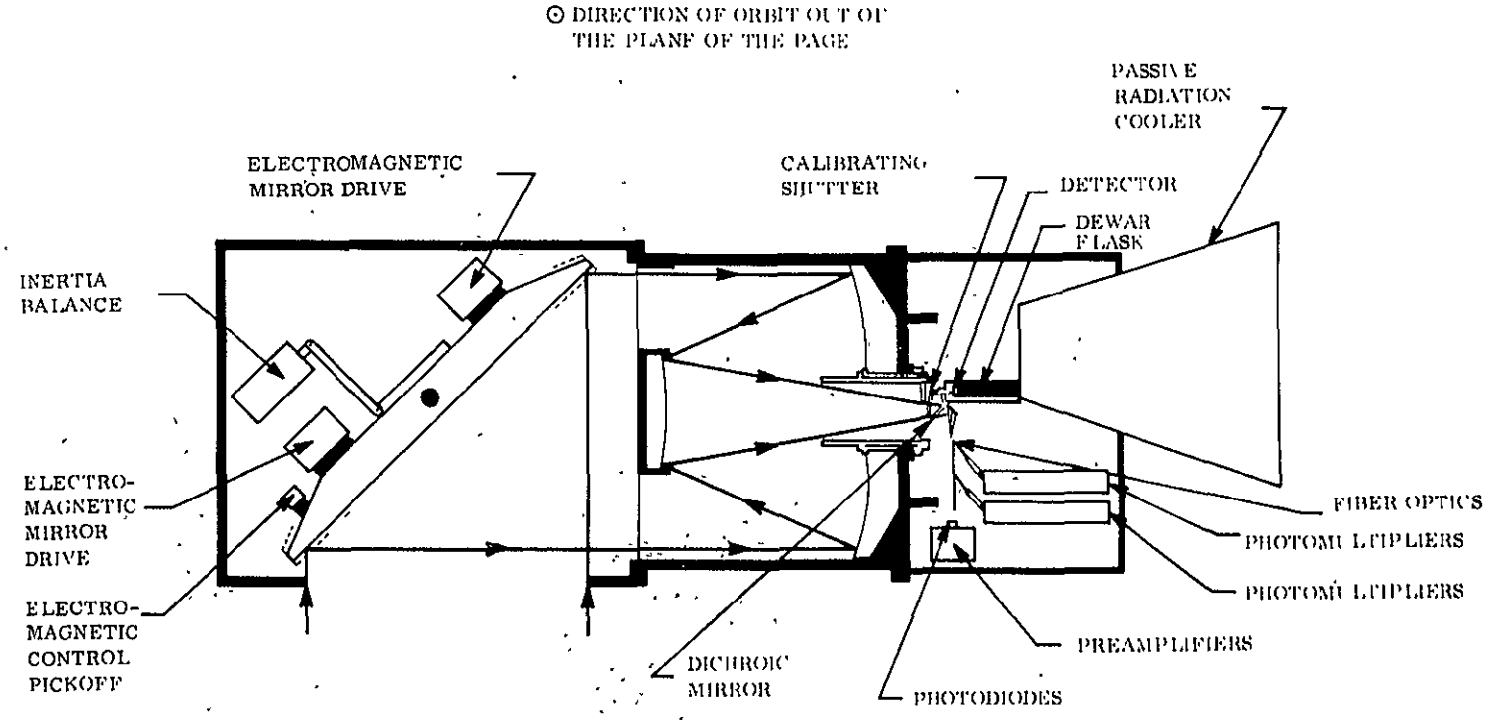

Figure 3.4-1. Multispectral Scanner Diagram

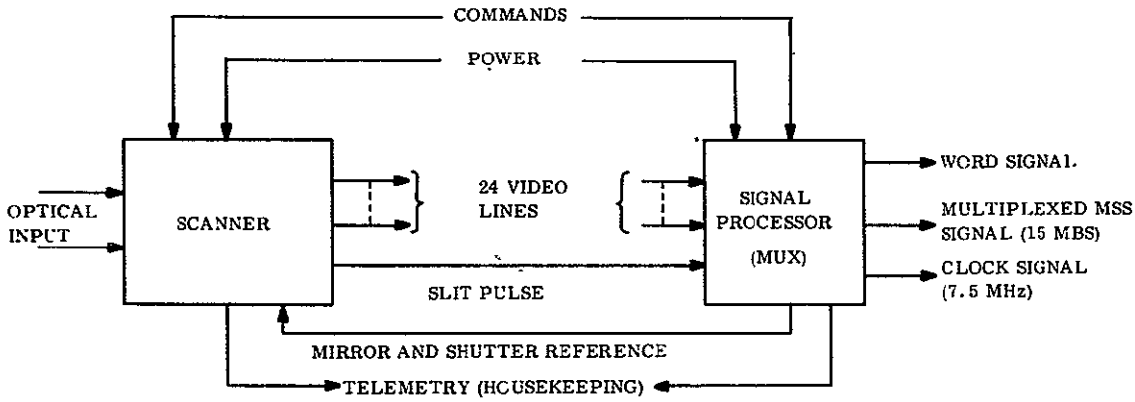

Figure 3.4-2. Block Diagram - Multi-Spectral Scanner

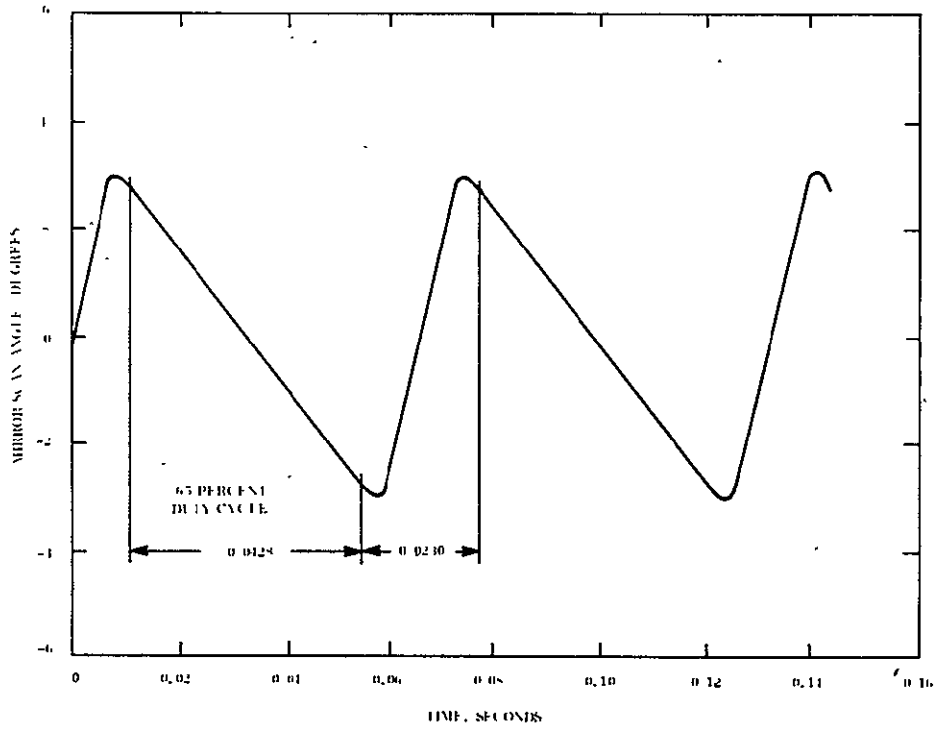

Figure 3.4-3. Scan Mirror Angle versus Time

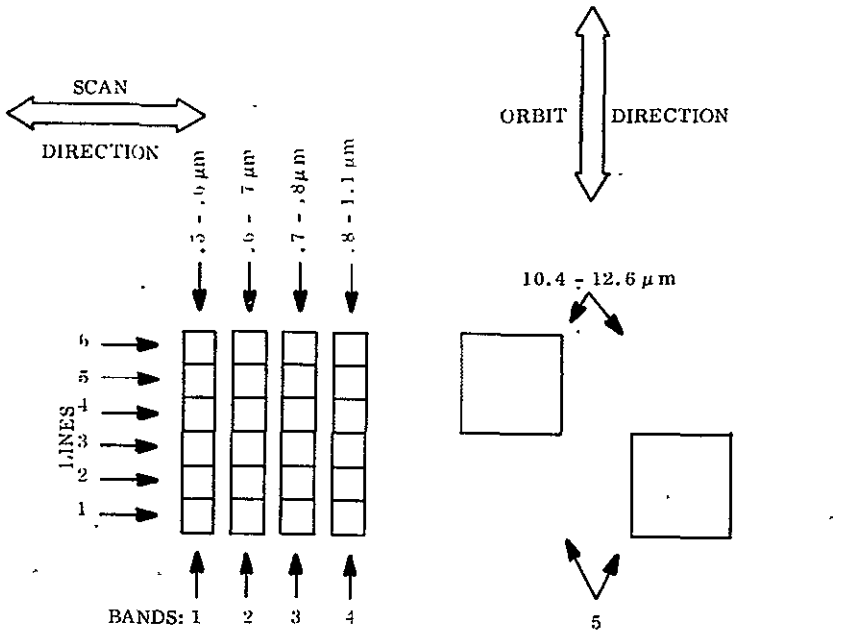

NOTE: The squares represent the IFOV's of each of the 26 channels.

Figure 3.4-4. Multispectral Scanner Image Plane Diagram

A gray scale, secondary calibration, is provided by incandescent high stability lamps. Since the lamps are viewed by all detectors, calibration will allow gain normalization of the spacecraft sensor. This event schedule is shown in Table 3.4-1.

MSS operation can be either real time or stored. In either mode the individual parallel signals from the detectors, in analog form, are converted by the signal processor (or multiplexer) into a serial PCM data stream. The multiplexer block diagram is shown in Figure 3.4-5. It samples the data according to format indicated in Figure 3.4-6 and converts it to a serial bit stream (PCM-NRZ-L) at 15 Mbps. In the real-time mode of operation, this data and clock output are provided to the spacecraft Wideband Communication Subsystem.

In the stored mode of operations, the MSS-MUX output is applied to the WBVTR where it is reconverted to an eight-level (encoded) FM signal, which is compatible with the basic recorder electronics (used normally for Return Beam Vidicon Subsystem recording). During playback of MSS data, the eight-level FM signal is converted back to PCM with a maximum expected S/N degradation of 1 db, and is applied to the spacecraft Wideband Communication Subsystem.

Due to a requirement on MSS to be able to compare the relative radiometric values of signal for the same resolution element in each spectral band, the spacing of optical fibers in the focal plane has been specially chosen (refer to Figure 3.4-7). This will allow commutator samples to be made coincident with the time interval between instantaneous field

Table 3.4-1. Multispectral Scanner Shutter/ Calibrator Event Schedule

Time*	Scan Angle, degrees	Motor Angle, degrees	Event
0.0115	+2.89	0.0	Start of scan period
0.0543	-2.89	117.0	Completion of scan period
0.0561	--	122.0	1. Start of blackbody surface into detector view 2. Start dc restore of Bands 1 to 4
0.0658	--	148.5	1. Completion of dc restore of Bands 1 to 4 2. Start of reference
0.0755	--	175.0	Completion of reference
0.0773	+2.89	180.0	1. Completion of blackbody surface in detector view 2. Start of new scan period
0.1201	-2.89	297.0	Completion of scan period
0.1219	--	302.0	1. Start of mirror into detector view 2. Start dc restore of Band 5 3. Start dc restore of Bands 1 to 4
0.1316	--	328.5	1. Completion of dc restore of Bands 1 to 4 2. Start of reference
0.1413	--	355.0	1. Completion of dc restore of Band 5 2. Completion of reference 3. Completion of mirror in detector view.
0.1430	+2.89	360.0	Start of new scan period Repeat

*Time is relative to mirror angle trace.

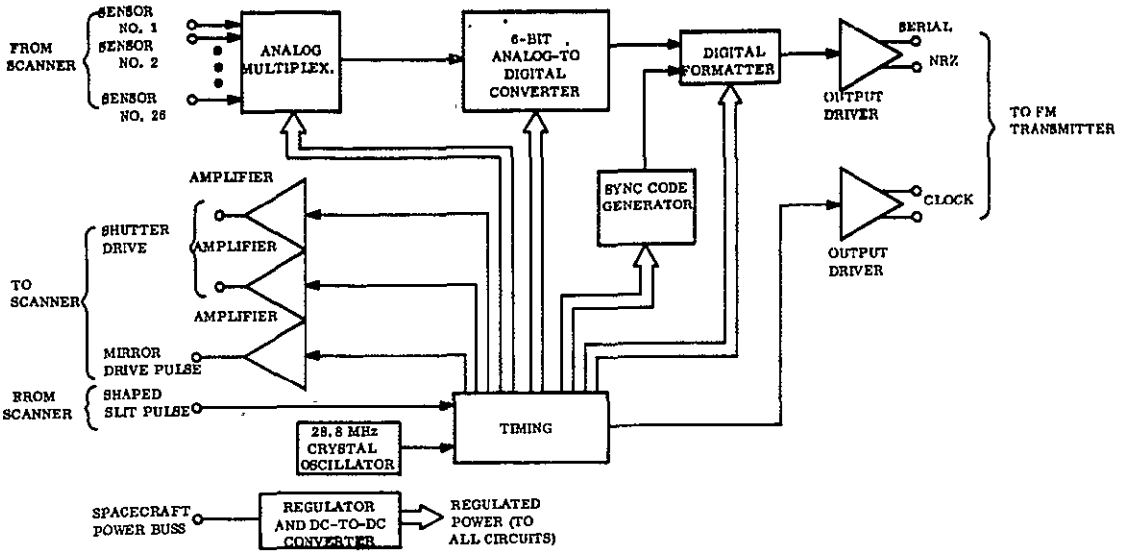

Figure 3.4-5. PCM Multiplexer Block Diagram

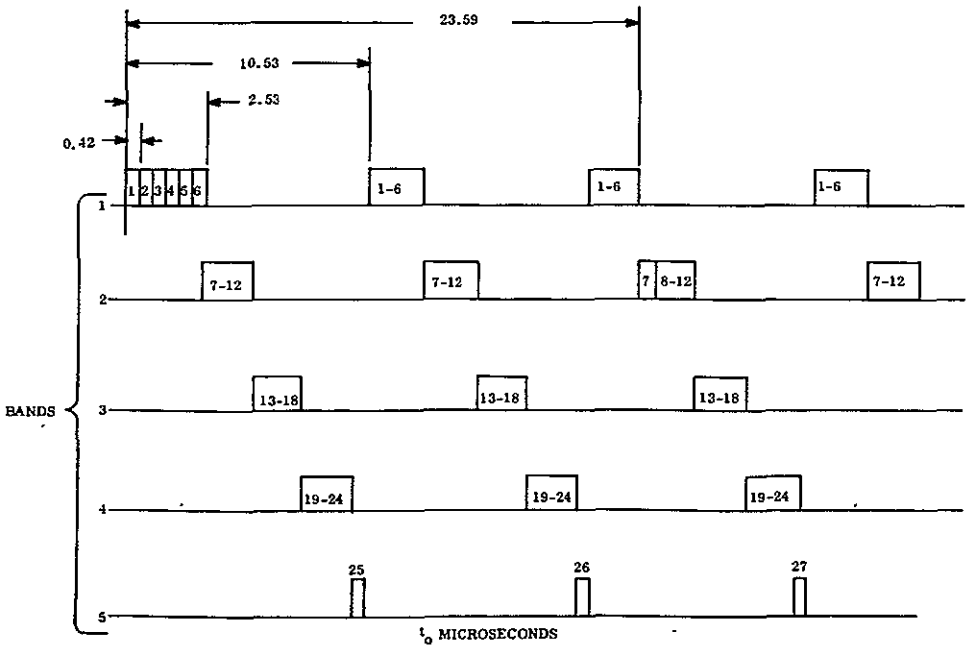

Figure 3.4-6. Commutator Sampling Format

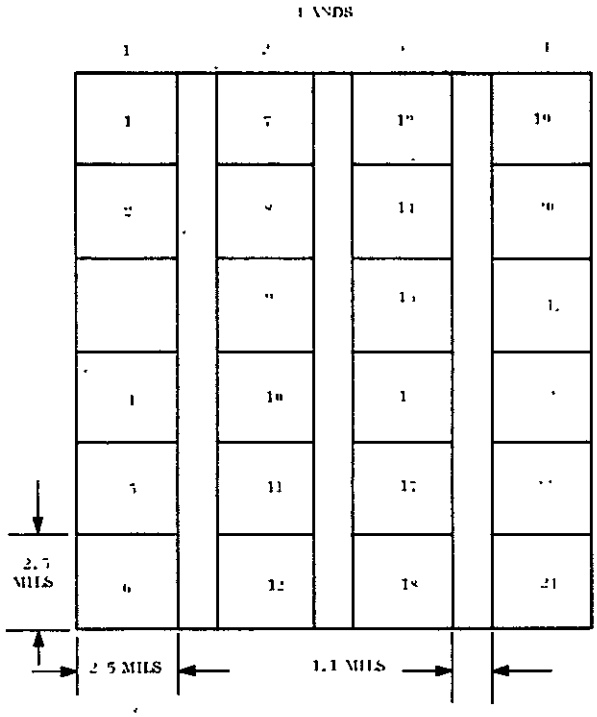

Figure 3.4-7. Fiber Matrix Layout

of view in adjacent bands, which will also mean that the commutator will sample exactly the same point on the ground, in each band, a known number of samples apart (or a known time interval). As a result, the ERTS computer can analyze the source point on the ground, in each band, simultaneously, by delaying the output of each band by the correct time interval, as illustrated in Figure 3.4-8.

3.4.2 GENERAL SPECIFICATIONS

1. Spectral bands

   a. Band 1 - 0.5 to 0.6 micrometers

   b. Band 2 - 0.6 to 0.7 micrometers

   c. Band 3 - 0.7 to 0.8 micrometers

   d. Band 4 - 0.8 to 1.1 micrometers

   e. Band 5 - 10.4 to 12.6 (ERTS-B only)

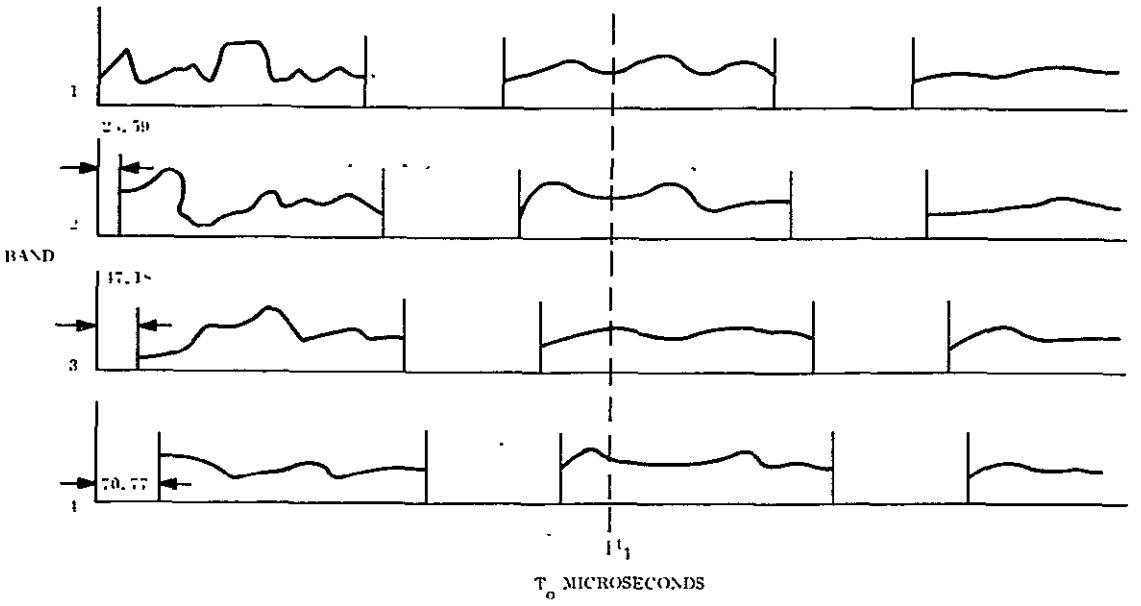

Figure 3.4-8. Required Delays

2. Quality imaging - Radiance levels from observables represented by agricultural crops in areas as small as 230 feet across should be measured with good relative fidelity among the reflective bands. The IR radiating band shall be suitable for assessing similar observables in areas as small as 600 feet across.

3. Minimum lighting condition - Sun zenith angle ≤ 55 degrees

4. Optics - Nine-inch Ritchey-Chretien, f/3.3 with 4-inch secondary mirror (Figure 3.4-1)

5. Scanning mechanism - Flat mirror oscillating at 15.2 Hz

   a. Scan efficiency - 65 percent (nominal)

   b. Deviation from linear - 0.2 percent of swath

   c. Alignment of lines - 30-feet, after correction

   d. Timing - See Figure 3.4-3

6. Number of lines scanned/scan - Six each in bands 1, 2, 3, and 4. Two in Band 5 (ERTS-B only)

7. Detectors

   a. Bands 1, 2, and 3 - photomultiplier tubes (PMT)

   b. Band 4 - silicon photodiodes (SiPD)

   c. Band 5 - intrinsic IR detector cooled to $\approx 80^{\circ}$K (ERTS-B only).

8. Instantaneous field of view

   a. Bands 1, 2, 3, and 4--0.077 milliradian

   b. Band 5--0.24 milliradian (ERTS-B only)

9. Video output rates

   a. Bands 1, 2, 3, and 4--61 kHz/channel

   b. Band 5--20 kHz/channel (ERTS-B only)

10. Cooling (ERTS-B only) - Two detectors cooled by a three-state radiation cooler to space. Initial operation at ≈ 80 °K with provisions for operating up to 100°K

11. Performance (estimated)

12. S/N Noise Ratio

	Band			
S/N Voltage Ratios	1	2	3	4
Bright Scene	140	103	62	73
Agricultural range	69	52	38	41

13. NE ΔT, Band 5 (ERTS-B) - 1.22° at 300°K

14. Radiometric reference

   a. Primary - Exposure to sunlight once per orbit

   b. Secondary - Calibrated lamps -8 intensity levels. One complete scale every 100 nm (Refer also to schedule, Table 3.4-1)

15. Corrected accuracy - Three percent

16. Size

a.	Scanner	Defined by Drawing HAC 11323-24469
b.	Signal Processor	Nimbus 2/2

17. Weight

		ERTS-A	ERTS-B
a.	Scanner	105 lbs (ERTS-A)	120 lbs (ERTS-B)
b.	Signal Processor	10 lbs (ERTS-A)	10 lbs (ERTS-B)

18. Uncompensated Angular Momentum

1×10^{-3} slug-ft^2 at 15.2 Hz (moment of inertia)

19. General Environment Requirements - S-320-G-1

3.4.3 POWER

Power: Voltage -24.5 $\pm$0.5V

Dissipation

		ERTS-A	ERTS-B
a.	Scanner	50 watts (ERTS-A);	55 watts (ERTS-B)
b.	Signal Processor	15 watts (ERTS-B);	15 watts (ERTS-B)

Power Profile

See Figure 3.4-9 for ERTS-A and Figure 3.4-10 for ERTS-B.

Maximum permissible transients input - -50 volts for 50 milliseconds

Maximum permissible noise input - 0.25 volts peak-to-peak (100 Hz to 1 MHz)

Maximum expected voltage feedback to power supply - 50 millivolts peak-to-peak, dc to 1 MHz into a 0.15 ohm power bus

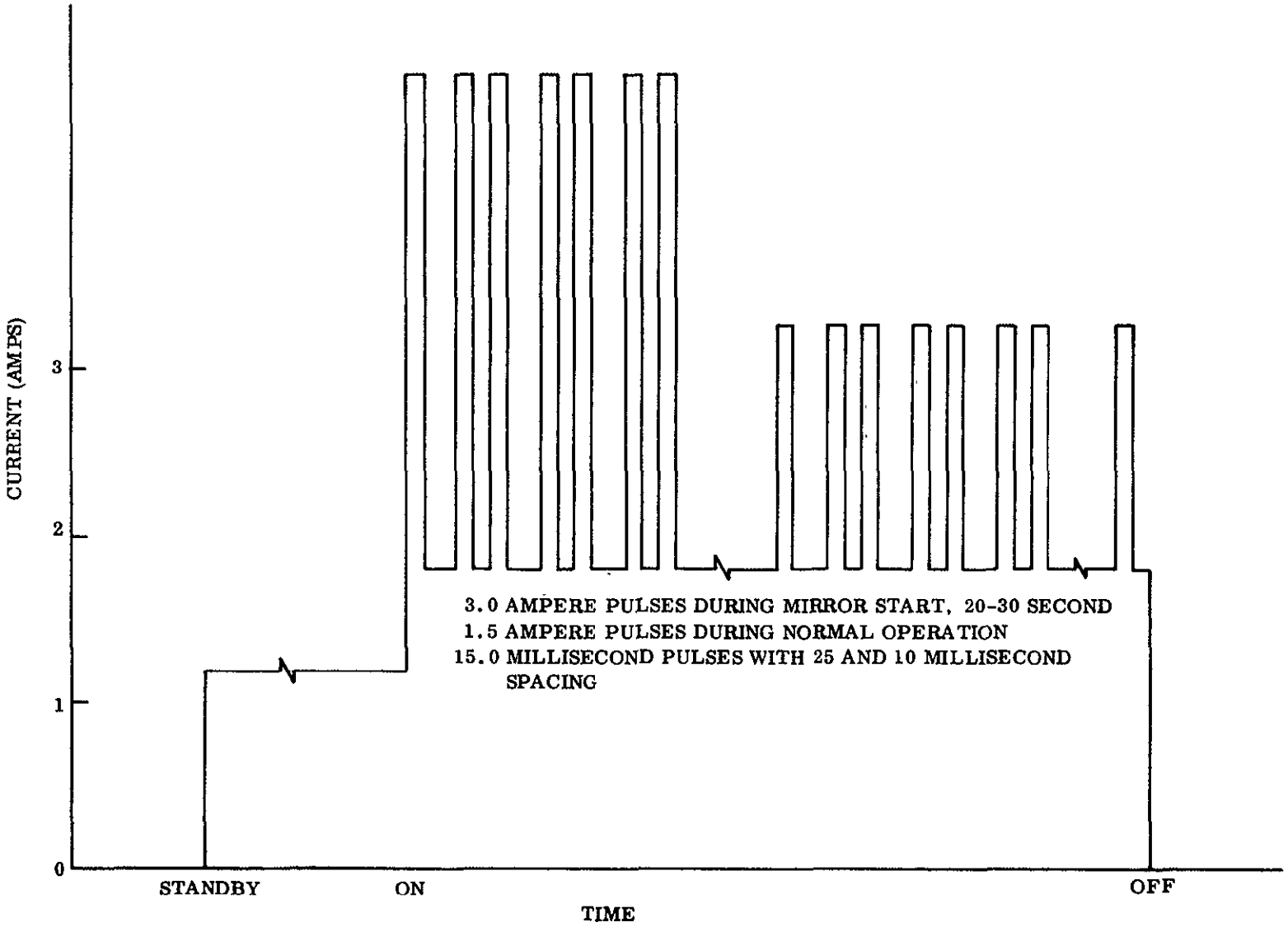

Figure 3.4-9. MSS Power Profile - ERTS A

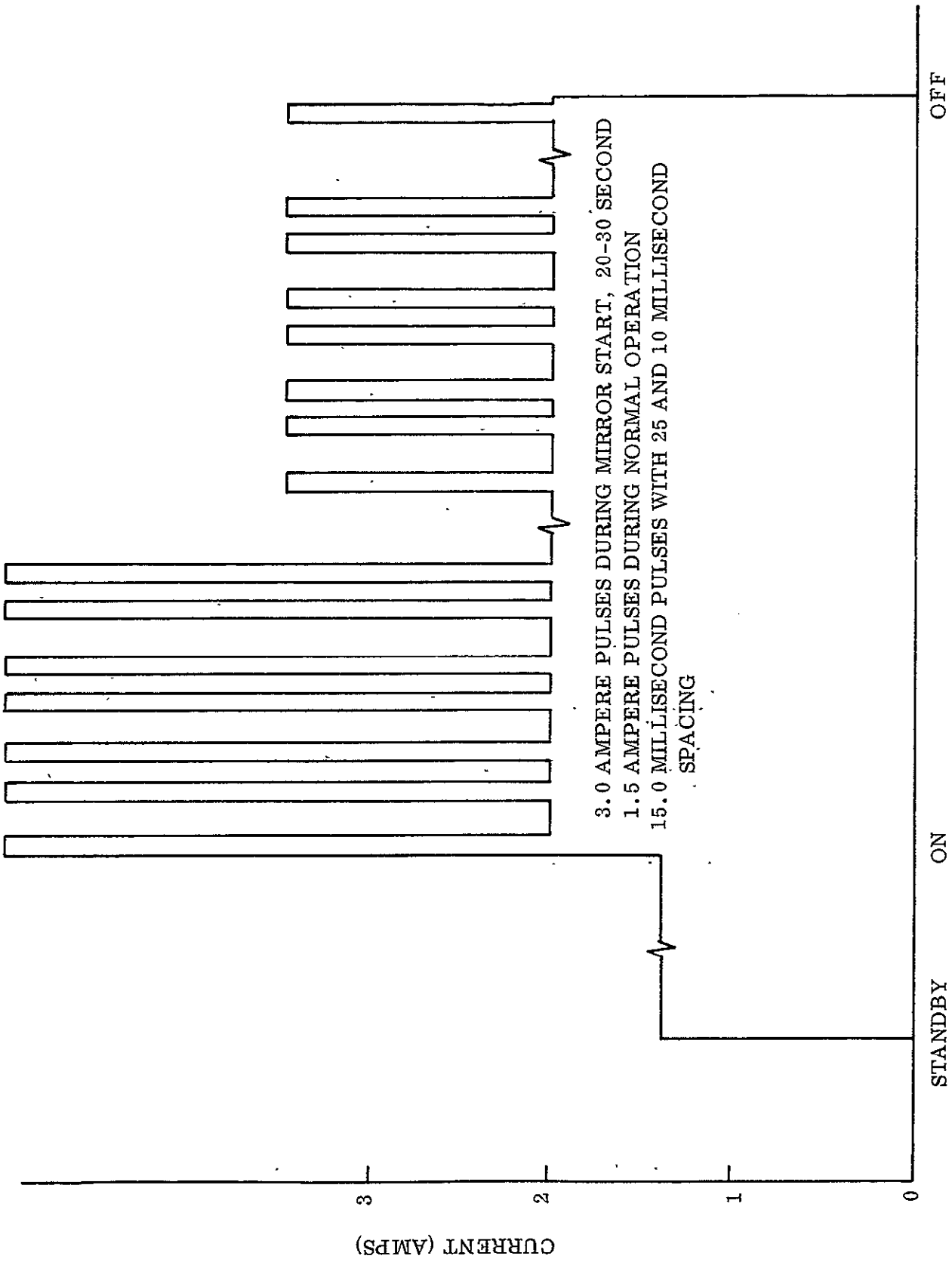

Figure 3.4-10. MSS Power Profile - ERTS B

Electrical Interconnections

a. The MSS interconnection wiring between the MSS and multiplexer

b. The spacecraft power, command and telemetry and Wideband Communication Subsystem

c. And the WBVTR's is shown in Figure 3.4-11.

3.4.4 THERMAL

The thermal interface between the MSS and spacecraft structure includes both conductive coupling through the mounting feet as well as radiative coupling to the interior of the torus section of the spacecraft. The mounting surface will be maintained at $20^{o}C \pm 10^{o}C$.

The total power dissipation in the MSS will be 50 watts (ERTS-A) or 55 watts (ERTS-B). The electronics will dissipate an additional 15 watts. The MSS will contain a radiator area for direct radiation to space. The remaining external area will be superinsulated.

3.4.5 TELEMETRY

The MSS Flight Subsystem is designed to provide outputs to the spacecraft Telemetry Subsystem. The characteristics of the telemetry outputs are as follows:

1. Analog

   a. Range - 0 to -6.375 Vdc

   b. Output impedance - 10K ohms maximum

   c. Effective accuracy - 8 bits

   d. Resolution - 25 millivolts

2. Digital (single bit words)

   a. OFF condition - -0.5 ± 0.5 Vdc

   b. ON condition - -7.5 ± 2.5 Vdc

   c. Output impedance - ON - 1M-ohm, maximum

   d. Output impedance -OFF - 50K ohm, maximum

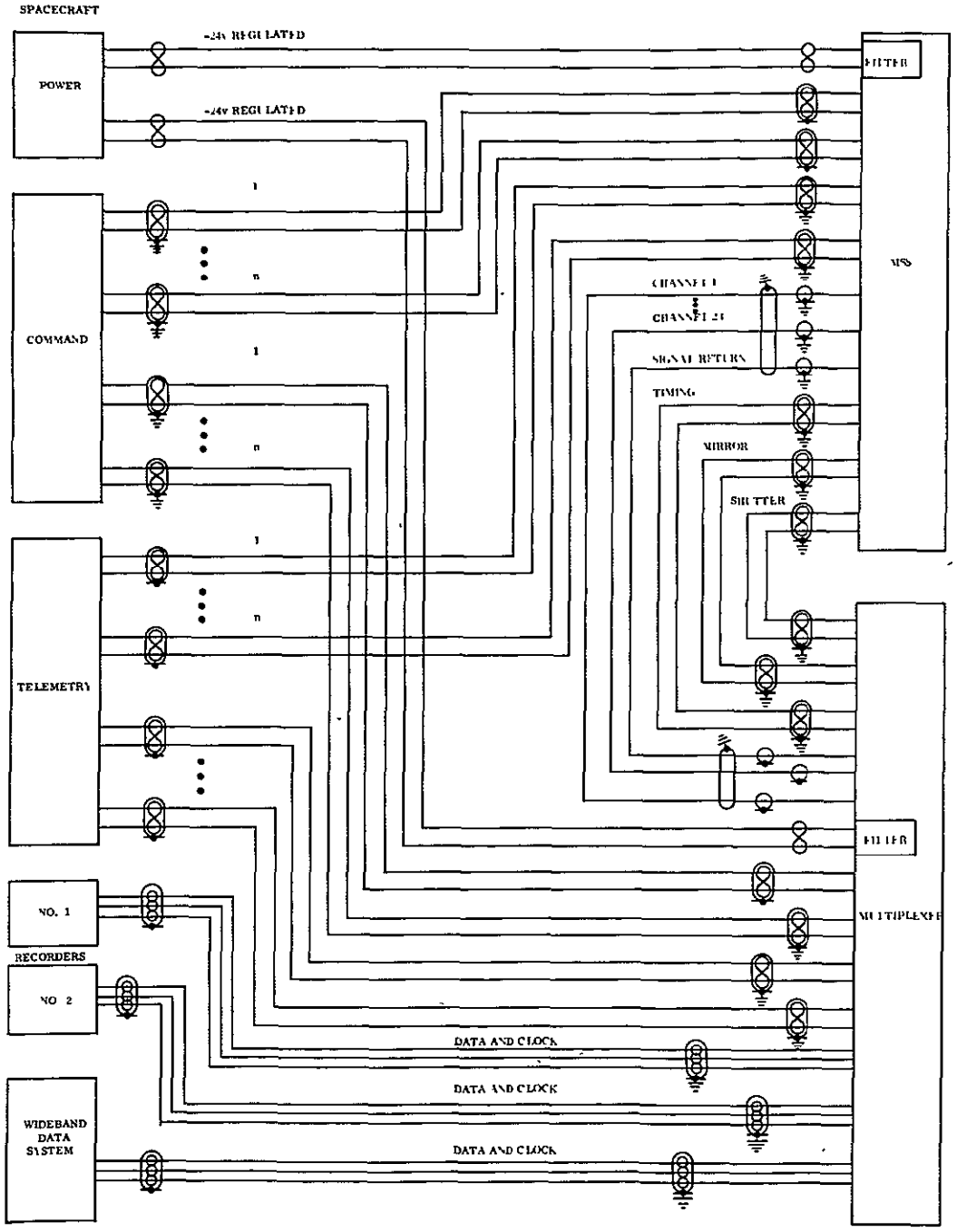

Figure 3.4-11. Electrical Interfaces

Table 3.4-2. Multispectral Scanner Flight Subsystem Telemetry Outputs

Item No.	Function	Type
1	Spectral Band 1 ON/OFF	Digital
2	Spectral Band 2 ON/OFF	Digital
3	Spectral Band 3 ON/OFF	Digital
4	Spectral Band 4 ON/OFF	Digital
5	Spectral Band 5 ON/OFF	Digital
6	Band 1 Gain LOW/HIGH	Digital
7	Band 2 Gain LOW/HIGH	Digital
8	Band 3 Gain LOW/HIGH	Digital
9	Band 4 Gain LOW/HIGH	Digital
10	Main Inverter A ON/OFF	Digital
11	Main Inverter B ON/OFF	Digital
12	Mirror Pick-Off ON/OFF	Digital
13	Band 1 High Voltage A ON/OFF	Digital
14	Band 1 High Voltage B ON/OFF	Digital
15	Band 2 High Voltage A ON/OFF	Digital
16	Band 2 High Voltage B ON/OFF	Digital
17	Band 3 High Voltage A ON/OFF	Digital
18	Band 3 High Voltage B ON/OFF	Digital
19	Scan Mirror Drive ON/OFF	Digital
20	Band 5 Focus ON/OFF	Digital
21	Band 5 Preamp Output Voltage	Analog
22	Calibration Lamp No. 1 ON/OFF - Critical sampling rate	Analog
23	Calibration Lamp No. 2 ON/OFF - Critical sampling rate	Analog
24	Rotating Shutter Drive ON/OFF	Digital
25	Silicon Photodiode Preamp Output	Analog
26	Silicon Photodiode Preamp Output	Analog
27	Silicon Photodiode Preamp Output	Analog
28	Silicon Photodiode Preamp Output	Analog
29	Silicon Photodiode Preamp Output	Analog
30	Silicon Photodiode Preamp Output	Analog
31	Low Voltage Supply Output	Analog
32	Low Voltage Supply Output	Analog
33	Low Voltage Supply Output	Analog
34	Low Voltage Supply Output	Analog
35	Low Voltage Supply Output	Analog
36	Spare T/M	Analog
37	Spare T/M	Analog
38	Spare T/M	Digital
39	Spare T/M	Digital
40	Spare T/M	Digital
		Spare
41	Temperature	Analog
42	Temperature	Analog
43	Temperature	Analog
44	Temperature	Analog
45	Rotating Shutter Housing Temperature	Analog
46	Calibration Lamp Base Temperature	Analog
47	Temperature	Analog
48	Temperature	Analog
49	Temperature	Analog
50	Temperature	Analog

3.4.6 COMMANDS

The MSS Flight Subsystem is designed to receive commands from the spacecraft command subsystem.

1. Command Pulse

   a. Amplitude - -23.5 ±1.0 V

   b. Pulse width - 40 ±5 msec (tentative)

   c. Current, load, maximum - 200 milliamperes

   d. Source Impedance - 30 ±5 ohms

2. Command Relays - twelve dc-type, latching relays

   NOTE: Neither relay input line will be grounded. Steering and suppression diodes will be used.

3.4.7 WIDEBAND VIDEO TAPE RECORDER INTERFACE

The MSS multiplexer will provide PCM data at 15 Mbps, a clock and word rate signal to each WBVTR. Except for the word rate signal, these signals will be identical to those supplied to the spacecraft Wideband Communications Subsystem.

3.4.8 MECHANICAL

The mechanical outline of the scanner head is shown in Figure 3.4-12. Mass Properties: The weight of the scanner is 105 pounds for ERTS A and 120 pounds for ERTS B. In both cases the multiplexer weight is 10 pounds. Centers of gravity were assumed at the physical centers.

3.4.8.1 Disturbance Torques

The scanner mirror will be balanced about its axis of movement.

No net torque levels exceeding 0.005 in-lb-seconds generated by the MSS Flight Subsystem shall be exerted on the spacecraft. Mirror impulses of 0.7 in-lb-seconds occur twice each mirror scan cycle, are opposite in direction, and are completely compensatory. The effect on a spacecraft having an inertia of 100 slug ft^2 will be a 15 Hz sawtooth displacement of ±4.6 microradians, maximum.

3.4.8.2 Pyrotechnics (tentative)

1. Uncage scanning mechanism

2. Uncap scanner optics

3. Uncap radiation cooler (ERTS-B only)

4. Uncage radiation cooler (ERTS-B only)

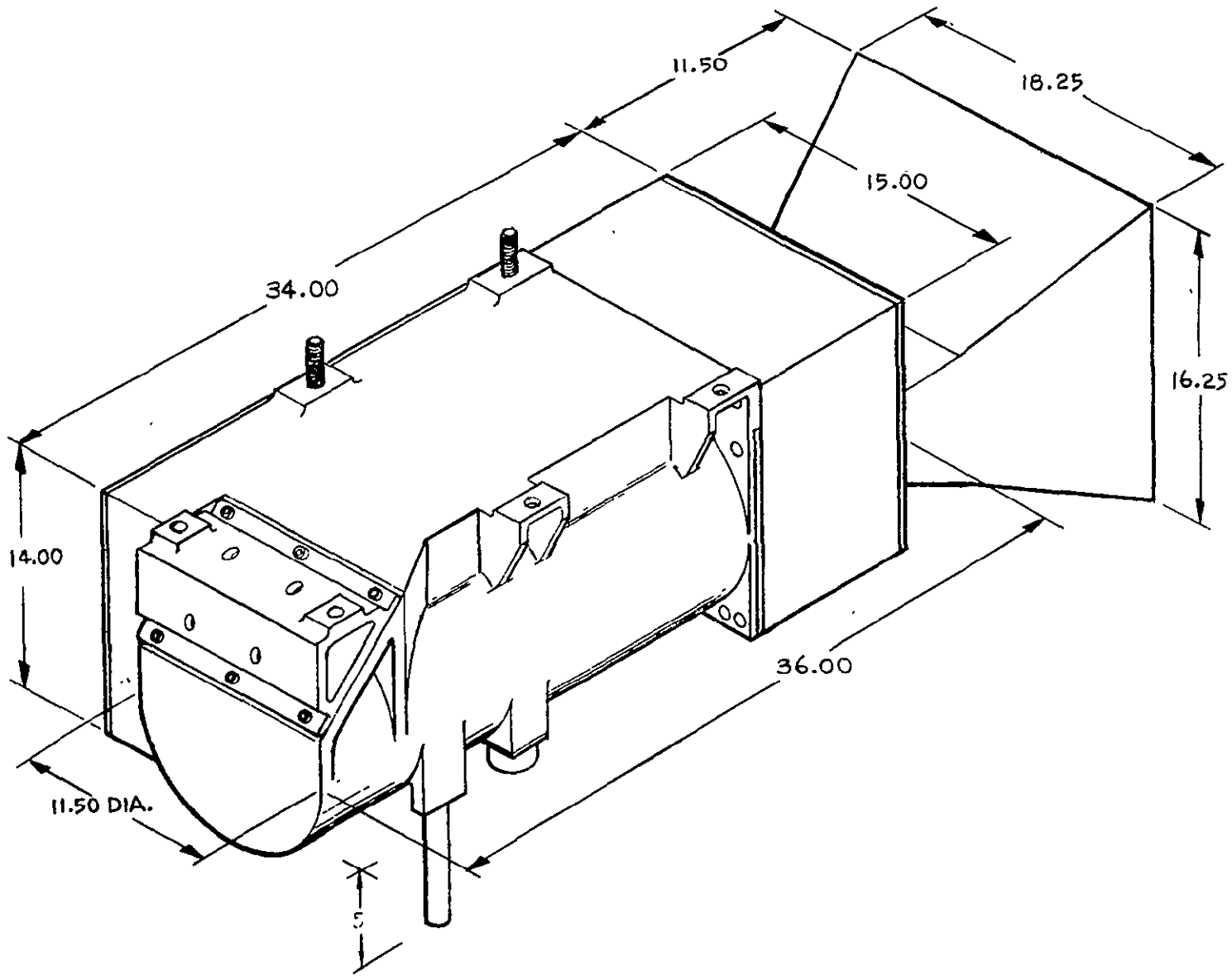

Figure 3.4-12. MSS Configuration 18 Jan. 1970

Table 3.4-3. Multispectral Scanner Flight Subsystem Command Relays

Command	Function	Command	Function
1	Multiplexer, ON	23	Mirror Pick-off, OFF
2	Multiplexer, OFF	24	Rotating Shutter Drive, ON
3	Spectral Band 1, ON	25	Rotating Shutter Drive, OFF
4	Spectral Band 2, ON	26	Calibration Lamp No. 1 ON
5	Spectral Band 3, ON	27	Calibration Lamp No. 2 ON
6	Spectral 4, ON	28	Select Calibration Sequence No. 1
7	Spectral Band 5, ON	29	Select Calibration Sequence No. 2
8	Spectral Band 1, OFF	30	Step Gain Band 1, Down
9	Spectral Band 2, OFF	31	Step Gain Band 2, Down
10	Spectral Band 3, OFF	32	Step Gain Band 3, Down
11	Spectral Band 4, OFF	33	Step Gain Band 4, Down
12	Spectral Band 5, OFF (ERTS-B only)	34	Spare command
		35	Spare command
13	Step Gain Band 1, UP	36	Spare command
14	Step Gain Band 2, UP	37	Spare command
15	Step Gain Band 3 UP	38	Band 1 HV Supply A
16	Step Gain Band 4, UP	39	Band 1 HV Supply B
17	Scan Mirror Drive, ON	40	Band 2 HV Supply A
18	Scan Mirror Drive, OFF	41	Band 2 HV Supply B
19	Step Band 5 Focus	42	Band 3 HV Supply A
20	Step Band 5 Focus Forward (ERTS-B only)	43	Band 3 HV Supply B
		44	Main Inverter A, ON
21	Step Band 5 Focus Reverse	45	Main Inverter A, OFF
22	Mirror Pick-off, ON	46	Main Inverter B, ON
		47	Main Inverter B, OFF
		48	Execute Command Sequence 1
		48+n	Execute Command Sequence n

3.4.8.3 Location

The following requirements shall apply to the location of the MSS and multiplexer units on the spacecraft:

1. The scanner shall be located on the side of the spacecraft shaded from the sun to take advantage of radiation cooling.

2. The radiation cooler shall be mounted so as to have an unobstructed view to black space.

3. The scanner shall be mounted so as to view the nadir within an elliptical cone of $\pm$15 degrees cross track and $\pm$10 degrees along track.

4. The multiplexer shall be mounted in close proximity to the scanner and to the spacecraft transmitter so as to reduce line lengths and corresponding signal attenuation.

3.4.8.4 Alignment (tentative)

	Initial		Recheck	
MSS to S/C Axes	Align. ($\pm^{o}$)	Accur. ($\pm^{o}$)	Align. ($\pm^{o}$)	Accur. ($\pm^{o}$)
Roll	0.05	0.008	0.10	0.01
Pitch	0.05	0.008	0.10	0.01
Yaw	0.05	0.008	0.10	0.01

3.5 WIDEBAND VIDEO TAPE RECORDER (WBVTR) SUBSYSTEM

3.5.1 SUBSYSTEM DESCRIPTION

The intended application for the recorder is to record and reproduce video signals from either the RBV camera or the multiplexed signal which is derived from the multispectral scanner. Reliable operation during 1 year in space orbit is required with a design goal of 4,000 full-length record and playback cycles. This goal is considered optimistic with respect to the critical head/tape interface; however, it is anticipated that a life of about 1,000 hours will be attained.

Two identical WBVTR subsystems are used, each consists of a tape transport module and an electronics unit. A block diagram of a subsystem is shown in Figure 3.5-1.

Each WBVTR is capable (by ground commanding) of recording either RBV video or MSS PCM. In the MSS mode the PCM input to the recorder is converted to an eight-level signal which can then be FM recorded. On playback, the PCM signal is again reconstructed. In the RBV mode, the pre and post recording signal processing is bypassed.

Two additional narrowband tracks are also provided, an auxiliary (AUX) track and a search track. The AUX track will accept a dc to 5-10 kHz input. This could be used for recording narrowband telemetry or time coded data for correlation with the stored wideband data. The search track contains prerecorded data. It will provide a digital readout in all modes of the position of the tape at 6-inch intervals to allow monitoring of the location of the data, for selective recording and reproduction. Because the "fast forward" and "rewind" speeds are 4-times the "record" or "playback" speeds, the prerecorded words will appear every 0.125 second and 0.500 second, respectively. In addition, during the "rewind" mode the bits comprising the digital words will appear in reverse order.

3.5.2 GENERAL SPECIFICATIONS

1. Recording Mode - FM
2. Scanning Principle - Transverse Scan
3. Head-to-Tape Speed - 1964 inches/second
4. Headwheel Rotary Speed - 18,750 rpm
5. Record/Playback Tape Speed - 12 inches/second
6. Rewind Tape Speed and High Speed Forward - 48 inches/second
7. Tape Length/Time - 2,000 feet/30 minutes
8. Tape Width - 2 inches
9. Transport Package Size (less mounting lugs) - 21.5 inches x 14.8 inches x 6.5 feet

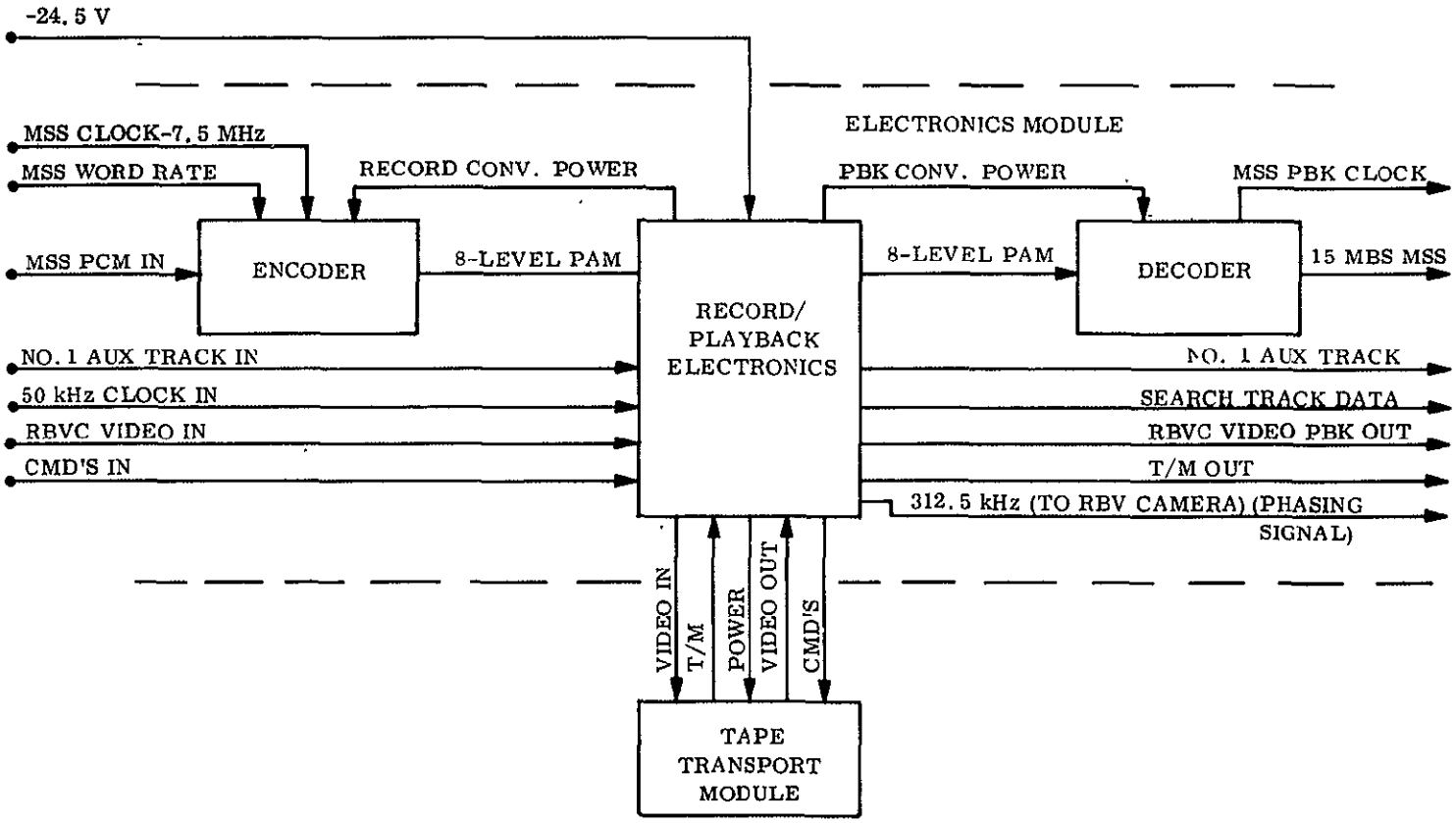

Figure 3.5-1. Tentative Wideband Video Recorder Block Diagram

10. Electronic Package Size (less mounting lugs) - 16.6 inches L x 16 inches W x 7.0 inches H

11. Estimated Total Weight - 70 lbs

3.5.2.1 Performance

1. Bandwidth, S/N - DC-4 MHz at 6 dB; S/N = 42 dB

2. S/N degradation (max.) - -1 dB

3. Linearity - ±3%

4. Drift - ±5% input to output

5. Transient Response - Approx. 5% peak overshoot

6. Input/Output Impedance

   a. RBV Mode - 75 ohms, coax

   b. MSS Mode - 50 ohms, balanced

   c. AUX Tracks - 600 ohms, coax

7. Switching Transients - below peak-to-peak noise

8. Jitter (MSS mode) - ~5 μsec p-p (phase) at 5.5 Hz

3.5.2.2 Input/Output Levels, RBVC Record Mode

1. Tip of Sync - 0V ± 0.05 v

2. Black Level, peak - minus 0.35 v ± 0.05 v

3. White Level, peak - minus 1.3 ± 0.1 v

4. Black Clip Level - minus 0.3 ± 0.05 v

5. White Clip Level - minus 1.65 ± 0.1 v

6. Video Signal Ouput Impedance - 75 ohms

3.5.2.3 Input/Output Levels, MSS Record Mode
(Later)

3.5.3 RECORDER OPERATIONAL SEQUENCES

3.5.3.1 RBV Mode

When operating with the Return Beam Vidicon (RBV) camera, the sequence of events is as follows:

1. At t_0 of the 25 second RBV picture interval, the recorder is commanded into "standby" (bring head wheel up to speed).

2. At $t_{11.5}$ the record signal(which activates the capstan and the record electronics) is received; when the tape is up to speed the head pressure "shoe" is applied.

3. At $t_{13.5}$, horizontal sync is recorded. This is done to provide ground sync prior to picture data.

4. At $t_{14.5}$, data is recorded.

5. At either t_{18}, $t_{21.5}$, $t_{25.0}$, depending on which cameras are operating, the record signal indicated in Step 2 is terminated, putting the recorder in the standby mode until receipt of the next record signals.

6. WBVTR generates 312.5 kHz signal, which is applied to the RBV cameras for phasing purposes.

3.5.3.2 MSS Mode

When operating with the MSS, the recorder will operate continuously. Operational commands will be supplied directly from the spacecraft.

3.5.4 POWER

Total Power Consumption

a.	Standby	
	Startup	265 watts (decreasing to average power in 6 seconds)
	Steady State	40 watts
b.	Record	
	Startup (From Standby)	119 watts (1 sec.)
	Steady State	85 watts
c.	Playback	
	Startup (From Standby)	115 watts (1 sec.) (estimated)
	Steady State	81 watts
d.	Wind (Headwheel Off)	
	Startup	120 watts (4 sec.)
	Steady State	40 watts

The Electronics Module consumes 30 watts of average power, without any major transients.

Typical power profiles for RBVC in various modes of operation are shown in Figures 3.5-2, 3.5-3, and 3.5-4. The external connector listing is shown in Figure 3.5-5.

3.5.5 THERMAL

Thermal dissipations by the individual modules depend on the operating mode. Total dissipation is as indicated in paragraph 3.5.2. Approximately constant dissipation is assumed for the electronics whenever the subsystem is operating.

3.5.6 TELEMETRY

Fourteen digital and 10 analog inputs are provided (see Table 3.5-1).

Table 3.5-1. Wideband Video Tape Recorder Subsystem Telemetry Inputs

Item No.	Function	Type	Item No.	Function	Type
1	Standby	Digital	15	Tape footage	Analog
2	Record	Digital	16	Pressure, internal, container	Analog
3	Playback	Digital			
4	Rewind	Digital	17	Temperature	Analog
5	Forward	Digital	18	Record Current, average	Analog
6	Primary end of tape	Digital			
7	Secondary end of tape	Digital	19	Playback Voltage, average	Analog
8	Primary start of tape	Digital			
9	Secondary start of tape	Digital	20	Servo Voltage	Analog
			21	Captain Motor Speed	Analog
10	Lap at beginning of tape	Digital	22	Motor Current (OC)	Analog
			23	Motor Current HWP	Analog
11	RBV/MSS mode	Digital	24	Motor Current, Capstan	Analog
12	Recorder current adjust, level 1	Digital			
13	Recorder current adjust, level 2	Digital			
14	Recorder current adjust, level 3	Digital			

3.5.7 COMMANDS

The commands required by the recorder are:

1. Standby - Headwheel only powered.

2. Record - Headwheel, capstan, and record circuitry are powered. When tape is up to speed, shoe is engaged. Previously recorded information is now being erased.

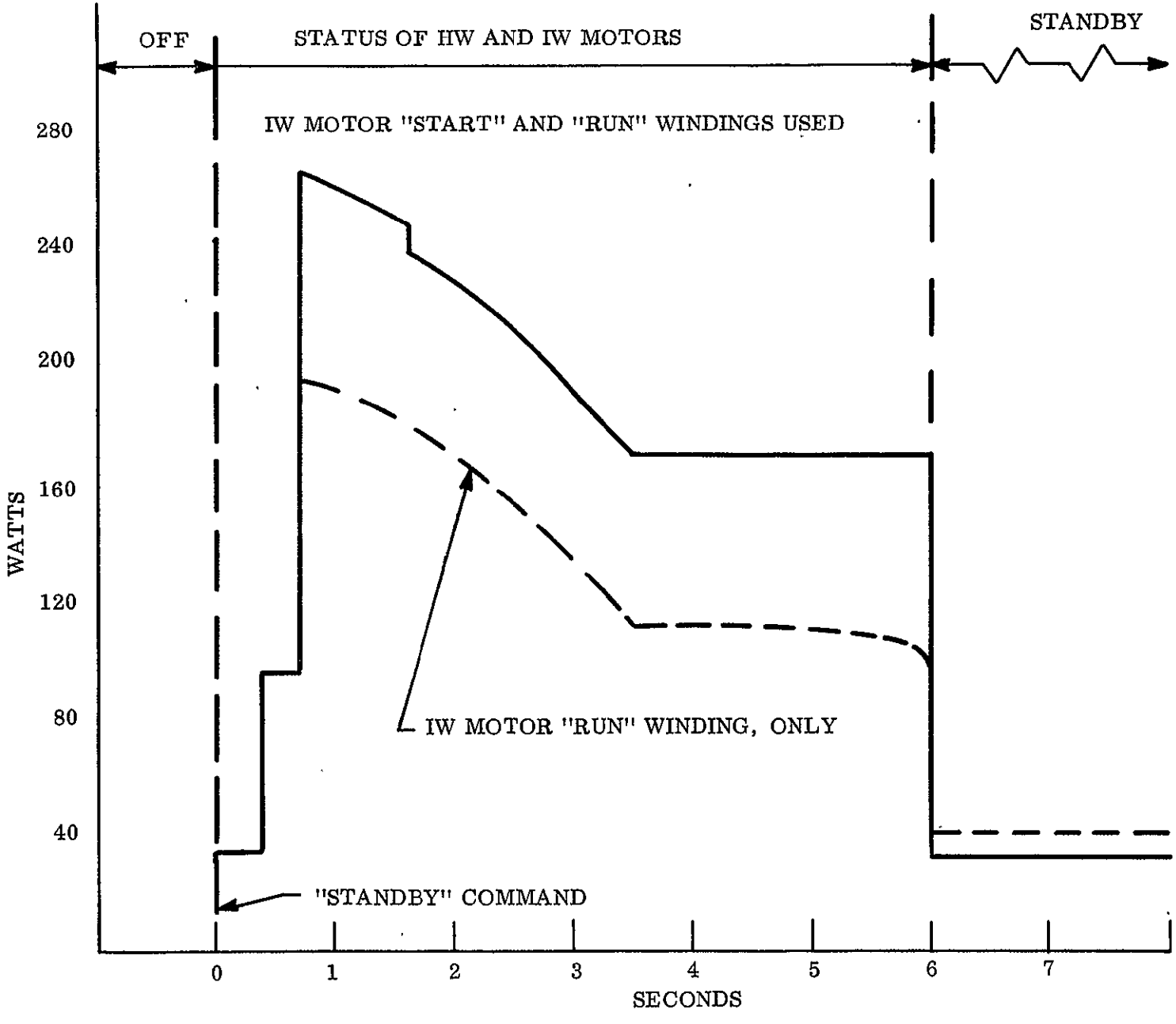

Figure 3-5-2. Power Profile Off-to-Standby Transition ERTS Video Recorder

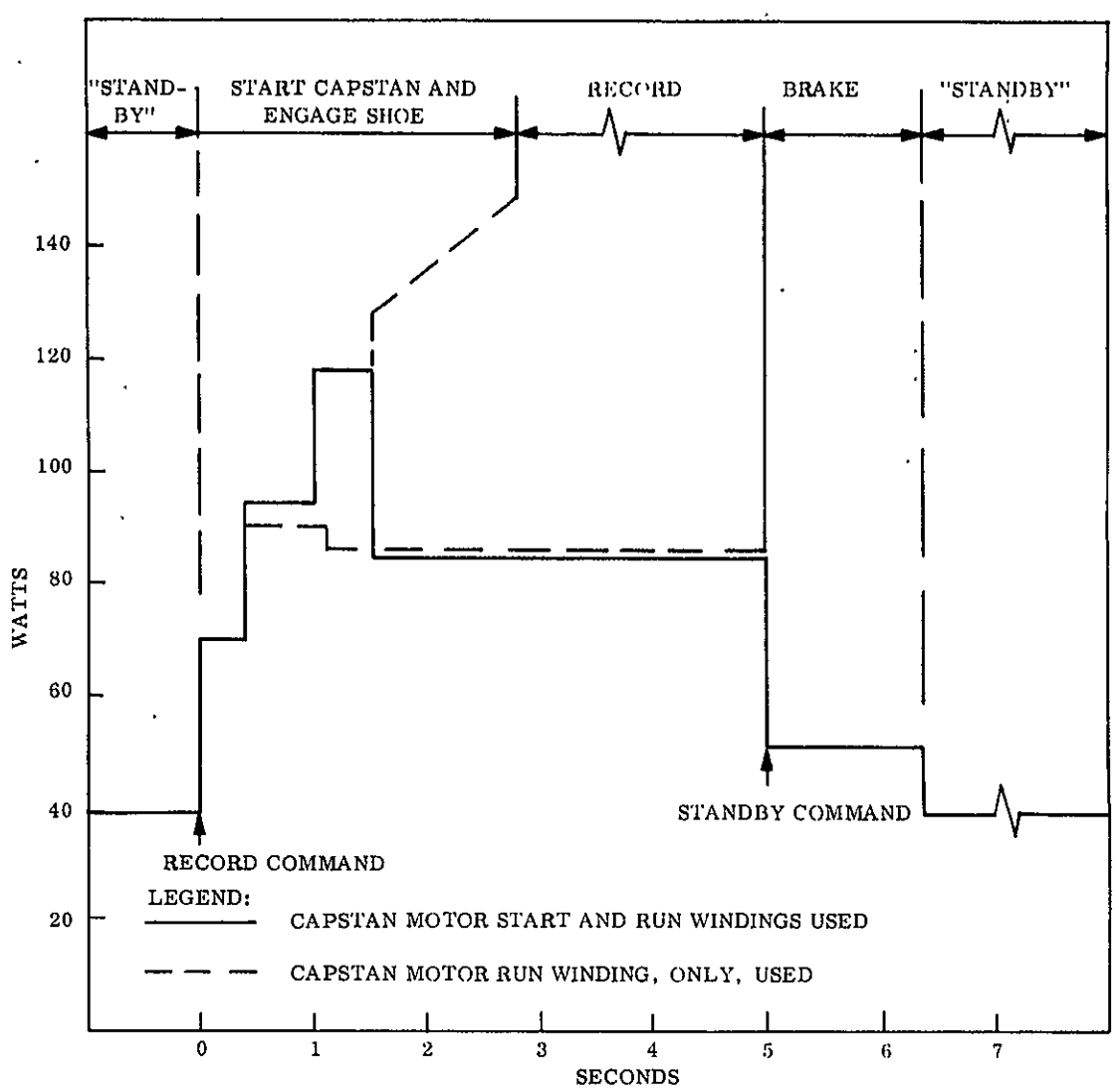

NOTE: PLAYBACK POWER IS 4 WATTS LESS THAN RECORD POWER

Figure 3.5-3. Power Profile Standby-to-Record-to Standby ERTS Video Recorder

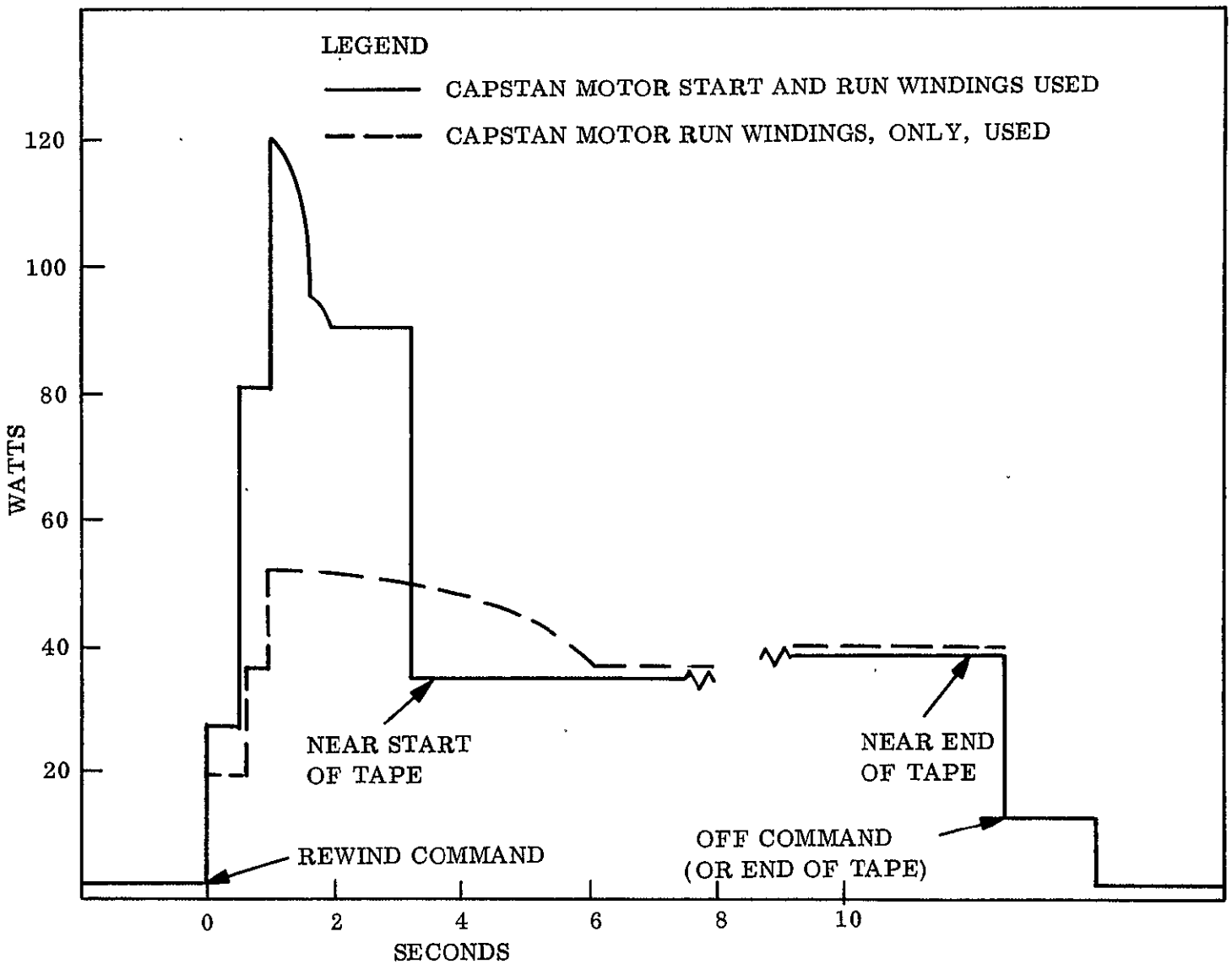

Figure 3.5-4. Power Profile Off-to-Rewind ERTS Video Recorder

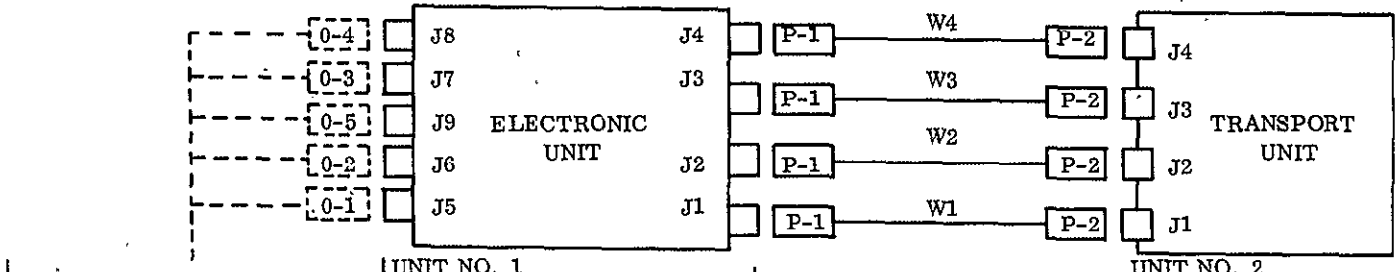

SPACECRAFT		UNIT NO. 1 ELECTRONICS UNIT		INTERCONNECTING CABLES		UNIT NO. 2 TRANSPORT UNIT	
DESIG-NATION	CONNECTOR*	DESIG-NATION	CONNECTOR*	DESIG-NATION	CONNECTOR*	DESIG-NATION	CONNECTOR*
		J-1	DS00-27PB7020	W1P1	DS07-27-SB-059-5020		
		J-2	DS00-27PC7020	W1P2	DS07-27-SB-059-5020	J-1	DM5605-27PB-797
				W2P1	DS07-27-SC-059-5020		
		J-3	DS00-3719PB7020	W2P2	DS07-27-SC-059-5020	J-2	DM5605-27PC-797
				W3P1	DS07-3719SB-059-5020		
		J-4	DS00-3719PC7020	W3P2	DS07-3719SB-059-5020	J-3	DM5605-3719-PB-4-797
				W4P1	DS07-3719SC-059-5020		
				W4P2	DS07-3719SC-059-5020	J-4	DM5605-3719-PB-4-797
0-1	DS07-1912S-059-5020	J-5	DS00-1912P7020				
0-2	DS07-37S-059-5020	J-6	DS00-37P7020				
0-3	DS07-3727S-059-5020	J-7	DS00-3727P7020				
0-4	DS07-3713S-059-5020	J-8	DS00-3713P7020				
0-5	DC3-5-00-000-A	J-9	DC-4-5-00-000-A				

*Connectors are identified by Deutsch part numbers.

Figure 3.5-5. WBVTR, External Connector Identification

3. Rewind - Shoe is retracted; unit rewinds at four times normal speed to the end of tape or until another command is received.

   NOTE: It is under consideration that the recorder be made capable of stopping itself at a preselected time code position.

4. Playback - Headwheel, capstan, and reproduce electronics are powered.

5. Fast Forward (Under Consideration) - Shoe is retracted; unit runs forward at rewind speed to a preselected point, end of tape, or receipt of another command.

6. Off - All systems are off

7. MSS - MSS mode of recording or playback

8. RBV - RBV mode or recording or playback

9. Record current adjust - Compensation for record head wear.

3.5.8 MECHANICAL

The outline drawings of WBVTR transport unit and electronics unit are shown in Figures 3.5-6 and 3.5-7, respectively.

3.5.8.1 Location

The location of WBVTR modules should be such as to assure short signal line lengths to corresponding feeding subsystems as well as transmitters.

3.5.8.2 Mounting

Tape unit may require mounting surface flatness to $\pm$ 0.005 inch.

3.5.8.3 Uncompensated Momentum

The momentum of the recorder headwheel is 0.0492 ft-lb-second. A compensation motor is currently provided (if necessary) which compensates this momentum except during start-up. The transient uncompensation is shown on Figure 3.5-8 for two conditions: using a starting winding and using only the run winding. The momentum vector is aligned parallel to the long dimensions of the tape transport.

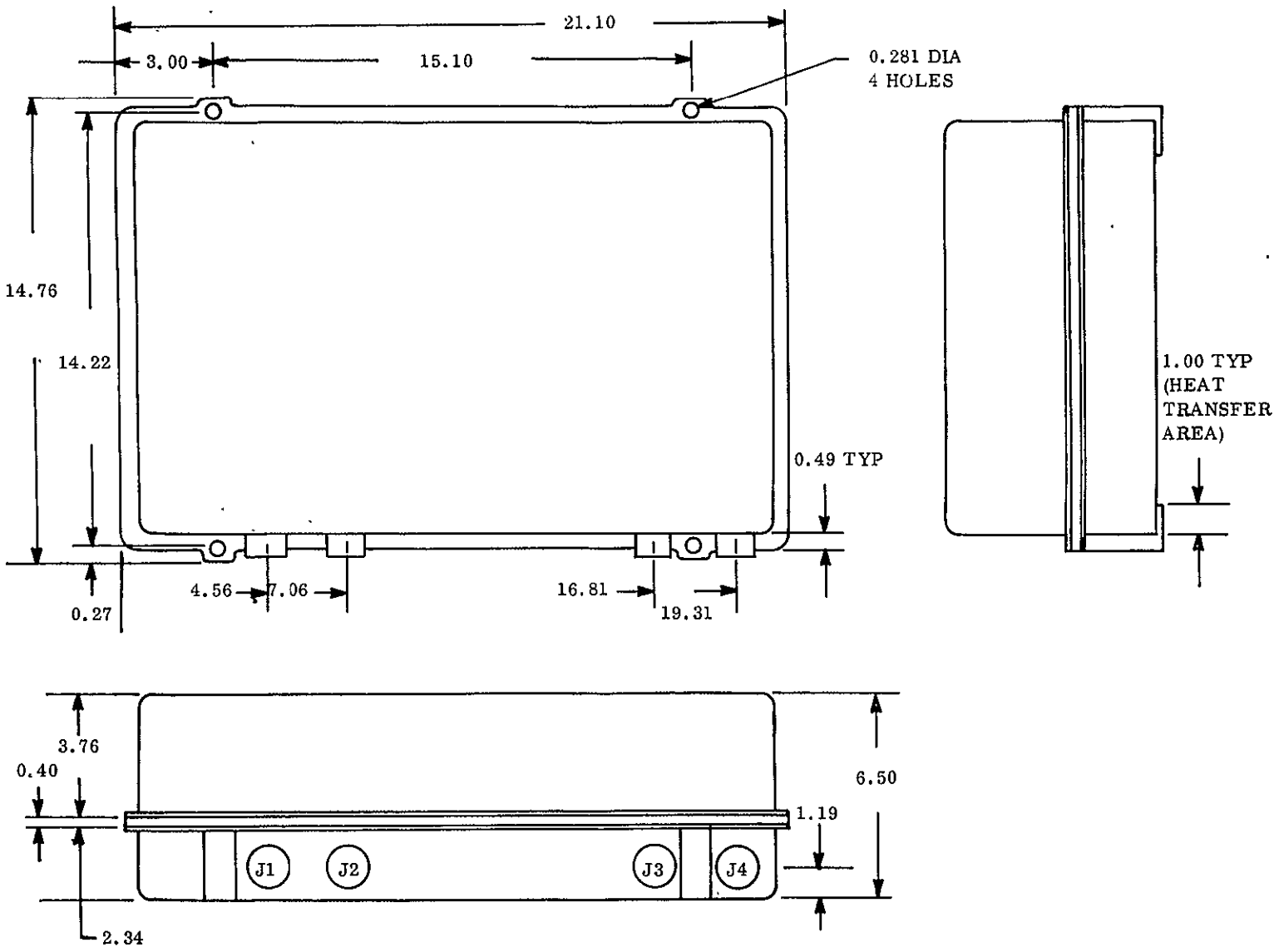

Figure 3.5-6. WBVTR Transport Unit ERTS

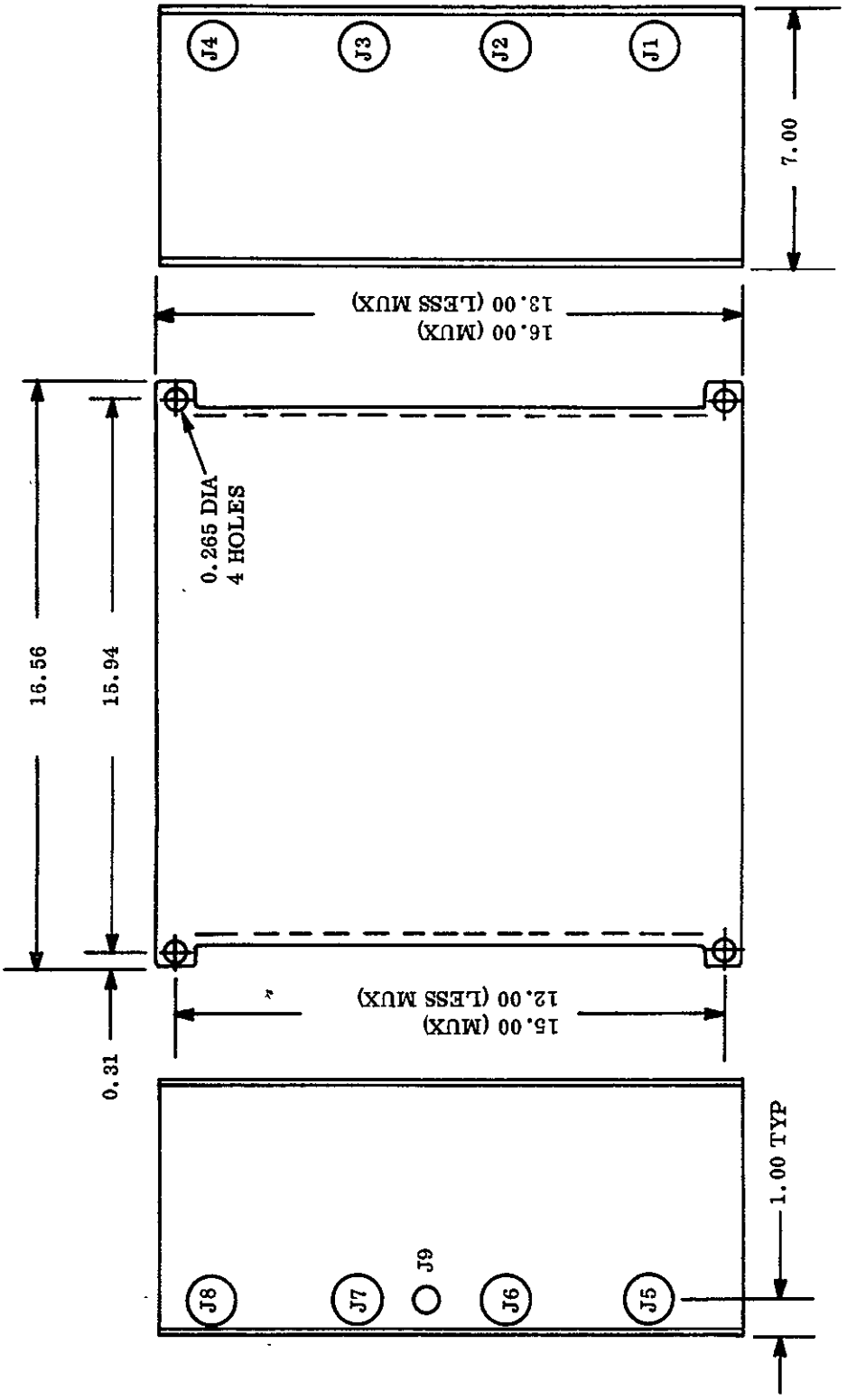

Figure 3.5-7. WBVTR Electronics Unit ERTS

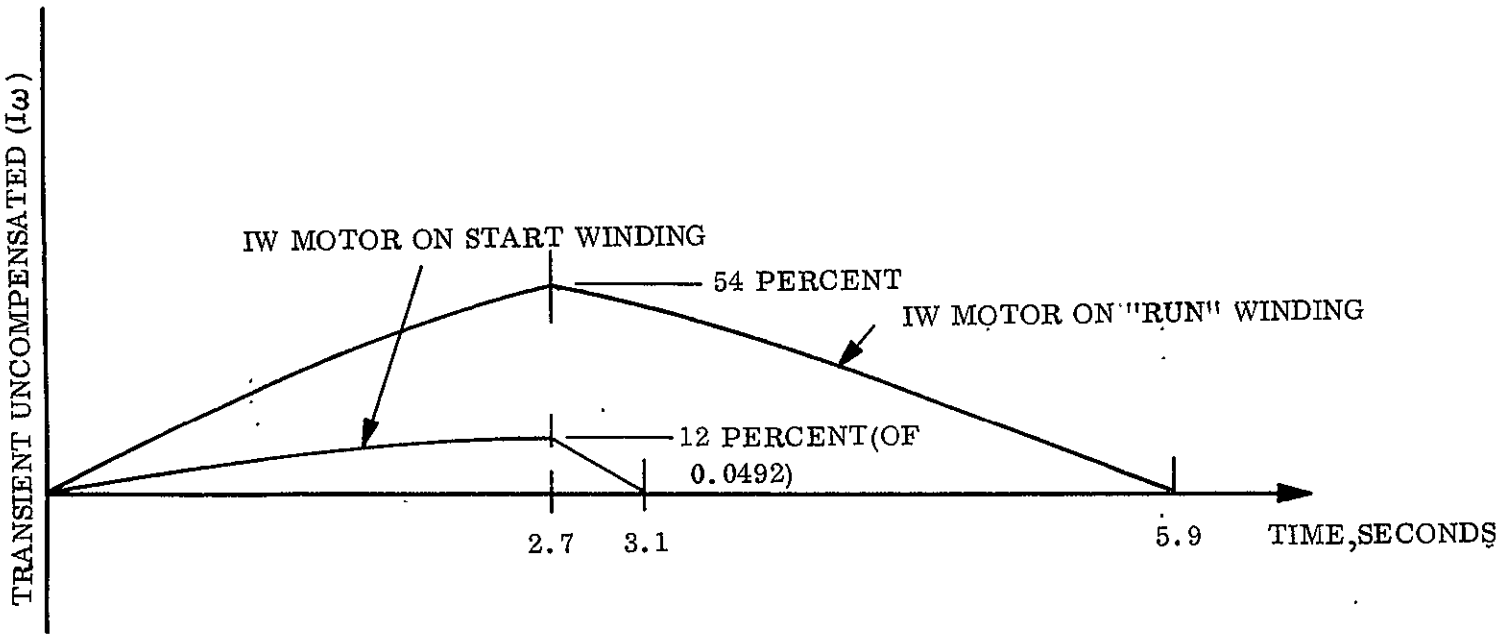

NOTE: 100 PERCENT = 0.0492 ft.-lb-sec

Figure 3.5-8. Headwheel Uncompensated Momentum

3.6 DATA COLLECTION SYSTEM (DCS)

3.6.1 SUBSYSTEM DESCRIPTION

The DCS for ERTS-A and B consists of three segments. The segments are: the Data Collection Platforms (DCP's), the Spacecraft Receiving Subsystem and the DCS Ground Preprocessing Equipment. An illustration of the system concept is shown in Figure 3.6-1.

The figure shows that the DCP's are colocated with sensors throughout the continental United States and its coastal waters. Each DCP accepts inputs from eight sensors. The analog inputs are multiplexed, using time division multiplexing (TDM). Each input is then coded, using pulse code modulation (PCM). A convolutional encoder then encodes the pulse train before it is passed on to the FSK modulator and the transmitter. The signal is transmitted to the spacecraft on a carrier at a frequency of 401.9 MHz.

The signal is received at the spacecraft through a crossed dipole antenna and passes to the DCS spacecraft receiver subsystem. The receiver is a double heterodyne receiver with a 3 dB overall noise figure, an IF bandwidth of 100 kHz and an output center frequency of 1.024 MHz. The 1.024 MHz signal is passed to the unified S-band (USB) premodulation processor where it is combined with other signals for relay to the ground over the USB downlink.

At the three receiving sites (Alaska, Corpus Christi, and NTTF), the USB downlink signal is received and demodulated. The DCS signal is stripped out of the composite baseband and routed to the DCS ground preprocessing equipment. In the preprocessing equipment, the PCM/FSK signal is detected and demodulated and then decoded and formatted for transmission over telephone lines to the Operation Control Center (OCC) and the NASA Data Processing Facility (NDPF). At the NDPF the data is formatted and prepared for dissemination to the users.

The system provides for a 1000 DCPs with 0.95 probability of receiving interference free data from each platform every 12 hours. The coding provided will assure that the probability of errors in a message being undetected is less than 0.05.

The DCPs are designed for production, at low cost, by normal commercial electronics manufacturers. Thus, members of the scientific community are not precluded from participation in the use of the DCS on the basis of cost. The spacecraft receiver subsystem will be of conventional design and packaged in a standardized module. The spacecraft receiver subsystem and crossed dipole antenna are described in more detail in the following paragraphs.

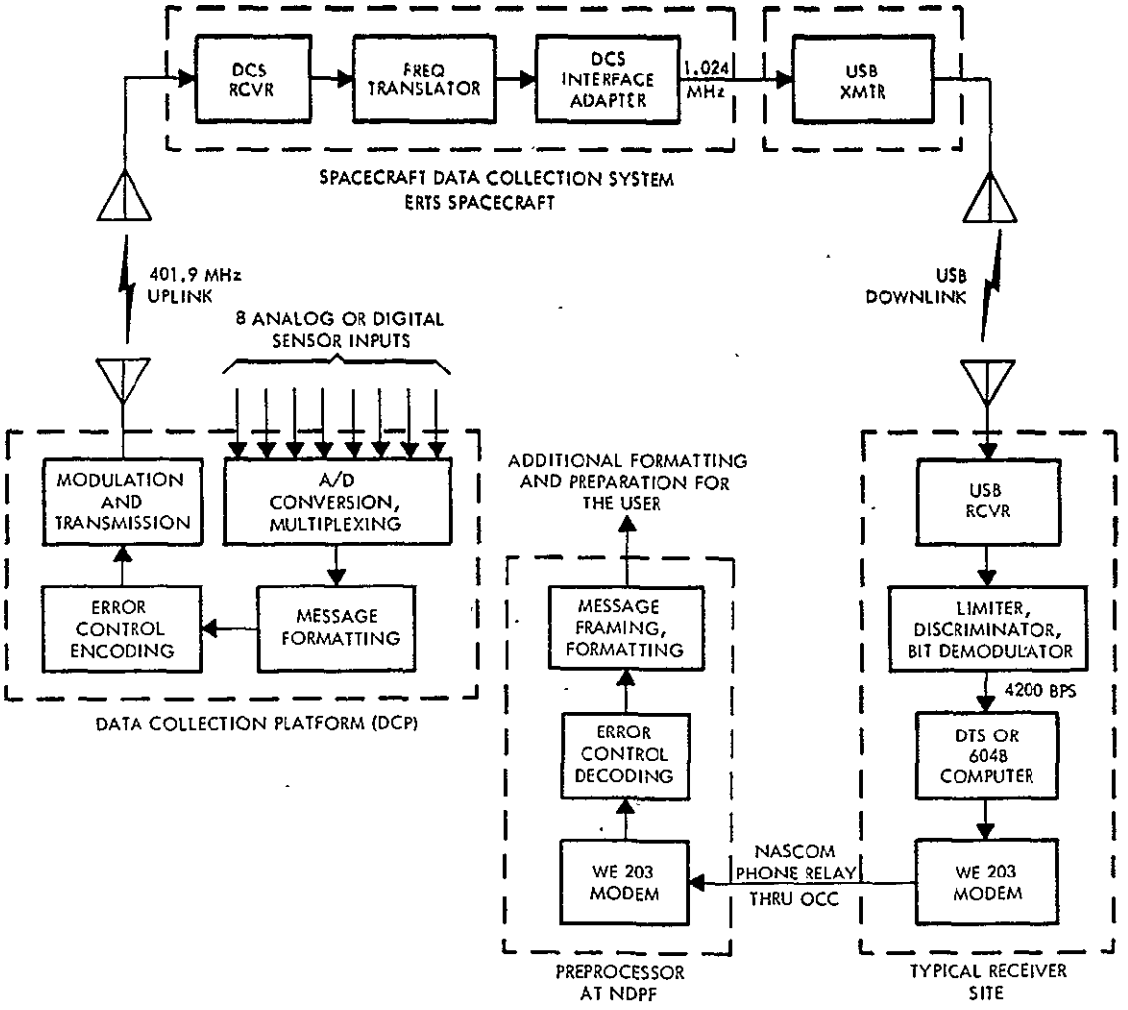

Figure 3.6-1. ERTS DCS Configuration

3.6.2 GENERAL REQUIREMENTS AND SPECIFICATIONS

Unit	Performance Parameter	Characteristics
Antenna	Type	Turnstile Dipole
	Impedance	50 ohms
	VSWR	1.5:1 (normal), 3:1 (prelaunch)
	Bandwidth (3 dB)	110 degrees
	Gain Over Isotropic	6 dB
	Polarity	Right Circular
	Frequency	401.9 MHz
Receiver	Size	1/0 Nimbus Module
	Weight	3 pounds
	Material	Aluminum
	Input Frequency	401.9 MHz
	Input Level	-121 dBm to -60 dBm
	IF Bandwidth	100 kHz
	Noise Figure	3 dB maximum
	Input VSWR	2.0:1
	Image Rejection	60 dB
	Spurious Response	60 dB below desired
	Local Oscillator Stability	0.002%
	Output Signal Center Frequency	1.024 MHz
	Output Voltage	2 volts, peak-to-peak
	Power Drain	1 watt, approximately
	Input Voltage	-24.5 vdc ± 1 volt
	Input Voltage Transients	-40 vdc
	Thermal-Power Dissipation	1 watt
	Telemetry Points:	
	1. Power ON & OFF	Digital B 1/16
	2. Temperature	Digital B 1/16
	3. Automatic Gain Control	Analog 1/16
	Commands:	
	1. Power ON	Change of state
	2. Power OFF	Change of state

3.6.3 POWER

The power required to operate the spacecraft receiver will be approximately 1 watt. The majority of this is required to raise the signal level to 2 volts (peak-to-peak) to drive the unified S-band preprocessor. The input voltage must be -24.5 vdc ± 1 volt. An internal regulator is used in the receiver to condition the spacecraft bus power.

3.6.4 THERMAL

The output power of the receiver is less than 100 mwatts. The power dissipated in therefore approximately 1 watt. The unit does not require any special cooling and does not contribute any significant heat to the spacecraft.

3.6.5 TELEMETRY

The health of the receiver may be determined from 3 measurements. They are:

1. Receiver ON or OFF
2. Temperature of the unit
3. Output signal power

3.6.6 COMMAND

Two commands are required, one to switch the unit on and one to turn it off.

3.6.7 DATA INTERFACE

The output of the receiver is a signal with a 100 kHz bandwidth, center frequency of 1.024 MHz at a level of 2 volts (peak-to-peak) when measurement across of 50-ohm load. The signal has the characteristics of a wideband (± 20 kc deviation) FM signal with an equivalent RMS test tone to white noise in a 100 kHz band of 4.6 dB.

3.6.8 MOUNTING REQUIREMENTS

The DCS receiver is housed in a Nimbus type 1/0 module and requires no special mounting provisions except that it should be reasonably close to the DCS antenna. The receiver has a power dissipation of only 1 watt and the four cables (command and power, telemetry, and antenna feed and USB connection cable) do not require special routing or shielding.

The DCS Antenna (Figure 3.6.8.2-1) which is placed in the earth facing surface is mounted so that the ground plane is as far above any protrusions as possible. This has resulted in the DCS antenna being lower down in the stowed configuration than the IRLS antenna used on similar vehicles. To accommodate the lower position, a change has been made in the reradiator, location on the adapter ring. This will maintain an adequate spacing between the reradiator and the DCS spacecraft antenna.

3.7 SUMMARY OF STUDY RESULTS, PAYLOAD SUBSYSTEMS

Many payload related studies have been conducted to assure successful integration into the spacecraft.

To facilitate easy locating of topics, a matrix was assembled indicating the results of the evaluation and location of this information in the report. This is shown on Tables 3. 7-1 through 3. 7-3.

3.8 RECOMMENDED CHANGES TO THE PAYLOAD SENSORS

As a result of analyses performed during the ERTS Phase B/C study, the following recommendations for modification of the sensor payloads are made for the purpose of improving the operational flexibility of these payloads.

3.8.1 ADDITION OF TIME CODE TO THE SENSOR DATA

To aid in image location and time/position correlation, the precise time of sensor operation must be known. Four basic approaches were considered for obtaining time information as a function of sensor operation. These approaches were:

1. Record all narrow band (NB) telemetry data on the auxiliary track of the wide band video tape recorder (WBVTR) when recording data.

   a. Real Time - on the ground

   b. Stored Mode - on the spacecraft

2. Record the pulse width modulated time code from the ERTS command clock on the auxiliary track of the WBVTR when recording sensor data.

   a. Real Time - on the ground

   b. Stored Mode - on the spacecraft

3. Record WWV on the auxiliary track of the ground tape recorder in either the real time or stored mode of operation.

4. Add time code to the sensors.

The approaches which require either NB telemetry data or time code to be recorded on the spacecraft (and ground, subsequently), or to record WWB on the ground along with the data impose rather extensive bookkeeping requirements, or duplicate processing of the NB telemetry data to correlate sensor operation with spacecraft time.

The recommended approach is to modify the RBVC and MSS sensors in a manner to permit the addition of time code to the video data from each sensor. This method of time annotation has the advantages of minimizing the bookkeeping, eliminating the need for processing

additional data, or for additional spacecraft equipment, and insuring that sensor data and time of sensor operation are forever inseparable. The manner in which the time code is added should be such that it is easily readable not only electronically but optically or visually. In addition, it is further desired that the last 10 bits be available for clocking into the telemetry system at least once per major frame.

3.8.2 RBVC SHUTTER EXPOSURE TELEMETRY MODIFICATION

If the time code modification to the sensors is not made, it is very important to know when the RBV camera shutter operated via telemetry. At present, this telemetry point is specified as an analog output, and the probability of sampling it is rather improbable because of its short duration. Because of this, it is recommended this telemetry point be changed to digital output type, with one "hold" period of a few seconds to insure that this event will get sampled.

3.8.3 AUTOMATIC OPERATION OF RBVC EXPOSURE

The RBV camera contains circuitry which permits operation at three discrete exposure times; i.e., 8, 12, and 16 milliseconds. In addition, there is another mode of operation known as the automatic operation mode.

The ERTS attitude control system has a drive for the solar paddle shaft. The shaft is always driven to a very specific point at which a maximum of solar illumination is intercepted by the solar cells, therefore, it is also in a fixed relationship to the earth's latitutde which can be used as an exposure determining input. Consequently, it is suggested the solar shaft be equipped with an appropriate signal transducer and thus provide the signal most likely needed for RBV automatic exposure mode of operation.

3.8.4 MSS TELEMETRY OUTPUT

In the GSFC Specification, S-731-P-100, dated June 1969, for the Multispectral Scanner System, the analog telemetry signal levels are specified to be between the voltage levels of 0 and -5 volts. This was verified during an MSS interface meeting with Hughes Aircraft Company on December 19, 1969. The digital words, however, are compatible with the Nimbus D telemetry system. It is recommended that the MSS analog signals also be made compatible with the Nimbus D telemetry system, which has a 0 to -6.375 volt range for analog signals.

TABLE 3.7-1. SUMMARY OF PAYLOAD STUDY RESULTS (RBVC)

TOPIC	RESULTS/STUDY	DISCUSSION IN VOLUME/SECTION
Alignment/Mounting	Mounting Requirements	2/2.3.4
	Field of View	2/2.3.4.1
	Component Placement	2/2.4.1.1
	Tests to Verify Alignment Maintenance	2/2.4.1.2
	Camera Mount Vibration	2/2.4.7.3
	Camera Mounting Thermal Distortion	2/2.4.7.4
	Mounting Design Description	2/2.5.4
Thermal Considerations	Camera Mount Thermal Distortion	2/7.4.2.4
	Heat Flow Rate Restrictions	2/7.2.4
	Heat Dissipation	2/7.3
	Thermal Problem Do Not Limit Time of Operation	2/7.4.1
	Thermal Balance	2/7.4.2.1
	RBVC Heat Rejection	2/7.4.2.3
Communication & Data Handling	Signal Conditioning	2/4.2.2
	Modes of Transmission	2/4.4.1.5.1
	Sensor Interface	2/4.4.1.5.3
	Wide Band FM Modulator Down Link Requirements	2/4.4.1.7
	Real Time Command Studies	2/4.4.2.2
	Telemetry & Command List	2/Appendix 4.A
	Video Switching Matrix	2/4.4.1.5.2
Attitude Control	Image Location Accuracy	2/5.2.1&1/4.3&4.4
	Pointing Accuracy	2/5.2.3.2
	Uncompensated Momentum	2/5.4.5
	Magnetic Disturbance	2/5.4.6
Power	Requirements	2/Table 8.2-1
	Regulated Power to Payload	2/8.3.1.4
	Operating Time, Day 9 (Worst Case)	2/8.3.2.2
	Baseline Power Profile	2/Figure 8.3-10
	Regulated Power Requirements	2/Table 8.4-1
	Peak Power	2/8.4.1.1
	RBV Camera Regulation and Conversion	2/8.4.1.1

TABLE 3.7-1. SUMMARY OF PAYLOAD STUDY RESULTS (RBVC) (Cont'd.)

TOPIC	RESULTS/STUDY	DISCUSSION IN VOLUME/SECTION
Test	EMC Tests SDM - Structural Tests Vibration, Shock, Thermal Model Test Schedule Payload Integration Alignment, Vacuum/Thermal Test Launch Configuration & RF Compatibility	
AGE	Alignment Requirements EAGE Check of Calibration Tie-in with Test Ground Station Bench Integration Test	

TABLE 3.7-2. SUMMARY OF PAYLOAD STUDY RESULTS (MSS)

TOPIC	RESULTS/STUDY	DISCUSSION IN VOLUME/STUDY
Alignment Mounting	Field of View Mounting Requirements Component Placement SDM - Tests Verify Alignment Maintenance Sun Glint Study Stimulator in Adapter Payload Design Description MSS Installation	
Thermal Considerations	Payload Operation Heat Flow Rate Restrictions Thermal S/S Description (MSS Heat Dissipation) Sensory Ring Thermal Analysis Thermal Problems Do Not Limit Time of Operation Thermal Balance MSS Heat Rejection Contamination of Second Stage Radiator Cone	
Communications & Data Handling	Payload Signal Conditioning MSS Transmission Link Modes of Transmission Video Switching Matrix Sensor Interface Wide Band FM Modulator Down Link Real Time Command Studies Telemetry & Command List	
Attitude Control	Uncompensated Momentum Magnetic Disturbance	
Power	Payload Power Requirements Regulated Power to Payload Operating Time, Day 9, Worst Case Baseline Power Profile Regulated Power Requirements MSS Regulation & Conversion	

TABLE 3.7-2. SUMMARY OF PAYLOAD STUDY RESULTS (MSS) (cont'd.)

TOPIC	RESULTS/STUDY	DISCUSSION IN VOLUME/STUDY
Test	EMC Tests SDM - Vibration, Shock, Thermal Tests Test Schedule Payload Integration, S/C Alignment and Thermal Vacuum Test Launch Configuration RF Compatibility	
AGE	Alignment Requirements EAGE Check of Calibration of Payload Sensors Test Ground Station; MSS Test Racks MSS Bench Test Equipment	

TABLE 3.7-3. SUMMARY OF PAYLOAD STUDY RESULTS (WBVTR)

TOPIC	RESULTS/STUDY	DISCUSSED IN VOLUME/SECTION
Mounting	Sensory Ring Assembly	
Thermal	Thermal S/S Description for WBVTR Heat Flow Rate Restrictions Payload Thermal Balance W.B.V.T.R. Heat Rejection	
Attitude Control	Effect of Uncompensated Momentum	
Power	Payload Power Requirements Regulated Power to Payload Baseline Power Profile Power Regulation and Conversion Peak Power	
Test	EMC Tests SDM - Structural, Vibration, Shock and Thermal Tests Test Schedule Payload Integration & Thermal Vacuum Test	
Use Management	Plan for Use of WBVTR, Operational Sequence, Tape Management	

SECTION 4

COMMUNICATION AND DATA HANDLING SUBSYSTEM (C&DH)

SECTION 4

COMMUNICATION AND DATA HANDLING SUBSYSTEM (C&DH)

This section deals with the following related subjects:

1. Imposed subsystem requirements
2. Specific study items dictated by subsystem requirements
3. Recommended designs as derived from the study results

The primary C&DH subsystem functions are conveniently classified as:

1. Wideband Telemetry
2. Command/Clock
3. Tracking and Narrowband Communications
4. Associated antennas

See Section 4.2 for definition of the above items. The following material is organized in the order listed above.

4.1 SUBSYSTEM REQUIREMENTS

The following requirements were either specified (GSFC No. S-701-P-3) or derived in this study for the various links.

4.1.1 WIDEBAND TELEMETRY

4.1.1.1 Return Beam Vidicon (RBV) link

1. Available RF carriers: 2229.5 and 2265.5 MHz
2. Video Bandwidth: 3.5 MHz
3. Modulation: Video/FM
4. Allowable signal degradation: 1 dB
5. Available RF bandwidth: 20 MHz
6. Transmitter power output: 20 watts, with a 10-watt commandable mode
7. Transmission of both real-time and recorded video

4.1.1.2 Multispectral Scanner (MSS) link

1. Available RF carriers: 2229.5 and 2265.5 MHz
2. Digital Bit Rate: 15 mbs
3. Modulation: PCM/FSK
4. Allowable BER: 10^{-5}
5. Available RF bandwidth: 20 MHz
6. Transmitter Power output: 10 watts, with a 20-watt commandable mode
7. Transmission of both real-time and recorded PCM.

In addition, the following constraints are imposed:

1. Simultaneous transmission of any two of the following signals:
   a. RBV Real-time
   b. MSS Real-time
   c. RBV Playback (WBTR No. 1)
   d. MSS Playback (WBTR No. 1)
   e. RBV Playback (WBTR No. 2)
   f. MSS Playback (WBTR No. 2)
2. Crosstalk between RBV and MSS to be compatible with signal degradation requirements.
3. Crosstalk between the wideband telemetry and the USB links to be compatible with performance requirements.
4. Cross-strapping will be employed to optimize system reliability
5. Antenna beam shaping will be employed to improve the available system signal margin:
   a. Near constant earth illumination for ± 60.6°
   b. Antenna gain - +4 dB for ±60.6°

4.1.2 COMMAND/CLOCK

A dual command system capability is required and is defined as follows:

4.1.2.1 Stadan Compatible

1. RF carrier: 154.2 MHz
2. Bandwidth: 30 kHz

3. Modulation: PCM/FSK-AM/AM
4. Bit rate: 128 bps
5. Antenna coverage: Spherical
6. ERTS-A address: $073_{(8)}$ and $103_{(8)}$
7. ERTS-B address: $021_{(8)}$ and $132_{(8)}$
8. Subcarrier: 8.0 kHz for a "0"; 8.6 kHz for a "1"

4.1.2.2 MSFN (USB) Compatible

1. RF carrier: 2106.4 MHz
2. Bandwidth: 3.6 MHz
3. Modulation: PCM/PSK/FM/PM
4. FM subcarrier: 70 kHz
5. PSK: Composite 2-kHz data and 1 kHz clock
6. Bit rate: 1 kbs
7. Sub-bit coding: 5 sub-bits to 1 data bit
8. Antenna coverage: Hemispherical

In addition, the following constraints were imposed:

1. Utility of existing MSFN ground station equipment without hardware modification
2. Minimum modification of existing software.
3. Real-time capacity: 412 commands
   Stored capacity: 30 commands
4. Fail-safe command execution
5. Redundant means for command verification
6. Means for override of individual stored commands
7. Low probability of a false command
8. Capability for 100 stored command executions between loadings
9. Available RF link margin: + 26 dB
10. RF link BER: 10^{-6}
11. Clock update to be known within 1 bit time of PCM telemetry rate
12. Generate system timing signal and a time code
13. A maximum growth potential consistent with spacecraft design constraints
14. Relative immunity from non-ERTS dedicated STADAN and MSFN ground stations

4.1.3 USB/VHF NARROWBAND

A dual tracking and telemetry capability defined as follows:

4.1.3.1 Stadan Compatible (VHF)

1. RF carrier: 137.86 MHz beacon
2. 100 mw of carrier power under all conditions for Minitrack
3. Bandwidth: 90 kHz emergency; 30 kHz normal
4. Modulation: PCM (2-phase/PM)
5. Emergency TLM record dump
6. Antenna coverage: Spherical

4.1.3.2 MSFN Compatible (USB)

1. RF carrier: 2287.5 MHz (coherent and non-coherent modes)
2. Bandwidth: 5 MHz
3. Carrier modulation: PM
4. Transmitter power: 1 watt
5. Available subcarrier and modulation
   a. 1.25 MHz - PCM/FM
   b. All IRIG proportional BW channels - PCM/FM
   c. 225 kHz (±7-1/2% or ± 15%) - PCM/FM
   d. 300 kHz (±7-1/2% or ± 15%) - PCM/FM
   e. 1.024 MHz - PCM/2-Phase
   f. 1.024 MHz - PCM/FM
   g. 576 kHz - PCM/PSK
   h. 768 kHz - PCM/PSK
6. Ranging: PRN code compatible with the Apollo Digital Ranging Equipment (DRE)
7. Downlink Data:
   a. DCS: 100 kHz IF
   b. RBV and MSS WBVTR auxiliary tracks (2): 100 bps (PCM/PDM time code)

c. Real-time housekeeping data - 1 kbs (PCM/2-Phase)

d. Stored housekeeping data: 24 kbs (PCM/2-Phase)

8. Antenna coverage: Hemispherical

In addition, the following constraints were imposed:

1. Sampling and encoding accuracy: 8 bits
2. TLM voltage range: 0 to -5 volts and 0 to -6.375 volts
3. Telemetry channel capacity:

   a. Analog: 408 @ 1/16
   33 @ 3/16
   24 @ 1/1
   2 @ 3/1
   Total 467 channels

   b. Digital: 160 @ 1/16
   70 @ 3/16
   20 @ 1/1
   5 @ 5/1

   c. Total 264 channels

4. Telemetry and tracking available during launch
5. Utility of existing ground station equipment without hardware modification
6. Minimum modification of existing software
7. A maximum growth potential consistant with spacecraft design constraints

4.1.3.3 Storage Capability

1. Capacity: 2 ERTS orbits
2. P-B/Record ratio: > 20 to 1
3. Existing space qualified operating life: 1 year

4.2 SUBSYSTEM DESCRIPTION

4.2.1 INTRODUCTION

A Communication and Data Handling subsystem based on the requirements described in Section 4.1 has been designed. This subsection presents a summary description of the subsystem. The following sections present detailed studies leading to this design; this description includes a hardware-oriented block diagram, together with a discussion of component functions and signal flow.

4.2.2 BLOCK DIAGRAM

4.2.2.1 Wideband Telemetry

Figure 4.2-1 illustrates the wideband telemetry hardware. This equipment interfaces with the ERTS spacecraft payload and the ground stations. The power, command and telemetry interfaces are not shown. The WBVTR search and auxiliary tracks contain low rate PCM data and are routed to the narrowband communications. The subsystem consists of four component types: (1) redundant signal conditioner, (2) redundant frequency modulator, (3) two power amplifiers, and (4) two shaped-beam antennas.

4.2.2.1.1 Signal Conditioner

The signal conditioner interfaces with the payload. It accepts stored and real-time signals from the MSS, the RBV, and the two associated wideband video tape recorders. The unit is commanded by the spacecraft command/clock and selects pairs of input lines. The unit conditions the inputs as follows:

	15 MBS MSS (PCM)	(3.5 MHz) RBV (Video)
Impedance matching	X	X
Digital reconstruction	X	
Premodulation filtering	X	X

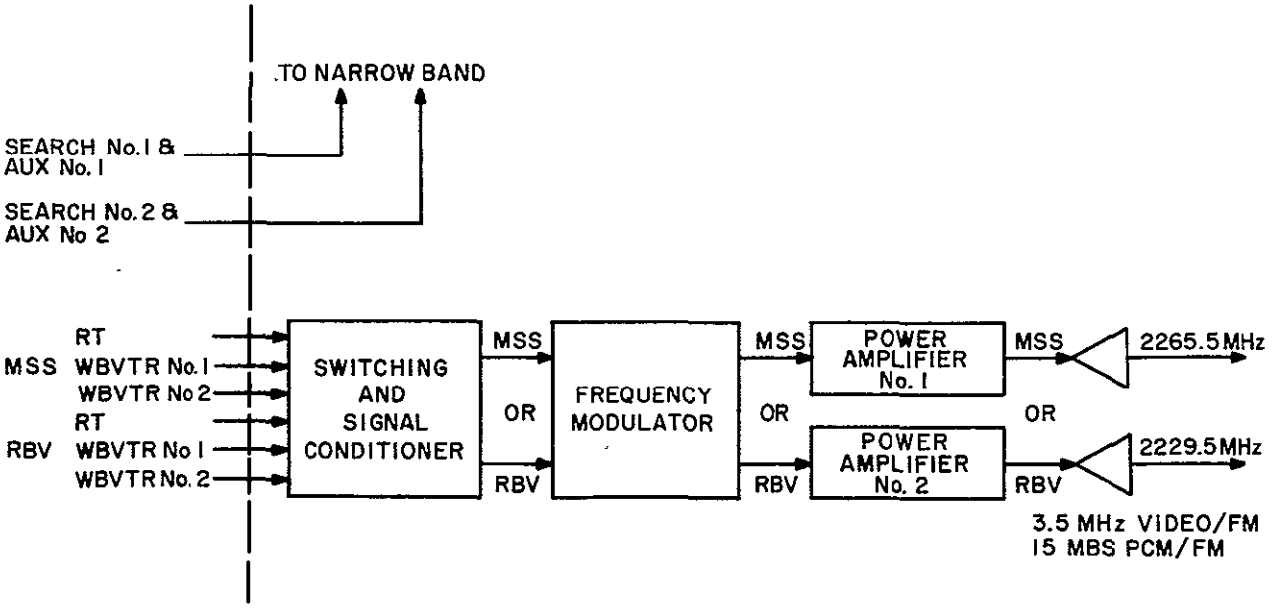

Figure 4.2-1. Wideband TLM Subsystem

The selected and conditioned MSS/RBV signals are routed to the frequency modulators.

4.2.2.1.2 Frequency Modulator

The frequency modulator consists of two identical commandable units. Each unit is capable of operation at either center frequency (2229.5 MHz or 2265.5 MHz) and will accept either MSS or RBV signals. The modulator routes a frequency modulated signal to the TWT power amplifiers. Cross-strapping switches are employed at the output lines.

4.2.2.1.3 Power Amplifier

Either of the two separate power amplifiers accepts the frequency modualted MSS or RBV inputs on command. The units employ TWT's with commandable (10-and 20-watt) power levels. RF bandpass filtering is included in each unit. A circulator is used for isolation in each PA. PA's contain individual power supplies.

4.2.2.1.4 Shaped-Beam Antennas

Two identical shaped-beam antennas are located on the underside of the spacecraft. A simple, compact turnstile design is used. One antenna is dedicated to PA No. 1 (and therefore 2265.5 MHz); the other is dedicated to PA No. 2. Near-constant earth illumination is achieved with a gain $\geq$ 4dB over a cone angle of $\pm$60.6 degrees.

4.2.2.2 Narrowband Communications

Figure 4.2-2 illustrates the narrowband communications hardware. This equipment interfaces with other spacecraft subsystems and the ground stations. It consists of the items shown exclusive of the DCS receiver and antenna.

4.2.2.2.1 PCM Telemetry Processor

The versatile information processor (VIP) has been selected because of its flexibility, growth capacity, reliability, and qualification status. The processor handles the following inputs:

1. Analog and digital spacecraft telemetry channels
2. A command/clock-generated clocking signal and PWM serial time code.

The telemetry inputs are multiplexed and encoded by the processor. This data is then formatted together with the time code and additional synchronization bits. The resulting real-time serial PCM/2-phase bit train is routed to either of two commandable narrowband tape recorders, the VHF transmitter, and the premodulation processor.

4.2.2.2.2 VHF Transmitter

This unit contains two commandable transmitters each capable of two power levels: 300 mw for real-time data and 2-watt for playback data. The transmitter receives real-time

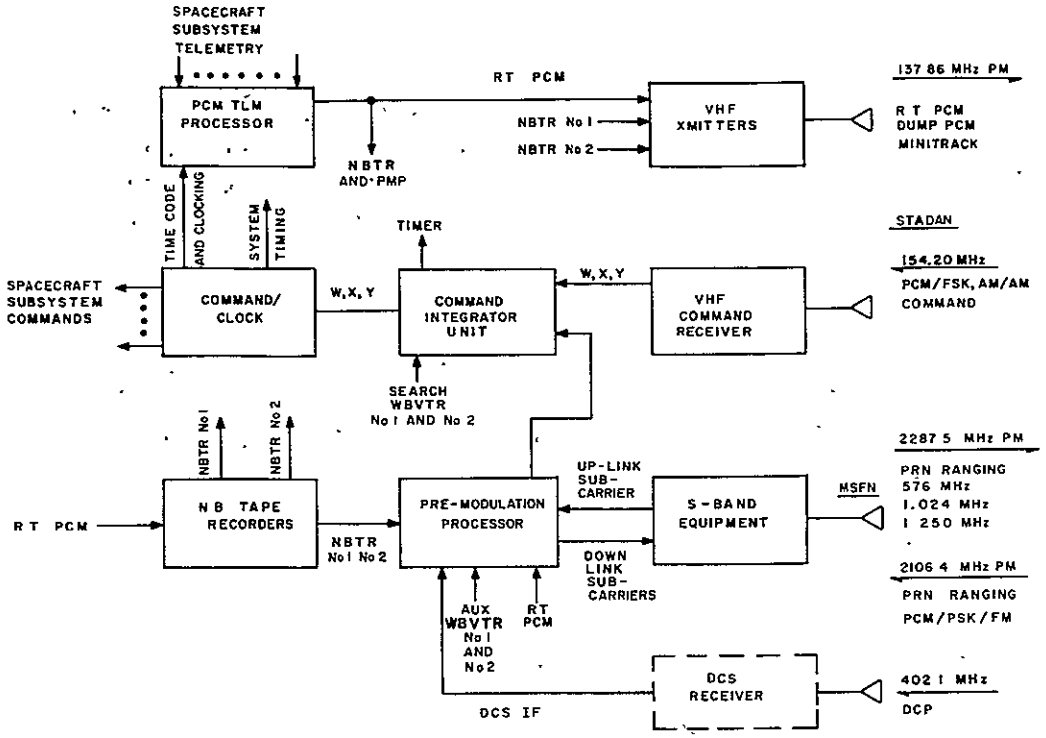

Figure 4.2-2. Narrowband Communications

2-phase TLM data from the PCM TLM Processor at a 1-kbs rate, or it receives stored 2-Phase TLM data from either of two commandable narrowband tape recorders. This data phase modulates a 137.86-MHz carrier in either of the two transmitters. The transmitters interface with the VHF quadraloop antennas and supply carrier power for Minitrack.

4.2.2.2.3 Command/Clock

The Nimbus D unit has been selected. The Command/Clock has complete hardware redundancy. The Command/Clock receives serial PCM data in a compatible format on three lines from the Command Integration unit: NRZ-L Data (w), NRZ-L Sync (x), and NRZ-L Enable (y).

The unit identifies valid commands, decodes the spacecraft address, and either stores or distributes spacecraft commands in real-time. It also implements previously stored commands. It contains a command decoder and relay matrix drivers for command implementation. In addition, a self-contained clock generates system timing signals and a time code.

4.2.2.2.4 Command Integrator Unit (CIU)

The CIU is designed to contain complete hardware redundancy. The unit integrates command signals from the VHF command receiver and the Premodulation Processor (PMP). The PMP uplink output is a 1-kbs PCM/PSK signal. The CIU demodulates this signal to

form NRZ-L sub-bit encoded data plus a 1-kbs clock. The resulting signal is sub-bit decoded to yield a 200-bps NRZ-L-Data (w) plus Clock (x). An enable (y) signal is also generated from the presence of the clock signal. This resulting signal is Stadan compatible and is OR'ed with the VHF command receiver output and routed to the Command/Clock.

The CIU also contains a backup timer for turning off the wideband power amplifiers and the S-band equipment. In addition, it contains a shift register for assembling the serial PCM data from the WBVTR search track.

4.2.2.2.5 VHF Command Receiver

The receiver interfaces with the command stub antenna at a 154.20-MHz carrier frequency. The receiver consists of two commandable units consisting of a front end, AGC, and a demodulator. The demodulator generates: (1) an enable (y) based on "presence of sub-carrier", (2) a clock (x) via detection of AM on the carrier, and (3) NRZ-L Data (W) via demodulation of the PCM/FM. The resultant signal (3 separate lines) is outputted to the C.I.U.

4.2.2.2.6 Unified S-Band Equipment

The S-band equipment interfaces with a single S-band antenna. The equipment forms a MSFN compatible redundant USB Transponder. It handles and turns around the PRN ranging signal, and routes the uplink command subcarrier to the PMP for demodulation. It also accepts a composite downlink baseband signal from the PMP.

4.2.2.2.7 Premodulation Processor

The PMP comprises a redundant subcarrier modulation and demodulation unit. It contains a 70-kc FM discriminator for command demodulation and FM subcarrier modulators and premodulation filters to handle the following downlink TLM signals:

1. Either of two NB tape recorders @ 24 kbs
2. One DCS IF @ 100 kHz BW
3. One RT TLM Channel @1 kbs
4. Two WB VTR auxiliary TLM channels @ 100 BPS

4.2.2.2.8 Narrowband Tape Recorders

Either of two commandable NBTR's accept real-time PCM/2-Phase inputs from the PCM TLM processor at 1 kbs. Playback is at a 24:1 ratio, and either recorder may be routed to both the PMP and the VHF transmitter.

4.2.2.2.9 Antennas

The Narrowband antennas have the following characteristics:

1. VHF Beacon and Telemetry
   a. Frequency: 137.86 MHz
   b. Pattern coverage: Spherical
   c. Minimum gain: -10 dB with 3-dB nulls
2. VHF Command

   Frequency: 154.2 MHz
   Pattern coverage: Spherical
   Minimum gain: 0 dB with 20-dB nulls
3. Unified S-Band

   Frequency: 2100 to 2300 MHz
   Pattern coverage: Hemispherical
   Gain: 0 dB for $\pm$60 degree cone

4.3 STUDY TASKS

This subsection lists the specific items studied during the ERTS Phase B/C contract. The study items are derived from the GSFC top-level subsystem requirements and were necessary to: (1) specify the C&DH operational parameters, (2) define hardware specifications, and (3) verify subsystem performance. The studies are classified as follows:

1. Wideband Telemetry
2. Command/Clock
3. Narrowband Communications
4. Associated Antennas

4.3.1 WIDEBAND TELEMETRY

4.3.1.1 System Analysis

1. Digital modulation methods (Binary FSK, Binary PSK, Multi-phase PSK, Multitone FSK) for the MSS link
2. FM parameters studies for MSS and RBV links
3. Link analyses for MSS and RBV links
4. Signal degradation in the MSS and RBV links
5. Premodulation filtering
6. RF filtering

7. Signal conditioning
8. Signal cross-coupling between the RBV and MSS links and between the MSS/RBV and USB links
9. Ground station capabilities assessment
10. Transmission modes
11. Power requirements
12. Link failure analysis and associated cross-strapping
13. Performance verification

4.3.1.2 Frequency Modulator

1. Alternative technical approaches
   a. Loop stabilized VCO
   b. Summed VCO and local oscillator
   c. FM/PM
2. State-of-the-art survey
3. In-depth analysis, design, breadboard, and test of approach (1a).

4.3.1.3 S-Band Power Amplifier

1. Solid-state versus TWT designs
2. Commandable power levels
3. Power summing
4. Vendor survey

4.3.1.4 Shaped Beam Antenna

1. Dual antenna versus diplexer plus one antenna
2. Beam shaping study
   a. Circular aperture
   b. Line source

4.3.2 COMMAND STUDIES*

1. Command integration — MSFN (USB) and Stadan
2. Real-time commands

*Also see breadboard test results, Appendix 4B.

a. Command functions required

b. Synchronization

c. Verification

3. Stored commands

a. Command functions required

b. Multiple execution

c. Command override and verification

4. Command format

5. Command loading

6. Error probabilities

7. Fail-safe design techniques

8. Accuracy of clock update

4.3.3 RANGING AND NARROWBAND TELEMETRY*

4.3.3.1 System Analysis

1. Tracking considerations

2. Modulation parameters

3. Signal degradation

a. Link analysis

b. Intermodulation

c. Ground stations

d. Hardware effects

4. DCS interface

5. VHF link analysis

4.3.3.2 S-Band Transponder

1. Alternative technical approaches

2. Vendor survey

4.3.3.3 PCM Telemetry Processor

1. Alternative approaches

*Also see breadboard test results, Appendix 4B.

a. Nimbus B PCM system

b. Nimbus D PCM system

c. Modifications of a and b

4.3.3.4 Narrow Band Tape Recorder

1. Alternative technical approaches
2. Vendor survey

4.3.4 ANTENNAS

1. Available designs
2. Separate transmit/receive antenna versus a diplexer and one common antenna
3. Pattern coverage
4. Pickups and re-radiators
5. Launch coverage

4.4 COMMUNICATIONS AND DATA HANDLING STUDIES

In this section, the study tasks outlined in paragraph 4.3 are presented in detail. These subjects are organized as in previous sections:

1. Wideband Telemetry
2. Command/Clock Equipment
3. Narrowband Communications
4. Antennas

4.4.1 WIDEBAND TELEMETRY

4.4.1.1 Summary of Principal Results

This study of the wideband telemetry links of the ERTS satellite was performed using the GSFC baseline design. Prominent among the GSFC suggested link parameters are the center frequencies for the two transmission links (the RF bandwidth, and the modulation method to be used for RBV and MSS information transmission). It is also stipulated that the signals supplied by each sensor can be impressed upon either carrier using the specified modulation method; further, a "commandable" 20-watt transmitter power is suggested for each transmission link. The requirements are summarized in Table 4.4.1-1. The results of the study show that the above requirements lead, essentially, to an optimum system.

TABLE 4.4.1-1. WIDEBAND TRANSMISSION LINK (MSS AND RBV)

	MSS	RBV
Center Frequency	2229.5	2265.5 MHz
RF Bandwidth	20	20 MHz
Transmitter Power	20*	20* Watt
Modulation	PCM/FSK	Video/FM

*Commandable power levels - 10 watts or 20 watts

This fact is substantiated by the results of detailed analyses, comparisons, and tradeoffs performed in the course of the study and recorded in the following paragraphs. In summary, they reflect the following conclusions:

1. A comparative analysis of digital modulation methods with a view to their applicability to the MSS transmission link, showed clearly the advantages of PCM/FSK for this application.

   PCM/FSK is, therefore, the selected modulation method for the transmittal of digital MSS data.

2. The RBV and MSS transmission links were analyzed with a view to assessing link performance, signal degradation, and transmitter power requirements. The analysis allowed the important conclusion that operation with 10.0-watt transmitter power is a valid, power saving mode which, under certain conditions results in negligible signal degradation.

   It is, therefore, concluded that the power amplifiers must be equipped with a power selection capability which will allow a 20-watt operation and a 10-watt operation.

3. A functional block diagram of the two parallel signal chains was evolved. Signal flow, signal level, and signal characteristics were determined at each point of the equipment chain. Furthermore, the parameters of each individual assembly were defined from the point of view of overall link performance, feasibility, and spacecraft compatibility. Their overall size, volume, weight, and thermal characteristics are in accordance with the requirements of the spacecraft environment.

4. Reliability was analyzed as well as its possible improvement without additional equipment. It was found that cross strapping among transmitter building blocks will increase the reliability, and it is therefore incorporated.

4.4.1.2 Digital Modulation Methods

4.4.1.2.1 PCM/PSK

The binary phase shift keying modulation method offers the following possibilities:

1. A signal of constant frequency is used. Its phase is shifted between 0 degree and 180 degrees, in accordance with the space and mark bit sequence. When received and detected coherently, PSK offers the best (minimum) C/N ratio for a given bit error probability. It is 3 dB better than the next best (and basically different) modulation method (differential PSK excluded) and thus leads to a saving in carrier power. This can be seen from Figure 4.4-1*, where bit error probability is plotted against the signal to thermal noise ratio. Coherent PSK has a 3 db advantage over coherent FSK. Note that in Figure 4.4.1-1, the noise power is measured in a bandwidth defined by the spectral requirements of the signal, i.e., the minimum bandwidth in which the signal can be contained.

2. The power advantage of PSK thus established, its limitations have to be considered. There are, indeed, practical limitations which apply, generally, to any detection scheme based on coherent processing of received signals. The problem resides in the difficulty associated with the generation and preservation of an accurate reference signal (including RF phase) at the receiver site for the demodulation of the received PSK signal. While a phase variation ($\Delta\varphi$) of the local reference would have no effect on the post detection noise, it will clearly reduce the amplitude of the detected signal by a factor cos $\Delta\varphi$ and thus adversely affect the bit error probability. For example, if the performance of a PSK link is to be kept constant within 1 db (i.e., admissible loss of 1 db in S/N ratio) as compared to the ideal

*Stein, S., Modern Communication Principles, McGraw Hill Book Co., pp 241, 1967.

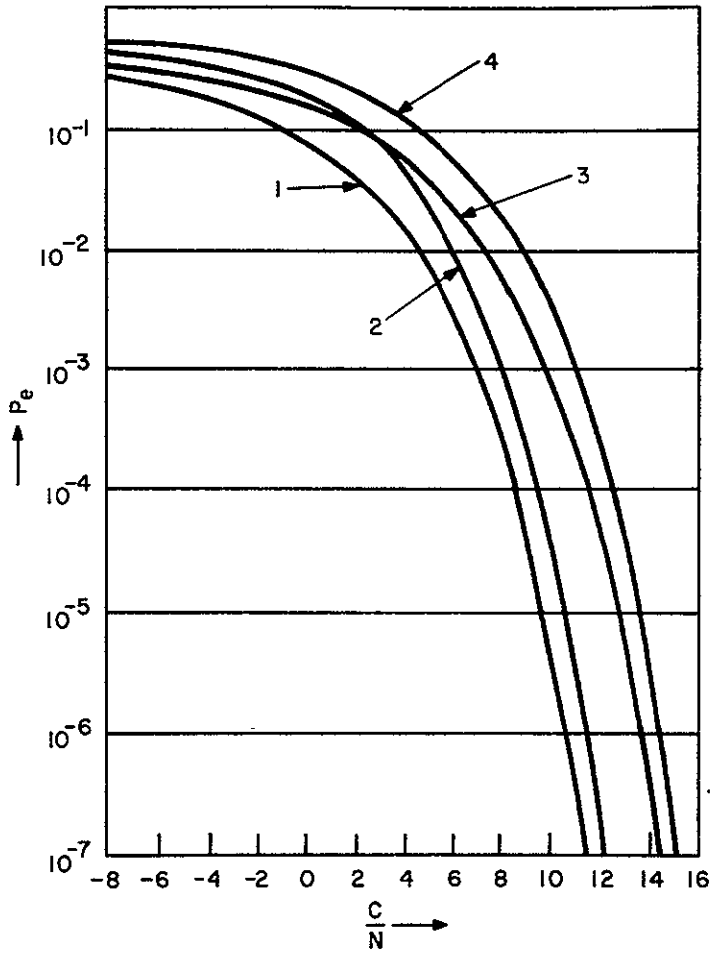

1. COHERENT PSK
2. DPSK
3. COHERENT FSK
4. NON COHERENT FSK

NOTE: $\frac{C}{N}$ IN BANDWIDTH WHICH CONTAINS THE SIGNAL

Figure 4.4.1-1. Bit Error Probability for Several Binary Systems

situation, $\Delta\varphi$ must be kept within ± 25 degrees, or (with f = 2229.5 mc) Δ t, the time delay variation over the entire link, should not exceed

$$\Delta t = \frac{\pm \Delta\varphi}{f} = \frac{\pm 0.44 \text{ radians}}{2229.5 \times 10^6}$$

$$\Delta t = \pm 0.2 \text{ nanoseconds}$$

Δ t includes the time delay variations of the received signal due to equipment instabilities (e.g., frequency drifts) as well as time delay variations due to varying parameters of the propagation medium. Clearly, this poses serious requirements on the transmission link as well as on the reference signal.

The reference signal can be locally generated. It contains no information and is merely used to obtain ideal conditions of signal detection. In most practical cases, however, the reference signal is obtained by phase locked loop techniques, i.e., by locking the locally generated reference to the received carrier. The net result is, in this case, a noisy reference which, when applied to the coherent detector, leads to a degradation of overall performance. Even with a C/N ratio well above the threshold required for acquisition and maintaining phase lock, adverse conditions may still affect the loop operation and thus degrade performance. The bit error probability P_e for PSK is given by:

$$P_e = 1/2 \, (1 - \text{erf}\sqrt{\gamma}) \qquad (1)$$

where:

$\gamma = \frac{S^2}{2N}$, S is the signal amplitude; and N is the noise power

The argument of the error function becomes $\sqrt{\gamma} \cos \Delta\varphi$ in case of phase variations of the reference signal.

4.4.1.2.2 PCM/DPSK

An alternative to the coherent PSK is the DPSK i.e., differentially coherent phase shift keying. As pointed out above, ideal PSK requires long term phase stability of the reference signal which can be obtained. e.g., by high quality phase correction loops. Here, instead, of importance is the equipment and transmission medium stability only over a short time interval, namely, the duration of one pulse. This is due to the fact that with DPSK the information is not encoded (and decoded) in terms of absolute phase positions of the RF signal. Rather, it is encoded in terms of the phase change between successive pulses, i.e., differentially; herein resides the essential difference from PSK. As a consequence, each pulse is used as a reference to the next pulse and thus has to maintain its phase stability only over two pulse intervals: the first, for its proper detection; the second, for its use as a reference for the detection of the next pulse. Under these conditions, a coherent detector can be used with the present pulse as signal input, and the former pulse as a

reference input. The reference signal is "noisy"; it is contaminated by noise to the same extent as the information carrying pulse. This accounts for the slight performance degradation of DPSK (1 db) as can be seen from Figure 4.4.1-1.

The expression for bit error probability of DPSK is given by*

$$P_e = 1/2\, e^{-\gamma} \qquad (2)$$

and differs from ideal PSK by the fact that the complementary error function of argument $\sqrt{\gamma}$ has been replaced by an exponential function of argument $-\gamma$. This leads to an advantage of ideal PSK over DPSK which is pronounced at low γ, but decreases rapidly as we move toward higher values of γ.

Clearly, DPSK will require additional equipment; namely, a differential encoder will become part of the transmitter, and a pulse storing and processing arrangement in the receiver instead of a phase lock loop.

4.4.1.2.3 PCM/FSK

The binary frequency shift keying technique produces an rf signal of constant amplitude, whose frequency is subjected to rapid transitions from frequency f_1 to frequency f_2, corresponding to mark and space, respectively, of the binary bit sequence.

There are two distinct modes of FSK operation: noncoherent and coherent. The former, in its simplest form, makes use of two separate CW oscillators whose frequencies correspond to mark and space, respectively. The modulation process is accomplished by switching between the two oscillators, thus obtaining a signal of frequency f_1 for mark and a signal frequency f_2 for space.

It is clear that this method does not preserve phase continuity of the rf signal during the transition time interval, i.e., the mark and space signals are noncoherent.

An alternative to the above method is the coherent FSK, where phase continuity of the rf signal is preserved. This can be accomplished by selective gating of one of a pair of locked oscillators, or by the use of a reactance modulator.

It is noted that these modes of operation give rise to an rf signal whose spectral composition is quite different in each case. In the coherent mode**, the energy spreads away from mid frequency as the deviation ratio m (m = frequency interval between mark and space, divided by the bit rate) increases and concentrates near the steady state mark and space frequencies. For integer value of m, the result is the sum of two on-off AM carriers located at mark and

*Stein, S., Modern Communication Principles, McGraw Hill Book Co., 1967.

**Bennett, W. R., and Davey, J. R., Data Transmission, McGraw Hill Book Company, 1965.

space frequencies and keyed in phase opposition. For other than integer values of m, there is no frequency component at the mark or space frequencies, and both even and odd sideband frequencies are present.

In the discontinuous phase case, we have the equivalent superposition of two AM waves on separate carriers rather than one simple FM wave on the average carrier. Here, the high order sideband components are inversely proportional to n, while in the continuous phase case they are proportional to n^2; the power spectra vary therefore with the second or fourth power of n respectively, where n designates the order of sideband component. As a consequence, the continuous phase case results in less sideband frequency spread and can be contained in a narrower bandwidth.

A more significant difference between the two modes of FSK lies in the methods that are applied for the recovery of the baseband signal.

In the case of coherent FSK, the equivalent of matched filter detection can be applied. Matched filtering represents the ultimate, perhaps, in processing of digital signals in additive Gaussian noise.

As in the PSK case, this process or its equivalent (the synchronous or coherent detection) is based on the availability in the receiver of an accurate replica of each of the two possible transmitted rf signals. The detection process itself corresponds to multiplying (in two mixers) the mark and space waveforms (only one is present at a time) with their respective locally available replicas, and passing the resulting waveforms through separate low-pass filters. A comparison is then made and the output signal is marked MARK or SPACE, depending on whether it is supplied by channel 1 or 2 of the detector.

Clearly, this method is not applicable in the case where discontinuous phase FSK is sent; the detection process cannot make use of the phase of the signal. The latter varies from pulse to pulse discontinuously, and its replica is not available at the receiver. The demodulation process to be employed in this case is incoherent in nature; it consists e. g., of two bandpass filters centered at the mark and space frequencies, followed by envelope detectors. Since, at a given time, only one filter will show detected signal, (the other filter will carry only noise), a simple decision device will be required to mark the output signal of filter No. 1, when it occurs, as mark, and the output signal of filter No. 2 as space. The enve - lopes at the detector output terminals are sampled once per information pulse. Normally, no threshold is needed; the outputs of the two signal paths are compared and the larger is marked as containing the signal.

It has been shown that coherent detection of continuous phase FSK has significant advantage over noncoherent detection FSK at relatively low S/N ratios, i. e., relatively poor error rates. This advantage is approximately 2 db at $P_e = 10^{-2}$; it shrinks to less than 1/2 db at $P_e = 10^{-5}$*. On the other hand, coherent FSK has to cope with the same difficulties as coherent PSK, but achieves less performance (a difference of approximately 3 db at both

*Stein, S., and Jones, J. J., Modern Communication Principles, McGraw Hill Book Co., 1967.

$P_e = 10^{-2}$ and $P_e = 10^{-5}$). Also, coherent PSK has no greater equipment requirements than coherent FSK, in fact probably less, since only one frequency is used. All this seems to indicate that if a coherent mode of information transmission and recovery is to be used, PSK is the stronger candidate. If, on the other hand, FSK is to be used instead of PSK for some reason, then the coherent detection process does not contribute more than 0.5 db in C/N savings at $P_e = 10^{-5}$. The penalty to be paid is the generation and maintenance of an exact and clean replica of the binary signals, in R. F. form, at the receiver site. Thus noncoherent FSK appears to have strong practical advantage.

Of course, a noncoherent detection process can be applied to an FSK signal which exhibits phase continuity. In terms of circuitry, this means that a discriminator (or a pair of filters, followed by envelope detectors) can be applied to the continuous phase FSK signal, generated in the spacecraft from a voltage controlled oscillator (VCO).

In our case, the selection of a continuous phase FSK modulation method has the advantage that the same modulator is used as in the RBV FM channel. This permits a certain amount of redundancy to be built into the transmitter without adding new (standby) equipment. By providing the necessary cross strapping circuitry and the capability of changing VCO center frequency, the RBV modulator can be made to accept MSS baseband signals and perform FSK modulation; and vice versa, the MSS modulator can accept and process RBV video signals thus rendering the two modulators completely interchangeable.

It is this significant advantage that has to be kept in mind when FSK is compared to the more power-efficient PSK method with its coherent detection requirements.

4.4.1.2.4 Four Phase (Quaternary) and Multiphase (M-ary) Signaling

We consider first the four-phase case. This case is of practical importance because it permits operation with two completely independent binary signals, with ideally no cross-talk between them. This effect is due to the orthogonality of the selected phase positions, for instance, 45 degrees or 225 degrees for one signal component, and 135 degrees or 315 degrees for the other.

Due to the orthogonality of the two information carrying signals, they can be accommodated in the bandwidth required for one; since each can carry the full information volume, this leads to an information rate augmented by a factor of 2. In the receiver, coherent PSK detection using an adequate reference will retrieve one signal component with its noise components; and, a second (quadrature) reference will retrieve the quadrature information signal with its independent noise components.

Consider the error rate probability. It is determined by ST/N_O, where S is the power associated with each signal component, N_O is the noise density, and T is the pulse length. In order to retain the same bit error probability as in the simple binary case, we have to double the power, use the same R. F. bandwidth and signal, and, at twice the initial information rate. Or, if the signaling rate is kept the same, the bit error probability will remain unchanged, if we keep the total signal power the same, but reduce the bandwidth by a factor of 2, assigning to each signal component half of the total information volume to be

transmitted, and half of the total available power. Thus a bandwidth saving can be realized, without paying a penalty in transmitter power, rate of information flow, or bit error probability. A penalty will be paid in equipment complexity; however, the spacecraft transmitter must employ a four-phase modulator, and the ground station must keep available two (orthogonal) reference signals.

The transition from the quaternary to the multiphase (m-ary) PSK case is not straightforward. We compare, again, with the binary case and find that now, with more than two pulse levels, we can transmit the same information volume with smaller pulse groups, i.e., the number of pulses transmitted per unit of time has decreased. As a direct consequence of this, we can now operate in less bandwidth.

A second direct consequence of the growth of m is the increased power requirements; in fact, if we endeavor to keep the accuracy of the recovered information as high as in the binary case, we must keep the level differences between pulses the same; which, since m has grown to more than 2 levels, leads to higher power requirements.

A quantitative comparison with the binary case needs a new definition of error probability. Clearly, one bit error will affect in different ways a binary and a m-ary system; hence, the use of word (or symbol) error probability instead of bit error probability appears more adequate. Symbol error probabilities must be considered as a function of the signal-to-noise ratio and when comparisons are to be made, the bandwidth and information rate associated with one m-ary case have to be rescaled in order for the comparison to be meaningful.

In the case of large m, where

$$\sin \frac{\pi}{m} \approx \frac{\pi}{m} \tag{3}$$

the symbol error probability can be written

$$P_s \cong 1\text{-erf} \left\{ \sqrt{K \gamma_b} \frac{\pi}{m} \right\} \tag{4}$$

*

where P_s is the symbol error probability; m is the number of phase positions that the signal vector can assume (usually, m is taken as a power of 2, i.e., $m = 2^{\overline{K}}$, $\overline{K}$ = integer) and γ_b is the SNR per information bit

$$\gamma_b = \frac{\gamma}{\overline{K}} = \frac{\gamma}{\log_2 m}$$

where γ is the SNR at the detector input terminals.

---

* Stein, S., Modern Communication Principles, McGraw Hill Book Co., 1967, pp 297

If P_S is to be maintained constant with increasing m, we have

$$K\gamma_b = \frac{\pi^2}{m^2} = \text{const}$$

and

$$\gamma_b = \frac{\text{const}}{\pi^2} \cdot \frac{m^2}{\log_2 m} \tag{5}$$

Thus, the SNR per bit (γ_b) must grow with m; more power is required with growing number of different pulse levels.

Note, however, that for constant information flow the signaling bandwidth will diminish. In fact, as we move from binary to m-ary signaling, the pulse length increases by $\log_2 m$, hence the attendant bandwidth is reduced by $(\log_2 m)^{-1}$.

A different case arises if the signaling bandwidth is to be preserved while expanding from binary to m-ary PSK signaling. Since R. F. bandwidth decreases, the information rate must be increased by the factor $\log_2 m$ in order to keep the signaling bandwidth constant.

Constant symbol error probability requires a SNR (and power) growth as $m^2/\log_2 m$ (see equation 5) if the information rate remains constant. Increased information rate by factor $\log_2 m$ leads to constant R. F. bandwidth and imposes an increased growth (m^2) of power.

If we keep information rate, signaling bandwidth, and symbol error probability constant while increasing m, the following can be stated: the power growth of $m^2/\log_2 m$ with attendant $1/\log_2 m$ bandwidth reduction will prevail with growing m; or, due to the diminishing rf bandwidth, the power growth will be more gradual.

The effect of growing m upon the symbol error probability is shown on Figure 4.4.1-2.

4.4.1.2.5 Multitone Signaling (Multiple FSK)

A completely different situation is created with multifrequency signaling. In this case, different frequencies are selected, each representing a pulse level of the modulating PCM pulse train.

Only noncoherent reception is considered. The difficulties associated with maintaining all necessary reference signals for coherent reception, as needed in a true multitone system, make its implementation impractical.

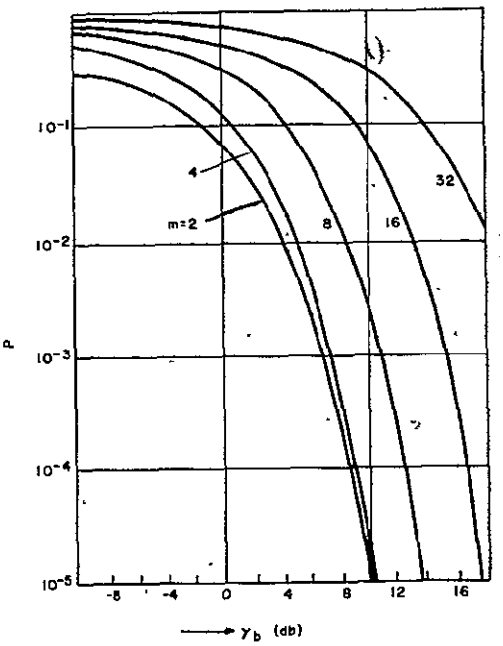

Figure 4.4.1-2. Coherent Multiphase Signalling*

In a coherent system we have, essentially, envelope detection and decision based on largest envelope output. We assume tone spacing and receiver filtering such that no crosstalk among filter outputs exists. If each pulse has a length T_m, the required tone spacing is $\frac{1}{T_m}$ and the -3 db bandwidth B_m occupied by the overall system (outermost tone pulses) is given by

$$B_m = \frac{m}{T_m} \tag{6}$$

Symbol error rate P_s is related to binary error rate P_b by

$$P_s = P_b \frac{2^K - 1}{2^{K-1}} \tag{7}$$

The symbol error probability is given by

$$P_s \leq \frac{m-1}{2} e^{-\frac{\gamma}{2}} \tag{8}$$

* Stein, S., Modern Communication Principles, McGraw Hill Book Co., 1967, pp 294

where; again,

$\gamma = K\gamma_b$; $m = 2^K$; and

γ, γ_b designate symbol SNR and SNR per information bit.

If we keep symbol pulse length T_m constant, and increase m (number of tones), the result is an increased rate of information transmission. At the same time, the required bandwidth will grow exponentially with K

$$B_m = \frac{2^K}{T_m} \tag{9}$$

and, in order to keep symbol error rate constant, (see equation 8), the signal power has to grow as ln m, linearly with K.

It can be shown that the bandwidth power tradeoff can be carried to the point where an arbitrarily small symbol error rate can be achieved at the expense of bandwidth; if the condition is satisfied that γ_b, the SNR per bit, exceeds 1.4 db. This is obtained by letting K grow toward infinity. The penalty paid is the bandwidth which increases exponentially with $2^K/K$. The value of K is normally determined by practical considerations, since the receiver complexity, i.e., the number of tone filters, also grows exponentially with K.

This is in sharp contrast to the multiphase mode of signaling described in the preceding section. Here, for a fixed information rate, the symbol error probability is maintained constant with increasing m, if the symbol SNR (γ) is increased as ln m or the energy per bit is decreased as $(\log_2 m)^{-1}$, while the associated bandwidth grows as m/k.

With m-ary phase keying, we have, under the same conditions, a SNR per bit (γ_b) which must grow with $m^2/\log_2 m$, while the bandwidth is reduced as $(\log_2 m)^{-1}$, i.e., the trends in power and bandwidth requirements are exactly opposite.

The effect of m upon the symbol error probability P_s is shown in Figure 4.4.1-3.

4.4.1.2.6 Conclusion and Recommendation

In view of the pertinent characteristics of the digital modulation methods which were briefly summarized in the preceding paragraphs, the PCM/FSK modulation method was recognized as the most appropriate for this application.

Its signal power disadvantage, pointed out in the discussion, is largely compensated by two advantages: the possibility of implementing a simple demodulation method (discriminator, e.g.,), and the possibility to have two identical modulators in the wideband transmitter, thus increasing equipment reliability without additional (standby) equipment.

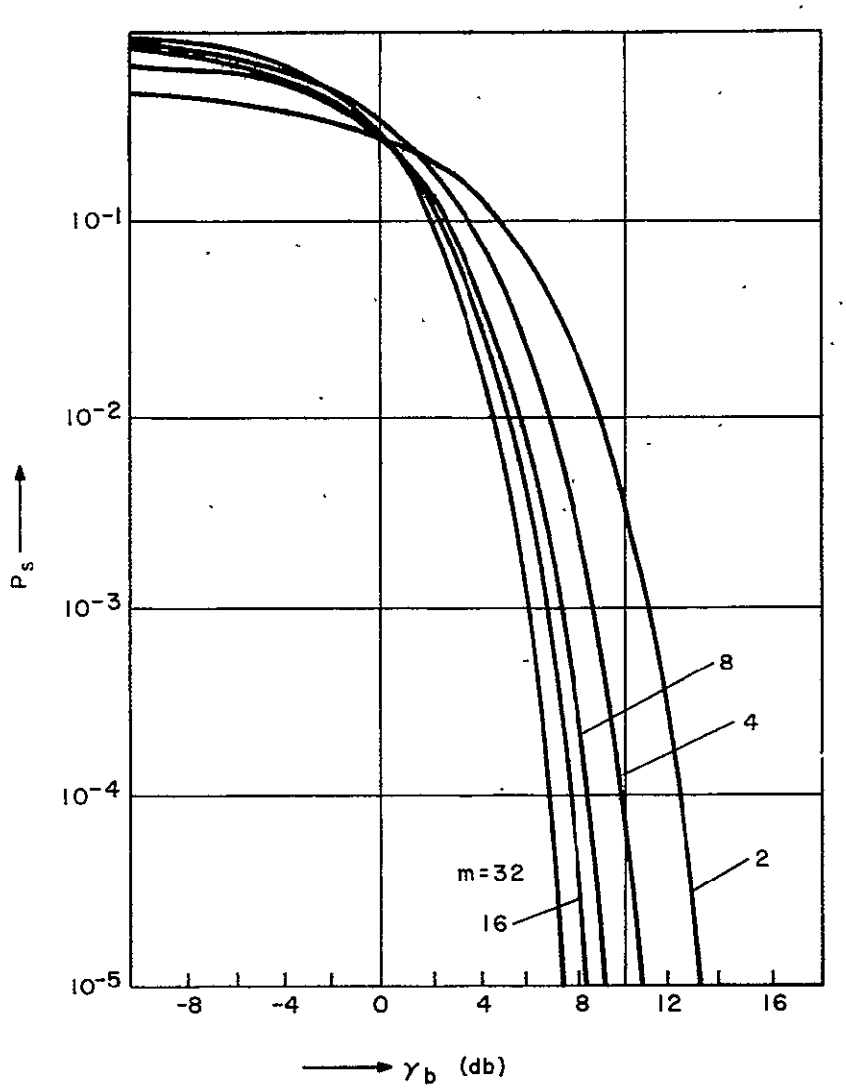

Figure 4.4.1-3. Noncoherently Detected Orthogonal Multitone Signalling*

* Stein, S., Modern Communication Principles, McGraw Hill Book Co., 1967 pp 302

4.4.1.3 The RBV Transmission Link

Three RBV cameras are operated simultaneously and supply a video signal which covers a frequency range from dc to 3.5 MHz. The camera output signal can be directed either into one of the two wideband video tape recorders (WBVTR 1 or 2) for recording and playback transmission, or into the input terminals of the wideband telemetry transmitter for real time transmission. In the ground station, a wideband discriminator operated well above threshold processes the received carrier embedded in thermal noise, recovering the video signal with attendant S/N post detection improvement.

4.4.1.3.1 Link Calculations

The wideband spacecraft-to-earth-station RBV telemetry link is examined at the specified transmission frequency of 2265.5 MHz. The assumption is made that the indicated 20 MHz RF bandwidth is equal to the noise bandwidth. Two earth stations are considered with their specified antenna gains, antenna noise temperatures and receiver noise temperatures; a requested 6 db safety margin is included in the calculations.

The results, for a single elevation angle of 5 degrees, and for a transmitter power of 20 watts, are shown in Table 4.4.1-2. The last two entries contain the FM improvement factor and the post detection S/N ratio (peak to peak signal to rms noise).

It should be noted that the numbers listed in the table are based on the following data:

1. Spacecraft antenna - a shaped beam antenna is used, mounted on the lower surface of the spacecraft with a 121.2 degree field of view. The beam shape is so chosen as to maintain a near constant power density field at the surface of the earth. At angles from ±60.2 degrees (which corresponds to 5 degree elevation angle) the antenna gain is 4.0 db or better. This number includes polarization losses due to pattern ellipticity.

2. A transmission loss of 1.35 db is shown. It is composed of losses between the output terminals of the power amp. and the input terminals of the antenna and includes losses in filters, connectors, cable, circulator, etc. A detailed summary and justification of this number is given in Section 4.4.1.8.1.1.

   Power losses due to tracking inaccuracies are not considered; neglected also are transmission line losses in the earth station. Atmospheric losses have to be accounted for: they grow from 0.07 db at zenith to 0.7 db at 5 degree elevation angle. The number of 0.7 db is used in this link calculation.

3. The free space losses were computed from the formula

$$L_{FS} = 20 \text{ Log } \frac{\lambda}{4\pi R} \qquad (4.4.1\text{-}1)$$

TABLE 4.4.1-2. RBV TRANSMISSION LINK

	5 Degree Elevation	
	30 Ft. Dish	85 Ft. Dish
Spacecraft transmitter power	43 dbm	43 dbm
Spacecraft antenna gain (includes polarization loss)	4.0 db	4.0 db
Transmission loss	-1.35 db	-1.35 db
Space loss[2)]	-169.8 db	-169.8 db
Receiver antenna gain	44.0 db[1)]	51.5 db[1)]
Antenna noise temperature	125°K[1)]	125°K[1)]
Receiver temperature	0[3)]	100°K[1)]
Noise power (20 MHz bandwidth)	-104.6 dbm	-102.1 dbm
System margin	-6 db[x]	-6 db[x]
Received power	-86.15 dbm	-78.65 dbm
Carrier-to-noise ratio	+18.45 db	+23.45 db
FM improvement (modulation index)	13.4 db (β=1.6)	+13.4 db (β =1.6)
Detected signal-to-noise ratio (peak-to-peak signal to RMS noise)	+38.85 db	+43.85 db

1) Numbers supplied by NASA
2) Including atmospheric loss
3) Receiver temperature is included in the antenna noise temperature of 125°K

where L_{FS} is in db, λ is the wavelength, and R is the range. With a spacecraft altitude H = 492 nm, an elevation angle α = 5 degrees, and the earth radius R_e = 3440 nm, the angle β at earth center is found from

$$\beta = \cos^{-1}\left(\frac{R_e}{R_e + H}\right) - \alpha \qquad (4.4.1\text{-}2)$$

and the range R follows from

$$R = (R_e + H) \frac{\sin \beta}{\sin (90 + \alpha)} \qquad (4.4.1\text{-}3)$$

Using:

R_e = 3340 nm

H = 492 nm

α = 5 degrees

we find

β = 24 degrees

R = 1620 nm

L_{FS} = 169.1 db for f = 2265.5 MHz (λ = 13.2 CW)

4. Thermal noise power in an equivalent noise bandwidth of 20 MHz is computed from

   N = -228.6 dbW per °K per cps

5. A "single-tone" FM analysis was conducted in order to define the last two entries in Table 4.4.1-2: modulation index and attendant FM improvement, and post detection peak-to-peak signal to RMS noise ratio. It is understood that the main advantage of such an analysis is its relative simplicity; its drawback resides in the fact that it represents a rather poor description of the complex modulating signal and the resulting modulation process. The obtained operational parameters (e.g., peak deviation) are, therefore, conservative. It is very likely that a higher deviation could be used, leading to a larger S/N improvement, with the main spectral components within the allotted 20 mc RF bandwidth, and with the carrier-to-noise ratio still well above threshold.

4.4.1.3.2 Selection of FM Parameters

Figure 4.4.1-4 shows the typical video signal. As can be seen, the picture signal amplitude (peak white to peak black) is 1.15 ±0.15 volt while the peak to peak signal (peak white to sync) is 1.50 ±0.1 volt. Thus, the sync signal represents approximately 20 percent of the entire signal or 25 percent of the picture signal, while the picture signal represents 1.2/1.5 = 80 percent of the total.

The video signal is fed into the FM modulator. A frequency modulated carrier signal is obtained which, amplified and filtered, is transmitted to the ground station. There, received, amplified and down converted, it is presented to the discriminator input terminals at whose output terminals the video signal is recovered.

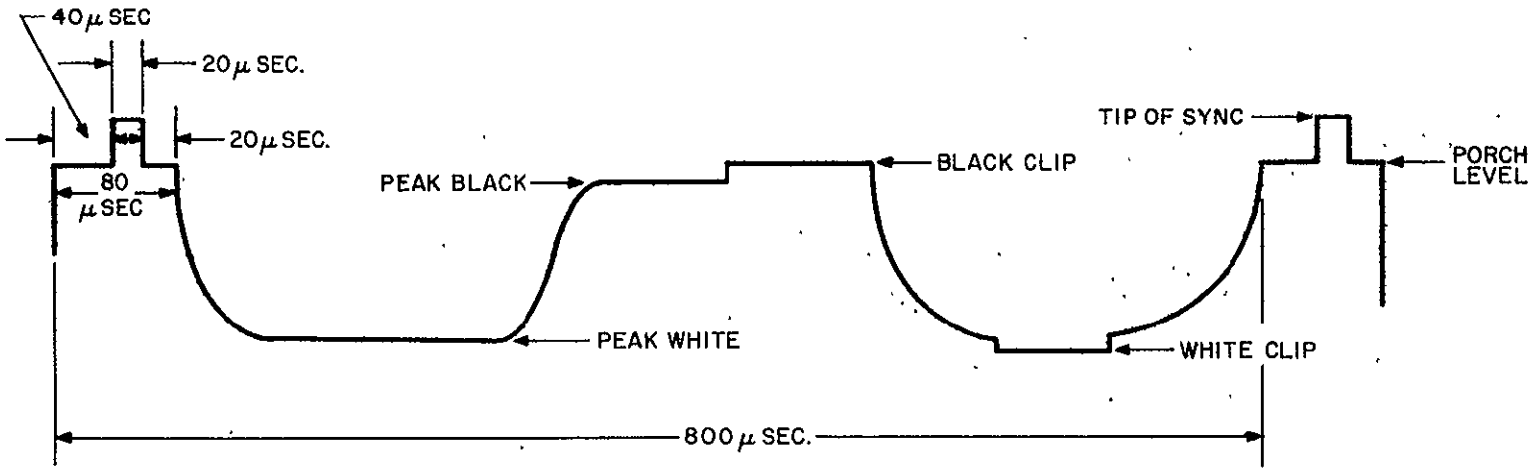

VOLTAGE LEVELS:

TIP OF SYNC	0±0.05 VOLTS
PORCHES	−0.3±0.05 VOLTS
BLACK CLIP	−0.3±0.05 VOLTS
PEAK BLACK	−0.35±0.05 VOLTS
PEAK WHITE	−1.5±0.1 VOLTS
WHITE CLIP	−1.65±0.1 VOLTS

Figure 4.4.1-4. Video Signal Characteristics (Typical Line)

Under these conditions, the signal-to-noise power ratio $(S/N)_o$ at the output terminals of the discriminator is given by

$$\left(\frac{S}{N}\right)_o = \frac{3}{2}\left(\frac{\Delta f}{f_m}\right)^2 \cdot \frac{B_{RF}}{f_m} \cdot \left(\frac{C}{N}\right) \qquad (4.4.1\text{-}4)$$

where

Δf is the peak deviation from center frequency of the RF signal

f_m is the modulating frequency

B_{RF} is the RF bandwidth, and

(C/N) is the carrier-to-noise ratio at the input terminals of the discriminator

The RBV video signal covers a video spectrum from 0 to 3.5 MHz. Since the RF bandwidth is given, the number of significant sidebands (pairs) within the bandwidth can be determined from $n = BW/2\ f_m$. A knowledge of the significant sidebands that can be accommodated in the given RF bandwidth leads to a determination of the modulation index which in turn yields the peak deviation.

Using f_m = 3.5 MHz and RF bandwidth = 20 MHz, n is found equal to 2.86. Thus, only two pairs of sidebands can be accommodated in the bandwidth of 20 MHz.

The exact modulation index can be obtained from an examination of the Bessel functions. Table 4.4.1-3 is a summary of pertinent Bessel functions, with arguments β from 0 to 1.7. We choose β such that the total sideband energy outside the RF bandwidth be no greater than approximately 1 percent of the total. With $\beta = 1.2$, e.g., an FM improvement factor of 12.3 (10.9 db) is realized with only $100 \times 2 \times (.032)^2$ (third pair of sidebands) = 0.2 percent RF energy outside the 20 MHz RF bandwidth. With $\beta = 1.4$ the corresponding numbers are 12.2 db improvement, and $100 \times 2 \times (.05)^2 = 0.5$ percent RF power outside the RF bandwidth.

A modulation index of 1.6 was selected. It results in a onesided peak deviation of 5.6 MHz and leads to a spectral composition shown on the next to the last line of Table 4.4.1-3. The total sideband energy outside the 20 MHz bandwidth (i.e. the energy contained in the third and fourth pair of sidebands) is approximately 1.1 percent.

The second column in the table is the Modulation Improvement Factor which is computed from

$$MIF = \frac{3}{2}\left(\frac{\Delta f}{fm}\right)^2 \cdot \frac{B_{RF}}{fm} \qquad (4.4.1\text{-}5)$$

The selected modulation index $\beta = 1.6$ results in a MIF of 22 (13.4 db).

TABLE 4.4.1-3. PERTINENT BESSEL FUNCTIONS

β	MIF	$I_0(\beta)$	$I_1(\beta)$	$I_2(\beta)$	$I_3(\beta)$	$I_4(\beta)$
1	8.55	0.765	0.440	0.115	0.019	0.002
1.2	12.3	0.671	0.498	0.159	0.032	0.005
1.4	16.7	0.567	0.542	0.207	0.051	0.009
1.5	19.2	0.512	0.558	0.232	0.061	0.012
1.6	22.0	0.455	0.569	0.257	0.073	0.015
1.7	24.8	0.398	0.578	0.282	0.085	0.019

Equation 4.4.1-4 is valid for a single sinusoidal modulating signal. When applied to a video signal, the following points should be borne in mind:

1. Since the picture signal, as stated above, is 80 percent of the entire peak-to-peak video signal, the picture S/N ratio at the detector output terminals will be equal to 0.8^2 times the S/N ratio of the peak-to-peak signal (-2 db).
2. A video signal which causes the same peak-to-peak FM swing as a single sinusoidal signal has a peak power 8 times larger than the average signal power of the sinusoid. The corresponding peak-to-peak signal to rms noise ratio is therefore by this factor larger than the rms S/N ratio computed from equation 4.4.1-1 (+9 db).

The last entry in Table 4.4.1-2 takes these two points into consideration.

The detected peak to peak rms signal to noise ratio for the 30 ft. dish, e.g., is computed from

$$\left(\frac{S}{N}\right) = 18.5 + 13.4 - 2 + 9 = 38.9 \text{ db}$$

as shown in Table 4.4.1-2.

4.4.1.3.3 Signal Degradation

The sensor output signal-to-noise ratios are given as 33, 33 and 25 db for camera I, II and III, respectively. The tape recorder S/N is specified as 42 db for the 4 mc channel, and 36 db for the 6 mc channel. Since the video peak-to-peak power is only 64 percent of the total, the recorder SNR will be degraded by that amount, i.e., it will be only 40 db in the 4 mc channel.

We consider the entire transmission link and examine the degradation suffered by the signal transmitted in real time, or upon playback.

The SNR at the output terminals of the earth station receiver is given by

$$\left(\frac{S}{N}\right)_o = \left[\frac{1}{(S/N)_S} + \frac{1}{(S/N)_R} + \frac{1}{(S/N)_{TL}}\right]^{-1} \qquad (4.4.1\text{-}6)$$

where

$(S/N)_S$ is the SNR of the sensor

$(S/N)_R$ is the SNR of the recorder

$(S/N)_{TL}$ is the SNR of the transmission link

The above is valid for playback transmission. When real time transmission takes place, the second term in equation 4.4.1-6 is set equal to zero.

Consider the case of camera I, upon playback.

$$\left(\frac{S}{N}\right)_S = 33 \text{ db} \; ; \left(\frac{S}{N}\right)_R = 40 \text{ db} \; ; \left(\frac{S}{N}\right)_{TL} = 38.9 \text{ db}$$

Then

$$\left(\frac{S}{N}\right)_o = \left[\frac{1}{2\cdot 10^3} + \frac{1}{10^4} + \frac{1}{7.8\cdot 10^3}\right]^{-1}$$

$$\left(\frac{S}{N}\right)_o = 31.4 \text{ db}$$

The signal has suffered a degradation of

$$33 - 31.4 = 1.6 \text{ db}$$

We consider next real time transmission and compute the degradation suffered by the video signal of camera I or II, as a function of the transmission link signal to noise ratio. We use equation (4.4.1-6), set $(S/N)_R = \infty$, and compute $(S/N)_o$ as a function of $(S/N)_{TL}$.

The results are shown on Figure 4.4.1-5: degradation D in db as a function of $(S/N)_{TL}$.

It can be seen that if the degradation is to be maintained equal to or smaller than 1 db, the $(S/N)_{TL}$ has to be in excess of 38.7 db. $(S/N)_{TL}$ over 42 db result in degradation of less than 0.5 db.

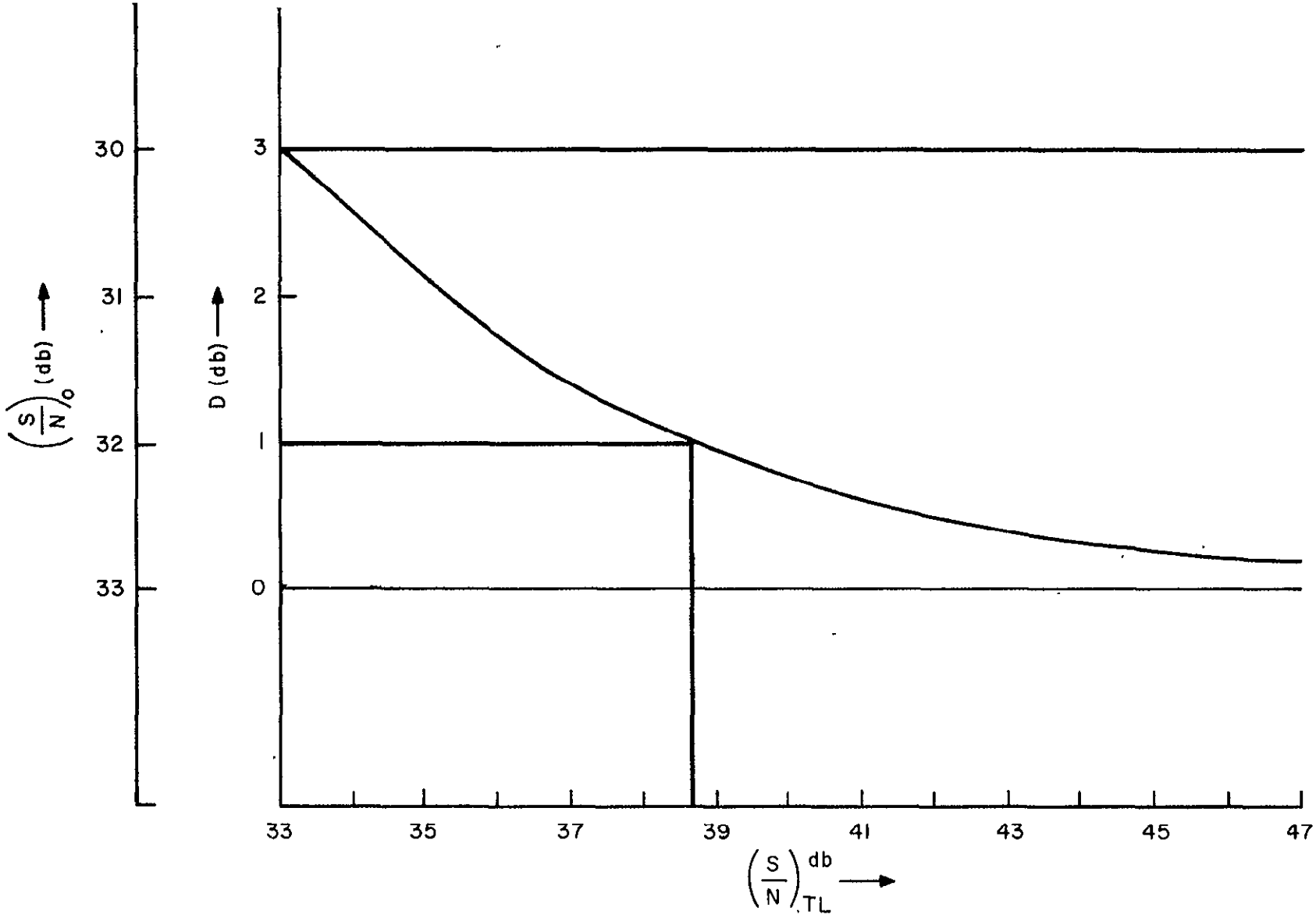

Figure 4.4.1-5. Signal Degradation (RBV); $(S/N)_S$ = 33 db

Comparing Figure 4.4.1-5 with the results of Table 4.4.1-2, we conclude that the signal degradation will we less than 1.0 db for operation with the 30 ft. dish. The degradation suffered by the camera III signals will be less significant due to its lower S/N ratio. This is accomplished with a transmitter power equal to 20 watts.

When the 85 ft. dish is used, the degradation will be 0.26 db. If a 10 watt transmitter is used, with attendant $(S/N)_{TL}$ reduction, the signal degradation will be approximately 0.75 db.

Based on the above numbers it is concluded that the real time RBV signal can be transmitted at a 10.0 watt power level when received by an 85 ft. dish.

When a 35 ft. dish is used for reception, a 20.0 watt power level will result in an 0.9 db signal degradation, while a 10.0 watt level will lead to a degradation of 1.8 db.

It is therefore recommended that for the RBV link a commandable 20/10 watt power amplifier be used which will result in most efficient operation.

4.4.1.3.4 Link Margin

It should be noted that the RBV link calculation contains safety margins in several important areas:

1. A NASA prescribed 6 db safety margin was included in the computation of the S/N ratio.
2. No signal preemphasis was considered. It is estimated that a moderate signal preemphasis will result in 1.5 db signal enhancement for a small increase in transmitter premodulation circuitry.
3. An antenna gain of 4 db was assumed for the worst case link calculation (5 degree elevation angle). Figure 4.4.1-6 shows the one-sided theoretical shaped-beam antenna pattern and its best analytical approximation. It can be seen, that while at θ = 60 degrees (S/C angle) the actual antenna gain will be only 0.4 db higher than the number used in the link calculation, this margin increases significantly with smaller angles, and at nadir it is 2.3 db. This indicates that over most of the spacecraft aspect angles a higher gain and therefore a better C/N ratio will be available. This margin, ΔG, is shown in Figure 4.4.1-7 as a function of θ.
4. The antenna noise temperature will improve as the elevation angle moves from 5 degree toward higher values. In fact, an improvement by a factor of approximately 2.4 is to be expected, at S-Band, at α = 45 degrees. This factor grows to 3.0 at α = 90 degrees. This effect results also in an improved S/N ratio.

The compound result of all these effects appears to point toward a possibility to operate into a 30 ft. dish with a 10.0 watt transmitter, if the attendant slightly higher signal degradation can be accepted, for a limited time, at lower elevation angles. In this case, it is of importance to know, what percentage the total transmitted RBV information will be subjected to a given degradation.

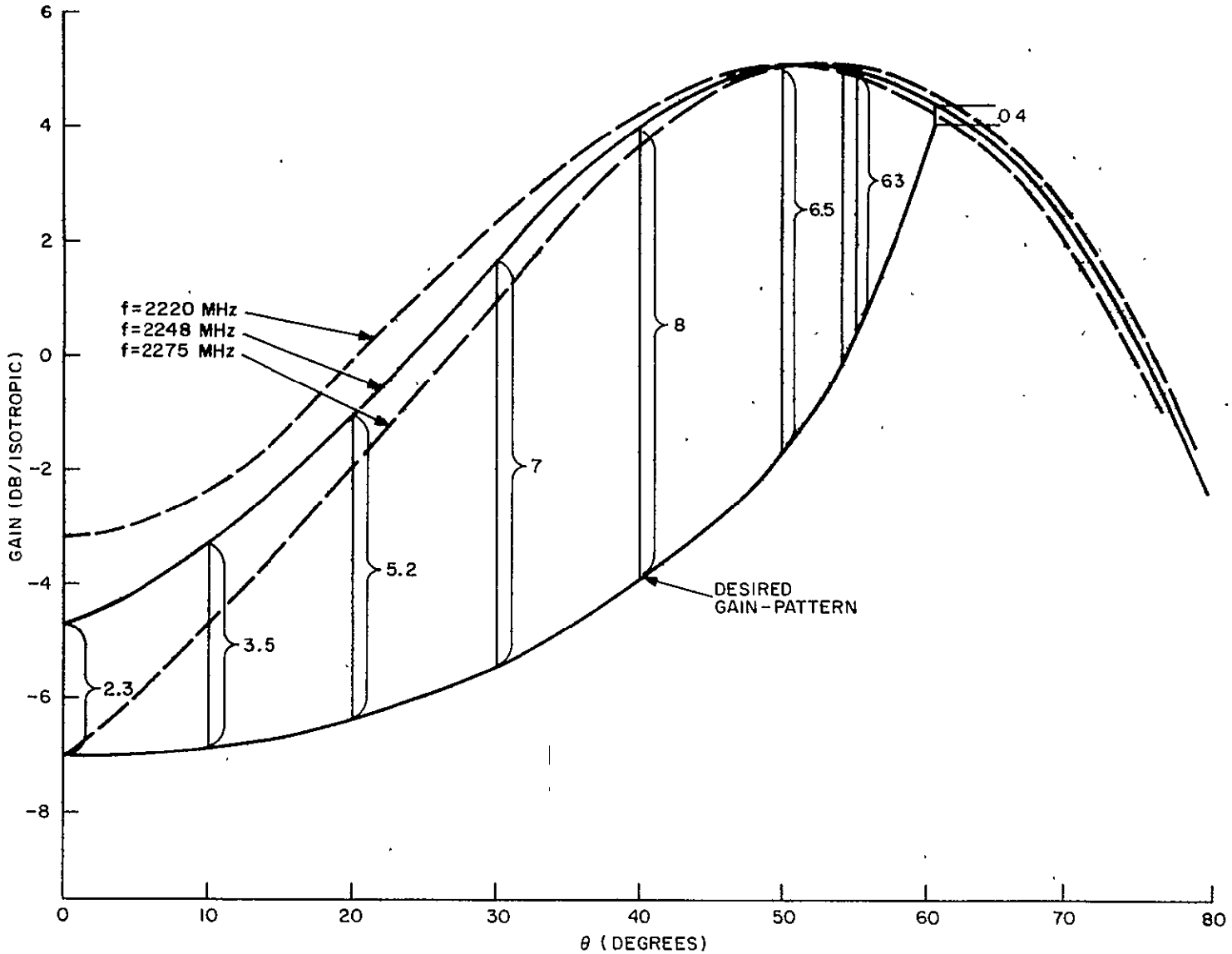

Figure 4.4.1-6. Calculated Gain Patterns for Single Radiator Above a Ground Plane

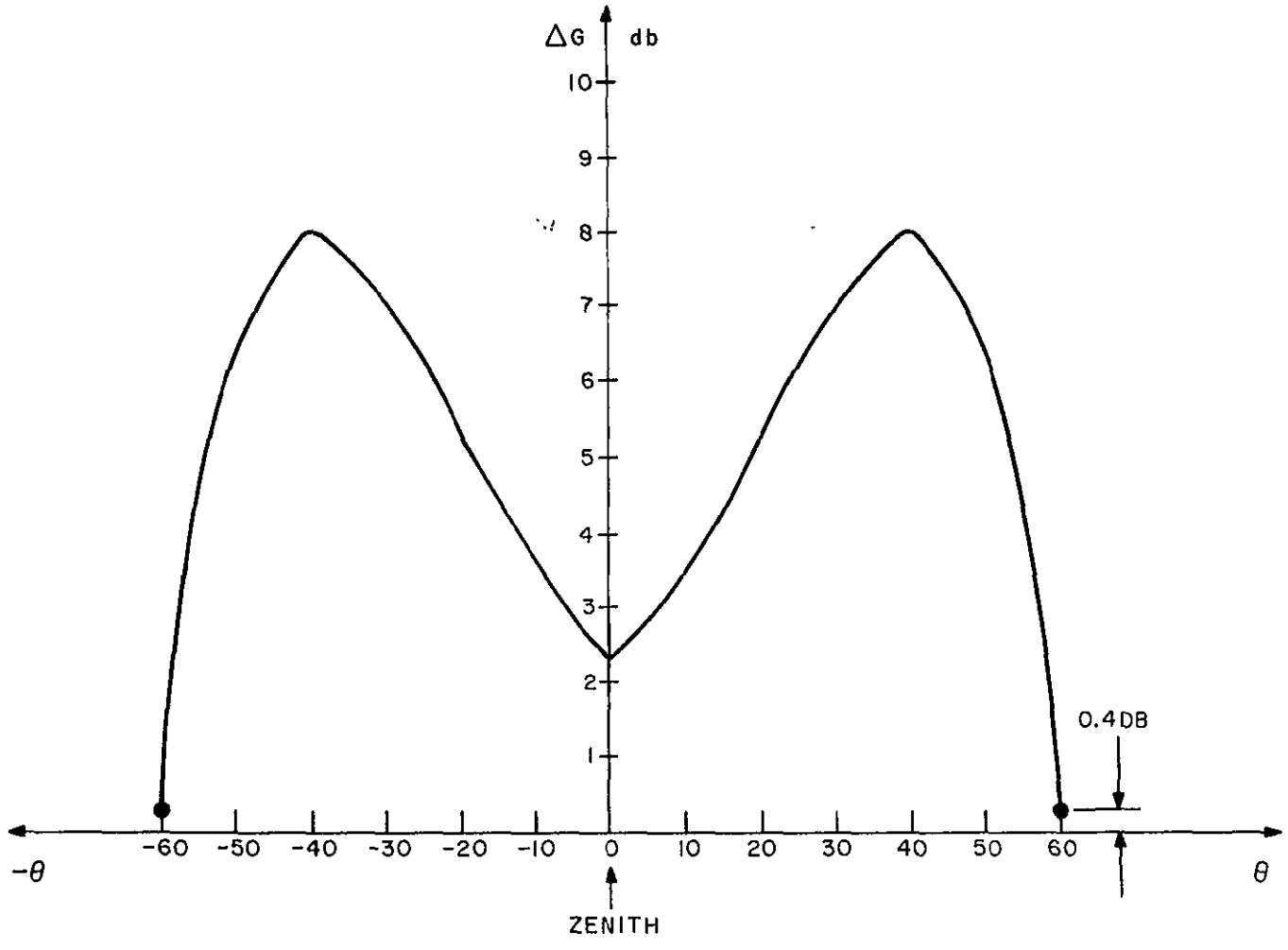

Figure 4.4.1-7. Antenna Gain Margin

The following curves clarify this point. Figure 4.4.1-8 shows the interdependence of the three angles: the elevation angle α, the S/C aspect angle θ and the angle at the center of the earth β. The curves are drawn for a satellite overhead pass, with α growing from 0 to 90 degrees, and back to 0, while β varies between ±29 degrees, and θ goes from +60 degrees to 0 degrees to -60 degrees. S/C altitude is 500 nm.

We assume that the wideband telemetry data are transmitted at a constant rate during the entire pass. Hence the volume of received data will grow linearly with β and reach 50 percent when $\beta = 0$. This is shown on a second abscissa axis of Figure 4.4.1-8 below the β-axis.

It can be seen that approximately 40 percent of the total data volume will be received at elevation angles $\alpha \leq 20$ degrees, which corresponds to $-55 \leq \theta \leq 55$ degrees.

This is shown more clearly on Figure 4.4.1-9. Here, information volume in percent and signal degradation in db are plotted over elevation angle, using the link margin afforded by the S/C antenna and shown on Figure 4.4.1-7. Using Figure 4.4.1-8 and Figure 4.4.1-9 the following conclusions can be drawn:

1. Operation with P_T = 20W will result in signal degradation considerably below 1.0 db.
2. When using a 10.0 watt transmitter, only elevation angles $5 \leq \alpha \leq 12$ degrees and $87 \leq \alpha \leq 90$ degrees will yield degradations over 1 db. In the first case approximately 23 percent of the information volume will be affected with $D \leq 1.65$ db, in the second case less than 4 percent will be affected with $D \leq 1.1$ db.

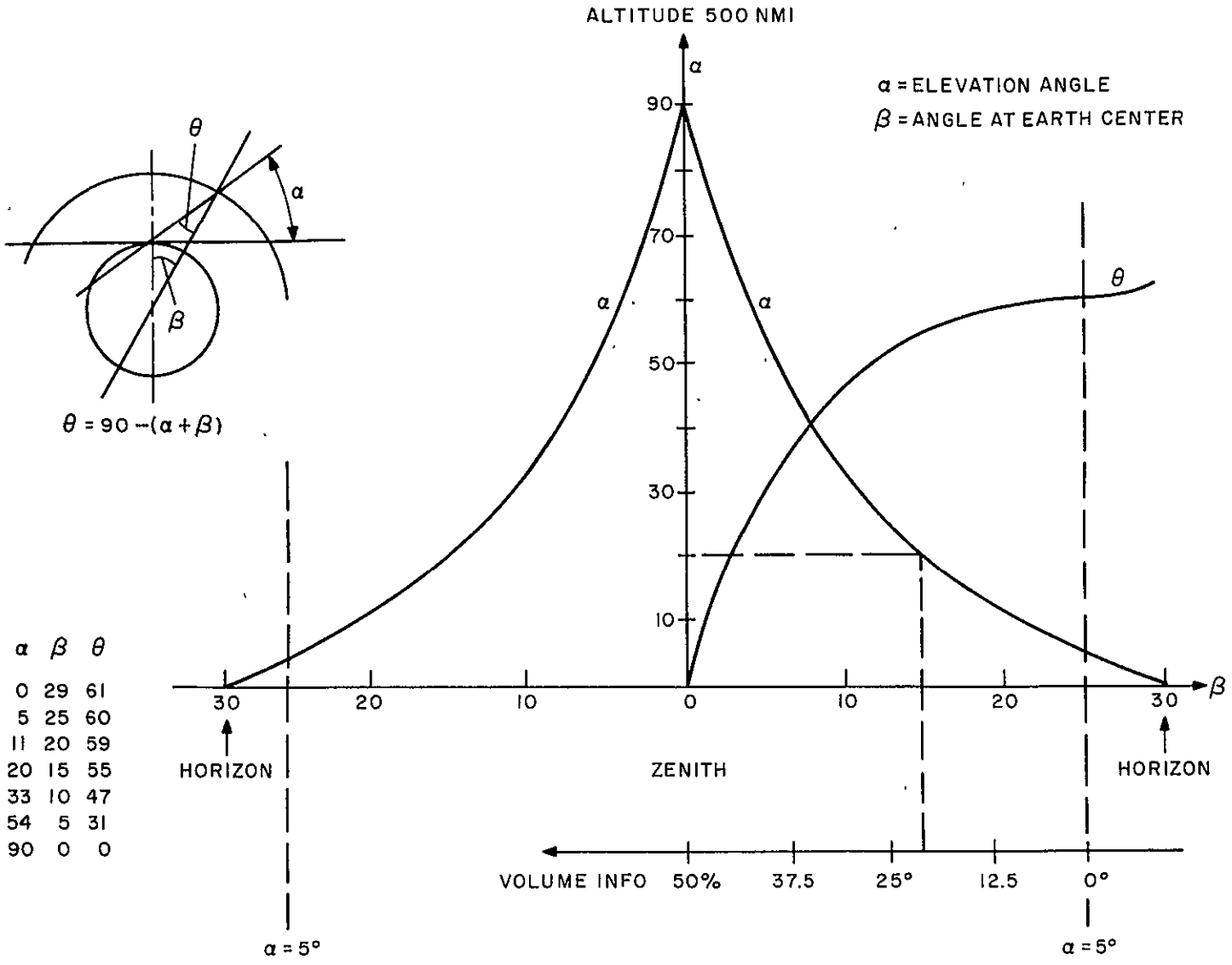

Figure 4.4.1-8. Interdependence of Elevation Angles

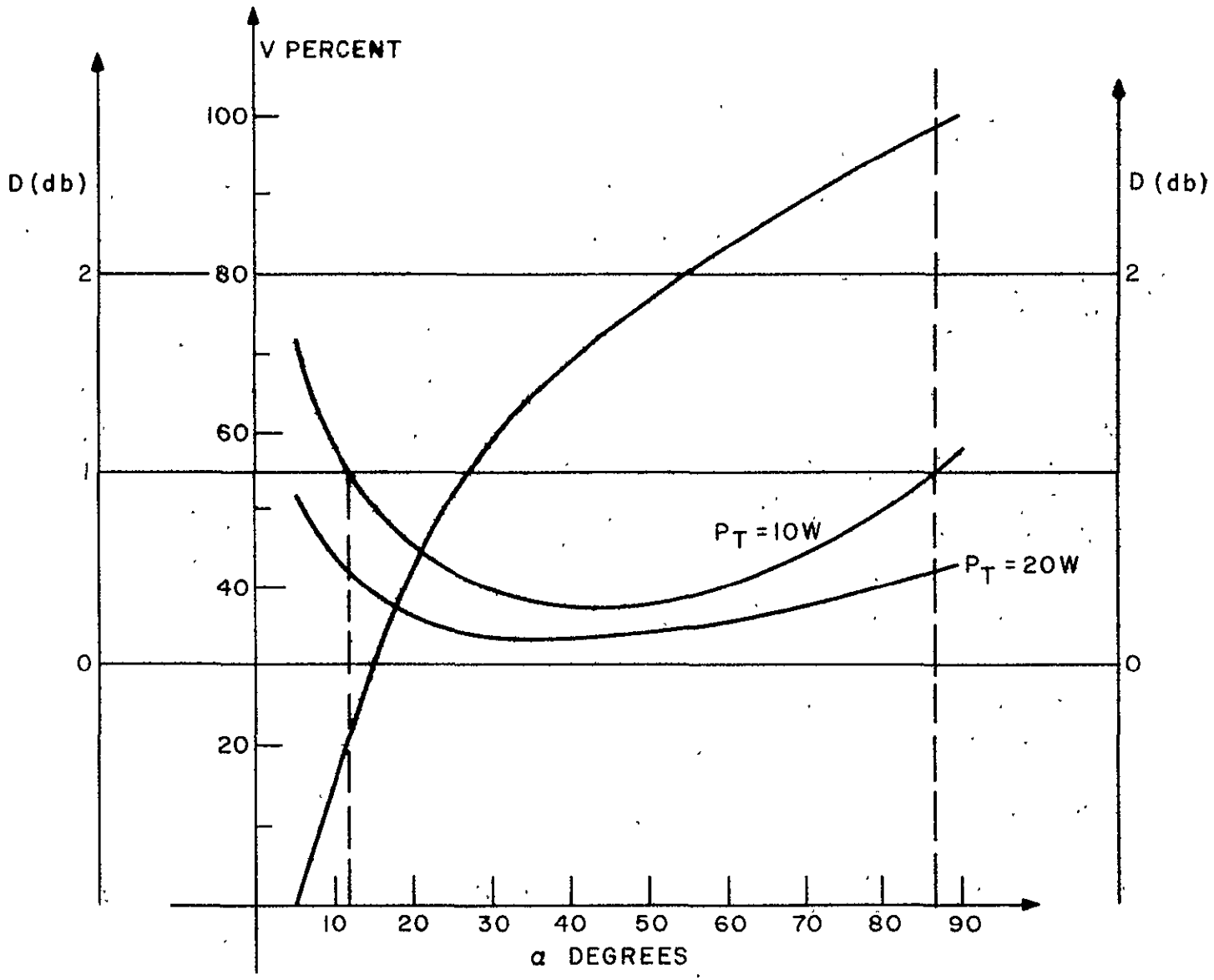

Figure 4.4.1-9. Relation of Information Volume and Signal Degradation to Elevation Angle

4.4.1.4 The MSS Transmission Link

The MSS transmission link is specified as a wideband PCM/FSK link, making use of 20 MHz bandwidth and situated at 2229.5 mc center frequency.

A binary NRZ bit stream at a rate of 15 mb per second is supplied by the electronic processor of the MSS Sensor. This bit stream is passed through a premodulation filter and applied to the input terminals of the FSK (FM) modulator. The obtained modulated RF signal is amplified, filtered, and fed into the input terminals of the antenna. In the ground station, the reverse process takes place: the modulated signal is RF processed by the receiver in an adequate RF bandwidth, and then applied to the FSK demodulator. The demodulated waveform is passed through a post-modulation filter at whose output terminals the original binary bit stream is recovered.

Once the modulation method is selected, the prime objective of the design lies in ensuring "best" bit error probability for the recovered bit stream leading to an optimal reconstruction of the information in the ground station. Best does not necessarily mean minimum; rather, if means an acceptably low bit error probability coupled with realistic performance estimate and reasonable equipment complexity.

The evaluation of the RF link is centered around a selected bit error rate $P_e = 10^{-5}$. It is known that bit error rate has a major influence upon the accurate reconstruction of the digital (and analog) sensor signal in the earth station. A review of the effects of P_e upon frame synchronization, acquisition time, false validation of sync acquisition as a function of sync code lengths and validation procedures, together with equipment complexity consideration, and trade offs, suggests[1] a $P_e = 10^{-5}$ as a best compromise.

The relation between a given bit error rate and the resulting PCM analog error, for a given binary word length N, has been investigated extensively.[2] A closed form analytical result is obtained from the rms analog error without parity check for a given N

$$E_{rms} = \left[\frac{P_e}{3}\,\frac{2^N + 1}{2^N - 1}\right]^{1/2}$$

which, with $P_e = 10^{-5}$, results in $E_{rms} = 0.18$ percent. This analog error is judged acceptable for the MSS data transmission.

In order to assess the possibility of operation at this low error rate, a link calculation for the MSS transmission was performed. No separate listing is given here of the link parameters

since they are essentially the same as shown in Table 4.4.1-A for the RBV link, with the following exceptions:

1. The nominal center frequency for the MSS link is 2229.5 MHz*. This slight difference in frequency results in reduced free space losses of 1.015^2 or 0.14 db.
2. The predetection bandwidth of the MSS link as shown later is limited to the bit rate, i.e., 15.0 MHz between the 3 db points. This leads to a 1.2 dB reduction in thermal noise power and a corresponding increase in C/N ratio.

Thus, the C/N ratio for the MSS link is:

	30-foot dish	85-foot dish
C/N	19.8 db	24.8 db

Clearly, achieving $P_e = 10^{-5}$ does not place a particular burden on the RF link. No matter which digital modulation method is employed above a threshold of approximately 9.0 db, the bit error probability decreases very rapidly with increasing C/N ratio. Theoretical and experimental investigations show that the carrier energy to noise density ratio (which is the same as the C/N ratio in an IF bandwidth equal to the bit rate) is 14.0 db for $P_e = 10^{-5}$, with discrimination detection[3]. Optimum (coherent) detection places the C/N requirements at 13.0 db for the same bit error rate[4], while experimental results indicate 13.5 db[5].

A conservative C/N of 14.0 db is assumed to be necessary for the attainment of the 10^{-5} error rate. Then, a margin of 5.8 db or 10.8 db is available when transmitting to a small or to a large earth terminal, respectively. These numbers have to be reduced by 1.5 db each, to account for signal degradation due to time delay distortion, as shown in detail in the next section. Thus, the C/N margin in the small station case will still allow us to operate with a 10.0 watt transmitter, satisfy the bit error requirements, and show a 5.8 - 4.5 = 1.3 db margin. This margin is significantly larger (6.3 db) in the case of the large earth station.

4.4.1.4.1 Phase Nonlineartities (Signal Degradation)

A nonlinear input-output characteristic will have a high distortion effect upon an AM wave. Distortion products may appear within the baseband which are difficult to remove by filtering.

An FM wave will suffer little under the same conditions. If the nonlinearity is expressed, e.g., as a third order polynominal, its effect on the FM wave will be the generation of second and third harmonic of the carrier wave, each carrying the distorted modulation. Filtering will remove the harmonics, and thus extract the FM wave centered at the carrier

* It is understood that either carrier frequency can be used for the MSS transmission. The link calculations are conducted at the nominal frequencies of the two channels.

frequency. The net effect of the nonlinear characteristic will be only a gain modification. The restriction to be observed here is that the sidebands centered around the carrier frequency and its second harmonic do not overlap, thus allowing a recovery of the FM wave by filtering.

Phase nonlinearities have a more significant effect upon FM waves.

Phase distortion is due to a deviation from direct proportionality of phase shift with frequency. A network with phase shift proportional to frequency causes no distortion to the FM waveform. Linear phase characteristics means that relative phase positions of the sidebands with respect to the carrier are retained throughout the transmission link, although delayed in time by the same amount, thus preserving the modulated RF waveform. With a nonlinear phase characteristic, the quadrature relationship carrier/odd order sideband is disturbed. The net result is that both phase and amplitude distortion is introduced into the detected signal.

Envelope delay is defined as the derivative of the phase characteristic $\theta(\omega)$ with respect to frequency, i.e.,

$$\text{Envelope delay} = \frac{d}{d\omega}\ \theta\ (\omega) \text{ seconds}$$

Envelope delay measures the time required to propagate a change in the envelope of the wave (i.e., the actual information bearing part of the signal) through the system. If $\theta(\omega)$ is proportional to frequency, the envelope delay is constant for all frequencies and there is no distortion of the transmitted signal.

In general, the derivative of the phase characteristic will not be constant but will contain terms that are function of frequency. The envelope delay distortion is equal to the envelope delay minus the constant delay term. Thus, if,

$$\theta(\omega) = b_1\ (\omega - \omega_c) + b_2\ (\omega - \omega_c)^2 + b_3\ (\omega - \omega_c)^3$$

The envelope delay is given by

$$\frac{d}{dt}\ \theta(\omega) = b_1 + 2b_2\ (\omega - \omega_c) + 3b_3\ (\omega - \omega_c)^2$$

and the envelope delay distortion

$$\text{EDD} = 2b_2\ (\omega - \omega_c) + 3b_3\ (\omega - \omega_c)^2$$

In the following, the cases of linear and quadratic time delay distortion are treated separately.

Analytical expressions are derived[6] which show transmission impairment (i.e. the required increase in C/N ratio at the detector input to compensate for the effect of phase distortion) as a function of a ratio d/T. Here, d is the difference in time delay between midband frequency and the maximum frequency off midband; T is the pulse length. It is found that, if we use a raised cosine spectrum of pulses at the detector input and quadratic delay distortion, curve 1 in Figure 4.4.1-10 will show the transmission impairment as a function of d/T. The same, for linear delay distortion, is shown on curve 2. The signal spectrum, and the significance of d in the linear and quadratic case are also shown.

With a pulse train of 15 mbps, a pulse length of 66 nsec is given, which has to be related to d. It was assumed that a d/T = 0.5 would lead to 1.3 db total signal degradation. d = 33 nsec would describe accurately the MSS transmission channel; $\frac{d}{T} = 0.5$ was partitioned between transmitter and ground station: a design goal of 15 nsec was allotted to the transmitter, while 18 nsec were expected to cover the total time delay distortion incurred in the ground station.

Note that the C/N ratio has to be increased by approximately 1.5 db to make up for this impairment.

4.4.1.4.2 Operational Parameters

If we consider a sequence of Mark-Space pulses, each of a duration $T = (15.10^6)^{-1}$ seconds, the resulting frequency spectrum will go to zero at $f_b = 15.10^6$; at $f = 7.5\ 10^6$ Hz, the fundamental component will have a normalized amplitude of $2/\pi$. Hence, an ideal filter bandwidth slightly above 7.5 MHz (1/2T) will pass the fundamental component. A bandwidth larger than (1/2T) will increase the steepness of the pulses, but will have little effect upon pulse height. Bandwidth below 1/2T will affect strongly the pulse height which will rapidly decrease with narrower bandwidth. In addition, the location of the leading or lagging edge will become less accurately determined.

The above considerations point at a premodulation filter which will pass the 7.5 MHz component with as little attenuation as possible. In addition, the phase characteristic up to and beyond this point should be linear. A limitation to the pass band of this filter arises from the consideration that it is this filter that will determine the spectral occupancy of the RF signal.

Experimental results with a quasi/random bit sequence show that no filtering leads to frequency splatter which reaches 60 db below the unmodulated carrier level at $f = 10.\ 1/2\ f_b = 75$ MHz off center frequency[7]; and 40 db are attained at $2 \times (1/2\ f_b) = 15$ MHz. Given the RBV - MSS frequency separation of 35 MHz between carriers, and 25 MHz from carrier to band edge, the resulting splatter in the RBV band will be only -45 db below the unmodulated carrier. The effect of a premodulation filter (3 db bandwidth equal to bit rate f_b) can be seen to restrict the splatter to below 65 db[8]. In both cases, the results are obtained experimentally with a one sided frequency deviation equal to $0.8 \times 1/2 \times f_b$. It is concluded that a premodulation filter shall be used with a 3 db bandwidth of 15 MHz (less than 1.0 db at 7.5 MHz). It will be of the Bessel type. The roll off in the stop band should be 18 db/octave.

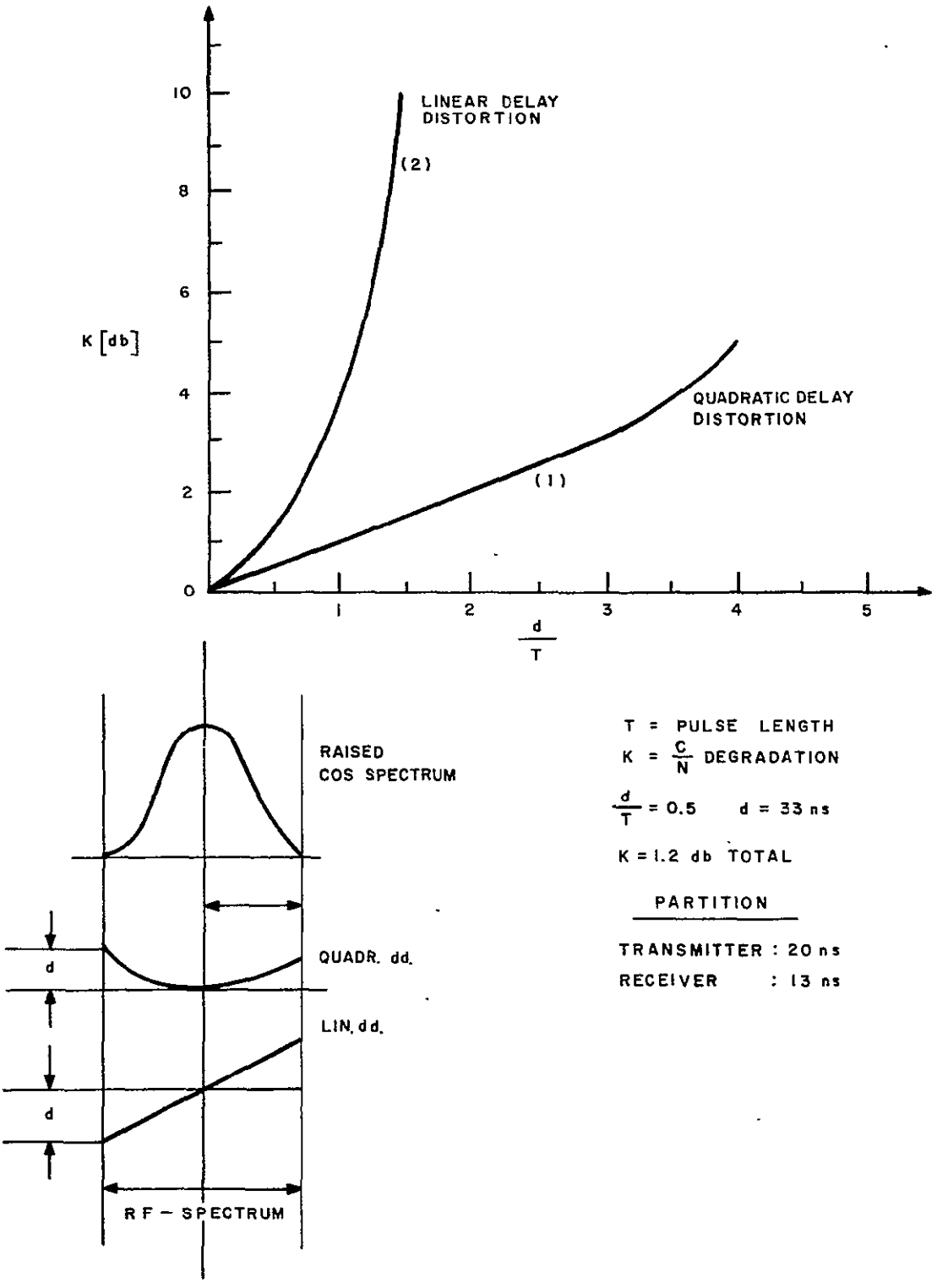

Figure 4.4.1-10. Link Time Delay Distortion

4.4.1.4.3 Frequency Deviation and RF Bandwidth

Both theoretical and experimental investigations show that there is an optimum frequency deviation which results in best bit error probability. The peak-to-peak deviation $2 \cdot f_d$ is related to the frequency interval Δf between mark and space frequency, and to the bit rate f_B by the following expression

$$\Delta f = 2 \cdot f_D = K \cdot f_B$$

where the constant K varies between 0.715 and 0.80, and f_D is the one sided frequency deviation.

Here, the experimental results[9] are accepted which indicate that best bit error rate performance is obtain with K = 0.75, and with the receiver IF bandwidth equal to the bit rate. This result is independent of carrier to noise ratio, and no advantage is gained by operating in a wider bandwidth.

The selected filter bandwidth must be examined from the viewpoint of transmitter (and/or receiver) center frequency stability and detuning effects.

The $\pm$ 0.005 percent center frequency stability of the modulator leads to a $\pm$ 113.2 kHz frequency variation (center frequency 2229.5 MHz). If we add to it a compound detuning effect of the same value due to not ideal matching, component aging, and thermal effects, we have a total of $\pm$ 226.4 kHz which can be well accommodated in the wide RF filter.

The analogous problem in the earth station is more complex. To the above frequency shift, we have to add the effect of the ground station local source frequency instability, and the Doppler effect. If we assume center frequency stability of $\pm$5 parts in 10^6, we obtain $\pm$11.3 kHz; the maximum Doppler shift will account for $\pm$50.5 kHz (at 5 degree elevation angle and 24000 ft/sec orbital velocity). Thus, the total frequency uncertainty for the ground station may be as high as $\pm$ 228.2 kHz and must be considered in devising the receiver filtering and detection equipment.

The video (post detection) filter used in the receiver has an optimum 3 db bandwidth equal to half the bit rate. This filter will follow the discriminator detector and be followed by either a sampling or integrating detector.

The RF bandpass filters in the transmitter will have little effect on the signal spectrum; feasibility and insertion loss considerations will dictate the 3 db bandwidth. A look at a measured spectrum[8] indicates a drop-off (20 db) at approximately 1/2 bit rate off center frequency, i.e., 9.0 MHz, and a frequency roll off at a rate of 18 db per octave. The flat portion of the spectrum is 25 db below the value of the unmodulated carrier. At the band edge of the RBV channel (25 MHz away from MSS carrier), the spectrum is 62 db below the unmodulated carrier. The spectrum indicates a good side band utilization with most of the RF energy contained within the 20 MHz filter limits.

A different case arises when the quasi random-bit rate used for the above spectrum test is replaced by a square wave modulating wave. This situation can occur during portions of the transmission period when bit patterns are formed corresponding to sync codes. It is considered in the next section.

4.4.1.4.4 Cross Talk

The case is considered when, for a limited interval of time, the MSS sensor electronics supplies a well defined (deterministic) sequence of Mark and Space symbols corresponding to an operational code. We have, then, the case of square wave modulation and, therefore, a different spectral picture of the FM modulated carrier: the spectrum consists of discrete lines, whose spacing and magnitude are determined by the modulating signal and the modulating process.

The energy contained in these spectral lines is far greater than the energy contained within a narrow frequency band of the FM spectrum during the time interval of data transmission. Therefore, this case is given particular consideration.

The cross talk can arise at two points of the signal chain:

1. It can take place at baseband. The video switching matrix is a point where, due to the finite isolation between the ports of the solid state switches, the MSS baseband signal can find a way to enter the RBV signal path. The RBV premodulation filter will strongly attenuate these signals; note that its passband is 4.0 MHz, while the fundamental component of the MSS signal may be higher, depending on the Mark-Space sequence. If we assume a 1-0-1-0 sequence, this fundamental component will be at 7.5 MHz at which frequency the RBV filter will have 18-22 db attenuation. A sequence of 1-1-0-0-1-1 will exhibit a lower fundamental frequency (by a factor of 2) and thus will be less attenuated.

   The RBV signals can also reach the MSS channel. The wider MSS premodulation filter will not offer any attenuation and they will reach the modulator input unchanged.

2. Cross talk between the modulators can take place if the modulated carrier of Modulator I can enter Modulator II. Particular attention is paid to the effect of the AFC loop and the selection of the discriminator center frequency (IF). The unmodulated carrier of the MSS channel can mix with the carrier of the RBV in the down converter, yielding a difference signal of f = 35 MHz. If the second harmonic of this signal falls within the passband of the IF amplifier-discriminator, it will lead to a VCO center frequency offset, possibly varying in time as the MSS carrier varies in the course of the prevailing modulation sequence.

The above effects take place within the transmitter. Their reduction and elimination requires careful isolation between transmitter components. Isolation better than 50 db will result in negligible RBV signal degradation.

In the following a more important source of cross talk is considered: it is due to the MSS signal sidebands that fall within the RBV band. They are radiated by the MSS antennas, received by the ground station, and can not be eliminated by filtering.

We first consider the spectral composition of several bit sequences.

4.4.1.4.4.1 Square Wave Spectral. The spectral components of a square-wave of peak amplitude I are written:

$$i = \frac{4.I}{\pi} \left\{ \sin \omega_1 t + \frac{1}{3} \sin 3 \omega_1 t + \frac{1}{5} \sin 5 \omega_1 t + - - - \right.$$

$$\left. - - - \frac{1}{n} \sin n\omega_1 t \right. \qquad (4.4.1\text{-}9)$$

where $\omega_1 = 2\pi f_1 = \frac{\pi}{T}$; T = pulse length; n odd

The spectrum is discrete, only odd harmonics of the fundamental ω_1 are present, and their magnitude decreases at a rate of 6 db/octave.

Even harmonics are, ideally, not present. They may be generated, however, with timing errors. The ratio of second harmonic to the fundamental is given by

$$\frac{i_2}{i_1} = \frac{\Delta t}{2/\pi}$$

Thus, an error of 1 percent leads to

$$\frac{i_2}{i_1} = \frac{0.01}{\frac{2}{\pi}} = 0.0157,$$

i.e., the second harmonic is approximately 36 db below fundamental.

The square wave FM spectrum is given by

$$i_c = \left| \frac{2I}{\pi\beta} \right| \sin \pi \frac{\beta}{2} \quad \text{(carrier)} \qquad (4.4.1\text{-}10)$$

$$i_n = \left| \frac{I \cdot \beta}{\beta + n} \right| \frac{\sin (\beta - n) \frac{\pi}{2}}{(\beta - n) \pi/2} \quad \text{(sidebands)} \qquad (4.4.1\text{-}11)$$

With very large β, in the limit, two steady state waves are produced, $\omega_o + \Delta\omega$ and $\omega_o - \Delta\omega$, i.e., we have a two-line spectrum. As β decreases each subcarrier $\omega_o + \Delta\omega$

becomes surrounded by a spectrum which has the appearance of the super-position of two square wave AM spectra centered at $\omega_o \pm \omega$.

As β decreases further these two square-wave spectra move closer to the carrier, the carrier component grows larger and the simplified AM picture loses validity. For $\beta < 1$ the spectrum is like a sinusoidal single tone, low β FM: the carrier predominates and all side bands are present.

Equation (4.4.1-11) shows the sideband configuration as a function of the modulation index β. It can be seen that if β is an odd (even) integer, all odd (even) sidebands are equal to zero, except the subcarriers. If β is not an integer, however, both odd and even sidebands are present, at intervals $\pm n \omega_1$.

Using Equations (4.4.1-10) and (4.4.1-11) the FM spectrum of a square-wave modulating signal was computed. This was done for three different bit sequences:

0 1 0 1

00 11 00 11 and

000 111 000 111

The results are summarized in Table 4.4.1-4.

Using Equation (4.4.1-9) the baseband spectrum of the same bit sequences was computed. It is shown in Table 4.4.1-5.

4.4.1.4.4.2 Baseband Cross Talk. Table 4.4.1-D contains the spectral composition of each of the three bit sequences, the relative level of each harmonic component, and the attenuation that the RBV filter would impress upon each harmonic. The RBV filter is shown in Figure 4.4.1-11; its 3 db point is at 4 MHz, its stopband attenuation is 24 db/octave. Clearly, all harmonic components of the 1010 MSS bit sequence lie in the RBV filter stopband and suffer attenuation. This is not so, however, with the 11 00 11 or the 111 000 111 bit sequence. Here the fundamental component lies well within the passband of the RBV filter and is not attenuated.

The above shows that the RBV filter can provide some protection for given bit patterns. In adverse cases, however, it is of little value. One has to rely, therefore, mainly on the isolation provided by the video switches. The amount of isolation needed can be assessed from the following considerations.

The RBV sensor S/N ratio at the terminals of the video matrix is 33 db. In order to keep the signal degradation less than 0.1 db, the sum of the interfering signals should be at least 50 db below the video signal. Since, as in the 111 000 111 case, more than one spectral component can find its way into the RBV channel, a switch isolation between ports of 60 db or better is required.

TABLE 4.4.1-4. SQUARE WAVE FM SPECTRAL COMPONENTS

	β = 0.75	β = 1.5	β = 2.25	β = 3.0
i_0	0.78	0.28	0.1	0.21
i_1	0.43	0.6	0.31	0
i_2	0.11	0.43	0.53	0.36
i_3	0.03	0.06	0.35	0.5
i_4	0.03	0.04	0.32	0.26
i_5	0.01	0.02	0.06	0

Bit Sequence

0	1	0	1	β = 0.75;	f_1 = 7.5 MHz
00	11	00	11	β = 1.5;	f_1 = 3.75 MHz
000	111	000	111	β = 2.25;	f_1 = 2.5 MHz
0000	1111	0000	1111	β = 3;	f_1 = 1.9 MHz

4.4.1.4.4.3 RF Cross Talk. The normalized spectral components of the FM signal resulting from the three different bit patterns are shown in Table 4.4.1-4. The frequency deviation is constant; the modulation index varies with the fundamental and results in different spectral compositions.

Table 4.4.1-4 shows the high energy content of the discrete spectral lines when compared to the FM spectrum obtained from a quasi random-bit stream. Consider, e.g., the 1010 bit sequence. The third harmonic, 22.5 MHz off the MSS carrier is only 2.5 mc off RBV band edge. Its power is 30 db below the unmodulated carrier, while the measured power of the data spectrum at this frequency, has been shown to be in excess of 60 db below the unmodulated carrier[8]. The same power level is associated with the fourth harmonic which falls well within the RBV filter passband.

It is understood that the MSS sidebands falling within the RBV band should be kept as low as possible. The above shows that during data transmission the danger of interference is negligible; the spectral components are 60 db below the unmodulated carrier. Adding to this the bandpass filter attenuation results in 60 +27 (3 pole filter) = 87 db which is adequate.

TABLE 4.4.1-5. BASEBAND SQUARE WAVE SPECTRA

Frequency MHz	Spectral Component	Level (db)	RBV Filter Attenuation	Total Attenuation
Sequence: 1 0 1 0 1 0				
7.5	Fundamental	0	27	27
22.5	3. Harmonic	-4.8	66	70.8
37.5	5. Harmonic	-7	80	87
52.5	7. Harmonic	-8.5	--	--
67.5	9. Harmonic	-9.4	--	--
Sequence: 11 00 11 00				
3.75	Fundamental	0	3 db	3 db
11.25	3. Harmonic	-4.8	38	2.8
18.7	5. Harmonic	-7	61	68.0
26.3	7. Harmonic	-8.5	72	80.5
34.0	9. Harmonic	-9.4	--	--
Sequence: 111 000 111 000				
2.5	Fundamental	0	1	1
7.5	3. Harmonic	-4.8	30	34.8
12.5	5. Harmonic	-7	45	52
17.5	7. Harmonic	-8.5	57	65.5
22.5	9. Harmonic	-9.4	67	76.4

The case of three particular bit patterns and the RF bandpass filter characteristic is shown on Figure 4.4.1-12. The question arises as to which pattern should be selected on the basis of minimum MSS-RBV channel interference. It is clear that it is the pattern which, when we take the RBV bandpass filter curve under consideration, will give us minimum interference

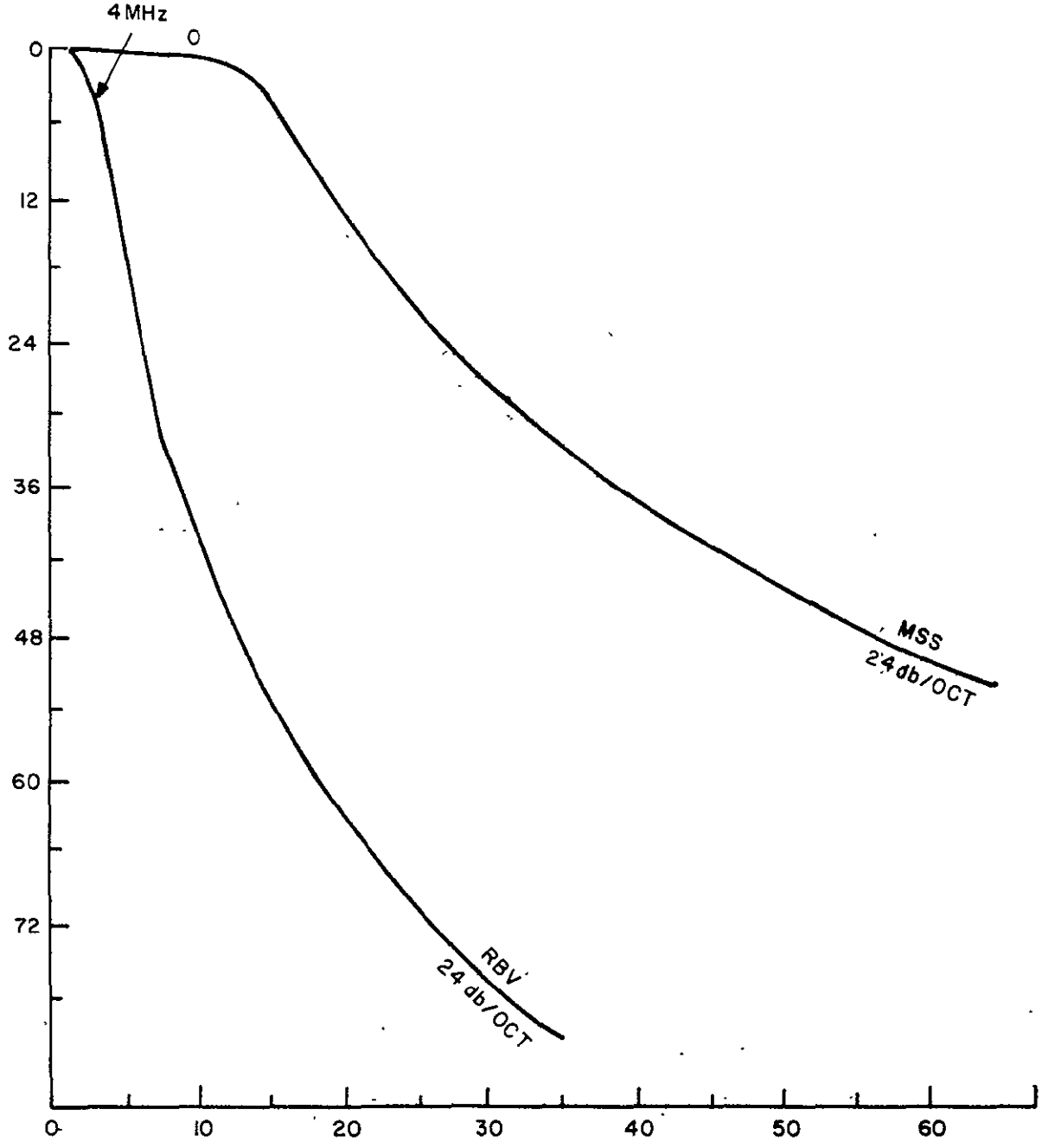

Figure 4.4.1-11. Video Cross Talk

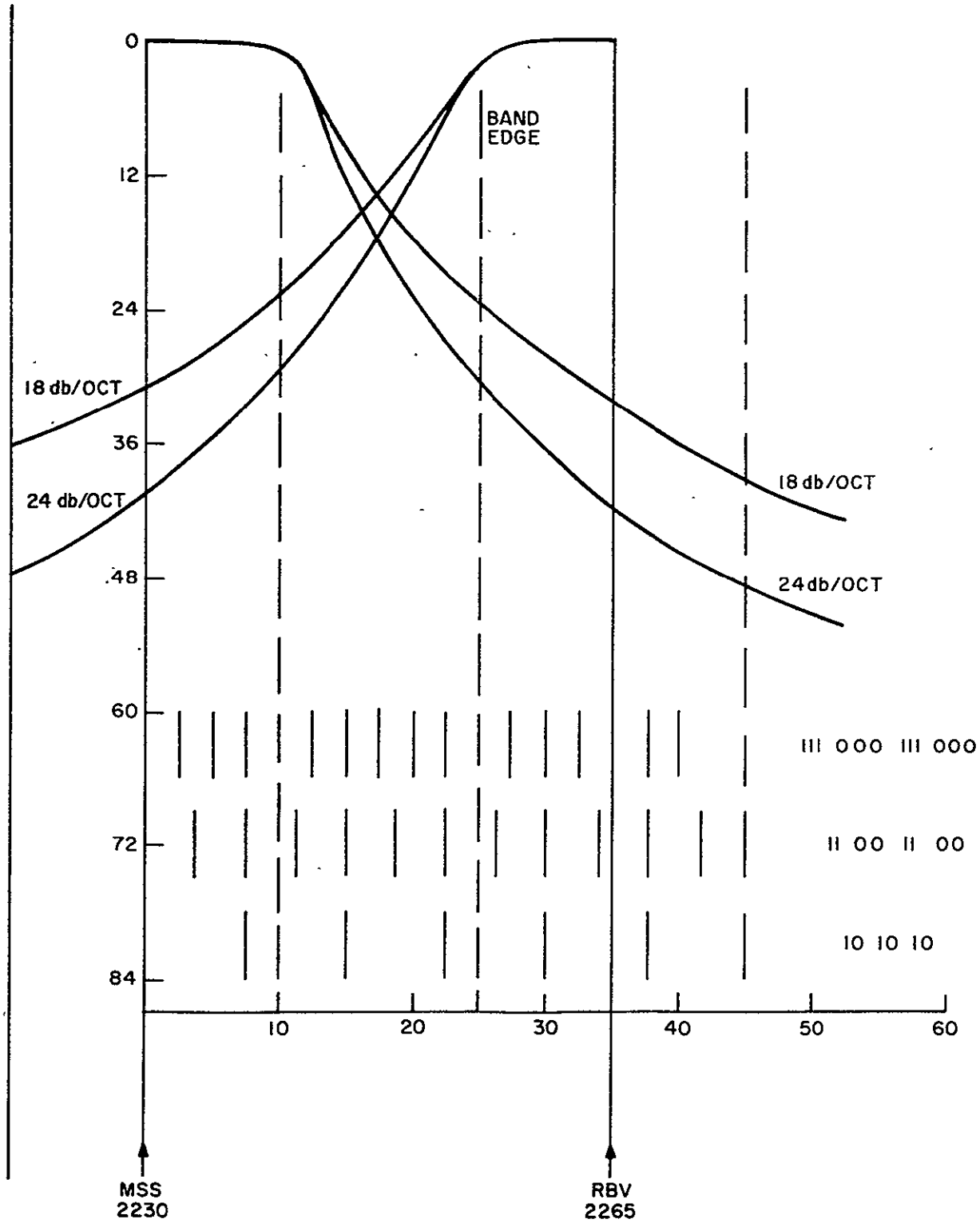

Figure 4.4.1-12. Three Bit Patterns and the RF Bandpass Filter Characteristic

power. This is a first approximation. It is based on superposition effects and neglects disturbances that can arise in the receiver due to non-linearities. This approximation is, however, justified as long as the interfering signals are very low.

A qualitative examination of the three bit patterns shows the following (see Figure 4.4.1-12 and Table 4.4.1-4):

1. Case 1 0 1 0 1 0: Components i_4 and i_5 are 30 db and 37 db, respectively, below carrier. MSS filter (3 pole) yields attenuation of 27 and 35 db. Hence, total attenuation is 57 and 72 db. The case of i_1, is more severe. Here the RBV filter will yield only 25 db attenuation. Although this spectral line is far from RBV center frequency and can be filtered out in subsequent receiver stages, its presence in the receiver RF portion may lead to serious disturbances.
2. Case 11 00 11 00. Here, five spectral lines fall within the RBV baseband at power levels, each more than 43 db below unmodulated carrier. The out of band significant sidebands (first and second), and the carrier, are attenuated 28, 22 and 30 db respectively.
3. Case 000 111 000: 9 sideband fall within the RBV band (sideband 10 to sideband 19). The power levels associated with these bands are not shown in Table 6. It is estimated that they are more than 50 db below the unmodulated carrier.

It should be noted that the above interference discussion is based on a perfect square wave modulating signal. Since the pre-modulation filter (3 db bandwidth of 15 MHz) reduces significantly the harmonics of the bit stream, it is expected that this will result in further sideband attenuation and, therefore, reduced interference.

The preceding qualitative examination results in the conclusion that the selected band pass filter characteristics and a selection of a minimum energy bit pattern (probably 111 000 111) will permit reduction of MSS interference below 50 db which will limit the RBV signal degradation to an acceptable value.

4.1.4.5 References

(1) MSS MUX/DIODEM/DEMUX, Final Study Report No. NAS 5-11624, Hughes Aircraft Co.

(2) Telemetry System Study, Final Report, Volume I, Aeronutronic, 1959

(3) Paul D. Shaft, Error Ratio of PCM-FM using Discriminator Detection, IEEE Trans SET, 1963, December, p. 131-37.

(4) S. Stein, Modern Communication principles.

(5) Telemetry Study, Final Report, Volume II, Aeronutronic, 1959.

(6) E. D. Sunde, BSTJ, March 1961, p. 353

(7) Aeronutronic Report, Vol. II, Fig. II-3-13

(8) Ibid, Fig. II-3-15

(9) Ibid, Fig. II-3-4

4.4.1.5 Wideband Transmission System Recommended Design - Block Diagram

The block diagram of the wideband telemetry system is shown on Figure 4.4.1-13.

A video switching matrix constitues the first building block in this diagram. Six input terminals are shown; two output terminals connect the video matrix to modulator No. 1 and modulator No. 2, respectively, thus establishing transmission channels No. 1 and No. 2. The switching matrix is discussed in more detail later.

Modulators No. 1 and No. 2 are identical in structure. Each consists of an AFC loop, built around a voltage controlled oscillator (VCO). The parts of the loop are a local microwave reference frequency source, and a down converter followed by a limiter, IF ampliifer, and a discriminator. The recovered modulation content at the output terminals of the discriminator is compared to a sample of the modulating signal. The difference between the two waveforms constitutes the VCO center frequency correction signal which is applied to the VCO input terminals along with the modulating signal.

The modulator is designed to operate at either 2229.5 MHz or 2265.5 MHz; the center frequency selection is performed by switching of the reference oscillator and the VCO control voltage. Further, each modulator can accept either the RBV video or the MSS PCM baseband signal and operate in the video/FM or PCM/FM mode with the proper frequency deviation. A detailed discussion of the modulator is included in 4.4.1.7.

Both power amplifiers may accept the output of either modulator. Two possibilities were considered for the power amplifiers: either TWT or solid state. The advantages of the TWT are known: high efficiency and high gain (resulting in low heat losses and small driver-amplifiers), and good output-input isolation (leading to small cross talk and proven reliability). These advantages are partially offset by the fact that the TWT is to be operated at two power levels--the penalty paid for this extended capability is a sacrifice in TWT efficiency.

The solid-state power amplifier is a serious contender. Among its advantages are potentially high reliability, modular construction, and hence, relatively easy selection of output power levels by de-energizing and disconnecting portions of the power amplifier modules. Its drawbacks are lower efficiency and higher susceptibility to cross talk.

Considering the higher efficiency and proven reliability of the TWT, it is the selected design. A detailed justification is given in paragraph 4.4.1.8.

4.4.1.5.1 Modes of Transmission

A list of all transmission modes is shown on Table 4.4.1-6. The two sensors and the two tape recorders, each one with an RBV and an MSS signal output, results in six discrete signal sources which can be applied to the two available (and interchangeable) transmitter channels in 22 different ways, assuming that the two channels are operated at the same time. This results in six different modes of transmission which are obtained by setting the video switching matrix in the proper mode.

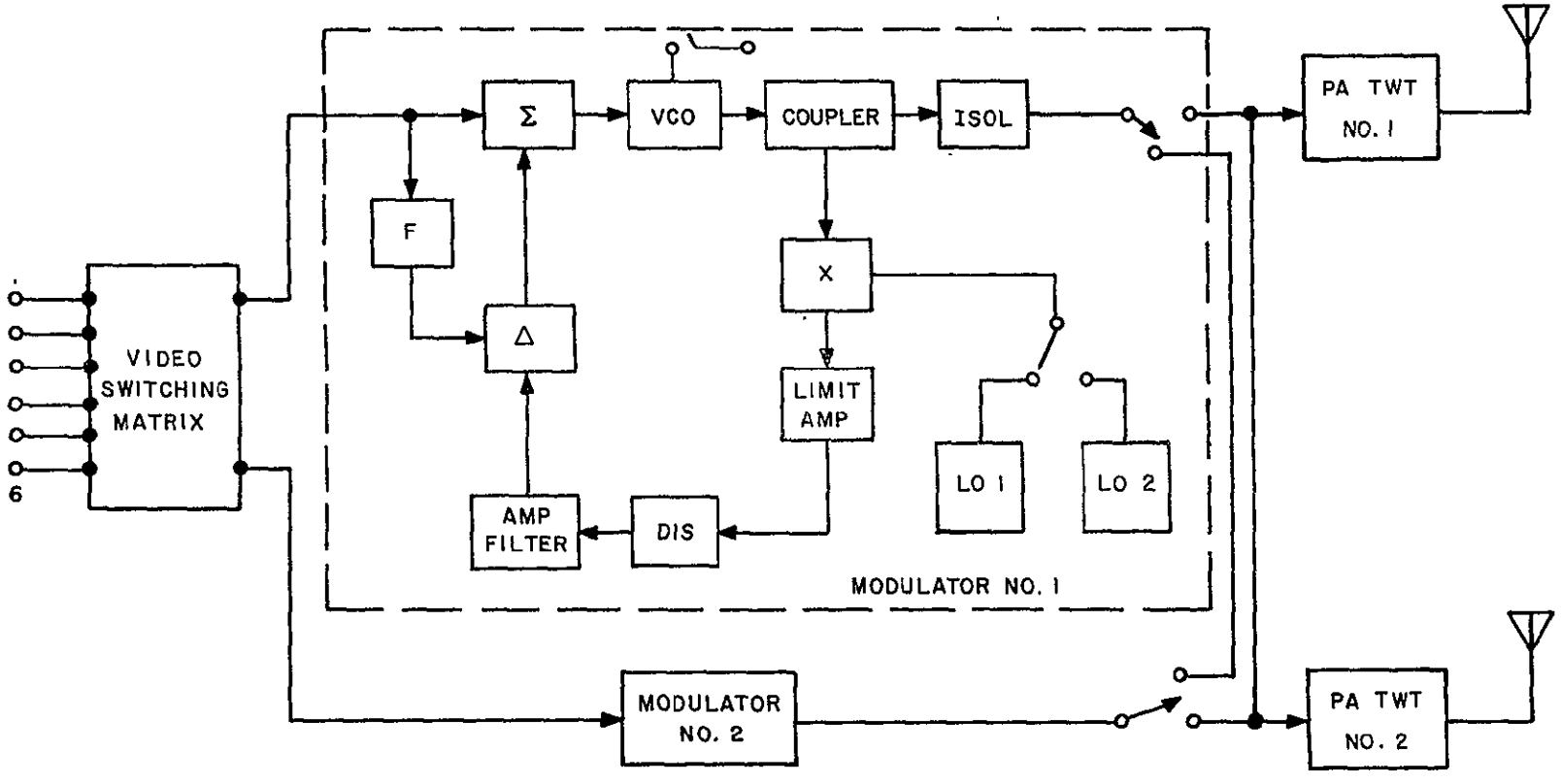

Figure 4.4.1-13. Recommended Wideband Telemetry - Block Diagram

TABLE 4.4.1-6. MODES OF TRANSMISSION

Combinations	No. 1	No. 2	No. 3	No. 4	No. 5	No. 6
1. RBV (RT)	*A or B*	A or B	A or B			
2. MSS (RT)	B or A			A or B	A or B	
3. WBVTR No. 1 (RBV PB) or WBVTR No. 1 (MSS PB)		B or A		B or A		A or B
4. WBVTR No. 2 (RBV PB) or WBVTR No. 2 (MSS PB)			B or A		B or A	B or A
	2	4	4	4	4	4

*A = Link A; B = Link B

4.4.1.5.2 Video Switching Matrix

The functional diagram of the video switching matrix is shown on Figure 4.4.1-14. Six input signals are shown derived from the sensors and the video tape recorders. These signals are routed via 4 three-position switches through the corresponding low pass filters and summing

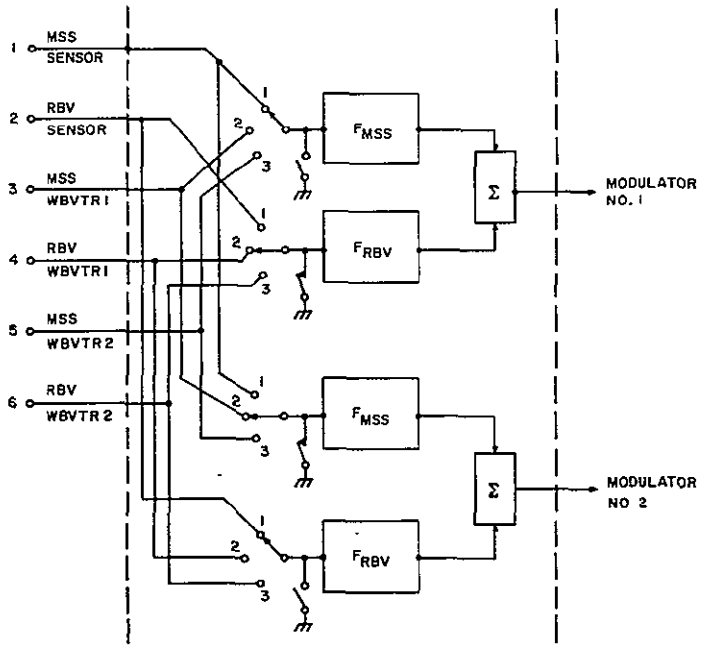

Figure 4.4.1-14. Video Switching Matrix

networks to the input terminals of the modulators. Thus, each signal can reach each modulator by proper switching; in addition, short circuit switches are provided to eliminate the case of one modulator receiving two input signals simultaneously.

The case shown in Figure 4.4.1-14 represents the switch settings for simultaneous MSS and RBV transmission.

1.4.1.5.3 Sensor Interface

The sensor interface is shown in Figure 4.4.1-15.

4.4.1.6 Reliability and Cross Strapping

The basic building blocks of the two wideband transmission chains are shown in Figure 4.4.1-16. Two antennas are assumed; each antenna is connected to one power amplifier via band pass filters, isolators, and cables. The filters and the antennas are entirely passive devices; the modulators and power amplifiers are active. The power amplifiers are TWTs; they have sufficient bandwidth to handle anyone of the modulated signals without any switching or adjustment; i.e., 2229.5 mc ±10 mc and 2265.5 ±10 mc. A video switching matrix receives and routes the six input signals to the input terminals of the modulators.

The basic functional diagram as shown in Figure 4.4.1-15 exhibits no cross strapping devices. Two signal chains are shown which consist of identical components i.e., modulators

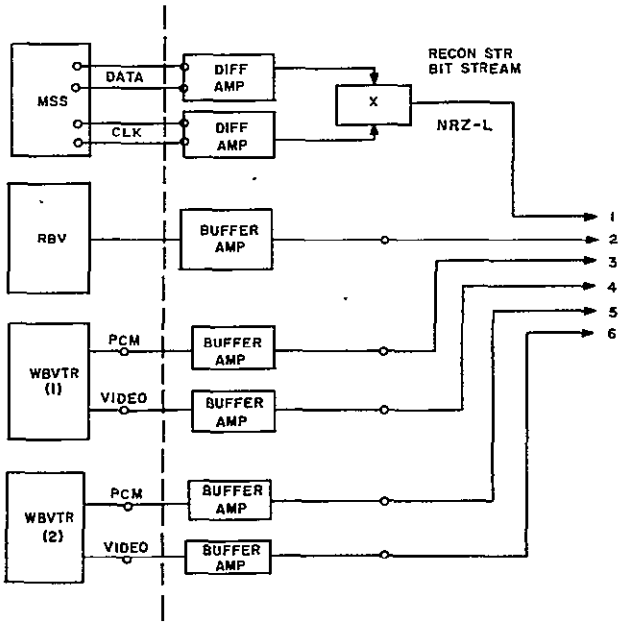

Figure 4.4.1-15. Sensor Interface

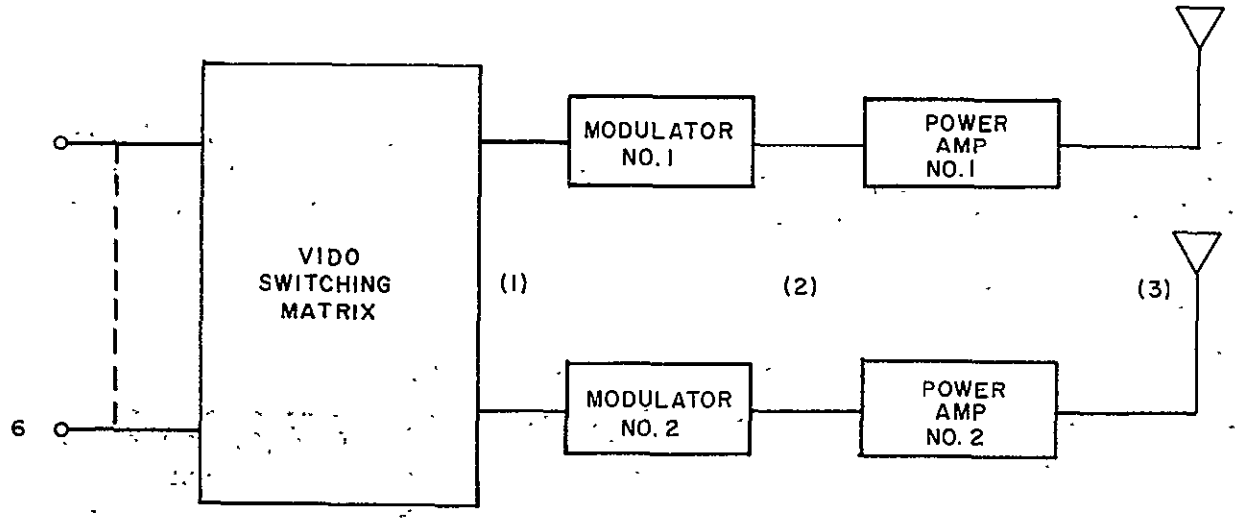

Figure 4.4.1-16. Wideband Transmission Chains

and power amplifiers. The points designated with (1), (2), and (3) show possible locations of the cross strapping switches.

4.4.1.6.1 No Cross Strapping

We examine first the case without cross strapping. Clearly, if the two chains to be operative at the same time and transmit simultaneously two information signals on two different carriers, all building blocks of Figure 4.4.1.-16 must be operational. A single failure of any one of the assemblies that are shown will result in failure to meet this requirement.

Survival of this mode of operation is therefore equal to the probability of survival of all assemblies. No cross strapping will alter this probability. On the contrary, introduction of cross strap switches while useful for other modes of operation will degrade the probability of survival of this "double transmission mode" because of the permanent inclusion of additional devices in the circuitry.

A second mode of operation, designated as "single transmission mode", can be envisioned. This mode can be selected by proper setting of the video switches which will feed a signal only into one of the two chains; in such a case, the other may be de-energized.

The feature of mode selection is lost when a single failure occurs as can be seen from Figure 4.4.1-16. A single failure in one of the signal chains will permanently disable this

signal chain, and thus limit the mode of transmission to the single transmission mode via the other chain. Thus, operation will be possible with only one carrier frequency. The video matrix will allow however, modulation of this carrier with any one of the six available base-band signals.

4.4.1.6.2 Failure Modes

Ten Failure modes are listed in Table 4.4.1-7 showing single failures of the modulators and power amplifiers, and double failures among the same. The second column shows the effect of these failures when no cross strapping is used. The first six failure listed modes result in a reduction to single transmission mode operation. The last four failure modes lead to complete failure of the wideband system.

TABLE 4.4.1-7. FAILURE MODES

No.	Failure	Effect (No Cross Strapping)	Effect (Cross Strapping At Point (2))
1	Power Amplifier No. 1	Channel f_1 disabled	Basically the same but increased flexibility
2	Modulator No. 1	Channel f_1 disabled	
3	Power Amplifier No. 2	Channel f_2 disabled	
4	Modulator No. 2	Channel f_2 disabled	
5	Power Amplifier No. 1 and Modulator No. 1	Channel f_1 disabled	Same
6	Power Amplifier No. 2 and Modulator No. 2	Channel f_2 disabled	Same
7	Power Amplifier No. 1 and Modulator No. 2	Both channels disabled	Only channel f_1 disabled
8	Power Amplifier No. 2 and Modulator No. 1	Both channels disabled	Only channel f_2 disabled
9	Power Amplifier No. 1 and Power Amplifier No. 2	Both channels disabled	Same
10	Modulator No. 1 and Modulator No. 2	Both channels disabled	Same

The question arises as to how can cross strapping alleviate this situation. Consider the following:

1. If a cross strapping switch is introduced in location (2) (Figure 4.4.1-16), only failure modes 9 and 10 will lead to complete shut down; failure modes 7 and 8 will not completely disable the entire system. By using the cross strap switch, the failed components can be circumvented and the operational ones connected in cascade so as to form a complete signal chain, at the right carrier frequency. This is the most significant gain of the cross strapping device.
2. Cross strapping will not alter the situation listed under failure modes 5 and 6.
3. In cases 1 to 4, with one single failure occurring, cross strapping will not basically alter the situation; operation with only one channel will be possible. It will allow, however, in case of one modulator failure, the use of either power amplifier and thus operation at f_1 or f_2; or, in the case of a power amplifier failure, either modulator can be used, at only one carrier frequency.

Thus, cross strapping offers significant gains in cases 7 and 8, and some advantages in cases 1 to 4. These are listed in the third column of Table 4.4.1-14.

4.4.1.6.3 Reliability Calculations

Let t denote elapsed mission time and p denote the fraction of elapsed time in which data are transmitted. We assume that:

1. PCM data and video data are transmitted for equal amounts of time. Thus, the components in each transmitter are powered under normal mode for a time $t = 1/2\ pt$
2. Each premodulation is powered for time $1/2\ pt$
3. The cross strap switches are powered for time pt
4. The failure rate for a component which is not powered (in dormant mode) is equal to 1/10 of its failure rate when in operating condition (powered mode).

In the following, expressions for the probability of survival for the following modes of operation are established:

1. Normal (dual) transmission mode, Pr (G)
2. Dual or single transmission mode, $\Pr\{G \cap D\}$

Then, the probability $\Pr\{D\}$ of the single transmission mode is given by:

$$\Pr\{D\} = \Pr\{G \cap D\} - \Pr\{G\}$$

Three distinct configurations were examined.

1. Configuration A - No cross strapping
2. Configuration B - Cross strapping between modulators/power amplifiers
3. Configuration C - Cross strapping between modulators/power amplifiers and video matrix/modulators.

The reliability models and the equations used for the computation of the probability of survival Pr $\{G\}$ and Pr $\{G \cap D\}$ are shown in Figures 4.4.1-17 through 4.4.1-19.

The frequency function for time-to failure f(t) of the configuration

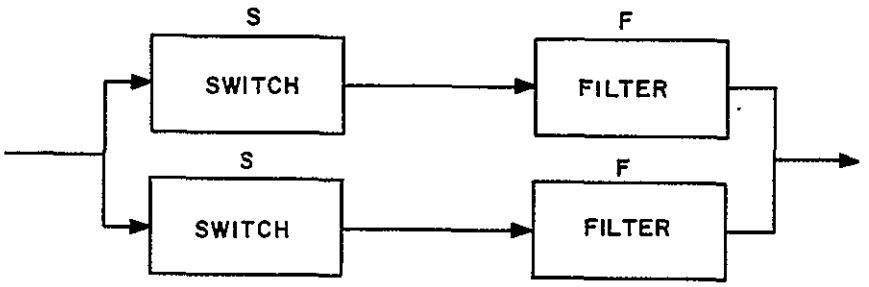

was approximated by

$$f(t) \cong \alpha e^{-\alpha t}$$

where

$$\alpha = -\frac{1}{8760} \ln \left\{ 2e^{-(\lambda_F + \lambda_S) 8760} - e^{-2(\lambda_F + \lambda_S) 8760} \right\}$$

that is

$$e^{-\alpha t} = 2 \cdot e^{-(\lambda_F + \lambda_S) 8760} - e^{-2(\lambda_F + \lambda_S) 8760}$$

This approximates the true probability density function with an exponential function, such that the cumulative probabilities of time-to-failure of the two are equal for t = 1 year.

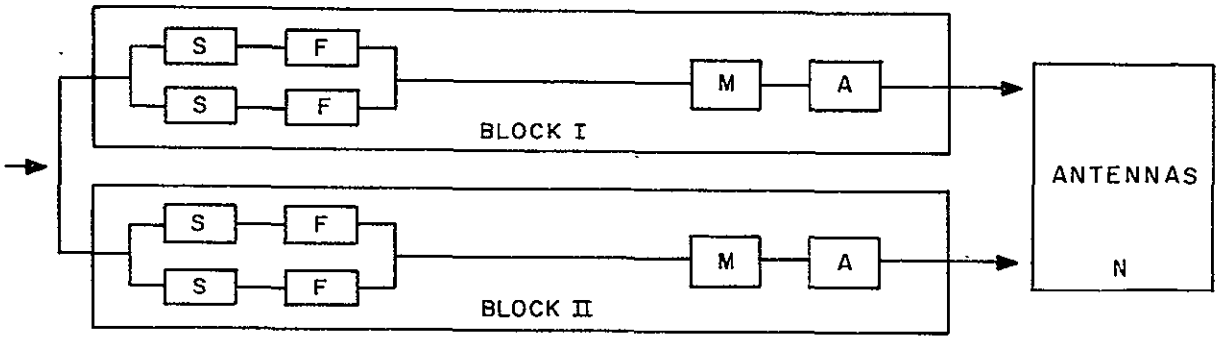

$$PR\{G\} = PR\{\text{BLOCK I} \cap \text{BLOCK II}\}\, R_N^2$$

$$PR\{GUD\} = PR\{G\} + R_N^2 \left[PR\{\text{BLOCK I} \cap \overline{\text{BLOCK II}}\} + PR\{\overline{\text{BLOCK I}} \cap \text{BLOCK II}\}\right]$$

Figure 4.4.1-17. Configuration A (No Cross Strapping)

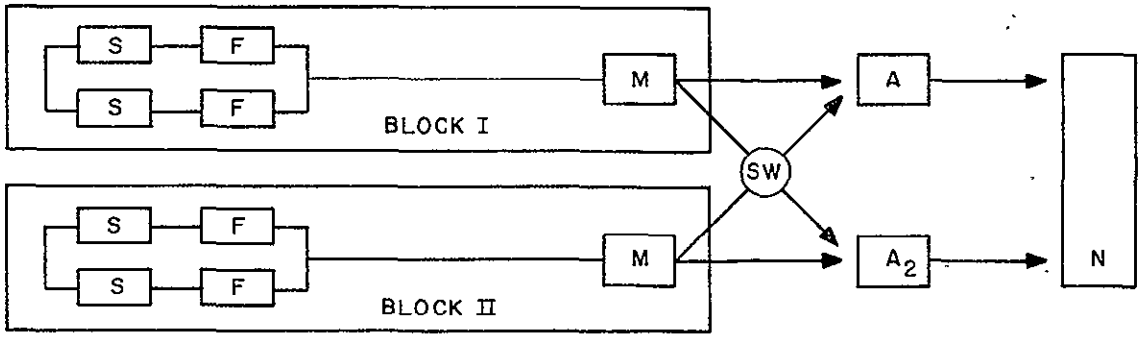

$$PR\{G\} = PR\{\text{BLOCK I} \cap \text{BLOCK II}\}\, R_A^2 R_N^2 R_{SW}$$

$$PR\{GUD\} = \frac{R_N^2 R_{SW}}{} \left[PR\{\text{BLOCK I} \cap \text{BLOCK II}\} + PR\{\text{BLOCK I} \cap \text{BLOCK II}\} + PR\{\text{BLOCK I} \cap \overline{\text{BLOCK II}}\}\right] \times \left[R_A^2 + PR\{\overline{A}_1 \cap A_2\} + PR\{A_1 \cap \overline{A}_2\}\right]$$

Figure 4.4.1-18. Configuration B (Cross Strapping Modulators/ Amplifiers)

Block I denotes success of all elements of Block I; The Sign Block I means that at least one element in Block I has failed.

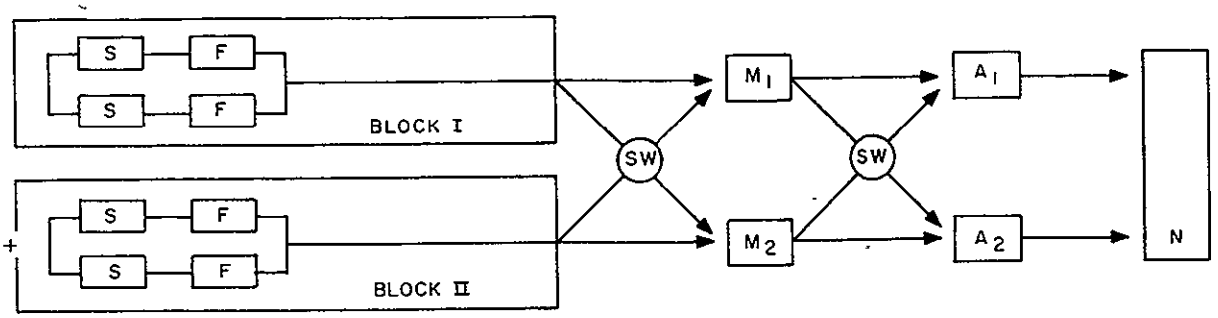

$$PR\{G\} = PR\{\text{BLOCK I} \cap \text{BLOCK II}\} R_M^2 R_A^2 R_{SW}^2 R_N^2$$

$$PR\{GUD\} = R_N^2 R_{SW}^2 \left[PR\{\text{BLOCK I} \cap \text{BLOCK II}\} + PR\{\text{BLOCK I} \cap \text{BLOCK II}\} + PR\{\text{BLOCK I} \cap \text{BLOCK II}\}\right] \times \left[R_M^2 + PR\{\bar{M}_1 \cap M_2\}\, PR\{M_1 \cap \bar{M}_2\}\right]\left[R_A^2 + PR\{A_1 \cap \bar{A}_2\} + PR\{\bar{A}_1 \cap A_2\}\right]$$

Figure 4.4.1-19. Configuration C

The following failure rates were used for the transmitter components.

Failure Rates

F	Filter	$\lambda_F = 0.1 \cdot 10^{-6}$
M	Modulator	$\lambda_M = 8.5 \cdot 10^{-6}$
A	Power Amplifier (TWT)	$\lambda_A = 17.0 \cdot 10^{-6}$
S	Switch	$\lambda_S = 0.02 \cdot 10^{-6}$
N	Antenna	$\lambda_N = 0$

The failure rates are based on:

F - Report ITT on solid-state S-band amplifier
M - Parts Count
A - Data from HAC
S - MIL Handbook - 217A

4.4.1.6.4 Numerical Results

Assuming that data are to be relayed throughout a 1 year mission, let T = 8760 and p = 1 in reliability equations. Recall that G denotes the state in which both data sets may be transmitted simultaneously; D denotes the state in which either may be transmitted upon command, but not simultaneously.

Table 4.4.1-8 shows the results obtained for the three configurations.

TABLE 4.4.1-8

Configuration	Pr (G)	PR (G Ω D)	Pr (D)
A	0.7821	0.9970	0.2149
B	0.7821	0.9983	0.2162
C	0.7820	0.9982	0.2162

Conclusion: The above numbers show that significant advantage can be realized in configuration (B) with one cross strapping switch. This configuration is, therefore, selected.

4.4.1.7 Wideband FM Modulator

4.4.1.7.1 Requirements

The downlink data requirements of the MSS and RBV payloads can be satisfied by a single frequency modulator having the following performance characteristics:

1. Center frequency: 2229.5 or 2265.5 MHz, selectable by command
2. Frequency stability: ±0.005% for 25° ±20°C temperature variation and sinusoidal modulation applied
3. Output power: 0.5 watts
4. Deviation range: ±6 MHz
5. Modulation response - dc: 10 MHz ±0.5 dB, 15 MHz ±3 dB
6. Modulation sensitivity: - 10 MHz/volt ±6 dB adjustable
7. Spurious outputs: 68 dB down from output level
8. Intermodulation: 40 dB down from full deviation

4.4.1.7.2 Study Tasks

The following tasks are covered in detail.

1. Survey of available hardware
2. Tradeoff, analysis, and tests of preferred approach.

4.4.1.7.2.1 Survey Of Available Hardware

Table 4.4.1-9 indicates the vendors surveyed, their present capability, response to ERTS specifications, and technical approach.

Because no vendor has advanced beyond the breadboard stage of equipment designed for the ERTS requirement, the selection of the hardware will be based upon the technical merit of the proposed design approach. This tradeoff is given under Task No. 2. Based upon the results of Task No. 2, GE proposes to integrate their preferred design with the video switching, line receivers, and premodulation filters into a single 2/0 assembly, thus greatly reducing cabling. Figure 4.4.1-20 is a block diagram of the redundant modulator and associated signal conditioner. The signal conditioner box contains the video switching, line receivers, buffer amplifiers, digital reconstructer and premodulation filters.

Because no proven modulator designs presently exist, GE plans to continue development work on in-house funds. This effort is scheduled to result in a prototype model by March 1970. It is expected, of course, that potential vendors will do likewise.

TABLE 4.4.1-9. VENDOR SURVEY

Vendor	Flight Hardware	Breadboard	Related Experience	Proposal	Technical Approach
Collins	-	-	-	*	FM Feedback
Cubic	-	-	-	-	
Conic	-	-	*	-	VCO and Crystal
GE/SSO	-	*	*	*	Hetrodyne/AFC
Hughes	-	-	*	-	
ITT	-	*	*	*	VCO and Crystal
Motorola	-	*	*	-	Hetrodyne/AFC
Philco	-	-	-	-	
Spacecraft	-	-	*	*	VCO and VCXO
Teledyne	-	-	*	*	VCO and Crystal
Watkins Johnson	-	-	-	-	Hetrodyne/AFC
RCA	-	-	-	-	
Bendix	-	-	-	-	

4.4.1.7.2.2 Tradeoff, Analysis, and Test on Preferred Approach

Preferred Approach - Heterodyne/AFC

The straightforward approach to meeting the requirements as shown in Figure 4.4.1-21 is to modulate a voltage controlled oscillator (VCO) directly at the required output frequency. Over the small deviation range required, about ±0.3% of output frequency, excellent linearity in the VCO tuning characteristic is easily obtained. A self-excited oscillator, however, is seldom capable of the 0.005 percent stability required. To stabilize the VCO frequency, a frequency control loop using a quartz crystal controlled oscillator and a discriminator at intermediate frequency is used. To prevent degeneration of the low-frequency response of the modulation, modulation components recovered at the output of the IF discriminator are cancelled before the frequency correction voltage is applied to the VCO.

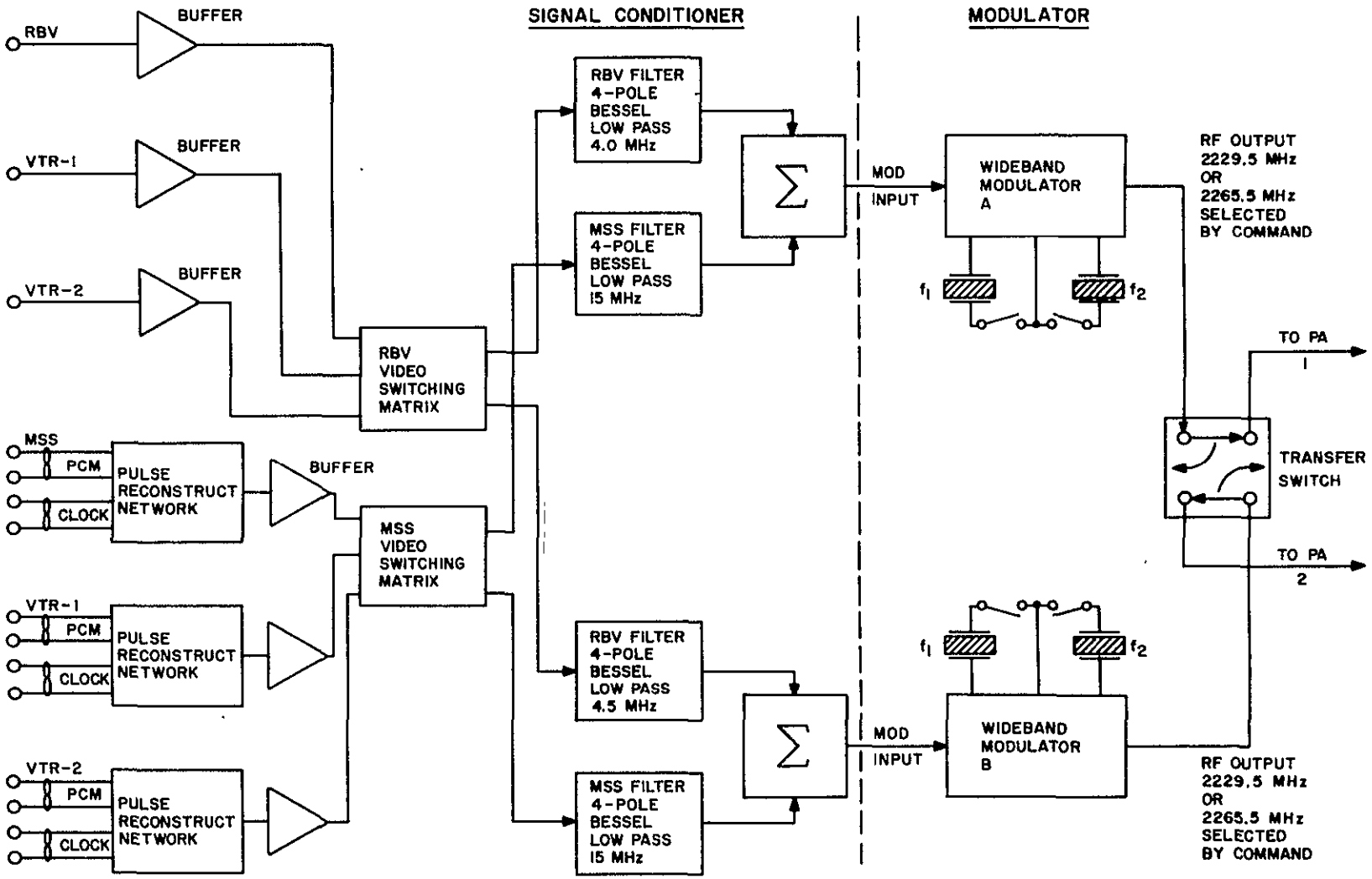

Figure 4.4.1-20. Recommended Frequency Modulator and Signal Conditioner

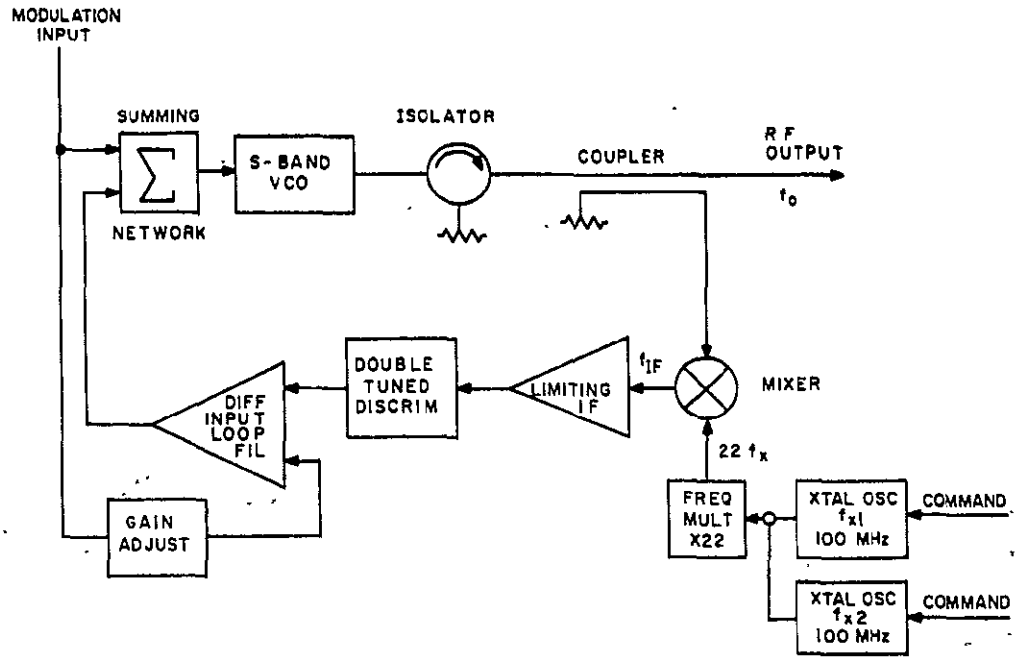

Figure 4.4.1-21. Block Diagram of Preferred Wideband Modulator

Loop Analysis

Referring to Figure 4.4.1-22, the output of the loop $F_o(S)$ is given by:

$$F_o(S) = E_V(S) + K_v \left\{M(S) + K_1 H(S) \left[K_2 M(S) + K_D (F_R - F_o(S)\right]\right\}$$

$$F_o(S) \left[1 + K_V K_1 K_D H(S)\right] = F_V(S) + K_V M(S)$$

$$+ K_V K_1 K_2 H(S) M(S)$$

$$+ K_V K_1 K_D H(S) F_R$$

Let

$$F_V(S) = F_R + F_e(S)$$

$$F_o(S) = F_R + \frac{K_V (1 + K_1 K_2 H(S)) M(S) + F_e(S)}{1 + K_1 K_V K_o H(S)}$$

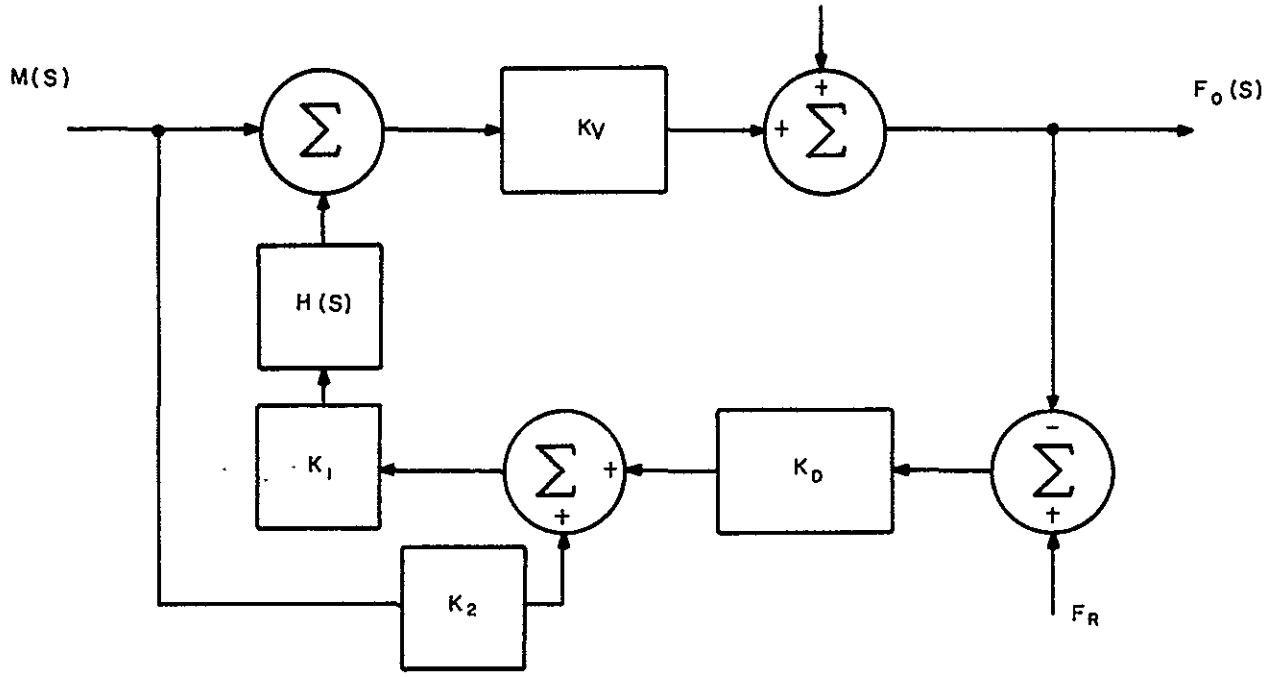

Figure 4.4.1-22. Loop Analysis Model

M(S) - Modulation input

$F_V(S)$ - Open loop frequency of VCO, Including both long and short term instabilities

$F_o(S)$ - Loop output frequency

F_R - Loop reference frequency

K_V - VCO modulation sensitivity in MHz/volt

K - Discriminator gain constant in volt/MHz

$K_1 H(S)$ - Loop filter response function. Typically:

$$H(S) = \frac{1}{1 + S\tau}$$

K_2 - Gain of modulation cancellation circuit

The function $F_e(S)$ represents excursions, both long and short term, from the nominal value F_R of the VCO open loop frequency. The loop reference frequency F_R is 22 F_X - F_{IF} where F_X is the basic crystal oscillator frequency and F_{IF} is the loop intermediate frequency.

The center frequency of the loop ($F_o(S)$ for M(S) = O) depends on F_R, $F_e(S)$, and the loop parameter $K_V K_D K_1$, which is the dc open loop gain. When modulation is applied, no shift in center frequency should occur, but in practice nonlinearities in the voltage/frequency characteristic of the S-band VCO causes center frequency shift. This shift, due to even order nonlinearities (square law, fourth-power law, etc.), is corrected by the control loop and may be viewed as a component of $F_e(S)$. Carrier shift is also caused by nonlinearity in the discriminator. These nonlinearities represent a slight offset in the IF frequency, and are corrected by the control loop.

$$\Delta f_o = \Delta f_R + \frac{\Delta f_e}{1 + K_{OL}}$$

$$= 22\ \Delta f_X - \Delta f_{IF} + \frac{\Delta f_e}{1 + K_{OL}}$$

$$K_{OL} = K_V K_D K_1$$

The values of Δf_X and Δf_e are know. Assuming K_{OL} = 1000, the value of Δf_{IF} can be computed, and a determination can be made as the feasibility of the calculated Δf_{IF}.

$$\left.\begin{aligned} \Delta f_X &= 0.001\% \\ \Delta f_e &= 1\% \end{aligned}\right\} \text{ Long-term drift}$$

$$\Delta f_e = 1\% \qquad \text{Non linearity}$$

$$\Delta f_{IF} = 0.005\%\, f_o - 22\ (0.001\%)\, f_X + \frac{2\%\ f_R}{1 + K_{OL}}$$

Assume

$$f_o \simeq 22\, f_X \simeq f_R$$

$$\frac{\Delta f_{IF}}{f_R} \simeq 0.002\%$$

$$\frac{\Delta f_{IF}}{f_{IF}} = \frac{2.200}{70}\ (0.002\%) = 0.064\%$$

The IF instability allocation of 0.064 percent f_{IF} is allocated 0.04 percent long-term instability and 0.024 percent center frequency shift.

In summary, the total instability of 0.005 percent for the wideband modulator dictates the following frequency stabilities of loop components:

1. Long-term drift/no modulation:
    a. VCO open loop frequency: ±1 percent f_R
    b. Crystal controlled source: ±0.001 percent f_R
    c. Center frequency of IF discriminator: ±0.040 f_{IF}
2. Modulation applied:
    a. VCO nonlinearity: ±1 percent f_R
    b. Discriminator nonlinearity: ±0.024 percent f_{IF}

In giving experimental results for the various components of the frequency loop, these requirements are compared with measured quantities.

4.4.1.7.3 Alternative Approaches

Figure 4.4.1-23 shows five alternative modulator configurations, along with the preferred design just described in detail. Each of these designs is intended to provide wide deviation frequency modulation while maintaining the center frequency stability of a crystal-controlled source.

Figure 4.4.1-23(a) is a generalized version of the selected configuration (heterodyne/AFC) in which the AFC loop operates on a VCO at a subharmonic of the desired output frequency. The frequency multiplier produces an output at the final output frequency. It is also possible to perform all the required power amplification at f_o/N and multiply to f_o at the output stage of the transmitter. This configuration offers no advantages in terms of linearity or modulation response over the selected design. At one time, when transistors for the S-band region were incapable of reasonable power output at good efficiency, the design of Figure 4.4.1-23(a) was optimum. At present, however, the availability of S-band transistors for oscillator service indicates that the design of Figure 4.4.1-23(a) is optimum for N = 1. The need for a frequency multiplier is eliminated resulting in decreased size, weight and complexity, while maintaining efficiency.

Figure 4.4.1-23(b) (VCO and Crystal) is related to Figure 4.4.1-23(a) in the sense that it uses a fixed crystal-controlled course to determine the output frequency. Frequency instabilities of the VCO like those of the IF discriminator, are scaled down in importance, since they are added to a stable frequency of relatively large magnitude.

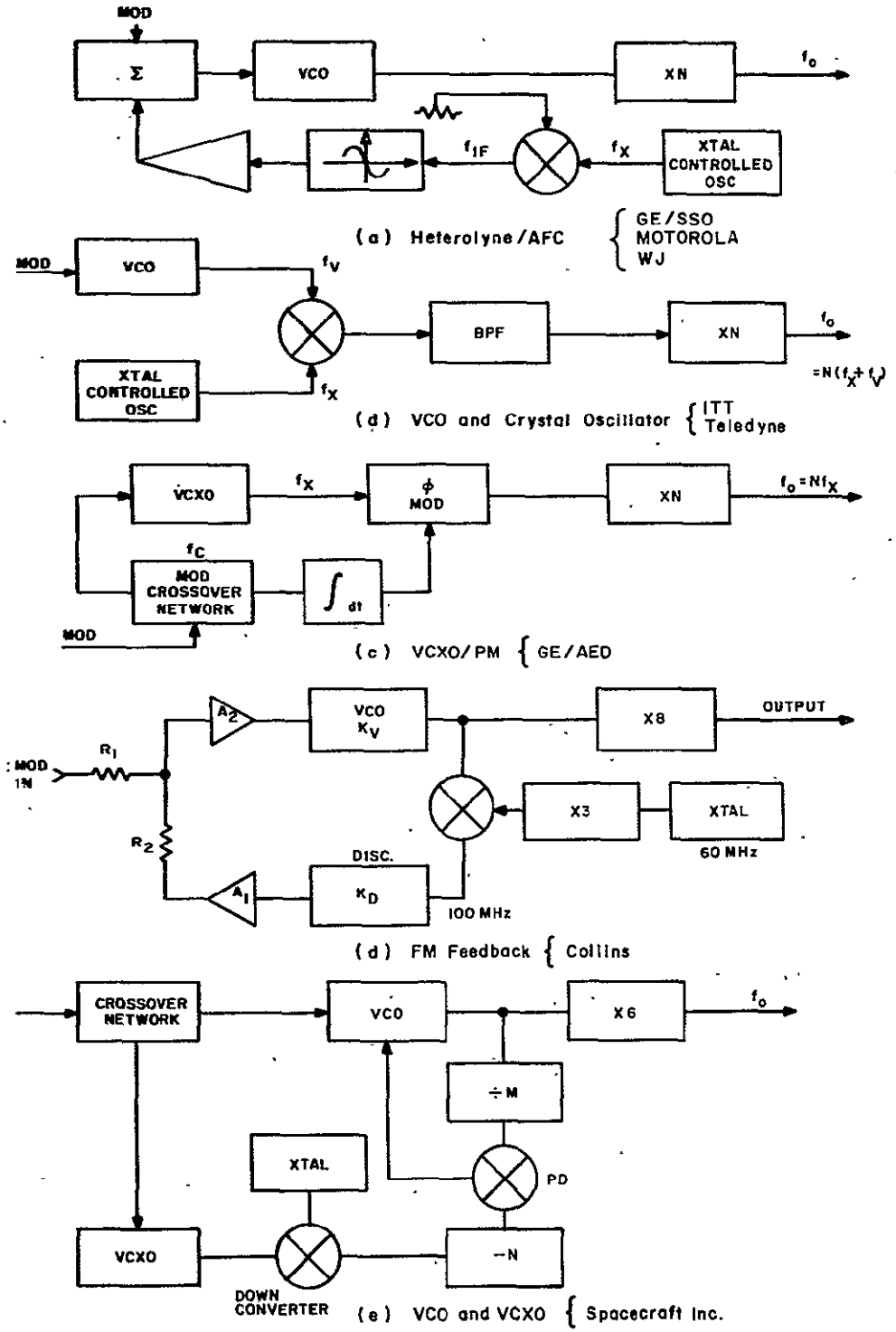

Figure 4.4.1-23. Alternative Configurations

To maximize frequency stability, then, it is desirable to make f_X as large as possible, while making f_V as small as possible. On the other hand, the VCO must be capable of linear deviation over $\Delta f_o/N$, and this criterion dictates that f_V be made as large as possible, consistent with frequency stability requirements. As an example:

$$f_o = 2200 \text{ MHz}$$

$$\Delta f_o = \pm 6 \text{MHz}$$

$$\Delta f_V/f_V = \pm 0.1 \text{ for 1-percent linearity}$$

$$f_V \text{ min} = 60 \text{ MHz if } N = 1$$

If the frequency stability of the output is to be 0.005 percent and $\delta f_X = 10^{-5} f_X$

$$5 \times 10^{-5} f_o = 10^{-5} f_X + \delta f_V$$

$$\delta f_V \simeq 4 \times 10^{-5} f_o = \frac{4 \times 10^{-5}}{60} \times 2250 f_V$$

$$\delta f_V \simeq 1.2 \times 10^{-3} f_V$$

The 60-MHz must have a frequency stability of 0.1 percent over its temperature range. This combination of modulation linearity and long term stability is not typically available. A standard VCO available off-the-shelf has ±5-percent linearity over a ±10-percent deviation, and 0.2-percent stability for temperatures of 0°C to 50°C.

ITT, however, has succeeded in achieving good linearity by using the new low frequency hyperabrupt varactors. Their Design Study Report, TD C69-59, dated 16 September 1969 indicates that they have achieved 0.2-percent linearity for a deviation of ±2.25 MHz at 250 kHz. The use of such a low VCO frequency, however, makes it impossible to separate the VCO frequency from the modulation input frequency without unacceptable frequency and phase distortion.

An additional problem arises in selecting the desired product at the output of the mixer. A microwave filter with a normalized bandwidth of 1 percent or less is required, and it must have excellent skirt selectivity to reject undesired conversion products.

The difficulty of obtaining an appropriate VCO and the formidable filtering problem make this approach unattractive.

In Figure 4.4.1-23(c) we show an interesting approach to the problem (VCXO/PM). It combines a voltage-controlled crystal oscillator (VCXO) and a phase modulator. The

long-term stability of the modulator is influenced by the VCXO alone, and the 0.005-percent goal is easily realized.

The VCXO is modulated by frequencies below the corner (f_c) of the crossover network. Frequencies above f_c are passed through an analog integrator and applied to a phase modulator.

The upper bound on f_c is the lowest modulating frequency at which spurious nodes are produced by the VXCO. Spurious nodes typically occur for modulating frequencies around 300 kHz.

The frequencies around f_c produce maximum phase deviation in the phase modulator. Higher frequencies are attenuated by the integrator circuit. The phase modulator may be assumed 1 percent linear for ±1.25 radians. The frequency deviation Δf at any modulating frequency f_M is:

$$f = \Delta \phi f_M = \pm 1.25 f_M$$

$$\Delta f = 6 \times 10^6 \text{ Hz at 2250 MHz}$$

$$\text{IF } f_X \simeq \frac{1}{30} (2250) \text{ MHz}$$

$$\Delta f = \pm 2 \times 10^5$$

$$f_C = \frac{2 \times 10^5}{1.25} \simeq 160 \text{ kHz}$$

The frequency deviation capability of the VCXO must then be ±200 kHz, which is 0.3 percent.

The problems with this approach are numerous. To obtain a VCXO with 0.3-percent deviation capability and 0.005-percent stability would require an additional crystal-controlled down conversion. There are problems in ensuring a smooth modulation response in the region of f_c. Finally, there is a requirement for high order frequency multiplication.

Figure 4.4.1-23(d) shows an approach proposed by Collins (FM feedback). The scheme is similar to 4.4.1-23(a) except that wideband feedback is used. The wideband feedback will linearize the VCO characteristic reducing distortion, incidental FM, and gain phase variations in the modulation baseband.

This approach suffers from practical limitations. Collins neglected to show: (1) how the IF frequency could be removed from the discriminator output without violating the phase/gain stability criterion (they are especially severe when one requires flat response in addition to stability) and (2) how circuit delay could be held to acceptable limits to allow flat response to 10 MHz.

Figure 4.4.1-23(e) shows Spacecraft, Incorporated's approach (VCO + VCXO). In this approach a VCO is phase-locked to a crystal oscillator. Low frequency modulation would normally be impossible because of the increasing phase excursion at the phase detector with decreasing frequency. This is overcome by also modulating the crystal at low frequency rates. The VCXO is down converted prior to being used as a reference in order to increase its percentage deviation. The xM and xN dividers are necessary in order to reduce the phase deviation into the phase detector. This approach is capable of satisfying the ERTS requirements, but it is far too complicated.

In summary, it appears that of the methods examined, the IF discriminator offers the simplest approach to satisfying the requirements. At present, it is possible to operate the modulator directly at the required output frequency, thus eliminating frequency multiplication.

4.4.1.7.4 Implementation

The breadboard model of the Wideband Frequency Modulator used (as much as possible) components on-hand at the beginning of the Phase B/C study. A voltage-controlled oscillator operating at S-band and a ferrite isolator were available from an in-house development program. A coaxial directional coupler of the type commonly used for microwave measurements was also used. A broadband mixer was purchased.

The following components of the modulator were designed and breadboarded in-house:

1. Crystal oscillator/buffer
2. Step recovery diode multiplier
3. Amplitude limiter
4. Double-tuned discriminator
5. Loop filter/modulator cancellation circuit

Of these, the limiter, discriminator, and loop filter circuits are most important.

4.4.1.7.5 Discriminator

The double-tuned discriminator is designed according to the method developed by Fancourt and Skwerzinski, and published by them in the Marconi Review in 1956. Their method for linearizing the discriminator characteristic is to choose the components of each tank circuit such that the square and cubic terms of the power series expansion vanish. Figure 4.4.1-24 shows the generic circuit with which we are dealing.

The discriminator consists of two amplifiers, each having an untuned input and tuned output. The voltages developed at the outputs of these amplifiers are rectified and added out of phase. The tuned circuits are tuned to different frequencies; the result is an input frequency/output voltage characteristic of the classic "S" shape. By adjusting the peak-to-peak separation, the tuned circuit Q's, and the relative magnitudes of the peaks, the central portion of the "S" curve can be linearized.

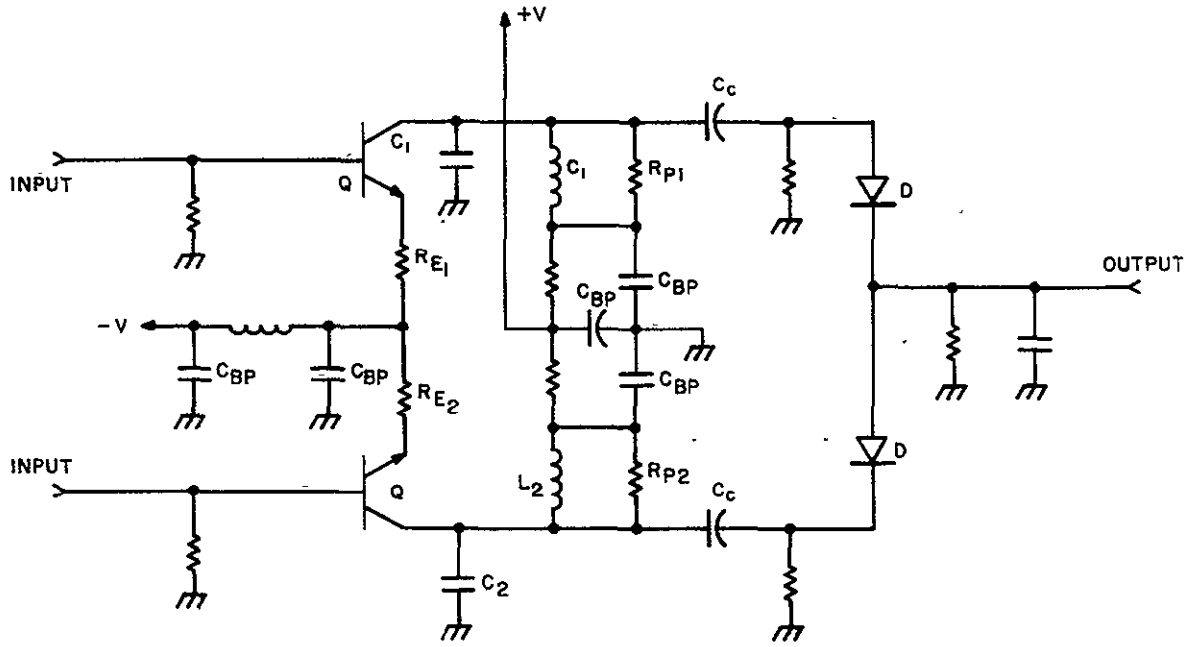

Figure 4.4.1-24. Double-Tuned Discriminator

Let f_o be the center frequency of the discriminator and f_1, f_2 the upper and lower peak frequencies, respectively. The output voltage V_o (f), where f is the input frequency is:

$$V_o(f) = \left\{ [Z, (f)] - [Z_2 (f)] \right\} g_m V_I$$

$$Z_1(\omega) = \frac{1}{\frac{1}{R_{P1}} + j\,\omega C_1 - \frac{j}{\omega L_1}}$$

$$Z_2(\omega) = \frac{1}{\frac{1}{R_{P2}} + j\,\omega C_2 - \frac{j}{\omega L_2}}$$

This expression assumes equal transconductance g_m of each amplifier and equal input signals $V_i \sin \omega t$.

Substituting

$$\frac{1}{L_1} = \omega_1^2 C_1$$

into the expression for Z

$$Z_1(\omega) = \frac{1}{\frac{1}{R_{P1}} \quad j\,\omega_1\,C_1\left[\frac{\omega}{\omega_1} - \frac{\omega_1}{\omega}\right]}$$

$$= \frac{R_{P1}}{1 \quad j\ \omega_1\,C_1\,R_{P1}\ \left[\frac{\omega}{\omega_1} - \frac{\omega_1}{\omega}\right]}$$

and likewise for $Z_2(\omega)$

$$Z_2(\omega) = \frac{R_{P2}}{1 + j\ \omega_2\,C_2\,R_{P2}\ \left[\frac{\omega}{\omega_2} - \frac{\omega_2}{\omega}\right]}$$

We recognize

$$W_1\,C_1\,R_{P2} = Q_{P1}$$

$$W_2\,C_2\,R_{P2} = Q_{P2}$$

Let

$$X_1 = Q_{P1}\left(\frac{\omega}{\alpha_1\,\omega_o} - \frac{\alpha_1\,\omega_o}{\omega}\right)$$

$$X_2 = Q_{P2}\left(\frac{\omega}{\alpha_2\,\omega_o} - \frac{\alpha_2\,\omega_o}{\omega}\right)$$

$$Z_1(\omega) = R_{P1}\left(1 + X_1^2\right)^{-1/2}$$

$$Z_2(\omega) = R_{P2}\left(1 + X_2^2\right)^{-1/2}$$

$$V_o(\omega) = g_m\,V_i\,R_{P1}\left[\left(1 + X_1^2\right)^{-1/2} - \frac{R_{P2}}{R_{P1}}\left(1 + X_2^2\right)^{-1/2}\right]$$

$$\frac{R_{P2}}{R_{P1}} = h$$

In theory, by appropriate choice of α_1, α_2, Q_1, Q_2 and h, linearity about ω_o may be optimized in the sense that square and cube law nonlinearities are reduced to zero. The parameters α_1, α_2, Q_1, Q_2 and h completely define the discriminator output response when normalized with respect to ω_o. One of these parameters may be chosen by the designer. The rest of the parameters are determined by the linearity optimization procedure of Fancourt and Skwerzinski.

The value of α_1 is chosen by applying the linearity requirement on the discriminator. The best case linearity is related to the magnitude of the fourth and fifth power terms of the power series expansion of V_o. Let Δ be an incremental departure from the discriminator center frequency ω_o.

$$v = \frac{\Delta}{\omega_o} = \frac{\omega - \omega_o}{\omega_o}$$

$$V_o(v) = g_m V_i R_{P1} \left[K_1 v + K_2 v^2 + K_3 v^3 + K_4 v^4 + K_5 v^5 + \ldots \right]$$

But $K_2 = 0$ and $K_3 = 0$ due to linearity optimization

Fancourt and Skwerzinski have plotted curves of K_4/K_2 and K_5/K_1 for various values of α_1 and the associated optimum values of α_2, Q_1, Q_2 and h_1. We concentrate on the fourth power term $K_4 v^4$. This term yields a dc term when $v = v(t) = v_{max} \sin \omega t$. The dc term is $3/8\ K_4 v^4{}_{max}$. The quantity v_{max} represents the normalized incremental maximum deviation from ω_o (in a given application). It was previously determined that an incremental dc shift of $0.00024\ \omega_o$ was tolerable

$$\frac{3}{8} \frac{K_4}{K_1} v^3_{max} = 2.4 \times 10^{-3}$$

The IF is 70 MHz, and the maximum deviation 6 is MHz

$$v_{max} = 8.6 \times 10^{-2}$$

$$v^3_{max} = 630 \times 10^{-6} = 6.3 \times 10^{-4}$$

$$\frac{K_4}{K_1} = \frac{8}{3} \times \frac{2.4 \times 10^{-3}}{6.3 \times 10^{-4}} = \frac{0.8}{0.8} \times 10 = 10$$

The value of α_1 corresponding to K_4 = 10k is 1.15. This value of α_1 is the smallest value consistent with the dc shift criterion. To get some idea of a more reasonable value let us attribute 25 percent of the total dc shift to fourth power nonlinearities

$$3/8 \frac{K_4}{K_1} v^3_{max} = 6 \times 10^{-4}$$

$$\frac{K_4}{K_1} = \frac{8}{3}$$

The value of α_1, corresponding to $K_4 = 3/8\ K$, is about 1.3. The double-tuned discriminator designed for this application has $\alpha_1 = 1.3$.

The parameters corresponding to α_1, = 1.300 are as follows:

$\alpha_2 = 0.7769$

$Q_1 = 2.703$

$Q_2 = 2.124$

$h = 0.8433$

For the IF of 70 MHz:

$f_o = 70$ MHz

$f_1 = 91.000$ MHz; $f_2 = 54.383$ MHz

The LC constants are:

$L_1 C_1 = 3.0588$ PF - μ H

$L_2 C_2 = 8.5647$ PF - μ H

We also have the relationship

$$\frac{R_{P2}}{R_{P1}} = h = \frac{Q_2 \alpha_1 C_1}{Q_1 \alpha_2 C_2}$$

$$\frac{C_2}{C_1} = \frac{1}{h} \frac{Q_2 \alpha_1}{Q_1 \alpha_2} = \frac{(2.124)(1.300)}{(0.843)(2.703)(0.777)}$$

$$\frac{C_2}{C_1} = 1.560$$

Letting

$$C_2 = 10 \rho F, \quad C_1 = 6.41 \text{ PF}$$

$$L_2 = 0.856, \quad L_1 = 0.476 \text{ hH}$$

$$P_{P2} = 758 \ \Omega, \quad R_{P1} = 896 \ \Omega$$

The discriminator design has not yet been subjected to temperature tests; however, a first-order prediction of thermal effects can be made. To a first approximation, the center frequency of the discriminator changes with the resonant frequencies of the two tank circuits. The center frequency stability 0.04 percent previously allocated must be satisfied over a ±20°C excursions from the 25°C nominal. Thus, the tank circuit frequencies are allowed a maximum termperature coefficient of ±0.002 percent/°C or 20 parts per million (ppm) per °C. Typical capacitors and inductors have temperature coefficients of ±25 to ±50 ppm/C. The fractional frequency deviation f/f_o of a parallel circuit is

$$\frac{\Delta f}{f_o} = -\frac{1}{2} \frac{\Delta L}{L} - \frac{1}{2} \frac{\Delta C}{C}$$

If inductors and capacitors having temperature coefficients which tend to cancel are chosen, the center frequency stability requirement is realizable.

4.4.1.7.6 Limiter

It is desirable to precede the frequency discriminator with an amplitude limiter. The limiter serves to prevent variations in IF signal level from influencing the performance of the discriminator. We have seen that the discriminator gain constant is proportional to the peak value of the input voltage. The basic limiter stage is an emitter coupled pair of transistors with a dc current source providing common-mode emitter biasing. Limiting action is achieved by adjusting the total bias current to a value insufficient to saturate either transistor

in the differential pair. Positive peaks of the output voltage are thus limited by cutoff, while negative peaks are limited by the current supply. A typical stage is shown in Figure 4.4.1-25 with the collector characteristic of one amplifier.

The small signal model of the differential amplifier is the same as for a single transistor.

The limiter designed for this application has two stages. Resistors in series with the emitters of the differential transistors have been used to stabilize the transconductance of the stage over the frequency range of interest. The transistor in use for breadboard purposes is the RCA 2N5179. Its small signal admittance parameters at 50 MHz and 100 MHz are:

	50 MHz	100 MHz
y_{ie}	$1 + j3$	$1 + j5$
y_{re}	$-j0.15 \times 10^{-3}$	$-j0.30 \times 10^{-3}$
y_{fe}	$50 - j8$	$47 - j18$
y_{oe}	$j0.5$	$j1.0$

The adjusted admittance parameters when an emitter resistor of R_E ohms is added are:

$$y_{11} = \frac{y_{ie} + \Delta y \; R_E}{1 + R_E \; \Sigma \; y_e}$$

$$y_{12} = \frac{y_{re} - \Delta y \; R_E}{1 + R_E \; \Sigma \; y_e}$$

$$y_{21} = \frac{y_{fe} - \Delta y \; R_E}{1 + R_E \; \Sigma \; y_e}$$

$$y_{22} = \frac{y_{oe} + \Delta y \; R_E}{1 + R_E \; y_e}$$

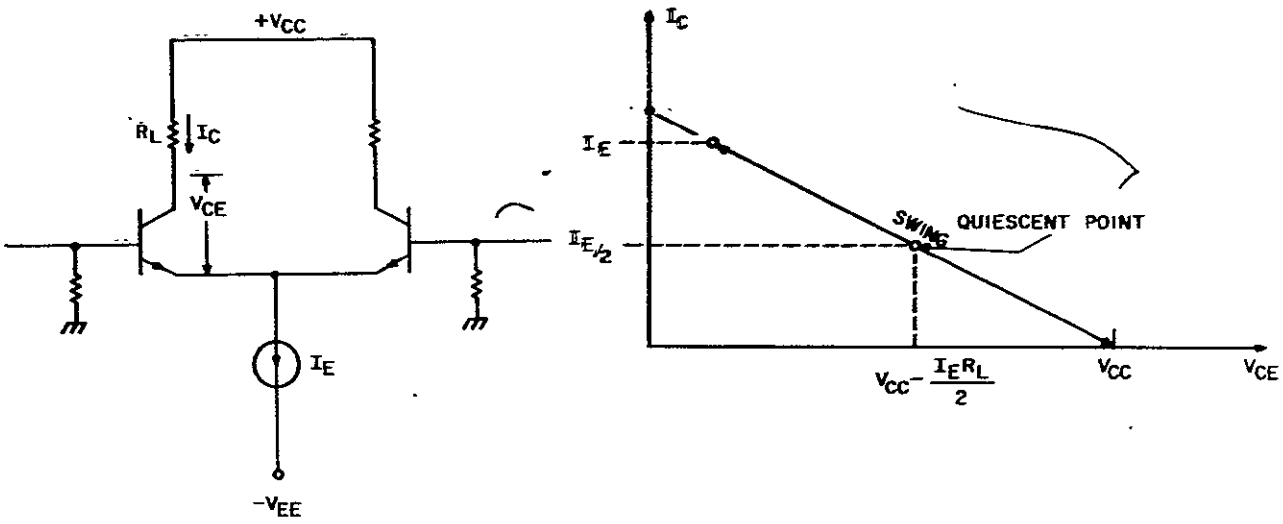

Figure 4.4.1-25

The corresponding numerical values for the 2N5179 with R_E = 100 ohms are 2N5179's with:

	50 MHz	100 MHz
y_{11}	0.64 $\angle 79.6°$	1.12 $\angle 93.3°$
y_{12}	0.156 $\angle -85.6°$	0.305 $\angle -78°$
Y_{21}	8.3×10^{-3} $\angle 5.6°$	8.65×10^{-3} $\angle -10.5°$
Y_{22}	0.21 $\angle 94.4°$	0.42 $\angle 102°$

Cascading two identical stages with an interstage admittance Y_1 and load admittance Y_2, we obtain the following voltage gain expression:

$$A_V = \frac{y_{21}^2}{(y_{22} + Y_L)(y_{11} + Y_1 + y_{22}) - y_{21}\, y_{12}} \qquad Y_1 = 2 \text{ mmhos}$$

The load Y_L is the input admittance of the double-tuned discriminator. To a first approximation $Y_L = y_{11} + 2$ mmhos, since the discriminator transistors are also 2N5179's with $R_E = 100\ \Omega$

$$A_V = \frac{y_{21}^2}{\left(y_{11} + y_{22} + 2 \text{ mmhos}\right)^2 - y_{12} y_{21}}$$

If a tuning inductor B_1 is added at the interstage the result is:

$$A_V^1 = \frac{y_{21}^2}{\left(y_{11} + y_{22} + 2 \text{ mmho}\right)^2 - j B_L \left(y_{11} + y_{22} + 2 \text{ mmho}\right) - y_{12} y_{21}}$$

where

$$B_L = \frac{1}{\omega_L}$$

choose B_L so as to make the denominator of A_V^1 purely real at 70 MHz. We make the approximation that:

$$y_{12} y_{21} \simeq - j \omega C_f$$

$$I_m \left[\left(y_{11} + y_{22} + 2\right)^2 - jB_L \left(y_{11} + y_{22} + 2\right) - y_{12} y_{21}\right]$$

$$= 2 \left(2 + y_{11}\right)\left(b_{11} + b_{22}\right) - B_L \left(y_{11} + 2\right) - \omega C_f$$

$$B_1 = 2 (b_{11} + b_{22}) - \frac{\omega C_f}{2 + y_{11}}$$

$$b_{11} + b_{22} \simeq \frac{f}{100} \text{ x } 1.6 \text{ mmhos}$$

$$\omega C_f = 2.6 \text{ x } \frac{f}{100} \text{ mmhos}$$

$$B_1(70 \text{ MHz}) = 2 (0.7 \text{ x } 1.6) - 0.7$$

$$= 1.5 \text{ mmhos}$$

$$L_1 \simeq 1 \mu H$$

The final circuit design is summarized in Figure 4.4.1-26.

4.4.1.7.7 DC Amplifier/Loop Filter

The dc amplifier is an integrated operational amplifier followed by a summing stage in which the modulation is added to the loop error signal. A circuit diagram is shown in Figure 4.4.1-27.

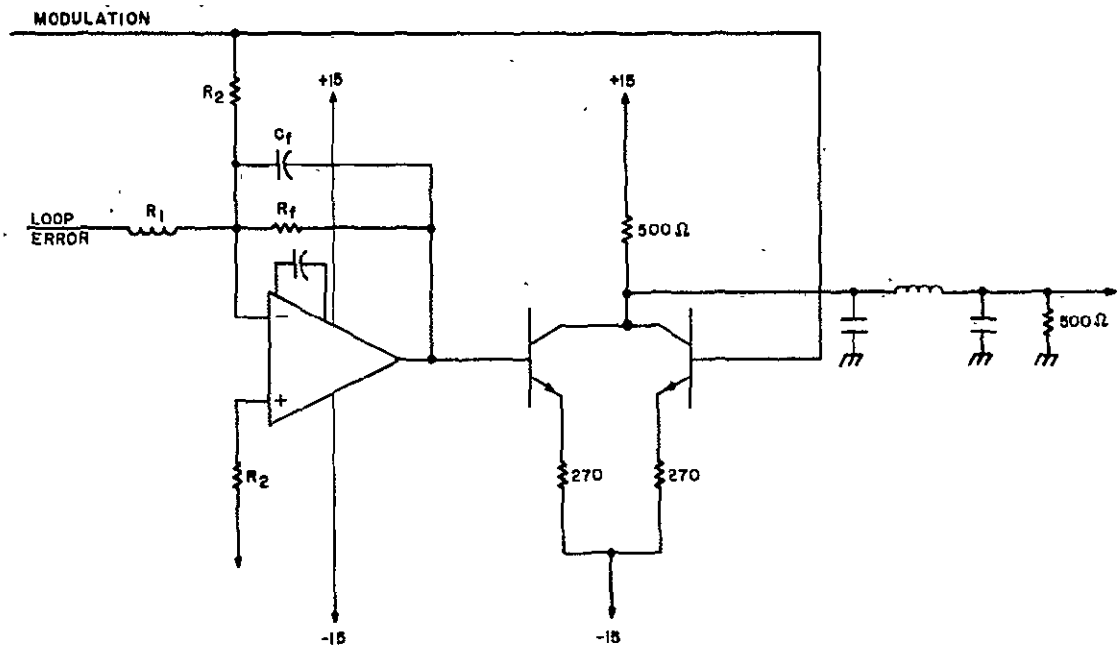

Figure 4.4.1-26. Cascaded Limiter

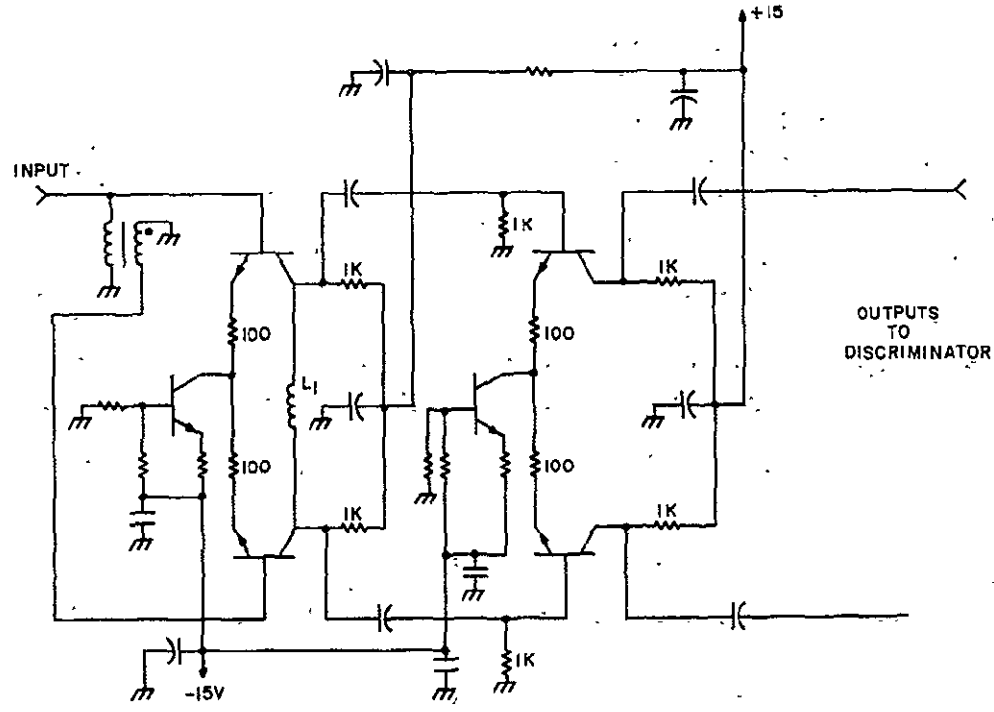

Figure 4.4.1-27. DC Amplifier

Recalling the analysis of the servo loop

$$K_1 = \frac{R_f}{R_1}$$

$$K_2 = \frac{R_1}{R_2}$$

The resistor R_L in series with the non-inverting input of the operational amplifier serves to equalize dc errors due to changes in the input offset current with temperature

$$\frac{1}{R_L} = \frac{1}{R_1} + \frac{1}{R_2} + \frac{1}{R_f} = \frac{1}{R_1} + \frac{1}{R_2}$$

The corner frequency of the active filter is

$$\frac{1}{R_f C_f}$$

The summing junction consists of two common emitter stages (each with transimpedance feedback) working into the same load. The three-pole low pass filter passes modulation but rejects any residual 70 MHz carrier leaking through the operational amplifier.

4.4.1.7.8 Crystal Oscillator/Multiplier

The oscillator is a crystal controlled common base Colpitts circuit as shown in Figure 4.4.1-28. The voltage developed across the collector tank is fed back through the capacitive voltage divider and the crystal to the emitter. The circuit oscillates in the vicinity of the series resonant frequency of the crystal. Tuning of the collector tank is relatively non-critical since the phase response of the crystal resonator is much steeper near resonance than that of the relatively low Q collector tank.

An inductor in parallel with the crystal resonates holder capacitance at the crystal frequency. If this capacitance is not resonated non-crystal controlled oscillations are possible.

The buffer amplifier is biased and tuned so as to produce 100 milliwatts of output at the oscillator frequency.

The frequency multiplier is a step recovery diode multiplier. The circuit is shown in Figure 4.4.1-29. At this writing only a design has been generated and no development work has been performed.

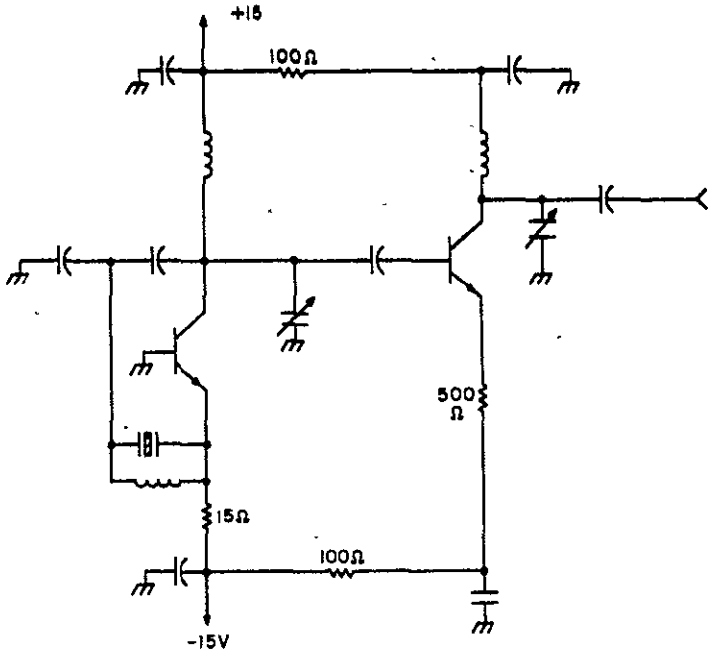

Figure 28. Oscillator Buffer

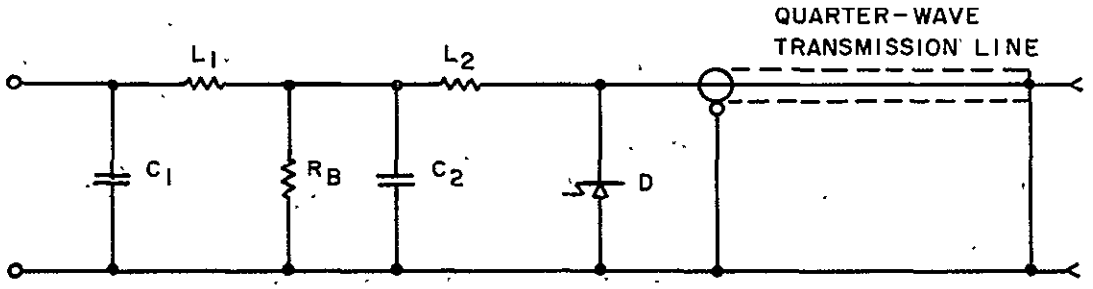

Figure 4.4.1-29. Step Recovery Diode Multiplier

4.4.1.7.9 Voltage Controlled Oscillator (VCO)

A modified VCO was purchased from Omni Spectra for a previous modulator program, and its characteristics are more than adequate when operating with a TWT amplifier.

4.4.1.7.10 Experimental Results

At this writing most of the critical components of the breadboard modulator have been evaluated at room temperature to determine their suitability in the AFC loop. Closed-loop tests have not yet begun. Temperature data is available on the Omni Spectra S-band VCO used in the breadboard.

These experimental results are significant since they establish the feasibility of the GE Design. They are, however, incomplete, and GE plans to continue its in-house development program. A final evaluation will be made by March 1970.

4.4.1.7-11 VCO Performance

Figures 4.4.1-30 and 4.4.1-31 show the tuning characteristics of the S-band VCO. Figure 4.4.1-31 also shows output power level as a function of tuning. The expanded tuning curve shows the excellent linearity to be had in the region of interest. When a power series is written in the form:

$$F_o(v) = K_V v \left(1 + K_2 v + K_3 v^2 + \ldots\right)$$

the square and cube coefficients are of the order of 0.01.

Over the temperature range of interest, -5° to 45°C, open loop frequency varies 3 Mhz and output power 0.5 dB. This variation in temperature is well within the ±1-percent range allocated in the carrier frequency stability budget (see Figure 4.4.1-32).

Modulation response as shown in Figure 4.4.1-33 is flat within 0.5 dB to 18 MHz, exceeding the present requirement.

4.4.1.7.12 Limiter And Discriminator Performance

Figure 4.4.1-34 shows the response of the limiter/discriminator to a sweep frequency input at a power level of -5 dBm. Similar curves result when the power input is lowered to -10 dBm, but the limiter is not fully saturated at that input level. Figure 4.4.1-34(a) shows that the output voltage, input frequency characteristic is relatively smooth from 30 to 110 Mhz, and that there are no polarity reversals other than that at the center frequency. This discriminator should allow initial lock-up of the loop for initial errors of ±20 MHz or more.

Figure 4.4.1-34(c) shows departure from linearity. (The linear component has been subtracted from display.) At 70 ±10 MHz the peak-to-peak error is 0.7 millivolt. The latter

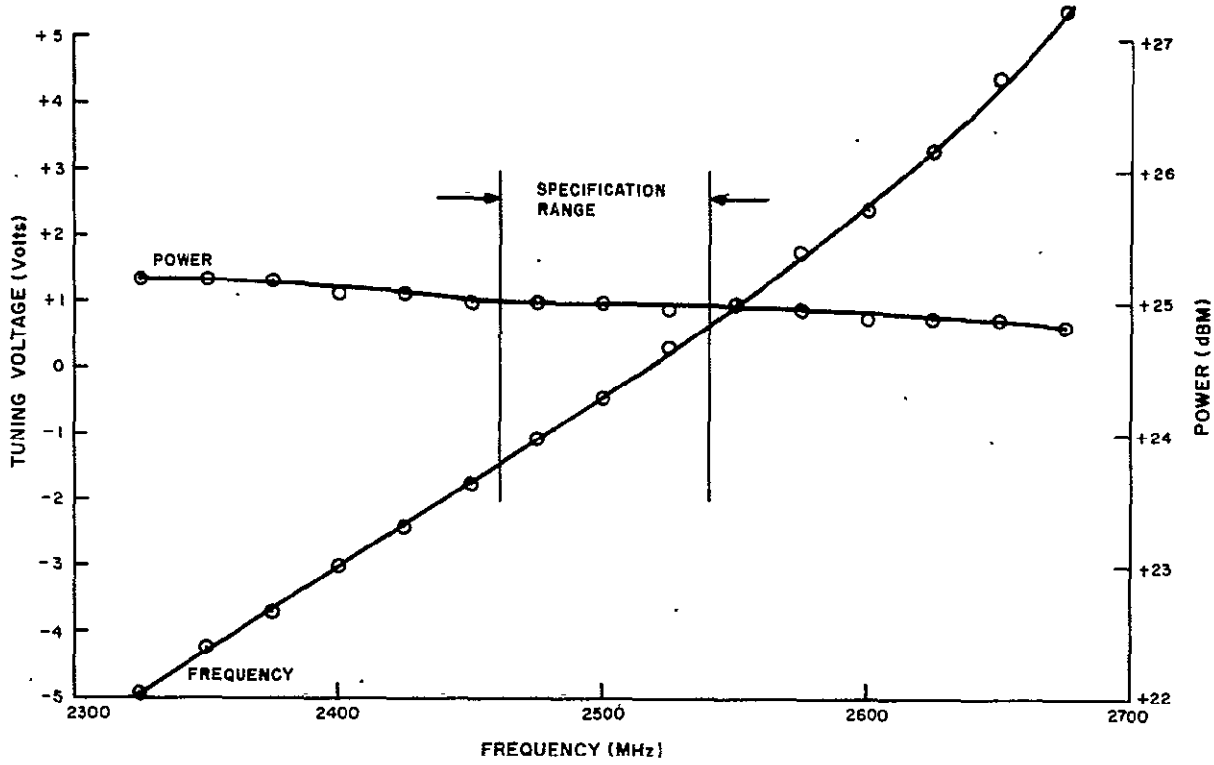

Figure 30. VCO Frequency — Power Versus Tuning Voltage

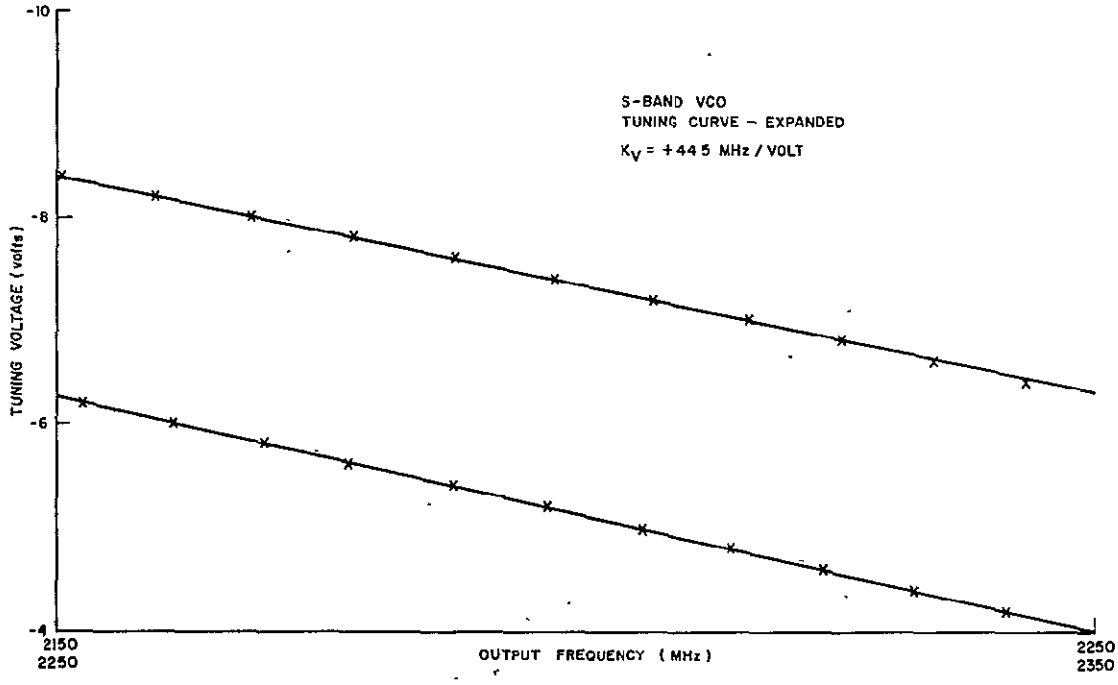

Figure 4.4.1-31. S-Band VCO Tuning Curve — Expanded

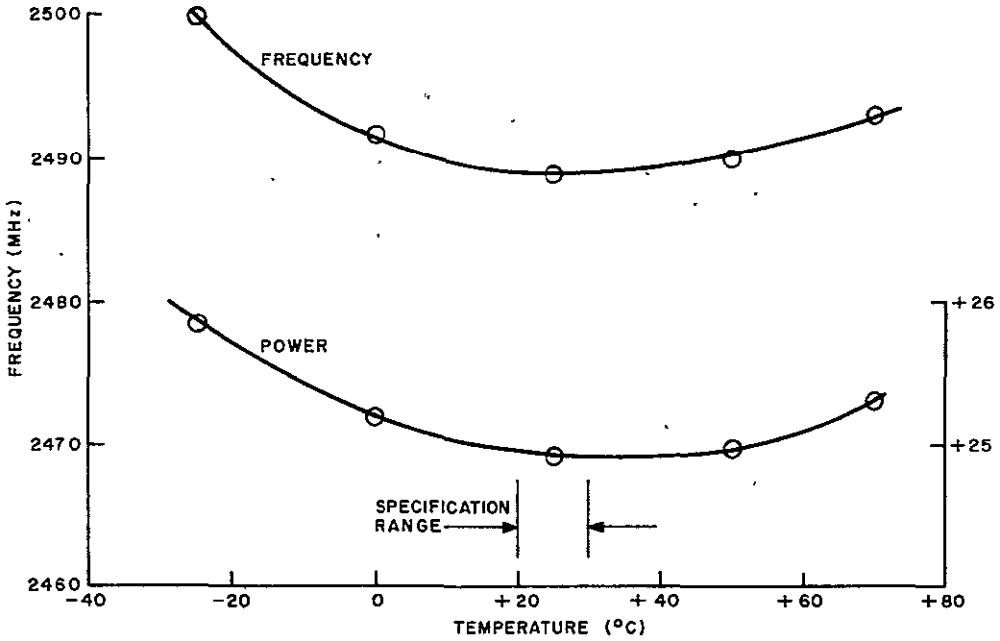

Figure 32. VCO Characteristics Versus Temperature

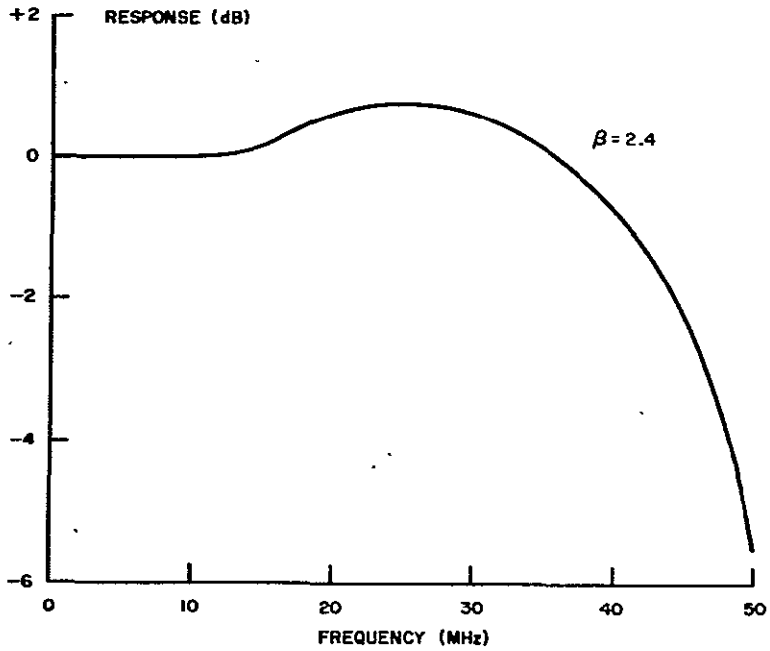

Figure 4.4.1-33. VCO Response

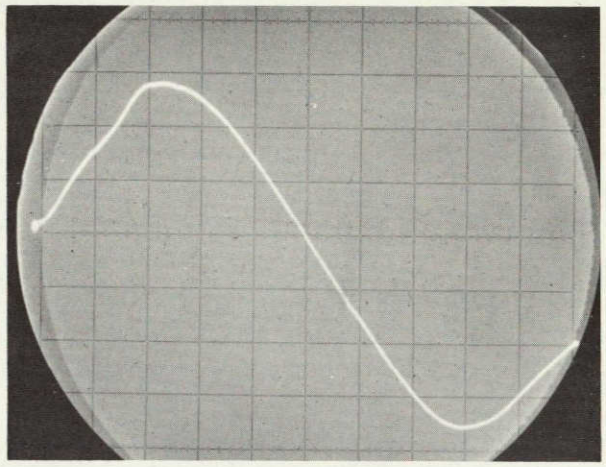

30 TO 110 MHz
SWEEP;
0.1 v/DIV
VERTICAL

A

K_o = -17 mv/MHz

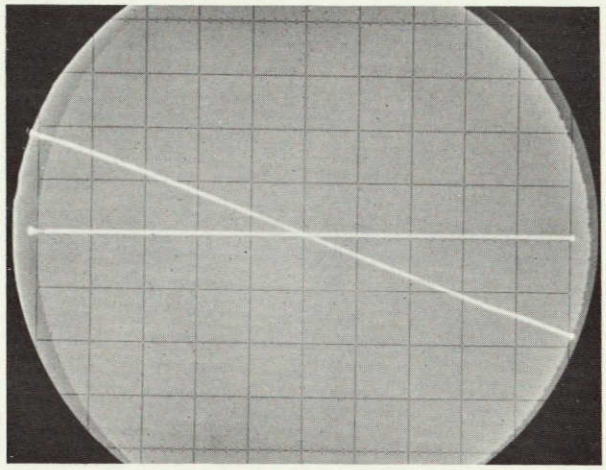

60 TO 80 MHz
SWEEP;
0.1 v/DIV
VERTICAL

B

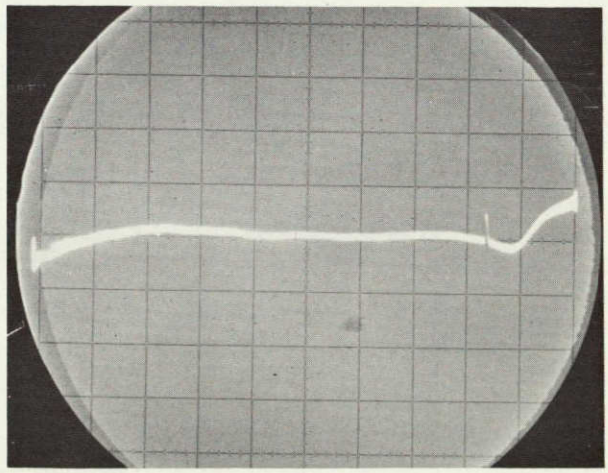

DEPARTURE FROM
LINEARITY;
60 TO 80 MHz
SWEEP;
5 mv/DIV (2.5 %
/DIV) VERTICAL;
MARKERS AT
64 AND 76 MHz

C

Figure 4.4.1-34. Limiter/Discriminator Response

figure corresponds to a linearity of 0.3 percent. Assuming this nonlinearity is square law, the dc shift contribution of the discriminator is well within the 0.18 percent low non-linearities.

4.4.1.7.13 Conclusions

The specified performance of the wideband modulator has not yet been verified, but a detailed analysis of the modulator is complete. Two crucial components of the modulator (and S-Band VCO and a highly linear IF discriminator) have been evaluated at room temperature and have been found to perform better than required to satisfy overall modulator specifications. Temperature data on the VCO shows satisfactory performance from -5° to +40°C.

GE plans to continue the study effort on in-house funds. A prototype modulator is scheduled for completion by March 1970. Analyses and tests performed to date have established that the design presented herein will meet all ERTS requirements.

4.4.1.8 Wideband Power Amplifiers

1. Requirements

Power output	10 and 20 watts min.
Power gain	27 dB min.
Bandwidth (1 dB)	2210 to 2285
Gain slope	±0.2 dB/20 MHz
Group delay variation	5 nsec/20 MHz
AM to PM conversion	15°/dB
Spurious	55 dB below 1 watt
Efficiency	25% min.
Noise figure	30 dB
Size	2/2 max.
Weight	8 lbs. max.
MTBF	100,000 hours

Figure 4.4.1-35 shows the recommended power amplifier design.

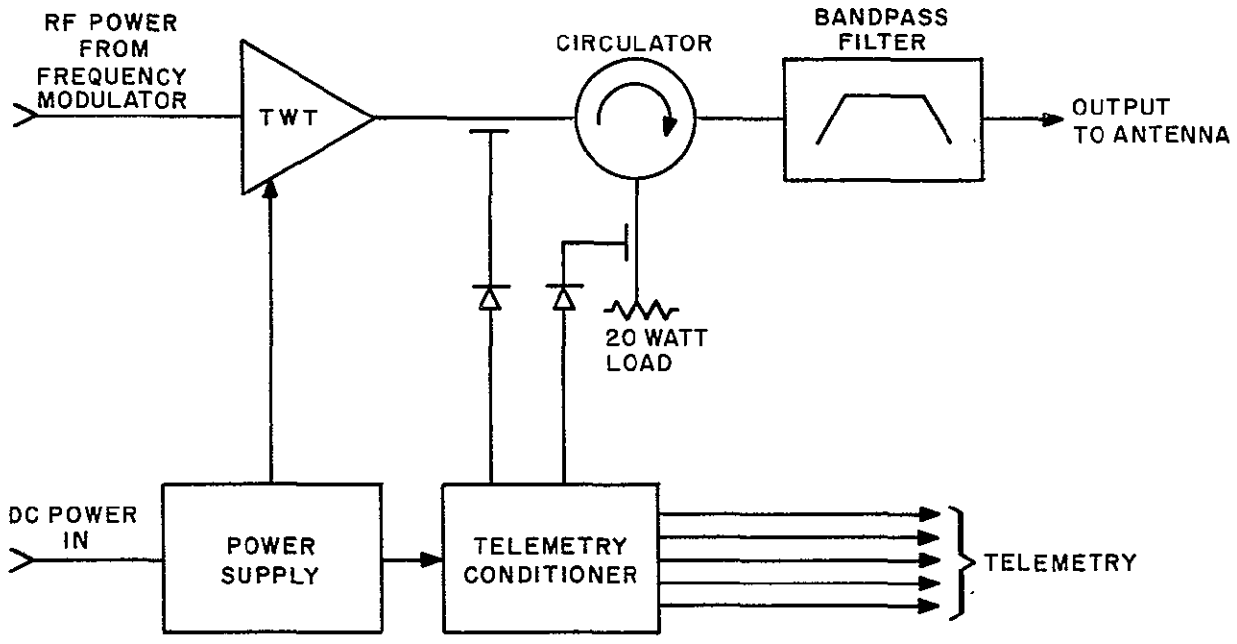

Figure 4.4.1-35. Recommended Power Amplifier Design

4.4.1.8.1 Study Tasks

The following items are covered in detail:

1. Survey of available hardware and synthesis of block diagram
2. Output filter requirements
3. Schematic techniques for dual power outputs.

The most serious requirement of the amplifiers is the need for two output power levels so that spacecraft prime power can be conserved during the majority of the data transfers. This dual power capability necessitates reductions in achievable efficiency and reliability and also increases the transmitter weight. Several techniques are available to accomplish power reduction and these effects are indicated below.

a. Change in Operating Voltages - The output power of both solid state and TWT amplifiers can be varied by voltage changes. In the case of solid state amplifiers this is most easily accomplished by varying the collector supply voltage to the final amplifying stages. This, however, necessitates the use of a power regulator that otherwise would be unnecessary since most manufacturers provide primary power isolation by floating the amplifier stages rather than incurring the loss of a DC to DC converter. Some manufacturers have suggested changing the output power by changing the bias on the output amplifiers. This method involves the risk of unstable operation since the bias of a high efficiency stage becomes more critical as the conduction angle is reduced in order to reduce power. Efficiency also suffers because reduced power is achieved by using a non-optimum conduction angle.

The output power of TWT's is varied by changing the collector voltage and one or more of the other electrode potentials. A tradeoff is involved between efficiency and complexity. Maximum efficiency at the high power mode is only possible if all voltages are changed for each mode. Moderate efficiency, on the other hand, can be obtained from two electrode voltage changes only. Unfortunately, all voltages do not change proportionally, thus adding to the complexity of the power supply.

b. Two Amplifiers Operated Singly or in Parallel - This method achieves higher efficiencies in both modes of operation but requires high power switching and an increase in weight and volume. This is offset partially by the enhanced reliability afforded in the low power mode by the standby redundant tubes. Various output switch configurations are available in both mechanical and solid state devices. A two junction circulator latching transfer switch, or mechanical transfer switch can be used in conjunction with a 3 dB hybrid to give Amplifier A, A + B, or 1/2 B outputs. Two transfer switches plus a hybrid will give A, B, and A + B. An alternate is provided by using a ferrite faraday rotator driven by orthogonal polarizations. This single device will give A, B, or A + B. This approach was used successfully on ATS 1, and 3 at C-Band. These parallel approaches require that the phase of both output signals remain within 15° of each other to keep the power loss under 0.1 dB. This has not always been successful on space flight programs involving TWT's since they are very phase sensitive to power supply changes.

All vendors contacted indicated a preference for voltage programming the power change. In light of the reliability problem of power summing TWT's and the weight advantage the voltage programming technique has been selected.

The efficiency requirement is difficult because we require output filtering and monitoring. In addition, the output power is referenced into a 1.5:1 load at worst phase and the input power varies ±1 dB. These requirements sum up to an expected output loss of 1.15 dB. These losses are tabulated in detail in Table 4.4.1-10.

c. Solid State VS TWT's - Solid State Amplifiers at present have a 9 percentage point disadvantage is regard to efficiency. The relative reliability of the two techniques is complicated. TWT's have a much higher proven MTBF but solid state amplifiers have a higher theoretical MTBF. The solid state MTBF's calculations usually ignore the part interconnections which can not compare in reliability with the welding techniques used in TWT's and their power supplies. In addition, most solid state designs use adjustable components such as multiple concentric ring variable capacitors of unproven reliability.

Table 4.4.1-11 compares the performance characteristics of the various amplifiers available. Several single mode units are also listed for comparison purposes.

The Watkins-Johnson 274-9 focused for maximum efficiency of 20 watts output gives the highest efficiency of all types surveyed. The 274-6 optimized by adjusting the helix pitch is an attractive alternate if one wishes to optimize the 10 watt mode. The ITT Solid State approach achieves a volume and weight saving at a large expense in efficiency.

1. Output Filter Requirements - Two types of requirements are placed upon the performance of the filter. These are external requirements such as MIL-STD 461A imposed to prevent electromagnetic interference and internal requirements imposed to enable proper functioning of the other spacecraft equipment. These requirements are discussed in the following sections and are displayed in graphical form for ease of interpretation.

a. MIL-STD 461A [(1)] MIL-STD 461A is imposed upon the equipment to prevent radio interference both internal and external to the spacecraft. The requirements for the spurious and harmonic radiated energy are plotted in Figure 4.4.1-36, curve (a). The ordinate is frequency normalized to the allotted channel bandwidth (10 MHz). The abscissa is attenuation of signal level in dB. Signal levels are referenced to the unmodulated carrier level of +13 dbw. Figure 4.4.1-36 shows that all spurious and harmonic energy outside the allotted channel must be greater than 70 dB down from the unmodulated carrier level. It is recognized that this does not regulate the information modulation on the carrier but outside the alloted channel.

(1) Military Standard, "Electromagnetic Interference Characteristics Requirements for Equipment", MIL-STD 461A, 1 August 1968.

Table 4.4.1-10. Estimated Output Losses

Inside Power Amplifier	Max	Min
Power Supply Regulation (1%)	-0.05 dB	-0.05 dB
Drive Variation (± 1 dB)	-0.10 dB	-0.10 dB
Cable Loss (0.5 ft ut. 141)	-0.10 dB	-0.10 dB
Circulator and Power Monitor	-0.20 dB	-0.20 dB
Band Pass Filter	-0.50 dB	-0.50 dB
Connector Interfaces (4 Pairs)	-0.20 dB	-0.20 dB
VSWR Loss TWT to Filter (1.30 to 1.30)	-0.15 dB	+.15
VSWR Loss Filter to Circulator (1.3 to 1.1)	-0.06 dB	+.06
VSWR Loss Circulator to Load (1.1 to 1.5)	-0.23 dB	+.23
Sub Totals	1.59 dB	0.71 dB
Average	1.15	
Outside Power Amplifier		
Connector Interface 1 Pair	0.05 dB	
Cable (3' 3/8 Spiral Line)	0.15 dB	
Totals	1.69 dB	0.81
Average	1.35 dB	

Table 4.4.1-11. Power Amplifier Performance

Vendor	Collins	Hughes	Hughes	ITT	Varian	WJ	WJ
Circuit Type	TWT Dual Mode	TWT Single Mode	TWT Dual Mode	Solid State Dual Mode	TWT Single Mode	TWT Dual Mode[2]	TWT Dual Mode[3]
Circuit eff.[1] 10 Watt Mode	32	—	25	20.8	—	36	32
Circuit eff. 20 Watt Mode	40	37.5	35	25.6	37.5	36	40
Power Supply eff.	80	90	82	—	88	85	85
Amplifier eff. 10 Watt Mode	25.6	—	20.5	20.4	—	35.1	27.2
Amplifier eff. 20 Watt Mode	32.0	33.7	28.7	25.6	33	35.1	34.0
DC Input 10 Watt Mode	39.1	—	48.8	48	—	28.5	36.7
DC Input 20 Watt Mode	62.5	59.7	69.8	78	60.6	65.5	58.9
Weight	8.4	7.0	9.0	5.5	9.0	10.0	10.0
Size	2/2	2/2	2/2	1/1	2/2	2/2	2/2

1. Power output of TWT divided by total DC input. (See Table 4.4.1-A for output losses)
2. WJ 274-6 optimized for both power modes.
3. WJ 274-9 optimized for high power mode.

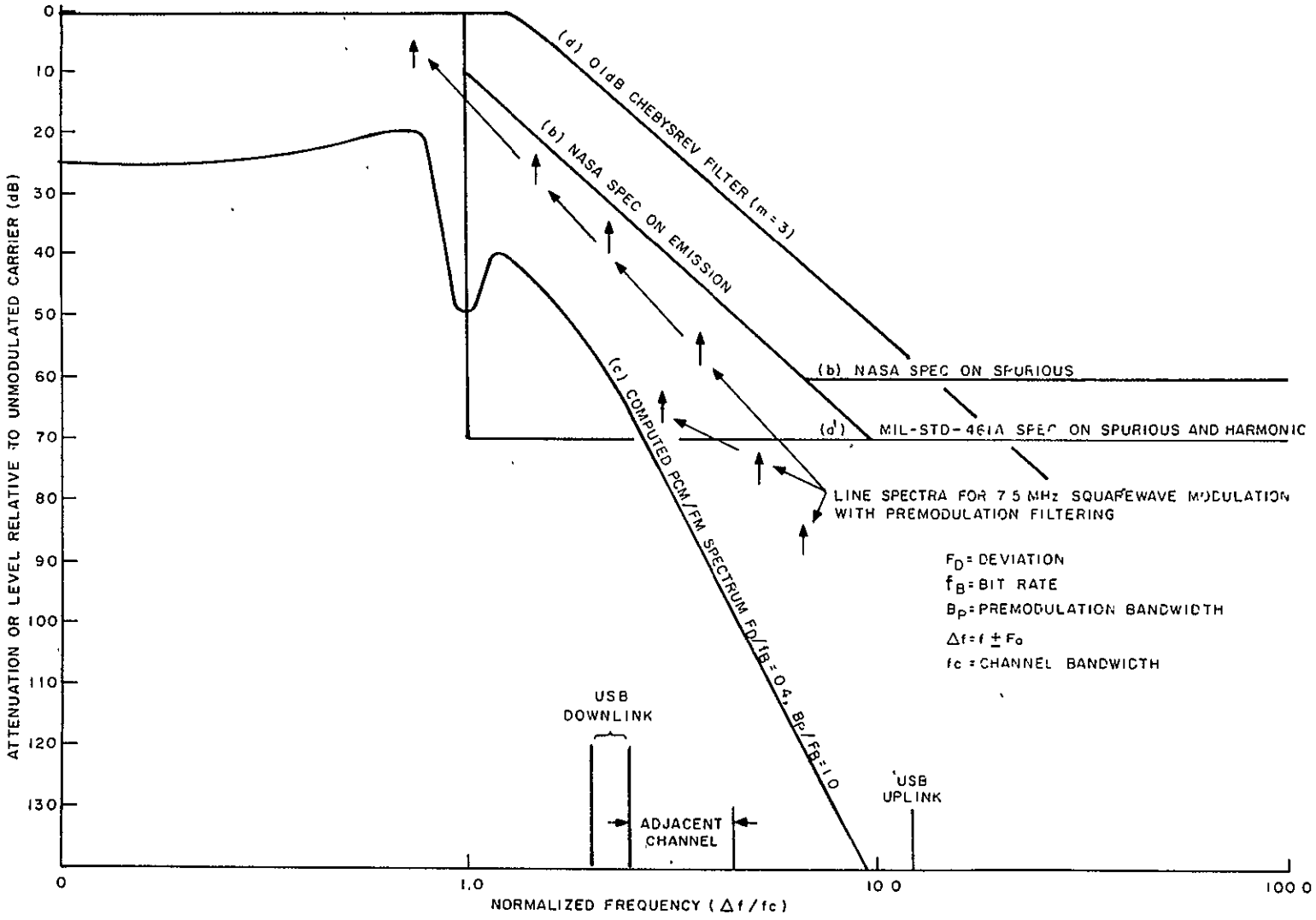

Figure 4.4.1-36. Filter Requirements, RF Spectra, and Filter Performance

b. Aerospace Data Systems Standards [2]. NASA specifications are also imposed on the spacecraft equipment. They not only specify spurious and harmonic energy but also information modulation outside the allotted channel. NASA specifications are plotted in Figure 4.4.1-B as in curve (b).

Since NASA places channels adjacent to each other without guard bands, the emissions at band edge must be 10 dB below unmodulated carrier level to prevent adjacent channel interference. The channel skirts must fall off by at least 18 dB per octave beyond this point until an attenuation of 60 dB is reached. At this point the spurious radiation specifications allow a -27 dBm maximum or 60 dB below unmodulated carrier level, whichever is greater. In order to meet both NASA and MIL-STD 461A, the emission from the filter must not be greater than the composite of curves (a) and (b).

c. Interference With USB Link - Although radiation requirements are imposed by NASA and military standards, this may not be sufficient to prevent interference with other on-board equipment such as the USB command up-link. The minimum detectable signal level for this receiver is -125 dBm. About 50 dB of isolation will be gained from antenna separation. Thus the maximum radiated power from the filter at 2106.4 MHz must not exceed -75 dBm. This level is 118 dB down from the unmodulated carrier level of 43 dBm. The relative position of the USB uplink channel is noted in Figure 4.4.1-36. An additional 57 dB attenuation is obtained from the R. F. Filter in the power amplifier. Spurious power amplifier output should therefore be 61 dB below the carrier at 2106.4 MHz. This presents no particular design problem.

Cross coupling from the USS link to the USB downlink appears to be no problem. In the case where the spectrum shown in Figure 4.4.1-36 applies, the radiated power within the downlink pass band is -43 dbw. In the case where the MSS is generating a 111 000 111 sequence discrete spectra are generated which are -34 dbw.

d. Interference with RBV Downlink - One other possibility for RF interference exists with the RBV downlink. This interference could be caused by modulation products from the MSS channel being received by the RBV ground equipment. Studies have been made in this problem and show that RF radiation from the MSS channel must be 60 dB below the RBV radiated energy to prevent interference at the ground terminal.

e. System and Interface Requirements - The remaining filter requirements are imposed by the assigned frequencies, assigned channel bandwidths, and equipment interface requirements. They are listed in Table 4.4.1-12 with some requirements determined in previous sections.

4.4.1.8.2 Study Task

The study effort for the filter was directed to finding a suitable design to meet the requirements listed in the output filter requirements section. This consisted of examining the

(2) Aerospace Data Systems Standards Part III Associated Standards Section I, "Radio Frequency and Modulation Standards for Space-to-Ground Telemetry", GSFC Data Systems Requirements Committee, November 4, 1965.

TABLE 4.4.1-12. FILTER REQUIREMENTS

Item	Requirements
Type design	*
Number of sections	*
Center frequencies	2230 MHz 2265 MHz
Bandwidth @ 0.25 dB	> 20 MHz
Bandwidth @ 13 dB	< 50 MHz
Insertion loss	< 0.5 dB
Max inband VSWR	< 1.5:1
Maximum time delay variation	5 nsec
Harmonic rejection	70 dB to 6.0 GHz

characteristics of various filter types, determining the typical expected performance of filter elements, performing sample design, and comparing computed results with the filter requirements.

4.4.1.8.3 Study Objective

The objective of the study was to determine the filter design specifications and find a suitable design to meet these specifications.

4.4.1.8.4 Transmitted RF Spectrum

Previous sections have considered the impact of standards and system specifications. We must also consider the impact of the transmitted spectrums and its relationship to the assigned channel.

Two types of data are to be transmitted; the MSS data and the RBV data. The MSS channel will have a deviation of ± 6 MHz and will have a 15 MHz four pole Bessel premodulation filter. The RBV channel will have n ± 3.5 MHz deviation and will have a 4 MHz four pole Bessel premodulation filter.

Since ERTS will have cross strapping for greater reliability each channel must be capable of transmitting the data for the widest system bandwidth. Therefore, we will consider the MSS data to be transmitted through both filter channels.

Two cases are considered for the transmitted RF spectrum. The first is a random PCM/FM data stream having a deviation of 0.4 of the bit rate and a premodulation filter with a cut off equal to the bit rate.(3) This approximates the operating data for the MSS case. The second is the line spectra for a 7.5 MHz square wave data stream into the modulator. This could be considered a worst case line spectrum for the MSS data stream. These two RF spectra are plotted in Figure 4.4.1-36 as curve (c) and the line spectra is plotted at 7.5 MHz separations.

4.4.1.8.5 Analysis

1. Design Considerations - The review of these filter requirements raises the question as to which of these requirements has the most effect upon the design. Some of these questions can be answered by reviewing the data presented in Figure 4.4.1-36. The following conclusions can be reached immediately:

a. The RF spectra will not exceed military or NASA specifications exclusive of filtering.

b. The RF spectra will not interfere with the RBV downlink exclusive of filtering.

c. Filter isolation of 43 dB at the USB uplink frequency will be required to prevent interference.

d. The requirement for an attenuation of 13 dB at 50 MHz and (3) above combine to specify a 16 dB/octave skirt selectivity for the filter (the filter must have at least 3 sections).

It is generally known that increasing the number of filter sections beyond four or five does not decrease the mid-band insertion loss. Conclusion (4) reached above sets a lower limit of three and a minimum mid-band insertion loss sets the upper limit of five on the number of filter sections required. Thus, the number of filter sections is fairly well fixed by the design requirements.

2. Characteristics of Various Filter Types - The initial analysis of the filter requirements and possible realization of the filter quickly revealed that the relatively narrow channel separations involved had a major impact on the type of filter that could fulfill the attenuation requirements.

The Bessel filter has an excellent time delay variation but the VSWR and insertion loss at the band edge is poor. The Butterworth filter has a better VSWR but, the insertion loss at band edge is poor. The Chebyshev and Elliptic filter have good skirt selectivity and good amplitude variation but the time delay variation is only fair. Realization of the elliptic filter can be somewhat difficult at microwave frequencies. No one filter type has all the desirable qualities required for the filter design. Therefore, Trade-offs must be made to meet all the requirements.

3. Unloaded Resonator Q - Any sample filter designs must incorporate the unloaded Q's of the filter elements and are a basis for design conclusions. An analysis of the expected unloaded

(3) Aeronautics Report U743, Vol. II, AD 234959.

Q's was performed and a figure of 4000 was determined to be reasonable. All the subsequent calculations are based on an unloaded Q of 4000.

Usually, the measured unloaded Q of a resonator will be about half of the calculated value. Therefore, the cavity should be designed for an unloaded Q of 8000. A sample calculation was performed for a coaxial cavity having this unloaded Q and the cavity was found to require a diameter of 1 1/2 inches. This cavity would have a height of about 1.3 inches. Physically realizing a filter should be no problem.

4. Sample Filter Calculations

1. Bessel Filter. Sample calculations for Bessel filters were performed using the required adjacent channel isolation for a design criterion. These designs showed that the Bessel filter VSWR and in-band amplitude variation were too extreme.

2. Butterworth Filter. Sample calculations for Butterworth filters were performed again using the required adjacent channel isolation for a design criterion. These designs showed that the amplitude variations in the data bandwidth were unacceptable.

3. Elliptic Filter. No designs were performed for the Elliptic filter because of the difficulty in realizing this type filter.

   Chebyshev Filter. Several paper designs for Chebyshev filters were performed using various combinations of ripple and number of filter sections. These designs showed that the requirements of Table 4.4.1-12 are realistic and feasible for a Chebyshev type filter. The results of one such design are given in Table 4.4.1-13 with the requirement as listed in Table 4.4.1-12 repeated for comparison purposes.

   The attenuation characteristic for this example filter is plotted as curve (d) on Figure 4.4.1-36. The curve shows that the skirt selectivity is adequate to meet the filter requirements. Note that the cut-off frequency greatly exceeds both the allotted channel and RF spectrum. This enables the filter time delay variation to meet the requirements.

5. Filter Spurious Responses - One additional specification should be mentioned. That is the harmonic rejection up to 12.4 GHz as is required by MIL-STD-462. Filters designed from distributed networks have spurious frequencies which usually begin at the third harmonic of the fundamental frequency. This frequency for the ERTS case is 6.7 GHz and will come within the MIL-STD-462 requirement. Therefore, the harmonic and spurious requirements are specified only to 6.0 GHz. Arrangements have been made to specify the emission from the TWT amplifier to comply with MIL-STD-462 in the frequency range of 6.0 to 12.4 GHz and enable the entire transmitter to meet the military standard.

4.4.1.8.6 Results

The results of the preceding analysis show that a conventional filter design should be followed for the MSS and RBV data channels.

TABLE 4.4.1-13. FILTER REQUIREMENTS AND SAMPLE DESIGN

Item	Requirements	Sample Calculation
Type Design	*	0.1 dB Chebyshev
Number of Sections	*	3
Center Frequencies	2229.5 MHz 2265.5 MHz	2229.5 MHz 2265.5 MHz
Bandwidth @ 0.25 dB	>20 MHz	22.2 MHz
Bandwidth @ 13 dB	<50 MHz	45 MHz
Insertion Loss	<0.5 dB	0.35 dB (Qu = 4000)
Max Inband VSWR	<1.5:1	1.32:1
Max Time Delay Variation	<5 nsec	3.0 nsec
Harmonic Rejection	70 dB to 6.0 GHz	---
Size	1/0	1/0

*To be determined by the manufacturer

4.4.1.8.7 Justification

The analysis of the filter problem has generated a set of requirements. Several filter types were analyzed and a design was selected. This design will meet the requirements set forth in Section X.15 and Section X.3.2.1. It is by no means the only design that will meet the requirements but it does show the feasibility of a filter to meet system requirements.

This Page Left Blank Intentionally.

4.4.1.9 Shaped Beam Antenna

4.4.1.9.1 Requirements

The design requirements for the shaped beam antenna are as follows:

1. Polarization: Right-hand circular
2. Frequency:
   a. 2229.5 MHz ± 10 MHz
   b. 2265.5 MHz ± 10 MHz
3. Power Handling: 25 watts CW
4. Beam Shape: Provide approximately constant power density on earth for a subtended angle on the spacecraft of 121.2 degree. Spacecraft nominal orbit is 492.4 nm.
5. Gain: $\gtrsim$4db (relative to an isotropic circularly-polarized radiator) at ± ±60 degrees with gains at lesser angles as per pattern shape.

4.4.1.9.2 Study Task

Conduct beam shaping analysis for wideband-telemetry subsystem to establish an antenna design which meets the design requirements and is compatible with the spacecraft configuration.

4.4.1.9.3 Beam Shaping Study

4.4.1.9.3.1 Objective. Conduct beam shaping analysis to establish an antenna design that satisfies the requirements of section 4.4.1.9.1 and is compatible with the spacecraft configuration.

4.4.1.9.3.2 Analysis

Desired Gain-Pattern Shape. The calculation of the desired gain-pattern shape includes consideration of such factors as the orbit geometry, the variation in path loss to earth, and the variation in atmospheric absorption. The ground station receiver system temperatures were assumed invariant for pattern computation purposes.

To perform this calculation, the coordinate system shown in Figure 4.4.1-37 was used. The ERTS spacecraft was assumed to be in a nominal orbit of 492.4 nm:

Using the law of cosines

$$R = (r + h)\cos\theta - \sqrt{(r + h)^2 \cos^2\theta - \left[(r + h)^2 - r^2\right]} \qquad (4.4.1\text{-A})$$

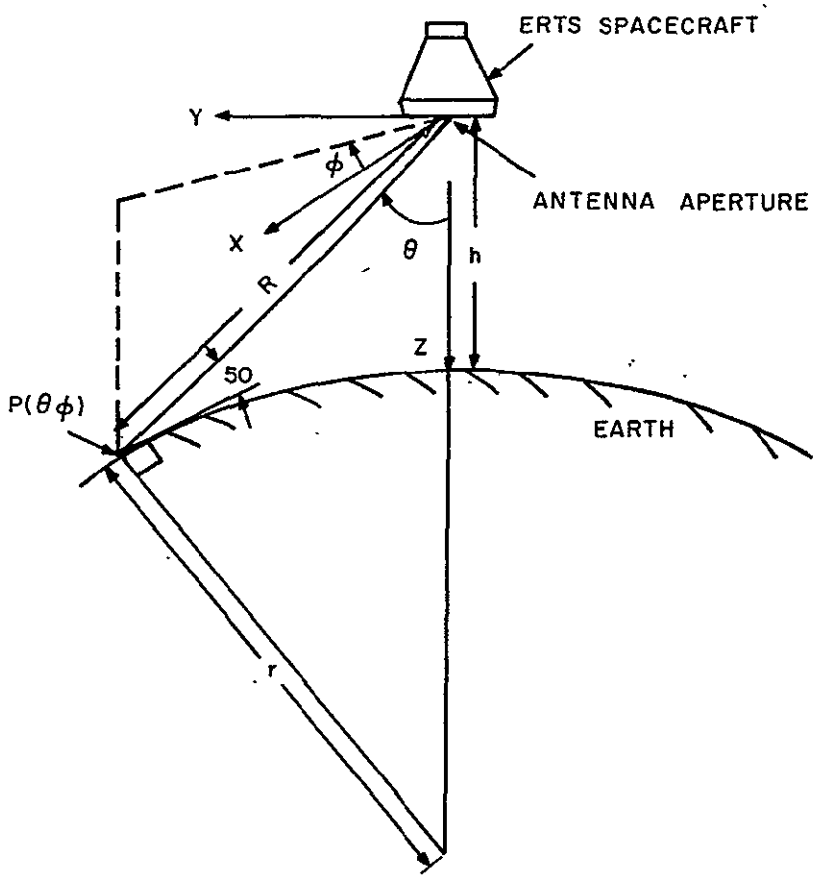

Figure 4.4.1-37. ERTS Geometry and Antenna Coordinate System

To illuminate the earth with constant power density within a cone whose subtended angle is 121.2 degrees, the electric field strength, E (θ), must be made proportional to the range R. Thus the desired field pattern expression (nomalized to unity at $\theta = 0^0$) becomes

$$E(\theta) = \frac{(r+h)\cos\theta - \sqrt{(r+h)^2\cos^2\theta - \left[(r+h)^2 - r^2\right]}}{h} \qquad (4.4.1\text{-B})$$

Utilizing equation 4.4.1-B and the atmospheric absorption loss data in Table 4.4.1-14 the desired pattern shape for the wideband-telemetry antenna is that given in Figure 4.4.1-38. The peak gain figure of 4 db (relative to a circularly-polarized isotropic radiator) at $\theta = \pm 60.6$ degree represents a minimum value based upon satisfactory overall subsystem performance.

In selecting a baseline-antenna design, two types of antenna configurations were studied. These were planar, circular-aperture configurations, and line-source configurations.

Circular Aperture Synthesis

An analysis of circularly-symmetric aperture distribution functions were investigated to approximate the desired gain-pattern shape. Using the circular aperture synthesis method developed by Ruze*, the radiation field and the gain expressions were derived, applied and their results assessed for aperture diameters out to 3.3 λ (wherein, λ is the free space wavelength).

TABLE 4.4.1-14. ATMOSPHERIC ABSORPTION VERSUS LOOK ANGLE θ

θ (degrees)	Atmospheric Absorption Loss (db)
0	0.07
17.4	0.09
34.2	0.11
42.0	0.15
49.2	0.17
55.3	0.25
57.7	0.30
59.5	0.40
60.6	0.70

*J. Ruze, "Circular Aperture Synthesis", IEEE Transactions on Antennas and Propagation, pp. 691-694, November, 1964.

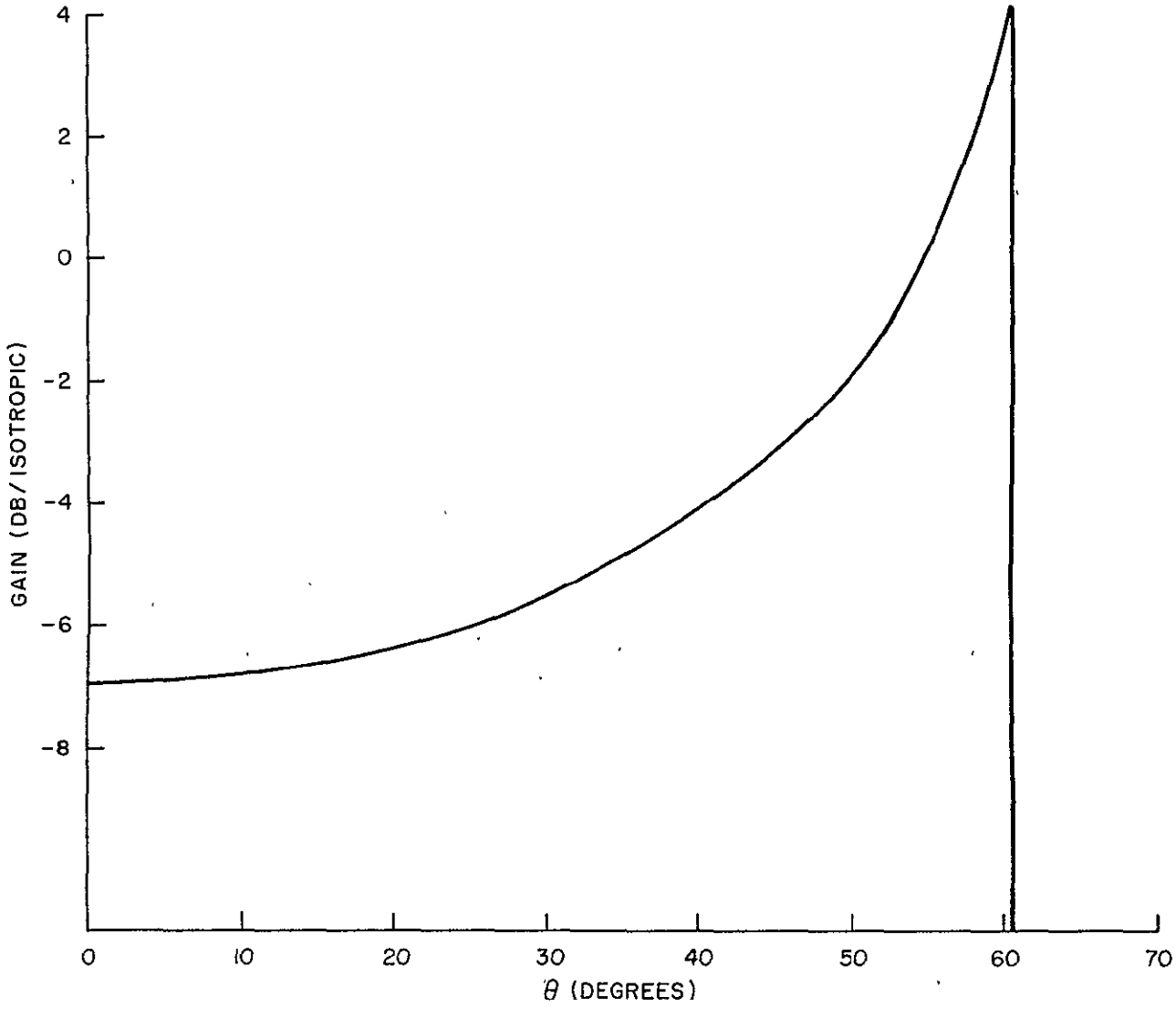

Figure 4.4.1-38. Desired Gain Pattern Shape for Wideband Telemetry S/S

The circularly symmetric aperture distribution function $A_N(r)$ is given by

$$A_N(r) = \frac{1}{\pi a^2} \sum_{j=1}^{N} \frac{Eo(\beta_j)}{J_o^2(\beta_j)} J_o(\beta_j r) \qquad (4.4.1\text{-C})$$

wherein a is the radius of the circular aperture,

r is a normalized radial coordinate in the aperture which satisfied $0 \leq r \leq 1$,

J_o is the Bessel function of the first kind,

β_j are roots of $J_1(\beta_j) = 0$, and

$Eo(\beta_j)$ are coefficients derived from the desired pattern shape.

The radiation field expression resulting from Equation 4.4.1-C is

$$E_N(\mu) = 2 \sum_{j=1}^{N} \frac{E_o(\beta_j)}{J_o(\beta_j)} \cdot \frac{\mu J_1(\mu)}{(\mu^2 - \beta_j^2)} (1 + \cos\theta), \qquad (4.4.1\text{-D})$$

wherein

$$\frac{2\pi a}{\lambda} \sin\theta.$$

And finally, the gain at an arbitrary angle θ_o can be expressed as,

$$G_N(\theta_o) = \frac{1}{4} \left(\frac{2\pi a}{\lambda}\right)^2 \frac{\left[E_N(\mu_o)\right]^2}{\left[\sum_{j=1}^{N} \frac{E_o^2(\beta_j)}{J_o^2(\beta_j)}\right]} \qquad (4.4.1\text{-E})$$

The subscript N denotes the number of terms of $A_N(f)$, $E_N(\mu)$ and $G_N(\theta_o)$ that are used to approximate the desired gain-pattern shape. Note that the radiation - field equation (and gain equation) includes the factor $(1 + \cos\theta)$ because the beam-shaping requirements extend out to $\theta = \pm 60.6$ degree.

The first pattern synthesized to approximate the desired pattern was for N = 2. The explicit pattern expression formulated was

$$E_2(\mu) = \left[\frac{2.466}{\mu} - \frac{21.811}{(\mu^2) - 14.684}\right] J_1(\mu) \quad (1 + \text{Cos}\,\theta) \qquad (4.4.1\text{-F})$$

The synthesis was tailored to provide maximum gain at $\theta = \pm 60.6$ degree. The calculated gain-pattern is compared with the desired pattern in Figure 4.4.1-39. As shown the desired gain in the vicinity of $\theta \approx 60$ degree cannot be obtained from this approximation and therefore this candidate design was discounted.

Using N = 3, the radiation field equation becomes,

$$E_3(\mu) = \left[\frac{2.466}{\mu} - \frac{7.132\,\mu}{(\mu^2 - 14.684)} + \frac{29.3\,\mu}{(\mu^2 - 49.224)}\right] J_1(\mu)\ (1 + \text{Cos}\,\theta) \qquad (4.4.1\text{-G})$$

Here, two gain-patterns were synthesized -- one, for maximum gain at $\theta = \pm 60.6$ degree and the other for minimum gain variation (as a function of frequency) at $\theta = \pm 60.6$ degree. These gain patterns are shown in Figure 4.4.1-40. They indicate that the desired gain at $\theta = \pm 60.6$ degree can be achieved from circular apertures whose diameters are $\approx 2.5\ \lambda$; however, the approximation for shaping is marginal and the gain in the vicinity of $\theta = \pm 15$ degree falls below the desired gain levels.

The last gain-pattern considered was for N = 4 using the field expression,

$$E_4(\mu) = \left[\frac{2.466}{\mu} - \frac{6.566\mu}{(\mu^2 - 14.684)} + \frac{10.82\,\mu}{(\mu^2 - 49.224)} - \frac{35.16\,\mu}{(\mu^2 - 103.51)}\right] J_1(\mu)\ (1 + \text{Cos}\,\theta) \qquad (4.4.1\text{-H})$$

A gain-pattern was calculated for the case wherein a gain of 4.65 db was provided at $\theta = \pm 60.6$ degree (see Figure 4.4.1-41). This gain figure is identical to that for the N = 3 ($2a/\lambda = 2.48$) example in Figure 4.4.1-D. It was chosen to observe the degree of improvement in pattern shaping over the N = 3 example. As indicated, the improvement is not significant and does not justify the enhancement in aperture diameter.

An alternative approach in satisfying the shaped-beam antenna requirements is to consider line source configurations which generate symmetric, end fire-type radiation patterns. Initial analyses indicated that the lack of available space between the spacecraft and adaptor precluded the use of line source array lengths that provided a clost approximation to the desired gain-pattern. Thus, detailed analysis was confined to shorter-length configurations which provided modest beam shaping. One such configuration (which is compatible with the spacecraft geometry) is a single, circularly-polarized radiator mounted above a ground plane.

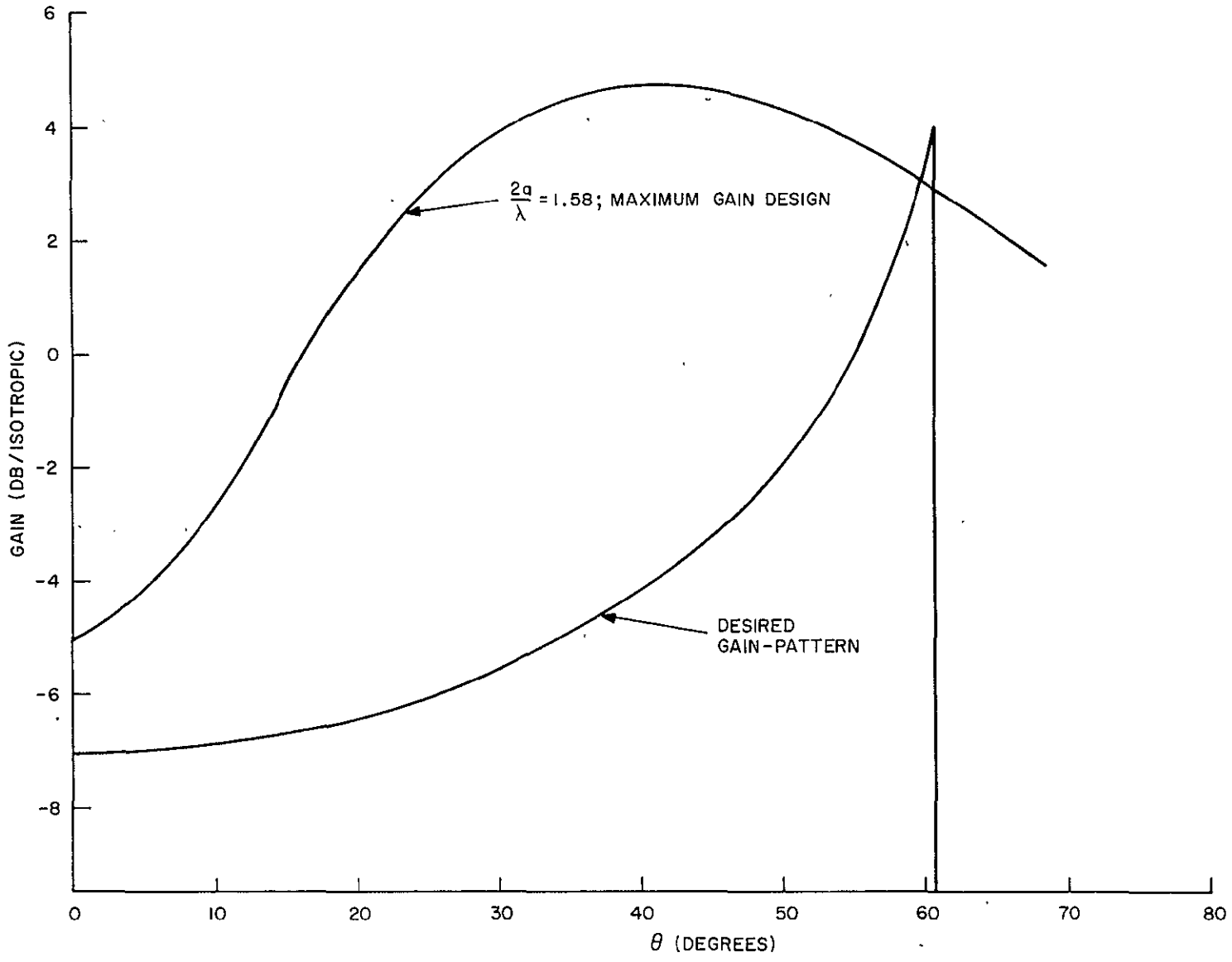

Figure 4.4.1-39. Calculate Circular Aperture Gain Pattern for N = 2

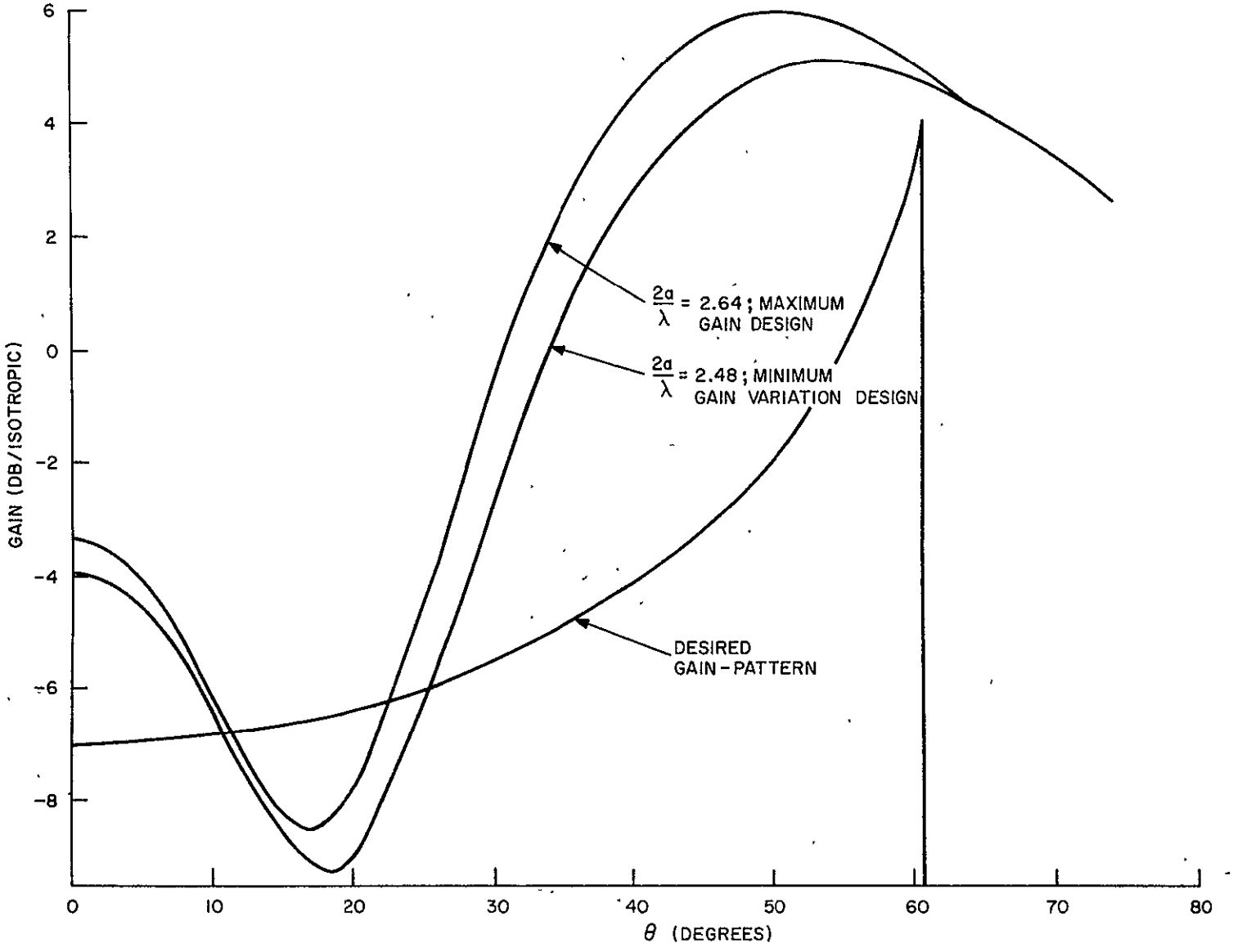

Figure 4.4.1-40. Calculate Circular Aperture Gain Pattern for N = 3

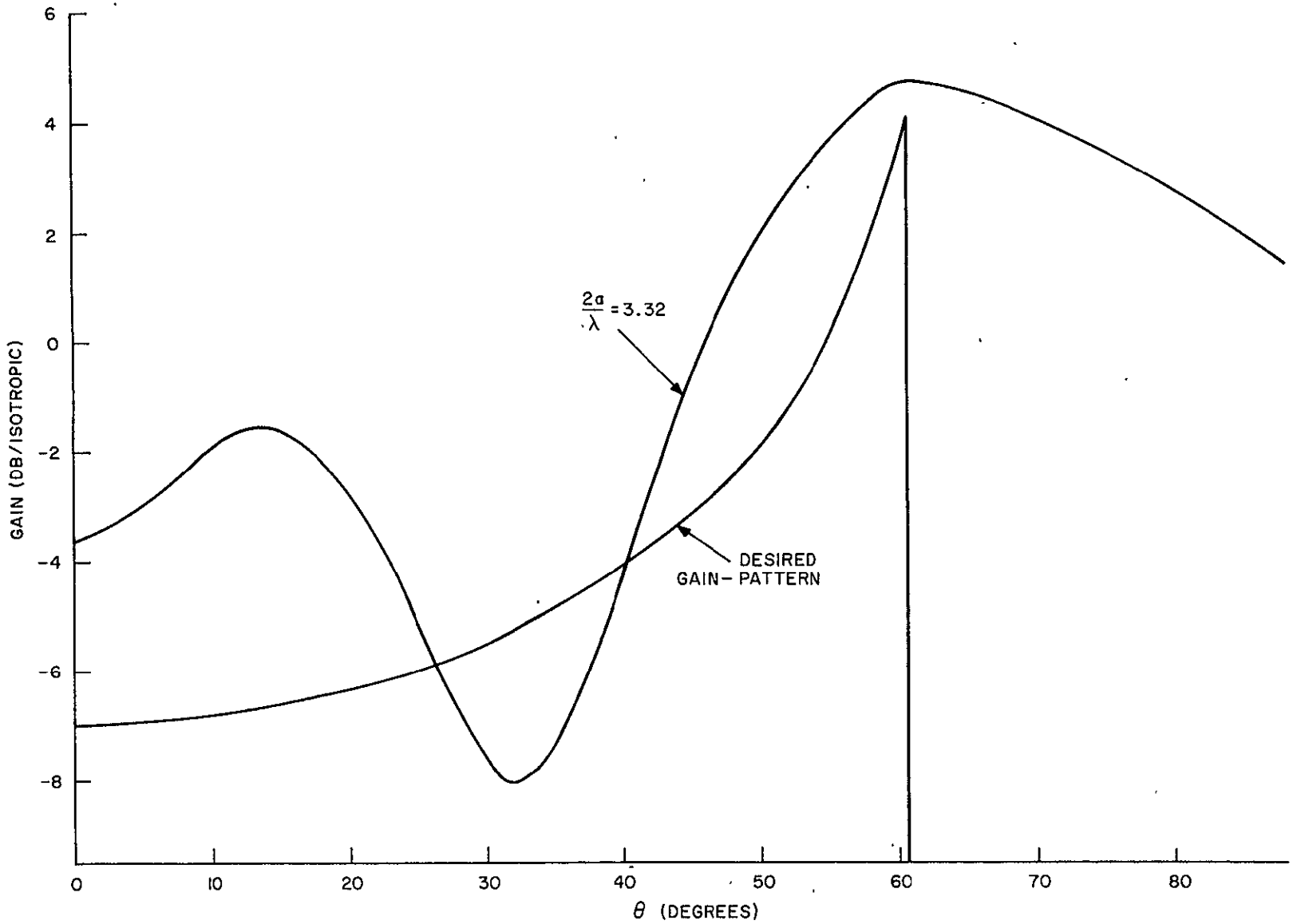

Figure 4.4.1-41. Calculate Circular Aperture Gain Pattern for N = 4

The total radiation field for this configuration can be expressed as

$$E_T(\theta) = k \sin\left(\frac{2\pi d}{\lambda} \cos\theta\right) \sqrt{1 + \cos\theta} \qquad (4.4.1\text{-I})$$

wherein, d is the spacing of the driven radiator above the ground plane.

Adjusting $2\pi d/\lambda$ = 164 degree at 2248 MHz yields the gain patterns shown in Figure 4.4.1-42. As shown, the approximation to the desired gain pattern is marginal, but the gain meets or exceeds the requirement within $\theta = \pm 60.6$ degree over the frequency band.

4.4.1.9.3.3 Selection of Antenna Design and Justification. The baseline design selected for the shaped-beam antenna is the single, circularly-polarized radiator mounted above a ground plane. The antenna configuration will consist of a driven turnstile mounted 2.4 inches above a reflector plate whose maximum diameter is 8 inches. The reflector-plate will be co-planar with the extended surface of the MSS box in order to satisfy coverage requirements.

This candidate design was chosen because it provides modest beam shaping with gain values that meet or exceed the desired gain-pattern curve. It represents a simple, reliable and low-cost approach. Furthermore, its size and weight are compatible with the spacecraft environment.

4.4.1.9.3.4 Recommended Antenna Subsystem. Two antenna subsystem approaches are possible to implement the RF portion of the wideband-telemetry subsystem. The first approach is a single-antenna subsystem consisting of one shaped-beam antenna and a diplexer tied to two separate transmitters. The second approach has two separate antenna subsystems, one for each of the two band pass channels (2229.5 ± 10 MHz and 2265.5 ± 10 MHz). Here, each subsystem contains a shaped-beam antenna, filter and transmitter.

From a cost and reliability standpoint, the second approach is recommended. Cost-wise, it is estimated that it will cost less to implement an additional (identical) shaped-beam antenna and a filter than to manufacture/buy and space qualify a diplexer. Reliability-wise, two separate RF channels afford redundancy and hence enhanced reliability. Finally, space is available on the spacecraft to accommodate an additional antenna and, with an interspacing of ~6 wavelengths, negligible interaction between antennas is anticipated.

For preliminary experimental results, see Appendix 4.C.

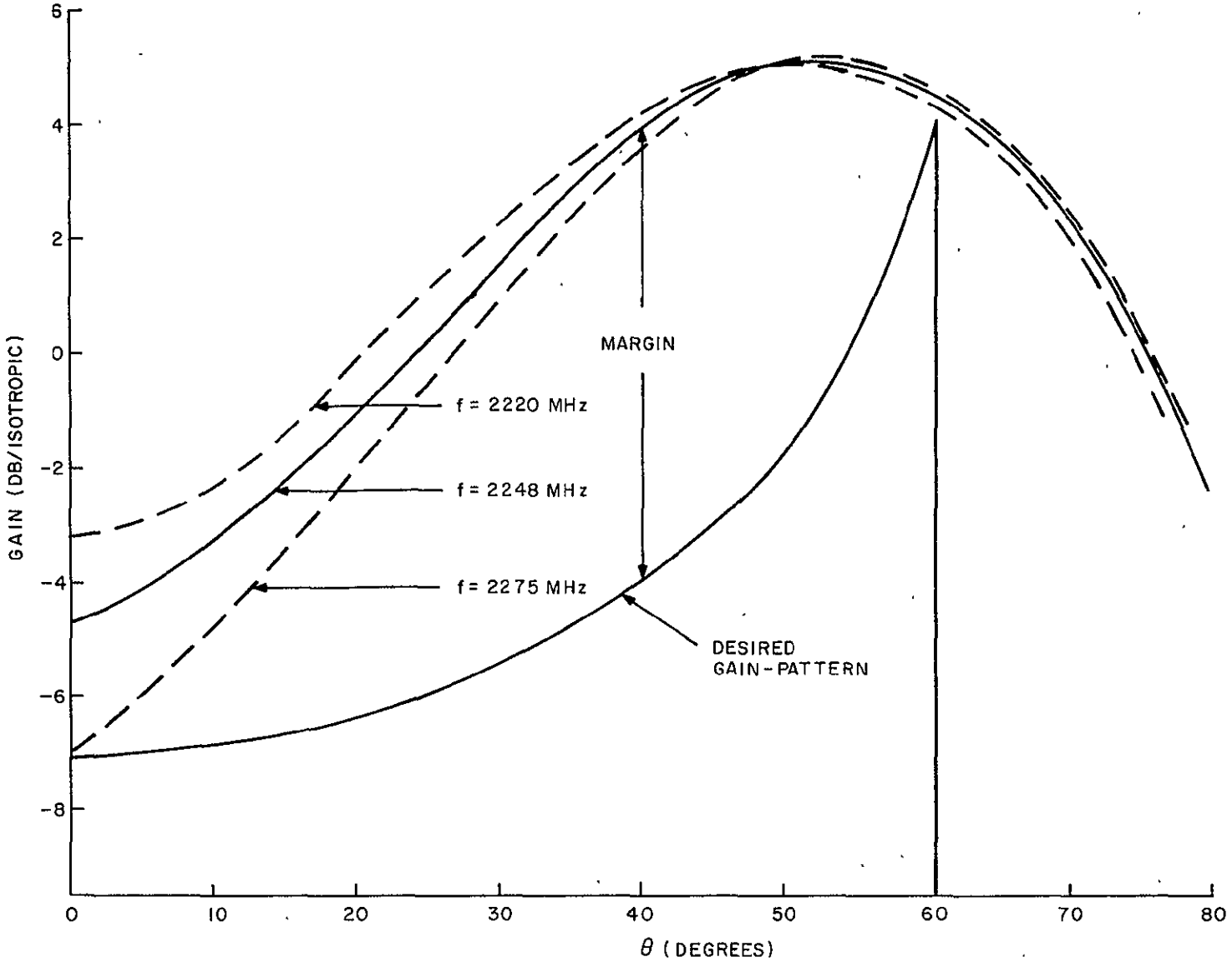

Figure 4.4.1-42. Calculate Gain-Patterns for Single Radiator above a Ground Plane as a Function of Frequency

4.4.2 COMMAND/CLOCK EQUIPMENT

4.4.2.1 Command Capability

4.4.2.1.1 Requirements and Constraints

1. Dual Command Links to permit the use of both MSFN and STADAN ground stations.
2. No hardware changes at ground sites. Use existing capability.
3. Process the signals from either of MSFN or STADAN ground stations to:
   a. Provide the same command capability from either site
   b. Avoid false commands and "lock out" when signals are simultaneously received from a MSFN and STADAN site. Assume one of the signals is unwanted (i.e., Non-ERTS).
4. The Command/Clock Subsystem should provide the following capability.
   a. Minimum of 412 real-time commands.
   b. Fail-safe command execution.
   c. Low probability of a false command.
   d. Capacity for 30 stored commands with (1) 100 executions of stored commands between loadings and (2) Verify and override capability.
   e. Redundant means of command verification.
   f. Generate clock frequencies and time code with time code up-date to be known within 1-bit time of PCM telemetry rate.
   g. Redundancy is required throughout the subsystem.
   h. Minimize changes to existing hardware designs and the complexity of new designs.
5. The maximum bit rate into the Command/Clock is approximately 500 bits/second.
6. An enable pulse must be provided to the Command/Clock unit along the data and sync. signals.

These items have been studied along with other topics in arriving at a recommended design. The results of these studies are presented in the following sections.

Figure 4.4.2-1 shows a simplified functional diagram of the recommended Command/Clock Subsystem. The system processes command signals from either a MSFN or STADAN site and provides the spacecraft timing signals and minitrack time code data. The equipment is completely redundant.

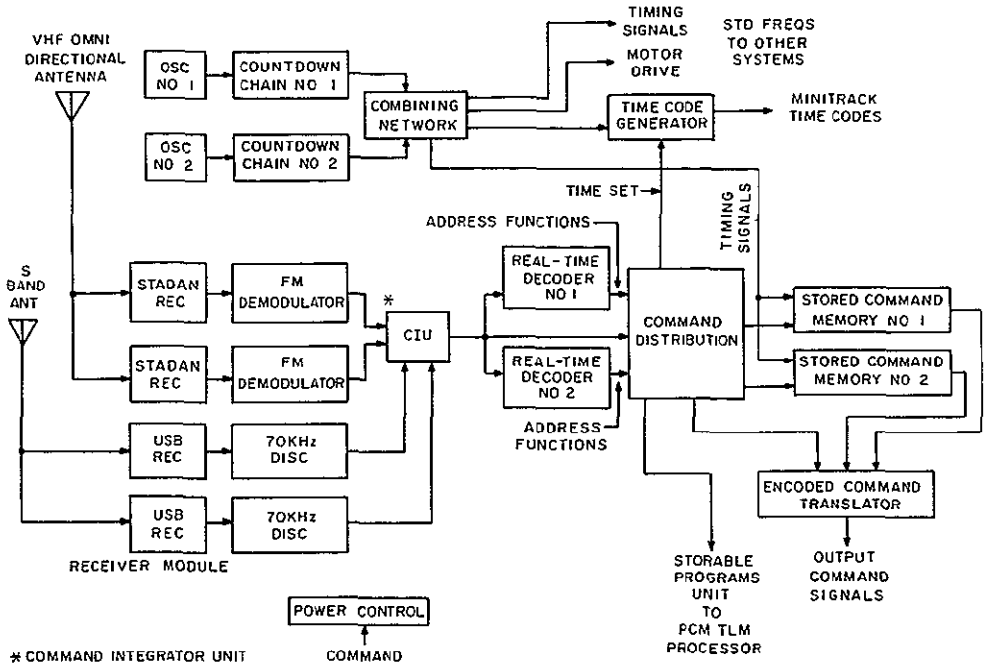

Figure 4.4.2-1. Command/Clock Subsystem

4.4.2.1.2 Command Integration

A study of the STADAN and MSFN/USB Command System capabilities was made in order to establish a dual integrated-command capability. The study included the feasibility of using the Command/Clock (unmodified Nimbus D configuration) as the Real-Time Command Decoder, Storage Unit, and Clock. The Command/Clock is particularly desirable since it conforms to the ERTS spacecraft equipment package design. The Command/Clock is also a space qualified unit, and meets or exceeds the ERTS requirements for command storage, total number of commands, clock format and stability.

4.4.2.1.2.1 Signal Compatibility. The MSFN sites transmit the command signals on an S-band carrier at 2.1064 GHz using PCM/PSK/FM/PM modulation. The digital signals are PSK modulated at a 1 KHz rate, but there exists the capability of sub-encoding the basic digital message so that the information rate transmitted can be considerably less than 1 Kbps.

The STADAN sites will be transmitting the commands at VHF on a 154.1 MHz carrier using PCM/FSK/AM/AM. A range of bit rates are available, but 128 bps has been chosen as the result of a trade-off between signal-to-noise ratio (i.e., bit error rate) and data rate.

Thus, the earliest point in the processing chain where the signals from the two receiving channels can be combined is the point where they have been demodulated to their PCM waveforms. The NRZ digital signal is provided at the output of FSK demodulator for the VHF STADAN receiver and the sub-bit decoder for the MSFN/USB receiver.

4.4.2.1.2.2 Reception of Simultaneous Signals from MSFN and STADAN Sites. Since the same up-link carrier frequencies are used by other spacecraft for both MSFN and STADAN sites, methods of minimizing interference have to be examined. The same FSK sub-carriers are used for other spacecraft at the STADAN, so the only uniqueness about the ERTS command signal from those sites are the digitally encoded spacecraft addresses.

The MSFN sites all use the 70 KHz FM sub-carrier and the same PSK sub-carriers (2 KHz for data and 1 KHz sync). Since sub-bit encoding is required to reduce the 1 K bps data rate below 800 bps for Command/Clock compatibility, a unique sub-bit code can be assigned to the ERTS spacecraft.

4.4.2.1.2.3 Enable Pulse. The Command/Clock unit requires an enable pulse to exist for the duration of a message. This is an additional precaution of preventing extraneous signals from entering the Command/Clock when a proper signal is not being received. Since this signal is not provided as part of the signal format at either the STADAN or MSFN sites, it must artifically be generated in the spacecraft.

4.4.2.1.2.4 MSFN/USB Sub-Bit Encoding. Considerations were given to 5 bit, 7 bit, and 8 bit sub-codes. Software is presently available to generate 5 bit sub-codes at the MSFN sites making the selection of this sub-code economically attractive. With 7 bits a Barker Code can be generated and would provide a larger Hamming distance between codes and thus making the decoding more secure. Eight bits was considered only because this provides an output data rate of 125 bps, which is nearly the equal to the STADAN data rate. There didn't appear to be any advantage to making the two data rates equal so the 8 bit sub-code was not chosen.

Additional spacecraft hardware and reprogramming cost for the MSFN sites required for the 7 bits more than offset the performance advantage so the 5 bit sub-code is recommended for the MSFN signal format.

It was decided to locate the sub-bit detector and decoder in the Command Integrator Unit to simplify the interface between the MSFN/USB receiver and the CIU.

4.4.2.1.2.5 Simultaneous Reception of MSFN and STADAN Signals. The objective is to prevent an unwanted signal in one receiver channel from interferring with the processing of an ERTS command signal in the other receiver channel. The case where both the interferring and desired signals are in the same receiver was not considered.

Two approaches were considered. The one approach is shown in Figure 4.4.2-2. The enable pulse is generated in the VHF STADAN receiver by sensing the presence of either of the FSK sub-carriers. The data, sync and enable signals each pass through NAND gates to OR gates where the signals are combined with the MSFN/USB digital outputs before being

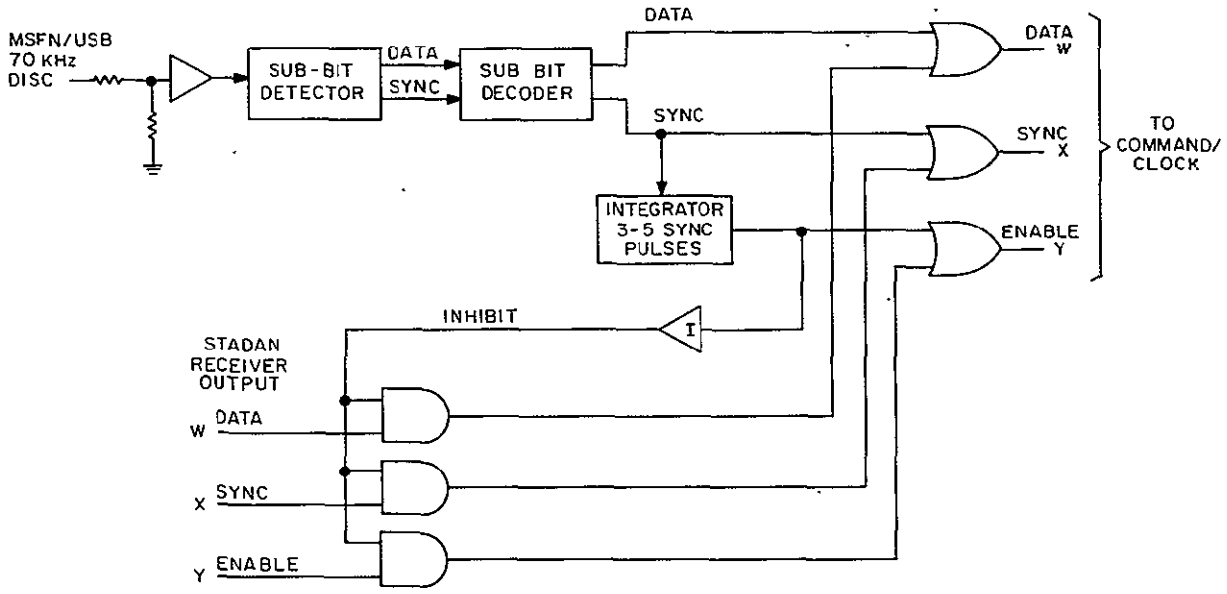

Figure 4.4.2-2. Functional Block Diagram of Command Integrator Unit (Shown in non-redundant configuration)

applied to the Command/Clock. The PSK output signal from the MSFN/USB FM Descriminator is applied to the PSK sub-bit detector and decoder. The output of the decoder is the 200 bps data stream and 200 Hz sync signal. A sync pulse is generated for each data pulse so that the 200 Hz sync is present only after proper sub-bit decoding of the 1 kbps data stream. Three to five pulses of the 200 Hz sync are integrated prior to generating an enable gate. The integration prevents dropping of the enable gate between sync pulses and avoids generating enable pulses due to spurious noise pulses. The enable pulse also used to inhibit the input from the STADAN receiver. The output format from the MSFN/USB sub-bit decoder is shown in Figure 4.4.2-3.

In this arrangement if an unwanted signal is being received from a STADAN site it will pass through the Command Integrator Unit but will be rejected in the Command/Clock decoder since it will have an improper spacecraft address. If a MSFN site sends an ERTS command to the spacecraft during this time, the inhibit circuit will be actuated shutting out the unwanted STADAN signal. On the other hand, an unwanted MSFN signal will be rejected by the sub-bit decoder since ERTS will be assigned a unique sub-bit code. The sub-bit provides the same security as the spacecraft address.

The second approach considered and is the one recommended provides a spacecraft address decoder in the STADAN data and sync lines following the inhibit NAND gates as indicated in Figure 4.4.2-4.

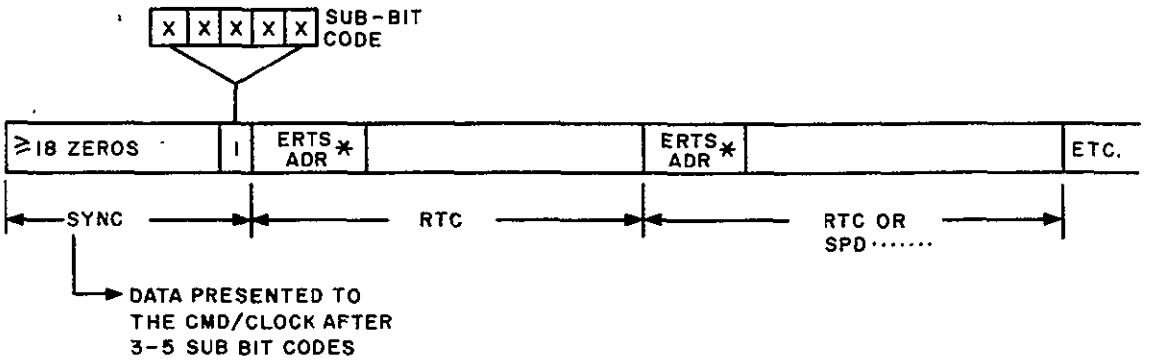

Figure 4.4.2-3. MSFN/USB Format

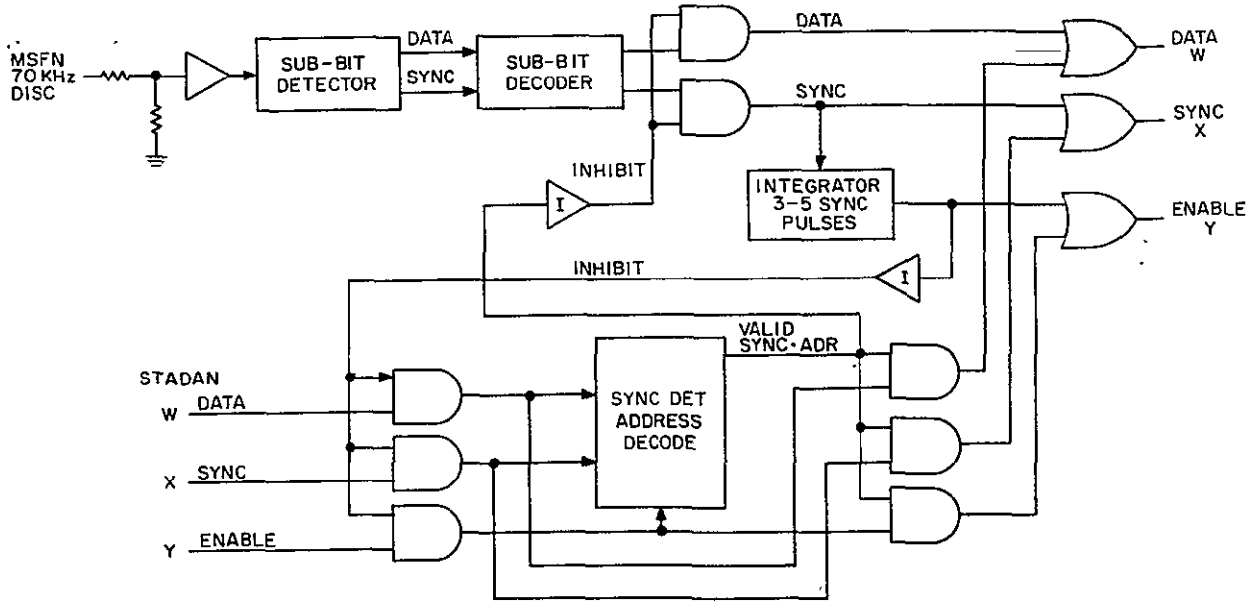

Figure 4.4.2-4. Recommended CIU Functional Block Diagram
(Shown in non-redundant configuration)

The decoder will recognize a STADAN sync word consisting of at least thirteen "zeros" followed by a "one" and followed by a 50 bit CIU command word. The first seven bits of the command word will be the ERTS Address for either COMDEC (command decoder) followed by 42 "zeros" and then a "one" (see Figure 4.4.2-5).

The enable Signal from the receiver/demodulator will be transmitted to the Command/Clock upon successful recognition of the sync and decoding of the ERTS-Address. Subsequent data will be transferred to the Command/Clock. The 42 "zeros" followed by a "one" (Figure 4.4.2-5) will be used as a sync for the Command/Clock and the following 50-bit command will be a Real Time Command which will be excuted by the appropriate command decoder (COMDEC) in the Command/Clock. Each COMDEC will be assigned a different address. The Addresses for ERTS-A will be $(073)_8$ and $(103)_8$. For ERTS-B the addresses will be $(021)_8$ and $(132)_8$. The CIU will respond to either ERTS-A address. An Address jumper plug will select the ERTS Addresses to which the CIU is to respond.

Once the CIU recognizes the Sync and ERTS Address the MSFN/USB decoded outputs will be inhibited until the Enable signal is removed from the CIU STADAN input.

The primary and redundant STADAN outputs (only one will be on at a time) are OR'ed together so that either section can provide an output to the Command/Clock. The OR'ed outputs from the STADAN sections are OR'ed with the output from the MSFN/USB sections.

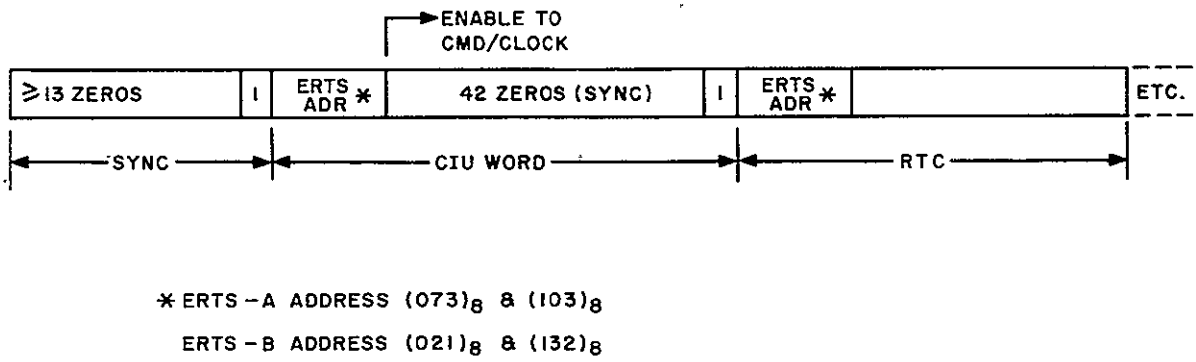

Figure 4.4.2-5. STADAN Format

4.4.2.1.3 Spacecraft Command Integrator Justification

The ERTS-A/B integrated command system will meet the ERTS-A/B requirements by the addition of a Command Integration Unit. By adding a Command Integrator Unit (CIU) the Calcomp Command/Clock can be used without altering its qualification status. The design of the CIU will not reflect any special requirements or restrictions on the Command/Clock, STADAN VHF receiver/demodulator, or MSFN/USB receiver/discriminator designs. Complexity of the CIU will be held to a minimum consistant with the provision for block redundancy and unique ERTS address recognition.

The ERTS-A/B integrated command system will not require special ground station equipment at either the STADAN or MSFN sites. In addition the use of a five-bit sub code will take full advantage of existing software by not placing any ERTS unique software restraints on the ground.

4.4.2.1.4 Command/Clock Description

Figure 4.4.2-6 presents a functional block diagram of the Command/Clock. The Command/Clock contains a redundant configuration of equipments for the purpose of generating spacecraft precision frequencies, storing and subsequently routing stored commands, and routing or executing real time commands. There is no "Power OFF" mode of operation. All major units are powered in "Exclusive OR" fashion; i.e., one (and only one) unit is operational at all times, except for the COMDECs and the COMSTORs. Special provision is made to power these units. Also, the COMSTORs can both be turned off. The primary functions of the major units comprising the Command/Clock are as follows:

1. Power Supplies - Two independent, redundant units designated primary and redundant, each capable of accepting the externally generated -24.5 vdc bus inputs and generating all internal secondary voltages required by the Command Clock. Both supplies are powered continuously.

2. COMDEC's - Two independent, identical units (designated primary and redundant), each capable of performing the command decoding functions of disabling or enabling command inputs, bit synchronization, data strobing, format checking and routing of both real time commands (executed when received) and stored commands (commands executed in accordance with the associated time tag). The COMDECs will operate in "Exclusive OR" configuration. A different 7-bit address selects the COMDEC required.

3. COMSTORS - Two independent, identical units (designated primary and redundant), each capable of storing time dependent (SPD) commands (capacity 15 commands each), continuously processing time tags, input error checking and command readout at command execution times. Readout of the memory can be commanded via encoded commands for command verification at the ground station. The COMSTORs can both be disabled or will operate in "Exclusive OR" fashion as commanded by encoded real time commands. When both powered, the outputs are time-phased to maintain isolation.

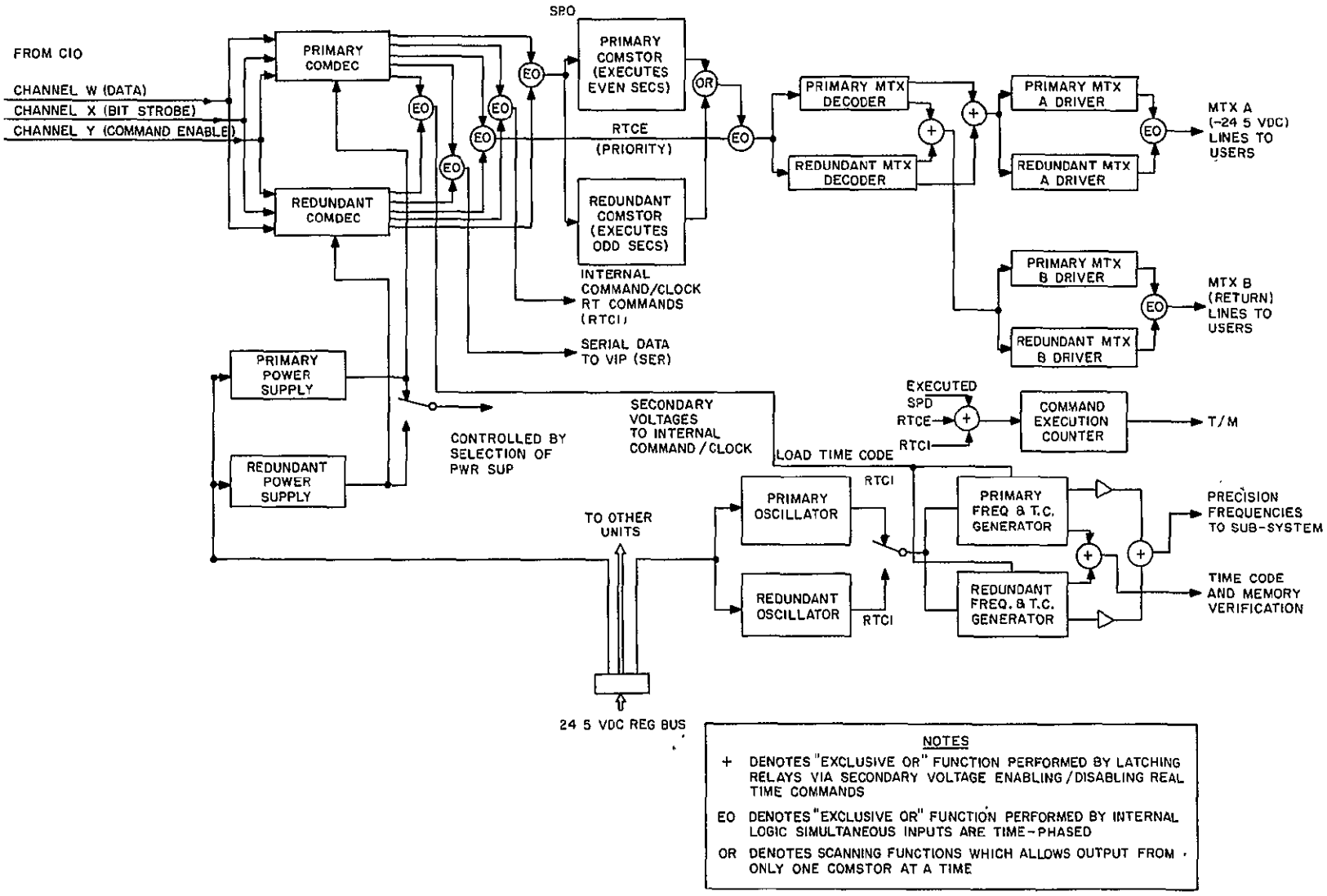

Figure 4.4.2-6. Command/Clock Functional Block Diagram

4. Matrix (MTX) Decoders - Two independent, identical units (designated primary and redundant), each capable of decoding and routing stored commands (from COMSTORs) or real time commands (from COMDECs) via strobe enabling pulses to the MTX Drivers. The decoders will operate in "Exclusive OR" configuration as commanded by encoded real time commands. Priority is assigned to the COMDEC (real time) inputs.

5. Matrix (MTX) Drivers - Two sets (A and B) of independent, identical units (designated primary and redundant), each capable of routing selective command strobe pulses to the interfacing subsystems. Enabling signals from the decoders are translated into a unique -24.5 vdc (MTX A) connection and a unique return (MTX B) connection. Associated latching functions are contained as required in the interfacing subsystems. The drivers will operate in "Exclusive OR" pair configurations as commanded by encoded real time commands. A total of 480 unique connections will be provided. There are 16 MTX A lines and 32 MTX B lines yielding 512 unique command connections; however; 32 connections are reserved for real time internal (RTCI) functions.

6. Oscillators - Two independent, identical units (designated primary and redundant), each capable of generating the precise base clock frequency for all spacecraft timing functions. The oscillators will both be continuously powered and their outputs will be enabled in "Exclusive OR" fashion as commanded by real time commands.

7. Frequency and Time Code Generators - Two independent, identical units (designated primary and redundant), each capable of accepting either oscillator input and continuously developing a 40-bit time code (resolution to one second) and a variety of precision frequencies for centralized time correlation of all spacecraft events. The precision frequencies are amplified and made available to all subsystems on an individual, buffered basis. The 40-bit time code is utilized as a time reference in the telemetry format and on the Minitrack tape.

8. Command Execution Counter - A single 6-bit counter that maintains a cumulative total (0 to 63) of all executed commands. The counter is reset by a real time command and its count status is telemetered for ground station command correlation.

4.4.2.2 Real Time Command Studies

4.4.2.2.1 Requirements and Objectives

1. Determine the command functions required for proper operation of the spacecraft and payload sensors. Identify whether a command is momentary, a change of state, or non-reversible.

2. Examine techniques which will provide a "fail safe" design in the execution of commands; particularly to ensure that a single occurrence of an erroneous command will not initiate a nonreversible command.

3. Determine necessary modifications (if any) to the candidate command subsystem designs to meet the above objectives and the "Aerospace Data Systems Standards" and "GSFC Specification, PCM Data Handling Systems, S-534-P-6".

4. Use existing space qualified designs where possible with minimum modification.

4.4.2.2.2 Required Commands

The operating functions of each spacecraft subsystem has been examined and the commands required to control these operations have been tabulated and presented in Appendix A. The type of each command is identified (i.e., momentary, change of state, or non-reversible), the location of the command relay, how the execution of the command is verified, and a brief functional description of the command. A detail description of the command function will be found in the section describing that particular subsystem.

Table 4.4.2-1 is a summary of this command list showing a total of 392 commands presently required for the spacecraft subsystems.

4.4.2.2.3 Command Evaluation

A prime objective of this study is to determine how existing space qualified designs can be adapted to the ERTS requirements.

The Command/Clock used on the Nimbus D program was selected for this evaluation study since it meets the spacecraft mechanical and electrical interface requirements and is most tractable to existing quality assurance facilities. The Command/Clock will be examined by considering the following items:

1. Compatibility with the "Aerospace Data Systems Standards"
2. Does it have the capacity for the number of commands listed in Table 4.4.2-1 with additional capacity for expansion.
3. Determine the probability of executing a false command to assess the fail safe capability.

TABLE 4.4.2-1. COMMAND LIST SUMMARY ERTS-A/B

Subsystem	COS	I	M	Total
Power	38		2	40
Attitude Control	56		1	57
Magnetic Moment Assy	14			14
Orbit Adjust	11	4		15
RBV Camera	36			36
Multispectral Scanner	52		13	65
Data Collection	2			2
Command/Clock	26	1	2	29
Command Integrator Unit	4			4
WB Video Tape Recorder	17			17
WB Telemetry	30			30
VIP	44		1	45
VHF Transmitter	11			11
VHF RCVR	4			4
Telemetry Recorder	6			6
Premodulation Processor	4			4
Unified S-Band Equipment	12			12
Totals	368	5	19	392

COS = Change of State
I = Irreversable
M = Momentary

4.4.2.2.3.1 Data Format. The Command/Clock is capable of receiving and processing five types of digital encoded commands. These are:

1. Real Time Commands External (RTCE)
2. Real Time Commands Internal (RTCI)
3. Stored Commands (Stored Program Data - SPD)
4. Time Code Data (TCD)
5. Serial Data (SER)

Figure 4.4.2-7 shows the input command format accepted by the Command/Clock, and also shows the digital encoding arrangement for these 5 types of commands.

The following definitions and operating constraints apply:

SYNC — All messages are preceded by a sync word consisting of a minimum of 13 "zeros" and a single "one" bit. Once Sync is established, the command message must immediately follow. The first word of the command message must be a Real Time Command.

ADDRESS BITS — The first word of each command must start with the seven bit ERTS address designation. A separate address will be assigned to the primary and redundant command decoders.

MODE BITS — Consist of three bits to designate the five types of commands. The single bit M1 is associated with Real Time Commands and designates the command for internal COMMAND CLOCK operations (RTCI) or external real time operations (RTCE).

PARITY BIT (P) — Odd parity is associated with all commands. Commands failing to comply with the odd parity bit are not processed. For commands other than real time, M1 is utilized as a parity bit.

KEY — Five bits that indicate which of the two Command Decoders (COMDEC's) will process the message. Each COMDEC is assigned a different key in the Nimbus program since all Nimbus spacecraft have the same spacecraft address word $(026)_8$. However a different spacecraft address will be assigned to the primary and redundant command decoders, in the ERTS program providing a dual means of selecting the desired Comdec unit for real time commands.

COMMAND BITS (C_9 through C_1) — Nine bits utilized to designate the 512 possible commands.

EXECUTION TIME BITS (D_{15} through D_1) — Fifteen bits utilized to designate the time span after loading when the associated Stored Command is to be executed. The fifteen bits provide for execution times from one second to over eighteen hours after storage.

ACTIVATE BIT (A) — Must be a "one" to enable stored command execution. After execution, the activate bit is set to zero to disable the command from subsequent execution except as described under RECYCLE BIT (R).

RECYCLE BIT (R) — When in "one" state, enables re-execution of the stored command at the time interval specified by RECYCLE TIME BITS. After command execution the status of R is examined and if a "one", the RECYCLE time bits are transferred to the EXECUTION BIT time positions and the ACTIVATE BIT is set to "one".

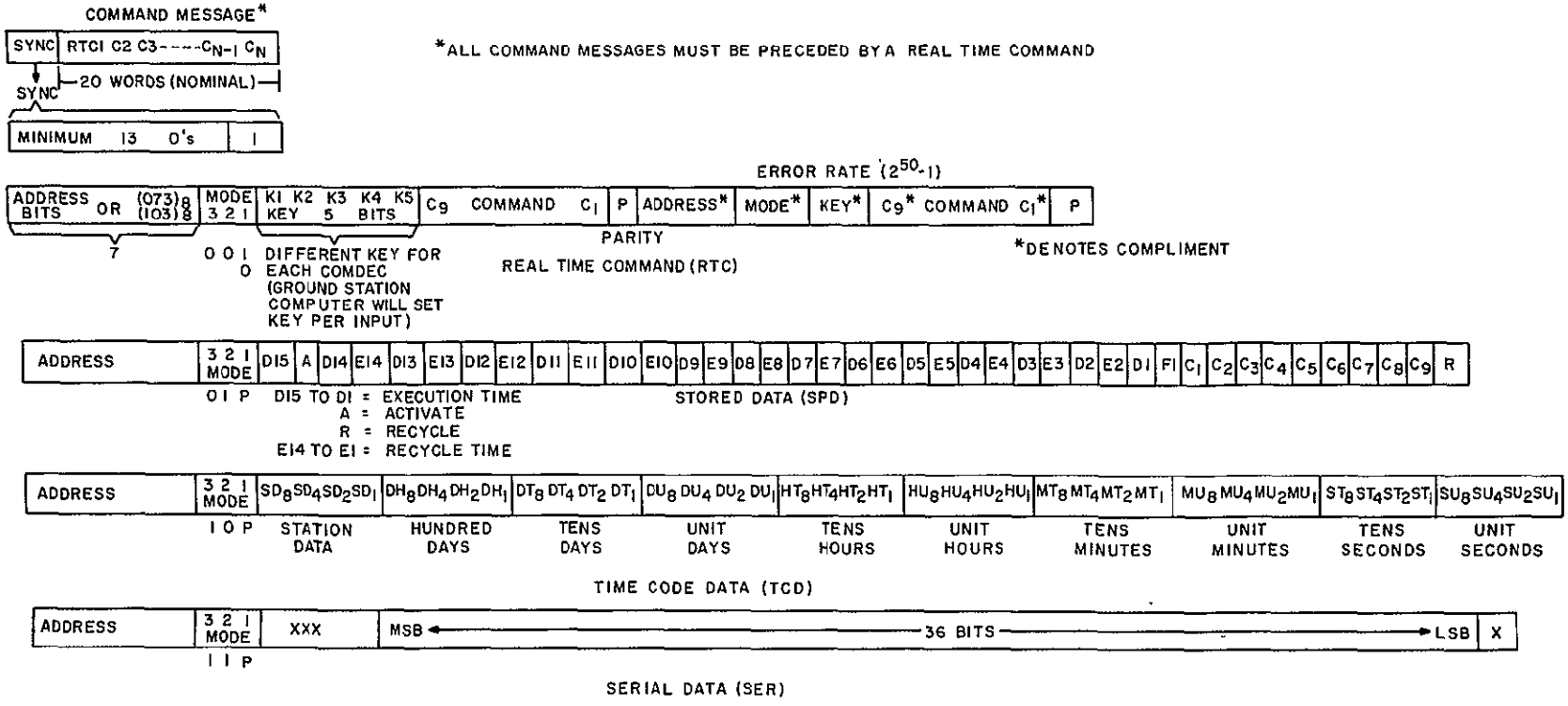

NOTES

1. ONLY THE 40 LEAST SIGNIFICANT BITS OF EACH COMMAND ARE STORED FOR THE SPD COMMANDS.

2. MODE M3 M2 MI
   - 1 1 1 REAL TIME COMMAND EXTERNAL (RTCE)
   - 1 1 0 REAL TIME COMMAND INTERNAL (RTCI)
   - 0 1 P COMSTOR DATA (SPD)
   - 1 0 P TIME CODE DATA (TCD)
   - — — P SERIAL DATA (SER)

3. ALL COMMANDS CONTAIN 50 HTS

Figure 4.4.2-7. Word Structure Transmission

RECYCLE TIME BITS (E_{14} through E_1) — Fourteen bits define the time span between the first time the command is executed and the time when the command is to again be executed. The fourteen bits provide for recycle times of from one second to over nine hours.

TIME CODE DATA (SD_8 through SU_1) — Forty bits of data are arranged into ten BCD character groups. The 10 characters allow for GMT specification of time in hundreds, tens, and units for days; tens and units for hours, minutes and seconds; and a four bit word (SD_8, SD_4, SD_2, SD_1) as an identifier or station data.

SERIAL DATA (MSD-- 36 BITS--LSB) — Thirty-six bits that define three 12 bit memory words intended for the reprogrammable PCM telemetry memory (external to the command clock).

ASTERISK BITS — Twenty-four bits associated with Real Time Commands provide a redundant basis for checking each of the ADDRESS, MODE, KEY, and COMMAND bits.

Figure 4.4.2-8 compares the format constraints as presented in the "Data Systems Standards" and the ERTS Command/Clock format. The Standards permit a 64 bit command word while the ERTS format uses only 50 bits for all types of commands.

4.4.2.2.3.2 Bit Synchronization. The Command/Clock receives the encoded commands from the Command Integrator in the form of three signals (W, X and Y). The three signals are command data (W), bit synchronization (X), and command enable (Y). Their time relationship and logical levels are shown in Figure 4.4.2-9. The bit synchronization occurs with the positive zero crossing (0 to -12 volts corresponds to a positive rising signal because of the -24 volt power supply on the ERTS spacecraft) at the 1/2 position of the bit period interval. The Command/Clock will accept an ± 11.5% jitter tolerance of the sync positive zero crossing when decoding a reconstituted data pulse with 6.5% rise and decay times. The standards permit the transmission of a synchronization signal with only 5% jitter tolerance relative to the center of the data pulse. Thus, the command decoder has a 2:1 safety factor relative data synchronization.

4.4.2.2.3.3 Command Verification. Three methods of spacecraft command verification are provided for real-time commands. The standards require only one method. However, the additional information on command activity and command status aides the ground data handling system in monitoring and analyzing the Spacecraft functions.

The three verification techniques are as follows:

1. Complement check. The first 25 bits of the command word is compared bit by bit against its complement (the last 25 bits of the real time command word) as the command is received by the command decoder. If a bit error occurs, the command is rejected and an error flag is provided to the telemetry PCM processor. The flag word is sampled by Telemetry PCM processor once every 0.2 seconds which is greater than the MSFN transmission word rate (i.e., .25 seconds). The

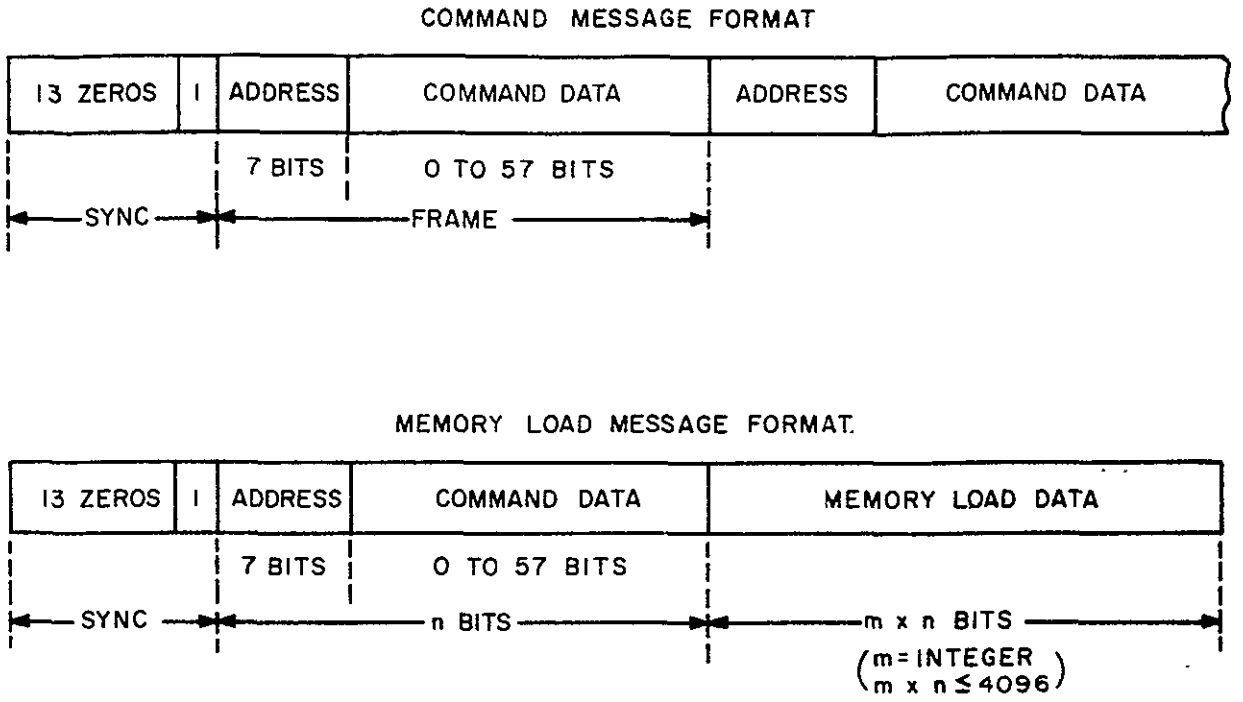

Figure 4.4.2-8. ERTS Command Format

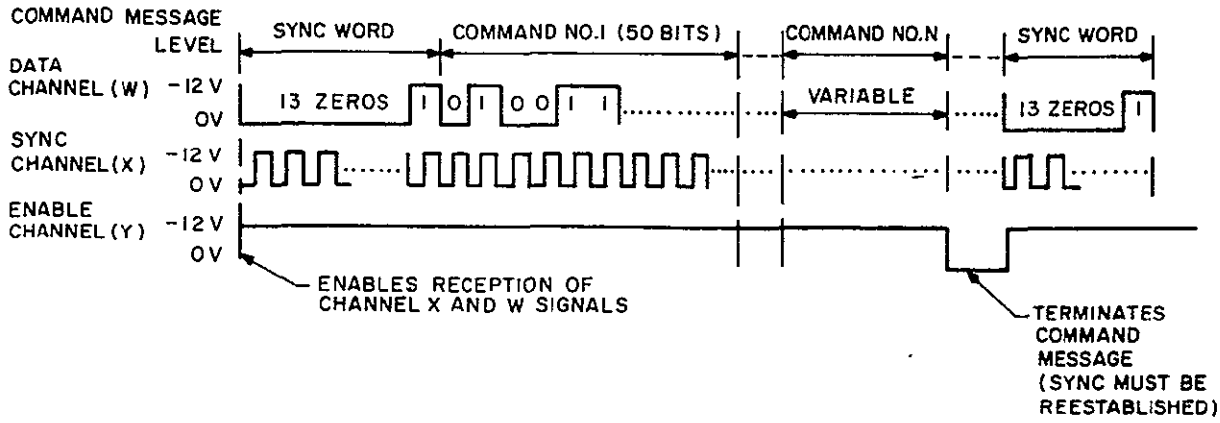

NOTES

1. COMMAND NO 1 WILL ALWAYS BE A RTCI COMMAND TO ENABLE SUBSEQUENT ROUTING AND/OR ESTABLISH THE EQUIPMENT CONFIGURATION OR OPERATIONAL MODE
2. CHANNEL W (DATA) BIT PATTERN IS SAMPLED AT CHANNEL X (SYNC) NEGITIVE TRANSITION TIME ("0" TO "1").
3. CHANNEL X WILL CONSIST OF A SQUARE WAVE LAGGING CHANNEL W BY ONE-HALF BIT TIME (128 Hz). STROBE ACTION IS POSITIVE GOING AT MID POINT OF DATA BIT
4. THE COMMAND TRANSMISSION RATE WILL BE 128 TO 200 BITS/SECOND.
5. ONLY ONE COPY OF EACH COMMAND WILL BE SENT

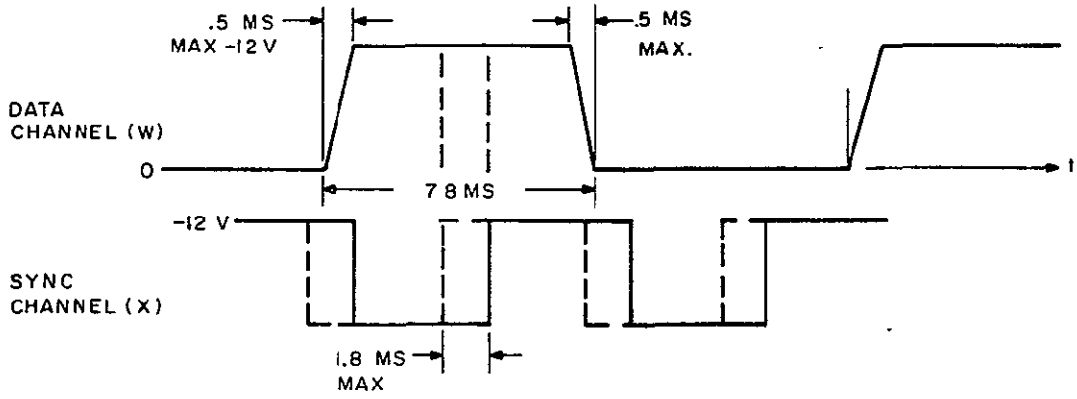

Figure 4.4.2-9. Command Signal Waveform Pattern

command error flag word is reset at the beginning of a new message, thus permitting the ground station to monitor the reception of each command word at nearly the word transmission rate.

2. Command Execution Counter. A single 6-bit counter maintains a cumulative total (0 to 63) of all executed commands (including stored commands). The counter can be reset by a real time command and its count status is telemetered for ground station command correlation.

3. Monitoring and Telemetring Command Relay Status. The status or relay state of each command relay is sampled by the PCM processor once a major frame.

4.4.2.2.3.4 Probability of a False Command. Prime concern is the execution of a non-reversible command. However, we will examine all real time commands. Examining the word structure in Figure 4.4.2-7 we see there are several ways in which a false command can be executed.

First, the conditions which must exist to execute a real time command must be examined:

1. The two halves of a 50 bit word must be complementary (i.e. corresponding bits must be complements).
2. Spacecraft Address (7 bits), Command Mode (3 bits), and Command Decoder Key (5 bits) are individually checked and must be correct.
3. Single bit parity for each half of the word is checked requiring two errors in each half of the word before parity is false.
4. The execution of a non-reversable command is accomplished by the execution of two independent real time commands.

Using the above ground rules and examining the word structure in Figure 4.4.2-7 we can state the way in which a false command can be executed:

Case 1. All bits correct except two corresponding command bits or a command bit and parity are in error, in each half of the word.

Case 2. A real time internal command executed as real time external command. This requires a mode bit error and command bit error in each half word.

Case 3. Stored, Time Code, or Serial data interpreted as a real time external command. This requires (a) two bits error in each half of the real time internal command preceeding the data which normally opens the proper gate for the data, (b) an error in the mode bit of the data word, (c) an additional bit error to give correct parity and (d) the 40 word bits correct in the data command.

Case 4. A command addressed to another spacecraft received correctly over the STADAN link. Assume the unwanted signal exceeds the receiver threshold, it must have three errors in the spacecraft address to be accepted and remaining 43 bits be correct.

The probability of error for the four cases in discussed below:

Case 1. We need four errors in a word with all other bits correct. Let p equal the probability a bit is in error and q = (1-p) equal the probability it is correct. Then the probability of 4 errors and 46 correct bits is,

$$\overbrace{p\ p\ p\ p}^{x}\qquad\overbrace{q\ q\ .\ .\ .\ .\ q}^{n-x} = p^{x}\,q^{n-x}$$

where x = 4 and n = 50 number of bits in the word.

The number of orders of bits is the number of permutations with the 9 command bits taken 2 at a time. (9 instead of 18 is used because the error must be the same in the command and its complement before being accepted.) Since each of these permutations are mutually exclusive events, the total probability of a false command in this manner is the probability of one trial times the number of ways it can occur. Thus,

$$Pe = \frac{M!}{X!\ (M-X)!}\ p^{x}\ q^{n-x}$$

M = number of bits in the command.

Assuming the probability of a bit error is 10^{-6}, (which is a performance requirement) the probability of a false command is:

$$Pe = \frac{9!}{2!(7!)}\ (10^{-6})^{4}\ (1-10^{-6})^{46}$$

$$= (36)\ .99984 \times 10^{-24}$$

$$Pe \approx 36 \times 10^{-24}$$

In the case where we restrict one error to the parity bit only 9 different ways can be obtained to get false command. The probability of error for case 1 is $(36 + 9) \times 10^{-24} = 45 \times 10^{-24}$.

Case 2. The mode bit error, is the same as the parity error so we get Pe for Case 2 $= 9 \times 10^{-24}$.

Case 3. Data word error is the probability of a mode bit and the 22 bits not including the command bits in the RTCI, times the probability the data word has "correct" errors. The probability of error is then given by:

$$Pe = (22)\ 10^{-24}\ \ 40 \times 10^{-12}\ \left(\frac{1}{2}\right)^{40}$$

$$= 8.8 \times 10^{-46}$$

The factor ($\frac{1}{2}$) assumes all 40 bits in the data word are equally likely ones or zeros (i.e., $p = \frac{1}{2}$), and since all 40 must be correct it is simply the product of these 40 events (i.e., the joint probability of 40 independent events).

Case 4. For the case of the unwanted receiver signal, we need to compute the joint probability that (a) we receive a "jamming" signal; (b) that it has the proper format, and (c) if these happen, the conditions previously stated in Case 4 occur. Thus, we can only compute the conditional probability that conditions (a) and (b) have been satisfied. Then,

$$Pe = \frac{7!}{3!\ (7-3)!} \quad (10^{-6})^{3} \quad (\tfrac{1}{2})^{43}$$

Again, this assumes ones and zeros are equally likely.

$$Pe = (36)\ 10^{-31}$$

To obtain the total probability of a false real-time command we shluld add the probabilities of each case since they are mutually exclusive events.

Case 1 and 2 are by far the largest so we can ignore cases 3 and 4. Thus, the probability of a single false command is 5.4×10^{-23}.

The probability of the joint occurence of two consecutive false commands required to actuate a non-reversable command, is the square of the Pe for a false command, times the probability two consecutive real time commands are sent without checking the status of the non-reversable relay states between the two commands. This is indeed an unlikely occurence.

4.4.2.3 Stored Command Studies

4.4.2.3.1 Study Requirements

The following three items were examined during the support of the system requirements:

1. Provisions for storing 30-digital commands.
2. Capability of multiple execution (up to 100) from among the 30-stored commands.
3. Capability to override and verify-stored commands.

The functions and capability of the present-command storage unit in the command/clock will be presented to show how it meets these requirements as well as the command storage requirement imposed by the systems study given in Section 4.5 of Volume I. That section will present the rationale establishing the requirement for 30 stored commands.

Stored Command Functions - Two stored-command modules (COMSTOR's) are designated primary and redundant, operating in association with the real-time command modules. Each is capable of being independently loaded, and verified. Overriding commands can be accomplished in either unit. The following is a description of these functions:

1. Loading

   The command/clock provides storage capacity for 15-stored data (SPD) commands in each COMSTOR, for a total capacity of 30 unique 40-bit memory words. A real-time command internal (RCTI) "Comstor ON and Fill" designates and initializes the selected COMSTOR and permits loading of the stored data in consecutive memory locations starting at memory word one and progressing to word fifteen. The loading of one COMSTOR does not interfere with the operation of the other COMSTOR.

2. Verification

   The contents of each COMSTOR is verified by sending an RCTI (COMSTOR VERIFY). When the command/clock is in the "verify" mode, all command-output registers are inhibited from command execution. The stored words are read out at one word per second starting at word No. 1, and routed to the PCM Telemetry processor instead of the Time Code Data. At the beginning of the verification sequence, the clock subtracts 16 seconds from the time tag of each stored command to compensate for the time consumed in the verification process.

3. Override

   If during the verify mode an error or errors are detected by the ground station computer, the operator has two methods of overriding the erroneous-command words as follows:

   a. Reload the entire contents of the memory as previously described under loading, or

b. Override individual commands by using a RTCI called "Comstor Copy". This command permits a storage location to be skipped by reinserting (or copying) the word in a storage location back into the same location. Thus, if storage location, say three wished to be changed but the first two words in storage remain unchanged then the sequence of Commands would be as follows:

(1) "Comstor ON and FILL"

(2) "Comstor copy" (location No. 1)

(3) "Comstor copy" (location No. 2)

(4) New Command (location No. 3)

After reloading the Comstor unit, the contents would again be verified to assure proper commands are stored.

Receipt of an RCTI for "COMSTOR ACTIVATE" enables the COMSTOR to execute the stored (SPD) commands within its memory. If during a verification sequence, an RTCI for "COMSTOR ACTIVATE" is received the command clock holds this command until completion of verification, then executes the command. The COMSTOR decrements the execute time tag of each (SPD) command every two seconds until zero is reached, then executes the command pulse on the specific MTXA and MTXB lines designated by the C_1 through C_9 bits. The time for first execution of each stored command (measured from insertion time to first execution) is 18 hours maximum, in increments of two seconds. If the recycle bit is "one", each stored command will be re-executed in a cyclic manner starting at the first execution time. The recycle period is nine hours maximum, measured in increments of two seconds. A six-bit counter maintains a status count of all executed real-time commands. The counter, since its contents are telemetered via PCM Telemetry, can be utilized as a status detector for the execution of the RTCI associated with the SPD commands programmed to execute in a given time interval.

4.4.2.4 Fail-Safe Design Techniques and Operating Philosophy

Fail-safe design falls into two categories. The first is assuring that real time and stored commands will be correct with high probability, and second, that there is an adequate procedure for controlling the operation and power to the primary and redundant units in the spacecraft.

The probability of a false command and reliability of the command subsystem is discussed in Sections 4.4.2.2.3.4 and 4.4.2.5.2 respectively. The intent of this discussion is to describe the operating procedures for controlling critical functions and high power dissipation subsystems.

This Page Left Blank Intentially

Figure 4.4.2-10.

1. Nonreversible Commands. The nonreversable commands on the ERTS spacecraft are activated by two independent real-time commands. Prior to activating these nonreversable functions, the operating procedures will be to monitor the status of all command relays after the transmission of each real-time command. This assures that if a nonreversable command relay is inadvertently actuated, it will be monitored and reset prior to execution of any additional commands. Thus, it will be virtually impossible to erroneously execute both of the real-time commands necessary to activate a nonreversable function.

2. Command Philosophy. The Command Subsystem is completely redundant from the command receivers (i.e. STADAN and USB) to the output of the command/clock. All primary units will be normally powered and the redundant units unpowered until the primary unit fails. The two exceptions are the command-storage units (Comstor) and command decoders which are both normally powered.

   The concern of this study is to assure that the redundant units can be switched "in" or power applied to them in case of failure of the primary unit and that power is switched off high-power loads when not in use.

3. Command Receiver Channels. The requirements to receive command signals from either a MSFN or STADAN ground station along with receiver redundancy leads us to dual redundant receiver channels. The earliest point in the processing chain of these two receiver channels where the signals are enough alike to be combined is the output of the demodulators and sub-bit decoder for the STADAN and MSFN/USB receiver channels respectively. The signals cannot be combined earlier because of the different modulation techniques used at the STADAN and MSFN station. Figure 4.4.2-11 shows a block diagram of the two receiver channels. The intent of this arrangement shown is to provide redundancy for each unit or subassembly.

   The method of control of the units is to switch power supply voltage ON or OFF to the prime or redundant channel instead of switching the signal lines.

   The objectives are as follows:

   1. Prevent additional signals and noise from being added to the system by the unused subassembly.
   2. Conserve power by removing unused units.
   3. Avoid placing relay contacts in a signal line where contact resistance could significantly degrade the command subsystem performance.

   Relay contact resistance is a variable which could influence the voltage or current to a unit, but by proper design of the equipment its performance can be made insensitive to these variations in supply voltage.

4. Control of Redundant Receiver Subassemblies. The dual redundancy provided by the STADAN and MSFN/USB receiver channels permits the flexibility of having one receiver channel control the operation of the other channel. The concept is to have all the primary STADAN and MSFN/USB subassemblies powered at all times permitting for example, the STADAN ground station to switch in a redundant MSFN/USB

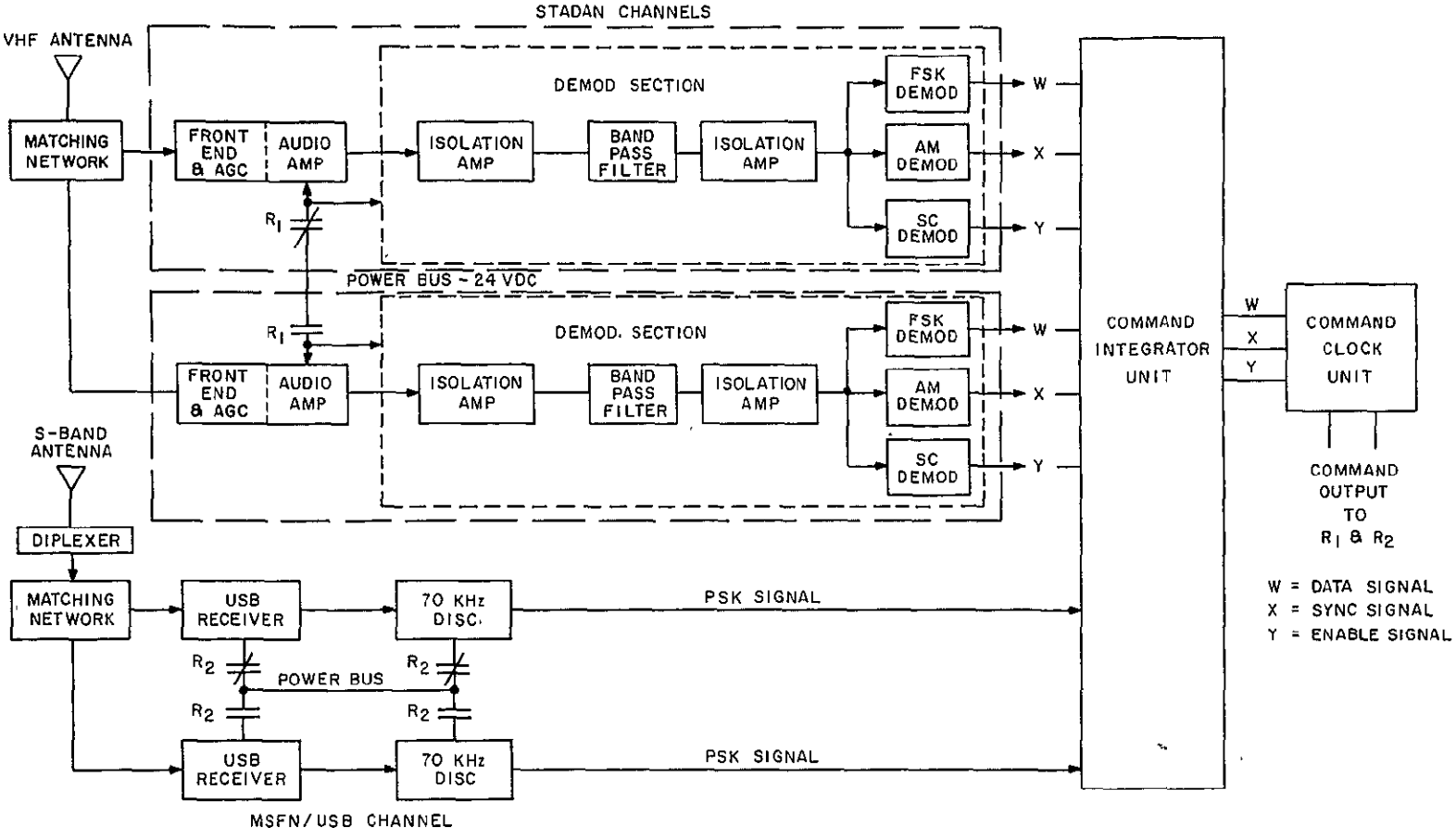

Figure 4.4.2-11. Command Receivers Block Diagram

receiver unit in case a MSFN/USB primary unit fails and vice versa. This assumes that the time delay in issuing commands by using this technique will be tolerable. That is, a failure in one of the MSFN receiver subassemblies may not be detected until it was flying over a MSFN site which would be sensed by a drop in AGC voltage and output signal. The corresponding redundant unit could not be switched in until it was in view of the next STADAN site. A standard encoded-digital command would be used to control this failure replacement function as indicated by relay contacts R1 and R2. A major assumption made by NASA during the Nimbus Programs is that only one failure will occur between the issuing of emergency or corrective commands to the spacecraft. This ground rule has also been used in the design of the ERTS emergency control system.

5. Critical Controls. Since there is dual redundancy in the command receivers (i.e. two redundant receiver channels), the critical section of the command subsystem is that portion of the Command Integrator Unit after STADAN and MSFN signals have been combined and the Command Decoder in the Command/Clock. A failure in the decoder prevents all commands from being executed. Therefore, the output "OR" gates in the Command Integrator Unit and both Command Decoders (Comdecs) will be powered continuously.

   Another critical spacecraft function is the Power Regulator. In case of a loss in voltage in the primary Power Regulator, an emergency command is used to switch in the redundant unit. This is actually a backup command since the redundant Power Regulator is automatically switched in with loss of voltage on the primary unit. The power to perform the switching is supplied by the auxiliary bus. The same auxiliary bus supplies power to the two receiver channels, the Command Integrator, and the command portion of the Command/Clock.

4.4.2.5 Determination of Spacecraft Clock Time

It is required that the time of the spacecraft-clock update be known to within a one-bit time of the PCM telemetry data rate. Since the PCM telemetry data rate is 1 K bps the spacecraft time should be known to within one millisecond. The final objective is to use the accuracy with which spacecraft time is known to aid in accurately locating image data with respect to the ground areas over which it was taken.

1. Frequency Generation. The Command Clock generates the spacecraft standard precision frequencies, two-phase motor drive signals, as well as the time-code data. The primary and redundant 3.2 MHz oscillators from which the all output frequencies are derived, have a frequency stability of five parts in 10^7 or better over a period of 230 hours, measured 0° C to 50° C at sea level.

   The output signals from the clock are coherent-square waves with transition times of less than six microseconds, or 10 percent of one cycle period, whichever is less. By coherent, we mean their positive or negative transitions (i.e. zero crossings) occur at the same time as indicated in Figure 4.4.2-13. The square waves are 97 to 100 percent symmetrical for frequencies 200 KHz and below and 90 percent to 100 percent symmetrical above that value. Symmetry is defined as shown in Figure 4.4.2-12.

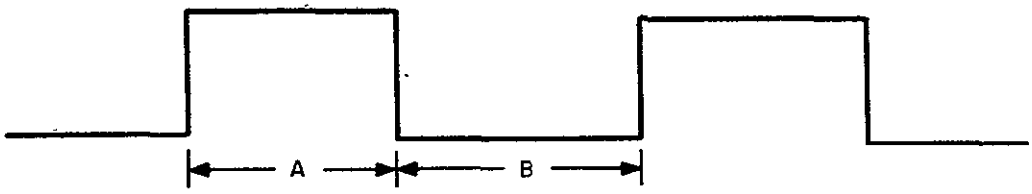

Figure 4.4.2-12. Coherent Square Wave Diagram

$$\% \text{ symmetry} = \frac{A}{B} \times 100\%;$$

Clock Characteristics

The clock provides an accurate time reference in seconds, minutes, hours, and days, and provides stable frequencies for use by experiments and subsystems. See Figure 4.4.2-13.

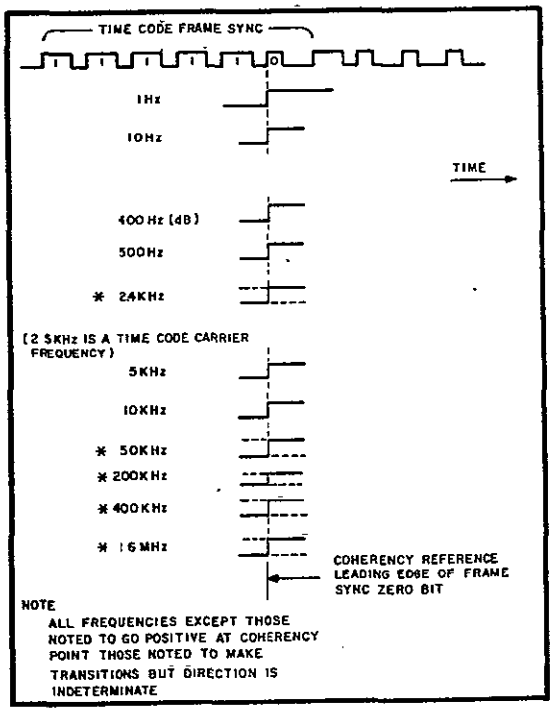

Figure 4.4.2-13. Clock Functions & Coherency Chart, Nimbus Clock

Accurate time reference is usable by the experiment in following two ways:

1. Stored Commands. The clock provides a reference for the command system so that a limited number of commands can be executed at a predetermined time.

2. Time Identification. Spacecraft time is provided at 100 pps to the PCM T/M Processor for placement in the PCM T/M Processor matric, providing correlation of all PCM T/M Processor data.

Frequencies provided by the clock are 1, 10, and 500 Hz; 2.4, 5, 10, and 50 KHz; and 0.4, and 1.6 MHz. In addition, two-phase clock signals (Phase B leads Phase A by 90 degrees) are provided at 100 and 400 Hz, and two-phase motor drive signals are provided at 400 Hz. All clock frequencies are coherent-square waves; the coherency is defined in the coherency chart.

2. Time Code Generation. The time code is stored in a 40-bit shift register in BCD format, and is up-dated once a second by the positive transition of the 1 Hz square wave. Standard-time code format is used where the first 9-BCD characters (i.e. 36 bits) give the time in units of seconds to hundreds of days and the 10th, 4-bit character is the station ID.

   The digital time-code signal is pulse width modulated at 100 pps, using the standard Minitrack format. That is, every tenth of a second, six sync bits and one 4-bit BCD character are generated, with each bit being 1/100 of a second in duration. Thus, in one second all 10-BCD characters are formatted and transmitted to the PCM Telemetry processor and tape recorders in a sequential manner with the least significant bit first (i.e. unit seconds).

   In the PCM telemetry processor the first five sync bits are stripped off the Minitrack format and the 4-bit BCD time-code characters along with one sync bit are loaded sequentially into 10-bit shift register. That is, two sequential 5-bit characters are loaded at a time. These two-BCD characters and their sync bits are transferred to the output shift register of the PCM processor as part of the telemetry format every 0.2 seconds starting 0.1995 seconds after the positive transition of the 1 Hz square wave. Thus, two BCD time-code characters appear periodically every 0.2 seconds in the telemetry output format which is transmitted down to the ground station.

   The PCM telemetry processor is driven by the 400 KHz square wave from the Command/Clock and the major frame of the telemetry format is synchronized by

the positive transition of the 1 Hz square wave with an accuracy (i.e. jitter) of less than one microsecond. Thus, the generation of the time code and the PCM processor telemetry format are all coherently related to the positive transition of 1 Hz square wave supplied by the clock (or more precisely coherent with the 3.2 MHz reference oscillators). The ground station would then synchronize to the leading edge of the major frame sync and compare this with the phase of the GMT clock located in the ground station. The accuracy with which this can be done is limited by the signal-to-noise ratio of the two signals and knowledge of the signal time delays.

4.4.2.5.1 Effect of Signal-to-Noise on Time Position Measurement

Assume the received digital signal waveform at the ground terminal approaches a raised cosine shape in order to reduce the sideband energy. The digital pulse is shown in Figure 4.4.2-14. The equation for the digital pulse is:

$$g(t) = \frac{A}{2} + (1 + \text{Cos}\ \pi\ f_b t);\ -T < t < T \qquad (4.4.2\text{-}1)$$

$$f_b = \frac{1}{T}$$

The threshold level for pulse recognition is set at A/2, which is half the peak pulse height, and the largest slope on the waveform. A noise wave of relatively small instantaneous value V_n, displaces the time detection by τ, where

$$\frac{V_n}{\tau} = g\ (-\frac{T}{2}) = \frac{\pi\ f_b A}{2} \qquad (4.4.2\text{-}2)$$

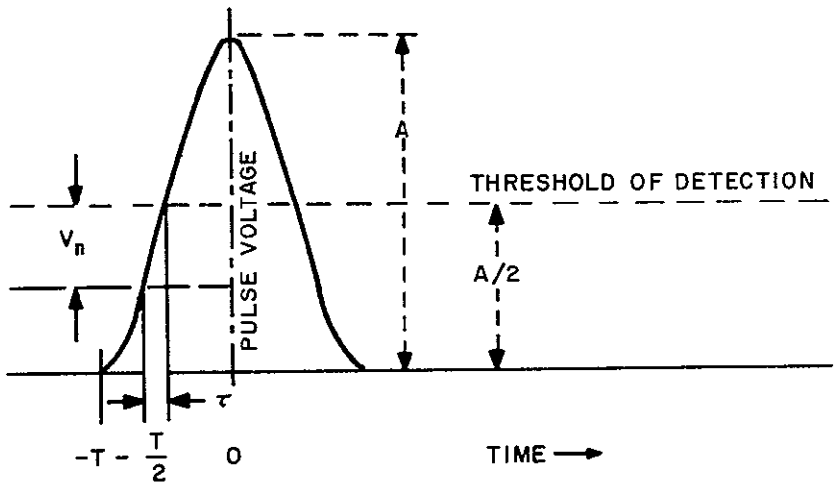

Figure 4.4.2-14. Digital Pulse Position Error Diagram

The mean square deviation produced by the noise is:

$$\langle \tau^2 \rangle = \frac{4 \langle Vn^2 \rangle}{(\pi f_b A)^2} \qquad (4.4.2\text{-}3)$$

$$\langle \tau^2 \rangle = \frac{4 \sigma_n^2}{(\pi f_b A)^2} \qquad (4.4.2\text{-}4)$$

The mean-square power in the pulse is:

$$P_s = \frac{1}{2T} \int_{-T}^{T} g^2(t)dt = \frac{3A^2}{8Tf_b} = \frac{3A^2}{8} \qquad (4.4.2\text{-}5)$$

Multiplying and dividing Equation (4.4.2-4) by Ps,

$$\langle \tau^2 \rangle = \frac{4 \sigma_n^2}{(\pi f_b A)^2} \frac{3A^2}{Ps\ 8} \qquad (4.4.2\text{-}6)$$

$$= \frac{3}{2} \pi^2 \frac{T^2}{\frac{Ps}{\sigma_n^2}}$$

In terms of signal-to-noise ratio,

$$\langle \tau^2 \rangle = 0.15198 \frac{T^2}{\left(\frac{S}{N}\right)} \qquad (4.4.2\text{-}7)$$

The rms value of the time jitter is:

$$\text{rms} = \frac{0.39\ T}{\sqrt{S/N}} \quad \text{where } T = 0.5 \text{ milliseconds in our case.} \qquad (4.4.2\text{-}8)$$

For an signal-to-noise ratio of only 10 db, τ rms is approximately 62 microseconds.

4.4.2.5.2 Errors Due to Uncertainty of Time Delay

The mean-time delays encountered in the spacecraft-telemetry circuits, propagation time and ground signal processing delay would have to be inserted prior to comparison. The task

is then to measure and compute the mean value for these transmission time delays as well as their variance or standard deviation about these means.

Since the spacecraft circuit delays will be measured prior to launch, it is assumed that these values will not significantly change over the lifetime of the spacecraft. Next, we will try to estimate these mean values and the expected jitter or variance about these means.

Time Delay Calculations

Figure 4.4.2-15 shows functionally the transmission of the time code from the clock to the ground station for comparison with the station for comparison with the station GMT clock. The total time delay from the point where the 1 Hz signal synchronizes the telemetry format to the point where it is compared with the GMT phase is given by:

$$T_T = T_{PCM} + T_{TD} + T_{PT} + T_{RD} - T_{GMT} \qquad (4.4.2\text{-}9)$$

where

T_{PCM} = time delay within the processor

T_{TD} = Transmission delay through the telemetry transmitter to the antenna

T_{PT} = propagation delay

T_{RD} = ground reception delay to the point of comparison

T_{GMT} = delay from the GMT clock to the point of comparison

The mean value of the time delay is:

$$\overline{T_T} = \overline{T_{PCM} + T_{TD} + T_{PT} + T_{RD} - T_{GMT}} \qquad (4.4.2\text{-}10)$$

where

$\overline{T_T}$ represents the ensemble average. Since the mean of the sum is equal to the sum of the means:

$$\overline{T_T} = \overline{T_{PCM}} + \overline{T_{TD}} + \overline{T_{PT}} + \overline{T_{RD}} - \overline{T_{GMT}} \qquad (4.4.2\text{-}11)$$

The more interesting statistical parameter is the variance or standard deviation about the mean value. The variance is given by:

$$\overline{(T_T - \overline{T}_T)^2} = \overline{[(T_{PCM} - \overline{T}_{PCM}) + (T_{TD} - \overline{T}_{TD} + T_{PT} - \overline{T}_{PT}) + (T_{RD} - \overline{T}_{RD}) - (T_{GMT} - \overline{T}_{GMT})]^2} \qquad (4.4.2\text{-}12)$$

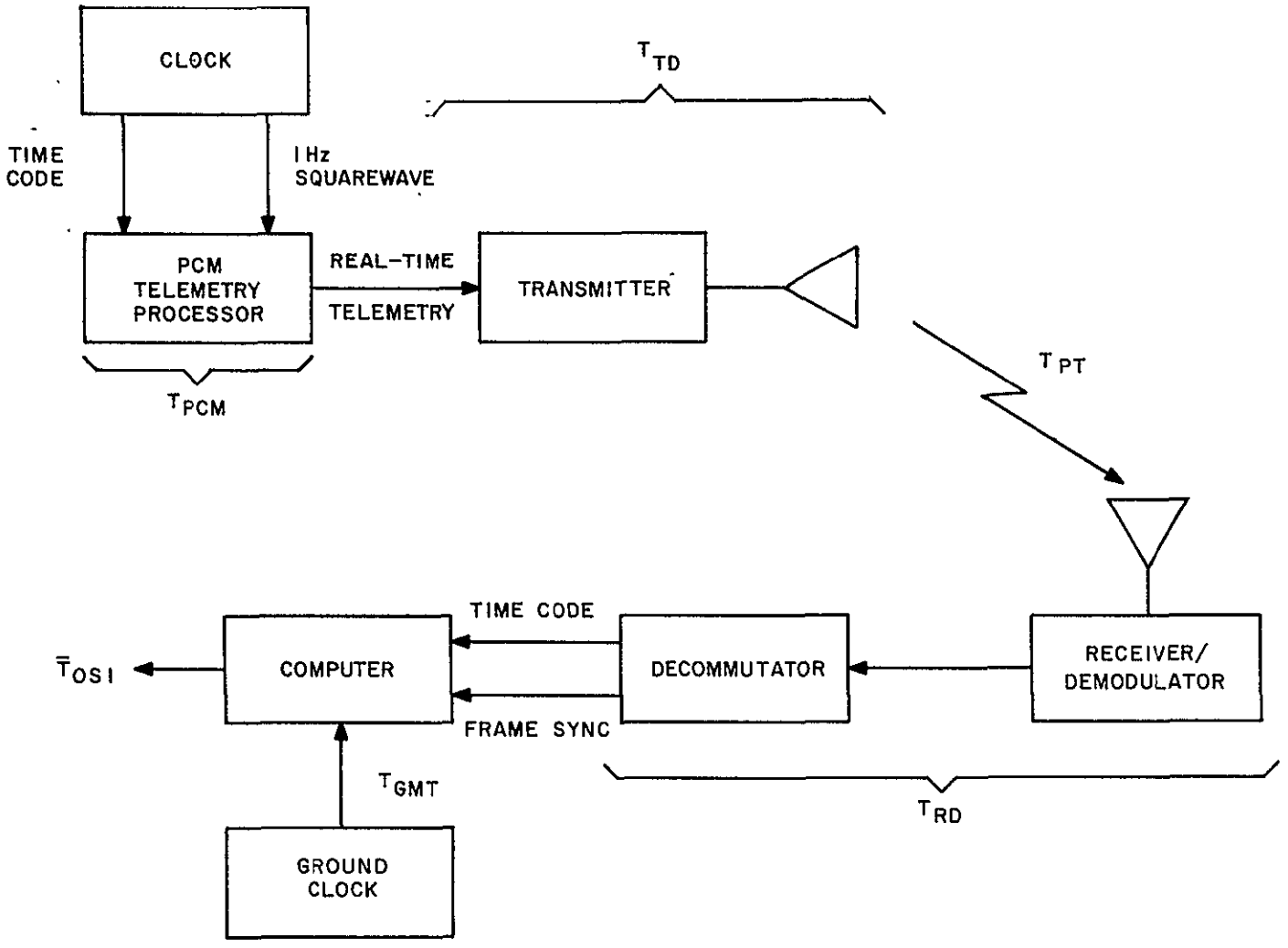

Figure 4.4.2-15. Time Code Time Delay Block Diagram

Since these time delays are independent, the cross product terms are zero and the variance becomes,

$$\overline{(T_T - \overline{T}_T)^2} = \overline{(T_{PCM} - \overline{T_{PCM}})^2} + \overline{(T_{TD} - \overline{T_{TD}})^2} + \overline{(T_{PT} - \overline{T_{PT}})^2} + \overline{(T_{RD} - \overline{T_{RD}})^2} + \overline{(T_{GMT} - \overline{T_{GMT}})^2} \quad (4.4.2\text{-}13)$$

which is simply the sum of the variances:

$$\sigma T_T^2 = \sigma T_{PCM}^2 + \sigma T_{TD}^2 + \sigma T_{PT}^2 + \sigma T_{RD}^2 + \sigma T_{GMT}^2 \quad (4.4.2\text{-}14)$$

The standard deviation is the square root of σT_T^2 or σT_T.

The mean values and standard deviations are given in Table 4.4.2-2.

TABLE 4.4.2-2. MEAN VALUES AND STANDARD DEVIATIONS

Parameter	Mean Value in Milliseconds	Standard Deviation in Microseconds
PCM Bi Phase Generator	10 (one word length)	less than 1
Transmitter & Transmission Line	≈0.5	≈1
Propagation Delay	10 max	*50-100
Ground Receiver	≈0.5	≈1 - 2
GMT Clock to Comparator	≈0.2	≈1 - 2
Estimated T_T	= 21.2	σT_T = 100

*This assumes propogation delay can be measured on the ground by measuring the round-trip time delay of the ranging signal at the MSFN sites.

One uncertainty is the position of the spacecraft relative to the ground station. The mean values of all other delays can be accurately measured.

Summary - Assuming signal-to-noise ratio of 10 db at the output of the ground receiver demodulator and a standard deviation of 100 microseconds about the expected mean delay, the total standard deviation about the true phase difference between the spacecraft clock and station GMT is approximately 118 microseconds.

4.4.2.5.2 Command Subsystem Reliability

The reliability for the Command Subsystem was computed using the functional failure diagram shown in Figure 4.4.2-16. The estimated probability of successful operation for one year for all functions is 0.99425. The command/clock unit has a probability of success of 0.99468 for one year's operation.

Assumptions

1. Reliability computed for one-year mission time.
2. In standby redundancy, the standby element is assumed to have 1/10 normal (powered) failure rate.

Probability of success for standby-redundancy reliability is given by,

$$R = 10\left[e^{-\lambda t} - e^{-1.1\lambda t}\right] + e^{-\lambda t}$$

λ = failure rate (See Table 4.4.2-3)

4.4.2.6 Clock Acceleration and Tests

The ERTS Clock does not permit the capability to accelerate the timekeeping section to count through one year in a short period of time. To incorporate this requirement would result in considerable redesign of the time-code section. However, the operation of time-code section can be completely checked out by allowing the timekeeping computation to overflow or reset back to zero. This is mechanized by loading or setting the register near the maximum time (days, hours, minutes, and seconds) and allowing the normal count cycle to count up to absolute maximum and overflow to all zeros. This method checks all gating logic and carry logic employed within the entire counting sequence for the most stringent operating condition.

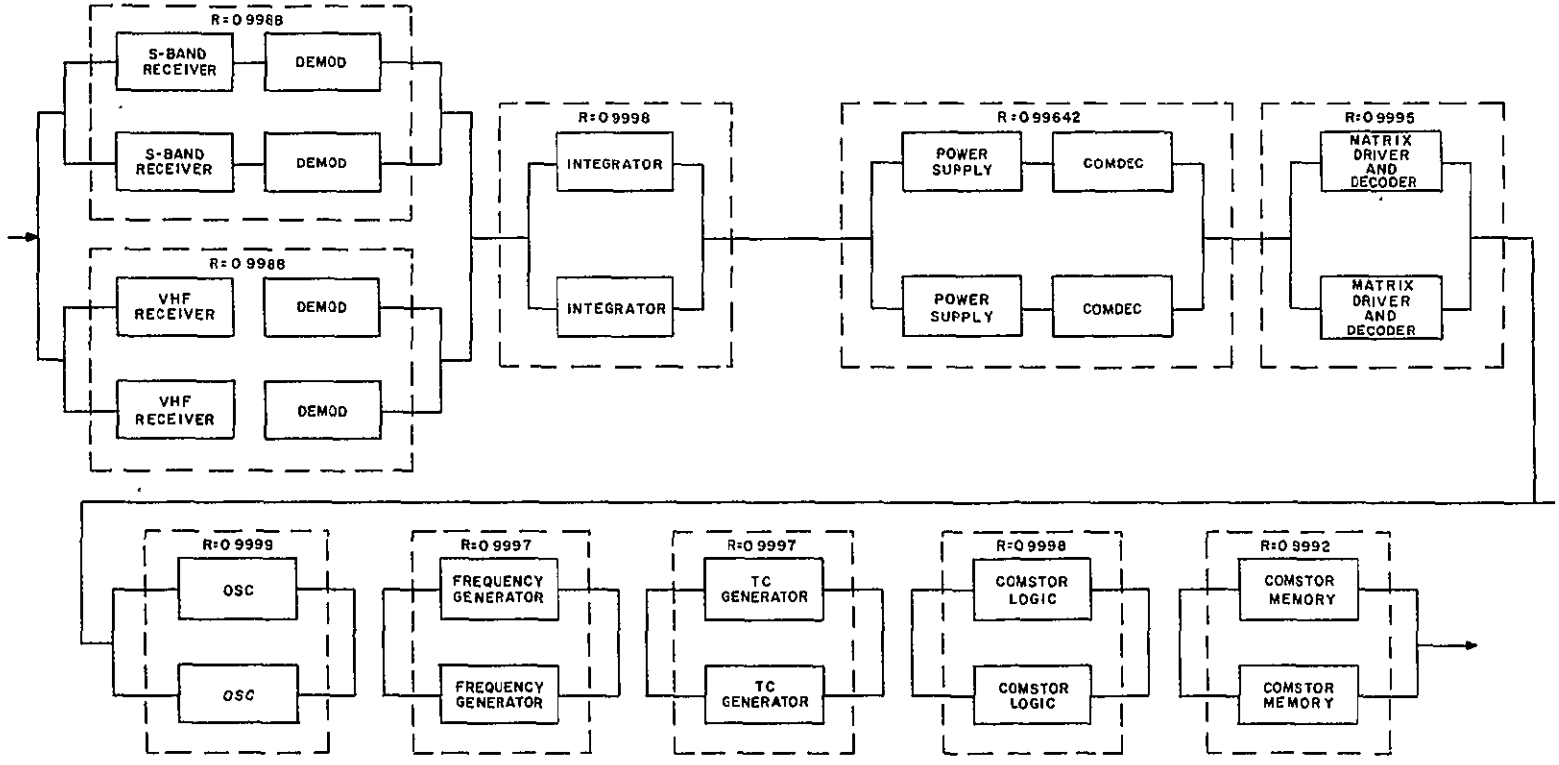

Figure 4.4.2-16. Command Subsystem Reliability Block Diagram

TABLE 4.4.2-3. COMMAND SUBSYSTEM FAILURE RATE

Component	Failure Rate $\lambda \times 10^6$	Source
S-Band Receiver	1.60480	ORI 469 - p. 113
Demodulator	3.82950	ORI 469 - p. 113
VHF Receiver	1.60480	ORI 469 - p. 113
Integrator	1.5 (est)	Rates derived conservatively from MIL-HDBK-217A supplied by vendor. Reduced by 1 order of magnitude.
Power Supply Unit	5.83400	
Conidec	3.64750	
Matrix Driver and Decoder	3.34100	
Cannistor Logic	1.45700	
OSC	3.17700	
Frequency	1.06924	
TC Generator	2.49000	
Nine Switching Relays for Power Supply	0.47000	

4.4.3 NARROWBAND COMMUNICATIONS

4.4.3.1 Tracking

4.4.3.1.1 Minitrack Tracking (VHF)

4.4.3.1.1.1 Requirements

It is necessary to transmit a suitable minitrack beacon signal to allow tracking by STADAN ground stations. The requirements for this beacon signal are as follows:

1. Nominal beacon frequency: 137.86 MHz
2. Frequency stability: 0.003 percent
3. Effective radiated power in carrier component: sufficient to provide -120 dBm at minitrack receiver for satellite elevation angles of 5 degrees, or more
4. Modulation: Modulation components at 50 ±5 Hz, 100 ±5 Hz, and 200 ±5 Hz shall be at least 35 dB below the average power output, within a 10 kHz band centered on the carrier.

4.4.3.1.1.2 Studies and Analysis

This section presents the analysis and trade-offs leading to specifications for hardware which satisfies the requirements listed in Section 4.4.3.1.1.1. For the first two requirements, beacon carrier frequency and frequency stability, no analysis is required; these requirements can be used directly to specify hardware parameters. It is noted that the stated requirements are extremely feasible for existing off-the-shelf hardware.

4.4.3.1.1.2.1 Required Transmitter Power in Carrier Component

Section 4.4.3.1.1.1 states that the power in the unmodulated carrier component of the downlink signal shall be greater than -120 dBm at the minitrack receiver input. This can be achieved by transmitting an unmodulated carrier signal with "sufficient" (to be determined presently) radiated power. However, it is also necessary (see Section 4.4.3.2.1.1) to transmit data on a downlink carrier at 137.86 MHz. Since simultaneous operation of two independent transmitters at the same nominal center frequency is undesirable due to probable mutual interference, it is necessary to satisfy both the tracking function and the data transmission function using the same transmitter. Since the data to be transmitted (again see Section 4.3.3.2.1.1) is PCM-split-phase and is phase-modulated on the carrier, it is possible to provide an unmodulated carrier component of sufficient power and the necessary data sidebands by judicious choice of total transmitter output power and peak phase deviation of the carrier signal by the data signal.

Consider the data-modulated carrier signal $s_T(t)$ at the transmitter output terminals:

$$s_T(t) = \sqrt{2 P_T} \cos (\omega_T t + \beta_D d(t) + \theta) \qquad (4.4.3\text{-}1)$$

Where

P_T = transmitter output power

ω_T = transmitter frequency (137.86 MHz times 2π nominally)

β_D = Zero-to-peak phase deviation of the carrier in radians

$d(t)$ = binary function of time taking on a value of either +1 or -1

θ = arbitrary reference phase

It can be assumed with no loss of generality that $\theta = 0$. Hence, Equation (4.4.3-1) can be expanded, using trigonometric identities:

$$s_T(t) = \sqrt{2P_T} \left[\cos (\omega_T t) \cos (\beta_D d(t)) - \sin (\omega_T t) \sin (\beta_D d(t)) \right] \qquad (4.4.3\text{-}2)$$

Since $\cos (\theta) = \cos (-\theta)$, the first term of equation (4.4.3-2) is independent of the data signal value, $d(t)$; all data information is contained in the second term. Hence, one can write:

$$s_T(t) = \sqrt{2P_T} \left[\cos (\beta_D) \cos (\omega_T t) - \sin (\omega_T t) \sin (\beta_D d(t)) \right] \qquad (4.4.3\text{-}3)$$

Clearly the first term represents an unmodulated carrier component. Calling the power in this component P_{TC}, it follows that:

$$P_{TC} = P_T \cos^2 (\beta_D) \qquad (4.4.3\text{-}4)$$

Now the unmodulated carrier power at the minitrack receiver input, P_{RC}, is related to the value for P_{TC} by a link calculation equation:

$$P_{RC} = \frac{P_{TC} G_T G_R}{L_T L_{FS} L_R M_S} \qquad (4.4.3\text{-}5)$$

Table 4.4.3-1 defines each parameter in Equation (4.4.3-5) and presents the nominal value and adverse tolerance for each parameter. Note that

$$L_{FS} = -(37.8 + 20 \log_{10} f + 20 \log_{10} r) \text{ dB} \qquad (4.4.3\text{-}6)$$

TABLE 4.4.3-1. TRACKING LINK CALCULATION

Parameter	Description	Nominal Value	Adverse Tolerance
P_{TC}	Carrier Power at Transmitter Output	P_{TC} dBm	-
L_T	Transmitting Circuit Loss	- 1 dB	-
G_T	Transmitting Antenna Gain (Incl. Polarization Loss)	-10 dB	-3 dB
L_{FS}	Free Space Loss	-144.9 dB	-
G_R	Receiving Antenna Gain	22 dB	-
L_R	Receiving Circuit Loss	0 dB	-
M_S	System Margin	- 6 dB	-
P_{RC}	Received Tracking Power	(P_{TC} - 139.9) dBm	-3 dB
R_{RC} Required	P_{RC} Required at 5 degrees	-120 dBm	-
	Margin at 5°	(P_{TC} - 19.9) dB	-3 dB

where

f = 137.86 (carrier frequency in MHz)

r = 1642 (slant range in nm)

From Table 4.4.3-1, P_{RC} equals (P_{TC} - 142.9) dBm in the worst case; hence, choosing

P_{TC} = 22.9 dBm

yields the minimum required value for P_{RC}.

4.4.3.1.1.2.2 Modulation Components

The modulation requirement in Section 4.4.3.1.1.1 states that components at 50 ±5 Hz, 100 ±5 Hz, and 200 ±5 Hz shall be at least 35 dB below the average power output. In order to insure that this requirement is met, it is necessary to examine the frequency spectrum

of the two different data signals which are transmitted on the minitrack beacon transmitter (see Section 4.4.3.2.1.1). In both cases, a PCM-split-phase signal is transmitted. Assuming random data, the power spectrum G(f) of the baseband signal is given by

$$G(f) = \frac{2}{R_D} \frac{\sin^4 (\pi f/2R_D)}{(\pi f/2R_D)^2} \quad \text{Watts/Hz}$$

where R_D equals one kHz for real-time telemetry and 24 kHz for stored telemetry. Figure 4.4.3-1 shows a logarithmic plot of G(f).

The worst case for interference is the one kbps case. Although there are no spectral components, approximately $2\frac{1}{2}$ percent of the total power is below 200 Hz. This is only 16 dB below the total data power, or about 21 dB below the unmodulated carrier. However, the power in a one Hz bandwidth around 200 Hz is about 42.2 dB below the unmodulated carrier.

There is no interference problem with the 24 kbps stored telemetry signal, since its power is spread over a bandwidth 24 times as great as in the one kbps case.

Hence, even without premodulation filtering of either data signal, no interference with the minitrack tracking receiver should occur. However, to insure this, the frequency response of the VHF transmitter phase modulator can be suppressed below 205 Hz. This will not significantly degrade the detection process for either data signal.

4.4.3.1.2 Mark 1 Ranging (USB)

4.4.3.1.2.1 Requirements

Capability must be provided to receive and demodulate a pseudo-random-noise (PRN) ranging signal which has been phase-modulated on the uplink USB carrier. The demodulated PRN signal shall be remodulated on the downlink USB carrier with a fixed time delay from reception to retransmission.

4.4.3.1.2.2 Studies

In order to provide the above capability, redundant USB coherent transponders are part of the narrowband communication equipment. Studies concerning this equipment are described in Section 4.4.3.5.

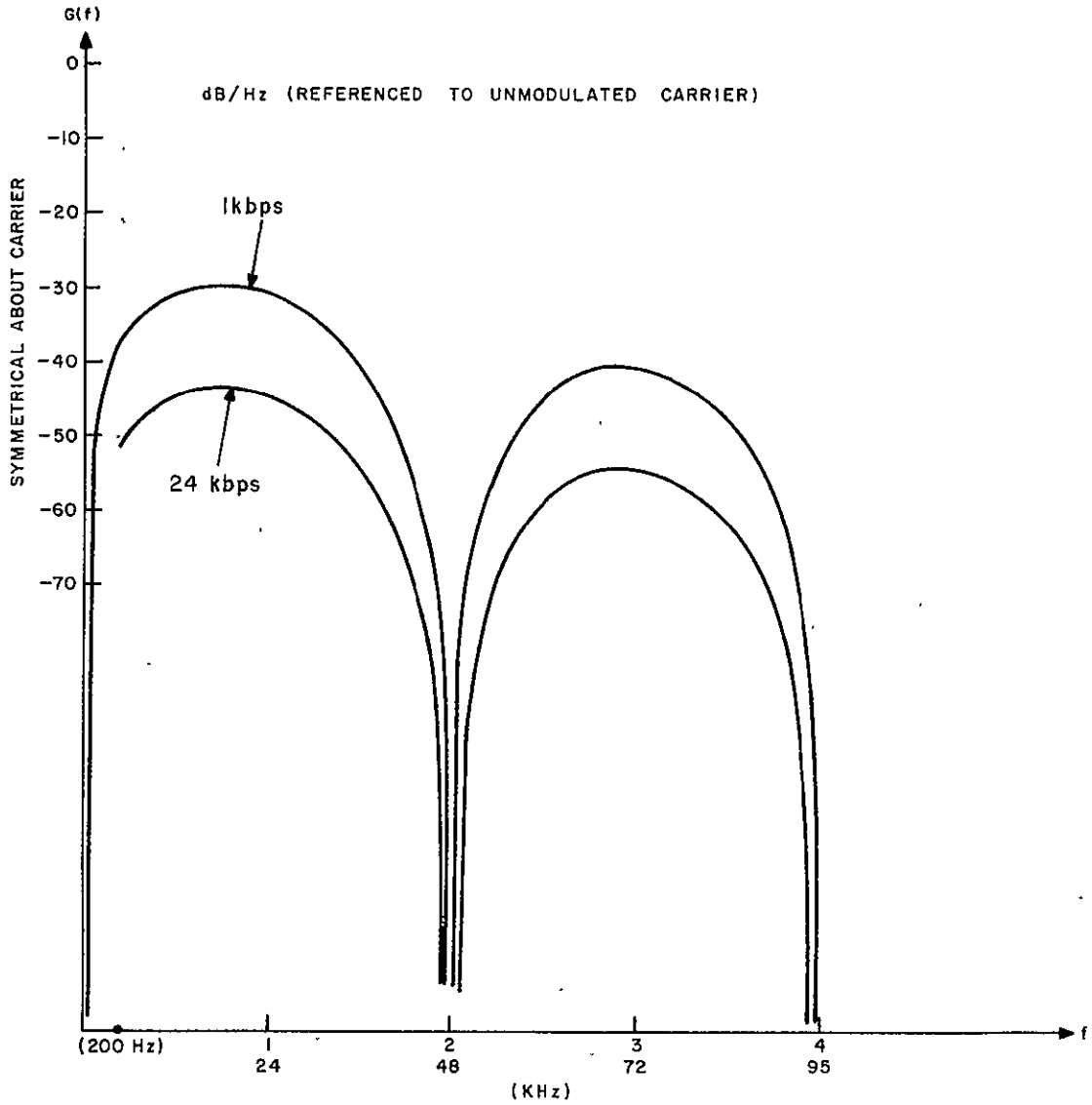

Figure 4.4.3-1. PCM-Split-Phase Spectrum

4.4.3.2 Telemetry Links

4.4.3.2.1 VHF Link

4.4.3.2.1.1 Requirements

It is necessary to transmit either the real time PCM housekeeping telemetry signal or the stored PCM housekeeping telemetry signal via a VHF transmitter channel. Following are general requirements:

Transmitter Center Frequency: 137.86 MHz ±.003 percent

Channel Bandwidth: 30 kHz, real-time telemetry data
90 kHz, stored telemetry data

Following is a description of each signal:

Real-Time Telemetry

Signal Description: PCM-split-phase-L

Bit Rate: 1 kilobit per second

Probability of Bit Error Upon Detection: Less than 10^{-6}

Stored Telemetry

Signal Description: PCM-split-phase-L

Bit Rate: 24 kilobits per second

4.4.3.2.1.2 Studies and Analyses

4.4.3.2.1.2.1 Required Transmitter Power in Data Sidebands

Section 4.4.3.1.1.2.1 presented the equation of the RF signal transmitted on the VHF downlink when a data signal is phase-modulating the transmitter. Examination of equation (4.4.3-3) shows that the second term on the right-hand-side represents the data sidebands. Calling the transmitted power in the data sidebands P_{TD}, it follows that

$$P_{TD} = P_T \sin^2(\beta_D) \qquad (4.4.3\text{-}7)$$

where the notation remains the same as in Section 4.4.3.1.1.2.1. The received power P_{RD} in the data sidebands at the ground station can be determined from P_{TD} in a link calculation similar to Equation (4.4.3-5) and Table 4.4.3-1. In fact,

$$P_{RD} = \frac{P_{TD} G_T G_R}{L_T L_{FS} L_R M_S} \qquad (4.4.3\text{-}8)$$

Table 4.4.3-2 shows an evaluation of Equation (4.4.3-8). The received data signal power is seen to be (P_{TD} - 142.9) dBm in the worst case for a S/C elevation angle of 5 degrees (slant range of 1642 nm). The required value for P_{RD} is now determined for the real time telemetry signal and the stored telemetry signal.

TABLE 4.4.3-2. DATA LINK CALCULATION (VHF)

Parameter	Description	Nominal Value	Adverse Tolerance
P_{TD}	Data Power at Transmitter Output	P_{TD} dBm	-
L_T	Transmitting Circuit Loss	- 1 dB	-
G_T	Transmitting Antenna Gain (Incl. Polarization Loss)	- 10 dB	-3 dB
L_{FS}	Free Space Loss	-144.9 dB	-
G_R	Receiving Antenna Gain	22 dB	-
L_R	Receiving Circuit Loss	0 dB	-
M_S	System Margin	- 6 dB	-
P_{RC}	Received Data Power	(P_{TD} - 139.9) dBm	-3 dB

Real-Time Telemetry Signal

A requirement is that the probability of bit error for the detected real-time telemetry signal be less than 10^{-6}. Figure 4.4.3-2 shows the theoretical probability of bit error versus E/N_o, which is the ratio of signal energy per bit to the noise spectral density at the detector input. For a probability of bit error less than 10^{-6}, the theoretical curve shows a required E/N_o of 10.5 dB. Allowing an additional 2.5 dB for detector losses yields an overall requirement of 13.0 dB. Now,

$$P_{RD_{Req'd}} = \left(\frac{E}{N_o}\right)_{Req'd} R_D N_o \qquad (4.4.3\text{-}9)$$

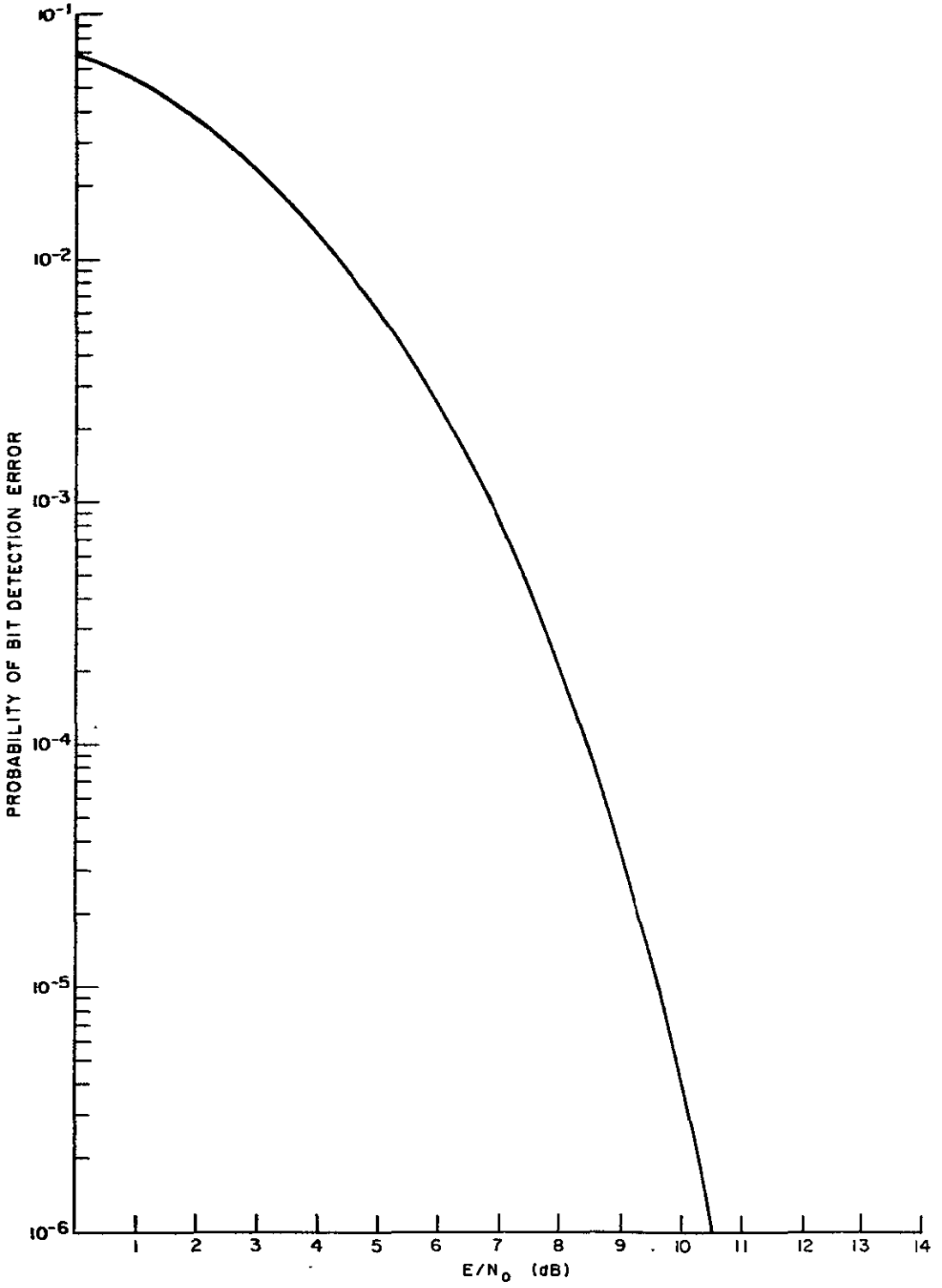

Figure 4.4.3-2. P_e versus E/N_o, Ideal Coherent PCM/PM

Where

R_D = Data Rate

N_o = Noise Power Density

The system temperature is specified by GSFC to be 1600°K, yielding an N_o of -166.4 dBm/Hz. For R_D = 30 dB-Hz, it is found that

$$P_{RD\ req'd} = -123.4\ dBm \qquad (4.4.3\text{-}10)$$

Comparing the actual P_{RD} with P_{RD} req'd, it is concluded that:

$$P_{TD\ req'd} \geq 19.5\ dBm$$

Stored Telemetry

There is no requirement on the allowable probability of bit error for this signal. A P_e of 10^{-4} is arbitrarily chosen. This requires a theoretical E/N_o of 8.4 dB. Allowing another 3.3 dB for detector losses and premodulation filtering (see Section 4.4.3.2.1.2.3) yields an overall required E/N_o of 11.7 dB. Then, for a bit rate of 24 kbps,

$$P_{RD\ req'd} = (11.7 + 43.8 - 166.4)\ dBm$$

$$= -110.9\ dBm$$

and

$$P_{TD\ req'd} \geq 32.0\ dBm$$

4.4.3.2.1.2.2 Required Total Transmitter Power

In Sections 4.4.3.1.1.2.1 and 4.4.3.2.1.2.1, the required values for P_{TC} and P_{TD} were calculated. Clearly, sufficient total power should be provided in the transmitter so that the minimum required values can be provided. The following three operational modes exist:

1. Tracking only — $P_{TC} \geq 22.9$ dBm
2. Tracking Plus Real-Time Telemetry — $P_{TC} \geq 22.9$ dBm; $P_{TD} \geq 19.5$ dBm
3. Tracking Plus Stored Telemetry — $P_{TC} \geq 22.9$ dBm; $P_{TD} \geq 32.0$ dBm

We must pick values for P_T and β_D in Equations (4.4.3-4) and (4.4.3-7). Note that β_D will not be a fixed number, but will have some tolerance, varying between $\beta_{D\ Min.}$ and $\beta_{D\ Max.}$

In order to insure that both tracking and data functions are successful, Equations (4.4.3-4) and (4.4.3-7) should be rewritten as:

$$P_{TC} = P_T \cos^2 \beta_{D\ Maximum} \qquad (4.4.3\text{-}11)$$

$$P_{TD} = P_T \sin^2 B_{D\ Minimum} \qquad (4.4.3\text{-}12)$$

With a modulation index tolerance of ±5 percent, the following numbers have been found to satisfy the requirements, as shown in Table 4.4.3-3. Note that the chosen power levels of 300 milliwatts and 2 watts provide the 6 dB system margin required by GSFC.

4.4.3.2.1.2.3 Bandwidth Utilization

The VHF downlink signal must be confined to a fixed RF bandwidth centered at 137.86 MHz. When real-time telemetry is being transmitted, the allowable RF bandwidth is 30 kHz. When stored telemetry is being transmitted, the allowable RF bandwidth is 90 kHz. The RF signal power spectrum must be down at least 10 dB at the bandwidth limits and must fall off faster than 18 dB per octave outside the bandwidth.

The entire allotted bandwidth cannot be used by signal spectra. Doppler shifts (±3 kHz) and oscillator instabilities (±5.5 kHz, for .003 percent and .001 percent spacecraft and ground station, respectively) utilize ±8.5 kHz or 17 kHz total. Hence, the signal spectrum must be down 10 dB at 6.5 kHz from dc for the real time telemetry signal and fall off at or faster than 18 dB per octave, referenced to one-half the assigned bandwidth, beyond that. Similarly, the signal spectrum must be down 10 dB at 36.5 kHz from dc for stored telemetry and fall off at or faster than 18 dB beyond that.

The worst case for spectrum occupancy will be when all zeros or all ones are transmitted in a long stream, so that the data will be a square wave of frequency equal to the data rate. For real time telemetry, the 7th harmonic will be the first exceeding band edge and its level will be down -17.8 dB (at 7 kHz). The level of each succeeding odd harmonic will be down $10 \log_{10} (8/n^2 \pi^2)$ with respect to the total power. For each octave of 15 kHz, there will be at least 7 odd harmonics. Hence, the rate of fall-off will be about 42 dB per octave of 15 kHz, which exceeds the requirement. Clearly, no premodulation-filtering or post-modulation filtering is required for the real-time telemetry mode.

For stored telemetry, the third harmonic will be the first exceeding the band edge. This harmonic will be down about 10.5 dB (at 72 kHz). This exceeds the bandwidth specification by about 20 dB.

A solution which will degrade performance little (.5 dB E/N_0 increase) is a premodulation filter with 3 dB point at 36 kHz, a roll-off exceeding 18 dB per octave of 36 kHz, and linear phase (3 pole). This will satisfy the bandwidth requirements.

TABLE 4.4.3-3. VHF TRANSMITTER POWER AND MODULATION INDEXES

	Transmitter Power		Nominal β_D	β_D maximum	β_D minimum	P_{TC}	P_{TD}	Extra Tracking Margin	Extra Data Margin
	(dBm)	(MW)	(Degrees)	(Degrees)	(Degrees)	dBm	dBm	dB	dB
Tracking Only	24.8	300	0	-	-	24.8	-	1.8	-
Tracking Plus Real Time Telemetry	24.8	300	35	36.7	33.3	22.9	19.6	0.0	0.1
Tracking plus Stored Telemetry	33.0	2000	68	71.4	64.6	23.0	32.1	0.1	0.1

4.4.3.2.2 Unified S-Band (USB) Downlink

4.4.3.2.2.1 Requirements

4.4.3.2.2.1.1 General Requirements

The Unified S-Band Downlink shall provide capability to transmit all narrowband data signals plus the received PRN range code (see Section 4.4.3.1.2.1) using a design compatible with an existing Manned Space Flight Network (MSFN) ground station. General requirements are as follows:

Carrier Phase Coherence: The carrier shall be coherent with the USB receiver VCO when a USB Uplink signal is locked up in the receiver phase-lock-loop. When no uplink signal is present, the carrier shall be coherent with a free-running L.O. onboard the spacecraft.

Carrier Frequency: 2287.5 MHz ±.0015 percent, non-coherent mode

240/221 times USB uplink carrier frequency, coherent mode

Carrier Modulation: Phase Modulation

Carrier RF Bandwidth: 5 MHz maximum

RF Spectrum Constraints: No spectral components within ±120 kHz of the carrier during acquisition at ground station.

4.4.3.2.2.1.2 Data Signals

It is necessary to transmit the following signals simultaneously on the Unified S-Band downlink carrier:

1. DCS Receiver IF Output
2. Real time PCM housekeeping telemetry
3. PWM time code from WBVTR No. 1 Auxiliary Track
4. PWM time code from WBVTR No. 2 Auxiliary Track

In addition to these signals, capability must exist to transmit the stored PCM housekeeping telemetry from a narrowband tape recorder (NBTR) during playback. Hence, during NBTR playback, five individual signals must be transmitted on the USB downlink carrier. Following is a description of the characteristics of each signal.

DCS Receiver IF Output

Signal Description: Frequency - modulated sine wave

Signal Bandwidth: 100 kHz, centered at some IF frequency to be chosen

Amplitude Modulation: No More than 10 percent

Overall S/N at Ground Station: zero dB in 100 kHz bandwidth

Real-Time PCM Housekeeping Telemetry

Signal Description: PCM-split-phase-L signal

Signal Level: 0 to .64 volts from 100 ohm source

Bit Rate: 1 kilobit per second

Probability of bit error upon detection: Less than 10^{-6}

PWM Time Code

Signal Description: PWM signal

Pulse repetition rate: 100 pps

Pulse Duration: Either 2 ms or 6 ms (2 ms = "0"; 6 ms = "1")

Signal Level: 0 to -5 volts from 100 ohm source

Probability of bit error upon detection: Less than 10^{-6}

Stored PCM Housekeeping Telemetry (NBTR Playback)

Signal Description: PCM-split-phase-L Signal

Signal Level: 0 to -5 Volts from 100 ohm source

Bit Rate: 24 kilobits per second

Probability of Bit Error Upon Detection: Less than 10^{-6}

4.4.3.2.2.1.3 Subcarriers/Subcarrier Modulation

In order to transmit all five signals simultaneously on the USB downlink carrier, it is necessary to employ several subcarriers. Due to the important requirement that the USB downlink signal must be demodulated using unmodified equipment existing at MSFN ground stations before the ERTS-A launch, the choice of subcarriers and subcarrier modulation has been limited to those suggested to GE by GSFC (*) at the beginning of the study. For review, these recommended subcarriers are presented below:

Subcarrier	Modulation on Subcarrier
All IRIG proportional bandwidth subcarrier channels	PCM/FM

*Bradley, Walter D., U.S. Government memorandum, "Meeting on November 10, 1969, concerning ERTS Unified S-Band Link, "November 13, 1969

Subcarrier	Modulation on Subcarrier
225 kHz (±7 1/2 percent or ±15 percent)	PCM/FM or FM**
300 kHz (±7 1/2 percent or ±15 percent)	PCM/FM or FM**
1024 kHz	PCM/PSK or PCM/FM**
1250 kHz	PCM/FM or FM**
576 kHz	PCM/PSK
768 kHz	PCM/PSK

The last two choices have not yet been implemented at the MSFN stations, but it is GE's understanding that such implementation will occur prior to launch of ERTS-A.

**The memo in the previous footnote had suggested only PCM/FM: however, frequency-modulating several low-frequency IRIG channels on any of these subcarriers would be acceptable.

4.4.3.2.2.2 Studies and Analyses

4.4.3.2.2.2.1 Composite Downlink Signal Design

The USB downlink signal, $s_r(t)$, received at a ground station is of the form

$$s_R(t) = \sqrt{2C} \cos \left[\omega_c t + \sum_{i=1}^{n} \theta_i \cos (\omega_{si} t + \varphi_i(t)) + \theta_{n+1} U(t) + n(t) \right] \qquad (4.4.3\text{-}13)$$

where

C = received total power

ω_c = carrier frequency

θ_i = Peak phase deviation of carrier due to i-th subcarrier

θ_{n+1} = peak phase deviation of carrier due to ranging signal

ω_{si} = i-th subcarrier frequency

$\theta_i(t)$ = information which is angle-modulated on i-th subcarrier

$U(t)$ = two level (±1) squarewave ranging signal

$n(t)$ = Gaussian bandlimited noise (density N_{oc})

Equation (4.4.3-13) can be expanded via trigonometric identities into the form

$$s_R(t) = \sqrt{2C} \left\{ \prod_{i=1}^{n} J_o(\theta_i) \cos(\theta_{n+1}) \cos \omega_c t \right.$$

$$+ \cos(\theta_{n+1}) \sum_{i=1}^{n} \prod_{\substack{j=1 \\ i=j}}^{n} J_o(\theta_j) J_1(\theta_i) \quad X$$

$$\left. [\cos((\omega_c + \omega_{si})t + \varphi_i(t)) - \cos((\omega_c - \omega_{si})t + \varphi_i(t))] \right. \qquad (4.4.3\text{-}14)$$

$$+ \prod_{i=1}^{n} J_o(\varphi_i) \sin(\varphi_{n+1}) U(t) \sin \omega_c t$$

$$+ \text{intermod terms}$$

$$+ n(t)$$

The first term in Equation (4.4.3-14) represents the unmodulated carrier component of the signal. The summation of terms represents the data-modulated subcarriers. The third term on the right represents the ranging sidebands. The remaining terms represent intermodulation of different subcarriers which are of no use (if not interferring) in the normal linear detection process. Note that each subcarrier has an upper and a lower sideband.

Figure 4.4.3-3 shows a typical demodulation scheme. The power in the i-th subcarrier, P_{Rsi} at the phase demodulator output, is given by

$$P_{Rsi} = C\left(2 J_i^2(\varphi_i)\right) \prod_{\substack{j=1 \\ j=i}}^{n} J_o^2(\varphi_j) \qquad (4.4.3\text{-}15)$$

The power in the ranging signal is given by

$$P_{R(n+1)} = C \sin^2(\theta_{n+1}) \prod_{i=1}^{n} J_o^2(\theta_i) \qquad (4.4.3\text{-}16)$$

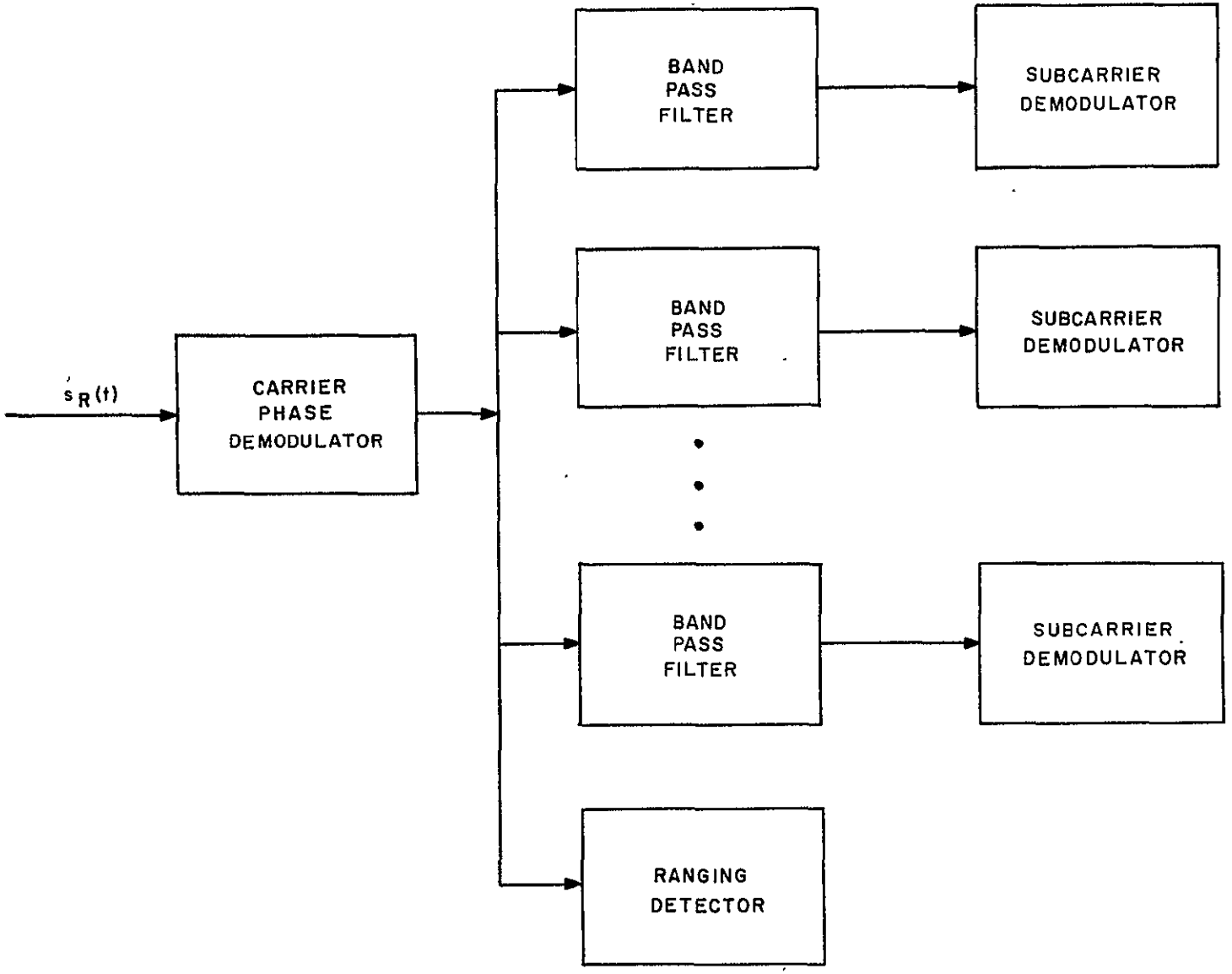

Figure 4.4.3-3. Typical USB Downlink Demodulation Scheme

The noise power density entering the ith subcarrier demodulator N_{oi}, is the same as the noise power density for the receiver, N_{oc}. In order to determine the correct design for the θ_i (and, therefore, the P_{Rsi}), it is useful to determine the value of the ratio

$$\left(\frac{S}{N_o}\right)_i = \frac{P_{R\,si}}{N_{oi}} = \frac{P_{R\,si}}{N_{oc}} \qquad (4.4.3\text{-}17)$$

required at each subcarrier demodulator for a particular type of data signal and subcarrier modulation. Then the θ_i can be chosen to allocate the carrier power appropriately into the various subcarrier signals.

4.4.3.2.2.2.1.1 Choice of Subcarriers/Subcarrier Modulation

The significant parameters of the various subcarrier channels are the type of modulation allowable and the available IF bandwidth for each. Based on consideration of bandwidths alone, the possible subcarriers for each data signal can be reduced. Then, based on intermodulation considerations and S/N_o requirements, the final choice can be made. Table 4.4.3-4 shows a summary of the available IF bandwidths for each subcarrier.

Examination of the right column of Table 4.4.3-4 shows that only the 1024 KHz channel has sufficient bandwidth to contain the DCS Receiver signal. It is shown in Section 4.4.3.2.2.2.1.2.2 that the best design in the 1024 KHz channel is to make the nominal IF frequency of the DCS receiver output signal equal to 1024 KHz. Although the actual frequency of this signal may change from 1024 KHz by ±50 KHz, it is a constant-amplitude frequency-modulated sine wave which is an ideal subcarrier signal for subsequent phase modulation on the carrier. This design also removes the necessity of providing a 1024 KHz VCO.

TABLE 4.4.3-4. IF BANDWIDTHS AVAILABLE FOR SUBCARRIERS

Subcarrier	IF Bandwidths Available
IRIG Subcarriers	.15 or .30 times center frequency
225 KHz	33.75 KHz, 67.5 KHz
300 KHz	45 KHz, 90 KHz
1024 KHz	6 KHz, 150 KHz, 600 KHz, unlimited*
1250 KHz	20 KHz, 35 KHz
576 KHz	Sufficient for at least 24 kbps split-phase PCM/PSK
768 KHz	

*The use of the 1024 KHz channel is limited by surrounding subcarriers, such as the 1250 KHz channel.

Now, the stored PCM housekeeping telemetry is a PCM-split-phase signal at 24 kbps data rate, hence, at least 72 KHz is required for an IF bandwidth. This eliminates the 1250 KHz channel from further consideration, leaving the 225 KHz, 300 KHz, 576 KHz, and 768 KHz channels as candidates. It can be shown that PCM/FM requires 2.2 dB greater S/N_0 than PCM/PM; moreover, Section 4.4.3.2.2.2.4 will show that 576 KHz is a good choice to minimize intermodulation interference. Since the 576 KHz channel also allows use of PCM/PSK, this channel shall be chosen for the stored PCM housekeeping telemetry signal.

This leaves three narrowband signals: the real time PCM housekeeping telemetry and two PWM time code signals. It is obvious that any subcarrier, except the very lowest-frequency IRIG subcarriers, can handle any of these signals; however, due to the ban on subcarriers below 120 KHz, a desire to minimize the number of subcarriers on the carrier, and the intermodulation analysis in Section 4.4.3.2.2.2.4, it has been found that the best design is to put each of these three signals on a low-frequency IRIG subcarrier using PCM/FM, sum the output of each IRIG VCO, and frequency-modulate the 1250 KHz subcarrier channel in a narrowband fashion (PCM/FM/FM). This limits the highest IRIG channel usable to at most half of 35 KHz, which is channel 13. Channel 13 is chosen for the real-time PCM housekeeping telemetry since its bandwidth is greater than the PWM time code. Channels 11 and 12 are chosen for each time code signal.

4.4.3.2.2.2.1.2 Required S/N_0 for each Subcarrier Channel

4.4.3.2.2.2.1.2.1 576 KHz Channel

The stored PCM housekeeping telemetry signal is a PCM-split-phase-L signal at a 24 kilobit-per-second rate. It is used to bi-phase modulate a 576 KHz subcarrier. The subcarrier phase deviation is chosen to vary over $\pm\pi/2$ radians; hence, all the subcarrier power is available for the bit detection process. Although the bit rate is not coherent with the subcarrier phase, bit sync can still be obtained at the detector in a doubling loop at twice the bit rate. Resulting ambiguities in the 1 or 0 decision are resolved automatically by certain data combinations when split-phase coding is employed.

For a perfect detector of PCM/PSK, the required ratio E/N_0 of energy per bit (in the subcarrier) to noise power density at the detector input was shown in Figure 4.4.3-2 versus the probability of error in detecting the bit. For a probability of bit error less than 10^{-6}, E/N_0 must be greater than 10.5 dB for a perfect detector. Allowing 2.5 dB for real detector losses, the actual E/N_0 should be greater than 13.0 dB to insure a probability of bit error less than 10^{-6}. Now,

$$\frac{E}{N_0} = \frac{ST}{N_0} \qquad (4.4.3\text{-}18)$$

where

S = Average power in the subcarrier

T = Bit period = $(\text{data rate})^{-1}$

hence,

$$\left(\frac{S}{N_o}\right)_1 = \left(\frac{E}{N_o}\right)\frac{1}{T} = 13.0 \text{ dB} + 43.8 \text{ dB-Hz} \qquad (4.4.3\text{-}19)$$

or,

$$\left(\frac{S}{N_o}\right)_1 = 56.8 \text{ dB-Hz}$$

where

$(S/N_o)_1$ is the required S/N_o for the 576 KHz subcarrier.

4.4.3.2.2.2.1.2.2 1024 KHz Channel

The 1024 KHz channel is used for the DCS Receiver IF output signal. This signal consists of a sinusoid of center frequency $f_{IF} \pm 50$ KHz which is frequency-modulated by both a desired information signal and random noise. The downlink transmission adds more noise to the information signal.

The data collection system processor at the ground station extracts the information signal from the noise. The overall S/N at the input to the ground station processor must be zero dB in a 100 KHz bandwidth centered at f_{IF}.

The total problem is that of a linear repeater relay satellite. The DCP-to-S/C link at 401.9 MHz adds some noise to the signal, and the S/C-to-ground station link (via the USB downlink carrier) adds the rest. Given the overall S/N requirement of zero dB, and the fact that the S/N at the DCS Receiver IF output is 3 dB, one can calculate the S/N due to the USB downlink alone as follows: For a linear repeater relay link,

$$\left(\frac{S}{N}\right)_{\text{overall}} = \frac{1}{\left(\frac{N}{S}\right)_u + \left(\frac{N}{S}\right)_d \left[1 + \left(\frac{N}{S}\right)_u\right]} \qquad (4.4.3\text{-}20)$$

where

$$\left(\frac{S}{N}\right)_{\text{overall}} = \text{Zero dB}$$

$$\left(\frac{S}{N}\right)_u = 3 \text{ dB for DCP-to-S/C link}$$

$\left(\frac{S}{N}\right)_d$ = S/N for S/C-to-ground station link

Solving for $(S/N)_d$ yields

$$\left(\frac{S}{N}\right)_d = \frac{1 + \left(\frac{N}{S}\right)_u}{\left(\frac{N}{S}\right)_{Overall} - \left(\frac{N}{S}\right)_u} \qquad (4.4.3\text{-}21)$$

Inserting

$$\left(\frac{N}{S}\right)_u = .5$$

$$\left(\frac{N}{S}\right)_{overall} = 1$$

yields

$$\left(\frac{S}{N}\right)_d = 3 = 4.8 \text{ dB}$$

Now the method of using the 1024 KHz channel has not yet been determined. The simplest fashion is to make f_{IF} = 1024 KHz, so that the DCS Receiver output is already appropriate to directly phase-modulate the USB downlink carrier. In such a case,

$$\left(\frac{S}{N}\right)_d = \frac{S}{N_o B_{IF}} \qquad (4.4.3\text{-}22)$$

where

B_{IF} = 100 KHz

therefore,

$$\left(\frac{S}{N_o}\right)_2 = \left(\frac{S}{N}\right)_d B_{IF} \qquad (4.4.2\text{-}23)$$

where

$(S/N_o)_2$ = S/N_o required for 1024 KHz channel

hence

$$\left(\frac{S}{N_o}\right)_2 = 54.8 \text{ dB-Hz}$$

Another way to utilize the 1024 KHz channel would be to make f_{IF} equal to 50 KHz and frequency-modulate the DCS Receiver IF output onto a 1024 KHz subcarrier. However, such a practice would require at least twice the bandwidth and a higher value of S/N_o due to the threshold characteristics of the 1024 KHz phase-lock discriminator. For example, using such a scheme, a peak subcarrier deviation of at least $\sqrt{2/3}$ times 100 KHz would be required to prevent an overall loss in the FM process. This would yield an IF bandwidth of $2(1+\sqrt{2/3})$ 100 KHz preceding the subcarrier discriminator. Assuming a threshold of zero dB (which is optimistic), the required S/N_o in the 1024 KHz channel would have to be 55.6 dB, which is .8 dB higher than the "no-subcarrier" case. Actually, the S/N_o would have to be greater than this to prevent threshold noise spikes. Hence, it is clear that the optimum method is as described previously. Note that the bandpass limiter in the DCS Receiver prevents amplitude modulation on the DCS Receiver IF output.

4.4.3.2.2.2.1.2.3 1250 KHz Channel

This channel is used to transmit the real-time PCM housekeeping telemetry and the PWM time code stored on the auxiliary track of each wideband video tape recorder. Each of the three signals is frequency-modulated on a separate IRIG subcarrier. The modulated IRIG subcarriers are pre-emphasized and summed to frequency modulate the 1250 KHz subcarrier. Figure 4.4.3-4 shows a block diagram of this modulation scheme.

In order to determine the required S/N_o for the 1250 KHz channel, it is necessary to determine the optimum pre-emphasis schedule for the three IRIG subcarriers. This is done by choosing the design approach that the required detection performance for all three data signals shall be achieved for the same value of S/N_o.

The performance equations for the real-time PCM housekeeping telemetry signal (PCM/FM/FM) and time code signals (PCM/PWM/FM/FM) shall now be developed. The development refers to Figure 4.4.3-5 which shows a block diagram of the detector scheme for the three 1250 KHz-channel data signals.

PCM/FM/FM

The rms signal-to-noise ratio, $(S/N)_{13}$, at the input to the IRIG channel 13 discriminator is given by:

$$(S/N)_{13} = \frac{3\Delta f_{c13}^{\ 2}}{(f_{u13}^{\ 3} - f_{\ell 13}^{\ 3})} \left(\frac{S}{N_o}\right)_3 \qquad (4.4.3\text{-}24)$$

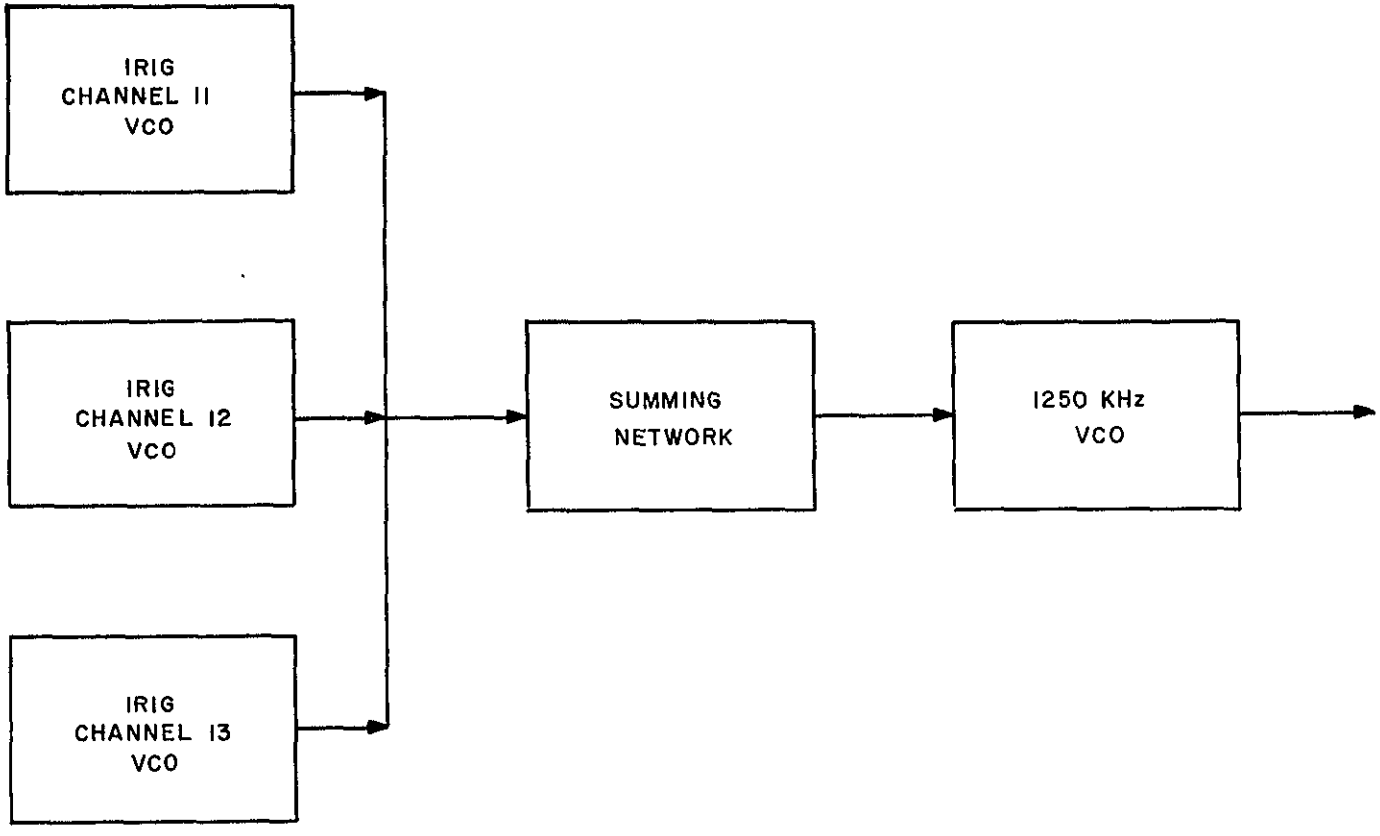

Figure 4.4.3-4. 1250 KHz Channel Modulation Scheme

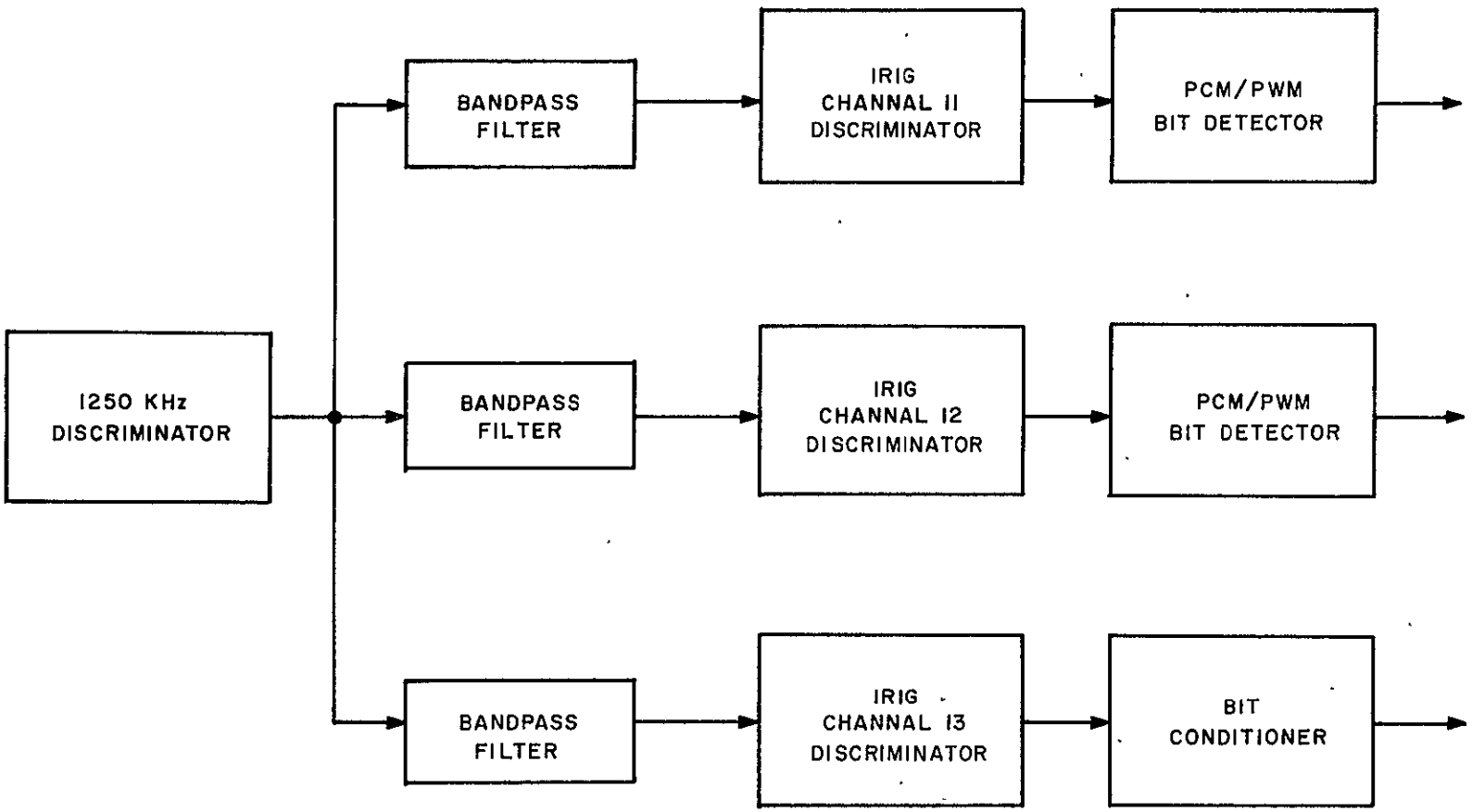

Figure 4.4.3-5. 1250 KHz Channel Demodulation Scheme

where

Δf_{c13}^{2} = peak frequency deviation of 1250 KHz subcarrier due to IRIG channel 13 subcarrier

f_{u13} = upper IF frequency limit of IRIG channel 13 discriminator

$f_{\ell 13}$ = lower IF frequency limit of IRIG channel 13 discriminator

$\left(\frac{S}{N_o}\right)_3$ = S/N_o for 1250 KHz channel

Figure 4.4.3-6 shows the probability of bit error versus $(S/N)_{13}$ when $(f_{u13} - f_{\ell 13})$ = the bit rate. The theoretical value for $P_e = 10^{-6}$ is seen to be 12.7 dB. Allowing an additional 3.3 dB for detector imperfections yields $(S/N)_{13}$ = 16 dB as a requirement for $P_e = 10^{-6}$.

PCM/PWM/FM/FM

It is assumed that the PWM Wavetrain is sampled halfway between the short pulse end and the long pulse end, as shown in Figure 4.4.3-7. The probability of error is the probability that the noise has an amplitude greater than one-half the signal level in the opposite direction. Assuming that the noise is zero-mean gaussian at the input to the system, it is still zero-mean gaussian at the sampler. The rms noise power at the i-th sampler (i = 11, 12) is given by

$$\sigma_i^2 = \frac{2 f_{si}^{\,2} f_a^{\,3}}{3 \Delta f_{ci}^{\,2}} \left[\frac{1}{(S/N_o)_3}\right], \quad i = 11, 12 \qquad (4.4.3\text{-}25)$$

where

f_{si} = center frequency of i-th IRIG channel

Δf_{ci} = peak frequency deviation of 1250 KHz subcarrier due to i-th IRIG channel subcarrier

f_a = baseband bandwidth of PWM signal (500 Hz)

The probability of error P_e in the sampling decision is given by

$$P_e = \int_{\Delta f_{si}}^{\infty} \frac{1}{\sqrt{2\pi}\,\sigma_i} \exp\left(-\frac{x^2}{2\sigma_i^2}\right) dx \qquad (4.4.3\text{-}26)$$

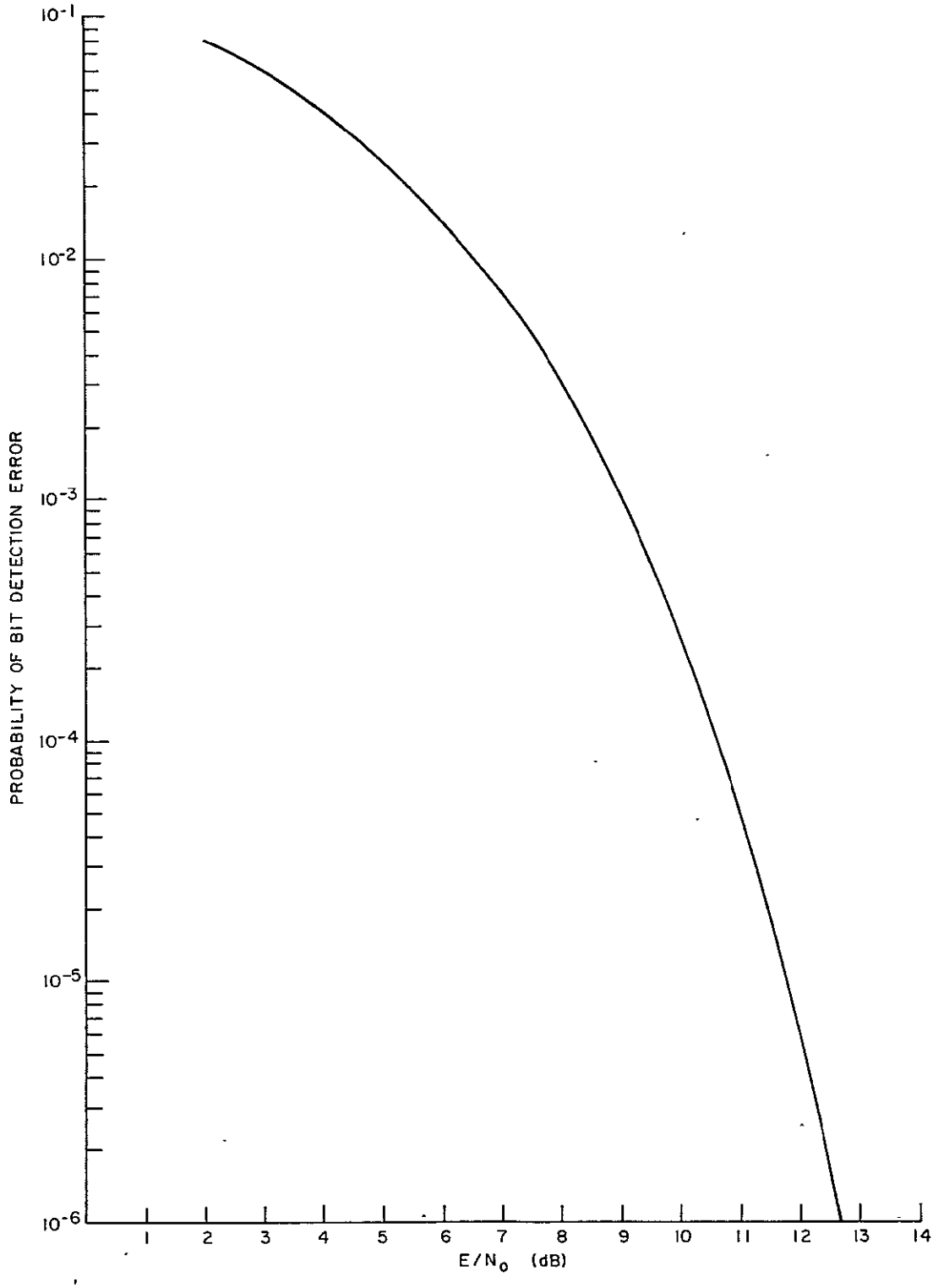

Figure 4.4.3-6. P_e versus E/N_o, Ideal PCM/FM

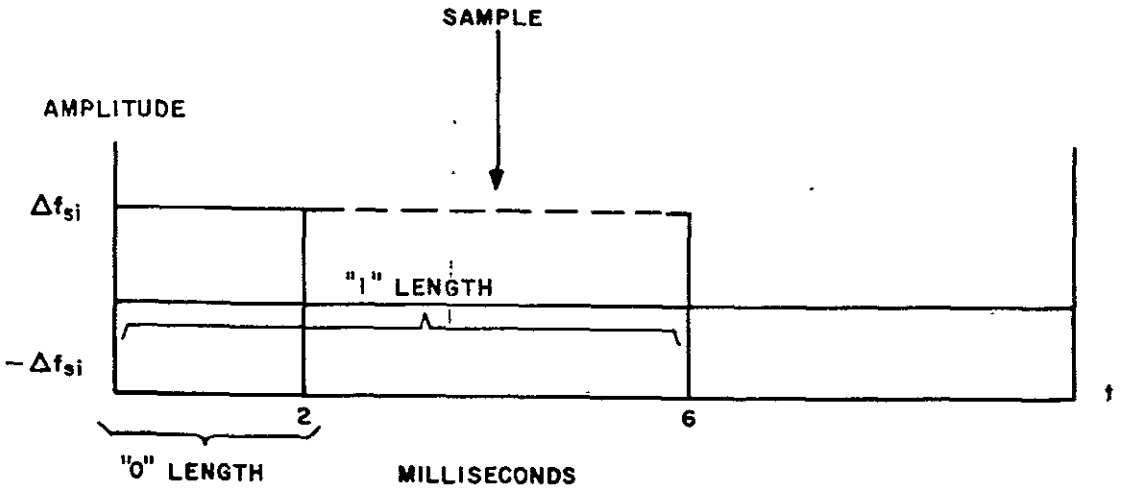

Figure 4.4.3-7. Sampling PCM/PDM Waveforms

where

Δf_{si} = signal level for long pulse

$-\Delta f_{si}$ = signal level for short pulse

If we choose $P_e \leq 10^{-6}$, then

$$\frac{\Delta f_{si}}{\sigma_i} \geq 4.75 \qquad (4.4.3\text{-}27)$$

Hence, at threshold,

$$\left(\frac{S}{N_o}\right)_3 = \frac{2\,(4.75)^2\ f_{si}^{\ 2}\ f_a^{\ 3}}{3\,\Delta f_{si}^{\ 2}\ \Delta f_{ci}^{\ 2}} \qquad (4.4.3\text{-}28)$$

Now, we have three equations in S/N_o. Each contains its own Δf_{ci}, i = 11, 12, 13, representing the deviation of the 1250 KHz channel by that IRIG subcarrier. We can solve for Δf_{ci} in each case in terms of S/N_o and other parameters whose values are known. Then, we make use of the fact that

$$\sum_{i = 11,12,13} \Delta f_{ci} = \Delta f_{c\ max} \qquad (4.4.3\text{-}29)$$

to solve for the individual Δf_{ci}'s.

Note that to find $\Delta f_{c\ max}$, use is made of the fact that the overall information bandwidth on the 1250 KHz channel is 15 KHz. To operate in a narrowband FM mode (thereby keeping the IF bandwidth to less than 35 KHz), the peak frequency deviation of the 1250 KHz subcarrier due to all IRIG subcarriers must be no more than .7 times 15 KHz, or approximately 10 KHz. This corresponds to an overall modulation indix of .7 on the 1250 KHz subcarrier. Now, we implement what we have just discussed.

$$\Delta f_{c11} = \frac{4.75\, f_{s11}\, f_a^{3/2}}{\Delta f_{s11}} \left(\frac{2}{3}\right)^{1/2} \left[\frac{1}{(S/N_o)_3}\right]^{1/2} \qquad (4.4.3\text{-}30)$$

$$\Delta f_{c12} = \frac{4.75\, f_{s12}\, f_a^{3/2}}{\Delta f_{s12}} \left(\frac{2}{3}\right)^{1/2} \left[\frac{1}{(S/N_o)_3}\right]^{1/2} \qquad (4.4.3\text{-}31)$$

$$\Delta f_{c13} = (f_{u13}^3 - f_{\ell 13}^3)^{1/2} \left(\frac{2}{3}\right)^{1/2} \left(\frac{S}{N}\right)_{13}^{1/2} \left[\frac{1}{(S/N_o)_3}\right]^{1/2} \qquad (4.4.3\text{-}32)$$

$$\sum_{i = 11,12,13} \Delta f_{ci} = 10{,}000 \qquad (4.4.3\text{-}33)$$

The following values are applicable:

$f_a = 500$

$f_{s11} = 7{,}350$

$\Delta f_{s11} = 550$

$f_{s12} = 10{,}500$

$\Delta f_{s12} = 790$

$f_{u13} = 15,000$

$f_{\ell 13} = 14,000$

Using these values, the following data is obtained:

$\Delta f_{c11} = 1100$ Hz

$\Delta f_{c12} = 1100$ Hz

$\Delta f_{c13} = 7800$ Hz

and

$(S/N_o)_3 = 54.4$ dB

It is necessary to check that the IRIG channels 11 and 12 discriminators are above threshold (channel 13 is at 16 dB, which is far above threshold). It is found that each of these discriminators has a 3 dB C/N input, which is 3 dB above threshold for a phase-lock discriminator.

Finally, it is noted that for an $(S/N_o)_3 = 54.4$ dB, the 1250 KHz discriminator (phase-lock type) is almost 10 dB above its threshold of 0 dB in 45 dB-Hz.

4.4.3.2.2.2.2 Modulation Indices

4.4.3.2.2.2.1 Criteria for Selection of Modulation Indices - Several factors have been taken into account in the selection of the proposed indices of phase modulation of the carrier by the subcarriers. These are described below for both the downlink and uplink.

In the downlink, the primary goal is to meet the requirements of each channel with a minimum of transmitted power. This, in turn, requires that the percentage of useful subcarrier power contained in the transmitted signal be maximized and that the margins in all channels be identical. These can be achieved only under a fixed set of conditions, i.e., for a given number of subcarriers and for fixed carrier phase deviations by all subcarriers.

For the proposed system, transmission of from two to five subcarriers is possible, the latter including turnaround ranging and the retransmitted command signal when ranging and command are performed simultaneously. Minimum relative power is contained in the subcarriers when all five are present; therefore, this mode has been used in the optimization procedure.

The other variables affecting the optimization procedure are the voltage levels at the modulator and the modulator conversion gain (radians per volt). Both of these variations tend to de-optimize the balance of useful power in the transmitted signal. In addition to causing imbalance in the subcarriers, they also cause a general reduction in useful signal power; i.e., if the resultant modulation indices decrease, power is diverted from the subcarriers to the carrier and if the resultant modulation indices increase, power is diverted to the intermodulation products. The approach here has been to define the nominal index values as those which produce maximum useful output power when the channels are balanced. Since the individual channel losses due to variations from this set of values are not symmetrical for positive and negative variations, the stated approach does not provide total optimization for worst-case variations. The gain that might be obtained by worst-case optimization, however, is relatively small and does not appear to warrant, at this time, the analytical iterations required for the optimization process.

In the previous discussion it has been stated that all channel margins should be equal to minimize transmitted power; however, this approach has not been rigidly applied to the ranging channel. The power required for the ranging channel is negligible compared to that required by the three data channels, and additional margin has been provided. The approach has been to provide for the ranging channel five percent of the value of the power in the strongest data channel. The retransmitted command signal is an unwanted signal; however, it must be considered in the downlink calculations. It has been allocated twice the power in the ranging channel. The associated modulation indices for the ranging and command channels are fixed by the uplink indices and the transponder turnaround ratio (radians downlink per radian uplink).

The uplink has significant margin in both the ranging and command channels for a wide range of modulation indices; therefore, within certain constraints, the selected values are not critical. These constraints are: (1) a positive SNR should be provided in the

range channel to minimize retransmission of noise and (2) the SNR requirements of the command channel must be met in the presence of the range channel interference.

For the first constraint the criterion used is that an SNR of at least 6 db is to be provided in the ranging IF bandwidth ($\approx$ 3 MHz) with or without the command signal present. For the second constraint, adequate command margin is assumed when the command channel has a 6 db margin taking into account the average power density of the ranging spectrum in the vicinity of the command signal. This average spectral density (assumes fine-structured ranging line spectra can be modeled as a continuous spectrum) is given by

$$N_{OR} = \frac{2P_R}{R_B} = \frac{2\,CL_{MR}}{R_B} \qquad (4.4.3\text{-}35)$$

where

P_R = Received range-channel power

R_B = Range signal bit rate (twice clock rate)

C = Total received power

L_{MR} = Range channel modulation loss

In addition to these constraints, a turnaround ratio of 0.3 radians downlink per radian uplink is assumed, and, as stated previously, the ranging and command downlink channels are allocated 5 percent and 10 percent of the value of the power in the strongest data channel, respectively.

4.4.3.2.2.2.2.2 Downlink Modulation Analysis - The basic modulation equation for five channels (4 sinewave and one squarewave) is (unmodulated subcarriers)

$$f(t) = \sqrt{2C}\cos\left[\omega t + \theta_A \cos \omega_A t + \theta_B \cos \omega_B t + \theta_C \cos \omega_C t + \theta_D \cos \omega_D t + \theta_E U(t)\right] \qquad (4.4.3\text{-}35)$$

where C is the total received power

ω is the carrier radian frequency

ω_N is the radian frequency of unmodulated subcarrier N

θ_N is the carrier phase deviation or modulation index for subcarrier N

U(t) is a two-level ($\pm$1) squarewave ranging signal

From this the relative signal power in each subcarrier and the carrier is found to be (see Section 4.4.3.2.2.2.1)

$$P_{CAR}/C = J_o^2(\theta_A) J_o^2(\theta_B) J_o^2(\theta_C) J_o^2(\theta_D) \cos^2\theta_E \quad (4.4.3\text{-}36)$$

$$P_A/C = 2J_1^2(\theta_A) J_o^2(\theta_B) J_o^2(\theta_C) J_o^2(\theta_D) \cos^2\theta_E \quad (4.4.3\text{-}37)$$

$$P_B/C = J_o^2(\theta_A) 2J_1^2(\theta_B) J_o^2(\theta_C) J_o^2(\theta_D) \cos^2\theta_E \quad (4.4.3\text{-}38)$$

$$P_C/C = J_o^2(\theta_A) J_o^2(\theta_B) 2J_1^2(\theta_C) J_o^2(\theta_D) \cos^2\theta_E \quad (4.4.3\text{-}39)$$

$$P_D/C = J_o^2(\theta_A) J_o^2(\theta_B) J_o^2(\theta_C) 2J_1^2(\theta_D) \cos^2\theta_E \quad (4.4.3\text{-}40)$$

$$P_E/C = J_o^2(\theta_A) J_o^2(\theta_B) J_o^2(\theta_C) J_o^2(\theta_D) \sin^2\theta_E \quad (4.4.3\text{-}41)$$

where $J_n(\theta)$ indicates nth order Bessel functions

The requirements for each channel are as derived in previous sections are:

$P_{CAR}/N_o \geq$ 45 db (carrier)

P_A/N_o = 56.8db (stored data)

P_B/N_o = 54.8 (DCS)

P_C/N_o = 54.4db (Real-time Data)

P_D/N_o = 46.8db (Command Turnaround)

P_E/N_o = 43.8db (Ranging Turnaround)

The power in each subcarrier relative to subcarrier A (strongest subcarrier) is then:

$P_{CAR}/P_A \geq$ -11.8db

P_B/P_A = - 2.0db

P_C/P_A = - 2.4db

P_D/P_A = -10.0db

P_E/P_A = -13.0db

At this point, then, it is necessary to determine the set of modulation indices that not only satisfies the relative subcarrier requirements, but also which provides maximum power in the subcarriers relative to the total transmitted power. This has been accomplished by computer as follows:

(1) a value of θ_A is selected

(2) the value of θ_B is then determined by satisfying the equation

$$\frac{P_B}{P_A} = \frac{J_o^2(\theta_A)\,2J_1^2(\theta_B)}{2J_1^2(\theta_A)\,J_o^2(\theta_B)} = 0.63\ (-2.0\text{db}) \qquad (4.4.3\text{-}42)$$

(3) θ_C and θ_D are determined in the same manner

(4) θ_E, the modulation index for the squarewave ranging signal is found from the equation

$$\frac{P_E}{P_A} = \frac{J_o^2(\theta_A)\sin^2\theta_E}{2J_1^2(\theta_A)\cos^2\theta_E} = 0.05\ (-13\text{db}) \qquad (4.4.3\text{-}43)$$

(5) the power in each channel is determined for the derived set of modulation indices (this set satisfies the relative subcarrier requirements but does not necessarily satisfy the maximum output power criterion)

(6) the entire procedure is repeated for increasing values of θ_A until the total power in the subcarriers reaches a maximum and begins to decrease.

That set of indices that produces maximum output power is selected as the desired set. For the given requirements, the optimum set is as given in Table 4.4.3-5. Also given in the table is the modulation loss (channel power relative to total transmitted power) for each channel for the given nominal modulation index values and the variations for operation at ±20 percent from the nominal index values. It can be noted that the resulting carrier level is 2.6 dB higher than the strongest subcarrier (stored data channel); thereby meeting the previously given requirement that it be no lower than 11.8dB below the strongest subcarrier.

4.4.3.2.2.2.3 Transmitter Power Requirements - Let C be the value of the total average power received at the ground station receiver. Let N_{oc} be the noise power density at the receiver input. From Equations (4.4.3-15) through (4.4.3-17), the ratio C/N_{oc} is related to each ratio $(S/N_o)_i$ by its modulation loss, that is,

$$(S/N_o)_i = (C/N_{oc})\,M_{Li} \qquad (4.4.3\text{-}44)$$

where the value for M_{Li} can be determined from Equations (4.4.3-15 through (4.4.3-17).

Section 4.4.3.2.2.2.1.2 determined the requirements for $(S/N_o)_i$. Section 4.4.3.2.2.2.2 determined the optimum values for the M_{Li}. Using these, the required value for C/N_{oc} will be the following:

$$(C/N_{oc}) = \max\left\{(S/N_o)_i / M_{Li}\right\},\ \text{all } i \qquad (4.4.3\text{-}45)$$

TABLE 4.4.3-5. MODULATION INDICES AND LOSSES (DOWNLINK)

Mode	Channel	Nom. Mod Index (Rad)	Nom. Mod Loss (dB)	Mod. Loss + 20 percent tolerance (dB)	Mod. Loss -20 percent tolerance (dB)
Five Subcarriers	Carrier	-	-4.9	-2.3	+1.8
	Stored Data	0.93	-7.5	-0.2	-0.3
	DCS	0.77	-9.5	-0.4	-0.0
	Real Time	0.74	-9.9	-0.4	-0.1
	Ranging	0.17	-20.2	-0.7	-0.1
	Command*	0.33	-17.5	-0.7	+0.5
Three Subcarriers	Carrier	-	-4.6	-2.2	+1.7
	Stored Data	0.93	-7.2	-0.0	-0.6
	DCS	0.77	-9.2	-0.2	-0.3
	Real Time	0.74	-9.6	-0.3	-0.2
	Ranging	0.0	-	-	-
	Command	0.0	-	-	-
Two Subcarriers	Carrier	-	-2.6	-1.2	+.9
	Stored Data	0.0	-	-	-
	DCS	0.77	-7.2	+.7	-2.0
	Real Time	0.74	-7.6	+.7	-1.9
	Ranging	0.0	-	-	-
	Command	0.0	-	-	-

*Command signal undesired but exists in downlink

However, the M_{Li} have, in general, been chosen so that

$$(S/N_o)_i/M_{Li} = (S/N_o)_j/M_{Lj} \quad (4.4.3\text{-}46)$$

Hence, the required value for C/N_o is seen to be (54.8 dB-Hz + 9.5 dB)

$$(C/N_o) = 64.3 \text{ dB-Hz}$$

req'd
nominal

An additional .4 dB must be added for transmitter modulation sensitivity change from the optimum setting.

In order to find the value of C as a function of the transmitter power P_T, a link calculation can be performed.

Table 4.4.3-6 shows a link calculation. From this table, it can be seen that a 6 dB system margin and a 1.9 dB "extra margin" exist under worst-case conditions when a transmitter power of 1 Watt (30 dBm) is chosen.

This extra margin will be allocated to modulation index variations from the ideal (derived in a previous section) caused by independent variations in the composite signal subcarrier amplitudes.

TABLE 4.4.3-6. USB DOWNLINK LINK CALCULATION

		Nominal	Adverse
Transmitter Power	dBm	30.0	-
Transmitting Circuit Less	dB	- 2.0	-
Transmitting Antenna Gain (Includes Polarization Loss)	dB	- 1.0	-3.0
Free Space Loss	dB	-169.3	—
Transmitter Frequency	MHz	2287.5	
Slant Range	N.M.	1642	
Receiving Antenna Gain (Includes Circuit and Point Losses)	dB	43.4	-
System Margin	dB	- 6.0	-
Receiver Total Power	dBm	-104.9	-3.0
Receiver Noise Power Density	dBm/Hz	-174.5	
System Temperature	Degrees K	250	
Received C/N_o	dB-Hz	69.6	-3.0
Required C/N_o	dB-Hz	64.3	+ .4
Extra Margin	dB	5.3	-3.4

4.4.3.2.2.2.4 Intermodulation Analysis - Phase modulation of a carrier by multiple subcarriers produces unwanted intermodulation products as well as the desired signals. These products not only reduce the useful transmitted power but also interfere with the desired signals. If the spectral components appear within the carrier search band (±120 KHz from carrier), if they are of sufficient amplitude, and if their associated spectra are sufficiently narrow (in the order of the loop bandwidth), they can interface with the carrier acquisition process by producing false locks. If they fall in any of the bands occupied by a desired subcarrier and are of sufficient amplitude they can interfere with the associated subcarrier information, producing higher error rates in digital channels and lower accuracy in the ranging process.

To evaluate the effects of intermodulation spurs on the communication channels it is first necessary to determine the nominal spur frequencies and their power levels. If these are such that a spur represents potential interference, it is then necessary to evaluate the nature of the interfering signal in relation to the desired signal and the detection process. This procedure will be carried out here in a sequence of steps so that the multitude of expected

spurs can be considered in a manner that quickly eliminates the majority that present no potential problems. In the first step, interference from the ranging and command channels will not be included; i.e., only spurs resulting from the stored data channel (ST) at 576 KHz, the Data Collection System Channel (DCS) at 1024 MHz, and the real time data channel (RT) at 1250 MHz will be considered. Included, however, are the second and third order spurs associated with these channels.

The frequencies and relative power levels of these spurs can be derived from the basic modulation equation

$$f(t) = \sqrt{2C} \cos (\omega t + \theta_A \cos \omega_A t + \theta_B \cos \omega_B t + \theta_C \cos \omega_C t) \qquad (4.4.3\text{-}47)$$

where C is the total receiver power

ω is the radian frequency of the carrier

ω_N is the radian frequency of subcarrier N

θ_N is the carrier phase deviation or modulation index of subcarrier N

Letting $N = \theta_N \cos \omega_N t$, the above can be expanded to the form

$$\begin{aligned} f(t) = \sqrt{2C} \cos \omega t \quad & [\cos A \cos B \cos C \\ & - \cos A \sin B \sin C \\ & - \sin A \sin B \cos C \\ & - \sin A \cos B \sin C \ ] \\ + \sqrt{2C} \sin \omega t \quad & [\sin A \sin B \sin C \\ & - \sin A \cos B \cos C \\ & - \cos A \cos B \sin C \\ & - \cos A \sin B \cos C \ ] \end{aligned} \qquad (4.4.3\text{-}48)$$

But

$$\cos N = \cos (\theta_N \cos \omega_N t) = J_o(\theta_N) + 2 \sum_{\substack{K=2 \\ K \text{ even}}}^{\infty} (-1)^{\frac{K}{2}} J_K(\theta_N) \cos K\omega_N t \qquad (4.4.3\text{-}49)$$

and

$$\sin N = \sin(\theta_N \cos \omega_N t) = 2 \sum_{\substack{K=1 \\ K \text{ odd}}}^{\infty} (-1)^{\frac{K+1}{2}} J_K(\theta_N) \cos K\omega_N t \qquad (4.4.3\text{-}50)$$

where $J_K(\theta_N)$ is the K^{th} order Bessel function. It is noted that the K^{th} order Bessel function is associated with the frequency $K\omega_N$. If the given relationships for cos N and sin N are substituted into the previous equation, and the products taken, all possible frequency components can be obtained. Limiting the infinite series to include third order and lower terms, it is found that the frequency components of the signal are described by the notation

$$[0, \omega_A, 2\omega_A, 3\omega_A][0, \omega_B, 2\omega_B, 3\omega_B][0, \omega_C, 2\omega_C, 3\omega_C] \qquad (4.4.3\text{-}51)$$

where a resultant frequency can be equal to any frequency of the first bracket, plus or minus any frequency of the second bracket, plus or minus any frequency of the third bracket. The above defines 172 unique frequencies. To reduce the number to include only those that are in the vicinity of a desired channel, a computer program was incorporated to indicate any spur frequency within 200 KHz of the carrier, within 50 KHz of the ranging channel (496 KHz), and within 100 KHz of any of the data channels (576 KHz, 1024 KHz, and 1250 KHz). These spur frequencies are given in Table 4.4.3-7. The "order" sequence given in the table indicates the basic frequencies from which the spur was derived. For example, in the first row, the sequence 1, 3, 2 indicates that the spur at 4 KHz was derived from a combination of the first order ST frequency (576 KHz), the third order DCS frequency (3072 KHz), and the second order RT frequency (2500 KHz). For this case 4 KHz = 576 - 3072 + 2500 KHz.

The relative power level of any spectral component in the predetection double sideband spectrum is given by (each component and its image component relative to the carrier are considered separately)

$$P_{xyz}/C_C = J_x^2(\theta_A) J_y^2(\theta_B) J_z^2(\theta_C) \qquad (4.4.3\text{-}52)$$

where x, y, and z are the orders of the channel A, B, and C frequencies producing the component. A sequence x, y, z can denote four frequencies (and their image frequencies) if x, y, and z are nonzero, two frequencies if one of the three are zero, and one frequency if two of the three are zero (the carrier component is obtained for x, y, and z equal to zero).

This equation gives relative predetection signal power; i.e., before carrier phase lock is obtained. It is therefore directly applicable for evaluation spurs in the vicinity of the carrier during the acquisition procedure. After acquisition, the appropriate equations are

$$P_{xyz}/C = 2J_x^2(\theta_A) J_y^2(\theta_B) J_z^2(\theta_C) \cos^2 \phi \quad (\text{for } x + y + z = \text{odd}) \qquad (4.4.3\text{-}53)$$

TABLE 4.4.3-7. SUMMARY OF INTERMODULATION SPURS

Freq (KHz)	Order ST	Order DCS	Order RT	Channel, Cntr. Freq, and Level (dB)	Spur Level (dB)	Quadrature Component	Remarks*
4	1	3	2	Carrier	-63		Negligible
26	3	2	3	0 to 120 KHz	-89	Not	Negligible
94	3	3	1	Acq. Range	-76	Applicable	Negligible
98	2	0	1	(-7)	-27		A
124	1	2	2		-47		Negligible
128	2	1	0		-27		B
448	1	1	0	Range	-13	X	C
452	0	2	2	596 KHz	-41	X	D
474	2	3	3	(-21)	-87	X	Negligible
478	3	0	1		-38	X	E
478	3	0	1	Stored	-38	X	Negligible
546	3	1	1	Data	-44		Negligible
550	2	2	3	576 KHz	-71		Negligible
572	0	3	2	(-8)	-57		Negligible
580	2	3	2		-71		Negligible
670	2	3	1		-58	X	Negligible
674	1	0	1		-13	X	F
926	2	1	1	DCS	-30	X	Negligible
930	3	2	1	1024 KHz	-56	X	Negligible
998	3	1	3	(-10)	-73		Negligible
1028	1	2	2		-44		Negligible
1050	3	3	3		-102		Negligible
1122	2	1	1		-30	X	Negligible
1152	2	0	0	Real	-18	X	G
1156	3	3	2	Time	-85	X	Negligible
1254	1	3	3	1250 KHz	-77		Negligible
1276	3	2	2	(-10)	-69		Negligible
1344	3	3	0		-66	X	Negligible
1348	2	0	2		-37	X	Negligible

* See text for comments A thru G

and

$$P_{xyz}/C = 2J_x^2(\theta_A)\, J_y^2(\theta_B) J_z^2(\theta_C) \sin^2 \phi \quad \text{(for } x + y + z = \text{even)}$$

(4.4.3-54)

where ϕ is the carrier loop phase error. In the following discussions it is assumed that a phase error of up to 10 degrees can occur. This has little effect on the "in-phase" channels (x + y + z = odd) since $\cos^2 10^\circ \approx 1$. However, the "quadrature" channels, rather than having zero output, will have twice their pre-acquisition power levels minus about 15 db ($\sin^2 15^\circ \approx -15$db).

In Table 4.4.3-7 all power levels exclude the effect of ϕ; however, the quadrature channels are noted and the assumed 15 dB loss will be taken into account in the following discussion where applicable. All values given are relative to total received power; in addition, the level of the channel with which interference is possible is given relative to total power. Spur levels given are for positive 20 percent modulation tolerances since this case gives maximum spur levels and minimum channel levels. Also, the levels of spurs around the carrier are for the case where only the three subcarriers are transmitted, as would be the case during carrier acquisition. The levels of spurs near the other channels are for the case where turnaround ranging and command signals are also present; spurs produced by the ranging and command signal, however, are not given in the table and will be discussed separately later.

A majority of the spurs indicated in Table 4.4.3-7 have such low levels that they can immediately be discounted as potential interference and are indicated negligible in the remarks column. To evaluate several of the remaining spurs, it is necessary to consider their spectral characteristics. A first order approximation can be obtained by first determining the characteristics of the basic channel components causing the spur. The equation for angle modulation of a single subcarrier, N, is

$$f(t) = \sqrt{2C}\ \cos\left\{\omega t + \theta_N \cos\left[\omega_N t + \theta_m(t)\right]\right\} \qquad (4.4.3\text{-}55)$$

$$= \sqrt{2C}\ \cos\omega t \left\{\cos\theta_N \cos\left[\omega_N t + \theta_m(t)\right]\right\} \qquad (4.4.3\text{-}56)$$

$$- \sqrt{2C}\ \sin\omega t \left\{\sin\theta_N \cos\left[\omega_N t + \theta_m(t)\right]\right\}$$

where the nomenclature is the same as used previously with the addition of $\theta_m(t)$, which is the phase deviation of the subcarrier caused by the data modulation.

This can be expanded further as

$$f(t) = \sqrt{2C}\ \cos\omega t \left\{J_o(\theta_N) - 2J_2(\theta_N)\cos\left[2\omega_N t + 2\theta_m(t)\right] + \cdots\right\} \qquad (4.4.3\text{-}57)$$

$$- \sqrt{2C}\ \sin\omega t \left\{2J_1(\theta_N)\cos\left[\omega_N t + \theta_m(t)\right] - 2J_3(\theta_N)\cos\left[3\omega_N + 3\theta_m(t)\right] + \cdots\right\}$$

Insight into the spectral characteristics can be obtained by evaluating the cases where the modulation is (1) PSK and (2) FM.

For PSK, $\theta_m(t) = X(t)\frac{\pi}{2}$, where X(t) is a two-level signal (± 1). Therefore

$$f(t) = \sqrt{2C}\cos\omega t \left\{J_o(\theta_N) - 2J_2(\theta_N)\cos 2\omega_N t + \cdots\right\} \qquad (4.4.3\text{-}58)$$

$$- \sqrt{2C}\sin\omega t \left\{2J_1(\theta_N)\cos\left[\omega_N t + X(t)\frac{\pi}{2}\right] - 2J_3(\theta_N)\cos\left[3\omega_N t - X(t)\frac{\pi}{2}\right] + \cdots\right\}$$

(Equation intentionally omitted) (4.4.3-59)

From this, the spectral components are noted to be unmodulated sinewaves at even multiples of the subcarrier frequency and bi-phase modulated sinewaves at odd multiples of the subcarrier frequency.

For FM, $\theta_m(t) = y(t)\,\omega_m t$, where y (t) is the modulating signal. Then,

$$f(t) = \sqrt{2P_t}\cos\omega t \left\{J_O(\theta_N) - 2J_2(\theta_N)\cos\left[2\omega_N t + 2y(t)\,\omega_m t\right] + \ldots\right\}$$

$$-\sqrt{2P_t}\sin\omega t \left\{2J_1(\theta_N)\cos\left[\omega_N t + y(t)\,\omega_M t\right]\right. \qquad (4.4.3\text{-}60)$$

$$\left. -2J_3(\theta_N)\cos\left[3\omega_N t + 3y(t)\,\omega_M t\right] + \ldots\right\}$$

This shows that modulated sinewaves exist at all multiples of the subcarrier frequency. The deviation of each spur frequency, however, is proportional to the nominal spur frequency. Therefore, the width of the spectra associated with FM signals are to a first approximation equal to K times the spectral width of the desired subcarrier, where K is the order of the spur.

When a spur results from the product of multiple subcarriers, the resultant spectrum is the convolution of the spectra of the individual subcarriers. For example, the spectrum for a spur of order x, y, z = 1, 3, 2 is obtained by convolution of the spectra associated with the first order frequency of channel A (ω_A), the third order frequency of channel B ($3\omega_B$), and the second order frequency of channel C ($2\omega_C$).

For the given channels (ST, DCS, and RT) the spectra are:

ST (order 1): split-phase PSK spectrum; bit rate = 24 Kbps

ST (order 2): sinewave

ST (order 3): same as order 1

DCS (order 1): 100 KHz band containing FSK signals appearing randomly in time and frequency. Each signal is 4.2 Kbps for a period of 38 milliseconds with a peak to peak frequency deviation of 50 KHz.

DCS (order 2): same as order 1 but spread over twice the bandwidth with 100 KHz peak-to-peak deviation

DCS (order 3): same as order 1 with "times-three" spectral spreading

RT (order 1): FM/FM signal. Low peak deviation of subcarrier by three sub-subcarriers in the vicinity of 10 KHz. Will contain spectral line at subcarrier frequency.

RT (order 2): same as order 1 with "times-two" spectral spreading

RT (order 3): same as order 1 with "times-three" spectral spreading

Following, then, is a discussion of the spurs indicated in Table 4.4.3-7.

A. Frequency: 98 KHz

Level: -20 db relative to carrier

Order: 2, 0, 1

Spectrum: RT channel translated to 98 KHz

Comments: RT subcarrier spectral line presents possible false lock point. Should give relatively high SNR in 700 Hz loop bandwidth.

B. Frequency: 128 KHz

Level: -20 dB relative to carrier

Order: 2, 1, 0

Spectrum: DCS channel translated to 128 KHz

Comments: Spectral components can appear down to 78 KHz. Duration of any signal is too short to maintain false lock but might cause momentary lock indication and interfere with the normal acquisition procedure.

C. Frequency: 448 KHz

Level: +8 dB relative to ranging clock subcarrier, -7 dB including quadrature phase error loss.

Order: 1, 1, 0

Spectrum: convolution of ST PSK spectrum and DCS spectrum; noise-type spectrum that can reach the range channel frequency. If 40 KHz wide noise spectrum is assumed in vicinity of ranging phase-locked loop of 40 Hz bandwidth, the interference will be reduced 30 db to a level of -37 dB.

Comments: Does not appear to be a problem

D. Frequency: 425 KHz

Level: -20 dB relative to range clock subcarrier; -35 dB including quadrature phase error loss

Order: 0, 2, 2

Spectrum: convolution of second order DCS and second order RT channel; basically noise type spectrum.

Comments: Should not cause interference

E. Frequency: 478 KHz

Level: -27 dB relative to range clock subcarrier; -42 dB including quadrature phase error loss

Order: 3, 0, 1

Spectrum: convolution of third order ST PSK spectrum with RT spectrum; noise type spectrum

Comments: Negligible

F. Frequency: 674 KHz

Level: -5 dB relative to ST channel; -20 dB including quadrature loss

Order: 1, 0, 1

Spectrum: convolution of ST PSK spectrum with RT FM/FM spectrum; noise type spectrum

Comments: center of spectrum 98 KHz from ST channel; negligible spectral components reach ST channels

G. Frequency: 1152 KHz

Level: -8 dB relative to RT channel; -23 dB including quadrature phase use

Order: 2, 0, 0

Spectrum: sinewave

Comments 98 KHz from RT center frequency; will be filtered out in discriminator with 35 KHz bandwidth

---

In summary, it appears that carrier acquisition is the only process that might be affected by spurs resulting from inherent intermodulation products. It should be noted, however, that the interfering signals for both cases A and B above depend on the presence of the stored data (ST) channel at 576 KHz. If this subcarrier is not applied until after carrier acquisition, it appears that no inherent spur problems exist for the cases considered this far.

Next, the potential interference due to the presence of the range clock signal will be considered. Its spectrum consists of lines at odd multiples of the clock frequency (496 KHz). The level of the fundamental is -21 dB.

Since any spur produced by the cross product of this component with any other spectral component results in an even lower level, the range channel presents little potential as an interfering signal. The highest level spurs are those produced by the cross product with any one of the other high level first order frequency terms; however, the resulting signals in this case are quadrature terms and are eliminated unless a carrier phase exists. Under the previous assumption of a maximum 10 degree phase error, these components are reduced 15 dB. Since the range channel itself operates with a low signal level, a potential problem could exist if a line frequency spur is produced that falls back in the ranging channel;

however, no such spurs were found to exist. The same is true relative to the third harmonic which is at a level of -31 dB.

The last potential interfering signal to be considered is the downlink command signal at 70 KHz. Its level is -18 dB and its second order component is down 38 dB. Again, because of its low level, it was not found to be a potential source of interference.

4.4.3.2.2.2.5 Amplitude Modulation of Subcarriers

In Equation (4.4.3-14), it was assumed that the subcarriers were of constant amplitude. Any amplitude modulation of a subcarrier can be represented as a time-varying modulation index, $\theta_i(t)$, for that subcarrier. As can be seen in the first term on the right of Equation (4.4.3-14), if $\theta_i(t)$ is not a constant, the carrier will be amplitude modulated by the term $J_o(\theta_i(t))$. Assume $\theta_i(t)$ can be represented by a constant θ_i plus a sine wave of amplitude $\Delta\theta_i$. The actual percent amplitude modulation of the carrier, R_{AMi} will be given by

$$R_{AMi} = \frac{J_o(\theta_i + \Delta\theta_i) - J_o(\theta_i - \Delta\theta_i)}{2 J_o(\theta_i)} \qquad (4.4.3\text{-}61)$$

Table 4.4.3-8 shows the values for R_{AMi} using the modulation indices from Section 4.4.3.2.2.2.2 and the subcarrier amplitude modulation levels θ_i shown in the table. The rms power in the AM sidebands is given by $\frac{1}{2} R^2_{AMi}$. This is also shown in Table 4.4.3-8.

Table 4.4.3-8: Amplitude Modulation of Carrier

Channel	θ_i (rad)	$\Delta\theta_i$ (%)	$\Delta\theta_i$ (rad)	$J_o(\theta_i)$ (actual)	$J_o(\theta_i - \Delta\theta_i)$ (actual)	$J_o(\theta_i + \Delta\theta_i)$ (actual)	R_{AMi} (actual)	$(20 \log R_{AMi} - 3)$ dB
576 KHz	.93	5	.045	.7952	.8136	.7761	2.35%	-35.6
1024 KHz	.77	10	.077	.8572	.8835	.8285	3.15%	-33.0
1250 KHz	.74	5	.037	.8677	.8800	.8548	1.45%	-39.8

4.4.3.3 Command Links

4.4.3.3.1 VHF Uplink

4.4.3.3.1.1 Requirements. It is necessary to receive and demodulate uplink command data which is modulated on a VHF carrier. Following is a list of general requirements:

1. Received Carrier Frequency: 154.2 MHz ± 0.005 percent
2. Modulation: PCM/FSK-AM/AM
3. Carrier Modulation Index: 80 percent AM (peak)
4. Command Subcarriers: 8.0 kHz and 8.6 kHz
5. Command Bit Rate: 128 bps
6. Probability of Error in Detecting Command Bits: less then 10^{-6}

4.4.3.3.1.2 Studies and Analyses

a. Receiver Sensitivity - Receiver sensitivity shall be defined as the value of received total RF power at the receiver input terminals (not the hybrid terminals) which yields a zero dB signal-to-noise ratio in the receiver IF noise bandwidth.

Given a peak antenna temperature and the receiver IF noise bandwidth, receiver sensitivity places a requirement on the overall noise figure of the receiver.

Calling P_R the value of received total power at the receiver input, the minimum value for P_R under the conditions stated by GSFC, $P_{R\ min}$, will be calculated. P_{Rmin} will define the receiver sensitivity. Now, in equation form,

$$P_R = \frac{P_T G_T G_R}{L_T L_{FS} L_P L_R M_S M_{SS}} \qquad (4.4.3\text{-}62)$$

Table 4.4.3-9 defines the parameters in Equation (4.4.3-62) and lists values for each. It can be seen that $P_{Rmin} = -115.2$ dBm

Hence, the receiver sensitivity must exceed -115.2 dBm.

b. Receiver IF Noise Bandwidth - The receiver IF bandwidth must be wide enough to pass the command information on the 8.0 kHz and 8.6 kHz subcarrier under all frequency uncertainties and doppler conditions. Doppler (±3.5 kHz) and frequency uncertainties (+5.5 kHz) added to the highest command subcarrier frequency require at least ± 18 kHz IF bandwidth. The actual IF bandwidth has been assumed to be at least ±20 kHz to insure linearity across the subcarrier frequencies. Hence, the noise bandwidth is at least 40 kHz.

TABLE 4.4.3-9. VHF COMMAND UPLINK CALCULATION

Parameter	Description	Value
P_T	Transmitter Power	53.0 dBm
L_T	Transmitting Circuit Loss	—
G_T	Transmitting Antenna Gain	12.0 dB
L_P	Polarization Loss	-3.0 dB
L_{FS}	Free Space Loss	-147.2 dB
	Carrier Frequency	154.2 MHz
	Slant Range (0°)	1913 nm
G_R	Receiving Antenna Gain	0.0 dB
L_R	Receiving Circuit Loss	-4.0 dB
M_S	System Margin	-6.0 dB
M_{SS}	Single Margin above Threshold	-20.0 dB
P_R	Received Carrier Power	-115.2 dBm

c. Receiver Noise Figure - The maximum allowable receiver noise figure F_R can be calculated from the receiver sensitivity, P_{Rmin}, the receiver IF noise bandwidth, B_{IF}, and the antenna temperature, T_a. Since the command antenna is isotropic, it sees mostly galactic noise, and T_a is estimated to be 1260°K. Hence from

$$P_{Rmin} = k \left[T_a + (F_R - 1)\ 290°K\right] B_{IF} \qquad (4.4.3\text{-}63)$$

one can calculate that

$$F_R = 1 + \left[\frac{P_{Rmin}}{k\ B_{IF}} - T_a\right] /290 \qquad (4.4.3\text{-}64)$$

where k = Boltzman's constant = 198.6 dBm/degree K-Hz

Hence

$$F_R = 15.7 = 12 \text{ dB}$$

is the maximum allowable noise figure for the VHF receiver. An actual noise figure of 7 dB will improve the receiver sensitivity an additional 3.5 dB. Note that if the noise figure is specified at the hybrid input, it can be 3 dB higher.

d. Effects of Command Antenna Nulls - The link calculation summarized in Table 4.4.3-9 assumed a zero dB receiving antenna gain. The actual receiving antenna gain may be as low as -20 dB. However, the signal margin, M_{SS}, which has been assigned 20 dB, will insure that the system margin of 6 dB still exists even when the receiving antenna gain is as low as -20 dB.

e. Probability of Error in Detecting Command Bits - In addition to having sufficient sensitivity, the command receiver must demodulate the command bits with a probability of bit error less than 10^{-6}. The modulation technique employed is non-coherent FSK. Figure 4.4.3-8 shows a curve of the probability of bit error. For a probability of bit error less than 10^{-6}, the E/N_0 must be theoretically greater than 14.2 dB. Allowing 4 dB additional for detector losses, the required E/N_0 is 18.2 dB.

Now

$$\frac{E}{N_0} = \frac{ST}{N_0} \qquad (4.4.3\text{-}65)$$

Here, T = (1/128) seconds, N_0 is -161.2 dBm/Hz for a 12 dB receiver noise figure and antenna temperature of 1260°K. Hence, S, the power in the FSK subcarriers, must be greater than -121.9 dBm. Now, the subcarrier power is at least 70 percent of half the carrier power. Hence, if the minimum carrier power is -115.2 dBm, the minimum subcarrier power

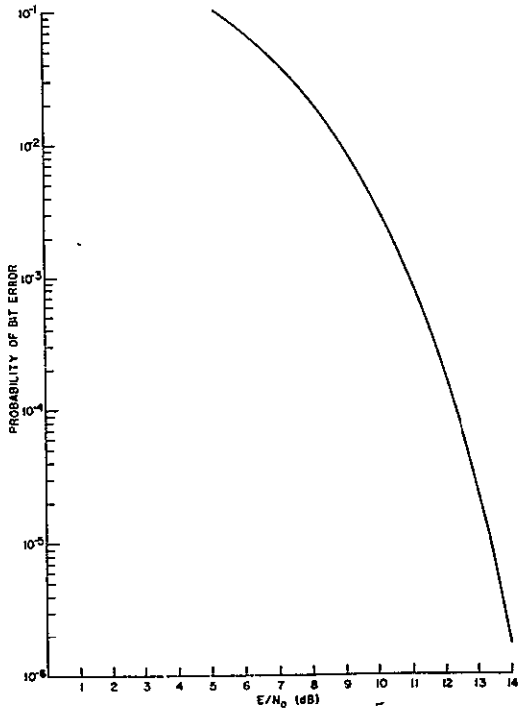

Figure 4.4.3-8. Pe versus E/N_0, Ideal Noncoherent FSK

will be 4.5 dB less, or -119.7 dBm. This gives a 2.2 dB margin over the required subcarrier power. Note that if a 7 dB noise figure receiver is used, the margin would be 3.5 dB more.

4.4.3.3.2 USB Uplink

1. Requirements - If is necessary to receive and demodulate the uplink USB signal from Manned Space Flight Network (MSFN) ground stations containing a carrier component, pseudo-random-noise (PRN) ranging signal, and command data subcarrier (70 kHz). The carrier must be acquired and tracked in a phase-lock-loop. The PRN signal and command subcarrier must be demodulated in a discriminator. Following are general requirements:

1. Received Carrier Frequency: 2106.40625 MHz ± .004 percent
2. In-Lock Tracking Range: ±90 kHz
3. In-Lock Tracking Rate: ±35 kHz
4. Modulation on Carrier: Phase
5. Information Bandwidth: 1.5 MHz
6. Command Subcarrier Frequency: 70 kHz
7. Command IF Bandwidth: 20 kHz
8. Command Information Bandwidth: 4 kHz

1. Studies and Analyses

a. Receiver Threshold - In order to determine the threshold for the phase-lock-loop receiver, it is necessary to perform a link calculation from MSFN ground stations to the spacecraft at an elevation angle of zero degrees. This is shown in Table 4.4.3-10. From this table, one can see that the minimum power expected in the carrier component is -103.7 dBm including a 6 dB system margin and 20 dB signal margin. Hence, the receiver threshold must be at or below this number.

b. Uplink Modulation Analysis - The nominal downlink ranging and command modulation indices determined in Section 4.4.3.2.2.2.2 are 0.17 and 0.33 radians, respectively. For the assumed turnaround ratio of 0.3 radians downlink per radian uplink the uplink modulation indices are:

$$\theta_R = 0.565 \quad \text{(Range Channel)}$$
$$\theta_C = 1.1 \quad \text{(Command channel)}$$

The modulation losses are then as given in Table 4.4.3-11 (assuming five percent modulation tolerances) as derived from the equations:

$$P_{CAR}/C = J_o^2(\theta_C)\cos^2\theta_R \qquad \text{(carrier)} \qquad (4.4.3\text{-}66)$$

TABLE 4.3.3-10. USB UPLINK CALCULATION

Parameter	Worst Case Value
Transmitter Power	63.0 dBm
Transmitting Circuit Loss	-
Transmitting Antenna Gain	43.0 dB
Free Space Loss	-169.9 dB
Carrier Frequency	2106.4 MHz
Slant Range (0°)	1913 nm
Receiving Antenna Gain (includes Polarization Loss)	-4.0 dB
Receiving Circuit Loss	-5.0 dB
System Margin	-6.0 dB
Signal Margin above Threshold	-20.0 dB
Received Total Power	-98.9 dBm
Carrier Modulation Loss	-4.8 dB
Received Carrier Power	-103.7 dBm

TABLE 4.3.3-11. MODULATION INDICES AND LOSSES (UPLINK)

Channel	Nom. Mod. Index (rad)	Nom. Mod Loss (dB)	Mod. Loss +5% Tol. (dB)	Mo. Loss -5% Tol. (dB)
Carrier	-	-4.3	-0.5	+0.5
Ranging	0.565	-8.3	+0.1	-0.1
Command	1.1	-5.0	+0.1	-0.3

$$P_R/C = J_o^2(\theta_C) \sin^2 \theta_R \quad \text{(range channel)} \qquad (4.4.3\text{-}67)$$

$$P_C/C = 2J_1^2(\theta_C) \cos^2 \theta_R \quad \text{(command channel)} \qquad (4.4.3\text{-}68)$$

Link calculations of Section 4.4.3.2.2.2.3 indicate that an SNR of 10.9 dB (including 6 dB system margin and 0.1 dB negative modulation index tolerance is available in the range-channel IF for the given modulation parameters; therefore, the constraint requiring at least 6 dB is satisfied.

The constraint on command SNR in the presence of ranging can also now be checked. The received command power is given by

$$P_C = C\, L_{MC} \tag{4.4.3-69}$$

where C is total received power and L_{MC} is the command channel mod loss. The ranging spectrum noise power density was given previously and is

$$N_{OR} = \frac{2\, C\, L_{MR}}{R_B} \tag{4.4.3-70}$$

where L_{MR} is the range channel mod loss and R_B is the range signal code bit rate ($\approx 10^6$ bits/second). Then, the command signal-to-noise-power-density ratio is

$$\frac{P_C}{N_{OR}} = \frac{C\, L_{MC}}{2\, C\, L_{MR}/R_B} = \frac{R_B}{2}\,\frac{L_{MC}}{L_{MR}} \tag{4.4.3-71}$$

In db, for the worst case,

$$\frac{P_C}{N_{OR}} = -3 + R_B + L_{MC} - L_{MR} = -3 + 60 + (-5) - (-8.2) = 60.2 \text{ dB}$$

Since command threshold is defined as a 10 dB SNR in 20 KHz ($P_C/N_o = 53$ dB-Hz), a margin of 7.2 dB is provided relative to the ranging channel noise; thereby meeting the constraint that the margin be at least 6 dB. Note that when commands only (no ranging) are transmitted on the uplink, the command threshold (P_C/N_o = 53 dB-Hz) is achieved with a 6 dB system margin, 20 dB signal margin above threshold, and 7.3 dB extra margin under worst-case conditions.

c. Probability of Bit Error in Detected Command Bits - USB Uplink - The output signal from the 70 kHz command subcarrier discriminator is the sum of a 2 kHz sine wave phase-shift-keyed by a 1 kHz sub-bit data stream plus a 1 kHz sine wave coherent with the data transitions, plus noise. The 2 kHz PSK'ed signal is demodulated in the Command Integrator Unit. The theoretical required E/N_o for a bit error rate of 10^{-6} is 10.5 dB, as seen from Figure 4.4.3-2 of Section 4.4.3.2.1.2.1. Allowing an additional 2 dB for demodulator losses yields a required E/N_o of 12.5 dB. Since the noise spectral density out of the discriminator is not white, an average value $\bar{N}_o$ will be computed. The total noise N in a 4 kHz bandwidth out of the discriminator is given by:

$$N = \frac{f_m^{\,3}\, N_o}{3\, P_c} \tag{4.4.3-74}$$

where

$f_m = 4$ kHz

$P_c/N_o = 53$ dB (from Section 4.4.3.3.2.2.2)

The value for $\overline{N}_o$ is then N/f_m or

$$\overline{N}_o = \frac{f_m^2 N_o}{3 P_c} \qquad (4.4.3\text{-}75)$$

The signal power S in the data signal is one-half the total signal power out of the discriminator, or

$$S = \frac{\Delta f_c^2}{4} \qquad (4.4.3\text{-}76)$$

The signal energy E equals S times the bit rate, R_B. Hence,

$$\frac{E}{\overline{N}_o} = \frac{3 \beta^2 P_c}{4 N_o R_B} \qquad (4.4.3\text{-}77)$$

where $\beta = \Delta f_c/f_m$. For $\beta = 1.5$, we have

$$\left(\frac{E}{\overline{N}_o}\right)_{\text{actual}} = 25 \text{ dB}$$

Since the required E/N_o is only 12.5 dB, it is obvious that a 10^{-6} probability of bit error will be achieved.

4.4.3.4 VHF/USB Recommended Design

Based on the requirements, studies, and analyses in Sections 4.4.3.1 through 4.4.3.3, a recommended design has been determined. Figure 4.4.3-9 shows a block diagram of this design. The components have been grouped in four black boxes: VHF Transmitters, VHF Command Receivers, Unified S-Band Equipment, and Premodulation Processor. The grouping has been done as shown to maximize use of existing black box designs. Block redundancy with little crosstrapping has been provided to insure successful operation throughout the mission lifetime without increasing the design complexity. Only one of each type of component operates at a time.

The VHF transmitters provide the minitrack tracking beacon plus the capability to transmit either real-time PCM housekeeping telemetry data or stored PCM housekeeping telemetry

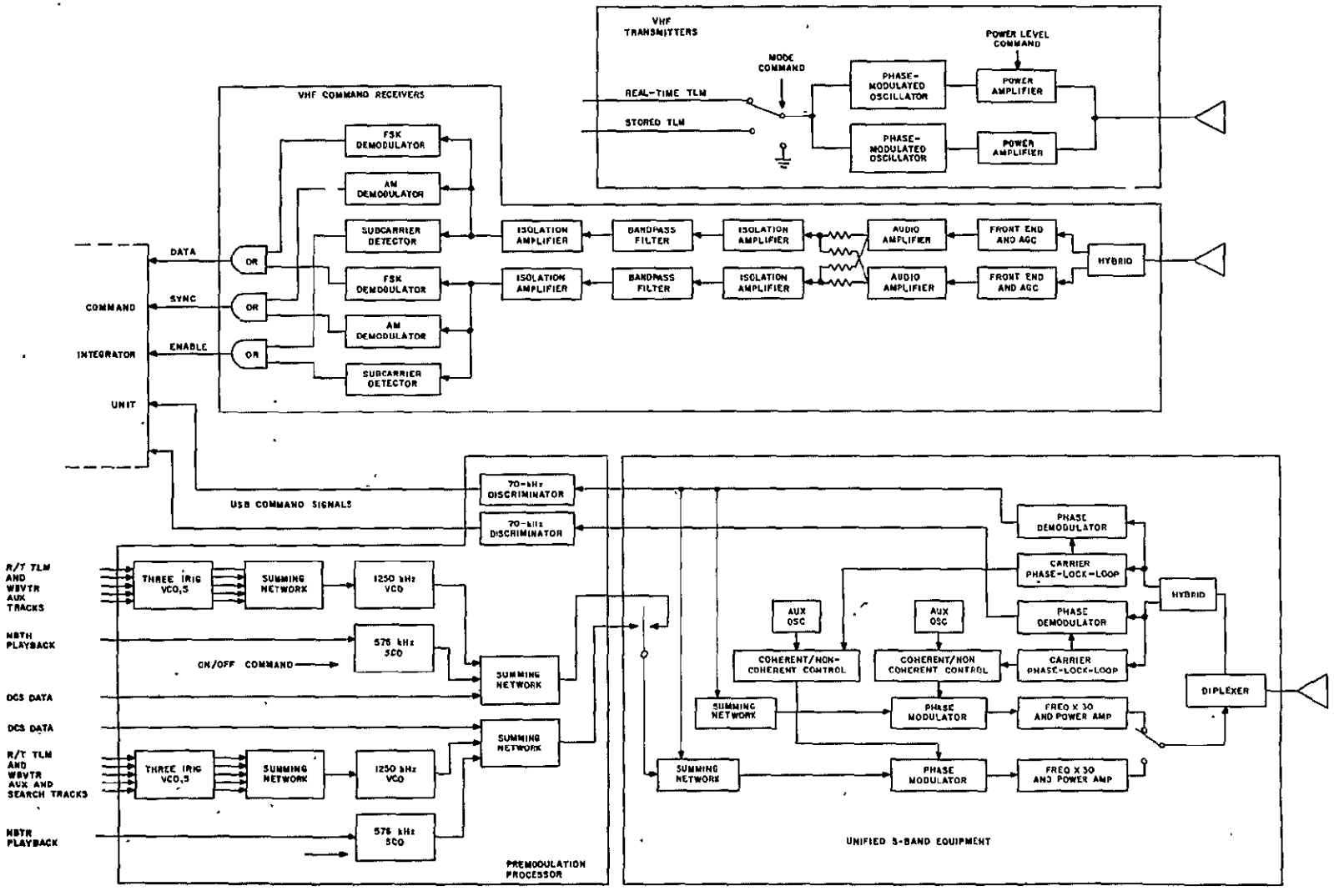

Figure 4.3.-9. VHF/USB Subsystem

data. The transmitter output power is 300 milliwatts in the tracking only mode and tracking plus real-time data mode. The transmitter output power is switched automatically to 2 watts for the tracking plus stored data mode.

The VHF Command Receivers receive and demodulate the uplink VHF command signal from STADAN ground stations.

The Unified S-Band Equipment (USBE) receives and demodulates the USB uplink command and ranging signal from MSFN ground stations. It accepts the composite baseband signal from the Premodulation Processor and phase-modulates this, along with the turn-around ranging (and command) signal, on the USB downlink carrier. The USB downlink carrier is coherent with the received USB uplink carrier (if present). Capability to transmit the composite baseband signal on a downlink carrier generated internally is also present. Switching between transponder (coherent) transmission and non-coherent transmission is performed automatically in the USBE when received carrier lock is indicated.

The Premodulation Processor accepts all five narrowband data signals and combines them into a suitable composite baseband signal for downlink transmission on the USB downlink carrier. It also premodulation filters the stored PCM housekeeping telemetry signal for downlink transmission via the VHF downlink carrier. Finally, it discriminates the 70 kHz command subcarrier from the received USB uplink signal and provides the recovered data signal to the Command Integrator Unit.

4.4.3.5 Unified S-Band Transponder

4.4.3.5.1 Requirements

1. MSFN Compatible

Frequencies	
Receive	2106.4 MHz
Transmit	2287.5 MHz
Tracking Threshold	-115 dBm
Dynamic Range	80 dB
Ranging Channel Band Width	1.5 MHz
Transmit Power	1.0 Watt
Modulation	PM/±3.0 Radians/1.5 MHz Rate (3 dB)
Frequency Stability (Open Loop)	$\pm 3.0\ 15 \times 10^{6}$
Modulation Sensitivity:	1 rad/volt ± 15 percent

2. Study Task - Survey available hardware and assess its compatibility with ERTS interface.

4.4.3.5.2 Available Hardware

Table 4.4.3-12 lists both flight proven and developmental hardware that could be adopted to meet ERTS requirements. The table indicates that the Apollo Block II USB flight hardware and the Collins baseboard come closest to meeting the ERTS requirement. The Philco hardware is DSIF compatible and the Hughes is DSIF or SGLS compatible.

4.4.3.5.3 Proposals

Three of the companies listed in Table 4.4.3-12 have submitted proposals for the ERTS requirement. Their proposed performance is compared in Tables 4.4.3-13 and 4.4.3-14. The Motorola approach consists of making the following modifications to the Apollo Block II flight hardware.

1. New external case for unmodified WBE modules (except as noted in No. 5 and No. 6).
2. Delete FM transmitter and antenna track modules.
3. Replace antenna receiver switch with 3 dB hybrid.
4. Design and include a diplexer
5. Replace 3 Ø 400 Hz supplies with new DC to DC converters
6. Repackage the LM power amplifier multiplier module to the USBE configuration.

The only new hardware designs required are the hybrid, diplexer, and power converter.

The Collins proposal offers basically a new design giving the same performance as Motorola production hardware. The weight differential is probably not significant since Motorola's is based largely on measurements and Collins is predicted. The DC total power difference is more significant even though their technical backup appears optimistic.

The Philco proposal offers a new advanced, microelectronics design giving across the board rf performance improvement along with a 2:1 reduction in weight and DC power over the Motorola Block II. Their power and weight claims are all substantiated in a technical proposal and very consistent with their production ALSEP S-Band Receiver and Transmitter.

TABLE 4.4.3-12. EXISTING HARDWARE APPLICABLE TO ERTS WB REQUIREMENTS (All Units are fully redundant)

Parameter	ERTS Req.	Motorola Block II	Motorola Advanced	Collins	Philco Mariner	Philco Viking Receiver	Hughes Surveyer	Hughes Tac-Sat
Status	Qualified	Production	Breadboard	Brassboard	Production	Breadboard	Production	Production
Rec. Freq.	2106.4 MHz	2106.4 MHz	2106.4 MHz	2106.4 MHz	2115 MHz	2115 MHz	2113 MHz	1800 MHz
Noise Figure (dB)	-	10.5	6.0	8.0	8.0	8.3	12.0	13.0
Tracking Threshold (dBm)	-122	-134	-130	-135	-152	-151	-	-
Tracking Range (kHz)	±90	±90	±89	±90		-	-	-
Dynamic Range (dB)	80	97	-	80		-	-	-
Ranging Channel Bn (MHz)	1.5	1.5	4.0	2.8	1.5	1.8	-	-
Predetection Bw (kHz)	-	15		10	4.5	4.5	13	-
Receiver Input Power (W)	-	5.54	1.6	10	11.7	1.8	1.8	5.0
Trans Freq (MHz)	2287.5	2287.5	2287.5	2287.5	2297	None	2295	
Trans Power Out (W)	1.0	0.25	20.0	5.5W	0.25W	-	0.1	0.07
Trans Modulation	±3 Rads 1.5 MHz PM	±3 Rads 1.5 MHz PM	- 10 MHz		3 MHz	-	-	-
Trans Input Power (W)		11.46		78	18	-	4.3	9.6
Size (in^3)	706	1200.0	368	400		-	34.3	715
Weight (lbs)	-	32.0	20	12.4	32.7	-	7.9	13.4

TABLE 4.4.3-13. COMPARISON TABLE OF PROPOSED DESIGNS

Parameter	Motorola	Collins (A)	Collins (B)	Philco
Precent Redesign from flight proven hardware	20%	100%	100%	100%
Percent Redesign from brassboard hardware	NA	20%	40%	50%
Size (Nimbus Module)	4/4	4/4	4/4	3/0
Weight (lbs)	20.95	17.4	17.4	17.4
Receiver Power (watts)	7.0	3.8	3.8	2.1
Transmitter Power (watts)	21.0	16.3	11.8	13.5
Total Power (watts)	28	21.1	15.6	15.6

TABLE 4.4.3-14. DETAILED SPECIFICATION COMPARISON

Parameter	Specification	Philco	Collins	Motorola
Receiver				
Noise Figure (dB)	-	+1 max.	10.4	11.4
Threshold (dBm)	-122	-130	-122	-134
Input Sig. Range (dBm)	-122 to -37	-130 to -20	-122 to -38	-134 to -37
Image Response (dB)	-	-60	-	-
Input VSWR	-	1.5:1 max	-	-
False Lock Margin (dB)	-	30 min	-	-
Frequency Stability	$\pm 2/10^5$	$\pm 1/10^5$	$\pm 2/10^5$	$\pm 2/10^5$
Tracking Range (kHz)	±90	±120	±90	±90
Static Phase Error (°)	±15	±8	±15	±15
Tracking rate (kHz/Sec)	35	60	35	35
Predetection BW (kHz)	-	20	16	-
Loop BW at Threshold (kHz)	-	2.0	0.8	0.8
Phase Det BW (kHz)	2	2	2	2
AGC Range (dBm)	-120 to -51	-130 to -30	-120 to -51	-120 to -51
AGC BW (Hz)	-	100	-	
AGC Accuracy (dB)	20	10	20	20
Subcarrier BW (kHz)	20 min	20	20	20
Subcarrier Stability (dB)	±9 max.	±3	±4	±4
Subcarrier S/N (dB)	10	16	10	10
Subcarrier Lin (%)	1	1	1	1
Ranging Freq. (MHz)	1.5 kHz to 1.5 MHz	1.5 kHz to 1.5 MHz	100 Hz to 1.5 MHz	1.5 kHz to 1.5 MHz
Power Input	-	2.1	3.8	7.0
Transmitter				
Power Output (w)	1	1	1.12	1.0
Load VSWR	1.3 1	1.3:1	1.3:1	1.3:1
Spectral	-	-60	-	-50
Modulation				
Freq. Res. (3 dB)	300 Hz - 1.5 MHz	DC to 1.5 MHz	300 Hz to 1.5 MHz	300 Hz to 1.5 MHz
Sens rad/volt	0.2 - 1.0	0.2 - 1.0	0.2 - 1.0	0.2 - 1.0
Stability %	±20	±10	±20	±20
Lin %	±10	±5	±10	±10
Max Dev (rad)	6.0 p-p	6.0 p-p	6.0 p-p	6.0 p-p
Frequency Stability				
Long Term	$15/10^6$	$13/10^6$	$15/10^6$	$15/10^6$
Short Term	-	$2/10^{10}$		
VCO Phase Noise	6° RMS Max	4° RMS Max	6° RMS	6° RMS max
Power Input	-	13.5	16.3	21.0

4.4.3.6 PCM Telemetry Processor

4.4.3.6.1 Introduction

The purpose of this study was to generate a preliminary design for an ERTS A/B PCM Telemetry Processor for a one-year operating mission. Two previously developed PCM systems the Nimbus D-VIP and Nimbus B PCM, were studied as a base for developing the ERTS PCM unit.

The VIP is a highly flexible, high reliability, maximum data handling capability system. Most of the effort on VIP was directed toward determining what capabilities would be eliminated from VIP in order to save cost.

The Nimbus B PCM is a simple fixed format system with less capability than is required for ERTS. The reliability figure of the Nimbus B is substantially lower than the VIP because there is less system redundancy. The Nimbus B redundancy scheme was structured around a six-month mission requirement. The study effort on Nimbus B was directed toward determining what changes and additions would be necessary to meet ERTS requirements.

4.4.3.6.2 System Capability Comparison

Table 4.4.3-15 compares ERTS requirements with the capabilities of the existing Nimbus B PCM system, a VIP with only a bit rate change, and a VIP operating in 1024 Mode (with no memory).

4.4.3.6.3 Modification to VIP

Several modifications of the VIP telemetry system, necessary for converting it to the ERTS application, were considered.

1. Output Bit Rate Change to 1 k bps

a. VIP Change. The change from 4 k bps to 1 k bps can be accomplished by changing the input clock frequency to the Memory Sequencer from 1.6 MHz to 400 kHz.

b. Test Set Modification. Logic changes to the clock generation logic are required. A DPDT switch is used in the test set to control NAND gates for routing the existing 1.6 MHz or the 400 kHz out as clock rate. The second pole of this switch controls two other NAND gates which route either the existing 800 kHz or the 200 kHz to the bit rate and word rate countdown logic.

2. Word Length Change from 10 Bits/Word to 8 Bits/Word

a. VIP Change. The following methods of implementing this change were considered:

1. Make the change to 8 bits with minimum cost impact.
2. Retain a 10-bit word, making the last two bits parity bits.

TABLE 4.4.3-15. SYSTEM CAPABILITY COMPARISON

	Nimbus B	VIP	VIP-1024 Mode	ERTS Requirements
Bit Rate	500 bits/sec	1000 bit/sec or 2000 bits/sec	1000 bits/sec or 2000 bits/sec	1000 bits/sec
Channel Capacity and Sampling Rates	455 Analog Ch. 434 at 1 sample/16 sec 21 at 1 sample/sec 343 Digital Channel 280 at 1 sample/16 sec 63 at 1 sample/sec	* 576 Analog 320 Digital "B" 16 Digital "A"	960 Channel Commands 1 sample/10.24 sec	481 Analog Channels 422 at 1 sample/16 sec 31 at 3 sample/16 sec 28 at 1 sample/sec 253 Digital Channels 146 at 1 sample/16 sec 73 at 3 sample/16 sec 34 at 1 sample/sec
Resolution	7 bits/word	10 bits/word	10 bits/word	8 bits/word
Reprogramming Capability	Fixed Format Only	All formats changeable until launch. One format re-programmable after launch	Fixed Format Only	Unknown
Time Code Capability	42 bits/16 sec	100 bits/sec	None Usable	100 bits/sec
Reliability	.525 probability of success for one yr operation	.808 probability of success for one yr operation	.965 probability of success for one yr operation	

*The VIP is designed for an 832 Channel analog capacity, 64 channels per card. Of the 13 cards that space is provided for in the VIP, only 9 were actually wired in. The sampling rates in VIP are selectable with the program stored in memory.

(1) Change to 8 Bits with Minimum Cost Impact. The system changes which would result from this "minimum-impact" means of changing from 10-bit words to 8-bit words are minor and do not significantly affect either the cost or reliability of the VIP. However, the impact on the Bench Test Equipment is somewhat extensive.

The Digital Multiplexer/Formatter cards will not require any changes. The input gates and control logic for bits 9 and 10 can simply be left off the cards.

It would be possible to remove a few components from the VIP Digital Coder if only 8 bits were coded rather than 10. The cost saving would be quite small, however, and the additional time required for design considerations and the advantages of retaining the capability of coding 10 bits probably justify retaining the present design.

The "Digital Address, Serial Data Register and Control" card will not require any re-design unless the "Digital A" data will be adversely affected by receiving 10 input shift pulses rather than 8. The 10 input shift pulses will be required to position the data properly in the 10-bit serial data register. Only the 8 Most Significant Bits of this register will be sampled.

The five-stage counter in the "Digital Command Generator" will have to be changed from a five-stage counter to a four-stage counter in order to reduce the word length from 10 bits to 8 bits. The bit 9 and 10 stages of the Output Register and Time Code Converter would be unnecessary and could be removed.

(2) Eight Bit Word with Parity Generator. This second alternative is slightly more complex, but may be justified because of the increased flexibility. Parity can be counted such that the total number of ONEs in a word is odd or even, whichever is desired.

The primary disadvantage of adding the two parity bits is the additional transmission time required. The two parity bits will also replace the last two bits of the time word, possibly resulting in the loss of time information.

The advantage of retaining the 10-bit word is that, in addition to having a parity check, it would allow for the possibility of changing back to a 10-bit data word resolution by by-passing the parity generator, possibly by changing a few card jumperwires.

This change does not substantially affect either the cost or reliability of the VIP.

3. Reduction of Channel Capability. Consideration was given to a possible reduction of the number of digital and analog channels in the VIP. The VIP is structured such that the removal of one card removes either 64 analog channels, 80 digital "B" channels, or 8 Digital "A" channels. Present information indicates that one Analog card and both of the Digital "A" cards will not be required.

4. Modifications to Memory and Memory Sequencer. Consideration was given to the cost savings that might result from the following changes:

1. Eliminate mode selection by ground command
2. Eliminate ground command selectable bit rate
3. Eliminate reprogramming capability
4. Reduce capacity of Memory Section 1.

It was determined that by reducing the program to a single fixed format as described for the ERTS system, the VIP non-programmable memory (Section I) can be reduced from 512 words by 10 bits to approximately 150 words by 10 bits. Also, the scratch-pad memory can be reduced from 8 words to four words. The scratch-pad would consist of four words (ten bits each), one for each of the three subcommutated sampling rates (those channels addressed less than once per second) and one to keep track of the minor frame count. A group of simple instructions similar to those in the VIP would be used to generate the various commands necessary to derive the channel addresses.

The elimination of the reprogrammable memory and the reduction in size of the non-programmable memory does not permit the removal of a significant portion of the memory electronics. Consequently, the net cost saving made possible by this reduction of memory capability is not sufficient to justify the reduction in system capability.

The "probability of success" for one year of operation for the present Nimbus B is 0.525. The addition of the new circuitry (the new box housing the memory for generating a flexible format, plus additions to the PCM and TME units) would cause this reliability figure to fall below 50 percent.

Because of the extensive redesigned requirement, which would result in an essentially new and non-qualified system, and the low "probability of success" figure, the Nimbus B approach is not recommended.

4.4.3.6.4 Nimbus B Expansion for ERTS

An Expansion Capability Study for Nimbus B was conducted. This study covered the changes which would have to be made to Nimbus B to meet ERTS requirements. Among these changes are:

1. Increased bit rate
2. Increased resolution for 7 bits/word to 8 bits/word
3. Higher encoding rate
4. More flexible format.

A new Time Code Converter would have to be added to Nimbus B and the number of Analog Channels would have to be expanded to meet ERTS requirements. The Time Code Converter

addition is necessary because the Nimbus B format includes only six 7-bit Time words per 16 second major frame. The ERTS requirements are for 100 bits of Time Code and Sync per second. An additional box would be required to generate a new format.

Table 4.4.3-16 lists the areas of design change and new design that would be required for a Nimbus B. These design changes are so extensive that the result would be essentially a new system. Because of the large number of changes required, the use of a modified Nimbus B would not result in a cost saving compared to an essentially unmodified VIP.

4.4.3.6.5 VIP Reduced Operating Mode

During the Reprogram Cycle, the formatter directs a sequential sampling of all gates. Ten stages of the formatter's eleven-stage counter are used to obtain sequential gate addresses (the eleventh stage is not used in the Nimbus D Configuration). Beginning at gate address 0, the counter effects a transfer of gate data into the VIP serial bit stream. Data contained at each address are as follows:

Address	Data
0 through 15	Digital A
16 through 31	Random
32 through 63	Digital B
64 through 639	Analog
640 through 895	Analog expansion (output zeroes)
896 through 958	Random
959	Time Code
960 through 1023	Value (binary count 960 to 1023)

When this Reprogram Cycle command is given, the VIP operates without direction from memory and sequentially samples all data channels each 10.24 seconds at a 1 k bps. If it is desired to sample any given channel more frequently the channel would have to be wired into more than one time slot.

This format will not contain the sync words or the Time Code that exists during the normal VIP mode. A sync pattern could be generated during the digital "B" portion of the 10.24-second format by wiring in the appropriate bits. The Time Code will be lost since only one 10-bit word is sampled during each 10.24-second format. Normally, 1024 bits of Time information are sampled during this period of time. The sampling of the one 10-bit word will not occur synchronously with the incoming time information.

The cost saving which would result from operating in this mode is about 20 percent of the cost of the VIP system. However, the limitations make it an unattractive mode for the ERTS PCM.

TABLE 4.4.3-16. NIMBUS 'B' MODIFICATIONS TO MEET "ERTS" REQUIREMENTS

Status	P.C. Card Location	P.C. Card Function	Electrical Redesign				Mechanical Redesign				Test Fixture, Test Specs, Documentation Redesign				Remarks
			Total	Major	Minor	None	Total	Major	Minor	None	Total	Major	Minor		
Existing Nimbus 'B' PCM	1A1	Programmer/Power Supply 'A'	X(1)				X				X				
	1A2	A/D Converter-Output Register 'A'	X(1)				X				X				
	1A3	10 Stage Counter/Command Gen. 'A'		X(2)			X				X				
	1A4	Digital Data Gates and G.P.A's 'A'		X(2)			X				X				
	1A5	Sub Com Matrix 'A'				X			X				X		60 Analog Ch, 28 Dig. Ch.
	1A6	Sub Com Matrix 'B'				X			X				X		60 Analog Ch, 28 Dig. Ch.
	1A7	Sub Com Matrix 'A'				X			X				X		60 Analog Ch, 28 Dig. Ch.
	1A8	Sub Com Matrix 'B'				X			X				X		60 Analog Ch, 28 Dig. Ch.
	1A9	Prime Matrix 'A' and 'B'				X			X				X		32 Analog Ch, 0 Dig. Ch.
	1A10	Sub Com Matrix 'A'				X			X				X		60 Analog Ch, 28 Dig. Ch.
	1A11	Sub Com Matrix 'B'				X			X				X		60 Analog Ch, 28 Dig. Ch.
	1A12	Sub Com Matrix 'A'				X			X				X		60 Analog Ch, 28 Dig. Ch.
	1A13	Sub Com Matrix 'B'				X			X				X		60 Analog Ch, 28 Dig. Ch.
	1A14	10 Stage Counter/Command Gen. 'B'		X(2)			X				X				
	1A15	Digital Data Gates and GPA's 'B'		X(2)			X				X				
	1A16	A/D Converter-Output Register 'B'	X(1)				X				X				
	1A17	Programmer/Power Supply 'B'	X(1)				X				X				
Added 'ERTS' Requirements		Time Code Converter 'A' and 'B'	X(3)				X				X				
		Serial Digital Interfaces 'A' and 'B'	X(3)				X				X				
		New Format Programmer 'A' and 'B'	X(4)				X				X				
		Additional Power Supply 'A' and 'B'	X(4)				X				X				
Nimbus B TMR Unit		Relay Control Logic (2 P.C. Cards)	X(4)				X				X				
		Summing Amplifiers 'A' and 'B'		X(4)			X				X				
		Recorder Read/Write Amps 'A' and 'B'	Delete				Delete				Delete				

Connected for 'ERTS' Requirements

Notes:
① Redesign for integrated circuits and planar P.C. cards to meet 'ERTS' requirements
② Redesign for 'ERTS' 8 bit data words and new fixed programmer
③ Redesign similar to existing VIP circuits
④ ERTS new design

4.4.3.6.6 Technical Discussion of Recommended System

Because of cost considerations or changed ERTS requirements, all of the changes to VIP which were originally considered were rejected, with the exception of the change in bit rate from 4 k bps to 1 k bps (the VIP, previously ground switchable from 4 k bps to 8 k bps will now be switchable from 1 k bps to 2 k bps).

The recommended system is, therefore, an unmodified VIP. The following is a description of the VIP operation.

1. Preliminary Technical Description. The purpose of the VIP is to arrange input data into a predetermined time sequence for transmission to ground stations.

The VIP is a highly flexible system with the following salient characteristics:

1.	High Reliability	Each section is redundant with power cross-switching capability for high-reliability operation.
2.	Flexible Bit Rate	Ground switchable from 1 k bps to 2 k bps.
3.	Large Data Handling Capability	Capability for 832 Analog Channels with an expansion capability for 832 additional channels
4.	High Resolution	10 bits/word
5.	Flexible Format	All formats can be changed by altering memory content up until launch. One format reprogrammable after launch.

Figure 4.4.3-10 is a block diagram of the VIP subsystem. The VIP subsystem comprises six major functional areas: memory, memory sequencer, analog multiplexer coder, digital multiplexer formatter and reprogrammer. The digital multiplexer and formatter are contained physically within the same module.

Rather than a hard-wire approach, the VIP uses a memory and memory sequencer as controlling units in generating required sampling sequences. The memory contains a stored program of instructions which are transferred to, and acted upon by the memory sequencer to set up known frame sequences. In implementing this procedure, the sequencer first calls for the contents of a specific memory location (address). The address is transferred to the sequencer and decoded. The decoded word is an instruction that either (1) effects a transfer of data from an experimenter or housekeeping circuit to the formatter (gate data) or (2) effects the transfer of the memory word itself to the formatter (value data). Value data may be either a synchronizationor identification word. This sequencing continues according to the stored program in memory. A major frame marker is supplied to experiment circuits to enable their synchronization with the frame sequence.

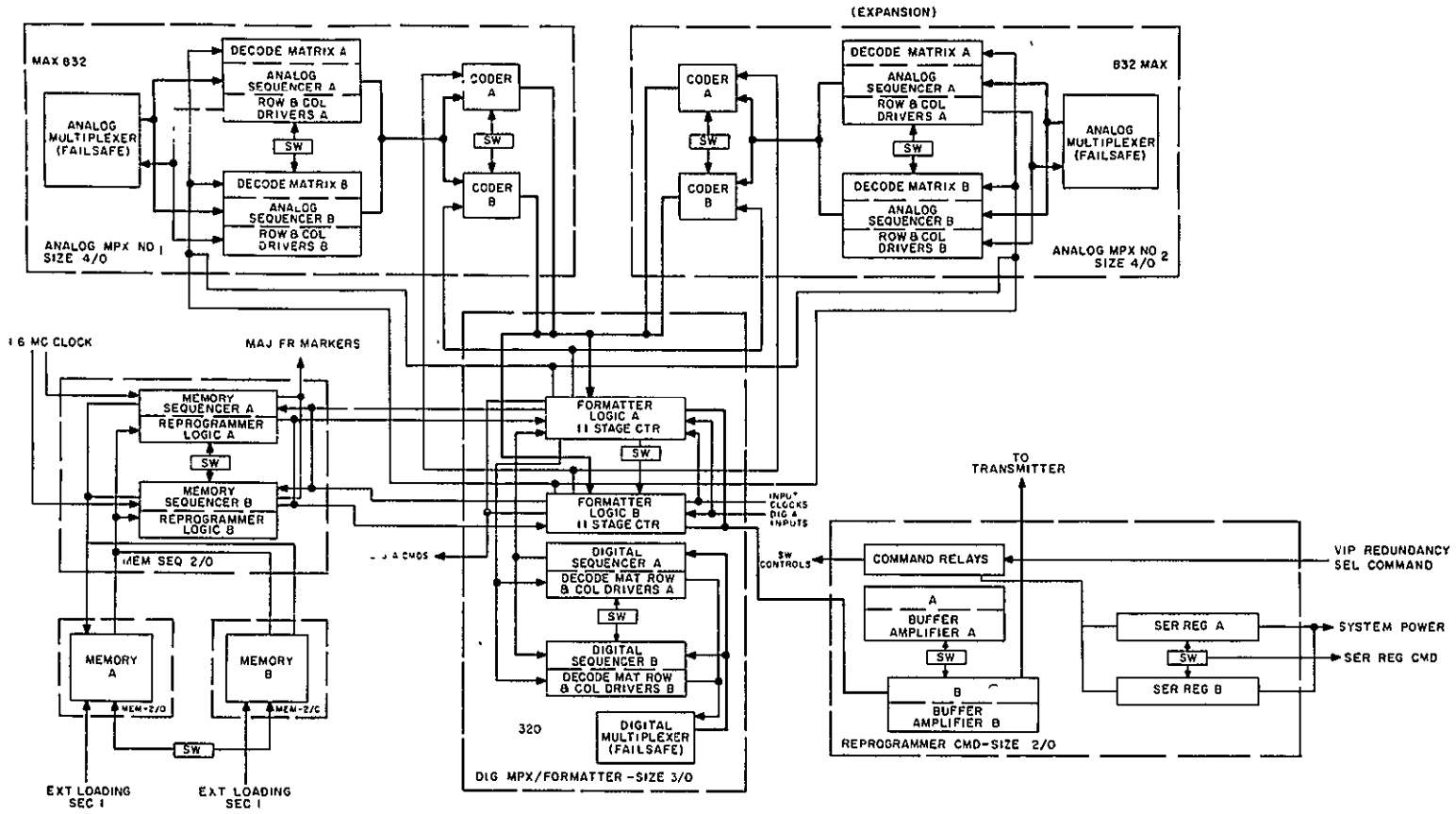

Figure 4.4.3-10. Versatile Information Proceddor (VIP)

Formatting data from the memory sequencer, and experiment and housekeeping circuits is coordinated by the formatter. This unit serially transfers the data to the recorder and to the programmer.

VIP split phase data from the formatter and the modulated time code from the command clock subsystem are buffered within the reprogrammer. Split phase data and the time code are available at the output. Ground commands operate relays within the reprogrammer to effect program control and to switch between redundant VIP modules. Series regulators, which are also contained within the reprogrammer, regulate -24.5 vdc primary power to -20.0 vdc power for use within the VIP subsystem. Reprogram data is hard wired through the module and applied to the memory sequencer.

Reliability of the VIP subsystem is increased by the use of redundant components. Redundancy features of the VIP are shown in Figure 4.4.3-10. Control of redundancy modes is initiated by ground command to the command clock subsystem, which in turn commands relays in the reprogrammer. The reprogrammer applies or removes power to the modules to set up the commanded configuration.

Components of the VIP subsystem which are not redundant are designed in a failsafe arrangement. That is, failure of a component results in a minimum loss of data.

4.4.3.6.7 Telemetry Format

1. Constraints and Requirements

   1. Output data rate will be 1 k bps, because of upper bound on the bit transmission rate.
   2. Input analog signals will be encoded to 10-bit resolution (8-bit accuracy required).
   3. Constraints imposed by existing PCM telemetry processor design:
      a. Analog gates 576 (expandable to 832 gates)
      b. Digital A (10-bit word) 16
      c. Digital B (single bit) 320
      d. Time Code Data - 10-bit input shift register
      e. 10-bit format word.

2. Functional Description. There are four independent formats available in the VIP telemetry which can be reprogrammed up through final spacecraft tests. In addition to the standard housekeeping format which will be discussed here, there will be special spacecraft troubleshooting formats. The design of these special formats will be accomplished during Phase D as the detailed of the component troubleshooting requirements become available.

The format can be considered a M x N matrix of 10-bit words arranged in rows and columns. The format is generated row by row by starting in row 1, column 1 and proceeding sequentially through the matrix until the Mth row is completed with the encoding of word M,N. The format is then repeated with the starting synchronized with the 1 Hz reference signal.

A row is referred to as a minor frame and the entire matrix is called the major frame. The signal leaving the PCM telemetry processor is a serial data stream of 1 k bps or 100 words per second.

Thus, the telemetry signal is a word sequence occurring periodically at the major frame rate. In this case the major frame period is simply MXN/100 words/sec.

a. Time Code Data. The time code is a 40-bit BCD word that is updated once a second and pulse-width modulated in minitrack format in the command/clock at 100 pps. The minitrack format contains ten 10-bit words with the first 6 bits of each word containing sync data and the last 4 bits is a BCD character of the time code. Thus one BCD character is transmitted to the PCM processor every 0.1 second in sync with the 1 Hz reference signal.

The constraints of using a 10-bit word in the format, including all time code data and restricting of the time code data input register to 10 bits, puts several bounds on the format.

Since only two BCD time code words can be stored in the input register we are restricted to loading a single BCD character into a 10-bit format word once every 0.1 second or two BCD characters every 0.2 second. The second arrangement is the obvious choice for efficiency of format words. The restrictions imposed by the input time code data rate and the output word rate from the formatter are indicated in Figure 4.4.3-11. This is a timing diagram starting at a major frame which occurs at the positive transition of the 1 Hz reference square wave. This is coincident with the updating of the time code data shown at the top of the figure. Also indicated is a minor frame of 20 words and the time relationship with the time code bits. The first two words of the format are for synchronization and the eleventh word is for minor frame identification. With these choices we see that the two BCD time code characters can be inserted into words 20, 23, 24, or 25. Starting at word 26 sync bit and a new 4-bit BCD character will be loaded into the input shift register, which requires the first 10 bits to be unloaded into the output format register by that time.

In order to incorporate an integer number of time code words (i.e., ten BCD characters) in the format, the major frame must be an integer number of seconds. To synchronize the start of the major frame with the positive transition of the 1 Hz signal, we must place the last two BCD characters of the major frame into the last word of the format (as shown in word 20). The other pairs of the BCD characters could be randomly placed in words 20, 23, 24, or 25 modulo 20 words, if it is so desired. However, for simplicity of processing the format in the ground data handling system, we will locate time code data in word 20 and every 20th word (i.e., modulo 20) from there on.

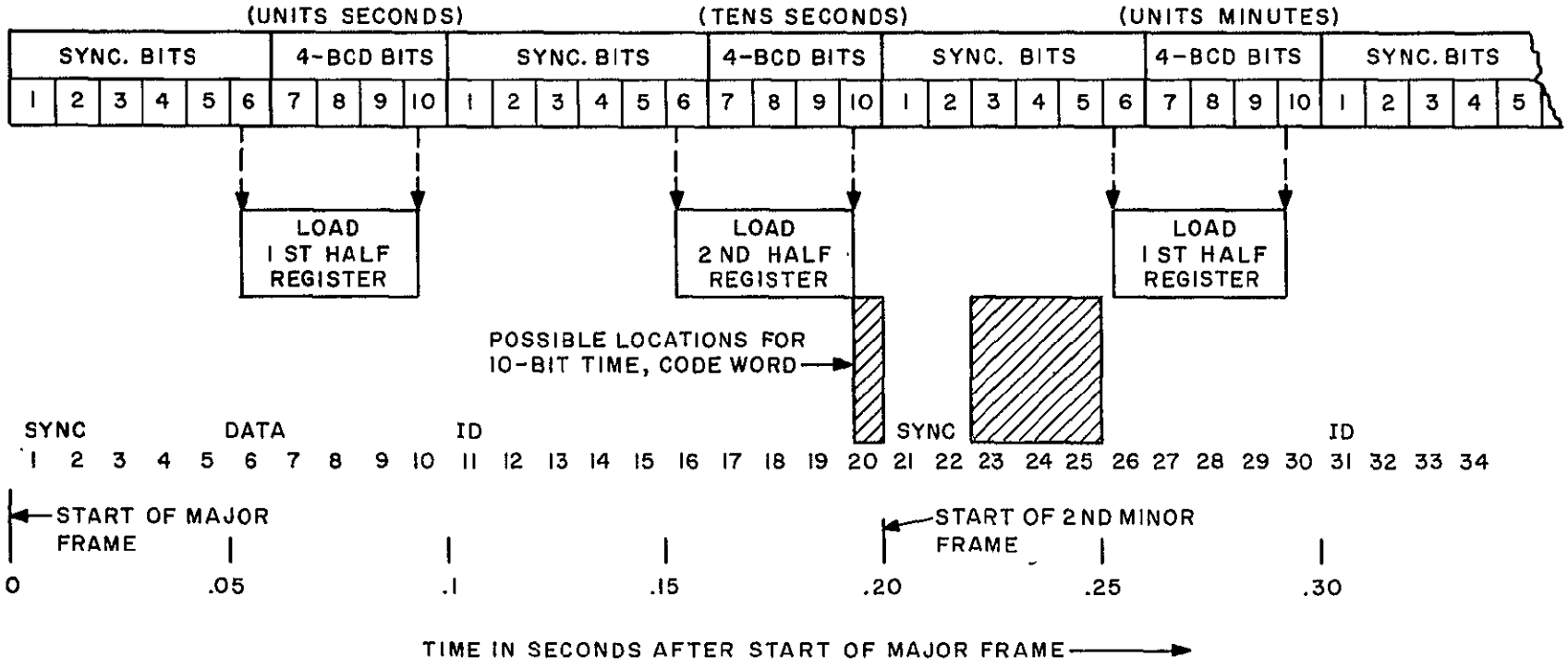

Figure 4.4.3-11. Time Relationship between Time Code Signal and Format Words

(1) Format Size

(a) Minor Frame Size. For most efficient format programming the optimum periodicity of the minor frame is equal to the maximum sampling rate of any of the telemetry points. In examining the data points the time code data is the highest at 5 Hz. All other data points are at a slower rate. Thus 0.2 second has been selected as the minor frame duration.

Each minor frame will contain twenty 10-bit words, the first two are for minor frame synchronization and the 20th word is time code data. The minor frame identification has been positioned in word eleven to allow maximum time separation between minor frame sync and identification for ground data handling ease. Thus, each minor frame will have 16 data words in addition to a time code data.

(b) Major Frame Size. We will develop expressions relating the major frame size and time period to the number of data points and minor frame parameters.

The number of words in the format is given by

$$N_W = \sum_{i=1}^{M} \frac{S_i D_i}{W} \qquad (4.4.3\text{-}78)$$

where

D_i = number of bits for the i th data point

S_i = number of times a data point is sampled in a major frame

W = number of bits in a format word = 10 bits

M = number of data points.

The time period of a major frame is

$$T_f = N_R T_M \ , \qquad (4.4.3\text{-}79)$$

where

N_R = number of rows or minor frames

T_M = time period of a minor frame.

The number of times a data point is sampled in a major frame is

$$S_i = R_i T_f \ , \qquad (4.4.3\text{-}80)$$

where

R_i = rate at which the point is sampled.

Thus the number of words in the format is

$$N_W = \sum_{i=1}^{M} \frac{R_i D_i}{W} T_f \qquad (4.4.3\text{-}81)$$

$$N_W = \frac{T_f}{W} \sum_{i=1}^{M} R_i D_i \quad . \qquad (4.4.3\text{-}82)$$

There are four types of data points sampled by the PCM processor. The number of bits each data type occupies in a 10-bit format word is shown below:

	Data Type	Number of bits in a word
1.	Time code	10
2.	Analog	10
3.	Digital A	10
4.	Digital B	1

The number of rows or minor frames is given by

$$N_R = \frac{NW}{20} \quad . \qquad (4.4.3\text{-}83)$$

Substituting (4.4.3-83) into (4.4.3-79) to solve for major frame time, we get

$$T_f = \frac{NW}{20} \ (.2) \qquad (4.4.3\text{-}84)$$

$$T_f = NW \times 10^{-2} \quad . \qquad (4.4.3\text{-}85)$$

Substituting for NW we get

$$T_f = (63.4\ T_f + 474.9)\ 10^{-2} \qquad (4.4.3\text{-}86)$$

$$T_f\ (1 - .634) = 4.749 \qquad (4.4.3\text{-}87)$$

$$T_f = \frac{4.749}{.366} \qquad (4.4.3\text{-}88)$$

$$= 12.96 \text{ seconds}$$

$\therefore$ T_f = 13 seconds minimum.

Substituting into NW we get

$$NW = 825 + 474.9 = 1299.9 \text{ words} \qquad (4.4.3\text{-}89)$$

$\therefore$ NW = 1300 words.

Table 4.4.3-17 gives the number of words in the telemetry format.

TABLE 4.4.3-17. NUMBER OF WORDS IN TLM FORMAT

Data Type	M_i Number of TLM points	D_i Bits/point	R_i Sample Rate (Hz)	$R_i D_i M_i$ Bits/second	$\frac{R_i D_i M_i}{W}$ words/second
1. Time Code	1	10	5	50	5
2. Analog	a. 2	10	3	60	6
	b. 28	10	1	280	28
	c. 31	10	$3/T_f$	$310/T_f$	$31/T_f$
	d. 422	10	$1/T_f$	$4220/T_f$	$422/T_f$
3. Digital A	4	10	1	40	4
4. Digital B	a. 4	1	5	20	2.0
	b. 34	1	1	34	3.4
	c. 73	1	$3/T_f$	$73/T_f$	$7.3/T_f$
	d. 146	1	$1/T_f$	$146/T_f$	$14.6/T_f$
5. Sync. + ID	3	10	5	150	15

$$\text{Total word rate} = 63.4 + \frac{474.9}{T_f}$$

$$\text{Total number of words } (N_w) = 63.4\, T_f + 474.9$$

The total available words in the format is the word rate being generated times the major frame time. The word rate

$$R_W = \frac{\text{words per minor frame}}{T_m} \qquad (4.4.3\text{-}90)$$

$$= \frac{20}{0.2} = 100 \text{ words/seconds.}$$

The total number of words available in the format is

$$N_T = R_W T_f \qquad (4.4.3\text{-}91)$$

$$= 1300 \text{ words.}$$

This leaves no room for expansion in the format. Since it is possible to use some existing Nimbus software at the ground stations it was decided to go to a 16 second major frame period. Thus the total available words in the format is

$$N_T = 1600 \text{ word positions available.} \qquad (4.4.3\text{-}92)$$

The number word positions used is,

$$N_W = (16)\ 63.4 + 475 \qquad (4.4.3\text{-}93)$$

$$= 1030 + 475$$

$$= 1505 \text{ word positions used.}$$

This leaves 95 unused positions for expansion.

The number of rows or minor frames is the total number of words divided by the number of columns, which is equal to the number of words in a minor frame.

$$N_R = \frac{N_T}{N_C} = 80 \qquad (4.4.3\text{-}94)$$

where

N_C = number of columns.

(c) Frame Parameter Summary. In summary, the recommended format is shown in Figure 4.4.3-12. The parameters are:

Minor Frame

Size: Twenty 10-bit words

1st two words for synchronization

11th word for identification

20th word time code data

16 additional data words

Period: 0.2 second.

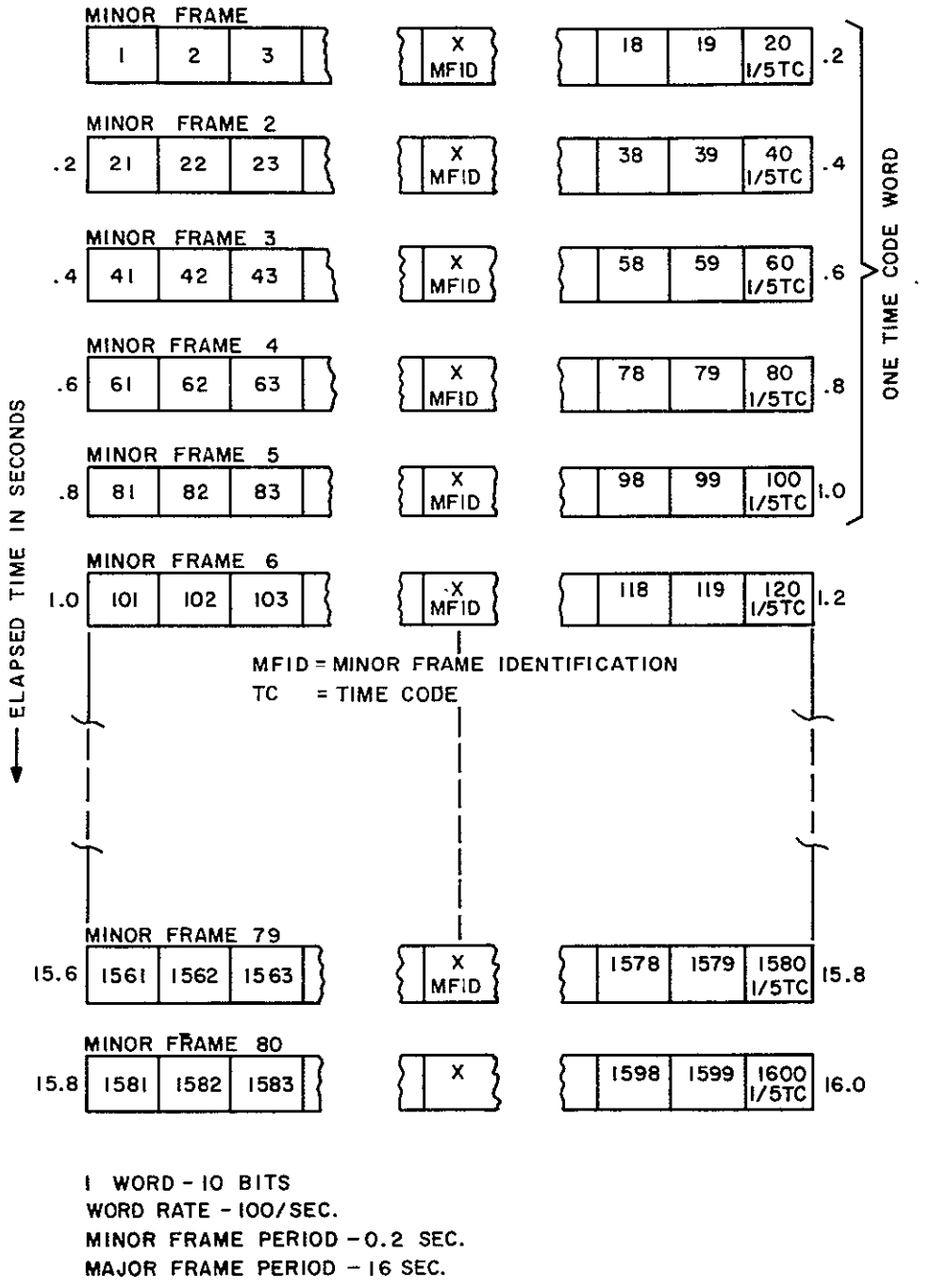

Figure 4.4.3-12. ERTS VIP 20 x 80 Matrix

Major Frame

Size Matrix: 80 Rows (i.e., minor frames) x 20 columns to provide 1600 - 10 bit words

Actual use: 1505 words

Period: 16 seconds.

3. PCM Frame Synchronization. Frame synchronization bits are added to the format in order to provide the ground data handling system with a means of accurately identifying a minor frame and properly process the data unit. There are two problems of properly identifying the synchronization word:

1. The probability of falsely identifying a group of data bits as the synchronization word and thereby losing telemetry data
2. The number of errors due to noise, preventing proper identification of the synchronization word.

The procedure for synchronizing the telemetry format by the ground data handling system will be described, followed by calculation of the synchronization parameters.

4. GDHS PCM Frame and Subframe Synchronization Procedure. The Telemetry processing system will be capable of executing a SEARCH, VERIFY and LOCK technique to achieve sync on the input data under three different sets of sync parameters as described in Table 4.4.3-18. The frame and subframe sync strategy will be performed by hardware with the parameters controlling the hardware sequence inserted from either the front panel or from the central processor (computer). The procedure to be used will be the SEARCH, VERIFY, and LOCK technique as detailed below. This is applicable to both forward and reverse-ordered data at bit rates up to 32 k bps.

TABLE 4.4.3-18. TLM PROCESSOR SYNC PARAMETERS

	No. Syncs		Allowable No. Bit Errors		Allowable Bit Slippage	No. MFID Checks	
	Good Advance	Bad Return to SEARCH	SYNC	MFID		Good Advance	Bad Return to SEARCH
SEARCH	1		e_1			1	
VERIFY	N_2	1	e_2	E_x	b_2	M_2	1
LOCK		N_3	e_3	E_y	b_3		M_3

a. Normal Mode and Normal Sub-Modes

(1) Sync Pattern Synchronization

(a) Sync Search Mode - The hardware will scan the serial bit stream to locate a 20-bit sync pattern. The number of bit errors allowable in the sync pattern shall be e_1. When an acceptable sync pattern has been identified, the decom will enter the SYNC VERIFY mode and visually indicate the condition on the processor console.

(b) Sync Verify Mode - The decom will continue to check serial input data and identify sync patterns, separated by 18 words $\pm b_2$ bits. The number of bit errors allowable in a sync pattern shall be e_2. When N_2 successive correct sync patterns have been received, the decom will enter the SYNC LOCK mode and indicate the condition on the processor console. If any sync pattern does not meet the above criteria, the decom will return to the SYNC SEARCH mode. In SYNC VERIFY and SYNC LOCK modes, the program will only look for sync patterns at the expected point (18 words $\pm b_n$ bits after the last sync pattern).

(c) Sync Lock Mode - The decom will continue to check sync patterns continuously. The separation shall be 18 words $\pm b_3$ bits, and the allowable sync pattern bit errors shall be e_3. If the above criteria are not met, the minor frame will be flagged, and processing and output will continue as if sync were good. Data words shall be referenced to the last received sync word position. If N_3 successive sync patterns do not meet the above criteria, the decom shall return to the SYNC SEARCH mode.

(2) Minor frame identification word synchronization - The MFID word is located at a known position from the sync pattern. Upon identification of a sync pattern MFID checks will be also initiated. MFID checks and modes are independent of sync pattern checks and modes except as indicated to the following paragraphs.

(a) MFID SEARCH Mode - The decom will test the MFID word against limits. If it is acceptable, the program will advance to the MFID VERIFY mode.

(b) MFID VERIFY Mode - The decom will check MFID words in a specified column and verify that each successive MFID word value is augmented by 1. E_x-bit errors shall be allowed in the MFID word. (When stored data is being processed, the sequence will be reversed). When M_2 successive correctly augmented MFID words have been received, the decom shall advance to the MFID LOCK mode, provided that the SYNC LOCK mode has been achieved. If during the sequence any MFID word is out of sequence, the program will return to the MFID SEARCH mode. A console switch option will be provided to also cause an out of sequence MFID to return to decom to the SYNC SEARCH Mode.

(c) MFID LOCK Mode - The decom will continue to check MFID words per proper sequencing. E_x bit errors shall be allowed in the MFID word. If any MFID words are out of sequence, they will be corrected before being used for data decommitation. If M_3 successive incorrectly augmented MFID words are received, the decom will return to the MFID SEARCH mode. The console switch option specified in MFID VERIFY mode will also cause the decom to return to the SYNC SEARCHmode, if M_3 successive incorrectly augmented MFID words are received.

(3) Synchronization parameters - The sync parameters will be stored in a table in memory. There will be at least three tables for use with data of high, medium, and low bit error rates (see Table 4.4.3-18).

(4) Data distribution - Data distribution and processing will be inhibited until the program has achieved both the SYNC LOCK and MFID LOCK modes.

b. Emergency (1024) and VIP Memory Verify Modes. The sync procedure is identical to the normal mode, except there are no MFID word checks. Sync pattern length and separation are different from those for Normal Mode. To handle these two modes the frame synchronizer word capacity shall be 1024 words for the Emergency Mode and 640 words for the Memory Verify Mode.

c. Summary of Analysis. The objective of this section was to examine the synchronization sequence in order to estimate the amount of data that may be lost under various conditions. Since the size of the synchronization word has to be in increments of 10 bits, (the format word size) two cases were examined:

Case I 20-bit sync word

Case II 10-bit sync word.

Below is summarized the average loss of data as a result of synchronization errors.

Mode	False Sync	True Sync Falsely Dismissed
Search	One frame	One frame
Verify	* $2N_2$ (False Lock)	$(1 + \frac{N_2}{2})$ frames

*Assumes $N_3 = N_2$

The probability of false synchronization, true sync falsely dismissed, and false lock were calculated for 10-bit and 20-bit sync words. The results are tabulated below:

	10-Bit Word	20-Bit Word
Probability of False Sync	10^{-2}	2×10^{-5}
Probability of True Sync Dismissed	0.09	0.26
*Probability of False Lock	10^{-3}	3×10^{-5}

*Assumes a probability of a bit error is 0.05; bit slippage b = 1 bit; $N_2 = 3$ and $e_1 = 0$ for the 10-bit word and 2 for the 20-bit word.

The probability of a bit error was chosen to obtain a worst case condition. Normally, the bit error is expected to be approximately 10^{-6}, which greatly reduces the dismissal of true sync and false lock. Even with this high bit error condition, the 20-bit word appears adequate for false lock where the greatest loss of data (i.e., 6 frames for $N_2 = 3$) can occur. In addition, there is significant performance difference between the 10 and 20-bit sync words that the larger word was selected for the telemetry format.

4.4.3.7 Digital Tape Recorder

4.4.3.7.1 Objective

Review proposals from various vendors to determine the availability of an existing space qualified digital magnetic tape recorder.

4.4.3.7.2 Vendor Ground Rules

A component specification, SVS 7746, was written specifying the system requirements. Each vendor was informed that preference would be given to existing space qualified magnetic tape recorders. Minor changes for reasons of compatibility would be considered; however, no development or major changes would be undertaken. Recorder interface requirements such as size, weight, and power were purposely listed as "later" in order to ensure complete vendor response.

4.4.3.7.3 Requirements

1. System

   Two-orbit record capability (200 minutes)

   Playback to record ratio > 20:1

   One year operating life

   Existing and space qualified.

2. Recorder

   Start/Stop Time < 10 seconds

   One channel

   1 k Bit - Split phase

   Input/output polarity indentical

   Drop units 1×10^6

   Pulse rise/fall time

      Record 10 microseconds (10-90%)

      Playback 1 microsecond (10-90%)

Pulse jitter - later - Vendor to state

Size - later - Vendor to state

Weight - later - Vendor to state

Power - later - Vendor to state

4.4.3.7.4 Vendor Response

1. No Bid. The following vendors no-bid the proposal at this time:

B&K Instrument Inc.

CBS Laboratories

CDC Space Defense

Dlevite Corp.

Fairchild Industrial Products

Honeywell A&O

Litton Data Systems

Raymond Engineering

Texas Instruments

Teledyne Telemetry

2. Technically Inadequate Bids. The following vendors proposals were technically inadequate and would not permit a proper engineering evaluation.

a. Borg Warner Controls. Data sheets consisting of a summary of recorder characteristics for three models of their basic model 310 recorder were offered. No documentation was presented on the flight status, design modification or system description.

b. Ampex. Ampex does not at this time have an applicable standard product magnetic tape recorder. A development program for a magnetic disc recorder was offered.

c. Bell & Howell. Proposal consisted of a letter and a technical proposal for an FM recorder offering a development program.

4.4.3.7.5 Vendor Review. Table 4.4.3-19 lists the recorder parameters as offered by the vendors.

1. Leach. Leach proposal consists of a modified MTR 2000 recorder. Modifications for data interface, control function are the primary changes necessary to conform to performance.

TABLE 4.4.3-19. VENDOR COMPARISON

Vendor	Weight (max)	Size (max)	Power - watts (max)		Tape Packing Density (Bits/Inch)	Jitter	Error Rate	Max No. of Consecutive Drop Outs	Start/Stop Times (max) (seconds)		Record Speed (IPS)	Reproduce Speed (IPS) (**)	Tape Length (Feet)	Tape Width (Inches)	Tape Thickness (Mil)	Temperature (Operating)	Motor	Operating Life (Hrs)	MTBF (Hrs)
			Record	Reproduce **					Record	Reproduce									
Leach Corporation	13 lbs	7.20 x 8.20 x 6.75' 398.5 Cubic inches	7.3	14.5	700	Bit to bit 10^{7} peak to peak	2 bits in 10^{6}	30 bits	2	5	1.41	48.7	1500 (t)	0.25	1.0 (nominal)	-5 C to 45 C (23 F to 114 F)	1 AC motor and duplex magnetic clutch	5000 (t) (14,000 demonstrated)	22,200
Odetics	10 lbs	10.87" x 7.75' x 4.5" 380 Cubic inches	3.0	10	1520	Less than 1"	1 bit in 10^{7}				66	21.1	2000 (min)	0.25		to 55 C	1 DC motor	12,000 (Projected)	
Radio Corporation of America	17 lbs	14.25 x 12.0 x 7.5 1350 Cubic inches	4	10.0	1240	±1" of average bit period measured over 10,000 bits	1 bit in 10^{6}		2.5 Start 0.5 Stop	2.5 Start 1.5 Stop	.805	27.8	980 (940 useable)	0.5		-5 C to 45 C (23 F to 114 F)	2 motors Two phase 400 Hz Synchronous Hysteresis		
Tele-dynamics	9 lbs	8.5 x 6 x 2	4	10	2000		1 bit in 10^{6}	4	< 2	< 2	5	16	525 (t)	.25			2 motors Two phase 100 Hz Hysteresis Synchronous	10,000 (Projected)	27,472

*Excluding connectors
**Parameters will reduce due to change from 12.1 to 24.1

2. Tele-Dynamics. The proposal as offered is for the development of a fluid film recorder. No flight or complete engineering models have been built or tested as of this date.

3. Odetics. The magnetic tape recorder as offered in the proposal is presently under development. No flight models have been built or tested as of this date.

3. RCA. The RCA proposal consists of a modified HDRSS tape recorder system. The reduction from five channels to one channel allows the signal processing circuits to be housed along with the tape transport in a single enclosure instead of 2 housing in the standard HDRSS. The HDRSS tape magnetic tape recorder is one of series of tape recorders that RCA has developed and flown.

4.4.3.7.6 Selection/Justification

Odetics and Tele-Dynamics proposals were eliminated due to the fact that both were offered as development programs. Each vendor proposal offers potential improvement in certain recorder parameters; mechanical interfaces, projected life, etc., however, both are in the primary engineering phases and still require extensive development.

Leach and RCA proposals both require modifications to existing magnetic tape recorders to meet the requirements of this program. A review of technical literature indicates that there is no recorder available for procurement without some modifications. At this time the Leach unit is recommended for ERTS use.

1. Leach

   Data Interface

   Control function

   Record/Reproduct Ratio

2. RCA

   Package in one housing

   Record/Reproduce Ratio

A GE design limit of 10 watts average was established for the digital tape recorder. Each of the proposed recorders meets this limit. Size of the RCA tape recorder severely limits where it may be mounted within the vehicle.

Leach's use of the hard-faced ferrite magnetic bands and low tape packing density will give a better error rate and tape wear, thereby achieving longer life. RCA's tape recorder requires a special command to allow cleaning of the magnetic heads by use of an abrasive layer to insure the required magnetic head to tape life.

The proposed Leach MTR 2000 satellite recorder has been configured in 34 different ways and over 260 units have been delivered in the past five years. Only the basic reel layout, tape path and tape tensioning scheme have stayed nearly the same. Life is being extended by proper choices of magnetic heads, clutches, motors, guiding techniques, lubricants, etc. A 14,000 life test was completed 15 January 1970. With the indication of extended life capabilities and the ability of making numerous configurations to the basic model, the Leach space qualified recorder has been selected for the ERTS program.

4.4.3.7.7 Method of Recording

1. Biphase Saturation Recording. Biphase recording is far superior to standard return to zero and nonreturn to zero techniques because of the narrow bandwidth of the recorded signal and better match to magnetic reproduce head systems. Where 800 bit per inch packing densities represent a practical limit in return to zero or nonreturn to zero, biphase can provide reliable operation well above the proposed 2000 bits per inch. (Biphase systems have demonstrated satisfactory performance to 10,000 bits/linear inch).

The theoretical reason for this better performance is as follows: The ability to read pulses stored on a magnetic tape depends on the detection of the presence or absence of a pulse in noise. Every bit is associated with a particular cell which is represented by a length of tape (1/2 mil in this sytem). An analysis of the playback voltage is necessary to determine the polarity of the voltage for each cell. The polarity alone, not the shape of the pulse, is of importance here. Once this is determined, efforts to maximize the ratio of peak signal to rms noise are required.

A rectangular pulse of a width of τ second and a height of 1 volt has a frequency spectrum as shown below.

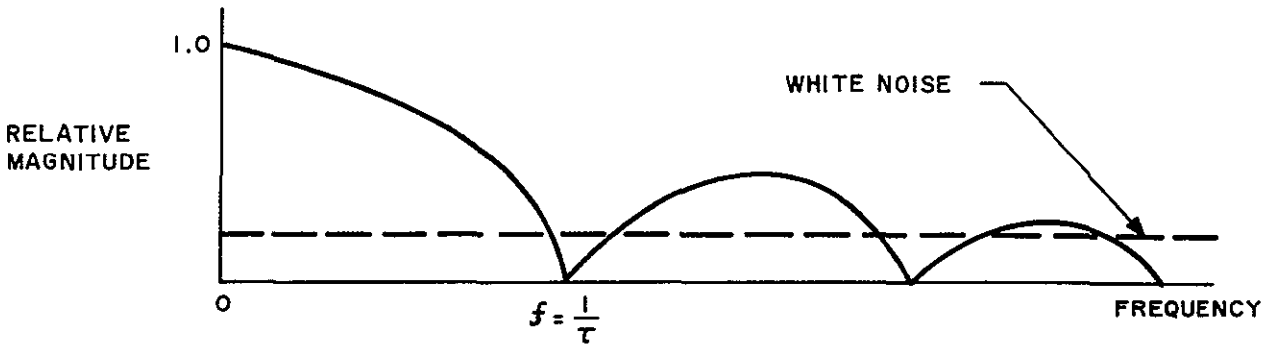

The frequency spectrum of noise can be assumed to be constant. If the system transfer function matches the input spectrum, the maximum noise attenuation possible for the complete signal is being transmitted. A mathematical derivation of this is as follows:

Input Signal = f(t)

Transformed Input = $F(j\omega) = \int_{-\infty}^{\infty} f(t)\, \epsilon^{-j\omega t}\, dt$

System Transfer Function = $H(j\omega)$

Output = $G(j\omega) = F(j\omega)\, H(j\omega)$

Time Output = $g(t) = \frac{1}{2\pi} \int_{-\infty}^{\infty} G(j\omega)\, \epsilon^{j\omega t}\, d\omega$

$$g(t) = \frac{1}{2\pi} \int_{-\infty}^{\infty} F(j\omega)\, H(j\omega)\, \epsilon^{j\omega t}\, d\omega$$

$$d\omega = 2\pi\, df$$

$$g(t) = \int_{-\infty}^{\infty} F(j\omega)\, H(j\omega)\, \epsilon^{j\omega t}\, df$$

At a specific instant of time, t_o the output is:

$$g(t\omega) = \left| \int_{-\infty}^{\infty} F(j\omega)\, H(j\omega)\, \epsilon^{j\omega t_o}\, df \right|$$

The two-sided ($-\infty$ to $+\infty$) power spectrum of "white noise" is:

$$G_H^1(\omega) = \frac{\eta}{2} \left| H(j\omega) \right|^2$$

where η = watts/cps

The output noise power across a one ohm resistor is N_H, where:

$$N_H = \frac{\eta}{2} \int_{-\infty}^{\infty} \left| H(j\omega) \right|^2 df$$

The $\sqrt{N_H}$ is the RMS output noise. The maximized ratio is:

$$\frac{\text{Peak Signal}}{\text{RMS Noise}} = \frac{\left| g(t_o) \right|}{\sqrt{N_H}}$$

Squaring this and dividng by a constant does not change the maximum. The input energy E, used as a constant yields:

$$\frac{(\text{Peak Signal})^2}{E\ (\text{RMS Noise})^2} = \frac{\left| g(t_o) \right|^2}{E\, N_H}$$

Where $E = \int_{-\infty}^{\infty} f^2(t)\, dt = \int_{-\infty}^{\infty} |F(j\omega)|^2\, df$

Substituting:

$$\frac{\text{Peak Signal}}{\text{RMS Noise}} = \frac{|g(t_o)|^2}{E\, N_H} = \frac{\left| \int_{-\infty}^{\infty} F(j\omega)\, H(j\omega)\, \epsilon^{j\omega t_o}\, df \right|^2}{\left\{ \int_{-\infty}^{\infty} |F(j\omega)|^2\, df \;\; \frac{\eta}{2} \right\} \int_{-\infty}^{\infty} |H(j\omega)|^2\, df}$$

Using Schwarz's inequality which is:

$$\left| \int_{-\infty}^{\infty} X(\omega)\, Y(\omega)\, d\omega \right|^2 \leq \int_{-\infty}^{\infty} |X(\omega)|^2\, d\omega \int_{-\infty}^{\infty} |Y(\omega)|^2\, d\omega$$

and identifying:

$$X(\omega) = F(j\omega)\, \epsilon^{j\omega t_o}$$

$$Y(\omega) = H(j\omega)$$

It can be shown that the ratio:

$$\frac{\eta}{2} \frac{\text{Peak Signal}}{\text{RMS Noise}} = \frac{\eta}{2} \frac{|g(t_o)|^2}{E\, N_H}$$

is a maximum if

$$H(j\omega) = K \left[F(j\omega)\, \epsilon^{-j\omega t_o} \right]^*$$

$$\boxed{H(j\omega) = KF^*(j\omega)\, \epsilon^{j\omega t_o}}$$

where the star indicates conjugate. This last equation shows that to maximize peak signal to rms noise ratio, the system transfer function should be the complex conjugate of the input

frequency spectrum. This is what is meant by a matched filter. The possible spectrum of an NRZ or RZ magnetization pattern is:

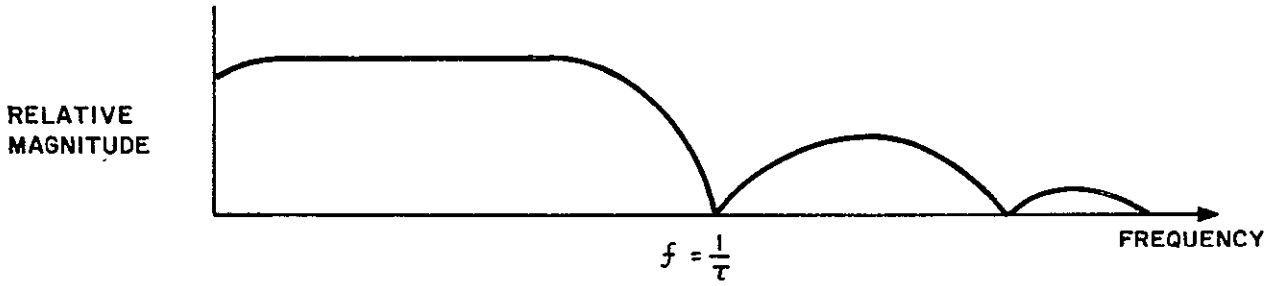

This is arrived at qualitatively where τ is the width of the narrowest pulse encountered and where it is assumed that a train of similar bits will generate wide pulses which contain low frequency components.

The case of phase modulation produces a frequency spectrum thusly:

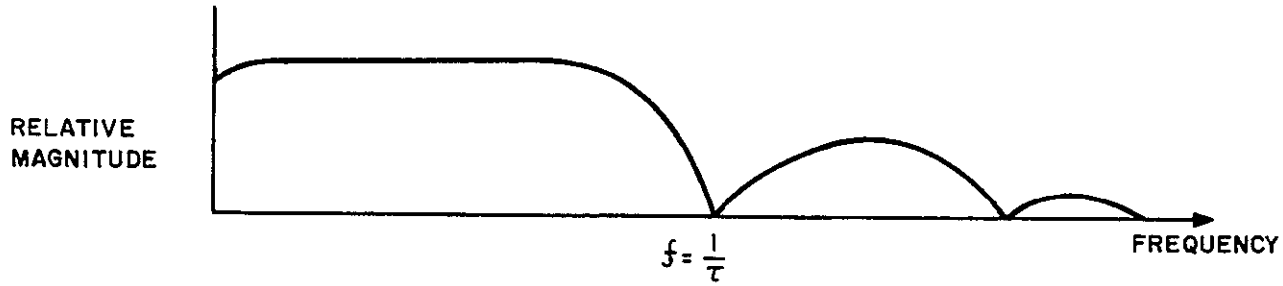

No low frequency components are used here. Considering the reproduce head characteristics:

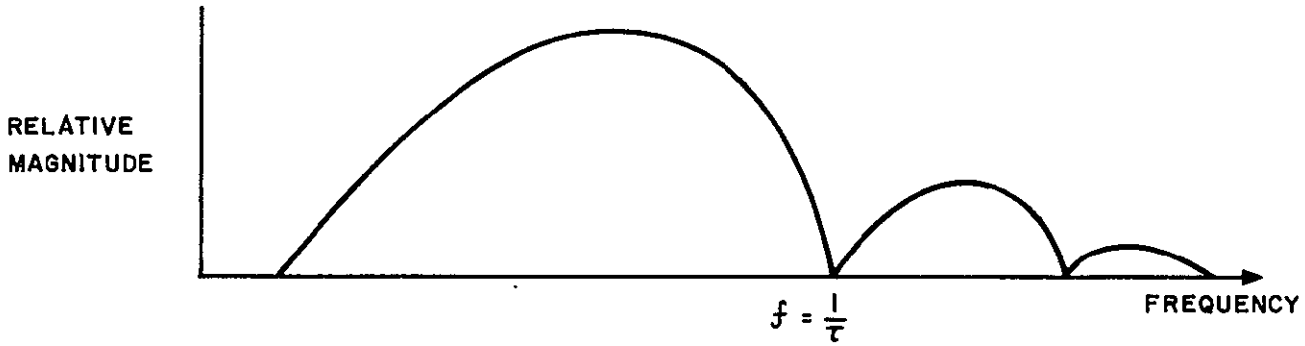

It can be determined that the efficacy of the biphase modulation format is due to stored information which is a better match to the system characteristics than it would be for an nonreturn to zero or return to zero format.

2. Choice of Record/Playback Ratio. It has been demonstrated that recording PCM-split-phase signals is far superior to recording PCM-NRZ or PCM-RZ signals. Furthermore, use of PCM-split-phase signals as input and output for the narrowband tape recorder (NBTR) will eliminate need for NRZ-to-split-phase (and vice versa) electronics in the recorder. Therefore, the output signals from the PCM Telemetry Processor and from the NBTR will be split-phase. The one disadvantage with this approach is that a split-phase signal requires at least 1.5 times the bandwidth of NRZ signals for satisfactory transmission. If the bandwidth increase is restricted to 1.2 times the NRZ case, then an additional 4 dB transmitter power would be required to transmit PCM-split-phase signals of the same bit error rate as PCM-NRZ signals.

The restricting factor in choosing the playback/record ratio is the VHF transmitter RF bandwidth available to transmit the NBTR playback signal. It is shown in Section 4.3.3.2.1.2.3 that 36 kHz of baseband bandwidth is available. This corresponds to a PCM-split-phase signal bit rate of 24 k bps. Since the input signal to the NBTR (real-time PCM telemetry from the PCM Telemetry Processor) has a bit rate of one k bps, this dictates a playback/record ratio of 24 to 1. This is well in excess of the ERTS requirement of greater than 20 to 1.

4.4.4. NARROW BAND ANTENNAS

The problem of providing spacecraft antenna subsystems for the various RF links has been studied and baseline antenna designs have been established. The effects of the vehicle structure and sensor packages on the anticipated antenna radiation patterns has also been studies. Radiation pattern requirements have been developed and reviewed in conjunction with the mission and test requirements. Anticipated antenna performance parameters have been derived and related to the basic system requirements.

The orbit geometry of the spacecraft with respect to the various ground stations determines the basic antenna radiation pattern requirements. For a spacecraft with 3-axis stabilization where the Z axis points toward the center of the Earth, the angle between the Z axis and the line-of-sight to the Earth's horizon is 60.9 degrees and has a slant range of 1915 nm. This geometry indicates that the spacecraft antennas must provide adequate pattern coverage to ±60 degrees from the Z axis and symmetrical about the Z axis. The absolute gain of the antenna is determined from signal margin considerations and the path loss (slant range) to the ground station. The curves in Figure 4.4.4-1 show the slant range and spacecraft elevation angle as a function of the ground elevation angle. In addition, the dB markings on the slant range curve indicate the decrease in path loss in dB from the maximum range of 1915 NM. The ideal antenna radiation pattern should then have maximum gain at a spacecraft angle of 60 degrees and taper to a -12 dB null area at an angle of 0 degrees. In practice, this type of pattern coverage is difficult to obtain with a reasonable antenna aperture particularly at VHF and low UHF frequencies. In addition, if a widebeam, omnidirectional antenna has appreciable gain at spacecraft elevation angles approaching 90 degrees then the interference effect of reradiation from adjacent spacecraft structure becomes important. Thus, a reasonable compromise is usually to provide an antenna with a single lobe radiation pattern of wide beamwidth (80 to 200 degrees) and yet provide decoupling from the spacecraft structure by minimal radiation towards the 90 degrees and above elevation angles.

A possibility exists that the spacecraft may lose attitude control and orbit in an unstabilized or conceivably an upside down mode. For this emergency condition, it is imperative that a command and telemetry link be established although not necessarily on a 100 percent coverage basis. Two command and telemetry RF links are available, one at VHF and one at S-Band.

The antenna problem is to provide a spherical radiation pattern while not compromising the principal 120 degree conical coverage or requiring RF switching of antenna radiators. The design approach at S-Band would be the use of two antennas both simultaneously energized thru a 3 dB power divider. One antenna would be mounted on the earth-side of the spacecraft and would provide the principal 120 degree conical pattern coverage; the other antenna would be mounted on the space side of the spacecraft and would provide a radiation pattern of maximum beamwidth and yet not provide an annoying interference pattern in the principal 120 degree cone region. The concept is pictured in Figure 4.4.4-2. Several disadvantages are apparent: For a normal mission 1/2 of the transmitter output power is continuously wasted; severe polarization losses will occur because of the inability to provide circular polarization over the spherical region; the pattern interference region will be essentially a blind area; and the solar panels, by their size and motion, will provide an undesirable modulation of the secondary pattern and perhaps portions of the principal pattern.

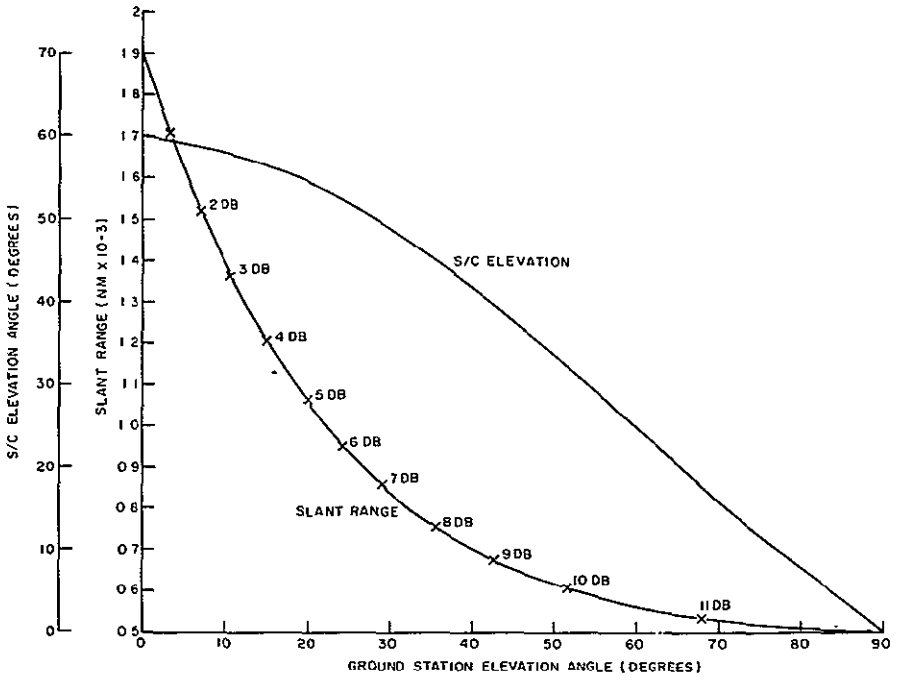

Figure 4.4.4-1. Slant Range and Spacecraft Elevation Angle or a Function of Ground Elevation Angle

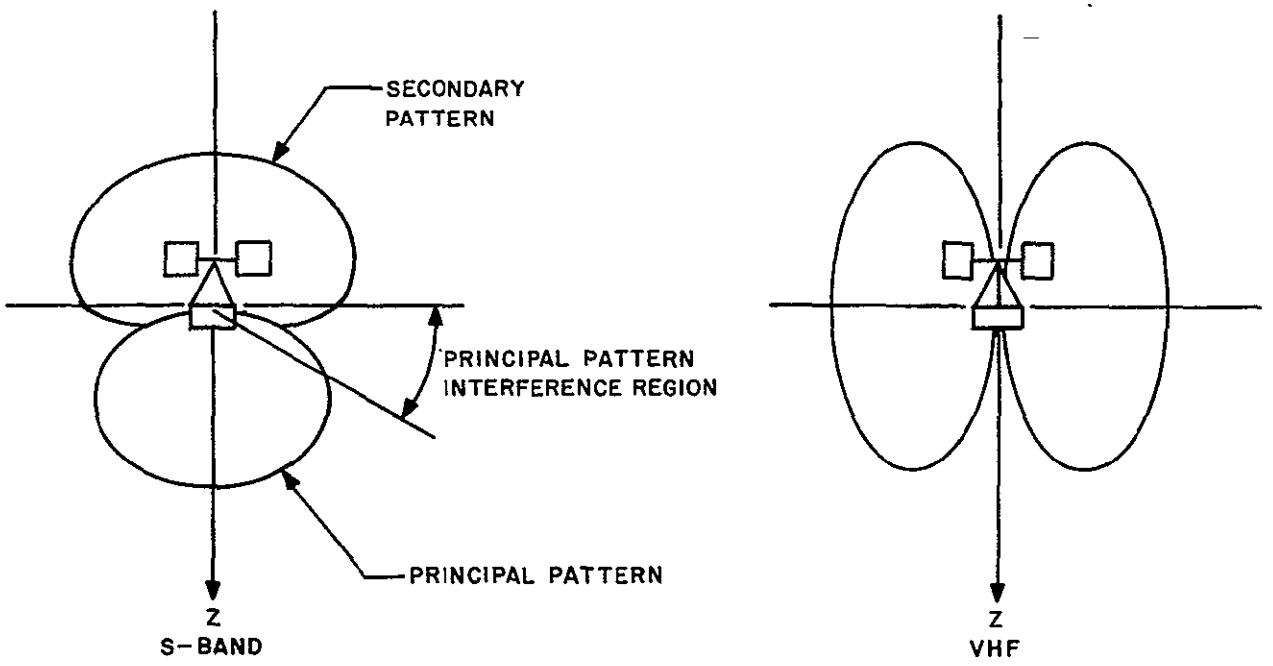

Figure 4.4.4-2. S-Band and VHF Antenna Patterns

At VHF, the problem of providing spherical pattern coverage becomes easier because the wavelength is comparable to the spacecraft dimensions. The problem was solved on the Nimbus vehicles by providing two antenna systems. For the command link, a monopole mounted atop the spacecraft excites a dipole-type pattern shown in Figure 4.4.4-2. For the telemetry link, an array of four antennas provides spherical coverage withsufficient gain so that acceptable signal-to-noise ratios can be obtained with a polarization diversity ground receiver. These antennas are discussed in greater detail in Section 4.4.4.1. Thus, the baseline approach is to provide spherical pattern coverage for the VHF TT&C links and the 120 degree conical coverage for the S-Band TT&C links.

Figure 4.4.4-3 shows the baseline antenna systems as they would be oriented on the spacecraft. Three structural features of the spacecraft can have a significant effect upon the orientation and performance of the antennas. The rotation of the solar paddles has a modulating effect on the radiation patterns of the VHF Command and VHF Beacon antennas. The solar paddles represent a large conductive surface area and significant RF energy is scattered over the spherical volume. The pattern modulation effect has been evaluated on the Nimbus vehicles and will be discussed further in Section 4.4.4.1.

The MSS sensor package on the bottom of the sensory ring assembly presents a large blockage area to the three adjacent antennas. The effect of the large package is to force the antennas away from the sensory ring for a clear field of view. Since the three antennas must have a radiation pattern with good symmetry about the Z axis and elevation angles around 60 degrees the proximity of adjacent conductive structure becomes important. The final orientation and placement of the antennas can only be determined after a radiation pattern measurement program using an RF equivalent mock-up of the spacecraft.

When the spacecraft is sitting on the launch-pad, reliable RF links must be established with the ground station to permit open-loop testing of the various transmitters and receivers. The launch shroud which encloses the spacecraft will be essentially RF transparent if it is similar to the Nimbus shroud. The VHF TT&C link antennas will be under the shroud and direct radiation to the ground station will occur. The DCS, USB, and Wideband antennas will be enclosed in essentially a metal drum formed by the spacecraft sensory ring, launch adapter cylinder, and booster interface plate. Although some leakage radiation will be present, it cannot be considered as a predictable or reliable source of radiation. Therefore, some method of coupling to the three spacecraft antennas must be provided.

During the powered flight and orbit injection phases of the mission, it may be a requirement to provide both VHF and S-Band tracking and telemetry coverage. The VHF telemetry antennas because of their location on the periphery of the sensory ring will radiate through the launch shroud during the powered flight phase and radiate into free space after shroud separation. It is expected that near spherical pattern coverage will exist even though the second stage booster is attached and the spacecraft solar paddles are folded and latched.

The S-Band antenna for powered flight coverage must be a separate antenna system because the spacecraft antenna is enclosed by the launch adapter. Two design approaches are considered; first, a pick-up and reradiator antenna system mounted in the launch adapter and second, a separate antenna system on the spacecraft.

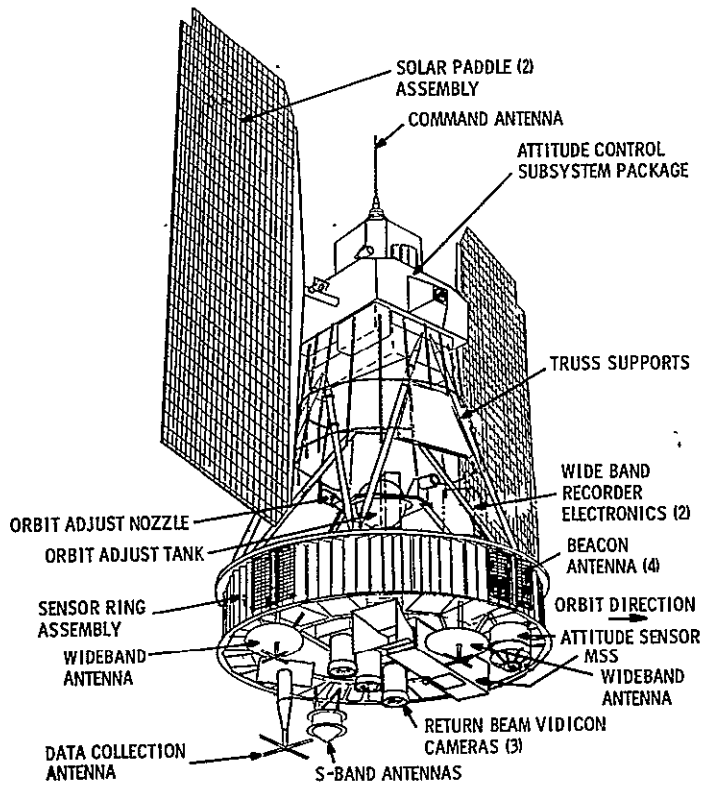

Figure 4.4.4-3. Baseline Antenna System

The pick-up and reradiator approach consists of coupling to the spacecraft antenna by a small antenna mounted in the launch adapter. The small antenna is then coupled through coaxial cables to two monopole antennas mounted diametrically opposite on the outside surface of the adapter. The monopole antennas, during the boost and coast phases, would provide good pattern coverage off the front, rear and both sides of the spacecraft providing one monopole antenna was pointing towards earth. If the roll position of the vehicle places the two monopole antennas in the horizontal plane, the interference pattern of the two antennas will intercept the Earth and provide unrealiable coverage. Thus, the roll orientation of the vehicle would control the placement of the monopole antennas on the adapter. In fact, if there are no roll maneuvers during the expected S-Band tracking of the vehicle, a single monopole could be used, rather than two. A major disadvantage would be the low antenna gain. For example, the monopole gain would be approximately +1 dB above circular-polarized isotropic and the pick-up antenna coupling and cable loss would be 4 to 6 dB; thus, the effective antenna gain would be -3 to -5 dB CPI. If two monopole antennas were used, the gain would be 3 dB less or -6 to -8 dB CPI.

Mounting the monopole or monopoles on the periphery of the spacecraft sensory ring would eliminate the coupling loss to the pick-up antenna. An RF switch could be used to couple the transmitter directly to the monopoles and provide a single monopole gain of approximately +0 dB CPI, 3 dB less for a pair of monopoles.

4.4.4.1 VHF TT&C Antennas

The antenna system requirements for the VHF TT&C links are two fold; first, adequate coverage of the 120 degree conical region during normal flight profiles is required and, second, spherical pattern coverage is required to provode for an emergency or unstabilized flight condition. The problem was solved on the Nimbus vehicles by using two separate antenna systems; one antenna for the command receiver and one antenna system for the tracking beacon and telemetry transmitter.

Although our baseline antenna design shows two separate antenna systems, the feasibility of diplexing the command receiver and telemetry transmitter into one antenna was studied. Two candidate antenna radiators, both flight-proven designs, were considered for diplexing.

Nimbus E antenna radiation pattern studies have indicated that the loop antenna and the monopole antenna would both provide acceptable radiation pattern characteristics when mounted on the bottom of the sensory ring, i.e., near the RBV cameras. Unfortunately, the anticipated bandwidth of the radiators limits their usefulness for the diplexing application. The two frequencies are 138 and 154 MHz, more than 10 percent separation. The Nimbus loop antenna has a bandwidth of approximately 1 percent because of the large amount of capacitive loading that is used to reduce the physical size of the antenna. Thus, it should not be considered for diplexing. The monopole antenna normally has adequate bandwidth to provide an acceptable impedance match at the two frequencies; however, when the antenna is mounted in an environment similar to the bottom area of the sensory ring, strong coupling occurs with the adjacent spacecraft structure. The coupling is manifested by an apparent reduction in the impedance bandwidth of the radiation. The coupling results in two problems; first, the measure impedance of the antenna will be controlled primarily by the adjacent spacecraft

configuration, thus flexibility of configuration modifications is hampered; and second, it is difficult to obtain good diplexer isolation performance with high >2:1 VSWR loads. Therefore, it was felt that diplexing would be a risky solution and was discarded.

The selected VHF beacon and telemetry antenna is the Nimbus flight proven antenna array of four low-profile loaded loop antennas spaced around the periphery of the sensory ring. The antennas elements are fed with a corporate feed harness to provide even power division and proper element-to-element phasing. The radiation pattern has been optimized to provide the greatest percentage of spherical coverage when used with a polarization diversity recieving antenna.

Figures 4.4.4-4 and 4.4.4-5 are power contour graphs of the VIP-Beacon antenna array used on Nimbus D. Although the graphs were taken for 136.5 MHz they are representative of the patterns expected at 137.84 MHz. The graphs show the gain contours referenced to isotropic over the complete sphere in spherical coordinates. Phi (ϕ) is the vehicle azimuth angle where $\phi = 270$ degrees is the direction of flight. Theta (θ) is the vehicle elevation angle where $\theta = 0$ is the -Z axis and $\theta = 180$ degrees is the +Z or earth-pointing axis. The 120 degree conical coverage region extends from $\theta = 120$ to 180 degrees and all ϕ angles. The two graphs show the worst case patterns for the worst position of the solar paddles. $\psi = 90$ degrees is that angle where the plane of the solar paddles is perpendicular to the Z azis. It should be noted that the worst case gain at the elevation angle of 60 degrees ($\theta = 120$ degree) is -13 db when both right-circular and left-circular diversity receiving antennas are considered. In addition, the polarization null areas are essentially filled-in by power of the other polarization. The antenna gain in the upper hemisphere is quite poor; however, margin calculations indicate that -13 dB of gain is needed for the minimum gain ground antenna and maximum slant range. Considering other ground antenna options suggests that the spacecraft antenna gain can go to -19 dB at maximum slant range for satisfactory communications.

The selected command antenna is the Nimbus flight-proven monopole radiator with an upper and lower ground plane assembly. The ground planes are used to tilt the linearly-polarized radiation pattern in the +Z direction or to provide better 120 degree conical coverage. The expected worst case antenna power contour graph is shown in Figure 4.4.4-6. The plane of the solar paddles is parallel to the Z axis for the worst case. The two null areas appearing at $\theta = 120$ degrees, $\phi = 240$ degrees are not present for other solar paddle positions. The minimum gain at $\theta = 120$ degrees is -20 dB from R.C. isotropic; this level will provide satisfactory communications with the minimum gain ground transmitting system. Additional gain of +27 dB is available at the ground sites. The typical gain at 120 degrees will be approximately -9 dB and this level will provide a comfortable margin.

A more useful technique for expressing the gain of a spherical coverage antenna is to compute the percentage pattern coverage for a particular gain value. Through integration of the gain contours over the 120 degree conical sector of the sphere, the percentage of the spherical surface area where the antenna gain exceeds or is less than a known value can be computed. This integration was performed for the Nimbus D command antenna and is plotted in Figure 4.4.4-7. The three curves show the effect of various solar paddles positions and also that the worst case paddle position for this analysis is $\theta = 90$ degrees rather than 0 degrees.

1. ANTENNA MODEL NO. VIP – BEACON	4. NUMBER OF ELEMENTS IN ARRAY: 4	7 PATTERN MEASUREMENT FREQUENCY 136 5 MHz
2 PSL RANGE REQUEST NO'	5. VEHICLE MOCKUP' NIMBUS – D	8' POLARIZATION COMPONENT RECORDED. RIGHT CIRCULAR
3 PSL PATTERN NO'S FROM TO	6. MODEL SCALE FULL	9 ARRAY PHASING STANDARD NIMBUS– BEACON
10. GAIN REFERENCE ISOTROPIC – RIGHT CIRCULAR		
11. REMARKS ψ=90° UNLESS OTHERWISE MARKED' ALL NO'S ARE MINUS.		

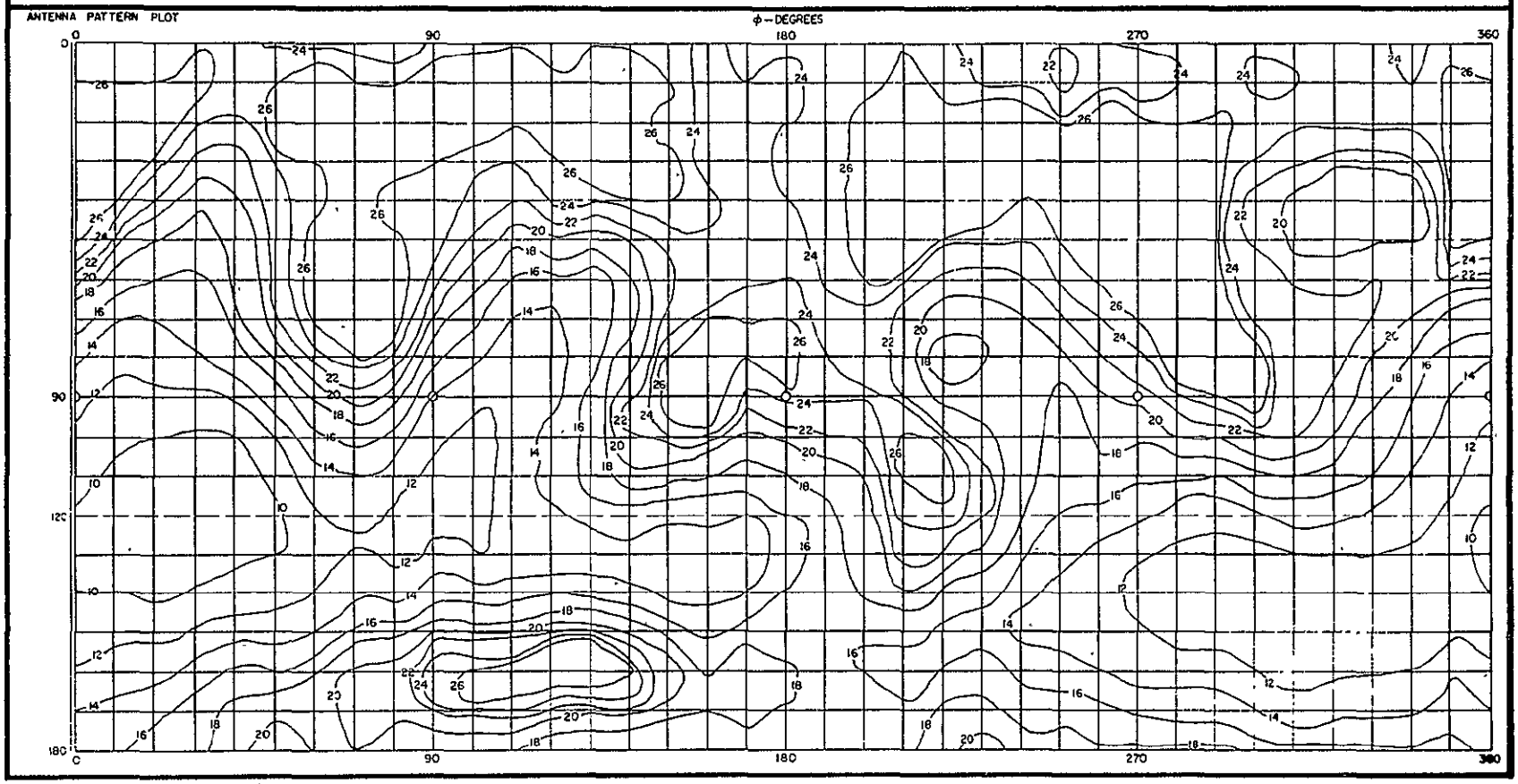

Figure 4.4.4-4. Power Contour Graph - VIP Beacon Antenna Right Circular Polarization - ψ = 90 Degrees

1 ANTENNA MODEL NO. VIP—BEACON	4. NUMBER OF ELEMENTS IN ARRAY: 4	7 PATTERN MEASUREMENT FREQUENCY 136.5 MHz
2 PSL RANGE REQUEST NO:	5 VEHICLE MOCKUP: NIMBUS—D	8 POLARIZATION COMPONENT RECORDED LEFT CIRCULAR
3 PSL PATTERN NO'S FROM TO	6. MODEL SCALE FULL	9. ARRAY PHASING. STANDARD NIMBUS - BEACON
10 GAIN REFERENCE. ISOTROPIC— L.C. POLARIZATION		
11 REMARKS $\psi = 90°$ UNLESS OTHERWISE MARKED: ALL NO'S ARE MINUS		

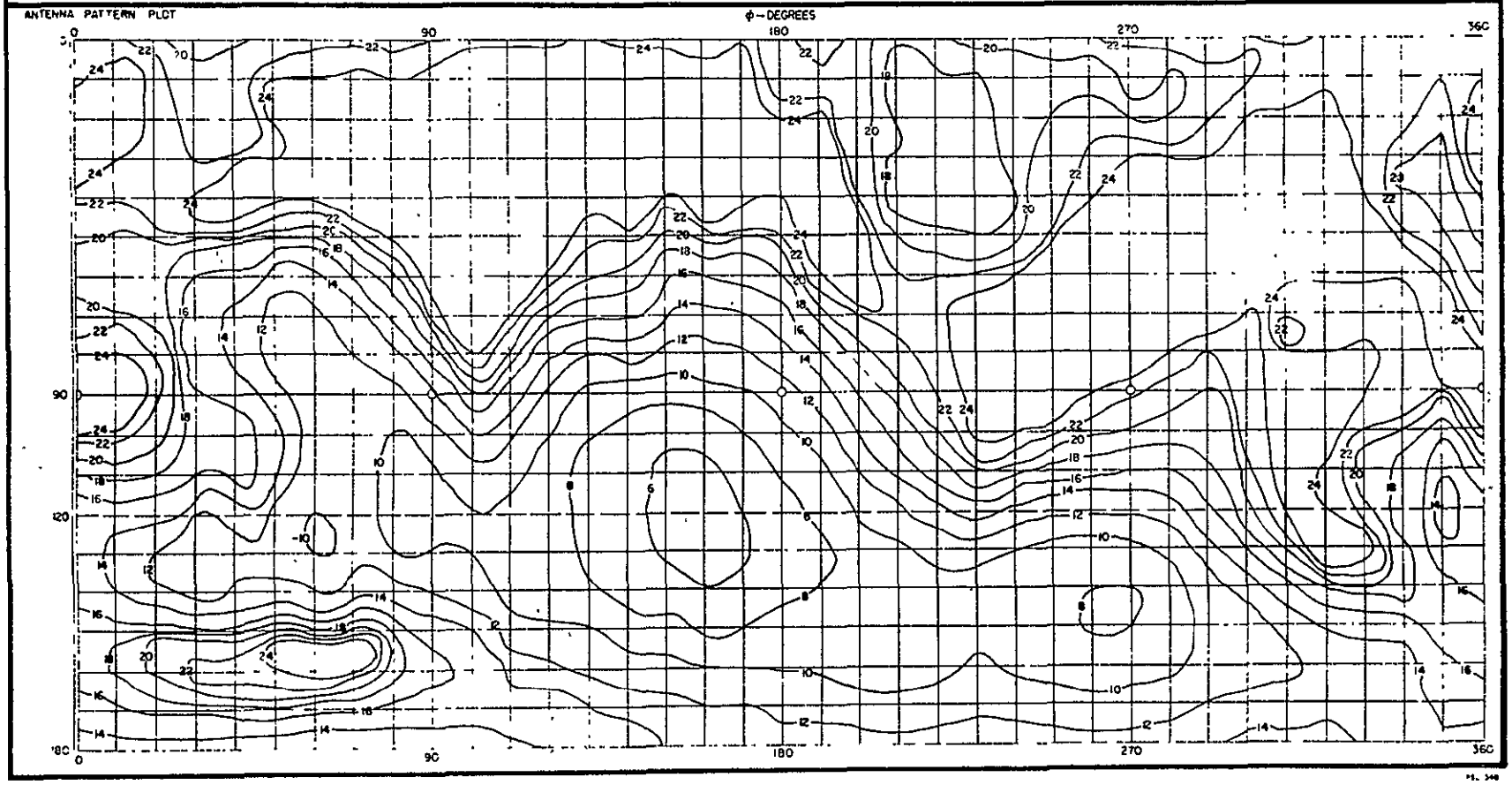

Figure 4.4.4.-5. Power Contour Graph - Left Circular Polarization - ψ = 90 Degrees

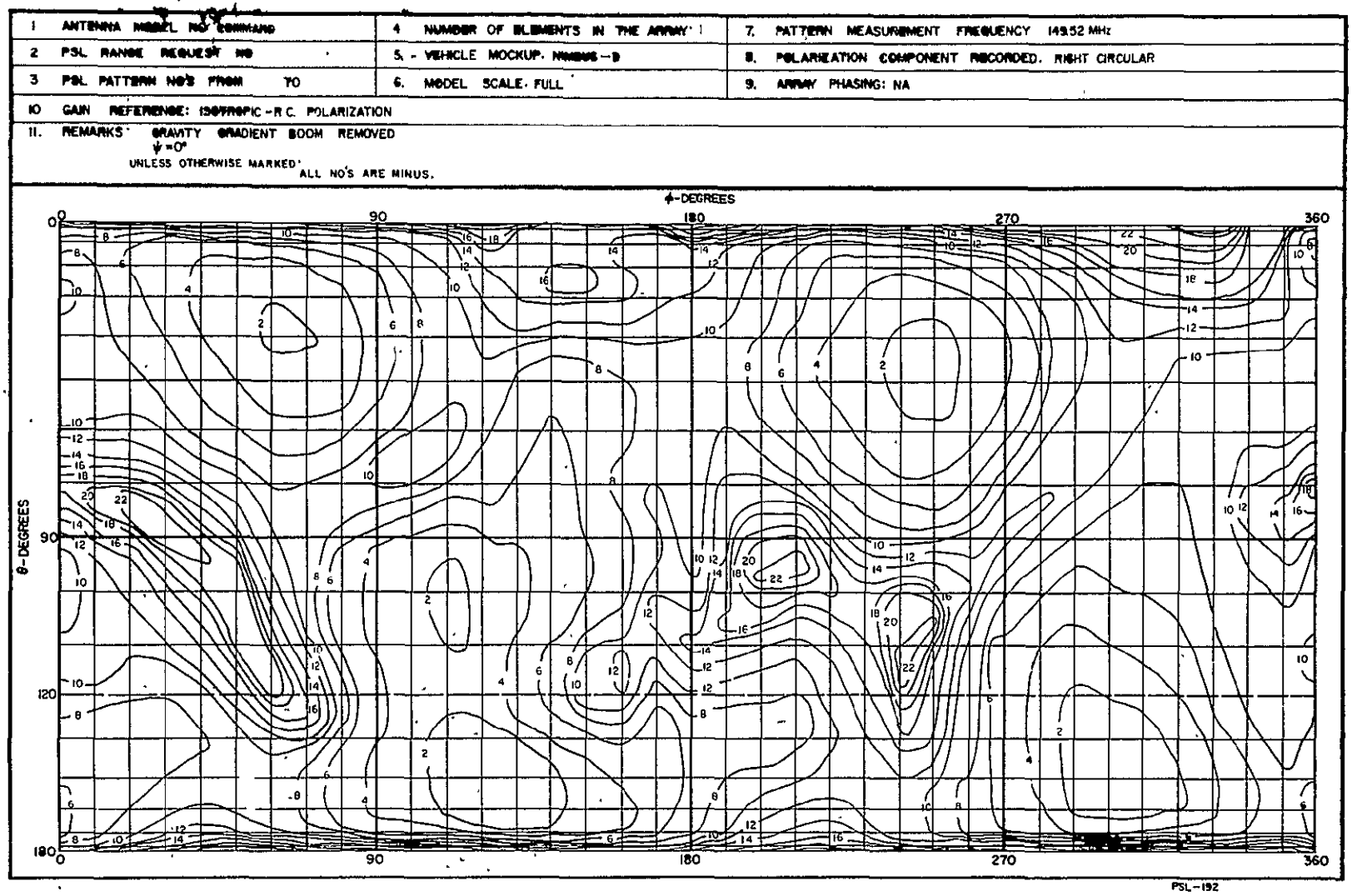

Figure 4.4.4-6. Power Contour Graph - Command Antenna - Right Circular Polarization $\psi = 0$ Degree

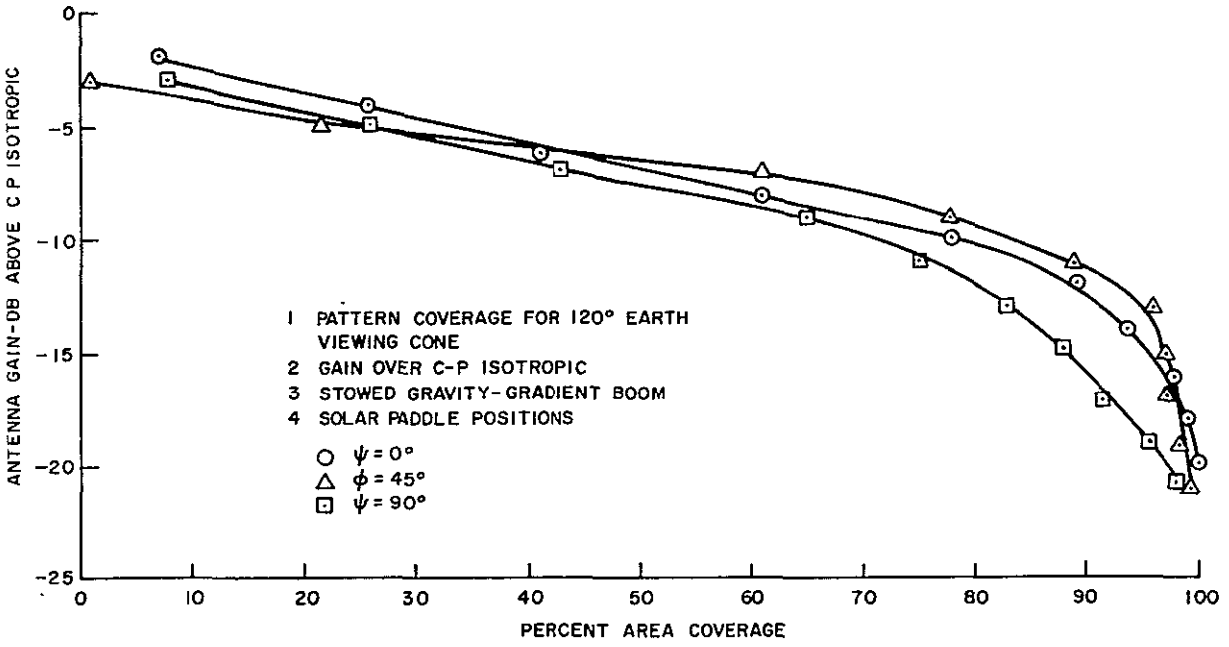

Figure 4.4.4-7. Nimbus D Command Antenna

The baseline VHF antennas, as described in the preceding paragraphs, represent flight-proven designs which have been subjected to extensive test and evaluation on the Nimbus programs.

The ERTS spacecraft, from the VHF antenna point of view, will be another Nimbus vehicle. Although frequency assignments are slightly different from the two antennas, the basic antenna performance parameters as discussed in the preceding paragraphs will apply to the ERTS spacecraft. The freqeuncy assignments are:

	Nimbus	ERTS	% Change
Command	149.52	154.20	+3.1
Beacon	136.50	137.86	+1.0

The impact of the minor frequency change on the design of the antennas is that the only antenna performance parameters which need be measured and evaluated are the input VSWR's on the spacecraft.

4.4.4.2 USB Antenna

The antenna requirements for the Unified S-Band link are to provide a right-circular polarized antenna with an azimuthally symmetric radiation pattern and which exhibits a gain of 0 dB or

greater at an elevation angle of 60 degrees. The Nimbus program has been using a broadband, cavity-backed conical- spiral antenna for their 1700 MHz links. The antenna performance has been measured at 1800 and 2250 MHz for the Nimbus E program. The indicated performance at 2250 MHz has shown that the antenna will provide an acceptable circularly-polarized radiation pattern with a gain of approximately -1 dB at the 60 degree elevation angle and +4 dB on beam peak. The radiation pattern is cardioid shaped and symmetrical about the Z axis.

The Nimbus antenna is shown as the baseline design primarily because of its flight-proven performance. It is recognized that the wideband antenna design should provide better radiation pattern characteristics on the horizon that a conical spiral antenna. An assessment of the wideband antenna will, therefore, be made early in the program.

4.4.4.3 DCS Antenna

The basic requirements of the DCS antenna are to provide for a circularly-polarized receiving antenna at 401.2 MHz and coverage of the 120 degree conical area. These requirements are almost identical to those imposed on the IRLS antenna on the Nimbus vehicle. The IRLS system transmits at 401.5 MHz and receives at 466.0 MHz with right-circular polarization. New Mexico State University performed an extensive feasibility study and development program for the IRLS antenna. With this background in mind, it is obvious that the baseline DCS antenna should be the flight-proven Nimbus IRLS antenna.

The antenna radiator is crossed-dipoles (turnstile) mounted approximately a quarter wavelength above a ground plane. The radiation pattern is a single lobe pattern which is symmetrical about the Z axis and has a gain of +6 dB on beampeak and 0 dB at ± 60 degree elevation angle. The radiation pattern will have some gain ripple in the area of the 60 degree elevation angle because of blockage and reradiation from the spacecraft structure and sensor packages. This ripple is not expected to be serious, $\approx$ 2 to 3 dB, and will be evaluated by radiation pattern tests.

4.4.4.4 Launch Adapter Reradiating System

The requirement for providing a luanch-pad RF link checkout capability for the spacecraft implies that some method of coupling to the spacecraft antennas be investigated. It was previously indicated that the VHF TT&C antennas will radiate through the shroud and would not require auxiliary coupling antennas.

Two methods of coupling are appropriate for this application. One method is to cut a slot in the adapter skin and thus provide a controlled coupling aperture for the adapter cavity; and the second method is to use small pick-up antennas near the spacecraft antennas and then provide external reradiator antennas on the outside of the adapter. Both coupling methods have been used on previous vehicles. The separate pick-up and reradiator antennas have been the more successful of the two approaches. Therefore, the pick-up and reradiator design has been selected as the baseline design.

Figure 4.4.4-8 shows the typical pick-up and reradiator antenna configuration. The pick-up antenna is a low profile loop antenna and typically provides 5 to 10 dB of coupling to the spacecraft antenna. The reradiator antenna is another low-profile loop and is connected to the pick-up coaxial cable. The typical radiation pattern for the reradiator antenna is shown in Figure 4.4.4-8 for both parallel polarization (E_p) and normal polarization (E_N). The reradiator antennas would be located on the adapter periphery such that the main-lobe of the E_p pattern points towards the ground station antenna.

There is a possible problem associated with energizing the transmitter in the launch configuration. The input VSWR of the USB and wideband antennas may be quite high because of the strong coupling to the adapter internal structure. This possible problem will be assessed during the design and test phase of the adapter reradiator system.

4.4.5 C&DH SUBSYSTEM RELIABILITY

The C&DH subsystem is quite large and complex. As the subsequent discussion will show, a great deal of redundancy is utilized to minimize the probability of degraded performance or failure. The success of redundancy in the design is shown by the achievement of the very high subsystem reliability of .9453 for successful performance for a one year mission.

It should be emphasized that this reliability is the probability of achieving all mission requirements. In addition, one degraded mode has been considered; it is discussed following the discussion of subsystm reliability.

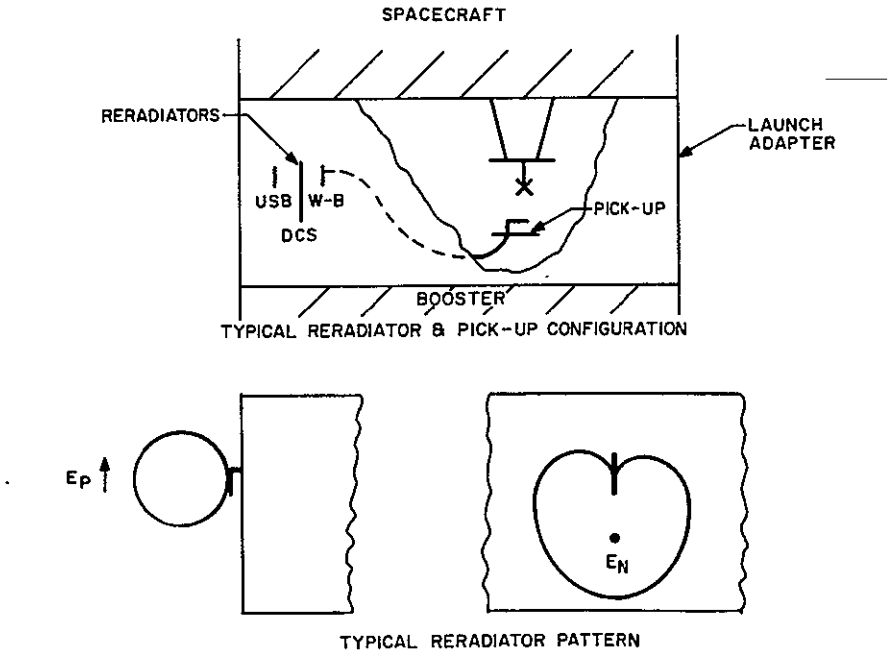

Figure 4.4.4-8. Typical Pick-Up and Reradiator Antenna Configuration

The components of the C&DH subsystem are shown in Table 4.4.5-1. In this table the VIP appears as a single component; it is broken down in Table 4.4.5-2.

TABLE 4.4.5-1. COMPONENTS OF C&DH SUBSYSTEM

Symbol	Component	Failure Rate or 1 Yr Rel. R	Source, Comments
A	VIP	R = .965006	Radiation Inc.
B	VHF Transmitter	1.0164	ORI 469, p. 202, reduced by one order of magnitude
C	PM Transponder	3.25	Colling Radio
D	Summing Networks	.0823 each	ORI 469, p. 201, reduced by one order of magnitude Compare ORI 541, p. 87
E	VCO (5)	.1784 each	ORI 469, p. 186, reduced by one order of magnitude
F	Buffer	.0823	Assumed equivalent to 1 summing network
G	S Band Receiver	1.6048	ORI 469, P.113, assumed equivalent to VHF Rcvr
H	Demodulator	3.8295	ORI 469, p. 113
I	VHF Receiver	1.6048	ORI 469, P, 113
J	Integrator	1.5	Estimated
K	Power Supply Unit	5.834	Rates supplied by vendor. Conservatively based on Mil-Hdbk-217A. Reduced by one order of magnitude for ERTS.
L	Comdec	3.6475	
M	Matrix Driver and Decoder	3.341	
N	Comstor Logic	1.457	
O	Comstor Memory	3.177	
P	OSC	1.069	
Q	Freq. Generator	2.795	
R	TC Generator	2.49	
S	Filter	.005	ITT
T	Modulator	.8452	Piece part analysis

TABLE 4.4.5-1. COMPONENTS OF C&DH SUBSYSTEM (Continued).

Symbol	Component	Failure Rate or 1 Yr Rel. R	Source, Comments
U	Power Amplifier	.5291	HAC
V	Antenna	.03	Estimated
W	Switch	.02	MIL-HDBK-217A

The Versatile Information Processor is built by Radiation Incorporated. Its components are shown in Table 4.4.5-2.

TABLE 4.4.5-2. COMPONENTS OF THE VIP

Symbol		One Year Reliability For Single Component
A	Memory	.5978
B	Memory Sequencer	.9660
C	11 Stage Counter	.9969
D	Multiplexer	.9887
E	Redundant Multiplexer Circuits	.9508
F	Coder	.9737
G	Formatter Logic	.9342
H	Reprogrammer	.9180
I	Transmitter	.9825
J	Isolator	.9903
K	Switching Circuit	.9999

The reliability block diagram of the VIP is shown in Figure 4.4.5-1.

The mathematical model for the reliability of the VIP is based on the assumption that all components are powered throughout the mission. The formula for the reliability of the

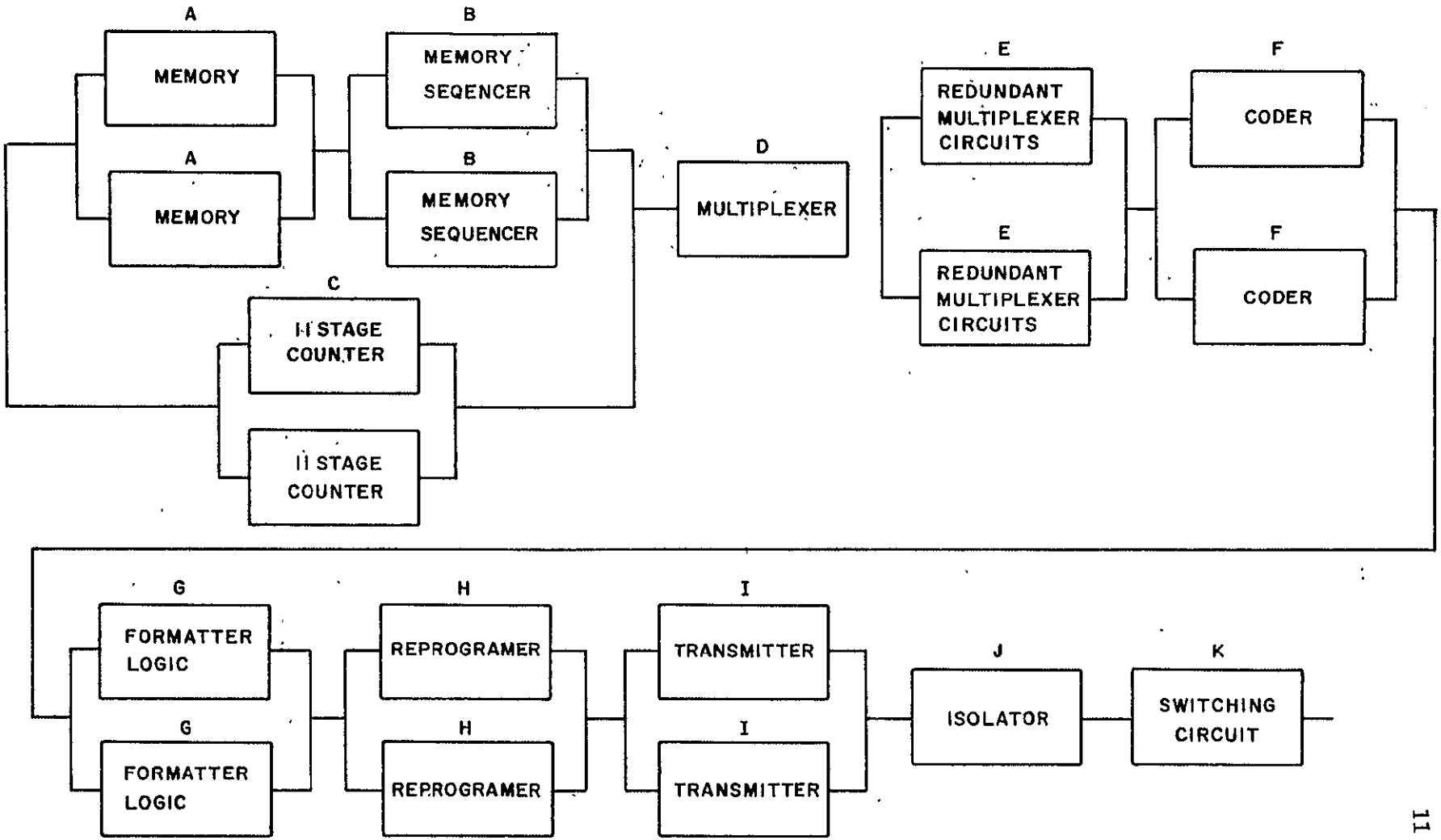

Figure 4.4.5-1. Reliability Block Diagram for VIP

VIP (letting R_X denote the one year reliability of component X, where the symbol is given in Table 4.4.5-2 is:

$$R_{VIP} = \left[\left(1 - 2R_A - R_A^2\right)\left(2R_B - R_B^2\right)\right]\left[1 - \left(2R_C - R_C^2\right)\right]$$

$$XR_D\left(2R_E - R_E^2\right)\left(2R_F - R_F^2\right)\left(2R_G - R_G^2\right)$$

$$X\left(2R_H - R_H^2\right)\left(2R_I - R_I^2\right)R_J R_K$$

The reliability block diagram for the entire C&DH subsystem is given in Figure 4.4.5-2.

The mathematical formula for the overall reliability of the C&DH subsystem uses the symbols for components given in Table 4.4.5-1 and Figure 4.4.5-2. For convenience of notation, let:

$R_X = e^{-\lambda_X T}$ = reliability of component X rate λ_X for time

$\Phi(\lambda) = 2e^{-\lambda T} - e^{-2\lambda T}$ = reliability of parallel redundant components with failure rate λ

$(\lambda) = e^{-\lambda T} + 10e^{-.02 \times 10^{-6} \times T}\left(e^{-\lambda T} - e^{-1.1\lambda T}\right)$ = reliability of primary plus standby paths with failure rate λ, where paths are identical.

The reliabilities of components S, T, V, and W are computed assuming a "powered" time of 1/2 year.

The subsytem reliability R is given by the following formula:

$$R = \left[1 - \left(1 - \Theta\left(\lambda_G + \lambda_H\right)\right)\left(1 - \Theta\left(\lambda_I + \lambda_H\right)\right)\right]\Phi\left(\lambda_J\right)$$

$$X\ \Theta\left(\lambda_K + \lambda_L\right)\Theta\left(\lambda_M\right)\Theta\left(\lambda_P\right)\left(\lambda_Q\right)\Theta\left(\lambda_R\right)\Phi\left(\lambda_N\right)$$

$$X\ \Phi\left(\lambda_O\right)\Theta\left(\lambda_B\right)\Theta\left(\lambda_C\right)\Theta\left(2\lambda_D + 5\lambda_E\right)\Theta\left(\lambda_F\right)$$

$$X\ R_A R_T^2 R_U^2 R_V^2 R_W\left(2R_S^2 R_W^2 - R_S^4 R_W^4\right)$$

R = .94534

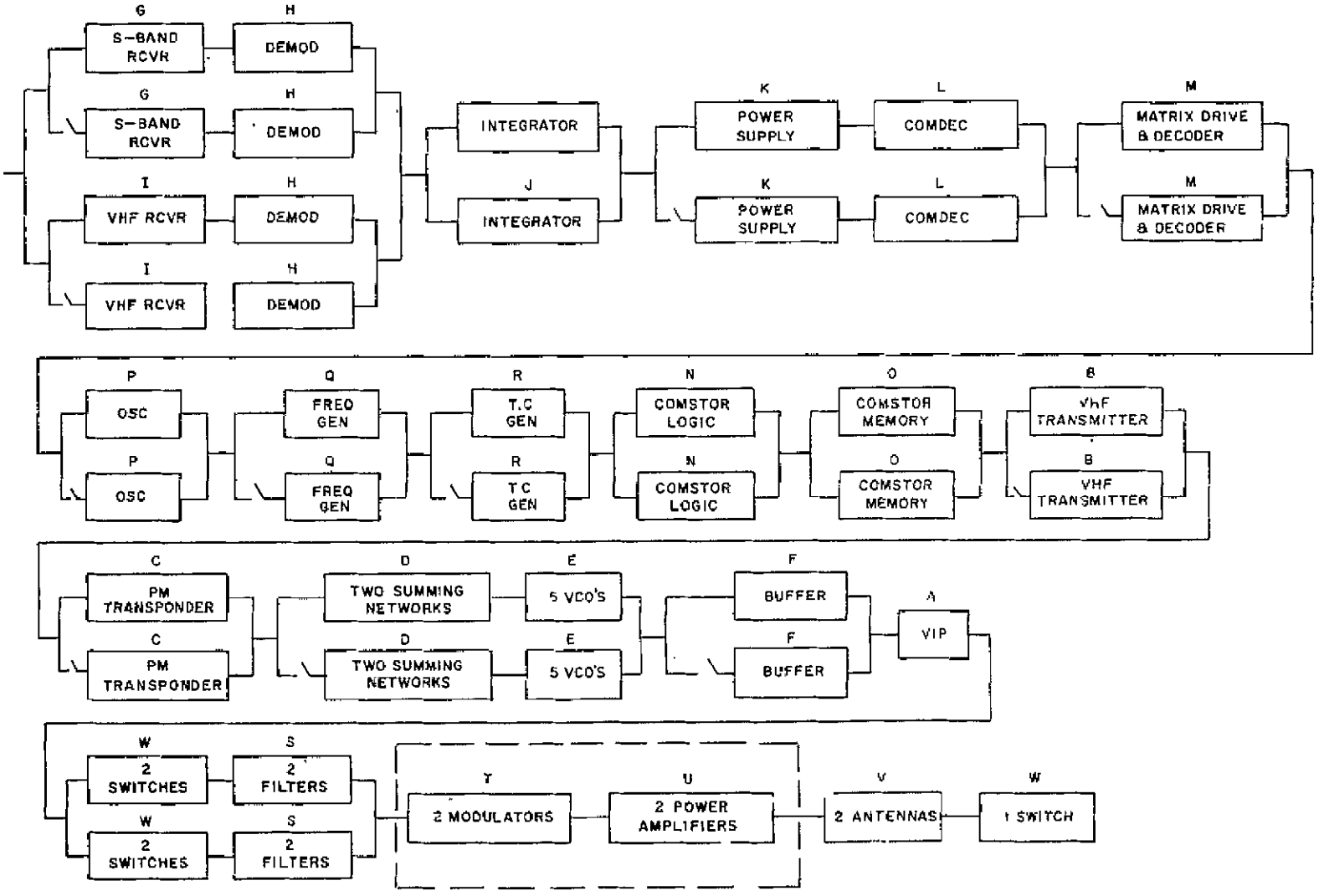

Figure 4.4.5-2. C&DH Subsystem Reliability Block Diagram

A deraded mode of operation was identified for the wideband transmitter. In normal operation, both PCM data and video data may be transmitted simultaneously. In the degraded mode, either may be transmitted upon command, but not both. The probability of operating at least in this degraded mode is .95840. This probability includes the probability of complete success (.9453) plus the probability of degraded operation only. This degraded mode of operation (shown in Figure 4.4.5-3) replaces the configuration (T and V) in Figure 4.4.5-2 with operating times adjusted to meet the requirements of degraded operation.

4.4.6 USE OF CROSS-STRAPPING IN NARROWBAND TELEMETRY DESIGN

The use of block redundancy has been considered essential to meet the ERTS reliability requirements. However, the decision whether to use cross-strapping between redundant components must be made. For the VHF downlink, cross-strapping can be achieved without significant additional complexity; hence, it is employed by using the PCM Telemetry Processor output and the narrowband tape recorder output to drive both VHF transmitters. For the USB downlink, however, complete cross-strapping requires considerable additional complexity. Moreover, the probability of succes for the premodulation processor (PMP) and USB Equipment (USBE) is increased only from 0.99946 without cross-strapping to 0.99950 with complete cross-strapping. Therefore, complete cross-strapping is not employed in the PMP or USBE. However, cross-strapping between the two redundant PMP outputs and the two USBE transmitter inputs can be achieved with the addition of a very reliable switch (failure rate approximately 0.02×10^{-6} per hour). This design increases the overall probability of success for the combined PMP and USBE functions.

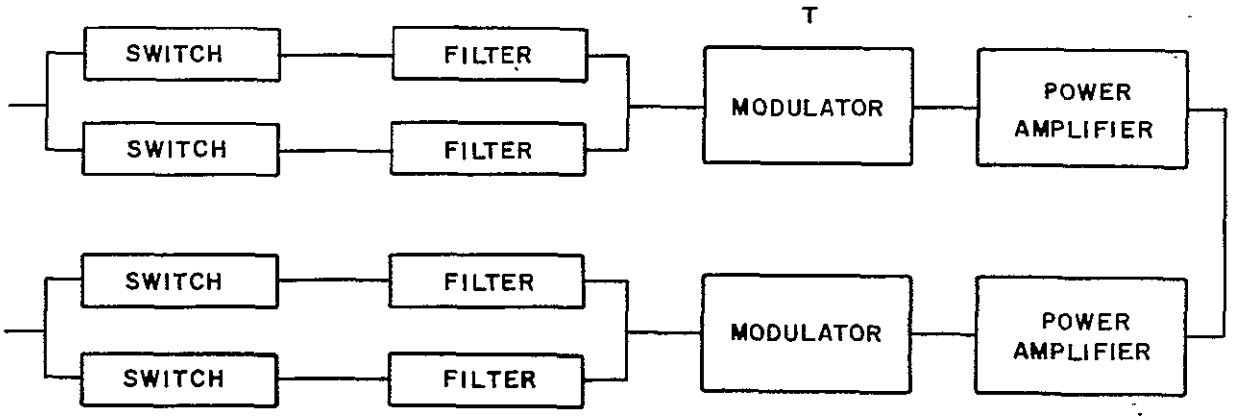

Figure 4.4.5-3. Degraded Mode

APPENDIX 4.A

ERTS COMMAND AND TELEMETRY LISTS

Telemetry and Command lists have been identified as a result of the ERTS system study (see Tables 4.A-2 through 4.A-18 and Tables 4.A-20 through 4.A-27). The command functions will be verified through telemetry as a means of validating ground commanding. Three categories of commands are identified:

1. Change of State (COS). This is defined as either an ON or an OFF for a specific function, i.e., PMP ON or PMP OFF.

2. Momentary (M). Momentary relay contact closure for the duration of the relay pulse lines, MA and MB.

3. Irreversible (I). Single command which would be executed only once, i.e., pyro firing.

The telemetry list for the ERTS spacecraft identifies the measurement name, type of signal to be monitored, and sample rate. The telemetry subsystem will convert each analog measurement to a ten-bit word. There are two digital type measurements; the one is one-bit word which indicates either sensor ON or sensor OFF; the Digital "A" is a serial read-out to the telemetry processor of 10 bits.

A summary precedes each command and telemetry list (see Tables 4.A-1 and 4.A-19).

Table 4.A-1. Command List Summary ERTS A&B

Subsystem	COS	I	M	Total
Orbit Adjust	9	4		13
Payload	105		13	118
Data Collection	2			2
Power	42		2	44
Command and Data Handling	156	1	3	160
Attitude Control	72		1	73
Totals	386	5	19	410

Command Type

COS - Change of state
I - Irreversible
M - Momentary

Table 4.A-2. Command List for Orbit Adjust Subsystem

Name	Type of Command	Location of Command Relay
Solenoid Valves Enable	COS	PSM
Actuate Solenoid Valve No. 1	COS	PSM
Actuate Solenoid Valve No. 2	COS	PSM
Solenoid Valves Reset	COS	PSM
Solenoid Valves Disable	COS	PSM
Arm Pyro Buss, Pri	COS	PSM
Arm Pyro Buss, Red	COS	PSM
Safe Pyro Buss, Pri	COS	PSM
Safe Pyro Buss, Red	COS	PSM
Fire Normally Open Valve, Pri	I	OA
Fire Normally Open Valve, Red	I	OA
Fire Normally Closed Valve, Pri	I	OA
Fire Normally Closed Valve, Red	I	OA

Table 4.A-3. Command List for Payload (RBV Camera)

Name	Type of Command	Location of Command Relay
Start Prepare	COS	(CC) Camera Controller
Camera 1, ON	COS	CC
Camera 2, ON	COS	CC
Camera 3, ON	COS	CC
Camera 1, OFF	COS	CC
Camera 2, OFF	COS	CC
Camera 3, OFF	COS	CC
Anode Mode	COS	CC
Target Mode	COS	CC
Beam IN	COS	CC
Beam OUT	COS	CC
Expose AUTO	COS	CC
Preset 8 MSEC	COS	CC
Preset 12 MSEC	COS	CC
Preset 16 MSEC	COS	CC
Single Cycle	COS	CC
Continuous (Normal) Cycle	COS	CC
Record Mode	COS	CC
Direct/Record Mode	COS	CC
Clock A (Spacecraft)	TBD	
Clock B (Spare)	TBD	
Calib. 1	COS	CC
Calib. 2	COS	CC
Calib. 3	COS	CC
Peaking IN	COS	CC
Normal	COS	CC
TBD		

Table 4.A-3. Command List for Payload (RBV Camera) (Cont'd)

Name	Type of Command	Location of Command Relay
TBD		
TBD		
TBD		
TBD		
RBV Power A, ON	COS	PSM
RBV Power A, OFF	COS	PSM
RBV Power B, ON	COS	PSM
RBV Power B, OFF	COS	PSM

Name	Type of Command	Location of Command Relay

Table 4. A-4. Command List for Payload (Multispectral Scanner)

Name	Type of Command	Location of Command Relay
Spectral Band 1, ON	COS	OPS PACKAGE
Spectral Band 2, ON	COS	OPS PACKAGE
Spectral Band 3, ON	COS	OPS PACKAGE
Spectral Band 4, ON	COS	OPS PACKAGE
Spectral Band 5, ON	COS	OPS PACKAGE
Spectral Band 1, OFF	COS	OPS PACKAGE
Spectral Band 2, OFF	COS	OPS PACKAGE
Spectral Band 3, OFF	COS	OPS PACKAGE
Spectral Band 4, OFF	COS	OPS PACKAGE
Spectral Band 5, ON	COS	OPS PACKAGE
Step Gain, Band 1, UP	COS	OPS PACKAGE
Step Gain, Band 2, UP	COS	OPS PACKAGE
Step Gain, Band 3, UP	COS	OPS PACKAGE
Step Gain, Band 4, UP	COS	OPS PACKAGE
Step Gain, Band 1, DOWN	COS	OPS PACKAGE
Step Gain, Band 2, DOWN	COS	OPS PACKAGE
Step Gain, Band 3, DOWN	COS	OPS PACKAGE
Step Gain, Band 4, DOWN	COS	OPS PACKAGE
Scan Mirror Drive, ON	COS	OPS PACKAGE
Scan Mirror Drive, OFF	COS	OPS PACKAGE
Step Band 5, Focus, ON	COS	OPS PACKAGE
Step Band 5, Focus, OFF	COS	OPS PACKAGE
Step Band 5, Focus, FORWARD	COS	OPS PACKAGE
Step Band 5, Focus REVERSE	COS	OPS PACKAGE
Mirror Pick-off, ON	COS	OPS PACKAGE
Mirror Pick-off, OFF	COS	OPS PACKAGE
Rotating Shutter Drive, ON	COS	OPS PACKAGE

Table 4.A-4. Command List for Payload (Multispectral Scanner) (Cont'd)

Name	Type of Command	Location of Command Relay
Rotating Shutter Drive, OFF	COS	OPS PACKAGE
Calib. Lamp No. 1, ON	COS	OPS PACKAGE
Calib. Lamp No. 2, ON	COS	OPS PACKAGE
Select Calib. Sequence No. 1	COS	OPS PACKAGE
Select Calib. Sequence No. 2	COS	OPS PACKAGE
Band 1 HV Supply A	COS	OPS PACKAGE
Band 1 HV Supply B	COS	OPS PACKAGE
Band 2 HV Supply A	COS	OPS PACKAGE
Band 2 HV Supply B	COS	OPS PACKAGE
Band 3 HV Supply A	COS	OPS PACKAGE
Band 3 HV Supply B	COS	OPS PACKAGE
Main Inverter A, ON	COS	OPS PACKAGE
Main Inverter A, OFF	COS	OPS PACKAGE
Main Inverter B, ON	COS	OPS PACKAGE
Main Inverter B, OFF	COS	OPS PACKAGE
MSS Power A, ON	COS	PSM
MSS Power A, OFF	COS	PSM
MSS Power B, ON	COS	PSM
MSS Power B, OFF	COS	PSM
Multiplexer, ON	COS	OPS
Multiplexer, OFF	COS	OPS
Execute Cmd Sequence 1	M	OPS
Execute Cmd Sequence 2	M	OPS
Execute Cmd Sequence 3	M	OPS
Execute Cmd Sequence 4	M	OPS
Execute Cmd Sequence 5	M	OPS

Table 4.A-4. Command List for Payload (Multispectral Scanner) (Cont'd)

Name	Type of Command	Location of Command Relay
Spare	COS	
Spare	COS	
Spare	COS	
Spare	COS	
Uncage Scanning Mech, PRIMARY	M	PSM
Uncage Scanning Mech, REDUNDANT	M	PSM
Uncage Rad Cooler, PRIMARY	M	PSM
Uncage Rad Cooler, REDUNDANT	M	PSM
Uncap Rad Cooler, PRIMARY	M	PSM
Uncap Rad Cooler, REDUNDANT	M	PSM
Uncap Scanner Optics, PRIMARY	M	PSM
Uncap Scanner Optics, REDUNDANT	M	PSM

Table 4.A-5. Command List for Wideband Video Tape Recorder

Name	Type of Command	Location of Command Relay
Standby VTR No. 1	COS	Recorder Control Box (RCB)
Record VTR No. 1	COS	RCB
Rewind VTR No. 1	COS	RCB
Playback VTR No. 1	COS	RCB
Fast Forward VTR No. 1	COS	RCB
VTR No. 1 OFF	COS	RCB
Record Current Adjust Command No. 1	COS	RCB
RBV Mode VTR No. 1	COS	RCB
MSS Mode VRR No. 1	COS	RCB
Standby - VTR No. 2	COS	RCB
Record VTR No. 2	COS	RCB
Rewind VTR No. 2	COS	RCB
Playback VTR No. 2	COS	RCB
Fast Forward VTR No. 2	COS	RCB
VTR No. 2 OFF	COS	RCB
RBV Mode VTR No. 2	COS	RCB
MSS Mode VTR No. 2	COS	RCB

Table 4.A-6. Command List for Data Collection (Cont'd)

Name	Type of Command	Location of Command Relay
DCS Power ON	COS	PSM
DCS Power OFF	COS	PSM

Name	Type of Command	Location of Command Relay

Table 4.A-7. Command List for Power Subsystem

Name	Type of Command	Location of Command Relay
		Battery Module
Battery No. 1 OFF	COS	No. 1
Battery No. 2 OFF	COS	No. 2
Battery No. 3 OFF	COS	No. 3
Battery No. 4 OFF	COS	No. 4
Battery No. 5 OFF	COS	No. 5
Battery No. 6 OFF	COS	No. 6
Battery No. 7 OFF	COS	No. 7
Battery No. 8 OFF	COS	No. 8
All Batteries ON	COS	Nos. 1 to 8
Trickle Charge NORMAL	COS	Power Control Module
Trickle Charge NORMAL	COS	Power Control Module
Switch PWM Regulator	COS	Power Control Module

Name	Type of Command	Location of Command Relay
Auxiliary Load No. 1 ON	COS	"Aux Load Contr (ALC)"
Auxiliary Load No. 2 ON	COS	ALC
Auxiliary Load No. 3 ON	COS	ALC
Auxiliary Load No. 4 ON	COS	ALC
Auxiliary Load No. 5 ON	COS	ALC
All Auxiliary Loads OFF 'A'	COS	ALC
All Auxiliary Loads OFF 'B'	COS	ALC
Shunt Load A OFF	COS	ALC
Shunt Load B OFF	COS	ALC
Shunt Loads C OFF	COS	ALC
Shunt Loads D OFF	COS	ALC

Table 4.A-7. Command List for Power Subsystem (Cont'd)

Name	Type of Command	Location of Command Relay
All Shunt Loads ON	COS	ALC
Comp Load No. 1 ON	COS	ALC
Comp Load No. 2 ON	COS	ALC
Comp Load No. 3 ON	COS	ALC
Comp Load No. 4 ON	COS	ALC
Comp Load No. 5 ON	COS	ALC
Comp Load No. 6 ON	COS	ALC
All Comp Loads OFF	COS	ALC
Verify TICK	M	
Verify TOCK	M	
Comp Load No. 8 ON	COS	PSM
Comp Load No. 8 OFF	COS	PSM
Comp Load No. 7 ON	COS	PSM
Comp Load No. 7 OFF	COS	PSM
Payload Reg Mod., ON	COS	PSM
Payload Reg Mod., OFF	COS	PSM
MSS Power A and RBV Power A BUSS ON	COS	PSM
MSS Power A and RBV Power A BUSS OFF	COS	PSM
MSS Power B and RBV Power B BUSS ON	COS	PSM
MSS Power B and RBV Power B BUSS OFF	COS	PSM
Switch PWM Regulator	COS	Payload Regulator Module

Table 4.A-8. Command List for C&DH Subsystem (Command/Clock)

Name	Type of Command	Location of Command Relay
Primary Comstor ON and Fill	COS	CMD/CLOCK
Primary Comstor VERIFY	COS	
Primary Comstor COPY	COS	
Primary Comstor OFF	COS	
Primary Comstor ACTIVE	COS	
Data Serial Transfer ON	COS	
Command Execution Counter RESET	M	
Select Primary Matrix Decoder	COS	
Select Primary Matrix A Drivers	COS	
Select Primary Matrix B Drivers	COS	CMD/CLOCK

Name	Type of Command	Location of Command Relay
Select Primary Oscillator	COS	CMD/CLOCK
Select Primary Frequency Generator	COS	
Load Time Code	M	
Redundant Comstor ON and Fill	COS	
Redundant Comstor Verify	COS	
Redundant Comstor Copy	COS	
Redundant Comstor OFF	COS	
Redundant Comstor Active	COS	
Select Redundant Matrix	COS	
Select Redundant Matrix A Drivers	COS	CMD/CLOCK

Table 4. A-8. Command List for C&DH Subsystem (Command/Clock) (Cont'd)

Name	Type of Command	Location of Command Relay
Select Redundant Matrix B Drivers	COS	CMD/CLOCK
Select Redundant Oscillator	COS	CMD/CLOCK
Select Redundant Frequency Generator	COS	CMD/CLOCK
Select Clock Primary Fuse	COS	ALC
Select Clock Backup Fuse	COS	ALC
Clock Data to Beacon ON	COS	PSM
Clock Data to Beacon OFF	COS	PSM
Comm. Enable (Separation Switch Bypass)	I	ALC

Name	Type of Command	Location of Command Relay

Table 4.A-9. Command List for Command Integrator Unit (CIU)

Name	Type of Command	Location of Command Relay
CIU A, ON	COS	PSM
CIU A, OFF	COS	PSM
CIU B, ON	COS	PSM
CIU B, OFF	COS	PSM

Name	Type of Command	Location of Command Relay

Table 4.A-10. Command List for C&DH Subsystem (VHF Receiver)

Name	Type of Command	Location of Command Relay
Receiver A, ON	COS	RCVR
Receiver A, OFF	COS	RCVR
Receiver B, ON	COS	RCVR
Receiver B, OFF	COS	RCVR

Name	Type of Command	Location of Command Relay

Name	Type of Command	Location of Command Relay
Transmitter A POWER ON	COS	VHF XMTR
Transmitter A POWER OFF	COS	VHF XMTR
Transmitter B POWER ON	COS	VHF XMTR
Transmitter B POWER OFF	COS	VHF XMTR
Transmitter A OUTPUT	COS	VHF XMTR
Transmitter B OUTPUT	COS	VHF XMTR
Normal TLM Mode	COS	VHF XMTR
Back-up Playback Mode	COS	VHF XMTR
0.3 W OUTPUT	COS	VHF XMTR
2.0 W OUTPUT	COS	VHF XMTR

Name	Type of Command	Location of Command Relay

Table 4. A-12. Command List for C&DH Subsystem (Wideband Telemetry)

Name	Type of Command	Location of Command Relay
Modulator		
Modulator A, ON	COS	WB MOD.
Modulator A, OFF	COS	WB MOD.
Modulator B, ON	COS	WB MOD.
Modulator B, OFF	COS	WB MOD.
Center Freq Select 1, A	COS	WB MOD.
Center Freq Select 2, A	COS	WB MOD.
Center Freq Select 1, B	COS	WB MOD.
Center Freq Select 2, B	COS	WB MOD.
PA Input Select A	COS	WB MOD.
PA Input Select B	COS	WB MOD.
Input MSS ON	COS	WB MOD.
Input MSS OFF	COS	WB MOD.

Name	Type of Command	Location of Command Relay
Modulator (Cont'd)		
Input VTR 1(D) ON	COS	WB MOD.
Input VTR 1(D) OFF	COS	WB MOD.
Input VTR 2 ON	COS	WB MOD.
Input VTR 2 OFF	COS	WB MOD.
Input RBV ON	COS	WB MOD.
Input RBV OFF	COS	WD MOD.
Input VTR 1(A) ON	COS	WB MOD.
Input VTR 1(A) OFF	COS	WB MOD.
Input VTR 2(A) ON	COS	WB MOD.
Input VTR 2(A) OFF	COS	WB MOD.
Input MSS ON	COS	WB MOD.
Input MSS OFF	COS	WB MOD.
Input VTR 1(D) ON	COS	WB MOD.
Input VTR 1 (D) OFF	COS	WB MOD.
Input VTR 2(D) ON	COS	WB MOD.

Table 4.A-12. Command List for C&DH Subsystem (Wideband Telemetry (Cont'd)

Name	Type of Command	Location of Command Relay
Modulator (Cont'd)		
Input VTR 2(D) OFF	COS	WB MOD.
Input RBV ON	COS	WB MOD.
Input RBV OFF	COS	WB MOD.
Input VTR 1(A) ON	COS	WB MOD.
Input VTR 1(A) OFF	COS	WB MOD.
Input VTR 2(A) ON	COS	WB MOD.
Input VTR 2(A) OFF	COS	WB MOD.
S-Band Power Amplifier		
Transmitter No. 1 Heater, POWER ON	COS	PA
Transmitter No. 1 HV POWER ON	COS	PA
Transmitter No. 1 POWER OFF	COS	PA
Select Transmitter 20 W OUTPUT	COS	PA

Name	Type of Command	Location of Command Relay
S-Band Power Amplifier (Cont'd)		
Select Transmitter 10 W OUTPUT	COS	PA
Transmitter No. 2 Heater POWER ON	COS	PA
Transmitter No. 2 HV POWER ON	COS	PA
Transmitter No. 2 POWER OFF	COS	PA
Select Transmitter No. 2 20 W OUTPUT	COS	PA
Select Transmitter No. 2 10 W OUTPUT	COS	PA
Transmitter No. 1 and No. 2 Heater POWER ON	COS	PA

Table 4.A-13. Command List for C&DH Subsystem (VIP)

Name	Type of Command	Location of Command Relay
Memory Write ON	COS	VIP
Matrix Verify Override ON	COS	VIP
Verify Memory OFF	COS	VIP
Memory Unit Select 'A'	COS	VIP
Memory Sequencer Unit Select 'A'	COS	VIP
Matrix Verify Override OFF	COS	VIP
Memory Write OFF	COS	VIP
Verify Memory ON	COS	VIP
A/D Converter Select 'A'	COS	VIP
Memory Unit Select 'B'	COS	VIP
Analog Multiplexer Select 'A'	COS	VIP
Memory Sequencer Unit Select 'B'	COS	VIP
Program Control Bit 21 ON	COS	VIP
Program Control Bit 20 ON	COS	VIP
Program Control Bit 21 OFF	COS	VIP
Clock Data to Beacon Override ON	COS	VIP
Digital Multiplexer Select 'A'	COS	VIP
A/D Converter Select 'B'	COS	VIP
Formatter Logic Select 'A'	COS	VIP
Analog Multiplexer Select 'B'	COS	VIP
VIP Data to Beacon	COS	VIP
Transmitter Buffer Amplifier Select 'A'	COS	VIP

Table 4.A-13. Command List for C&DH Subsystem (VIP) (Cont'd)

Name	Type of Command	Location of Command Relay
Program Control Bit 20 OFF	COS	VIP
Matrix Verify ON	COS	VIP
Digital Multiplexer Select 'B'	COS	VIP
Formatter Logic Select 'B'	COS	VIP
Power No. 1 ON	COS	VIP
Clock Data to Beacon	M	VIP
Pre-Reg 'A' ON	COS	VIP
Pre-Reg Output 'A'	COS	VIP
Force Program 0, 0 ON	COS	VIP
Power No. 2 OFF	COS	VIP
Memory Write/Verify Override ON	COS	VIP
Matrix Normal	COS	VIP

Name	Type of Command	Location of Command Relay
Transmitter Buffer Amplifier Select 'B'	COS	VIP
Power No. 1 OFF	COS	VIP
Clock Data to Beacon Override OFF	COS	VIP
Memory Write/Verify Override OFF	COS	VIP
Power No. 2 ON	COS	VIP
Force Program 0, 0 OFF	COS	VIP
Pre-Reg. 'B' ON	COS	VIP
Pre-Reg. Output 'B'	COS	VIP
Switched TLM Power OFF	COS	VIP
Switched TLM Power ON	COS	VIP
Ground to VIP	COS	VIP

Table 4.A-14. Command List for C&DH Subsystem (Telemetry Recorder)

Name	Type of Command	Location of Command Relay
POWER ON Recorder A	COS	Recorder
Receive Mode Recorder A	COS	
PB Mode Recorder A	COS	
POWER OFF Recorder A	COS	
POWER ON Recorder B	COS	
Receive Mode Recorder B	COS	
PB Mode Recorder B	COS	Recorder

Name	Type of Command	Location of Command Relay

Table 4.A-15. Command List for Unified S-Band Equipment

Name	Type of Command	Location of Command Relay
Receiver A POWER ON	COS	USB Equipment
Receiver A POWER OFF	COS	
Receiver B POWER ON	COS	
Receiver B POWER OFF	COS	
RANGING ON	COS	
RANGING OFF	COS	
Transmitter A POWER ON	COS	
Transmitter A POWER OFF	COS	
Transmitter B POWER ON	COS	
Transmitter B POWER OFF	COS	
Transmitter A VF OUTPUT SELECT	COS	USB Equipment
Transmitter B VF OUTPUT SELECT	COS	USB Equipment

Table 4.A-16. Command List for Premodulation Processor

Name	Type of Command	Location of Command Relay
Power A, ON	COS	PMP
Power A, OFF	COS	PMP
Power B, ON	COS	PMP
Power B, OFF	COS	PMP

Name	Type of Command	Location of Command Relay

Table 4.A-17. Command List for Attitude Control Subsystem

Name	Type of Command	Location of Command Relay
Unfused Power to Right SAD	COS	PSM
Fused Power to Right SAD	COS	PSM
Unfused Power to Left SAD	COS	PSM
Fused Power to Left SAD	COS	PSM
Pneumatics Reset	COS	CLB
Enable Pneumatics	COS	CLB
Disable Pneumatics	COS	CLB
Pneumatics Interlock Bypass	COS	CLB
Yaw Acquisition Mode	COS	CLB
Yaw Normal Mode	COS	CLB
Roll Unload Disable	COS	CLB
Roll Unload Enable	COS	CLB

Name	Type of Command	Location of Command Relay
Pitch Unload Disable	COS	CLB
Pitch Unload Enable	COS	CLB
Roll Tachometer Normal Gain	COS	CLB
Roll Tachometer High Gain	COS	CLB
Orbit Adjust Mode Disable	COS	CLB
Orbit Adjust Mode Enable	COS	CLB
Yaw Wheel Disable	COS	CLB
Yaw Wheel Enable	COS	CLB
Negative Pitch Momentum Bias	COS	CLB
Positive Pitch Momentum Bias	COS	CLB
Pitch Momentum Bias Mode Disable	COS	CLB

Table 4.A-17. Command List for Attitude Control Subsystem (Cont'd)

Name	Type of Command	Location of Command Relay
Pitch Momentum Bias Mode Enable	COS	CLB
Negative Pitch Positive Bias	COS	CLB
Positive Pitch Positive Bias	COS	CLB
0.25° Pitch Bias Enable	COS	CLB
0.5° Pitch Bias Enable	COS	CLB
1.0 Pitch Bias Enable	COS	CLB
2.0 Pitch Bias Enable	COS	CLB
0.25 and 0.5 Pitch Bias Disable	COS	CLB
1.0 and 2.0 Pitch Bias Disable	COS	CLB
Momentary Pneumatics Enable	M	CLB
Left SAD Enable	COS	Left SAD
Left SAD Enable	COS	Right SAD
Right SAD Enable	COS	Right SAD
Right SAD Disable	COS	Right SAD
Right SAD Normal Rate	COS	Right SAD
Right SAD High Rate	COS	Right SAD
Left SAD Normal Rate	COS	Left SAD
Left SAD High Rate	COS	Left SAD
RMP Heater and Elect. Power ON	COS	RMP
RMP No. 1 OFF	COS	RMP
RMP No. 1 Lower Motor Voltage	COS	RMP
RMP No. 1 Lower Motor Voltage	COS	RMP
RMP No. 1 Motor ON	COS	RMP
RMP No. 2 Heater OFF	COS	RMP

Table 4.A-17. Command List for Attitude Control Subsystem (Cont'd)

Name	Type of Command	Location of Command Relay
RMP No. 2 Heater and Elect. ON	COS	RMP
RMP No. 2 Lower Motor Voltage	COS	RMP
RMP No. 2 OFF	COS	RMP
RMP No. 2 Motor ON	COS	RMP
RMP No. 1 Control ON	COS	RMP
RMP No. 2 Control ON	COS	RMP
Front Scanner Disable	COS	CLB
Front Scanner Enable	COS	CLB
Rear Scanner Disable	COS	CLB
Rear Scanner Disable	COS	CLB
Attitude Sensor ON	COS	PSM
Attitude Sensor OFF	COS	PSM

Name	Type of Command	Location of Command Relay

Table 4.A-18. Command List for Attitude Control (Magnetic Moment Assembly)

Name	Type of Command	Location of Command Relay
Magnetic Moment Assembly (MMA) Pitch ON	COS	MMA
MMA Pitch OFF	COS	MMA
MMA Yaw ON	COS	MMA
MMA Yaw OFF	COS	MMA
MMA Roll ON	COS	MMA
MMA Roll OFF	COS	MMA
MMA Positive	COS	MMA
MMA Negative	COS	MMA
MMA Start	COS	MMA
MMA Enable	COS	MMA
MMA Power ON	COS	MMA
MMA Power OFF	COS	MMA
MMA Coarse Step	COS	MMA
MMA Fine Step	COS	MMA

Name	Type of Command	Location of Command Relay

Table 4.A-19. Telemetry List Summary ERTS A&B

Subsystem	Total	Digital A	Digital B				Analog			
		1/1	1/16	3/16	1/1	5/1	1/16	3/16	1/1	3/1
Mechanical	4		4							
Thermal	83						83			
Orbit Adjust	13		6				3		4	
Payload	182		80	9		3	68	20	2	
Data Collection	3		1				2			
Power	75			14	1		58		2	
C & DH	223	4	63	34	14	2	93	13		
Attitude Control	152		6	13	14		101		16	2
Totals	735	4	160	70	29	5	408	33	24	2

Table 4. A-20. Telemetry List for Mechanical Subsystem

Measurement Name	Type	Sampling Rate
Paddle Separation	Digital	1/16
Spacecraft Separation	Digital	1/16
Paddle Deployment	Digital	1/16
Paddle Latching	Digital	1/16

Table 4. A-21. Telemetry List for Thermal Subsystem

Measurement Name	Type	Sampling Rate
THERMISTORS		
Separator No. 1, Top Inboard	Analog	1/16
Separator No. 2, Bottom Outboard	Analog	1/16
Separator No. 3, Top Inboard	Analog	1/16
Separator No. 4, Bottom Outboard	Analog	1/16
Separator No. 5, Top Inboard	Analog	1/16
Separator No. 6, Bottom Outboard	Analog	1/16
Separator No. 7, Top Inboard	Analog	1/16
Separator No. 8, Bottom Outboard	Analog	1/16
Separator No. 9, Top Inboard	Analog	1/16
Separator No. 9, Top Outboard	Analog	1/16
Separator No. 9, Bottom Inboard	Analog	1/16
Separator No. 9, Bottom Outboard	Analog	1/16
Separator No. 10, Top Inboard	Analog	1/16
Separator No. 10, Top Outboard	Analog	1/16
Separator No. 10, Bottom Inboard	Analog	1/16
Separator No. 10, Bottom Outboard	Analog	1/16
Separator No. 11, Top Inboard	Analog	1/16
Separator No. 12, Bottom Outboard	Analog	1/16
Separator No. 13, Top Inboard	Analog	1/16

Table 4.A-21. Telemetry List for Thermal Subsystem (Cont'd)

Measurement Name	Type	Sampling Rate
Separator No. 14, Bottom Outboard	Analog	1/16
Separator No. 15, Top Inboard	Analog	1/16
Separator No. 16, Bottom Outboard	Analog	1/16
Separator No. 17, Top Inboard	Analog	1/16
Separator No. 18, Bottom Outboard	Analog	1/16
Upper Ring at Bay No. 1	Analog	1/16
Upper Ring at Bay No. 3	Analog	1/16
Upper Ring at Bay No. 5	Analog	1/16
Upper Ring at Bay No. 7	Analog	1/16
Upper Ring at Bay No. 9	Analog	1/16
Upper Ring at Bay No. 11	Analog	1/16
Upper Ring at Bay No. 13	Analog	1/16
Upper Ring at Bay No. 15	Analog	1/16
Upper Ring at Bay No. 17	Analog	1/16
Temperature Control Bellows No. 1	Analog	1/16
Temperature Control Bellows No. 2	Analog	1/16
Temperature Control Bellows No. 3	Analog	1/16
Temperature Control Bellows No. 4	Analog	1/16
Temperature Control Bellows No. 5	Analog	1/16
Temperature Control Bellows No. 6	Analog	1/16

Table 4. A-21. Telemetry List for Thermal Subsystem (Cont'd)

Measurement Name	Type	Sampling Rate
Temperature Control Bellows No. 7	Analog	1/16
Temperature Control Bellows No. 8	Analog	1/16
Temperature Control Bellows No. 10	Analog	1/16
Temperature Control Bellows No. 11	Analog	1/16
Temperature Control Bellows No. 12	Analog	1/16
Temperature Control Bellows No. 13	Analog	1/16
Temperature Control Bellows No. 14	Analog	1/16
Temperature Control Bellows No. 16	Analog	1/16
Temperature Control Bellows No. 17	Analog	1/16
Temperature Control Bellows No. 18	Analog	1/16
Center Section Radiator	Analog	1/16
Center Section Radiator	Analog	1/16
Center Section Radiator	Analog	1/16
Center Section Radiator	Analog	1/16
Main Beam Inboard of Separator No. 2	Analog	1/16
Main Beam Inboard of Separator No. 8	Analog	1/16
Main Beam Inboard of Separator No. 12	Analog	1/16
Main Beam Inboard of Separator No. 18	Analog	1/16
Main Beam Near Recorder A	Analog	1/16
Main Beam Near Recorder B	Analog	1/16

Table 4.A-21. Telemetry List for Thermal Subsystem (Cont'd)

Measurement Name	Type	Sampling Rate
Crossbeam Inboard of Separator No. 1	Analog	1/16
Crossbeam Between Bay No. 19 & 20	Analog	1/16
Crossbeam Inboard of MSPS	Analog	1/16
RBV Mount	Analog	1/16
MSPS Mount	Analog	1/16
Payload Mount	Analog	1/16
S-Band Transmitter	Analog	1/16
S-Band Transmitter	Analog	1/16
SHUTTER POSITION INDICATORS		
Shutter Assembly, Bay No. 1	Analog	1/16
Shutter Assembly, Bay No. 2	Analog	1/16
Shutter Assembly, Bay No. 3	Analog	1/16
Shutter Assembly, Bay No. 4	Analog	1/16
Shutter Assembly, Bay No. 5	Analog	1/16
Shutter Assembly, Bay No. 6	Analog	1/16
Shutter Assembly, Bay No. 7	Analog	1/16
Shutter Assembly, Bay No. 8	Analog	1/16
Shutter Assembly, Bay No. 10	Analog	1/16
Shutter Assembly, Bay No. 11	Analog	1/16
Shutter Assembly, Bay No. 12	Analog	1/16

Table 4.A-21. Telemetry List for Thermal Subsystem (Cont'd)

Measurement Name	Type	Sampling Rate
Shutter Assembly, Bay No. 13	Analog	1/16
Shutter Assembly, Bay No. 14	Analog	1/16
Shutter Assembly, Bay No. 16	Analog	1/16
Shutter Assembly, Bay No. 17	Analog	1/16
Shutter Assembly, Bay No. 18	Analog	1/16

Table 4.A-22. Telemetry List for Orbit Adjust Subsystem

Measurement Name	Type	Sampling Rate
Propellant Tank Temperature	Analog	1/16
Propellant Tank Pressure	Analog	1/16
Thrust Chamber No. 1 Temperature	Analog	1/1
Thrust Chamber No. 2 Temperature	Analog	1/1
Solenoid Valve No. 1 Temperature	Analog	1/1
Solenoid Valve No. 2 Temperature	Analog	1/1
PYRO BUSS Safed/Armed	Digital	1/16
N/O Valve PYRO Energized	Digital	1/16
N/C Valve PYRO Energized, Pri	Digital	1/16
N/C Valve Pyro Energized, Red	Digital	1/16
Line Pressure	Analog	1/16
Solenoid Valve No. 1 Coil Energized	Digital	1/16
Solenoid Valve No. 2 Coil Energized	Digital	1/16

Table 4.A-23. Telemetry List for Payload

Measurement Name	Type	Sampling Rate
RBV CAMERA NO. 1		
Vidicon Filament Current No. 1	Digital	1/16
G1 Voltage No. 1	Analog	1/16
Target Voltage No. 1	Analog	1/16
Anode Voltage Supply No. 1	Digital	1/16
G2 Voltage No. 1	Digital	1/16
Vidicon Cathode Current No. 1	Analog	1/16
Video Output No. 1	Analog	1/16
Focus Current No. 1	Analog	1/16
Alignment Currents No. 1	Analog	1/16
Horizontal Deflection Output No. 1	Analog	1/16
Vertical Deflection Output No. 1	Analog	1/16
Deflection Power Supply No. 1	Analog	1/16
Low Voltage Power Supply No. 1	Analog	1/16
-24.5 Volt Input Voltage No. 1	Digital	1/16
-28 Volt (Shutter) Current No. 1	Digital	5/1
Temperature - Faceplate No. 1	Analog	1/16
Temperature - Yoke/Focus Coil No. 1	Analog	1/16
Temperature - Electronics No. 1	Analog	1/16
Temperature - Low Voltage Power Supply	Analog	1/16

Table 4.A-23. Telemetry List for Payload (Cont'd)

Measurement Name	Type	Sampling Rate
RBV CAMERA NO. 1 (Cont'd)		
Anode/Target Mode (Command Verification) No. 1	Digital	1/16
Power On/Off (Command Verification) No. 1	Digital	1/16
One Cycle per Second Rephasing No. 1	Digital	1/16
Thermoelectric Cooler Current No. 1	Analog	1/16
RBV CAMERA NO. 2		
Vidicon Filament Current No. 2	Digital	1/16
G1 Voltage No. 2	Analog	1/16
Target Voltage No. 2	Analog	1/16
Anode Voltage Supply No. 2	Digital	1/16
G2 Voltage No. 2	Digital	1/16
Vidicon Cathode Current No. 2	Analog	1/16
Video Output No. 2	Analog	1/16
Focus Current No. 2	Analog	1/16
Alignment Currents No. 2	Analog	1/16
Horizontal Deflection Output No. 2	Analog	1/16
Vertical Deflection Output No. 2	Analog	1/16
Deflection Power Supply No. 2	Analog	1/16
Low Voltage Power Supply No. 2	Analog	1/16
-24.5 Volt Input Voltage No. 2	Digital	1/16

Table 4.A-23. Telemetry List for Payload (Cont'd)

Measurement Name	Type	Sampling Rate
-28 Volt (Shutter) Current No. 2	Digital	5/1
Temperature - Faceplate No. 2	Analog	1/16
Temperature - Yoke/Focus Coil No. 2	Analog	1/16
Temperature - Electronics No. 2	Analog	1/16
Temperature - Low Voltage Power Supply No. 2	Analog	1/16
Anode/Target Mode (Command Verification) No. 2	Digital	1/16
Power On/Off (Command Verification) No. 2	Digital	1/16
One Cycle per Second Rephasing No. 2	Digital	1/16
Thermoelectric Cooler Current No. 2	Analog	1/16
RBV CAMERA NO. 3		
Vidicon Filament Current No. 3	Digital	1/16
G1 Voltage No. 3	Analog	1/16
Target Voltage No. 3	Analog	1/16
Anode Voltage Supply No. 3	Digital	1/16
G2 Voltage No. 3	Digital	1/16
Vidicon Cathode Current No. 3	Analog	1/16
Video Output No. 3	Analog	1/16
Focus Current No. 3	Analog	1/16
Alignment Currents No. 3	Analog	1/16

Table 4.A-23. Telemetry List for Payload (Cont'd)

Measurement Name	Type	Sampling Rate
RBV CAMERA NO. 3 (Cont'd)		
Horizontal Deflection Output No. 3	Analog	1/16
Vertical Deflection Output No. 3	Analog	1/16
Deflection Power Supply No. 3	Analog	1/16
Low Voltage Power Supply No. 3	Analog	1/16
-24.5 Volt Input Voltage No. 3	Digital	1/16
-28 Volt (Shutter) Current No. 3	Digital	5/1
Temperature - Faceplate No. 3	Analog	1/16
Temperature - Yoke/Focus Coil No. 3	Analog	1/16
Temperature - Electronics No. 3	Analog	1/16
Temperature - Low Voltage Power Supply No. 3	Analog	1/16
Anode/Target Mode (Command Verification) No. 3	Digital	1/16
Power On/Off (Command Verification) No. 3	Digital	1/16
One Cycle per Second Rephasing No. 3	Digital	1/16
Thermoelectric Cooler Current No. 3	Analog	1/16
RBV CONTROLLER		
Clock Input	Digital	1/16
Horizontal Sync	Digital	1/16
Vertical Sync	Digital	1/16

Table 4.A-23. Telemetry List for Payload (Cont'd)

Measurement Name	Type	Sampling Rate
RBV CONTROLLER (Cont'd)		
Clock A/B (Command Verification)	Digital	1/16
Cycle Continuous/Single (Command Verification)	Digital	1/16
P3-Auto/P2-P1 (Command Verification)	Digital	1/16
P2-Auto/P3-P1 (Command Verification)	Digital	1/16
Mode Record/Direct-Record (Command Verification)	Digital	1/16
Mode Direct/Direct-Record (Command Verification)	Digital	1/16
Dynamic Beam Regulator In-Out (Command Verification)	Digital	1/16
Temperature-Camera Controller	Analog	1/16
MULTISPECTRAL SCANNER		
Spectral Band 1 ON/OFF	Digital	1/16
Spectral Band 2 ON/OFF		1/16
Spectral Band 3 ON/OFF		1/16
Spectral Band 4 ON/OFF		1/16
Spectral Band 5 ON/OFF		1/16
Band 1 Gain LOW/HIGH		1/16
Band 2 Gain LOW/HIGH		1/16
Band 3 Gain LOW/HIGH		1/16
Band 4 Gain LOW/HIGH	Digital	1/16

Table 4.A-23. Telemetry List for Payload (Cont'd)

Measurement Name	Type	Sampling Rate
Main Inverter A ON/OFF	Digital	1/16
Main Inverter B ON/OFF		1/16
Mirror Pick-off ON/OFF		1/16
Band 1 High Voltage A ON/OFF		1/16
Band 1 High Voltage B ON/OFF		1/16
Band 2 High Voltage A ON/OFF		1/16
Band 2 High Voltage B ON/OFF		1/16
Band 3 High Voltage A ON/OFF		1/16
Band 3 High Voltage B ON/OFF		1/16
Scan Mirror Drive ON/OFF		1/16
Band 5 Focus ON/OFF	Digital	1/16
Band 5 Preamp Output Voltage	Analog	1/16
Calibration Lamp No. 1 ON/OFF	Analog	1/1
Calibration Lamp No. 2 ON/OFF	Analog	1/1
Rotating Shutter Drive ON/OFF	Digital	3/16
Silicon Photodiode Preamp Output	Analog	3/16
Silicon Photodiode Preamp Output	Analog	3/16
Silicon Photodiode Preamp Output	Analog	3/16
Silicon Photodiode Preamp Output	Analog	3/16
Silicon Photodiode Preamp Output	Analog	3/16
Silicon Photodiode Preamp Output	Analog	3/16

Table 4.A-23. Telemetry List for Payload (Cont'd)

Measurement Name	Type	Sampling Rate
Low Voltage Supply Output	Analog	1/16
Low Voltage Supply Output	Analog	1/16
Low Voltage Supply Output	Analog	1/16
Low Voltage Supply Output	Analog	1/16
Low Voltage Supply Output	Analog	1/16
TBD	Digital	
TBD	Digital	
TBD	Digital	
TBD	Digital	
TBD	Digital	
Temperature	Analog	1/16
Temperature	Analog	1/16
Temperature	Analog	1/16
Temperature	Analog	1/16
Rotating Shutter Housing Temperature	Analog	1/16
Calibration Lamp Base Temperature	Analog	1/16
Temperature	Analog	1/16
Temperature	Analog	1/16
Temperature	Analog	1/16
Temperature	Analog	1/16

Table 4.A-23. Telemetry List for Payload (Cont'd)

Measurement Name	Type	Sampling Rate
MULTISPECTRAL SCANNER (Cont'd)		
Scanning Mech. Uncaged	Digital	1/16
Rad Cooler Uncaged	Digital	1/16
Rad Cooler Uncapped	Digital	1/16
Scanner Optics Uncapped	Digital	1/16
WIDEBAND VIDEO TAPE RECORDER		
Standby No. 1	Digital	1/16
Record No. 1	Digital	3/16
Playback No. 1	Digital	3/16
Rewind No. 1	Digital	3/16
Forward No. 1	Digital	3/16
Primary End of Tape No. 1	Digital	1/16
Secondary End of Tape No. 1	Digital	1/16
Primary Start of Tape No. 1	Digital	1/16
Secondary Start of Tape No. 1	Digital	1/16
Lap at Bot No. 1	Digital	1/16
RBV/MSS Mode No. 1	Digital	1/16
Record Current Adjust, Level 1, No. 1	Digital	1/16
Record Current Adjust, Level 2, No. 1	Digital	1/16
Record Current Adjust, Level 3, No. 1	Digital	1/16
Tape Footage No. 1	Analog	1/16

Table 4.A-23. Telemetry List for Payload (Cont'd)

Measurement Name	Type	Sampling Rate
WIDEBAND VIDEO TAPE RECORDER (Cont'd)		
Pressure, Internal, Container No. 1	Analog	1/16
Temperature No. 1	Analog	1/16
Record Current, Average No. 1	Analog	3/16
Playback Voltage, Average No. 1	Analog	3/16
Servo Voltage, No. 1	Analog	3/16
Capstan Motor Speed No. 1	Analog	3/16
Motor Current, DC No. 1	Analog	3/16
Motor Current, HWP No. 1	Analog	3/16
Motor Current, Capstan No. 1	Analog	3/16
Standby No. 2	Digital	1/16
Record No. 2	Digital	3/16
Playback No. 2	Digital	3/16
Rewind No. 2	Digital	3/16
Forward No. 2	Digital	3/16
Primary End of Tape No. 2	Digital	1/16
Secondary End of Tape No. 2	Digital	1/16
Primary Start of Tape No. 2	Digital	1/16
Secondary Start of Tape No. 2	Digital	1/16
Lap at Bot No. 2	Digital	1/16
RBV/MSS Mode No. 2	Digital	1/16

Table 4.A-23. Telemetry List for Payload (Cont'd)

Measurement Name	Type	Sampling Rate
WIDEBAND VIDEO TAPE RECORDER (Cont'd)		
Record Current Adjust, Level 1, No. 2	Digital	1/16
Record Current Adjust, Level 2, No. 2	Digital	1/16
Record Current Adjust, Level 3, No. 2	Digital	1/16
Tape Footage No. 2	Analog	1/16
Pressure, Internal Container No. 2	Analog	1/16
Temperature No. 2	Analog	1/16
Record Current, Average No. 2	Analog	3/16
Playback Voltage, Average No. 2	Analog	3/16
Servo Voltage, No. 2	Analog	3/16
Capstan Motor Speed No. 2	Analog	3/16
Motor Current, DC No. 2	Analog	3/16
Motor Current, HWP No. 2	Analog	3/16
Motor Current, Capstan No. 2	Analog	3/16

Table 4.A-24. Telemetry List for Data Collection Subsystem

Measurement Name	Type	Sampling Rate
Receiver AGC Voltage	Analog	1/16
Receiver Temperature	Analog	1/16
Input Power Buss	Digital	1/16

Table 4.A-25. Telemetry List for Power Subsystem

Measurement Name	Type	Sampling Rate
Battery No. 1 Discharge Current	Analog	1/16
Battery No. 1 Charge Current	Analog	1/16
Battery No. 1 Voltage	Analog	1/16
Battery No. 1 Temperature	Analog	1/16
Battery No. 2 Discharge Current	Analog	1/16
Battery No. 2 Charge Current	Analog	1/16
Battery No. 2 Voltage	Analog	1/16
Battery No. 2 Temperature	Analog	1/16
Battery No. 3 Discharge Current	Analog	1/16
Battery No. 3 Charge Current	Analog	1/16
Battery No. 3 Voltage	Analog	1/16
Battery No. 3 Temperature	Analog	1/16
Battery No. 4 Discharge Current	Analog	1/16
Battery No. 4 Charge Current	Analog	1/16
Battery No. 4 Voltage	Analog	1/16
Battery No. 4 Temperature	Analog	1/16
Battery No. 5 Discharge Current	Analog	1/16
Battery No. 5 Charge Current	Analog	1/16
Battery No. 5 Voltage	Analog	1/16
Battery No. 5 Temperature	Analog	1/16

Table 4.A-25. Telemetry List for Power Subsystem (Cont'd)

Measurement Name	Type	Sampling Rate
Battery No. 6 Discharge Current	Analog	1/16
Battery No. 6 Charge Current	Analog	1/16
Battery No. 6 Voltage	Analog	1/16
Battery No. 6 Temperature	Analog	1/16
Pulse Width Modulation (PWM) No. 1 Regulator	Digital	3/16
PWM No. 2 Regulator	Digital	3/16
Unregulated Bus Voltage	Analog	1/16
Regulated Bus Voltage	Analog	1/16
Auxiliary Regulator "A" Voltage	Analog	1/16
Auxiliary Regulator "B" Voltage	Analog	1/16
Solar Array Current	Analog	1/16
Regulated Bus Current	Analog	1/1
Battery No. 7 Discharge Current	Analog	1/1
Battery No. 7 Charge Current	Analog	1/16
Battery No. 7 Voltage	Analog	1/16
Battery No. 7 Temperature	Analog	1/16
Battery No. 8 Discharge Current	Analog	1/16
Battery No. 8 Charge Current	Analog	1/16
Battery No. 8 Voltage	Analog	1/16

Table 4.A-25. Telemetry List for Power Subsystem (Cont'd)

Measurement Name	Type	Sampling Rate
Battery No. 8 Temperature	Analog	1/16
Auxiliary Load No. 1	Digital	3/16
Auxiliary Load No. 2	Digital	3/16
Auxiliary Load No. 3	Digital	3/16
Auxiliary Load No. 4	Digital	3/16
Auxiliary Load No. 5	Digital	3/16
Shunt Load "A"	Digital	3/16
Shunt Load "B"	Digital	3/16
Shunt Load "C"	Digital	3/16
Shunt Load "D"	Digital	3/16
Tick Tock	Digital	1/1
Shunt Load No. 1 Current	Analog	1/16
Shunt Load No. 2 Current	Analog	1/16
Shunt Load No. 3 Current	Analog	1/16
Shunt Load No. 4 Current	Analog	1/16
Shunt Load No. 5 Current	Analog	1/16
Shunt Load No. 6 Current	Analog	1/16
Shunt Load No. 7 Current	Analog	1/16
Shunt Load No. 8 Current	Analog	1/16
Right Paddle Temperature	Analog	1/16

Table 4.A-25. Telemetry List for Power Subsystem (Cont'd)

Measurement Name	Type	Sampling Rate
Left Paddle Voltage "G"	Analog	1/16
Right Paddle Voltage "A"	Analog	1/16
Left Paddle Temperature	Analog	1/16
Right Paddle Voltage "F"	Analog	1/16
Left Paddle Voltage "J"	Analog	1/16
Trickle Charge Override	Digital	3/16
Thermistor No. 63 Top Outboard Power Control Module Temperature	Analog	1/16
Thermistor No. 64 Center Inboard Power Control Module Temperature	Analog	1/16
PWM No. 3 Regulator (Payload Regulator Module)	Digital	3/16
PWM No. 4 Regulator (Payload Regulator Module)	Digital	3/16
Payload Reg. Bus Voltage	Analog	1/16
Payload Unreg. Bus Voltage	Analog	1/16
Payload Reg. Bus Current	Analog	1/16
Payload Aux. Reg. Voltage	Analog	1/16
Payload Module Outboard Temp.	Analog	1/16
Payload Module Inboard Temp.	Analog	1/16

Table 4.A-26. Telemetry List for C&DH Subsystem

Measurement Name	Type	Sampling Rate
COMMAND/CLOCK		
Primary Power Supply ON/OFF	Digital	3/16
Redundant Power Supply ON/OFF	Digital	3/16
Power Supply Primary/Redundant	Digital	3/16
Primary Comstor ON/OFF	Digital	3/16
Redundant Comstor ON/OFF	Digital	3/16
Matrix Decoder Primary/Redundant	Digital	3/16
Matrix Driver A Primary/Redundant	Digital	3/16
Matrix Driver B Primary/Redundant	Digital	3/16
Frequency Gen Primary/Redundant	Digital	3/16
Select Oscillator Primary/Redundant	Digital	3/16
Serial Data Transfer ON/OFF	Digital	3/16
Serial Data Error	Digital	3/16
Primary W Channel Input (Data)	Analog	1/16
Primary X Channel Input (Strobe)	Analog	1/16
Primary Y Channel Input (Enable)	Digital	3/16
Redundant W Channel Input (Data)	Analog	1/16
Redundant X Channel Input (Strobe)	Analog	1/16
Redundant Y Channel Input (Enable)	Digital	3/16
Command Execute Counter Bit 1	Digital	3/16

Table 4.A-26. Telemetry List for C&DH Subsystem (Cont'd)

Measurement Name	Type	Sampling Rate
Command Execute Counter Bit 2	Digital	3/16
Command Execute Counter Bit 4	Digital	3/16
Command Execute Counter Bit 8	Digital	3/16
Command Execute Counter Bit 16	Digital	3/16
Command Execute Counter Bit 32	Digital	3/16
Primary Comstor Fill	Digital	1/1
Redundant Comstor Fill	Digital	1/1
Primary Comstor Activate	Digital	1/1
Redundant Comstor Activate	Digital	1/1
Primary Comstor Verify	Digital	1/1
Redundant Comstor Verify	Digital	1/1
Primary Comdec Data Error	Digital	5/1
Redundant Comdec Data Error	Digital	5/1
Primary Power Supply Temperature	Analog	1/16
Redundant Power Supply Temperature	Analog	1/16
Primary Oscillator Temperature	Analog	1/16
Redundant Oscillator Temperature	Analog	1/16
Primary Oscillator Output	Analog	1/16
Redundant Oscillator Output	Analog	1/16
100 kHz Master Clock	Analog	1/16

Table 4.A-26. Telemetry List for C&DH Subsystem (Cont'd)

Measurement Name	Type	Sampling Rate
10 kHz	Analog	1/16
2.5 kHz	Analog	1/16
1 Hz (A)	Digital	3/16
1 Hz (B)	Digital	3/16
400 Hz Ph A/Ph B	Analog	1/16
Primary +4 vdc	Analog	1/16
Redundant +4 vdc	Analog	1/16
Primary +6.4 vdc	Analog	1/16
Redundant +6.4 vdc	Analog	1/16
Primary -6.4 vdc	Analog	1/16
Redundant -6.4 vdc	Analog	1/16
Primary -23 vdc	Analog	1/16
Redundant -23 vdc	Analog	1/16
Primary 29 vdc	Analog	1/16
Redundant -29 vdc	Analog	1/16
COMMAND INTEGRATOR UNIT		
Primary Power ON/OFF	Digital	1/16
Redundant Power ON/OFF	Digital	1/16
Stadan Enable 1	Digital	1/1
Stadan Enable 2	Digital	1/1
MSFN Enable 1	Digital	1/1

Table 4.A-26. Telemetry List for C&DH Subsystem (Cont'd)

Measurement Name	Type	Sampling Rate
MSFN Enable 2	Digital	1/1
Secondary Voltage $+V_1$, 1	Analog	1/16
Secondary Voltage $+V_2$, 1	Analog	1/16
Secondary Voltage $+V_1$, 2	Analog	1/16
Secondary Voltage $+V_2$, 2	Analog	1/16
Temperature 1	Analog	1/16
Temperature 2	Analog	1/16
Search Track VTR No. 1 (First half of data)	Digital A	1/1
Search Track VTR No. 1 (Second half of data)	Digital A	1/1
Search Track VTR No. 2 (First half of data)	Digital A	1/1
Search Track VTR No. 2 (Second half of data)	Digital A	1/1
VHF RECEIVER		
Temperature No. 1 (Receiver 1)	Analog	3/16
Temperature No. 2 (Receiver 2)	Analog	3/16
Temperature No. 3 (PCM CMD Dem.)	Analog	3/16
AGC Receiver 1	Analog	3/16
AGC Receiver 2	Analog	3/16
Audio Amplifier 1	Analog	3/16
Audio Amplifier 2	Analog	3/16

Table 4.A-26. Telemetry List for C&DH Subsystem (Cont'd)

Measurement Name	Type	Sampling Rate
FSK Demodulator 1	Analog	3/16
FSK Demodulator 2	Analog	3/16
AM Demodulator 1	Analog	3/16
AM Demodulator 2	Analog	3/16
-24.5V Reg. Buss	Digital	3/16
Switched -24.5V Reg. Buss	Digital	3/16
VHF TRANSMITTER		
Transmitter A ON/OFF	Digital	1/16
Transmitter B ON/OFF	Digital	1/16
Input Signal Presence	Digital	1/16
Norm. TLM/Emergency Playback Mode	Digital	1/16
RF Output Level	Digital	1/16
Transmitter A/B Output Selected	Digital	1/16
Transmitter A Power Supply Voltage	Analog	1/16
Transmitter B Power Supply Voltage	Analog	1/16
Transmitter A Temperature	Analog	1/16
Transmitter B Temperature	Analog	1/16
VERSATILE INFORMATION PROCESSOR (VIP)		
Memory Sequencer DC/DC Converter A	Analog	1/16
Memory Sequencer DC/DC Converter B	Analog	1/16

Table 4.A-26. Telemetry List for C&DH Subsystem (Cont'd)

Measurement Name	Type	Sampling Rate
Memory Write Pulse A	Digital	1/16
Memory Write Pulse B	Digital	1/16
Memory Sequencer Module Temperature	Analog	1/16
Formatter DC/DC Coverter A	Analog	1/16
Formatter DC/DC Converter B	Analog	1/16
Digital Multiplexer DC/DC Converter A	Analog	1/16
Digital Multiplexer DC/DC Converter B	Analog	1/16
Formatter/Digital Multiplexer Module Temperature	Analog	1/16
Analog Multiplexer DC/DC Converter A	Analog	1/16
Analog Multiplexer DC/DC Converter B	Analog	1/16
A/D Converter DC/DC Converter A	Analog	1/16
A/D Converter DC/DC Converter B	Analog	1/16
Analog Multiplexer A/D Converter Module Temperature	Analog	1/16
Monitor Preregulator A	Analog	1/16
Monitor Preregulator B	Analog	1/16
Monitor Power A ON	Digital	1/16
Monitor Power B ON	Digital	1/16
Monitor Reporgram Relay	Digital	1/16
Monitor Bit Rate Status	Digital	1/16

Table 4.A-26. Telemetry List for C&DH Subsystem (Cont'd)

Measurement Name	Type	Sampling Rate
Monitor Memory Status (A or B)	Digital	1/16
Monitor Memory Sequencer Status (A or B)	Digital	1/16
Monitor A/D Converter Status (A or B)	Digital	1/16
Monitor Analog Multiplexer Status (A or B)	Digital	1/16
Monitor Digital Multiplexer Status (A or B)	Digital	1/16
Monitor Formatter Logic Status (A or B)	Digital	1/16
Monitor Buffer Amplifier Status (A or B)	Digital	1/16
Reprogrammer Module Temperature	Analog	1/16
Memory A DC/DC Converter	Analog	1/16
Memory A Module Temperature	Analog	1/16
Memory B DC/DC Converter	Analog	1/16
Memory B Module Temperature	Analog	1/16
Transmitter A ON/OFF	Digital	1/16
Transmitter B ON/OFF	Digital	1/16
Transmitter C ON/OFF	Digital	1/16
Transmitter D ON/OFF	Digital	1/16
Transmitter A Temperature	Analog	1/16
Transmitter B Temperature	Analog	1/16
Transmitter C Temperature	Analog	1/16
Transmitter D Temperature	Analog	1/16
Transmitter A RF Power	Analog	1/16

Table 4.A-26. Telemetry List for C&DH Subsystem (Cont'd)

Measurement Name	Type	Sampling Rate
Transmitter B RF Power	Analog	1/16
Transmitter C RF Power	Analog	1/16
Transmitter D RF Power	Analog	1/16
Transmitter A Modulated	Digital	1/16
Transmitter B Modulated	Digital	1/16
Transmitter C Modulated	Digital	1/16
Transmitter D Modulated	Digital	1/16
TELEMETRY RECORDER A		
Record Mode	Digital	3/16
Playback	Digital	3/16
Power ON/OFF	Digital	3/16
Record End of Tape	Digital	3/16
Playback End of Tape	Digital	3/16
Record Run/Start	Digital	1/1
Playback Run/Start	Digital	1/1
Recorder Pressure	Analog	1/16
Recorder Temperature	Analog	1/16
Motor Current	Analog	3/16
TELEMETRY RECORDER B		
Record Mode	Digital	3/16
Playback Mode	Digital	3/16

Table 4.A-26. Telemetry List for C&DH Subsystem (Cont'd)

Measurement Name	Type	Sampling Rate
Former Power Output No. 2	Analog	1/16
Reflected Power Output No. 2	Analog	1/16
Heater Status No. 2	Digital	1/16
HV Status No. 2	Digital	1/16
MODULATOR		
Input Power Buss A	Digital	1/16
Input Power Buss B	Digital	1/16
Modulator RF Power Output, A	Analog	1/16
Modulator RF Power Output, B	Analog	1/16
Center Frequency Status 1, A	Digital	1/16
Center Frequency Status 2, A	Digital	1/16
Center Frequency Status 1, B	Digital	1/16
Center Frequency Status 2, B	Digital	1/16
Temperature A	Analog	1/16
Temperature B	Analog	1/16
Temperature B	Analog	1/16
Pa Input Select A	Digital	1/16
Pa Input Select B	Digital	1/16
Mod. Input Select A	Digital	1/16
Mod. Input Select B	Digital	1/16
Input MSS/FLI-A	Digital	1/16

Table 4. A-26. Telemetry List for C&DH Subsystem (Cont'd)

Measurement Name	Type	Sampling Rate
Power ON/OFF	Digital	3/16
Record End of Tape	Digital	3/16
Playback End of Tape	Digital	3/16
Record Run/Start	Digital	1/1
Playback Run/Start	Digital	1/1
Recorder Pressure	Analog	1/16
Recorder Temperature	Analog	1/16
Motor Current	Analog	3/16
UNIFIED S-BAND EQUIPMENT		
Receiver A AGC Voltage	Analog	1/16
Receiver B AGC Voltage	Analog	1/16
Transmitter A Output Power Level	Analog	1/16
Transmitter B Output Power Level	Analog	1/16
Receiver A Static Phase Error	Analog	1/16
Receiver B Static Phase Error	Analog	1/16
Transponder A Temperature	Analog	1/16
Transponder B Temperature	Analog	1/16
Receiver A ON/OFF	Digital	1/16
Receiver B ON/OFF	Digital	1/16
Transmitter A ON/OFF	Digital	1/16
Transmitter B ON/OFF	Digital	1/16

Table 4.A-26. Telemetry List for C&DH Subsystem (Cont'd)

Measurement Name	Type	Sampling Rate
Ranging Mode ON/OFF	Digital	1/16
Transmitter VF Output Select A/B	Digital	1/16
PREMODULATION PROCESSOR (PMP)		
Power Supply A Voltage	Analog	1/16
Power Supply B Voltage	Analog	1/16
Section A Temperature	Analog	1/16
Section B Temperature	Analog	1/16
Section A ON/OFF	Digital	1/16
Section B ON/OFF	Digital	1/16
WIDEBAND TELEMETRY SUBSYSTEM		
S-BAND POWER AMPLIFIER		
Regulator Output Voltage No. 1	Analog	1/16
Helix Current No. 1	Analog	1/16
Cathode Current No. 1	Analog	1/16
Former Power Output No. 1	Analog	1/16
Reflector Power Output No. 1	Analog	1/16
Heater Status No. 1	Digital	1/16
HV Status No. 1	Digital	1/16
Regulator Output Voltage No. 2	Analog	1/16
Helix Current No. 2	Analog	1/16
Cathode Current No. 2	Analog	1/16

Table 4.A-26. Telemetry List for C&DH Subsystem (Cont'd)

Measurement Name	Type	Sampling Rate
Input VTR 1 (D)/FLI-A	Digital	1/16
Input VTR 2 (D)/FLI-A	Digital	1/16
Input RBV/FL2-A	Digital	1/16
Input VTR 1 (A) FL2-A	Digital	1/16
Input VTR 2 (A)/FL2-A	Digital	1/16
Input MSS/FL3-B	Digital	1/16
Input VTR 1 (D)/FL3-B	Digital	1/16
Input VTR 2 (D)/FL3-B	Digital	1/16
Input RBV/FL4-B	Digital	1/16
Input VTR 1 (A)/FL4-B	Digital	1/16
Input VTR 2 (A)/FL4-B	Digital	1/16

Table 4. A-27. Telemetry List for Attitude Control Subsystem

Measurement Name	Type	Sampling Rate
FORWARD AND REAR SCANNER SIGNAL PROCESSORS		
Fwd. Scan. Upside Down	Analog	1/16
Rear Scan. Upside Down	Analog	1/16
Fwd. Scan. Lead Earth Pulse	Analog	1/16
Fwd. Scan. Trail Earth Pulse	Analog	1/16
Rear Scan. Lead Earth Pulse	Analog	1/16
Rear Scan. Trail Earth Pulse	Analog	1/16
Fwd. Scan. Preamp. Card Temp.	Analog	1/16
Rear Scan. Preamp. Card Temp.	Analog	1/16
Fwd. Scan. Pressure	Analog	1/16
Rear Scan. Pressure	Analog	1/16
Fwd. Scan. Ref Processor Card Temp.	Analog	1/16
Rear Scan Ref. Processor Card Temp.	Analog	1/16
Fwd. Scan. Motor Temp.	Analog	1/16
Rear Scan. Motor Temp.	Analog	1/16
CONTROL LOGIC BOX		
Roll Coarse Error	Analog	1/1
Roll Fine Error	Analog	1/1
Roll Lead Amp. Output	Analog	1/1
Roll Diff. Tach. Amp. Output	Analog	1/1

Table 4.A-27. Telemetry List for Attitude Control Subsystem (Cont'd)

Measurement Name	Type	Sampling Rate
Roll Rear Motor Driver (CCW)	Analog	1/16
Roll Fwd. Motor Driver (CCW)	Analog	1/16
Roll Fwd. Motor Driver (CW)	Analog	1/16
Roll Rear Motor Driver (CW)	Analog	1/16
Pitch Motor Driver (CCW)	Analog	1/16
Pitch Motor Driver (CW)	Analog	1/16
Yaw Motor Driver (CW)	Analog	1/16
Yaw Motor Driver (CCW)	Analog	1/16
Roll Fwd. Flywheel Speed	Analog	1/16
Roll Rear Flywheel Speed	Analog	1/16
Roll Pneumatics Modulator	Analog	1/16
Roll Solenoid Duty Cycle	Analog	1/16
Pitch Solenoid Duty Cycle	Analog	1/16
Yaw Solenoid Duty Cycle	Analog	1/16
Roll (+) Solenoid	Digital	1/1
Roll (-) Solenoid	Digital	1/1
Pitch (+) Solenoid	Digital	1/1
Pitch (-) Solenoid	Digital	1/1
Yaw (+) Solenoid	Digital	1/1
Yaw (-) Solenoid	Digital	1/1

Table 4.A-27. Telemetry List for Attitude Control Subsystem (Cont'd)

Measurement Name	Type	Sampling Rate
Pitch Coarse Error	Analog	1/1
Pitch Fine Error	Analog	1/1
Pitch Flywheel Speed	Analog	1/16
Pitch Tach. Amp. Output	Analog	1/1
Pitch Pneumatic Modulator	Analog	1/1
0.25 and 0.5 Deg. and ± Pitch Bias	Analog	1/16
1 and 2 Deg. Pitch Bias	Analog	1/16
Pitch and Roll Unload and Pitch Mom. Bias Status	Analog	1/16
Low Volt. and Pneu. Interlocks	Analog	1/16
Interlock Bypass, and Yaw Fine Control Enable	Analog	1/16
Yaw Sun Sensor Mode Enable/Disable	Digital	3/16
Yaw Sun Sensor Amplifier	Analog	1/16
Yaw Tach. Amp. Output	Analog	1/1
Yaw Pneumatics Modulator	Analog	1/16
RMP No. 1 Control	Analog	1/16
RMP No. 2 Control	Analog	1/16
CLB ± 10V Supply	Analog	1/16
CLB ± 6V Supply	Analog	1/16
CLB Power Supply Voltage	Analog	1/16

Table 4.A-27. Telemetry List for Attitude Control Subsystem (Cont'd)

Measurement Name	Type	Sampling Rate
CLB Motor Driver Card Temp.	Analog	1/16
Rear Scanner OFF	Digital	1/16
Front Scanner OFF	Digital	1/16
Scanners ON	Digital	1/16
Orbit Adjust Mode Enable/Disable	Digital	1/16
YAW SUN SENSOR		
Rear Yaw Sun Sensor Case Temp.	Analog	1/16
Fwd. Yaw Sun Sensor Case Temp.	Analog	1/16
YAW RATE GYRO		
YRG Housing Temp.	Analog	1/16
YRG Wheel Speed	Analog	1/16
YRG Indicated Rate	Analog	1/1
RATE MONITORING PACKAGE NO. 1		
RMP Relay 1 Status No. 1	Analog	1/16
RMP Relay 2 Status No. 1	Analog	1/16
RMP Supply Voltage No. 1	Analog	1/16
RMP Motor Voltage No. 1	Analog	1/16
RMP Motor Current No. 1	Analog	1/16
RMP Heater Power No. 1	Analog	1/16
RMP Gyro Temperature No. 1	Analog	1/16

Table 4.A-27. Telemetry List for Attitude Control Subsystem (Cont'd)

Measurement Name	Type	Sampling Rate
RATE MONITORING PACKAGE NO. 1 (Cont'd)		
RMP Package Temperature No. 1	Analog	1/16
RMP Indicated Rate (Medium Resolution) No. 1	Analog	1/1
RMP Indicate Rate (High Resolution) No. 1	Analog	1/16
PNEUMATICS	Analog	1/16
Gas Tank Temperature	Analog	1/16
Manifold Temperature	Analog	1/16
Gas Tank Pressure (High)	Analog	1/16
Manifold Pressure (Low)	Analog	1/16
RATE MONITORING PACKAGE NO. 2		
RMP Relay 1 Status No. 2	Analog	1/16
RMP Relay 2 Status No. 2	Analog	1/16
RMP Supply Voltage No. 2	Analog	1/16
RMP Motor Voltage No. 2	Analog	1/16
RMP Motor Current No. 2	Analog	1/16
RMP Heater Power No. 2	Analog	1/16
RMP Gyro Temperature No. 2	Analog	1/16
RMP Package Temperature No. 2	Analog	1/16
RMP Indicated Rate (Medium Resolution) No. 2	Analog	1/1
RMP Indicate Rate (High Resolution) No. 2	Analog	1/16

Table 4.A-27. Telemetry List for Attitude Control Subsystem (Cont'd)

Measurement Name	Type	Sampling Rate
INITIATION TIMER		
Initiation Timer Reset ON/OFF	Digital	3/16
Initiation Timer Paddle Unfold	Digital	3/16
Initiation Timer T15	Analog	1/16
Initiation Timer T50	Analog	1/16
SOLAR ARRAY DRIVE	Analog	1/16
SAD Left Mtr. Winding Volt.	Analog	1/16
SAD Right Mtr. Winding Volt	Analog	1/16
SAD Left Phase Switch	Digital	3/16
SAD Right Phase Switch	Digital	3/16
SAD Left Tach. Output	Analog	1/1
SAD Right Tach. Output	Analog	1/1
SAD Left Rate Bias High/Normal	Digital	3/16
SAD Right Rate Bias High/Normal	Digital	3/16
SAD Left Mtr. Housing Temp.	Analog	1/16
SAD Right Mtr. Housing	Analog	1/16
SAD Left Mtr. Winding Temp.	Analog	1/16
SAD Right Mtr. Winding Temp.	Analog	1/16

Table 4. A-27. Telemetry List for Attitude Control Subsystem (Cont'd)

Measurement Name	Type	Sampling Rate
SOLAR ARRAY DRIVE (Cont'd)		
SAD Left Fwd. S/S Temp.	Analog	1/16
SAD Left Rear S/S Temp.	Analog	1/16
SAD Right Fwd. S/S	Analog	1/16
SAD Right Rear S/S Temp.	Analog	1/16
SAD Left S/S Preamp. Output	Analog	1/16
SAD Right S/S Preamp. Output	Analog	1/16
SAD Left -15V Converter	Analog	1/16
SAD Right -15 Converter	Analog	1/16
SAD Left Housing Pressure	Analog	1/16
SAD Right Housing Pressure	Analog	1/16
SOLAR ARRAY DRIVE OUTPUTS (EXTERNAL ISM)		
Cosine Pot. Left Signal Output	Analog	1/1
Cosine Pot. Right Signal Output	Analog	1/1
Segmented Switch Left ON/OFF	Digital	3/16
Segmented Switch Right ON/OFF	Digital	3/16
Day Signal ON/OFF	Digital	3/16
Night Signal ON/OFF	Digital	3/16
SAD Left Power Unfused/Fused	Digital	3/16
SAD Right Power Unfused/Fused	Digital	3/16

Table 4. A-27. Telemetry List for Attitude Control Subsystem (Cont'd)

Measurement Name	Type	Sampling Rate
ACS STRUCTURAL TEMPERATURES		
Temperature 6 Base Plate	Analog	1/16
Temperature 7 Base Plate	Analog	1/16
Temperature 8 Base Plate	Analog	1/16
Temp. 1 Thermal Box	Analog	1/16
Temp. 2 Thermal Box	Analog	1/16
Temp. 3 Thermal Box	Analog	1/16
Temp. 4 Thermal Box	Analog	1/16
Temp. 5 Thermal Box	Analog	1/16
ATTITUDE SENSING		
Roll Signal	Analog	3/1
Pitch Signal	Analog	3/1
Temperature	Analog	1/16
Sun Presence	Digital	1/16
Sun Presence	Digital	1/16
MAGNETIC MOMENT ASSEMBLY		
Pitch Set/Reset	Digital	1/1
Yaw Set/Reset	Digital	1/1
Roll Set/Reset	Digital	1/1
Polarity +	Digital	1/1

Table 4.A-27. Telemetry List for Attitude Control Subsystem (Cont'd)

Measurement Name	Type	Sampling Rate
MAGNETIC MOMENT ASSEMBLY (Cont'd)		
Polarity -	Digital	1/1
Start ON/OFF	Digital	1/1
Enable ON/OFF	Digital	1/1
Coarse/Fine Step	Digital	1/1
Pitch Moment	Analog	1/16
Yaw Moment	Analog	1/16
Roll Moment	Analog	1/16
Rod Temperature	Analog	1/16
Electronics Temperature	Analog	1/16
Reference Voltage	Analog	1/16

APPENDIX 4.B

ERTS COMMAND AND DATA HANDLING BREADBOARD TEST REPORT

4.B.1 INTRODUCTION

The proposed ERTS Command and Data Handling (C&DH) subsystem utilizes for the most part, flight-qualified MSFN-Unified S-Band and STADAN-VHF command equipment. There are, however, two basic requirements for the ERTS system which require some C&DH design modifications, and hence, breadboard design verification. First, it was required, for operational reasons, that the spacecraft command subsystem be capable of operating with a signal from either the STADAN-VHF command link or the MSFN-USB command link. Since the basic ground modulation techniques and data rates for these two links are different, it was necessary to design a spacecraft "Command Integrator Unit" which accepts inputs from either link and converts them to a signal compatible with the proposed Nimbus Command/Clock subsystem.

Second, the telemetry data requirements necessitated an additional subcarrier in the USB coherent downlink signal. The additional intermodulation products resulting from this subcarrier have been thoroughly analyzed. The objective of the breadboard testing performed here is to verify the spectral calculations and to experimentally evaluate the probability of a ground station false lock resulting from this additional subcarrier.

In order to evaluate these two new functions, a complete S-band and VHF C&DH Subsystem was breadboarded and tested. Implementation and evaluation of this breadboard, in the available time, was made possible by a joint effort between the General Electric Comapny and Collins Radio Company, utilizing to the greatest extent possible, existing USB, STADAN, and Nimbus checkout equipment. A simplified breadboard system function block diagram is shown in Figure 4.B-1, and photographs of the setup are shown in Figures 4.B-2, 4.B-3, and 4.B-4. The ground station simulation was provided by Collins and consists for the most part of a standard Apollo unified S-Band transponder test set. The pseudo random code Ranging Subsystem simulator provides for a complete system transit time measurement using a 500 kbps PRN ranging code. The pulse pattern generator and MSFN update generator provides the standard bi-phase modulated, subbit encoded command message, with the capability of generating any 64-bit command message. A baseband unit combines the PRN range code and the command signal (on the 70 kHz subcarrier) for modulation of the S-Band (2106.4 MHz) PM transmitter. This transmitter has a calibrated output attenuator capable of providing a singal at the transponder input of -20 dBm to -140 dBm. The S-Band transponder is also provided by Collins radio and is a modification of an engineering model USBE transponder developed on company funds. A detailed transponder breadboard block diagram is shown in Figure 4.B-5. The transponder is phasecoherent with a 221/240 trunaround ratio. Uplink 70 kHz data is demodulated in a 70 kHz. discriminator. The uplink ranging signal is demodulated, filtered and can be remodulated on the downlink for ranging measurements. The transponder also accepts a composite spectrum of modulated subcarriers (300 kHz, 1024 kHz, and 1250 kHz) for low-level phase modulation on the downlink transmitter Modulation levels on these subcarriers are individually controlled.

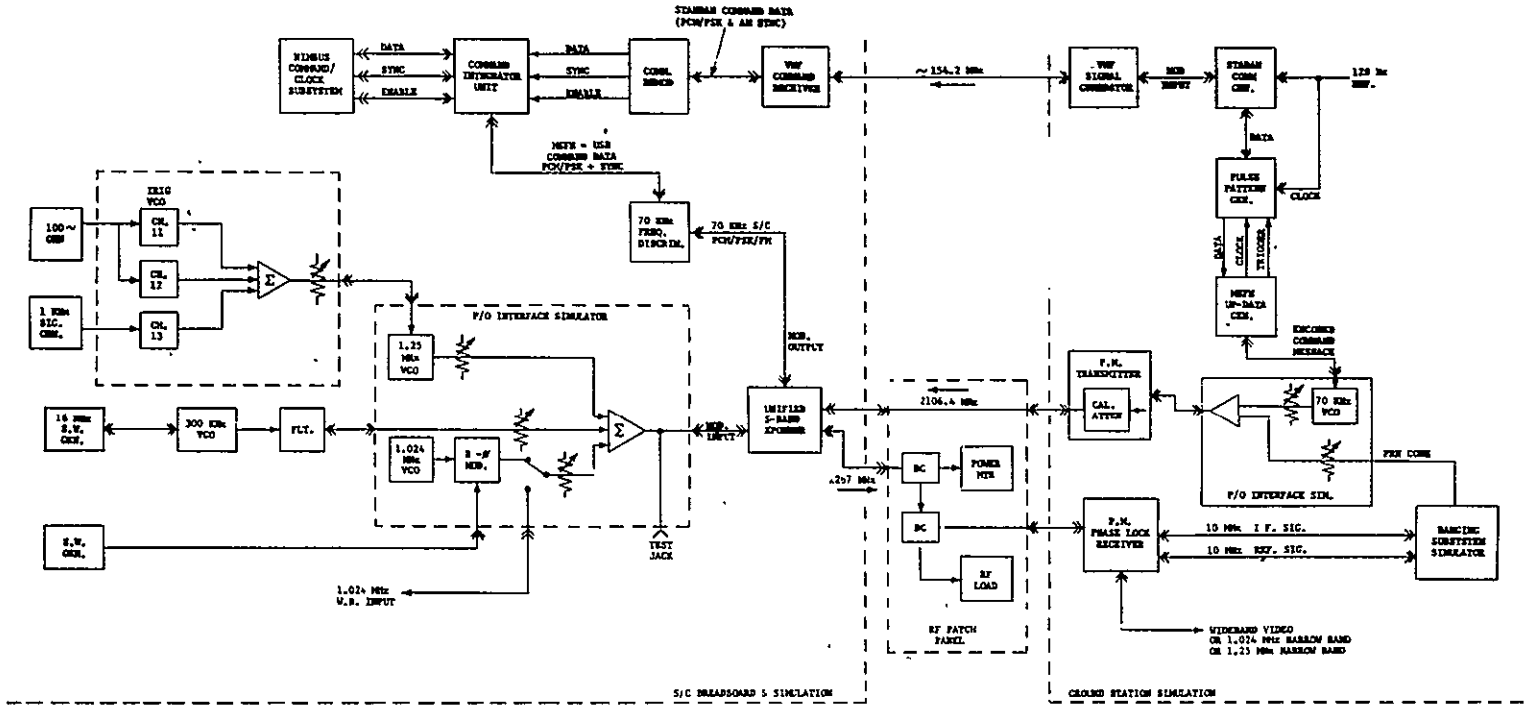

Figure 4.B-1. ERTS C&DH Subsystem Breadboard Block Diagram

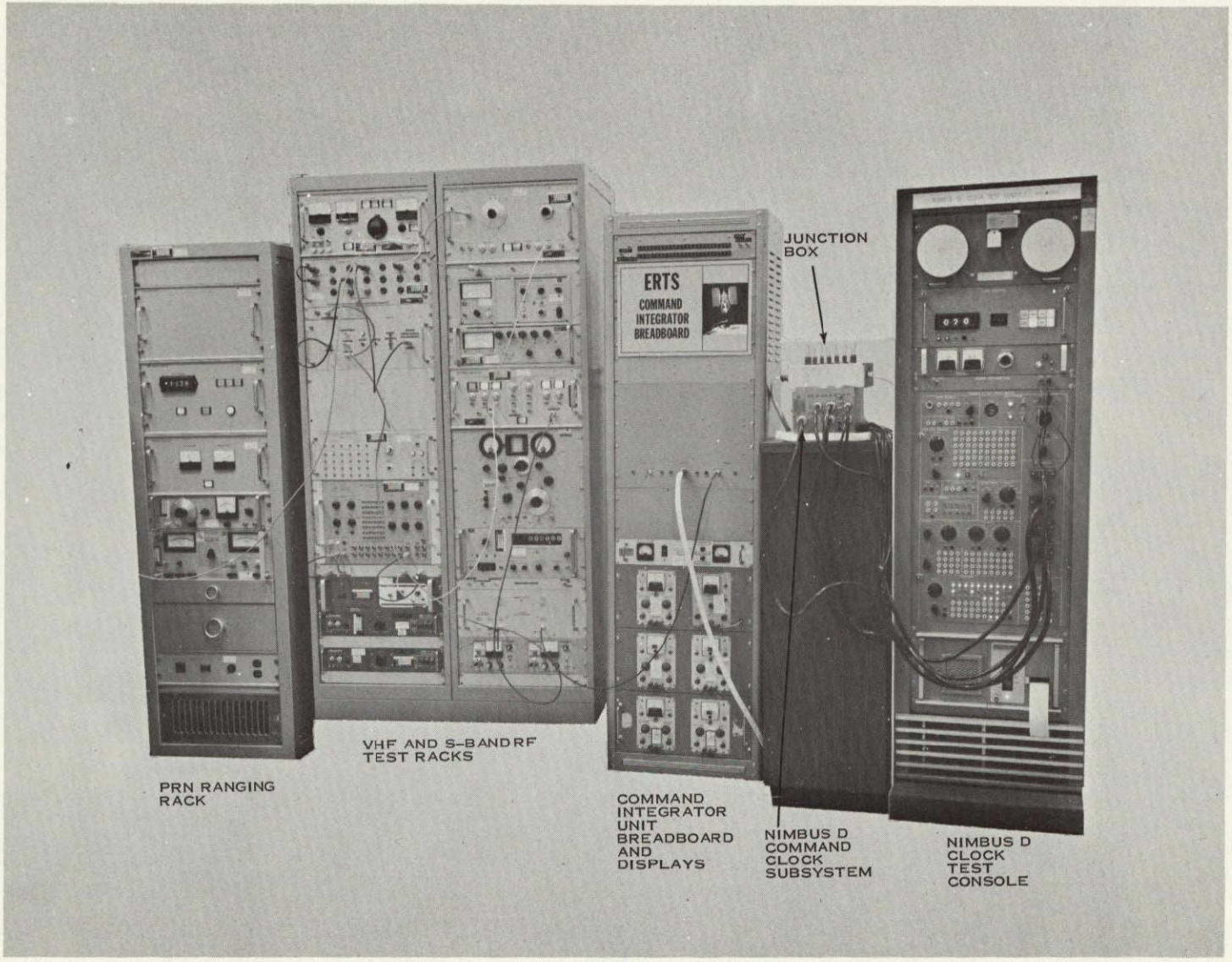

Figure 4. B-2. ERTS C&DH Subsystem Breadboard Set-up

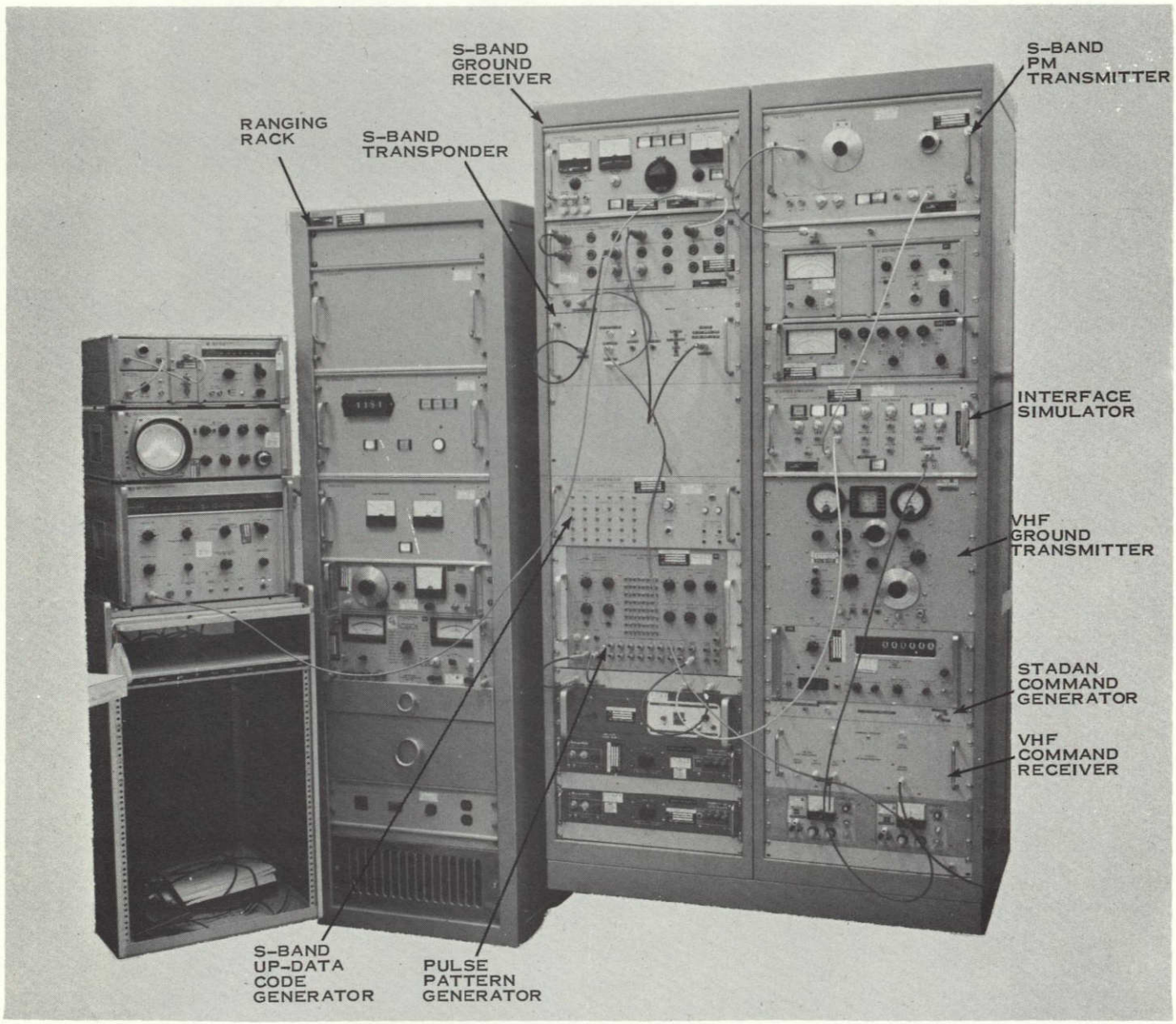

Figure 4. B-3. Ranging, Transponder and Ground Station Breadboard Racks

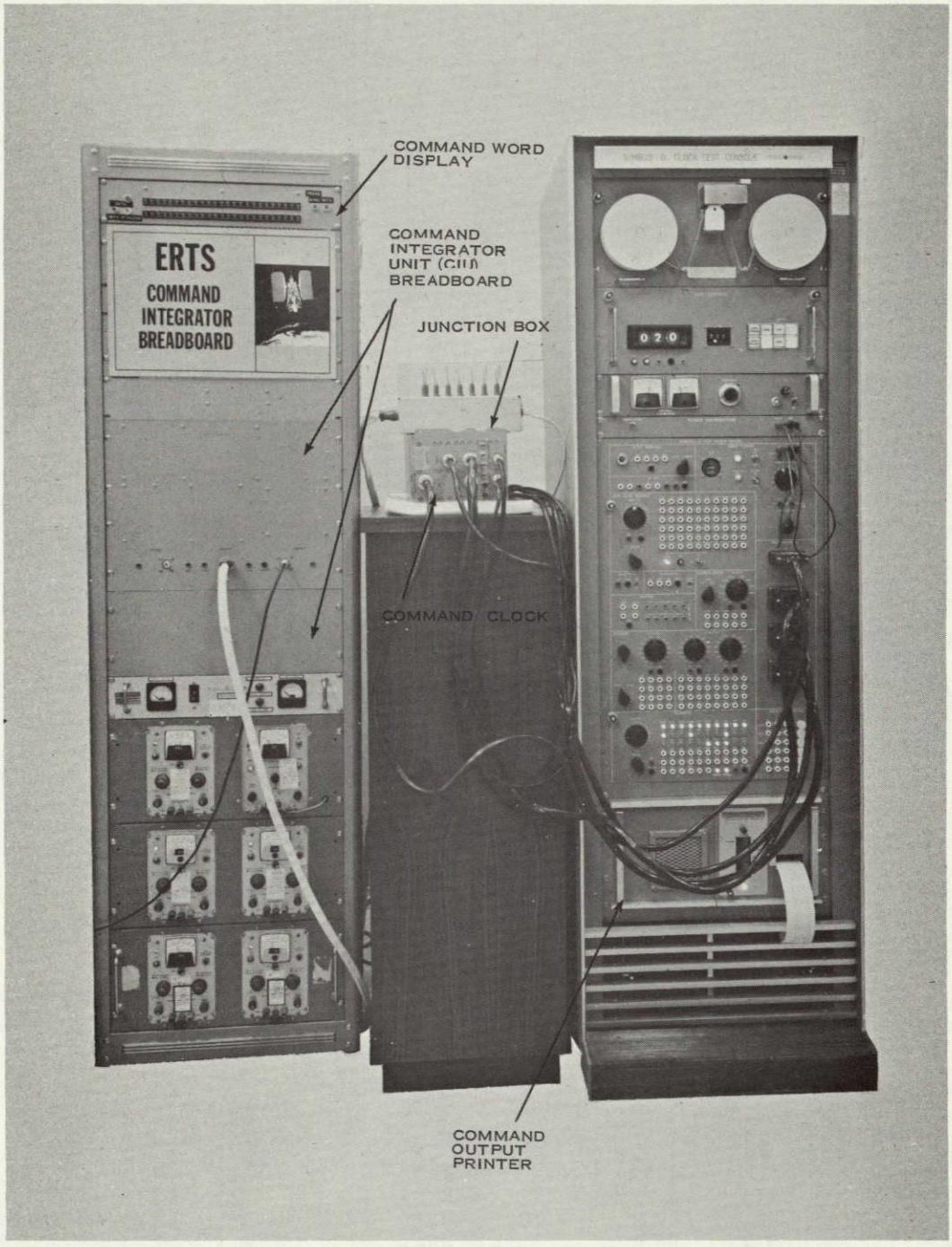

Figure 4. B-4. Command Integrator Unit (CIU) Breadboard, Nimbus D Command/Clock Subsystem, and Clock Test Console

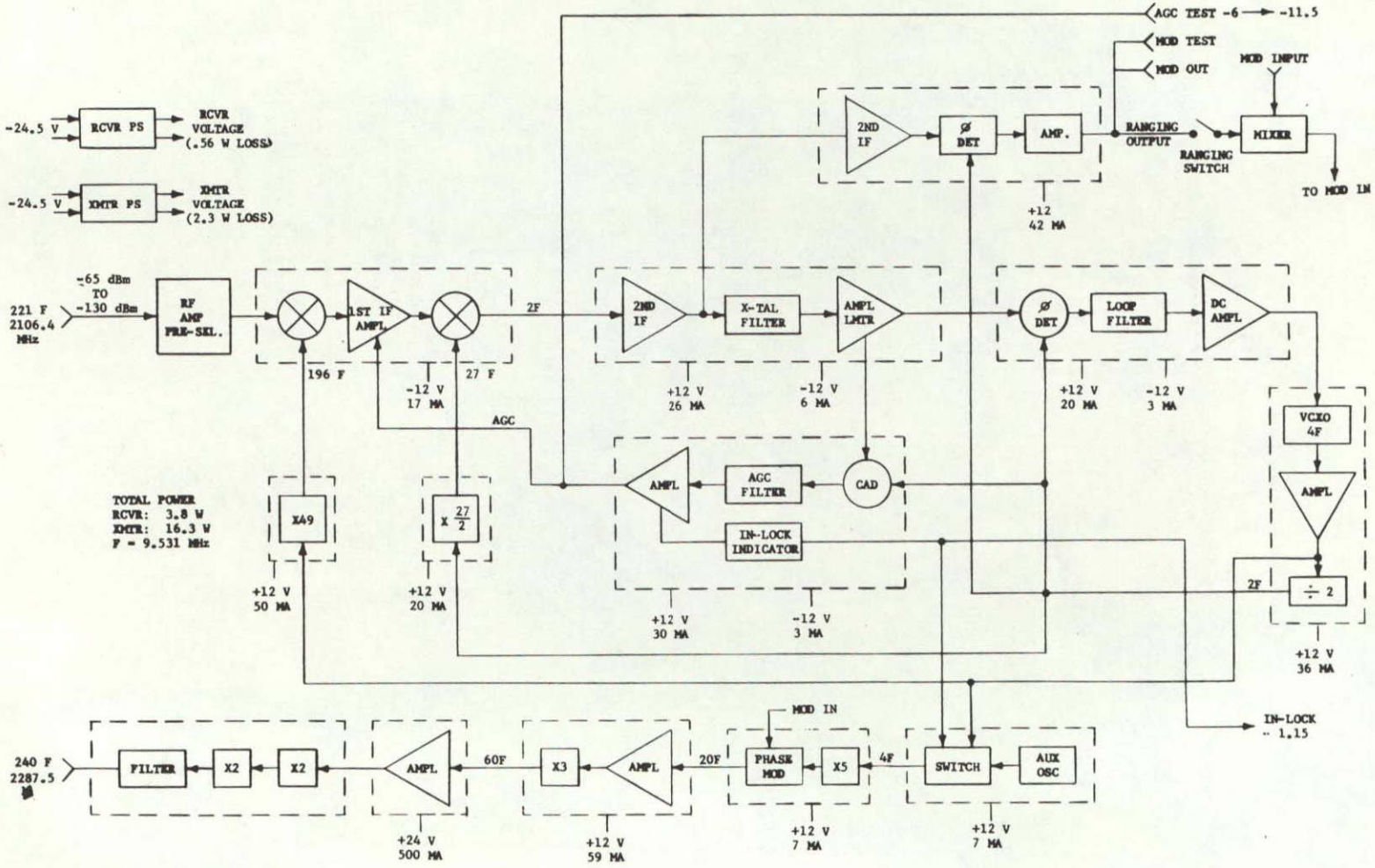

Figure 4.B-5. ERTS Breadboard USBE Transponder

A phase-locked, S-band ground receiver is also supplied as part of the Collins USB test set, which demodulates the three telemetry downlink subcarriers.

The pulse pattern generator can also supply the same 64-bit pulse sequence to a simulated STADAN command generator which uses them to FSK modulate a subcarrier (8.0 and 8.6 kHz) which is in turn 50 percent AM-modulated by a 128 Hz synchronization sinewave. This standard STADAN command signal is then AM-modulated on a VHF signal generator (HP model 608D) to simulate the STADAN VHF command uplink. This VHF signal is converted to baseband in a VHF command receiver breadboard, and then demodulated in an FSK demodulator breadboard to provide a "data" signal, a " sync" signal, and a third "enable" signal which simply indicates the presence of the 8 kHz signal. The proposed system will base the "enable" output on the presence of the correct data address, as well as a signal present; however, this design addition was made too late to incorporate in the breadboard.

The Command Integrator Unit (CIU) was breadboarded by GE, and accepts either the MSFN command signal (PCM/PSK + Sync) or the demodulated STADAN Command signal, and properly interfaces either signal with the Nimbus Command/Clock Subsystem. The Nimbus Command/Clock and associated display and checkout equipment was made available from the Nimbus test area by NASA and used to demonstrate the interface compatibility with either command link. A simplified block diagram of the CIU breadboard is shown in Figure 4.B-6.

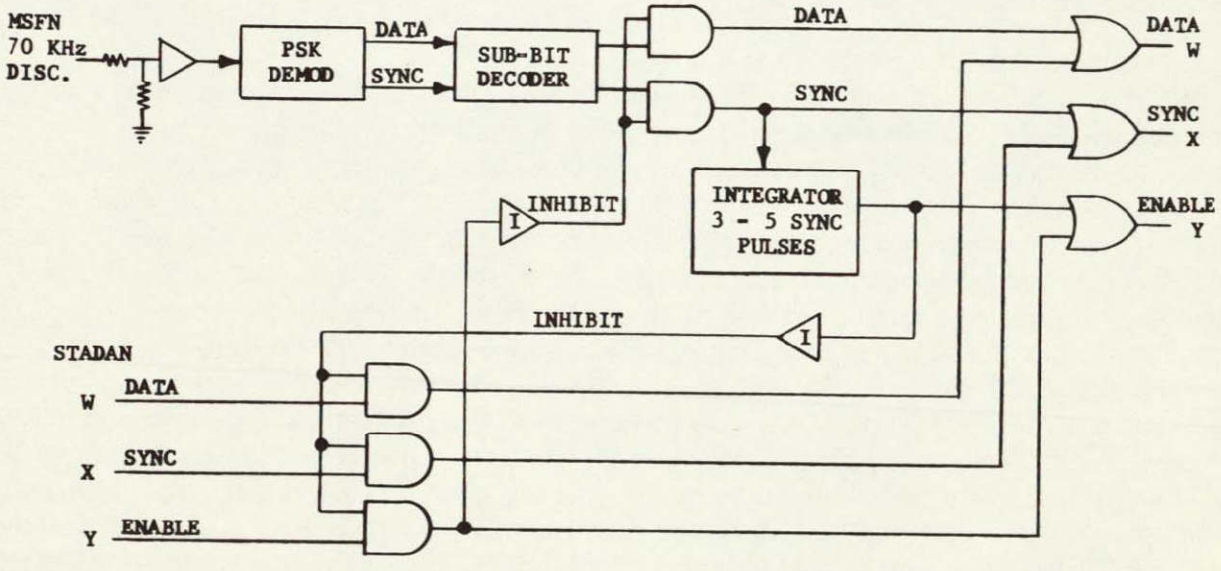

Figure 4.B-6. Functional Block Diagram of Command Integrator Unit (C10) Breadboard

4.B-2 TEST SUMMARY

The detailed test results are presented in Section 4.B-3. A brief summary of the tests and conclusions reached are presented here.

1. A 64-bit repetitive command message was generated and encoded in both the STADAN, VHF and MSFN Unified S-Band formats. The S-Band signal was received and demodulated in an S-Band transponder breadboard, and interfaced with the ERTS Command Integrator Unit (CIU) breadboard. The CIU output was checked and found compatible with the Nimbus Command/Clock Subsystem. Likewise, the VHF command signal was received in a receiver breadboard, and interfaced with the CIU. Recordings of input data versus CIU output data showed proper operation of both the MSFN and STADAN command links through the ERTS CIU breadboard unit.

2. Next, the Nimbus Command/Clock Subsystem and associated test rack were interfaced with the ERTS CIU breadboard output. A single, 64-bit command message (14 sync bits plus 50 command bits) was transmitted through both the VHF STADAN command link, and the MSFN S-Band command link, and produced correct command printouts on the Nimbus Command/Clock test rack printer.

3. The composite downlink S-Band telemetry spectrum was generated and all intermodulation products in a ±2 MHz band about the carrier recorded. Subcarriers used were 300 kHz, 1024 kHz, and 1250 kHz. Comparison of measured spectral components with computed values showed excellent agreement.

4.B.3 DETAILED TEST RESULTS

4.B.3.1 MSFN UNIFIED S-BAND COMMAND LINK

The USB command link was set up as shown in Figure 4.B-7. The PM transmitter output attenuator was adjusted for a nominal signal level at the USB transponder input of approximately -72 dBm (total signal power). Figure 4.B-8 shows recorded waveforms at key points in the breadboard. Photo 8A of Figure 4.B-8 shows the PCM NRZ 200 bps data at the pulse pattern generator output, along with subbit encoded data in the update generator. A subcode of 01101 corresponds to a data "1", and a 10010 corresponds to a data "0". Photo 8B of Figure 4.B-8 shows the modulated waveform at the 70 kHz discriminator output, which is identical to the output of the updata generator except for level. Photo 8C of Figure 4.B-8 shows the data and syncronization outputs of the CIU. Both data and syncronization outputs vary between 0^V and -15^V, with 0^V corresponding to a data "0" and -15^V to a data "1". The -15^V level is limited by the supply voltage level, and corresponds to an unloaded output level. This voltage drops by 4 to 5 volts when loaded into the Nimbus Command/Clock subsystem. As the photo shows, rise and fall times are significantly less than the 0.5 msec Command/Clock specification, and measured jitter on the syncronization sample edge (0 to -15^V transition) is an order of magnitude less than the 1.8 msec specification.

The breadboard also used an HP7858A, 8-channel chart recorder to simultaneously record the input data (pulse pattern generator output) and the CIU output "data", "sync", and "enable" lines. The pattern generator was set up for a 64-bit (eight-8bit words) repetitive pattern as shown in the following table.

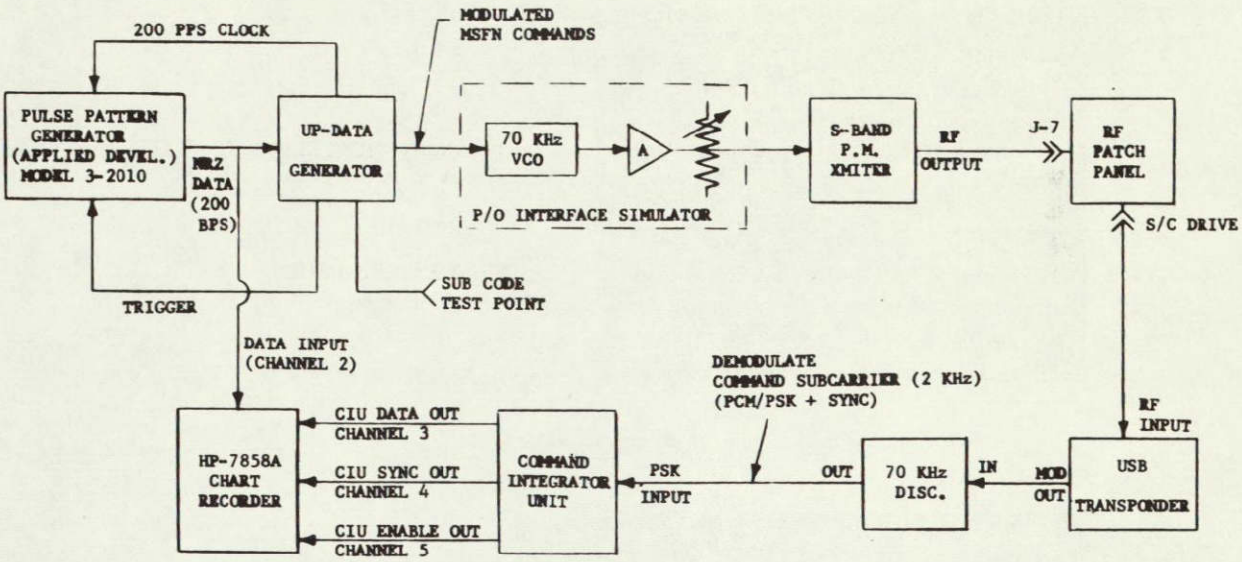

Figure 4.B-7. MSFN USB Command Breadboard Test

INPUT COMMAND MESSAGE								
Word \ Bit	1	2	3	4	5	6	7	8
1	1	1	1	1	1	1	1	1
2	0	0	0	0	0	0	0	0
3	1	0	1	0	1	0	1	0
4	0	1	0	1	0	1	0	1
5	1	1	1	1	1	1	1	1
6	0	0	0	0	0	0	0	0
7	1	1	0	0	1	0	0	1
8	0	0	0	0	0	0	0	0

The resulting recording is shown in Figure 4.B-9. Running the chart at maximum speed (200 mm/sec) allowed the data transitions to be separated; however, the approximate 100 Hz response of the recorder results in the squarewave forms (shown in Figure 8C) to be severely

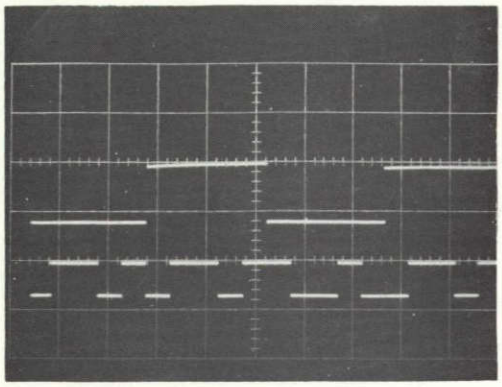

8A

DATA INPUT (PATTERN GEN. OUTPUT)
5V/cm & 2 m sec/cm

SUB CODE TEST POINT
5V/cm & 2 m sec/cm

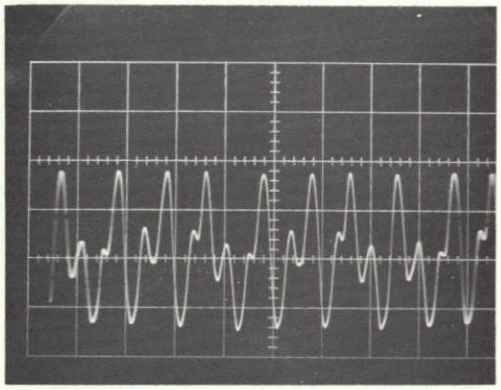

8B

OUTPUT OF 70 KHz DISCRIMINATOR
(XPONDER SIGNAL LEVEL - 72dBm)
2V/cm & 1 m sec/cm

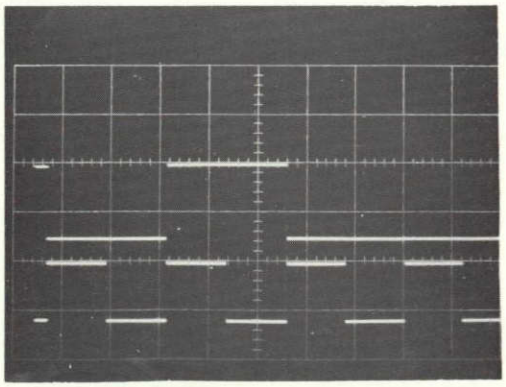

8C

CIU DATA OUTPUT (UNLOADED)
10V/cm & 2 m sec/cm (0V TO -15V)

CIU SYNC OUTPUT (UNLOADED)
10V/cm & 2 m sec/cm (0V TO -15V)

Figure 4. B-8. S-Band Command Channel Waveforms

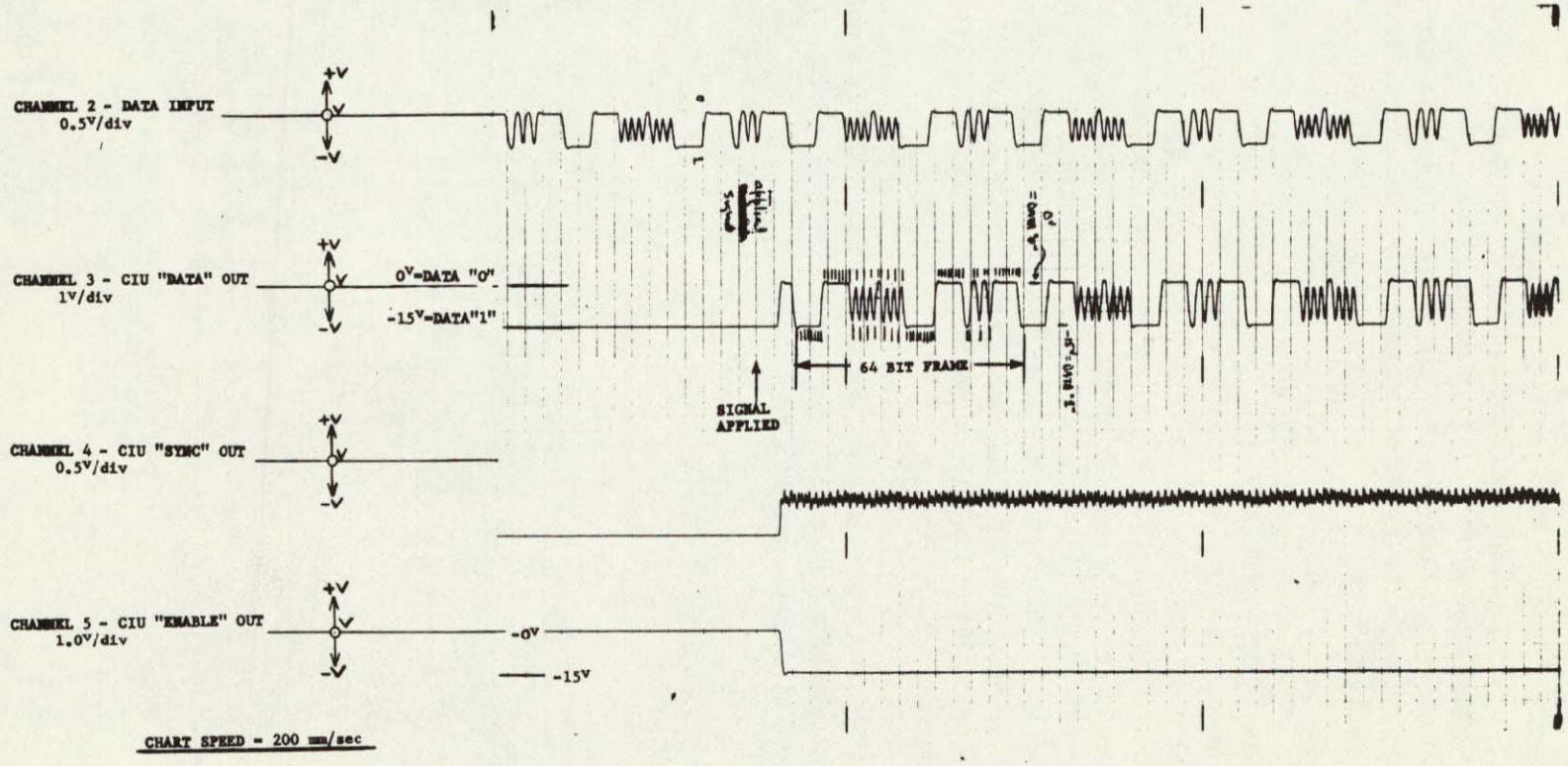

Figure 4. B-9. S-Band Command Channel Chart Recording

rounded. This is especially true for the sync signal which runs at a rate of 200 bps. It is still possible using the sync signal as reference to identify the output "1's" and "0's" which correspond exactly with the transmitted message shown above. A careful examination of the trace shows about a bit and a half delay between the transmitted and recreated data words. This results from a one bit delay in the subcode generator, and approximately a half-bit delay in the subbit decoder in the CIU.

4.B.3.2 STADAN VHF COMMAND LINK

The VHF command link was set up as shown in Figure 4.B-10, and waveforms at key points in the breadboard recorded (see Figure 4.B-11). Photo 11A of Figure 4.B-11 shows the STADAN modulated command signal (PCM/FSK/AM) at the VHF transmitter input, and also at the VHF command receiver output. A difference between the 8.0 kHz frequency and the 8.6 kHz frequency is seen because of the beat frequencies established in the chopped mode on the oscilloscope display. This frequency difference cannot be seen on a single line display. Photo 11B of Figure 4.B-11 shows the CIU data output as compared to the input FSK signal. A delay of 30 to 60 degrees (of the 128 Hz) can be seen between the FSK switching points and the data transition times.

Photo 11C shows the CIU data output and sync outputs, showing 0^{V} for a data "0" and approximately -15^{V} (supply voltage) for a data "1". As with the S-band system, both rise time and jitter are significantly better than the specified values.

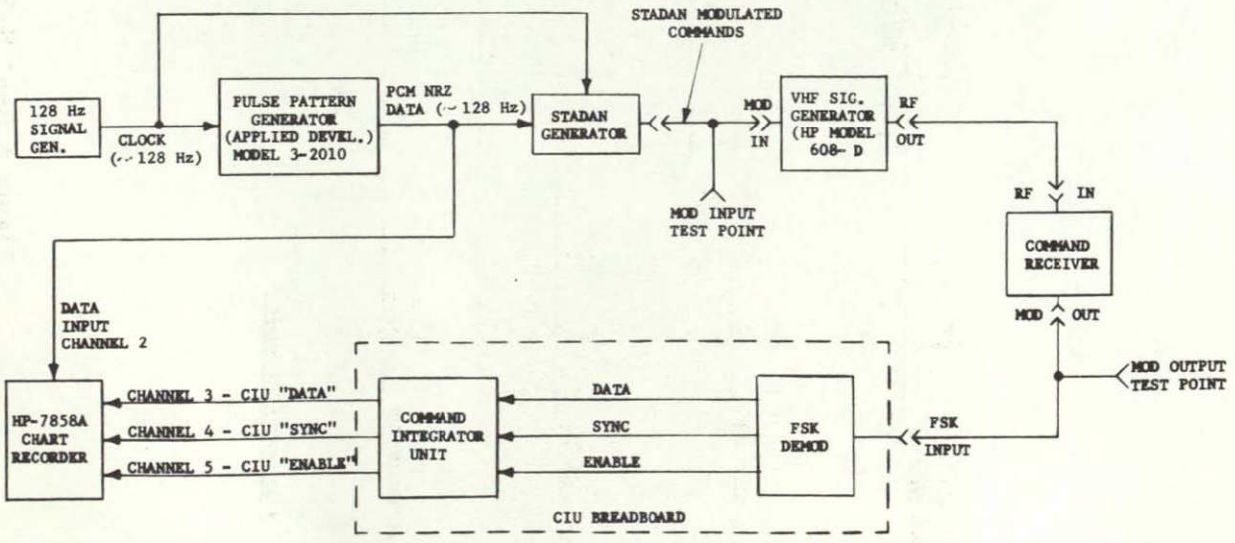

Figure 4.B-10. STADAN VHF Command Breadboard Test

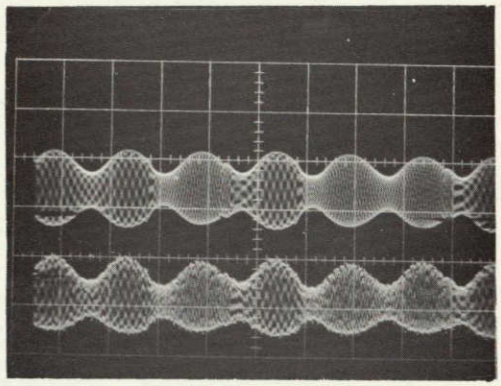

11A

5 m sec/cm sweep

VHF XMIR MODULATION
INPUT SIGNAL 1^V/cm

COMMAND RECEIVER MOD.
OUTPUT SIGNAL 2^V/cm

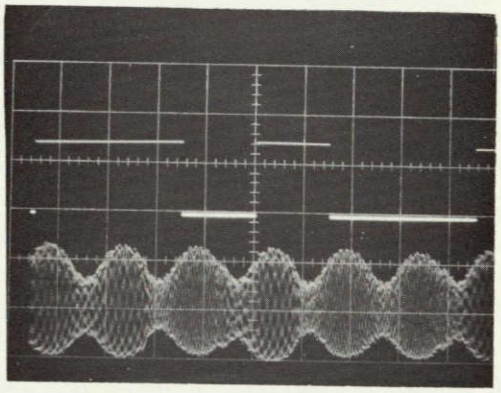

11B

5 m sec/cm sweep

CIU DATA OUTPUT SIGNAL
10^V/cm (0^V & -15^V)

CIU FSK INPUT SIGNAL
2^V/cm

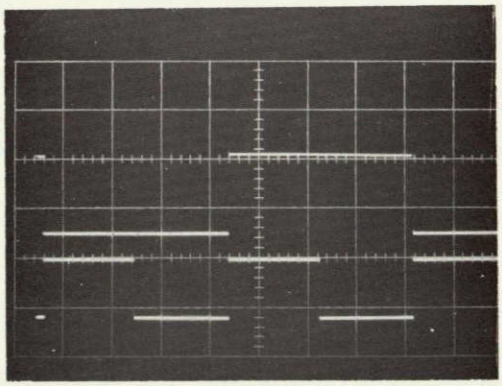

11C

2 m sec/cm sweep

CIU DATA OUTPUT SIGNAL
10^V/cm (0^V & -15^V)

CIU SYNC OUTPUT SIGNAL
10^V/cm (0^V & -15^V)

Figure 4. B-11. VHF Command Channel Waveforms

As in the S-Band system, a chart recording was taken showing "Data In", and CIU "data", "sync", and "enable" outputs (see Figure 4. B-12). The VHF recording is easier to read than the S-band Recording, because the bit rate is slower (128 Hz versus 200 Hz.) This is especially true in the 128-cycle sync signal. The true "data" and "sync" output waveform are shown in Photo 11C of Figure 4. B-11. The same data was transmitted as in the S-Band test, and the recording shows the same output sequence. A slight delay can be observed between the input data and the output data; but for VHF, this is much less than a bit delay.

4. B. 3. 3 NIMBUS COMMAND/CLOCK SUBSYSTEM INTERFACE TESTS

The Nimbus D command/clock subsystem was interfaced with the CIU breadboard as shown in Figure 4. B-13. The system was arranged so that a command message could be transmitted through either the S-band or VHF links and interfaced via the CIU breadboard with the Nimbus D Command/Clock subsystem. Figure 4. B-4 shows the CIU breadboard rack, the Nimbus C clock Subsystem, the interconnection junction box and the Nimbus D Clock Test Console. The J-Box allows the Nimbus Clock Subsystem to be connected to the test rack in a normal manner. Using the junction box, the CIU Data, Sync, and Enable outputs may be connected to the Nimbus Clock in place of those normally supplied by the test rack, all other lines remaining unchanged. This approach minimized the changes to the Nimbus Clock/Test Rack interface. As Figure 4. B- shows, a gating circuit has been added at the output of the pulse pattern generator. A push button switch on this panel gates out a single 64-bit word from the pattern generator to be transmitted through the system. When the message is not being transmitted, the S-band system transmits all ones, while the VHF system transmits all zeros. This single frame mode was necessary to simulate a realistic command sequence for the Nimbus Command/Clock subsystem with the test equipment available. The operating sequence is as follows:

1. The RF link (VHF or S-band) is interrupted (by removing the uplink RF or modulation) and the CIU enable drops to 0^{V} out.

2. The RF link is re-established and the CIU enable line to the Nimbus clock drop to -10^{V}. This starts the Nimbus Command/Clock looking for a sync word of 13 data zeros followed by a data one.

3. The message gate button is activated sending a single 64-bit word consisting of a 14-bit sync signal (13 zeros and a one) followed by a legitmate 50-bit command word.

4. The Nimbus Clock Test Rack printer records the commanded message.

5. The command message can now be recoded, and Steps 1 through 4 repeated.

Using the above procedure and the MSFN USB command link, the pulse pattern generator was set for the command word shown in Table 4. B-1. The resulting Clock Printout showed 777, corresponding to the command data number. This was repeated with the same result.

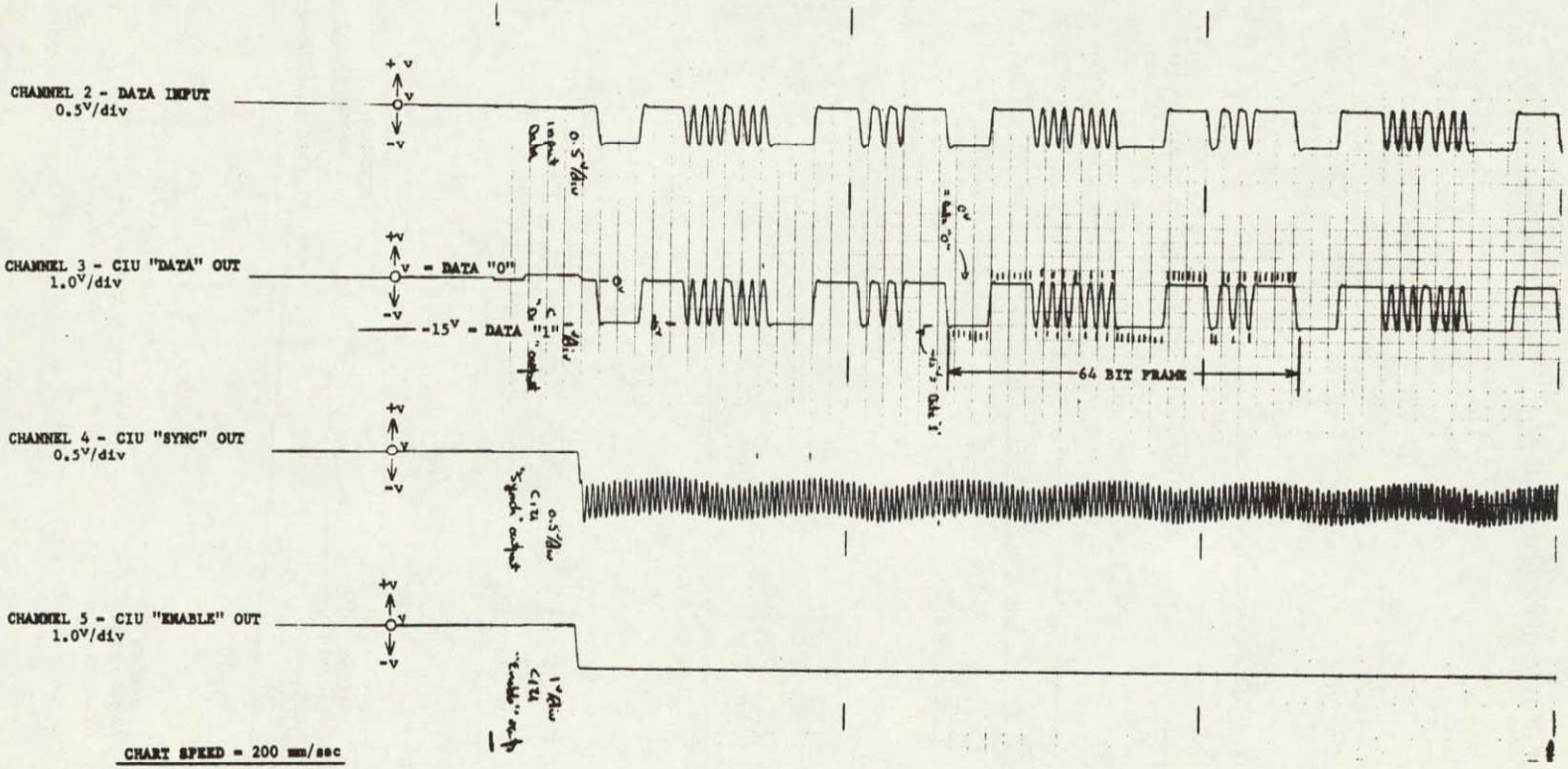

Figure 4. B-12. VHF Command Channel Chart Recordings

The Command "DATA" (9-bit number and 9-bit complement) was then changed from all ones to:

$$\underbrace{0\ 1\ 0}_{2} \qquad \underbrace{1\ 0\ 1}_{5} \qquad \underbrace{0\ 1\ 0}_{2}$$

Three printouts were obtained, all showing 252.

The same process was repeated, using the VHF STADAN command link with the following results:

9-Bit Number	Printout	No. Trials
$\underbrace{111}_{7}\ \underbrace{111}_{7}\ \underbrace{100}_{4}$	774	4
111 111 101	775	1
010 101 010	252	2

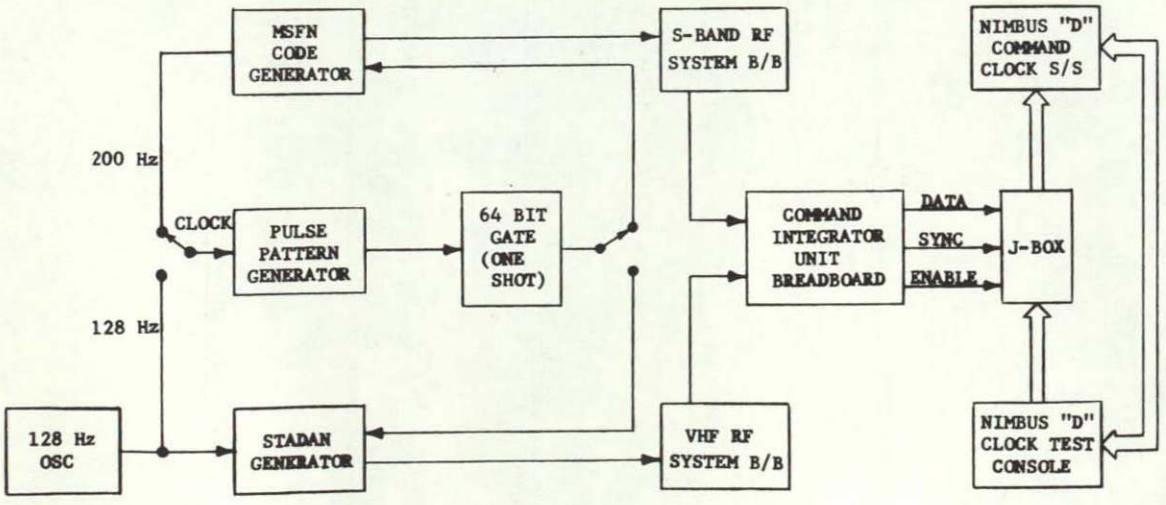

Figure 4. B-13. CIU - Command/Clock Interface Test

Table 4. B-1. Command Format

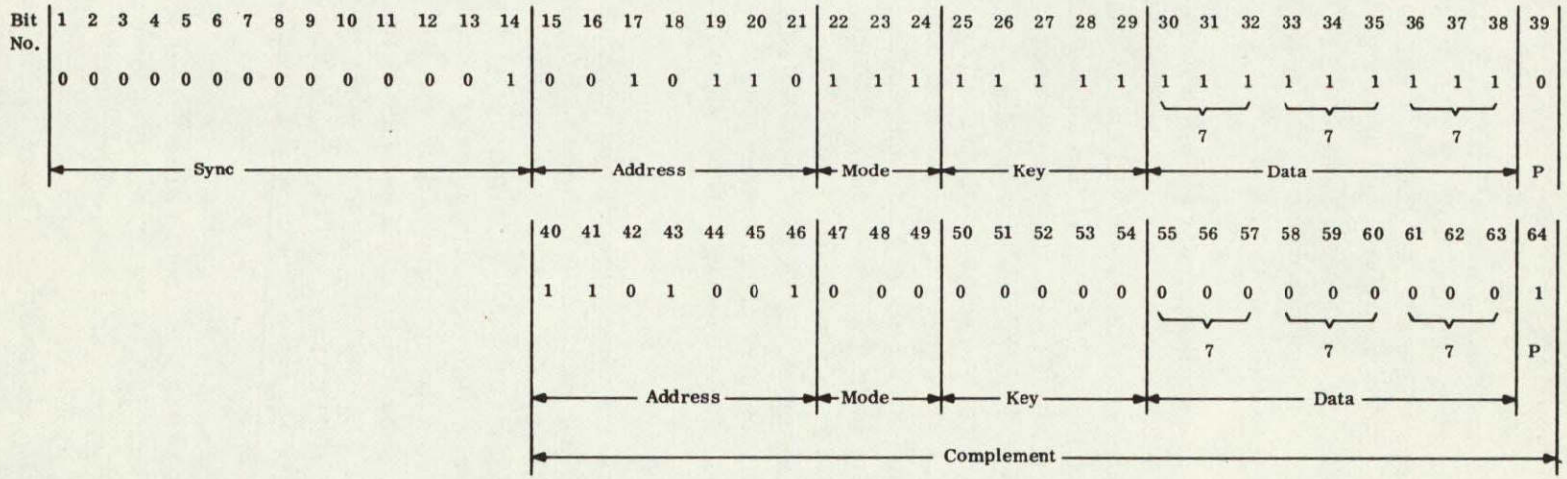

4.B.3-4 S-BAND DOWN-LINK SPECTRAL MEASUREMENTS

The MSFN Unified S-band breadboard was set up as shown in Figure 4.B-14. An HP model 8551B spectrum analyses RF unit, along with an HP 852A display unit was used to monitor the S-band transponder downlink spectrum, with various modulating subcarriers present. The downlink spectral displays were photographed and are displayed in Figures 4.B-15, 4.B-16, and 4.B-17. In all photos a sweep speed of 10 msec/division was used along with a a 1 kHz IF bandwidth. All displays also used a log scale providing 10 dB/major division on the vertical scale. The horizontal sweep range is recorded on each photo, and in each case the carrier component is in the center of the sweep.

The downlink subcarriers were applied one at a time and the modulation indexes set at the deviation shown in Table 4.B-2. Spectral measurements of the unmodulated carrier and the carrier, with each of the subcarrier tones applied one at a time, are shown in Figure 4.B-14, Photos A through D. Two points of interest in these photos should be noted. First, the unmodulated carrier shows a small ($\sim$ -50 dB with respect to the carrier) spurious carrier modulation at approximately 2.4 MHz. This is thought to be an oscillation caused by a slight mistuning of the final transmitter varactor stage, resulting from the equipment vibration in tranmission to the GE plant. This component was small enough that it did not effect the desired spectral measurements, so no effort has been made to correct it. The second point of interest is a slight assymetry in the higher-order sidebands of the 300 kHz modulated spectrum (Figure 4.B-14 Photo-D). Since the 1024 and 1250 kHz modulated spectra are perfectly symmetrical, this 300 kHz assemetry probably results from the higher modulation index, indicating a slight modulator nonlinearity at higher modulation levels. The first and second sideband terms in the photos can be seen to agree with the predicted levels in Table 4.B-2 to within 1 dB.

Figure 4.B-16 shows the spectra when two or three tones are applied simultaneously. Figures 4.B-16 Photos 16A and B, result from the use of 1024 and 1250 kHz subcarriers simultaneously. Figure 4.B-16, Photo 16B, is an expand horizontal base (300 kHz/cm) showing more detail around the carrier. This photo shows no internal products near the carrier, except the first-order difference frequency of 226 kHz (1250 kHz-1024 kHz) which is approximately 20 dB down from the carrier. Figures 4.B-16, Photos 16C and 16D, show the result when the 300 kHz subcarrier is added to the downlink. Figure 4.B-16, Photo 16D, is an expanded version (300 kHz/cm) of Figure 4.B-16, Photo 16C. This shows an additional first-order intermodulation (IM) product at 74 kHz (300 kHz-(1250-1024) kHz) about 26 dB down from the carrier. This agrees well with the computer IM product, as will be shown later.

Figure 4.B-17 shows the downlink spectrum, when the 70 kHz and PRN code are also transponded. Figure 4.B-17, Photo 17A, is the same as Figure 4.B-16, Photo 16D, only on a more expanded scale (100 kHz/cm) and has the 1024, 1250, and 300 kHz subcarriers applied. Figure 4.B-17, Photo 17B, shows the downlink spectrum with only the 70 kHz subcarrier being transponded (on 100 kHz/cm sweep). Figure 14.B-17, Photo 17C, combines Figure 4.B-17, Photos 17A and 17B, showing the composite downlink with 1024, 1250, 300 kHz subcarriers and the 70 kHz command subcarrier transponded. The 70 kHz spacecraft and the 74 kHz IM product can just be separated on this display. Figure 4.B-17, Photo 17D, shows the resulting spectrum when the 500 kbps PRN code is also transponded.

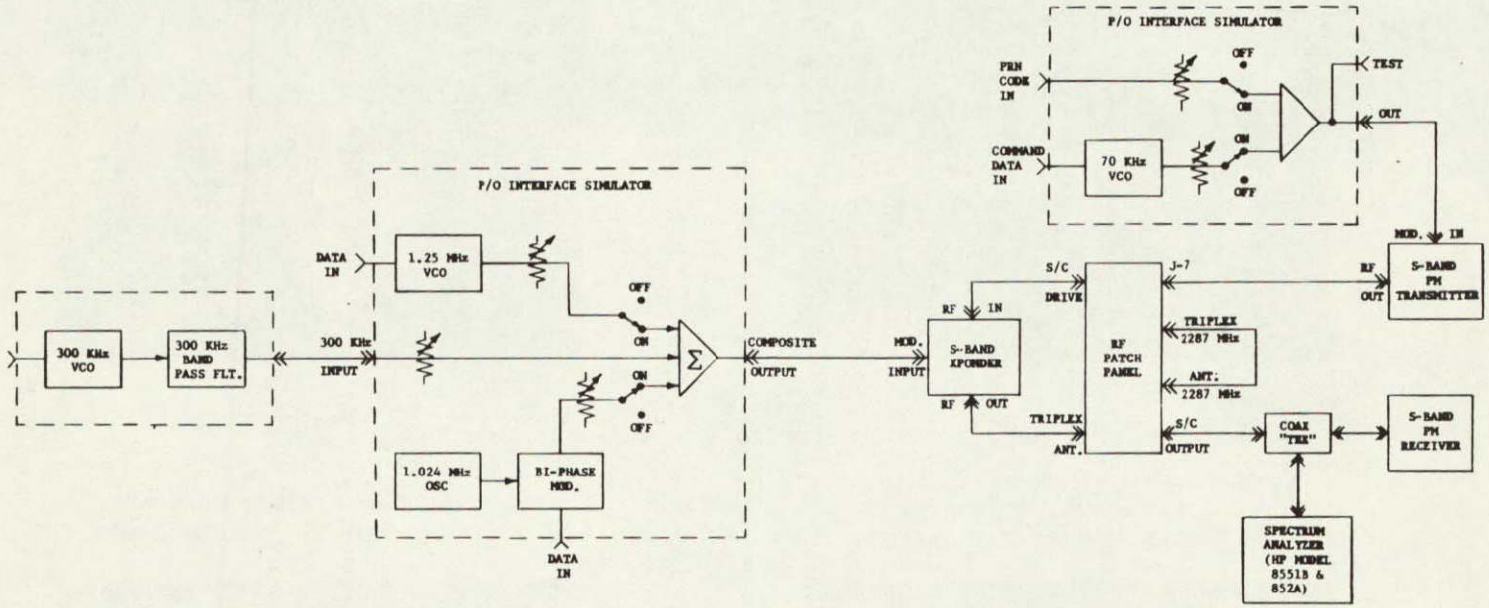

Figure 4. B-14. S-Band Downlink Spectral Test Set-up

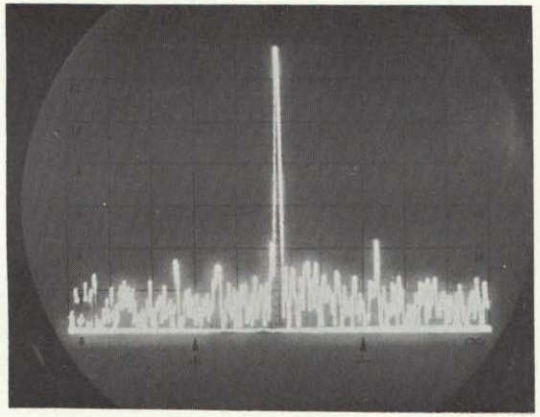

15A UNMODULATED CARRIER
1 MHz/cm sweep & 10 dB/cm scale

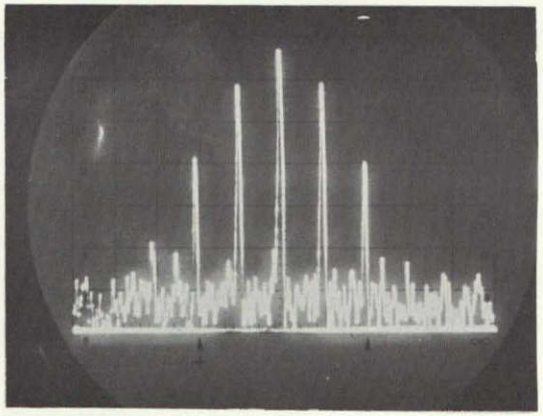

15C CARRIER + 1.024 MHz S/C
PM MODULATED 0.69 RAD.
1 MHz/cm sweep & 10 dB/cm scale

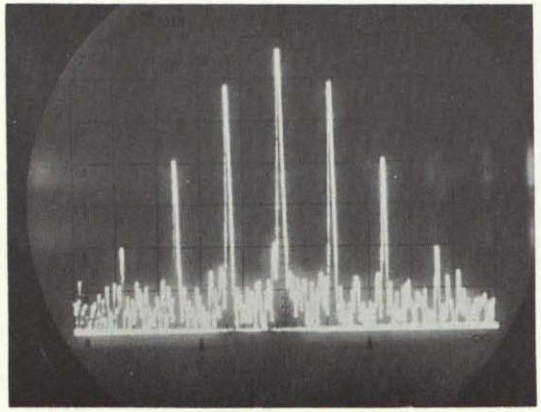

15B CARRIER + 1.250 MHz S/C
PM MODULATED 0.76 RAD.
1 MHz/cm sweep & 10 dB/cm scale

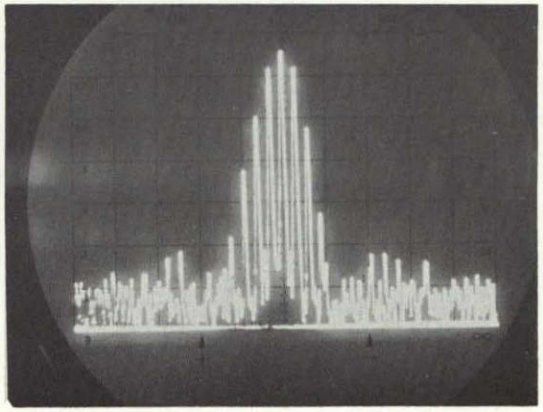

15D CARRIER + 300 KHz S/C
PM MODULATED 0.92 RAD.
1 MHz/cm sweep & 10 dB/cm scale

Figure 4. B-15. S-Band Single Tone Spectra

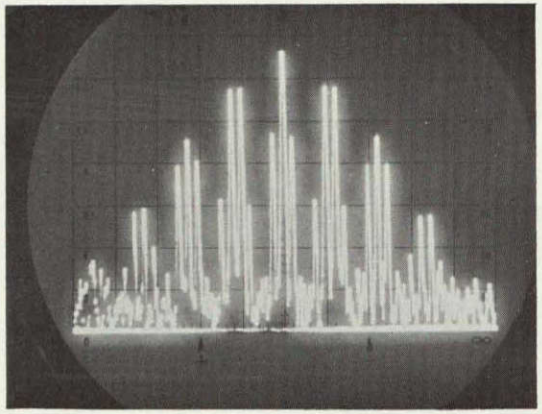

16A COMPOSITE 1024 & 1250 KHz S/C
PM MODULATED ON CARRIER
1 MHz/cm sweep & 10 dB/cm scale

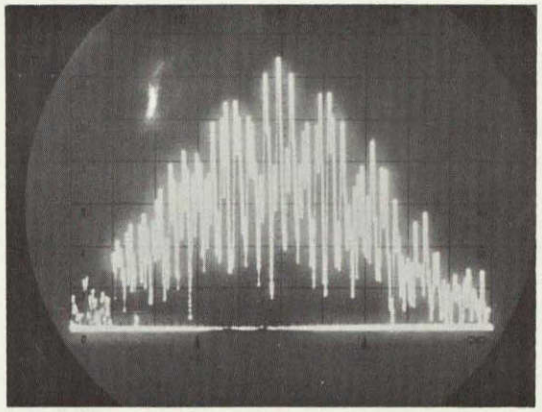

16C COMPOSITE 1024, 1250 & 300 KHz S/C
PM MODULATED ON CARRIER
1 MHz/cm sweep & 10 dB/cm scale

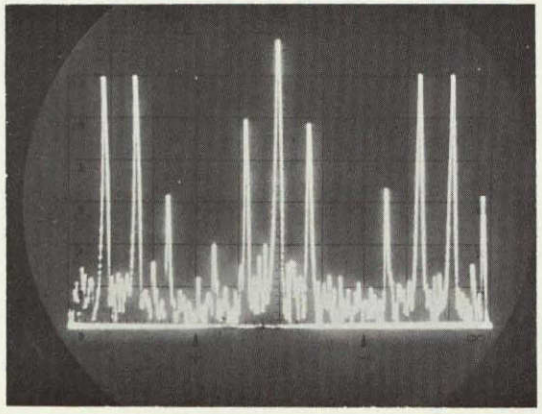

16B COMPOSITE 1024 & 1250 MHz S/C
PM MODULATED ON CARRIER
300 KHz/cm sweep & 10 dB/cm

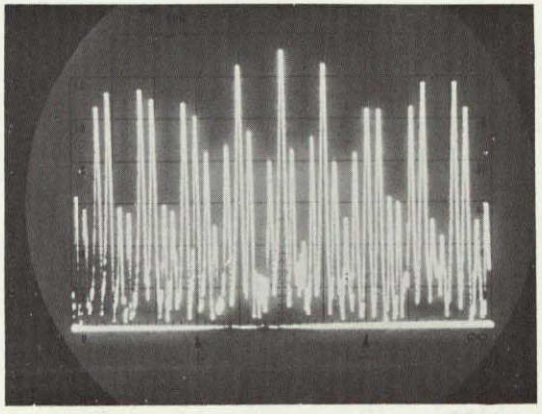

16D COMPOSITE 1024, 1250 & 300 KHz S/C
PM MODULATED ON CARRIER
300 KHz/cm sweep & 10 dB/cm scale

Figure 4. B-16. S-Band Composite Tone Spectra

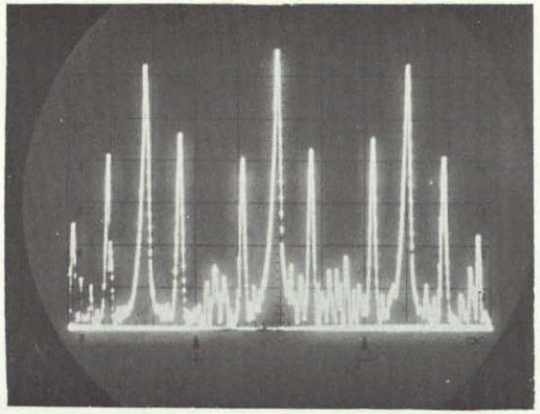

17A COMPOSITE 1024, 1250, & 300 KHz S/C
PM MODULATED ON CARRIER
100 KHz/cm sweep & 10 dB/cm

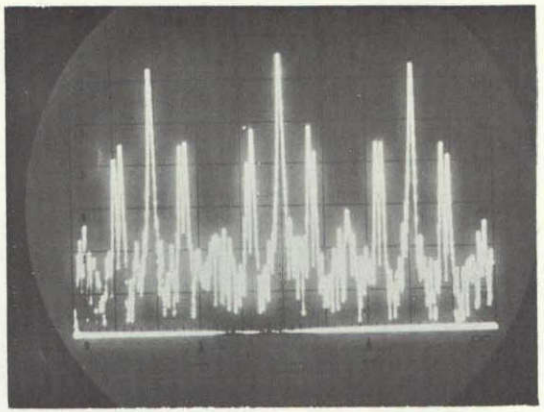

17C COMPOSITE 1024, 1250, & 300 KHz S/C
WITH 70 KHz TRANSPONDED ON DOWN LINK
(16A + 16B)
100 KHz/cm sweep & 10 dB/cm

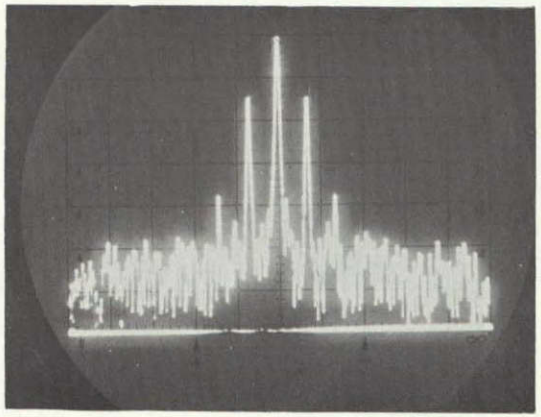

17B S-BAND DOWN LINK WITH 70 KHz
COMMAND S/C TRANSPONDED
100 KHz/cm sweep & 10 dB/cm

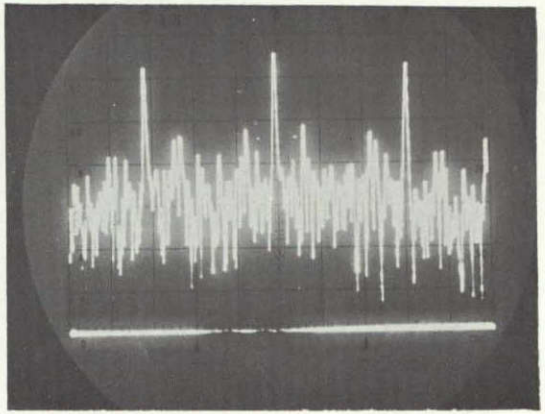

17D COMPOSITE DOWN LINK - 1024, 1250, 300 KHz
S/C PLUS 70 KHz & PRN CODE TRANSPONDED
100 KHz/cm sweep & 10 dB/cm

Figure 4.B-17. S-Band Composite Tone + Command Turn-around Spectra

Table 4. B-2. Downlink Modulation Indexes

Subcarrier Frequency	Modulation Index (Rad)	Carrier Component Level (dB)	First-Side Band-Level (dB)	Second-Side Band Level (dB)
300 kHz	0.92	-2.0 (0)	-7.7 (-5.7)	-20.4 (-18.4)
1024 kHz	0.69	-1.1 (0)	-9.8 (-8.7)	-24.8 (-23.7)
1250 kHz	0.76	-1.3 (0)	-9.0 (-7.7)	-23.7 (-22.4)
70 kHz (Transponded)	0.18 (down)	-0.1 (0)	-22.0 (-21.9)	-48.0 (-47.9)
PRN Code (Transponded) (500 kbps rate)	0.33 (down)	-0.2 (0)	-15.8 (-15.6)	-38.4 (-38.2)

In addition to the spectrum pictures, each of the measurable spectral components in the modulated downlink spectrum were recorded using the 30 kHz/cm sweep range on the analyzer. These measurements are recorded in Table in Table 4. B-3, and can be seen to agree with Photos 16C, 16D, and 17A. Also tabulated in Table 4. B-3 are the computed sideband levels expected from a perfectly linear PM modulator with the 1024, 1250, and 300 kHz subcarriers applied at the input. Since there are some amplitudes, as well as frequency discrepancies, between the measured and computed sidebands, the major components (everything above -40 dB) have been plotted in Figure 4. B-18. This plot shows good frequency agreement on some components but approximately a 35 to 40 kHz on other components. In speaking of the modulated terms, it is convenient to identify them by a mode number which identifies which fundamental tones mixed to produce the particular term of interest. The first number (in the mode number) represents the 300 kHz subcarrier; the second number, the 1024 kHz subcarrier; and the third number, the 1250 kHz subcarrier. Thus, the fundamental tones are:

Mode No.	Frequency (kHz)
100	300
010	1024
001	1250

Likewise, there are

110	$(1024 \pm 300) = 724$ or 1324
111	$300 \pm (1250 - 1024) = 74$ or 526 (All other terms are out of the range of interest.
021	$2(1024) - 1250 = 798$ Etc.

Looking at Figure 4. B-18, it is seen that the fundamental tones at 1024 kHz and 1250 kHz appear to be 35 to 40 kHz low when measured on the spectrum analyzer. These frequencies were not checked with a counter and may indeed be off several kHz. However, both subcarriers are low by about the same amount, and the 300 kHz appears to be on frequency. Thus, it would be expected that any IM product, depending on the difference of 1024 kHz and 1250 kHz, to be on frequency; while those terms, depending on only one of the two subcarriers, to be off by approximately 40 kHz. Another way to evaluate this is: all terms with mode numbers ending in -00, -11, -22, -33, --- should be close in frequency to the predicted frequency. However, those terms ending in -01, -10, -21, -12, --- (i.e., a difference of one) should have a measured frequency low by approximately 40 kHz. For those higher-order terms with a difference of two (i.e., -02, -20, -13, -31, etc.) a frequency error of approximately 80 kHz would be expected. When the data in Figure 4. B-18 and Table is corrected in this manner, excellent frequency agreement is registered between measured and computed terms.

There are also varying amplitude discrepancies between measured and predicted levels. Two factors help to explain this: First, we note that the 300 kHz fundamental is approximately 4 dB above the predicted level resulting from a slightly higher modulation used in the measurements than that used in the calculation. Thus, we would expect those IM terms which depend on the 300 kHz to be slightly higher than computed, which appears to hold true (see terms 200, 110, 210). The second factor is a slight spectral assymetry in the upper and lower sidebands (see Figure 4. B-16, Photos 16C and 16D) probably resulting from a slight modulation nonlinearity. Since only the terms on one side of the carrier were measured, this could account for several dB variations, especially in the higher-order terms.

In conclusion, the measured intermodulation (IM) product terms showed excellent agreement with the predicted values for all terms of interest.

APPENDIX 4.C

PRELIMINARY EXPERIMENTAL RESULTS

A breadboard model of the shaped-beam antenna, selected for pattern study, is shown in Figure 4.C-1. The turnstile is fed by a 50-ohm coax transmission line which contains a quarter-wavelength split-balun. The turnstile is located about 2.5 inches above an 8-inch diameter reflector plate. Measured axial-ratio patterns of this model at 2275 MHz, in a free space environment, are shown in Figure 4.C-2. The patterns were taken in the two principal planes ($\phi = 0°$, $90°$) and a diagonal plane ($\phi = 45°$) of the antenna to illustrate the beam-shaping obtained to-date. The $\phi = 0°$ and $90°$ -plane patterns correspond to the planes in which the orthogonal pair of dipoles are located. These patterns were taken with the arms of the turnstile tilted 30° from being co-planar. These results are shown to indicate that modest beam-shaping can be obtained with this antenna design. Work is proceeding to obtain the predicted beam shape and the gain. The results of this experimentation will be reported on in the Addendum to the study to be submitted in April 1970.

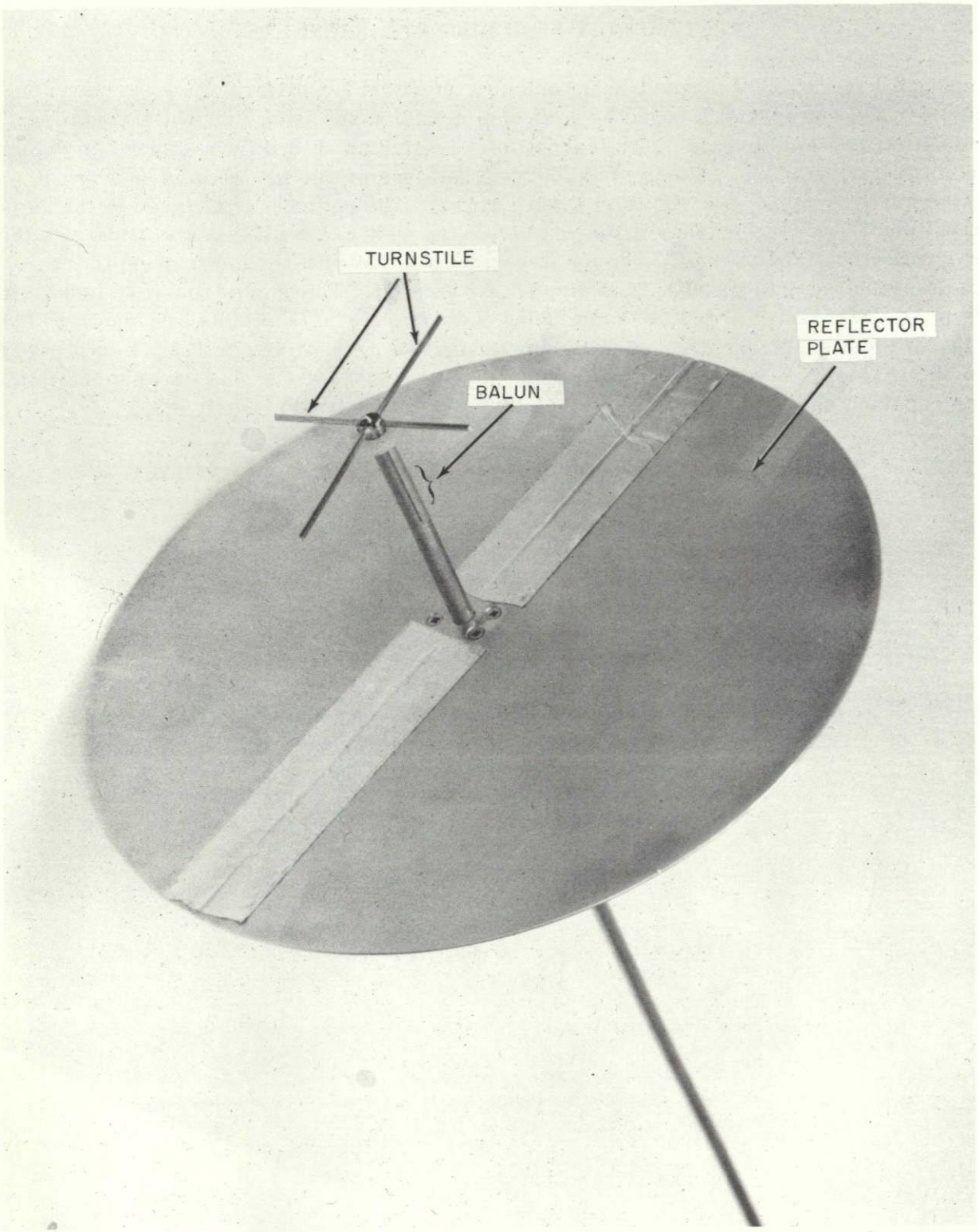

Figure 4.C-1. Breadboard Model of Shaped Beam Antenna

Table 4. B-3. S-Band Spectrum - Measured Versus Computed

Measured Data		Computed Data		
Frequency (kHz)	Level (dB)	Mode	Frequency (kHz)	Level (dB)
80	-25	111	74	-26
226	-25	011	226	-21
306	-6	100	300	-10
380	-26	210	424	-28
425	-60			
440	-58	322	448	-84
465	-44	022	452	-50
525	-27	111	526	-26
605	-15	200	600	-22
685	-15	110	724	-19
740	-58	021	798	-35
765	-40	323	802	-99
825	-37	211	826	-39
905	-16	101	950	-18
985	-12	010	1024	-13
1045	-58	222	1052	-68
1075	-43	121	1098	-42
1135	-45	311	1126	-55
1215	-13	001	1250	-12
1295	-16	110	1324	-19
1360	-58	311	1374	-55
1380	-45	220	1448	-46
1440	-43	012	1476	-35
1520	-15	101	1550	-18
1600	-29	210	1624	-31
1655	-58	211	1674	-39
1690	-35	120	1748	-34
1745	-45	112	1776	-41
1775	-60	031	1822	-55
1825	-30	201	1850	-30
1905	-30	020	2048	-28
1985	-30	102	2200	-32

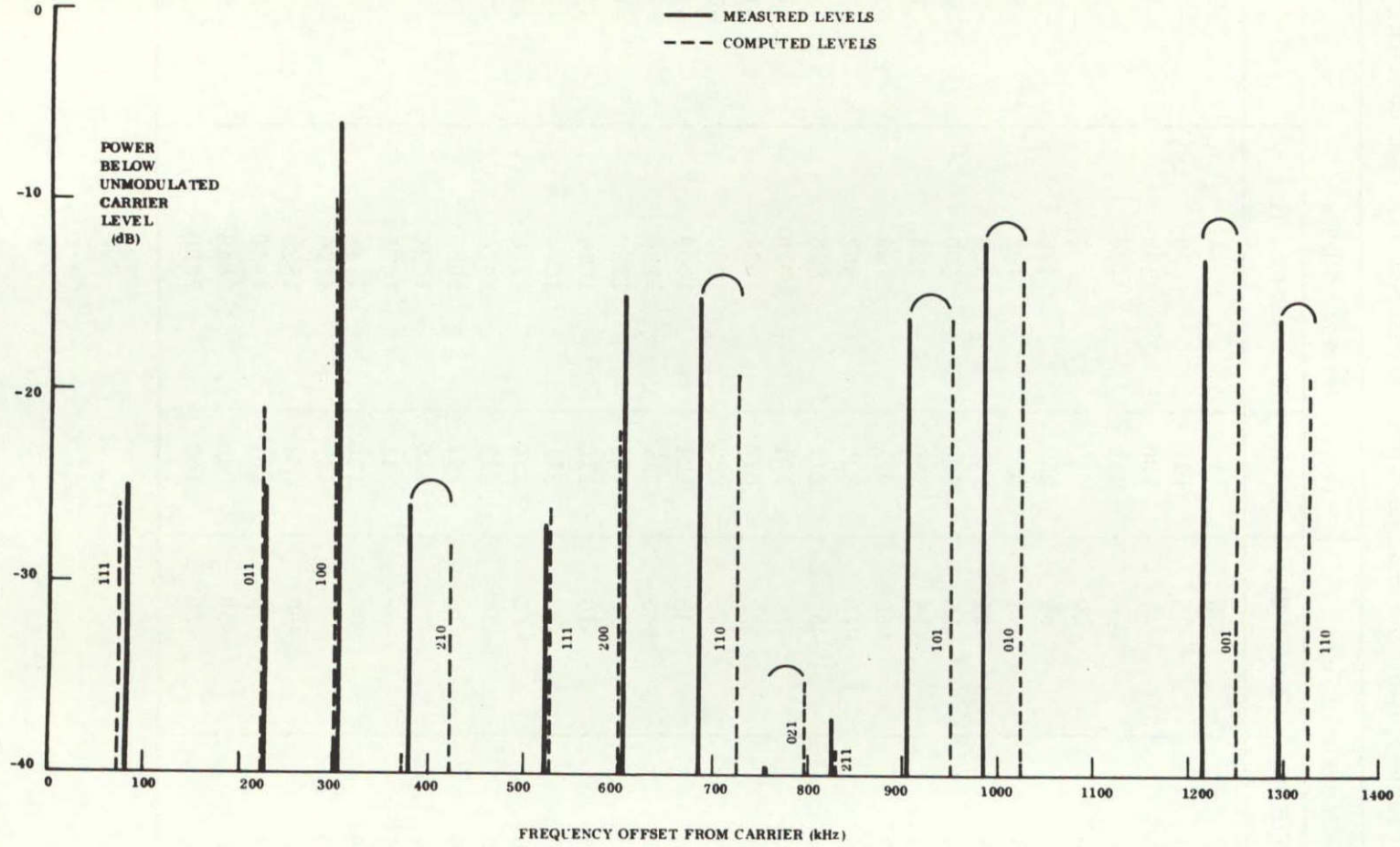

Figure 4. B-18. S-Band Composite Modulated Spectrum Measured Versus Computed

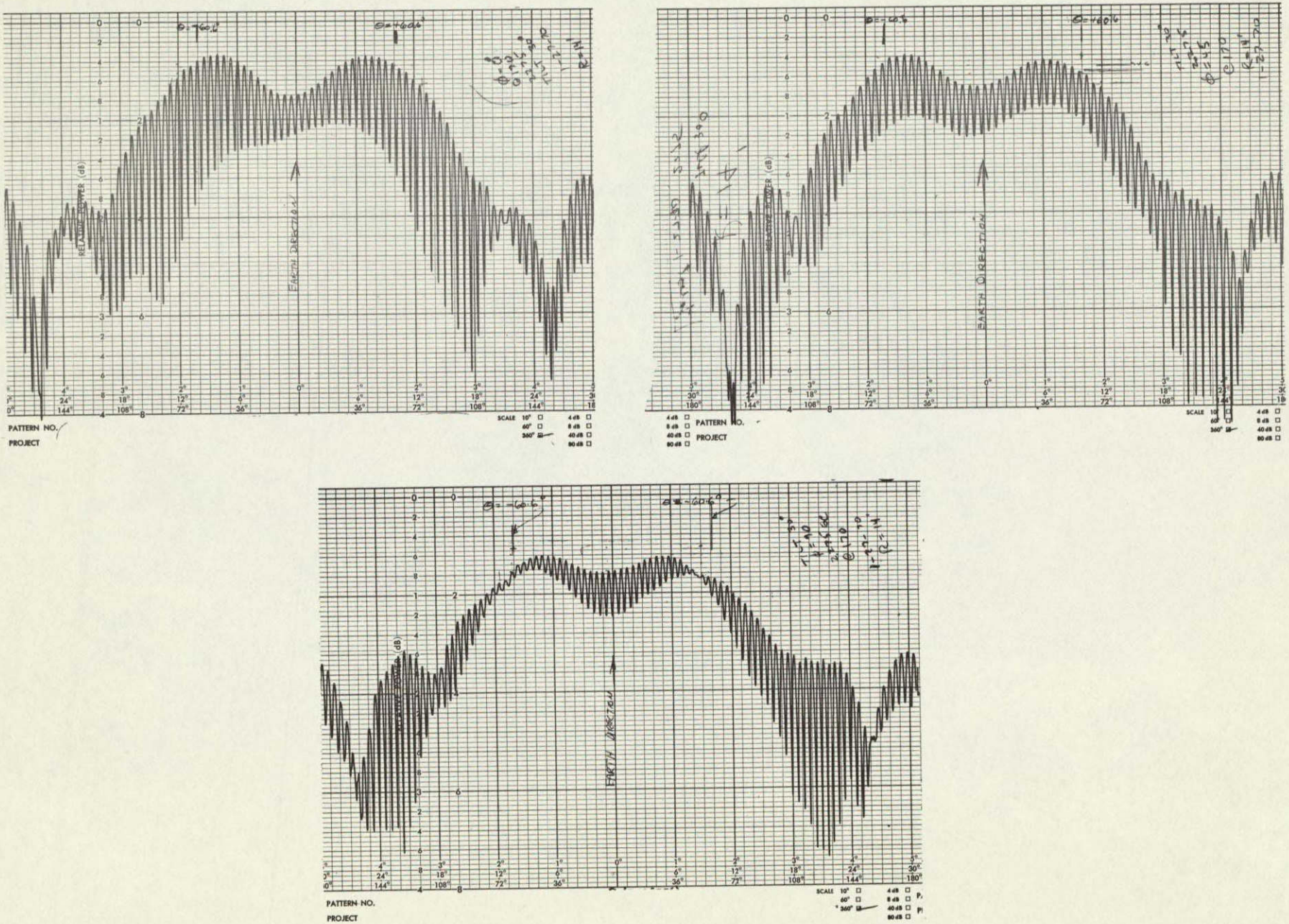

Figure 4.C-2. Measured Free-Space Radiation Patterns of Shaded-Beam Antenna at 2275 MHz

GENERAL ELECTRIC
SPACE DIVISION
SPACE SYSTEMS ORGANIZATION